

**REACTIVITY AND COORDINATION CHEMISTRY OF
RUTHENIUM(II) AMINOPHOSPHINE COMPLEXES WITH
H₂S, THIOLS, H₂O AND OTHER SMALL MOLECULES**

By

ERIN SHU FEN MA

B.Sc. (Hons.), University of British Columbia, 1994

A THESIS SUBMITTED IN PARTIAL FULFILLMENT OF
THE REQUIREMENTS FOR THE DEGREE OF
DOCTOR OF PHILOSOPHY

in

THE FACULTY OF GRADUATE STUDIES
(Department of Chemistry)

We accept this thesis as conforming
to the required standard

THE UNIVERSITY OF BRITISH COLUMBIA

August 1999

© Erin Shu Fen Ma, 1999

In presenting this thesis in partial fulfilment of the requirements for an advanced degree at the University of British Columbia, I agree that the Library shall make it freely available for reference and study. I further agree that permission for extensive copying of this thesis for scholarly purposes may be granted by the head of my department or by his or her representatives. It is understood that copying or publication of this thesis for financial gain shall not be allowed without my written permission.

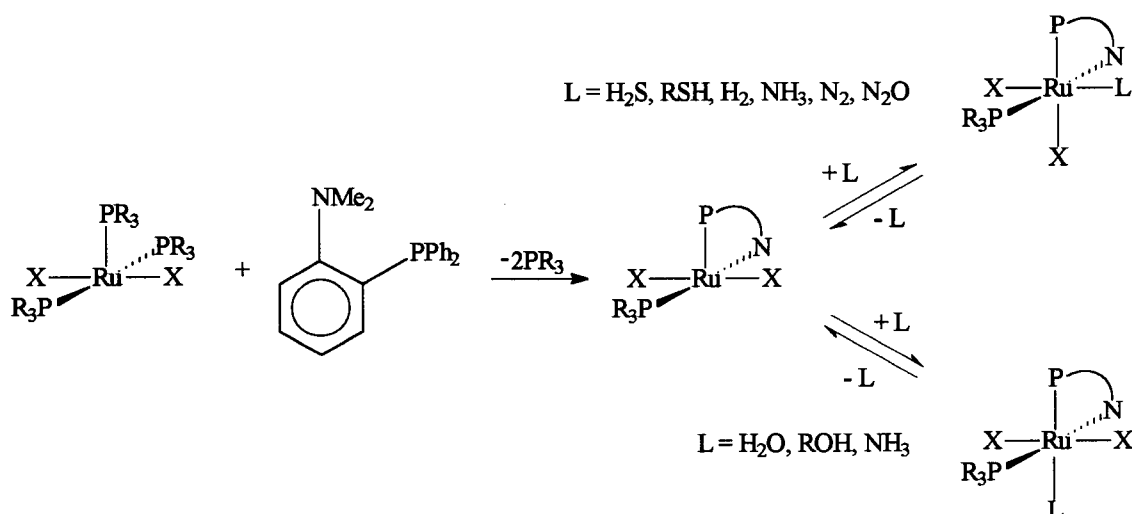
Department of Chemistry

The University of British Columbia
Vancouver, Canada

Date October 5, 1999

Abstract

The coordination of small molecules (H_2S , RSH , H_2O , ROH , H_2 , NH_3 , N_2 and N_2O ; R = alkyl) to the coordinatively unsaturated complexes $\text{RuX}_2(\text{P-N})(\text{PR}_3)$ ($\text{X} = \text{Cl}$, Br , I ; P-N = [*o*-(*N,N*-dimethylamino)phenyl]diphenylphosphine; $\text{R} = \text{Ph}$, *p*-tolyl), themselves prepared from $\text{RuX}_2(\text{PR}_3)_3$ and P-N , was investigated (see figure). The species containing the $\text{Ru}(\text{P-N})$ moiety were characterized spectroscopically, particularly by ^1H and $^{31}\text{P}\{^1\text{H}\}$ NMR and in some cases in conjunction with X-ray crystallography.



Cis- $\text{RuX}_2(\text{P-N})(\text{PPh}_3)(\text{L})$ species ($\text{X} = \text{Cl}$, $\text{L} = \text{H}_2\text{S}$, MeSH , EtSH ; $\text{X} = \text{Br}$, $\text{L} = \text{H}_2\text{S}$) were isolated from the reaction of $\text{RuX}_2(\text{P-N})(\text{PPh}_3)$ with excess L in acetone, and characterized crystallographically. The geometry of these complexes is pseudo-octahedral with the halogen atoms in mutual *cis* positions with the coordinated S-ligand *cis* to the P-atom of the P-N ligand and *trans* to a halogen atom; all H-atoms on the coordinated S-ligands were refined isotropically. The S-H bond lengths are of equal or shorter distances (1.20 - 1.34 Å) than those of free gaseous ligands (1.33 - 1.40 Å); in particular, the bond length of 1.03 Å for the coordinated MeSH complex is the shortest S-H distance yet reported. Of interest, the ^1H NMR spectrum of *cis*- $\text{RuX}_2(\text{P-N})(\text{PPh}_3)(\text{SH}_2)$ shows three-bond coupling of only one

proton of the coordinated H_2S to the P-atom of the P-N ligand ($\text{X} = \text{Cl}$, $^3J_{\text{HP}} = 3.5 \text{ Hz}$; $\text{X} = \text{Br}$, $^3J_{\text{HP}} = 4.3 \text{ Hz}$) at -50°C , and this represents an extension of the Karplus relationship to vicinal coupling within a P-Ru-S-H system.

The reaction of $\text{RuCl}_2(\text{P-N})(\text{PR}_3)$ with H_2O gave *trans*- $\text{RuCl}_2(\text{P-N})(\text{PR}_3)(\text{OH}_2)$, which was crystallographically characterized. The geometry is pseudo-octahedral with mutually *trans* Cl-atoms; the H_2O ligand is *trans* to the P-atom of the P-N ligand. The orientation of incoming monodentate ligand L in either *cis* or *trans* positions (see figure) is affected by the mutual *trans* influence of L and of the apical phosphine of $\text{RuX}_2(\text{P-N})(\text{PR}_3)$.

The thermodynamics for the reversible binding of H_2S , thiols, H_2 and H_2O to $\text{RuCl}_2(\text{P-N})(\text{PPh}_3)$, in solution, were determined using UV-Vis and NMR spectroscopies. The low ΔH° values (-22 to -54 kJ/mol) imply relatively weak Ru-L bond energies and the negative ΔS° values (-32 to -140 J/mol K) are consistent with binding of a small molecule at a metal site. Differential scanning calorimetry on solid state samples also allowed for determination of ΔH° values, and estimation of enthalpy changes for a *cis*- to *trans*-rearrangement in solution.

Cis- $\text{RuX}_2(\text{P-N})(\text{PPh}_3)(\text{SH}_2)$ ($\text{X} = \text{Cl}, \text{Br}$) reacted with NaSH or proton sponge (in the presence of added H_2S) to give initially $\text{Ru}(\text{SH})\text{Cl}(\text{P-N})(\text{PPh}_3)$ and then $\text{Ru}(\text{SH})_2(\text{P-N})(\text{PPh}_3)$. The mercapto species, however, are thermally unstable and were only observed by NMR spectroscopy at -78°C .

Reaction of 1 atm NH_3 with $\text{RuX}_2(\text{P-N})(\text{PPh}_3)$ ($\text{X} = \text{Cl}, \text{Br}$) in the solid state led to the formation of *trans*- $\text{RuX}_2(\text{P-N})(\text{PPh}_3)(\text{NH}_3)$ which, when dissolved in solution, subsequently isomerized to *cis*- $\text{RuX}_2(\text{P-N})(\text{PPh}_3)(\text{NH}_3)$. Evidence for bis- and tris-amine species, as well as for $[\text{RuX}(\text{P-N})(\text{PPh}_3)(\text{NH}_3)_2 \cdots \text{X}]$ with a 'strongly associated' halide, is also presented.

The formation of *cis*-RuCl₂(P-N)(PPh₃)(N₂O) was observed by NMR spectroscopy at -40°C when RuCl₂(P-N)(PPh₃) was subjected to 6 atm N₂O in CD₂Cl₂. The coordination of N₂O is of particular interest because of the rarity of such a reaction and because of the potential of discovering an effective catalytic oxidation system using N₂O as an O-atom donor. In fact, *cis*-RuCl₂(P-N)(PPh₃)(N₂O) appears to form *cis*-RuCl₂(P-N)(PPh₃)(η¹-N₂) and O₂ at T > -40°C. When the system was warmed to room temperature, O=PPh₃ and (μ-O)(μ-Cl)₂[RuCl(P-N)]₂ were formed. The crystallographically characterized μ-oxo complex was also formed when RuCl₂(P-N)(PPh₃) was reacted with O₂.

RuCl₂(P-N)(PPh₃) also reacted with HC≡CPh to give the crystallographically characterized *cis*-RuCl₂(P-N)(PPh₃)(=C=CHPh). The carbene complex reacted with H₂S and H₂O to give *cis*-RuCl₂(P-N)(PPh₃)(S=C(H)CH₂Ph) and a mixture containing RuCl(P-N)(PPh₃)(CH₂Ph)(CO) and RuCl₂(P-N)(PPh₃)(CO), respectively. The formulations of the products were based on ³¹P{¹H} NMR and IR spectroscopic data.

The reactions of RuCl₂(PR₃)₃ with aminophosphine ligands other than P-N were also explored: RuCl₂(BPN)(PR₃) (BPN = bis[*o*-(*N,N*-dimethylamino)phenyl]phenylphosphine) and RuCl₂(PAN)(PR₃) (PAN = 1-(*N,N*-dimethylamino)-8-(diphenylphosphino)naphthalene) were isolated and characterized; RuCl₂(AMPHOS)(PPh₃) (AMPHOS = (*R*)-(+)-*N,N*-dimethyl-1-[*o*-(dimethylphosphino)phenyl]ethylamine) was observed *in situ*; and an impure sample of RuCl₂(ALAPHOS)₂ (ALAPHOS = [(*S*)-2-(dimethylamino)propyl]diphenylphosphine) was isolated. PTN (tris[*o*-(*N,N*-dimethylamino)phenyl]phenylphosphine) did not react with RuCl₂(PR₃)₃.

Table of Contents

Abstract.....	ii
Table of Contents.....	v
List of Figures.....	xiii
List of Tables.....	xx
List of Symbols and Abbreviations.....	xxii
Table of Compound Numbers.....	xxvi
Acknowledgements.....	xxvii
 Chapter 1 Introduction.....	 1
1.1 Natural and Industrial Occurrences Sulfur Compounds	2
1.1.1 The Natural Sulfur Cycle.....	2
1.1.2 Hydrodesulfurization (HDS) and the Claus Process.....	3
1.2 Coordination Chemistry of H ₂ S and Thiols.....	5
1.2.1 Physical Properties of H ₂ S and Thiols.....	5
1.2.2 Reactions of H ₂ S and Thiols with Transition Metal Complexes.....	7
1.2.2.1 Mononuclear Mercapto and Thiolato Complexes.....	8
1.2.2.2 Bridging Mercapto and Thiolato Ligands.....	11
1.2.2.3 Recovery of H ₂ from H ₂ S using Pd ₂ X ₂ (μ ₂ -dpm) ₂	17
1.3 The Chemistry of Transition Metal Aminophosphine Complexes	19
1.4 Overview of Thesis	22
1.5 References	23
 Chapter 2 Experimental Procedures.....	 29
2.1 Materials.....	29
2.1.1 Gases	29
2.1.2 Solvents	29
2.1.3 Compounds.....	30
2.2 Instrumentation.....	30
2.2.1 Nuclear Magnetic Resonance Spectroscopy	30
2.2.2 Infrared Spectroscopy	31
2.2.3 Ultraviolet Spectroscopy.....	31
2.2.4 Thermal Analysis.....	32

2.2.5 Microanalysis	32
2.2.6 X-ray Crystallography	32
2.2.7 Gas Chromatography	33
2.2.8 Magnetic Susceptibility Studies	33
2.2.9 Conductivity Measurements	33
2.3 Syntheses of Ligands	34
2.3.1 [<i>o</i> -(<i>N,N</i> -Dimethylamino)phenyl]diphenylphosphine, P-N	35
2.3.2 Bis[<i>o</i> -(<i>N,N</i> -dimethylamino)phenyl]phenylphosphine, BPN	36
2.3.3 Tris[<i>o</i> -(<i>N,N</i> -dimethylamino)phenyl]phosphine, TPN	36
2.3.4 (<i>R</i>)-(+)- <i>N,N</i> -Dimethyl-1-[<i>o</i> -(diphenylphosphino)phenyl]ethylamine, AMPHOS ...	37
2.3.5 1-(<i>N,N</i> -Dimethylamino)-8-(diphenylphosphino)naphthalene, PAN	38
2.3.6 [(<i>S</i>)-2-(Dimethylamino)propyl]diphenylphosphine, ALAPHOS	39
2.3.7 <i>o</i> -Diphenylphosphineanisole, PO	41
2.4 Syntheses of Ruthenium Precursors	42
2.4.1 Dichlorotris(triphenylphosphine)ruthenium(II), RuCl ₂ (PPh ₃) ₃ (1)	42
2.4.2 Dichlorotris(tri- <i>p</i> -tolylphosphine)ruthenium(II), RuCl ₂ (P(<i>p</i> -tolyl) ₃) ₃ (2)	43
2.4.3 <i>Cis</i> -dichlorotetrakis(dimethylsulfoxide)ruthenium(II), <i>Cis</i> -RuCl ₂ (DMSO) ₄ (3) ...	43
2.4.4 Trichlorobis(triarylphosphine)(dimethylacetamide)ruthenium(III)·DMA solvate RuCl ₃ (PPh ₃) ₂ (DMA)(DMA) (4a) and RuCl ₂ (P(<i>p</i> -tolyl) ₃) ₂ (DMA)·(DMA) (4b) ..	43
2.5 Dichlorobis(<i>o</i> -diphenylphosphinoanisole)ruthenium(II), RuCl ₂ (PO) ₂ (5)	44
2.6 Syntheses of Ruthenium(II) Aminophosphine Complexes	44
2.6.1 Dichloro{[<i>o</i> -(<i>N,N</i> -dimethylamino)phenyl](diphenylphosphine)}- (triphenylphosphine)ruthenium(II), RuCl ₂ (P-N)(PPh ₃) (6a)	44
2.6.2 Dibromo{[<i>o</i> -(<i>N,N</i> -dimethylamino)phenyl](diphenylphosphine)}- (triphenylphosphine) ruthenium(II), RuBr ₂ (P-N)(PPh ₃) (6b)	45
2.6.3 Diiodo{[<i>o</i> -(<i>N,N</i> -dimethylamino)phenyl](diphenylphosphine)}- (triphenylphosphine)ruthenium(II), RuI ₂ (P-N)(PPh ₃) (6c)	45
2.6.4 Dichloro{[<i>o</i> -(<i>N,N</i> -dimethylamino)phenyl](diphenylphosphine)}- (tri- <i>p</i> -tolylphosphine)ruthenium(II), RuCl ₂ (P-N)(P(<i>p</i> -tolyl) ₃) (7a)	46
2.6.5 Dibromo{[<i>o</i> -(<i>N,N</i> -dimethylamino)phenyl](diphenylphosphine)}- (tri- <i>p</i> -tolylphosphine)ruthenium(II), RuBr ₂ (P-N)(P(<i>p</i> -tolyl) ₃) (7b)	46

2.6.6 Diiodo{[<i>o</i> -(<i>N,N</i> -dimethylamino)phenyl](diphenylphosphine)}-(tri- <i>p</i> -tolylphosphine)ruthenium(II), RuI ₂ (P-N)(P(<i>p</i> -tolyl) ₃) (7c)	47
2.6.7 Dichlorobis{[<i>o</i> -(<i>N,N</i> -dimethylamino)phenyl](diphenylphosphine)}-ruthenium(II), RuCl ₂ (P-N) ₂ (8)	47
2.6.8 Dichloro[(1-(<i>N,N</i> -dimethylamino)-8-(diphenylphosphino)naphthalene]-(triphenylphosphine) ruthenium(II), RuCl ₂ (PAN)(PPh ₃) (9)	48
2.6.9 Dichloro[(1-(<i>N,N</i> -dimethylamino)-8-(diphenylphosphino)naphthalene]-(tri- <i>p</i> -tolylphosphine)ruthenium(II), RuCl ₂ (PAN)(P(<i>p</i> -tolyl) ₃) (10)	48
2.6.10 Dichloro{(<i>R</i>)- <i>N,N</i> -dimethyl-1-[<i>o</i> -(diphenylphosphino)phenyl]ethylamine}-(triphenylphosphine)ruthenium(II), RuCl ₂ (AMPHOS)(PPh ₃) (11)	48
2.6.11 Attempts to Prepare Dichlorobis{[(<i>S</i>)-2-(dimethylamino)propyl]-(diphenylphosphine)}ruthenium(II), RuCl ₂ (ALAPHOS) ₂ (12)	49
2.6.12 Dichloro{bis[<i>o</i> -(<i>N,N</i> -dimethylamino)phenyl](phenylphosphine)}-(triphenylphosphine)ruthenium(II), RuCl ₂ (BPN)(PPh ₃) (13)	50
2.6.13 Dichloro{bis[<i>o</i> -(<i>N,N</i> -dimethylamino)phenyl](phenylphosphine)}-(tri- <i>p</i> -tolylphosphine) ruthenium(II), RuCl ₂ (BPN)(P(<i>p</i> -tolyl) ₃) (14)	51
2.7 Syntheses of Ruthenium(III) Aminophosphine Complexes	51
2.7.1 Trichloro{[<i>o</i> -(<i>N,N</i> -dimethylamino)phenyl](diphenylphosphine)}-(triphenylphosphine)ruthenium(III), RuCl ₃ (P-N)(PPh ₃) (15a)	51
2.7.2 Trichloro{[<i>o</i> -(<i>N,N</i> -dimethylamino)phenyl](diphenylphosphine)}-(tri- <i>p</i> -tolylphosphine) ruthenium(III), RuCl ₃ (P-N)(P(<i>p</i> -tolyl) ₃) (15b)	52
2.7.3 <i>Mer</i> -trichloro{bis[<i>o</i> -(<i>N,N</i> -dimethylamino)phenyl](phenylphosphine)}-ruthenium(III), <i>Mer</i> -RuCl ₃ (BPN) (16)	52
2.7.4 Di-μ-chloro-μ-oxo-bis{chloro[<i>o</i> -(<i>N,N</i> -dimethylamino)phenyl]-(diphenylphosphine)ruthenium(III)}, (μ-O)(μ-Cl) ₂ [RuCl(P-N)] ₂ (17)	53
2.8 Syntheses of Ruthenium(II) Complexes Containing Coordinated H ₂ S or Thiols:	
<i>Cis</i> -dichloro{[<i>o</i> - <i>N,N</i> -dimethylamino)phenyl](diphenylphosphine)}-(triarylphosphine)(ligand)ruthenium(II), <i>Cis</i> -RuX ₂ (P-N)(PR ₃)(L)	53
2.8.1 <i>Cis</i> -RuCl ₂ (P-N)(PPh ₃)(SH ₂)·(acetone) (18a)	54
2.8.2 <i>Cis</i> -RuBr ₂ (P-N)(PPh ₃)(SH ₂)·(acetone) (18b)	55
2.8.3 <i>In situ</i> Preparation of <i>Cis</i> -RuI ₂ (P-N)(PPh ₃)(SH ₂) (18c)	55
2.8.4 <i>Cis</i> -RuCl ₂ (P-N)(P(<i>p</i> -tolyl) ₃)(SH ₂)·(acetone) (19a)	56

2.8.5 <i>Cis</i> -RuBr ₂ (P-N)(P(<i>p</i> -tolyl) ₃)(SH ₂)·(acetone) (19b).....	56
2.8.6 <i>In situ</i> Preparation of <i>Cis</i> -RuI ₂ (P-N)(P(<i>p</i> -tolyl) ₃)(SH ₂) (19c).....	56
2.8.7 <i>Cis</i> -RuCl ₂ (P-N)(PPh ₃)(MeSH)·(acetone) (20).....	57
2.8.8 <i>Cis</i> -RuCl ₂ (P-N)(PPh ₃)(EtSH)·(EtSH)·(acetone) (21).....	57
2.8.9 <i>In situ</i> Preparation of <i>Cis</i> -RuCl ₂ (P-N)(PPh ₃)(RSH), R = <i>n</i> -Pr, <i>i</i> -Pr, <i>n</i> -Pn, <i>n</i> -Hx, and Bz (Pr = propyl, Pn = pentyl, Hx = hexyl, Bz = benzyl).....	58
2.9 <i>In situ</i> Preparation of Ru(L)X(P-N)(PPh ₃) (L = SH, OH, H) and Ru(L) ₂ (P-N)(PPh ₃) (X = Cl, Br; L = SH, OH, H).....	59
2.9.1 Ru(SH)Cl(P-N)(PPh ₃) (27a).....	59
2.9.2 Ru(SH)Br(P-N)(PPh ₃) (27b).....	60
2.9.3 Ru(OH)Cl(P-N)(PPh ₃) (28a).....	60
2.9.4 Ru(OH)Br(P-N)(PPh ₃) (28b).....	61
2.9.5 Ru(H)Cl(P-N)(PPh ₃) (29).....	61
2.9.6 Ru(SH) ₂ (P-N)(PPh ₃) (30).....	61
2.9.7 Ru(OH) ₂ (P-N)(PPh ₃) (31).....	62
2.9.8 Ru(H) ₂ (P-N)(PPh ₃) (32).....	62
2.10 Syntheses of Ruthenium(II) Complexes Containing Coordinated H ₂ O, MeOH, or EtOH.....	62
2.10.1 <i>Trans</i> -RuCl ₂ (P-N)(PPh ₃)(OH ₂) (33a).....	62
2.10.2 <i>Trans</i> -RuCl ₂ (P-N)(P(<i>p</i> -tolyl) ₃)(OH ₂) (33b).....	63
2.10.3 <i>Trans</i> -RuCl ₂ (P-N)(PPh ₃)(MeOH) (34).....	63
2.10.4 <i>Trans</i> -RuCl ₂ (P-N)(PPh ₃)(EtOH) (35).....	64
2.11 Syntheses of Ruthenium(II) Complexes with Other Coordinated Gases.....	65
2.11.1 <i>Cis</i> -RuCl ₂ (P-N)(PPh ₃)(η ² -H ₂) (36).....	65
2.11.2 Reactions with NH ₃	66
2.11.3 <i>Cis</i> -RuCl ₂ (P-N)(PPh ₃)(η ¹ -N ₂) (43).....	69
2.11.4 <i>Cis</i> -RuCl ₂ (P-N)(PPh ₃)(N ₂ O) (44).....	70
2.12 Synthesis and Reactions of Ruthenium(II) Carbene Complexes.....	70
2.12.1 <i>Cis</i> -RuCl ₂ (P-N)(PPh ₃)(=C=CHPh) (45).....	70
2.12.2 <i>Cis</i> -RuCl ₂ (P-N)(P(<i>p</i> -tolyl) ₃)(=C=CHPh) (46).....	71
2.12.3 <i>Cis</i> -RuCl ₂ (P-N)(PPh ₃)(=C=CHPhCH ₃) (47).....	71

2.12.4 <i>Cis</i> -RuCl ₂ (P-N)(PPh ₃)(SCHCH ₂ Ph) (48).....	72
2.12.5 Reaction of <i>Cis</i> -RuCl ₂ (P-N)(PPh ₃)(=C=C(H)Ph) (45) with H ₂ O.....	72
2.13 References	74
Chapter 3 Synthesis and Reactivity of Ruthenium Aminophosphine Precursors...	76
3.1 Introduction.....	76
3.2 Preparation of RuCl ₂ (P-N)(PR ₃) (R = Ph (6a), R = <i>p</i> -tolyl (7a))	76
3.2.1 Decomposition of RuCl ₂ (P-N)(PPh ₃) (6a) to (μ-O)(μ-Cl) ₂ [RuCl(P-N)] ₂ (17)	79
3.3 Metathesis Reactions	85
3.3.1 Synthesis and Characterization of RuBr ₂ (P-N)(PR ₃) (6b) and RuI ₂ (P-N)(PR ₃) (6c)	86
3.3.2 <i>In situ</i> Formation of Ru(OH)X(P-N)(PPh ₃) (X = Cl (28a), Br (28b)) and Ru(OH) ₂ (P-N)(PPh ₃) (31).....	88
3.3.3 <i>In situ</i> Reactions of 6a or 6b with NaSH·xH ₂ O	91
3.3.4 <i>In situ</i> Formation of Ru(H) ₂ (P-N)(PPh ₃) (32).....	92
3.4 Synthesis of RuCl ₂ (BPN)(PR ₃) (R = Ph (13), <i>p</i> -tolyl (14))	93
3.5 Synthesis of <i>Mer</i> -RuCl ₃ (BPN) (16)	96
3.6 The Reactions of TPN with Ru(II) and (III)	99
3.7 Characterization and Reactivity of RuCl ₂ (PAN)(PR ₃) (R = Ph (9), <i>p</i> -tolyl (10))	100
3.8 Attempted Synthesis and Reactivity of RuCl ₂ (AMPHOS)(PPh ₃) (11)	101
3.9 Attempted Preparations of RuCl ₂ (ALAPHOS) ₂ (12).....	104
3.10 Miscellaneous: Reactivity of <i>Trans</i> -RuCl ₂ (PO) ₂ (5) with H ₂ S.....	104
3.11 Summary	105
3.12 References	107
Chapter 4 Transition Metal H₂S AND Thiol Complexes: Synthesis and Characterization of <i>Cis</i>-RuX(P-N)(PR)(L); L = H₂S, Thiols.....	110
4.1 Introduction.....	110
4.1.1 Transition Metal H ₂ S Complexes.....	110
4.1.2 Transition Metal Thiol Complexes.....	115
4.2 Synthesis and Characterization of <i>Cis</i> -RuX ₂ (P-N)(PPh ₃)(SH ₂), X = Cl, Br, I	119
4.2.1 <i>Cis</i> -RuCl ₂ (P-N)(PPh ₃)(SH ₂) (18a)	120
4.2.2 <i>Cis</i> -RuBr ₂ (P-N)(PPh ₃)(SH ₂) (18b).....	131

4.2.3 <i>In situ</i> Preparation of <i>Cis</i> -RuI ₂ (P-N)(PPh ₃)(SH ₂) (18c) and <i>Cis</i> -RuI ₂ (P-N)(P(<i>p</i> -tolyl) ₃)(SH ₂) (19c)	135
4.3 The Synthesis and Characterization of <i>Cis</i> -RuCl ₂ (P-N)(PPh ₃)(RSH) Species (R = alkyl)	136
4.3.1 <i>Cis</i> -RuCl ₂ (P-N)(PPh ₃)(MeSH) (20)	136
4.3.2 <i>Cis</i> -RuCl ₂ (P-N)(PPh ₃)(EtSH) (21)	140
4.3.3 <i>In situ</i> Preparation of <i>Cis</i> -RuCl ₂ (P-N)(PPh ₃)(RSH) Species, R = <i>n</i> -Pr, <i>i</i> -Pr, <i>n</i> -Pn, <i>n</i> -Hx, Bz	145
4.4 Comparison of Coordinated S-H Vibrational Frequencies for 18a , 18b , 19a , 20 and 21	148
4.5 The UV-Vis Spectra of RuX ₂ (PN)(PR ₃) (X = halogen; PN = P-N, PAN or AMPHOS; R = Ph OR <i>p</i> -tolyl) and <i>Cis</i> -RuX ₂ (P-N)(PPh ₃)(L) (L = H ₂ S, MeSH or EtSH) Species	149
4.6 Solution Thermodynamics for Reversible Formation of H ₂ S and Thiol Complexes	152
4.7 The Ru-S Bond Strengths in the Solid State: DSC Experiments	156
4.8 The Acidity of RuCl ₂ (P-N)(PPh ₃)(H ₂ S): Proton Abstraction with Proton Sponge	158
4.9 Reaction of RuCl ₂ (P-N)(PPh ₃) with SO ₂	166
4.10 Decompositon of <i>Cis</i> -RuCl ₂ (P-N)(PPh ₃)(SH ₂)	167
4.11 Summary	168
4.12 References	169
Chapter 5 Coordination of H₂O and Alcohols to RuCl₂(P-N)(PPh₃)	173
5.1 Preparation of <i>Trans</i> -RuCl ₂ (P-N)(PR ₃)(OH ₂)	173
5.2 X-Ray Crystal Structures of <i>Trans</i> -RuCl ₂ (P-N)(PPh ₃)(OH ₂) (33a)	175
5.3 NMR Spectra <i>Trans</i> -RuCl ₂ (P-N)(PPh ₃)(OH ₂) (33a)	181
5.4 <i>Trans</i> Influence of Ligands and its Effect on ³¹ P NMR Chemical Shifts	186
5.5 UV-Vis Spectral Studies of the RuCl ₂ (P-N)(PPh ₃)/H ₂ O System	191
5.6 The Preparation of <i>Trans</i> -RuCl ₂ (P-N)(PPh ₃)(L) (L = MeOH (34) and EtOH (35))	195
5.7 DSC Data for Complexes Containing O-Donor ligands	198
5.8 Summary	201
5.9 References	202

Chapter 6	Reactions of $\text{RuCl}_2(\text{P-N})(\text{PPh}_3)$ with Dihydrogen, Ammonia, Nitrous Oxide, Alkynes, and Hydrogen Chloride	205
6.1	The Structure and Reactivity of $\text{Cis-RuCl}_2(\text{P-N})(\text{PPh}_3)(\eta^2\text{-H}_2)$ (36)	205
6.1.1	The Crystal Structure $\text{Cis-RuCl}_2(\text{P-N})(\text{PPh}_3)(\eta^2\text{-H}_2)$ (36)	206
6.1.2	Thermodynamic Studies of $\text{Cis-RuCl}_2(\text{P-N})(\text{PPh}_3)(\eta^2\text{-H}_2)$ (36) in Solution and in the Solid State	208
6.1.3	The pK_a of $\text{Cis-RuCl}_2(\text{P-N})(\text{PPh}_3)(\eta^2\text{-H}_2)$ (36)	211
6.2	Reactions of $\text{RuX}_2(\text{P-N})(\text{PPh}_3)$ ($\text{X} = \text{Cl}, \text{Br}$) with NH_3	214
6.2.1	Isolation of $[\text{RuX}(\text{P-N})(\text{PPh}_3)(\text{NH}_3)_2\cdots\text{X}]$ (37) in the Presence of Excess NH_3	214
6.2.2	The Solution Chemistry of $[\text{RuX}(\text{P-N})(\text{PPh}_3)(\text{NH}_3)_2\cdots\text{X}]$ (37)	216
6.2.3	The Solid State Reaction of $\text{RuX}_2(\text{P-N})(\text{PPh}_3)$ with NH_3	219
6.2.4	The Preparation of $[\text{RuCl}(\text{P-N})(\text{PPh}_3)(\text{NH}_3)_2]\text{PF}_6$ (41)	220
6.3	The Coordination Chemistry of N_2O	225
6.3.1	N_2O as a Potential Oxidant	225
6.3.2	The Reaction of $\text{RuCl}_2(\text{P-N})(\text{PPh}_3)$ with N_2O	229
6.4	Ruthenium Carbene Complexes: The Synthesis and Reactivity of $\text{Cis-RuCl}_2(\text{P-N})(\text{PR}_3)(=\text{C}=\text{C}(\text{H})\text{R}')$ ($\text{R}, \text{R}' = \text{Ph}, p\text{-tolyl}$)	235
6.4.1	Characterization of $\text{Cis-RuCl}_2(\text{P-N})(\text{PR}_3)(=\text{C}=\text{C}(\text{H})\text{R})$	235
6.4.2	The Reactivity of $\text{Cis-RuCl}_2(\text{P-N})(\text{PPh}_3)(=\text{C}=\text{C}(\text{H})\text{Ph})$ (45)	240
6.5	The Reaction of $\text{RuCl}_2(\text{P-N})(\text{PPh}_3)$ (6a) with HCl	243
6.6	The Catalytic Hydrogenation of $\text{PhC}(\text{H})=\text{NPh}$ Using Complexes Containing the $\text{Ru}(\text{P-N})$ Moiety	244
6.7	Summary	246
6.8	References	248
Chapter 7	General Conclusions and Recommendations for Future Research	253
7.1	References	256
Appendices		257
Appendix I	X-Ray Crystallographic Analysis of Bis[<i>o</i> - <i>N,N</i> -dimethylamino]phenyl]phenylphosphine, BPN	258
Appendix II	X-Ray Crystallographic Analysis of <i>Mer</i> - $\text{RuCl}_3(\text{BPN})$ (16)	261

Appendix III	X-Ray Crystallographic Analysis of $(\mu\text{-O})(\mu\text{-Cl})_2[\text{RuCl}(\text{P-N})]_2$ (17)	266
Appendix IV	X-Ray Crystallographic Analysis of <i>Cis</i> - $\text{RuCl}_2(\text{P-N})(\text{PPh}_3)(\text{SH}_2) \cdot (\text{acetone})$ (18a)	271
Appendix V	X-Ray Crystallographic Analysis of <i>Cis</i> - $\text{RuBr}_2(\text{P-N})(\text{PPh}_3)(\text{SH}_2) \cdot (\text{benzene})$ (18b)	276
Appendix VI	X-Ray Crystallographic Analysis of <i>Cis</i> - $\text{RuCl}_2(\text{P-N})(\text{PPh}_3)(\text{MeSH}) \cdot (\text{acetone})$ (20)	279
Appendix VII	X-Ray Crystallographic Analysis of <i>Cis</i> - $\text{RuCl}_2(\text{P-N})(\text{PPh}_3)(\text{EtSH}) \cdot (1.5\text{C}_6\text{D}_6)$ (21)	284
Appendix VIII	X-Ray Crystallographic Analysis of <i>Trans</i> - $\text{RuCl}_2(\text{P-N})(\text{PPh}_3)(\text{OH}_2) \cdot (2\text{C}_6\text{H}_6)$ (33a, I) and <i>Trans</i> - $\text{RuCl}_2(\text{P-N})(\text{PPh}_3)(\text{OH}_2) \cdot (1.5\text{C}_6\text{H}_6)$ (33a, II)	287
Appendix IX	X-Ray Crystallographic Analysis of <i>Cis</i> - $\text{RuCl}_2(\text{P-N})(\text{PPh}_3)(\eta^2\text{-H}_2)$ (36)	295
Appendix X	X-Ray Crystallographic Analysis of <i>Cis</i> - $\text{RuCl}_2(\text{P-N})(\text{PPh}_3)(=\text{C}=\text{CHPh})$ (45)	298
Appendix XI	Thermodynamic Calculations and Data for the Reversible Formation of <i>Cis</i> - $\text{RuCl}_2(\text{P-N})(\text{PPh}_3)(\text{L})$ (X = Cl, Br; R = Ph, <i>p</i> -tolyl; L = H_2S , MeSH, EtSH)	302
Appendix XII	Thermodynamic Calculations and Data for the Reversible Formation of <i>Trans</i> - $\text{RuCl}_2(\text{P-N})(\text{PPh}_3)(\text{OH}_2)$ (33a)	308
Appendix XIII	Thermodynamic Calculations and Data for the Reversible Formation of <i>Cis</i> - $\text{RuCl}_2(\text{P-N})(\text{PPh}_3)(\eta^2\text{-H}_2)$ (36)	316

List of Figures

Figure 1.1 The sulfur cycle in nature.	2
Figure 1.2 The most widely utilized methods for the synthesis of thiols.....	6
Figure 1.3 Some common coordination modes of SR^- ($\text{R} = \text{H}$ or alkyl) and S^{2-} ligands to transition metal centres (M).....	7
Figure 1.4 Formation of hydrido mercapto and bis(mercapto) Ru(II) phosphine complexes ...	9
Figure 1.5 Formation of <i>trans</i> - $\text{IrCl(H)(SH)(CO)(PPh}_3)_2$	9
Figure 1.6 Reactions of <i>trans</i> - $\text{Mo(N}_2)_2(\text{dppe})_2$ with thiols.....	10
Figure 1.7 Formation of five-coordinate, trigonal bipyramidal mercapto and thiolato complexes.	11
Figure 1.8 Reactions of H_2S with monomeric complexes to form di- and tri- μ_2 -SH dinuclear complexes.....	12
Figure 1.9 Reaction of $[\text{Ir(H)}_2(\text{MeCO})_2(\text{PPh}_3)_2][\text{BF}_4]$ with H_2S	13
Figure 1.10 Formation of dinuclear mercapto and thiolato-bridged complexes containing arene co-ligands.....	14
Figure 1.11 Clusters containing μ_2 - and μ_3 -SR bridged ligands.....	15
Figure 1.12 Formation of μ_2 -S and μ_2 -SMe dinuclear complexes.....	16
Figure 1.13 S-H bond activation in H_2S and thiols by (a) $\text{RhRe(CO)}_4(\mu\text{-dpm})_2$ and (b) $[\text{Pt}_3(\mu_3\text{-CO})(\mu\text{-dpm})_3]^{2+}$	17
Figure 1.14 Structure of intermediate formed during the reaction of $\text{Pd}_2\text{X}_2(\mu\text{-dpm})_2$ With H_2S en route to $\text{Pd}_2\text{X}_2(\mu_2\text{-S})(\mu\text{-dpm})_2$ and H_2	18
Figure 1.15 Homogeneous catalytic cycle for the recovery of H_2 from H_2S	19
Figure 1.16 Proposed transition state for the reconversion of $\text{Pd}_2\text{X}_2(\mu\text{-dpm})_2$ from $\text{Pd}_2\text{X}_2(\mu_2\text{-S})(\mu\text{-dpm})_2$	19
Figure 1.17 [<i>o</i> -(<i>N,N</i> -dimethylamino)phenyl]diphenylphosphine] (P-N)	19
Figure 1.18 Reaction of $\text{RuCl}_2(\text{P-N})(\text{PR}_3)$ with small molecules L.....	21
Figure 2.1 Ligands studied in this thesis work.....	34

Figure 3.1 The preparation of $\text{RuCl}_2(\text{P-N})(\text{PR}_3)$ ($\text{R} = \text{Ph}$ (6a), $\text{R} = p\text{-tolyl}$ (7a)).....	76
Figure 3.2 The ORTEP plot of $\text{RuCl}_2(\text{P-N})(\text{P}(p\text{-tolyl})_3)$ (7a)	78
Figure 3.3 The ORTEP plot of $(\mu\text{-O})(\mu\text{-Cl})_2[\text{RuCl}(\text{P-N})]_2$ (17).....	80
Figure 3.4 Antiferromagnetic coupling between two Ru centres through an O^{2-} ligand	83
Figure 3.5 UV-Vis spectrum of $(\mu\text{-O})(\mu\text{-Cl})_2[\text{RuCl}(\text{P-N})]_2$ (17) in DMSO at 25°C	84
Figure 3.6 The catalytic oxidation of PPh_3 to O=PPh_3 by 6a in the presence of O_2	85
Figure 3.7 Synthesis of $\text{RuBr}_2(\text{P-N})(\text{PPh}_3)$ (6b) and $\text{RuI}_2(\text{P-N})(\text{PPh}_3)$ (6c).....	86
Figure 3.8 $^{31}\text{P}\{^1\text{H}\}$ NMR spectra (81.0 MHz, C_6D_6 , 20°C) for (a) $\text{RuCl}_2(\text{P-N})(\text{PPh}_3)$ (6a), (b) $\text{RuBr}_2(\text{P-N})(\text{PPh}_3)$ (6b) and (c) $\text{RuI}_2(\text{P-N})(\text{PPh}_3)$ (6c).....	87
Figure 3.9 $^{31}\text{P}\{^1\text{H}\}$ NMR spectra (121.4 MHz) for the reaction of $\text{RuCl}_2(\text{P-N})(\text{PPh}_3)$ (6a) with NaOH in d_6 -acetone after (a) 2 h and (b) 20 h at 25°C	89
Figure 3.10 The substitution of Cl^- ligands by OH^- ligands.....	90
Figure 3.11 High field ^1H NMR spectrum (300 MHz) for the reaction of 6a with NaH in d_6 -acetone at 25°C	93
Figure 3.12 The ORTEP plot of BPN	94
Figure 3.13 Possible structures of $\text{RuCl}_2(\text{BPN})(\text{PR}_3)$	95
Figure 3.14 The ORTEP plot of <i>mer</i> - $\text{RuCl}_3(\text{BPN})\cdot\text{CHCl}_3$ (16).....	97
Figure 3.15 The ORTEP plot of TPN	99
Figure 3.16 Possible structures for $\text{RuCl}_2(\text{PAN})(\text{PR}_3)$	100
Figure 3.17 Synthesis of $\text{RuCl}_2(\text{AMPHOS})(\text{PPh}_3)$ (11).	102
Figure 3.18 Synthesis of $[(\text{PPh}_3)_2(\eta^2\text{-H}_2)\text{Ru}(\mu\text{-H})(\mu\text{-Cl})_2\text{Ru}(\text{H})(\text{PPh}_3)_2]$	102
Figure 3.19 Synthesis of $\text{Ru}(\text{H})\text{Cl}(\text{PPh}_3)_3$ using AMPHOS as the base.	103
Figure 3.20 Structure of $\text{RuCl}_2(\text{ALAPHOS})_2$ (12) (proposed) and $\text{RuCl}_2[\kappa^2(P,N)\text{-Ph}_2\text{PCH}_2\text{CH}_2\text{NMe}_2]_2$	104
Figure 3.21 Reactions of $\text{RuCl}_2(\text{PO})_2$ (5) with H_2S	105
Figure 4.1 The (a) preparation, (b) structure and (c) oxidation of $[\text{Ru}(\text{SH}_2)(\text{PPh}_3)(\text{'S}_4)]$	111

Figure 4.2 Formation of $[\text{Pt}(\text{PPh}_3)_2(\text{SH}_2)]$	112
Figure 4.3 Formation of $\text{W}(\text{CO})_5(\text{SH}_2)$	113
Figure 4.4 Formation of metal carbonyl H_2S salts.....	114
Figure 4.5 Formation of $[(\text{ThiCp})\text{Ru}(\text{PPh}_3)_2][\text{OTf}]$	114
Figure 4.6 Preparation of thiol complexes containing the electron rich CpM (M = Ru, Fe) moieties	116
Figure 4.7 Formation of $[\text{Ru}(\eta^3\text{:}\eta^3\text{-C}_{10}\text{H}_{16})\text{Cl}_2(\text{HSR})]$	117
Figure 4.8 Preparation of $[\text{IrH}(\text{SCH}_2\text{CH}_2\text{PPh}_2)(\text{HSCH}_2\text{CH}_2\text{PPh}_2)(\text{CO})]\text{Cl}$	118
Figure 4.9 <i>In situ</i> formation of $[\text{MH}(\text{CO})(\text{N-SH})(\text{PPh}_3)_2][\text{BF}_4]$	119
Figure 4.10 The ORTEP plot of <i>cis</i> - $\text{RuCl}_2(\text{P-N})(\text{PPh}_3)(\text{SH}_2)$ (18a).....	121
Figure 4.11 Bond distances between H-atom and C-atom of phenyl ring to indicate SH/ π interactions in $(\text{PhMe}_2\text{P})_3\text{Ru}(\mu\text{-SH})_3\text{Ru}(\text{SH})(\text{PMe}_2\text{Ph})_2$	123
Figure 4.12 $^{31}\text{P}\{^1\text{H}\}$ NMR spectra (202.47 MHz) of <i>cis</i> - $\text{RuCl}_2(\text{P-N})(\text{PPh}_3)(\text{SH}_2)$ (18a) in CD_2Cl_2 at various temperatures	125
Figure 4.13 ^1H NMR spectra (121.4 MHz) of <i>cis</i> - $\text{RuCl}_2(\text{P-N})(\text{PPh}_3)(\text{SH}_2)\cdot(\text{acetone})$ (18a) in C_6D_6	126
Figure 4.14 VT ^1H NMR spectra (500 MHz) of <i>cis</i> - $\text{RuCl}_2(\text{P-N})(\text{PPh}_3)(\text{SH}_2)$ (18a) in CD_2Cl_2 (under 1 atm H_2S) for the region δ 0.0 to δ 4.0	127
Figure 4.15 ^1H and $^1\text{H}\{^{31}\text{P}\}$ NMR spectra (500 MHz) of <i>cis</i> - $\text{RuCl}_2(\text{P-N})(\text{PPh}_3)(\text{SH}_2)$ (18a) in CD_2Cl_2 (under 1 atm H_2S) at -50°C for the region δ 0.2 to 1.6.....	128
Figure 4.16 ^1H NMR (500 MHz) signal at δ 1.49 for <i>cis</i> - $\text{RuCl}_2(\text{P-N})(\text{PPh}_3)(\text{SH}_2)$ (18a) with decoupler transmitter centred at 202.4685838 MHz with increasing ^{31}P decoupler power	129
Figure 4.17 The vicinal Karplus correlation. Relationship between dihedral angle (ϕ) and ^3J	130
Figure 4.18 End-on schematic view of the solid state structure of 18a	131
Figure 4.19 The ORTEP plot of <i>Cis</i> - $\text{RuBr}_2(\text{P-N})(\text{PPh}_3)(\text{SH}_2)$ (18b).	133
Figure 4.20 End-on view schematic view of the solid state structure of 18b	135

Figure 4.21 The ORTEP plot of <i>cis</i> -RuCl ₂ (P-N)(PPh ₃)(MeSH) (20).....	137
Figure 4.22 ¹ H NMR spectra of <i>cis</i> -RuCl ₂ (P-N)(PPh ₃)(MeSH)·(acetone) (20) in CD ₂ Cl ₂ (a) 20°C and (b) -50°C	139
Figure 4.23 The ORTEP plot of <i>cis</i> -RuCl ₂ (P-N)(PPh ₃)(EtSH) (21).....	141
Figure 4.24 ¹ H NMR spectrum (500 MHz) of 21 in CD ₂ Cl ₂ at 20°C	143
Figure 4.25 ¹ H NMR spectra of 21 (500 MHz, CD ₂ Cl ₂): (a) simulated spectrum; (b) expanded regions.	144
Figure 4.26 ¹ H NMR resonance of Ru-S-H _a in <i>cis</i> -RuCl ₂ (P-N)(PPh ₃)(EtSH) (21): (a) ¹ H NMR spectrum; (b) ¹ H{ ³¹ P}NMR spectrum (500 MHz, 20°C, CD ₂ Cl ₂).	145
Figure 4.27 ³¹ P{ ¹ H} NMR (300 MHz) spectra of <i>in situ</i> reactions of 6a with (a) <i>i</i> -PrSH and (b) <i>n</i> -PnSH in C ₆ D ₆ at 20°C.	147
Figure 4.28 The vibrational modes for H ₂ S (or any bent triatomic molecules).....	148
Figure 4.29 UV-Vis spectra for RuCl ₂ (P-N)(PPh ₃) (6a) and <i>cis</i> -RuCl ₂ (P-N)(PPh ₃)(SH ₂) (18a) in CH ₂ Cl ₂	151
Figure 4.30 Van't Hoff plots for the K equilibria (see p. 42) for (a) 18a , (b) 18b , (c) 19a , (d) 20 and (e) 21 in C ₆ D ₆	153
Figure 4.31 ¹ H NMR spectra in the region δ -0.5 to 4.5 (300 Mhz, C ₆ D ₆) for the equilibrium between 18a , 6a and H ₂ S at (a) 20°C, (b) 36°C and (c) 50°C.....	154
Figure 4.32 DSC curves for <i>cis</i> -RuCl ₂ (P-N)(PPh ₃)(L) complexes.....	157
Figure 4.33 Proposed reaction scheme for the loss of L from <i>cis</i> -RuCl ₂ (P-N)(PPh ₃)(L).....	158
Figure 4.34 Structure of a typical proton sponge.....	158
Figure 4.35 (a) , (b) Dihydrogen activation by Ru(II) complexes in the presence of added base, and (c) abstraction of proton from RuCl ₂ (P-N)(PPh ₃)(SH ₂).	159
Figure 4.36 ³¹ P{ ¹ H} NMR (300 MHz, CD ₂ Cl ₂) spectra for various Ru(II) complexes containing sulfur ligands: (a) RuCl ₂ (P-N)(PPh ₃)(SH ₂) at 20°C; RuCl ₂ (P-N)(PPh ₃) + 3PS + 1 atm H ₂ S at (b) 20°C, (c) -25°C, (d) -60°C and (e) -70°C	161
Figure 4.37 ¹ H NMR spectra (200 MHz, CDCl ₃ , r.t.) of (a) PS and (b) PSH ⁺ Cl ⁻	162

Figure 4.38 (a) Equilibrium for formation of $\text{RuCl}_2(\text{P-N})(\text{PPh}_3)(\text{SH}_2)$ (18a); (b), (c), (d) are subsequent equilibria en route to the formation of $\text{Ru}(\text{SH})_2(\text{P-N})(\text{PPh}_3)$ (30) in the presence of added PS	163
Figure 5.1 TGA spectrum of 33a	174
Figure 5.2 PLUTO plots of 33a (<i>trans</i> - $\text{RuCl}_2(\text{P-N})(\text{PPh}_3)(\text{OH}_2) \cdot 2\text{C}_6\text{H}_6$ (I) and <i>trans</i> - $\text{RuCl}_2(\text{P-N})(\text{PPh}_3)(\text{OH}_2) \cdot 1.5\text{C}_6\text{H}_6$ (II))	176
Figure 5.3 The ORTEP plot of $\text{RuCl}_2(\text{P-N})(\text{PPh}_3)(\text{OH}_2) \cdot 1.5\text{C}_6\text{H}_6$ (33a (II))	177
Figure 5.4 Rapid equilibrium between 6a and 33a	182
Figure 5.5 $^{31}\text{P}\{^1\text{H}\}$ NMR spectra of <i>trans</i> - $\text{RuCl}_2(\text{P-N})(\text{PPh}_3)(\text{OH}_2)$ (33a) in CD_2Cl_2 at various temperatures	183
Figure 5.6 $^{31}\text{P}\{^1\text{H}\}$ NMR spectra (20°C) of $\text{RuCl}_2(\text{P-N})(\text{PPh}_3)$ (6a) in d_6 -acetone with various H_2O concentrations	184
Figure 5.7 ^1H NMR spectra of <i>trans</i> - $\text{RuCl}_2(\text{P-N})(\text{PPh}_3)(\text{OH}_2)$ (33a) in CD_2Cl_2 at various temperatures	186
Figure 5.8 The relationship between Ru- P_A bond length (Å) and δP_A (in CDCl_3) for the complexes containing the Ru(P-N) moiety	188
Figure 5.9 Proposed mechanism for the formation of <i>cis</i> - $\text{RuCl}_2(\text{P-N})(\text{PPh}_3)(\text{SH}_2)$ (18a)	190
Figure 5.10 Species in equilibrium when 6a is dissolved in a coordinating solvent in the presence of H_2O	191
Figure 5.11 Spectral changes observed upon addition of H_2O to $\text{RuCl}_2(\text{P-N})(\text{PPh}_3)$ (6a) in CH_2Cl_2	192
Figure 5.12 Spectral changes observed upon addition of H_2O to $\text{RuCl}_2(\text{P-N})(\text{PPh}_3)$ (6a) in C_6H_6	192
Figure 5.13 Spectral changes observed upon addition of H_2O to $\text{RuCl}_2(\text{P-N})(\text{PPh}_3)$ (6a) in acetone	193
Figure 5.14 Spectral changes observed upon addition of H_2O to $\text{RuCl}_2(\text{P-N})(\text{PPh}_3)$ (6a) in THF	193
Figure 5.15 Solving K for the addition of H_2O to 6a at 25°C	194
Figure 5.16 ^1H NMR spectrum of <i>trans</i> - $\text{RuCl}_2(\text{P-N})(\text{PPh}_3)(\text{MeOH})$ (34) in CD_2Cl_2	196
Figure 5.17 ^1H NMR spectrum of <i>trans</i> - $\text{RuCl}_2(\text{P-N})(\text{PPh}_3)(\text{EtOH})$ (35) in CD_2Cl_2	197

Figure 5.18 DSC curves for <i>trans</i> -RuCl ₂ (P-N)(PPh ₃)(L)	199
Figure 5.19 DSC curves for <i>trans</i> -RuCl ₂ (P-N)(PPh ₃)(OH ₂) (33a) and <i>trans</i> -RuCl ₂ (P-N)(P(<i>p</i> -tolyl) ₃)(OH ₂) (33b)	200
Figure 6.1 The ORTEP plot of <i>cis</i> -RuCl ₂ (P-N)(PPh ₃)(η ² -H ₂) (36)	207
Figure 6.2 ³¹ P{ ¹ H} NMR spectrum (81.0 MHz) of 36 in equilibrium with 6a in C ₆ D ₆ at 20°C.	210
Figure 6.3 ¹ H NMR spectrum (200 MHz) of 36 in equilibrium with 6a in C ₆ D ₆ at 20°C	210
Figure 6.4 DSC curve for <i>cis</i> -RuCl ₂ (P-N)(PPh ₃)(η ² -H ₂) (36)	211
Figure 6.5 ³¹ P{ ¹ H} NMR (121.4 MHz, 20°C, CD ₂ Cl ₂) spectrum of the <i>in situ</i> reaction of RuCl ₂ (P-N)(PPh ₃) (6a) with 1.5 equiv PS under 1 atm H ₂	213
Figure 6.6 ¹ H NMR (121.4 MHz, 20°C, CD ₂ Cl ₂) spectrum in the region δ 2.0 to 4.0 of the <i>in situ</i> reaction of RuCl ₂ (P-N)(PPh ₃) (6a) with 1.5 equiv PS under 1 atm H ₂	213
Figure 6.7 Proposed structure of [RuX(P-N)(PPh ₃)(NH ₃) ₂ ···X] (37)	215
Figure 6.8 ¹ H NMR spectrum (CDCl ₃ , 300 MHz) of [RuCl(P-N)(PPh ₃)(NH ₃) ₂ ···Cl] (37a) under 1 atm NH ₃ at 20°C.	215
Figure 6.9 ³¹ P{ ¹ H} spectra (121.4 MHz, 20°C, CDCl ₃) for [RuCl(P-N)(PPh ₃)(NH ₃) ₂ ···Cl] (37a): (a) with 1 atm NH ₃ and (b) absence of excess NH ₃	217
Figure 6.10 Reversible conversion of [RuCl(P-N)(PPh ₃)(NH ₃) ₂ ···Cl] (37a) to <i>cis</i> -RuCl ₂ (P-N)(PPh ₃)(NH ₃) (39a).	218
Figure 6.11 ³¹ P{ ¹ H} NMR spectrum (121.4 MHz) of <i>trans</i> -RuCl ₂ (P-N)(PPh ₃)(NH ₃) (38a) after 5 min of being dissolved in CDCl ₃ at 20°C	220
Figure 6.12 ¹ H NMR spectrum (300 MHz) of <i>trans</i> -RuCl ₂ (P-N)(PPh ₃)(NH ₃) (38a) (after 5 min of being dissolved in CDCl ₃ at 20°C) in the region δ 0.0 to 4.0.	220
Figure 6.13 ³¹ P{ ¹ H} NMR spectra of (a) [RuCl(P-N)(PPh ₃)(NH ₃) ₂][PF ₆] (41) and (b) [RuCl(P-N)(PPh ₃)(NH ₃) ₂ ···Cl] (37a).	222
Figure 6.14 ³¹ P{ ¹ H} NMR spectrum for the <i>in situ</i> formation of [Ru(P-N)(PPh ₃)(NH ₃) ₃ ···Cl][PF ₆] (40a)	222
Figure 6.15 Reaction scheme for the preparation of NH ₃ complexes containing PF ₆ ⁻ ions. .	223

Figure 6.16 ^1H NMR spectrum of $[\text{RuCl}(\text{P-N})(\text{PPh}_3)(\text{NH}_3)_2][\text{PF}_6]$ (41).....	224
Figure 6.17 Potential catalytic cycle for the oxidation of organic substrates using N_2O	226
Figure 6.18 Stoichiometric formation of $\text{PhCH}_2\text{C}(\text{O})\text{Ph}$ utilizing N_2O	227
Figure 6.19 Transfer of the O-atom of N_2O into Ni-C bond.	228
Figure 6.20 Formation of Ru-OH complexes by O-atom insertion from N_2O	228
Figure 6.21 Possible coordination modes of N_2O to $(\text{dmpe})_2\text{Ru}(\text{H})_2$	229
Figure 6.22 $^{31}\text{P}\{^1\text{H}\}$ NMR spectrum (121.4 MHz, CD_2Cl_2) of (a) 6a , and the reaction of 6a with 6 atm N_2O at (b) 20°C , (c) -40°C , (d) -90°C and (e) 20°C after reaction time of 2 days.	231
Figure 6.23 $^{31}\text{P}\{^1\text{H}\}$ NMR spectra (121.4 MHz, CD_2Cl_2) for the reaction of 6a with (a) 6 atm N_2 at 20°C and (b) 6 atm N_2O at -40°C	232
Figure 6.24 Proposed reaction scheme for the formation of 17 and $\text{O}=\text{PPh}_3$ if N_2O is initially coordinated to 6a via the terminal N atom.....	233
Figure 6.25 The catalytic oxidation of PPh_3 by N_2O	234
Figure 6.26 Formation of a vinylidene complex from a 1-alkyne ligand.....	236
Figure 6.27 The ORTEP plot of <i>cis</i> - $\text{RuCl}_2(\text{P-N})(\text{PPh}_3)(=\text{C}=\text{C}(\text{H})\text{Ph})$ (45)	237
Figure 6.28 $^{31}\text{P}\{^1\text{H}\}$ NMR spectrum (81.0 MHz, 20°C) of <i>cis</i> - $\text{RuCl}_2(\text{P-N})(\text{PPh}_3)(=\text{C}=\text{C}(\text{H})\text{Ph})$ (45) in CDCl_3	239
Figure 6.29 ^1H NMR spectrum (200 MHz, 20°C) of <i>cis</i> - $\text{RuCl}_2(\text{P-N})(\text{PPh}_3)(=\text{C}_\alpha=\text{C}_\beta(\text{H})\text{Ph})$ (45) in CDCl_3	240
Figure 6.30 Proposed mechanism for the formation of <i>cis</i> - $\text{RuCl}_2(\text{P-N})(\text{PPh}_3)(\text{S}=\text{C}(\text{H})\text{CH}_2\text{Ph})$ (48) from 45 and H_2S	241
Figure 6.31 The reaction of <i>cis</i> - $\text{RuCl}_2(\text{P-N})(\text{PPh}_3)(=\text{C}=\text{C}(\text{H})\text{Ph})$ (45) with H_2O at 80°C in THF.	243
Figure 6.32 Reaction of $\text{RuCl}_2(\text{P-N})(\text{PPh}_3)$ (6a) with HCl : formation of $\text{RuCl}_3(\text{P-N})(\text{PPh}_3)$ (15a).	244
Figure 6.33 $^{31}\text{P}\{^1\text{H}\}$ NMR spectra for the reaction of $\text{RuCl}_2(\text{P-N})(\text{PPh}_3)$ (6a) with (a) 1 equiv HCl and (b) 5 equiv HCl in C_6D_6	244
Figure 7.1 Examples for the modification of P-N	255

List of Tables

Table 1.1 Some physical properties of H ₂ S and thiols.....	6
Table 3.1 Selected bond lengths (Å) for (μ-O)(μ-Cl) ₂ [RuCl(P-N)] ₂ (17)	81
Table 3.2 Selected bond angles (°) for (μ-O)(μ-Cl) ₂ [RuCl(P-N)] ₂ (17).....	81
Table 3.3 ³¹ P{ ¹ H} NMR data for the <i>in situ</i> reactions of RuX ₂ (P-N)(PPh ₃) (X = Cl, Br) with NaOH in d ₆ -acetone.....	91
Table 3.4 ¹ H NMR data for the <i>in situ</i> reactions of RuX ₂ (P-N)(PPh ₃) (X = Cl, Br) with NaOH in d ₆ -acetone.	91
Table 3.5 ³¹ P{ ¹ H} NMR spectroscopic data for RuCl ₂ (BPN)(PR ₃) in CDCl ₃	95
Table 3.6 ¹ H NMR chemical shifts for RuCl ₂ (BPN)(PR ₃) in CDCl ₃	95
Table 3.7 Selected bond lengths (Å) for <i>mer</i> -RuCl ₃ (BPN) (16)	98
Table 3.8 Selected bond angles (°) for <i>mer</i> -RuCl ₃ (BPN) (16).....	98
Table 4.1 Selected bond lengths (Å) for <i>cis</i> -RuCl ₂ (P-N)(PPh ₃)(SH ₂) (18a) and <i>cis</i> -RuCl ₂ (P-N)(P(<i>p</i> -tolyl) ₃)(SH ₂) (19a).....	122
Table 4.2 Selected bond angles (°) for <i>cis</i> -RuCl ₂ (P-N)(PPh ₃)(SH ₂) (18a) and <i>cis</i> -RuCl ₂ (P-N)(P(<i>p</i> -tolyl) ₃)(SH ₂) (19a).....	122
Table 4.3 Selected bond lengths (Å) for <i>cis</i> -RuBr ₂ (P-N)(PPh ₃)(SH ₂) (18b).....	134
Table 4.4 Selected bond angles (°) for <i>cis</i> -RuBr ₂ (P-N)(PPh ₃)(SH ₂) (18b)	134
Table 4.5 Selected bond lengths (Å) for <i>cis</i> -RuCl ₂ (P-N)(PPh ₃)(MeSH) (20).....	138
Table 4.6 Selected bond angles (°) for <i>cis</i> -RuCl ₂ (P-N)(PPh ₃)(MeSH) (20)	138
Table 4.7 Selected bond lengths (Å) for <i>cis</i> -RuCl ₂ (P-N)(PPh ₃)(EtSH) (21)	142
Table 4.8 Selected bond angles (°) for <i>cis</i> -RuCl ₂ (P-N)(PPh ₃)(EtSH) (21).....	142
Table 4.9 ³¹ P{ ¹ H} NMR chemical shifts (121.4 MHz) for <i>cis</i> -RuCl ₂ (P-N)(PPh ₃)(RSH) in the presence of added RSH.....	146
Table 4.10 ν _{S-H} (cm ⁻¹) frequencies (ν ₁ and ν ₃ bands) for H ₂ S and thiols, in the free gaseous state and upon coordination to Ru.....	149
Table 4.11 λ ₁ and λ ₂ UV-Vis bands for RuX ₂ (PN)(PPh ₃)(L) in CD ₂ Cl ₂	150

Table 4.12 Thermodynamic parameters for the formation of <i>cis</i> -RuX ₂ (P-N)(PR ₃)(L) in C ₆ D ₆	155
Table 4.13 ³¹ P{ ¹ H} NMR chemicals shifts of Ru(II) mercapto complexes in d ₆ -acetone. ...	165
Table 5.1 Selected bond lengths (Å) for <i>trans</i> -RuCl ₂ (P-N)(PPh ₃)(OH ₂)·2C ₆ H ₆ (I), <i>trans</i> -RuCl ₂ (P-N)(PPh ₃)(OH ₂)·1.5C ₆ H ₆ (II) and <i>trans</i> -RuCl ₂ (P-N)(P(<i>p</i> -tolyl) ₃ (OH ₂) (33b)	179
Table 5.2 Selected bond angles (°) for <i>trans</i> -RuCl ₂ (P-N)(PPh ₃)(OH ₂)·2C ₆ H ₆ (I), <i>trans</i> -RuCl ₂ (P-N)(PPh ₃)(OH ₂)·1.5C ₆ H ₆ (II) and <i>trans</i> -RuCl ₂ (P-N)(P(<i>p</i> -tolyl) ₃ (OH ₂) (33b)	180
Table 5.3 P _A and P _X chemical shifts for RuCl ₂ (P-N)(PPh ₃) (6a) and <i>trans</i> -RuCl ₂ (P-N)(PPh ₃)(OH ₂) (33a)	182
Table 5.4 Comparison of ³¹ P{ ¹ H} NMR chemical shifts and Ru-P bond lengths	187
Table 5.5 Ru-Cl bond lengths (Å) for <i>trans</i> -RuCl ₂ (P-N)(PR ₃)(L)	189
Table 5.6 Ru-Cl bond lengths (Å) for <i>cis</i> -RuCl ₂ (P-N)(PR ₃)(L)	190
Table 6.1 Selected bond lengths (Å) for <i>cis</i> -RuCl ₂ (P-N)(PPh ₃)(η ² -H ₂) (36)	208
Table 6.2 Selected bond angles (°) for <i>cis</i> -RuCl ₂ (P-N)(PPh ₃)(η ² -H ₂) (36)	208
Table 6.3 ³¹ P{ ¹ H} NMR data for Ru(II) ammonia complexes in CDCl ₃	217
Table 6.4 ¹ H NMR data for Ru(II) ammonia complexes in CDCl ₃	218
Table 6.5 Selected bond lengths (Å) for <i>cis</i> -RuCl ₂ (P-N)(PPh ₃)(=C=C(H)Ph) (45)	238
Table 6.6 Selected bond angles (°) for <i>cis</i> -RuCl ₂ (P-N)(PPh ₃)(=C=C(H)Ph) (45)	238
Table 6.7 Hydrogenation of PhC(H)=NPh using ruthenium aminophosphine complexes	246

List of Symbols and Abbreviations

δ	chemical shift (parts per million)
μ	descriptor for bridging
ϵ	extinction coefficient or molar absorptivity ($M^{-1} \text{ cm}^{-1}$)
κ	kappa, coordination of different atoms of ligand
λ	wavelength (nm)
ν	frequency (cm^{-1})
Λ_M	molar conductivity ($\text{ohm}^{-1} \text{ mol}^{-1} \text{ cm}^2$)
η^n	hapticity of degree n
(<i>R</i>)-	absolute configuration (Latin: rectus; right)
(<i>S</i>)-	absolute configuration (Latin: sinister; left)
°	degrees
*	chiral centre
≠	transition state
[]	molar concentration
$^{13}\text{C}\{^1\text{H}\}$	carbon-13-observed proton-decoupled (NMR)
$^1\text{H}\{^{31}\text{P}\}$	proton-observed phosphorus-31-decoupled (NMR)
$^{31}\text{P}\{^1\text{H}\}$	phosphorus-31-observed proton-decoupled (NMR)
Å	angstrom, 10^{-10}m
ALAPHOS	[(<i>S</i>)-2-(dimethylamino)propyl]diphenylphosphine
AMPHOS	(<i>R</i>)-(+)- <i>N,N</i> -dimethyl-1-[<i>o</i> -(dimethylphosphino)phenyl]ethylamine
anal.	analysis
atm	atmosphere(s)
b.p.	boiling point
bdpp	(2 <i>S</i> , 4 <i>S</i>)-2,4-bis(diphenylphosphino)pentane
binap	(<i>R</i>)- or (<i>S</i>)-2,2'-bis(diphenylphosphino)-1,1'-binaphthyl
BPN	bis[<i>o</i> -(<i>N,N</i> -dimethylamino)phenyl]phenylphosphine
br	broad
bu	butyl
bz	benzyl
calcd	calculated

<i>cct</i>	<i>cis, cis, trans</i>
chiraphos	2,3-bis(diphenylphosphino)butane
Cp	cyclopentadienyl
Cp*	pentamethylcyclopentadienyl
Cy	cyclohexyl
d	doublet
dd	doublet of doublets
ddd	doublet of doublet of doublets
diop	4,5-bis[(diphenylphosphino)methyl]-2,2-dimethyl-1,3-dioxolane]
dippe	1,2-bis(diisopropylphosphine)ethane
DMA	<i>N,N</i> -dimethylacetamide
dmpe	1,2-bis(dimethylphosphino)ethane
DMSO	dimethylsulfoxide
dpm, dppm	1,1-bis(diphenylphosphino)methane
dppb	1,4-bis(diphenylphosphino)butane
dppe	1,2-bis(diphenylphosphino)ethane
dppn	1,5-bis(diphenylphosphino)pentane
dppp	1,3-bis(diphenylphosphino)propane
dq	doublet of quartets
DSC	differential scanning calorimetry
e.e.	enantiomeric excess
equiv	equivalent(s)
Et	ethyl
h	hour(s)
HDS	hydrodesulfurization
hx	hexyl
Hz	Hertz, cycles per second
<i>i</i>	iso
IR	infrared (spectroscopy)
isn	isonicotinamide
isoPFA	1-[α - <i>N,N</i> -dimethylaminoethyl]-2-(diphenylphosphino)ferrocene
J	coupling constant (Hz)

K	equilibrium constant
L	litre
m	multiplet (NMR), medium (IR), milli-, meter
M	molarity (mol/L), mega-
<i>m</i>	meta
m.p.	melting point
Me	methyl
min	minute(s)
MNAA	2-(6'-methoxynaphth-2'-yl)acrylate anion
<i>n</i>	normal
N-S	pyridine-2-thiolate or quinoline-8-thiolate
NMR	nuclear magnetic resonance (spectroscopy)
NP ₃	tris(2-diphenylphosphinoethyl)amine
<i>o</i>	ortho
OTf	triflate
OTs	<i>p</i> -toluenesulfonate
<i>p</i>	para
P-N	[<i>o</i> -(<i>N,N</i> -dimethylamino)phenyl]diphenylphosphine
PAN	1-(<i>N,N</i> -dimethylamino)-8-(diphenylphosphino)naphthalene
Ph	phenyl
PN	aminophosphine ligand
pn	pentyl
PNP	1- <i>N,N</i> -bis[(diphenylphosphino)ethyl]propylamine
PO	<i>o</i> -diphenylphosphineanisole
PP ₃	tris(2-diphenylphosphinoethyl)phosphine
PPFA	1-[<i>N,N</i> - α -dimethylaminoethyl]-2-diphenylphosphinoferrocene
ppm	parts per million
Pr	propyl
PS	proton sponge or 1,8-bis(dimethylamino)naphthalene
psi	pounds per square inch
q	quartet
qn	quintet

r.t.	room temperature
s	singlet, second(s), strong (IR)
<i>t</i>	tertiary
t	triplet
T ₁	longitudinal relaxation time (NMR)
TGA	thermogravimetric analysis
THF	tetrahydrofuran
ThiCp	2-(thienylmethyl)cyclopentadienyl
TPN	tris[<i>o</i> -(<i>N,N</i> -dimethylamino)phenyl]phenylphosphine
TPP	tetraphenylporphyrin
triphos	1,1,1-tris(diphenylphosphinoethyl)ethane
trpy	2,2'2''-terpyridine
UV-Vis	ultraviolet-visible (spectroscopy)
VT	variable temperature
w	weak

Table of Compound Numbers

Number	Compound
1	$\text{RuCl}_2(\text{PPh}_3)_3$
2	$\text{RuCl}_2(\text{P}(p\text{-tolyl})_3)_3$
3	$\text{cis-RuCl}_2(\text{DMSO})_4$
4a	$\text{RuCl}_3(\text{PPh}_3)_2(\text{DMA}) \cdot (\text{DMA})$
4b	$\text{RuCl}_3(\text{P}(p\text{-tolyl})_3)_2(\text{DMA}) \cdot (\text{DMA})$
5	$\text{RuCl}_2(\text{PO})_2$
6a	$\text{RuCl}_2(\text{P-N})(\text{PPh}_3)$
6b	$\text{RuBr}_2(\text{P-N})(\text{PPh}_3)$
6c	$\text{RuI}_2(\text{P-N})(\text{PPh}_3)$
7a	$\text{RuCl}_2(\text{P-N})(\text{P}(p\text{-tolyl})_3)$
7b	$\text{RuBr}_2(\text{P-N})(\text{P}(p\text{-tolyl})_3)$
7c	$\text{RuI}_2(\text{P-N})(\text{P}(p\text{-tolyl})_3)$
8	$\text{RuCl}_2(\text{P-N})_2$
9	$\text{RuCl}_2(\text{PAN})(\text{PPh}_3)$
10	$\text{RuCl}_2(\text{PAN})(\text{P}(p\text{-tolyl})_3)$
11	$\text{RuCl}_2(\text{AMPHOS})(\text{PPh}_3)$
12	$\text{RuCl}_2(\text{ALAPHOS})_2$
13	$\text{RuCl}_2(\text{BPN})(\text{PPh}_3)$
14	$\text{RuCl}_2(\text{BPN})(\text{P}(p\text{-tolyl})_3)$
15a	$\text{RuCl}_3(\text{P-N})(\text{PPh}_3)$
15b	$\text{RuCl}_3(\text{P-N})(\text{P}(p\text{-tolyl})_3)$
16	$\text{mer-RuCl}_3(\text{BPN})$
17	$(\mu\text{-O})(\mu\text{-Cl})[\text{RuCl}(\text{P-N})]_2$
18a	$\text{cis-RuCl}_2(\text{P-N})(\text{PPh}_3)(\text{SH}_2)$
18b	$\text{cis-RuBr}_2(\text{P-N})(\text{PPh}_3)(\text{SH}_2)$
18c	$\text{cis-RuI}_2(\text{P-N})(\text{PPh}_3)(\text{SH}_2)$
19a	$\text{cis-RuCl}_2(\text{P-N})(\text{P}(p\text{-tolyl})_3)(\text{SH}_2)$
19b	$\text{cis-RuBr}_2(\text{P-N})(\text{P}(p\text{-tolyl})_3)(\text{SH}_2)$
19c	$\text{cis-RuI}_2(\text{P-N})(\text{P}(p\text{-tolyl})_3)(\text{SH}_2)$
20	$\text{cis-RuCl}_2(\text{P-N})(\text{PPh}_3)(\text{MeSH})$
21	$\text{cis-RuCl}_2(\text{P-N})(\text{PPh}_3)(\text{EtSH})$
22	$\text{cis-RuCl}_2(\text{P-N})(\text{PPh}_3)(n\text{-PrSH})$
23	$\text{cis-RuCl}_2(\text{P-N})(\text{PPh}_3)(i\text{-PrSH})$
24	$\text{cis-RuCl}_2(\text{P-N})(\text{PPh}_3)(n\text{-PnSH})$

Number	Compound
25	$\text{cis-RuCl}_2(\text{P-N})(\text{PPh}_3)(n\text{-HxSH})$
26	$\text{cis-RuCl}_2(\text{P-N})(\text{PPh}_3)(\text{BzSH})$
27a	$\text{Ru}(\text{SH})\text{Cl}(\text{P-N})(\text{PPh}_3)$
27b	$\text{Ru}(\text{SH})\text{Br}(\text{P-N})(\text{PPh}_3)$
28a	$\text{Ru}(\text{OH})\text{Cl}(\text{P-N})(\text{PPh}_3)$
28b	$\text{Ru}(\text{OH})\text{Br}(\text{P-N})(\text{PPh}_3)$
29	$\text{Ru}(\text{H})\text{Cl}(\text{P-N})(\text{PPh}_3)$
30	$\text{Ru}(\text{SH})_2(\text{P-N})(\text{PPh}_3)$
31	$\text{Ru}(\text{OH})_2(\text{P-N})(\text{PPh}_3)$
32	$\text{Ru}(\text{H})_2(\text{P-N})(\text{PPh}_3)$
33a	$\text{trans-RuCl}_2(\text{P-N})(\text{PPh}_3)(\text{OH}_2)$
33b	$\text{trans-RuCl}_2(\text{P-N})(\text{P}(p\text{-tolyl})_3)(\text{OH}_2)$
34	$\text{trans-RuCl}_2(\text{P-N})(\text{PPh}_3)(\text{MeOH})$
35	$\text{trans-RuCl}_2(\text{P-N})(\text{PPh}_3)(\text{EtOH})$
36	$\text{cis-RuCl}_2(\text{P-N})(\text{PPh}_3)(\eta^2\text{-H}_2)$
37a	$[\text{RuCl}(\text{P-N})(\text{PPh}_3)(\text{NH}_3)_2 \cdots \text{Cl}]$
37b	$[\text{RuBr}(\text{P-N})(\text{PPh}_3)(\text{NH}_3)_2 \cdots \text{Br}]$
38a	$\text{trans-RuCl}_2(\text{P-N})(\text{PPh}_3)(\text{NH}_3)$
38b	$\text{trans-RuBr}_2(\text{P-N})(\text{PPh}_3)(\text{NH}_3)$
39a	$\text{cis-RuCl}_2(\text{P-N})(\text{PPh}_3)(\text{NH}_3)$
39b	$\text{trans-RuBr}_2(\text{P-N})(\text{PPh}_3)(\text{NH}_3)$
40a	$[\text{Ru}(\text{P-N})(\text{PPh}_3)(\text{NH}_3)_3 \cdots \text{Cl}][\text{PF}_6]$
40b	$[\text{Ru}(\text{P-N})(\text{PPh}_3)(\text{NH}_3)_3][\text{PF}_6]_2$
41	$[\text{RuCl}(\text{P-N})(\text{PPh}_3)(\text{NH}_3)_2][\text{PF}_6]$
42	$[\text{RuCl}(\text{P-N})(\text{PPh}_3)(\text{NH}_3)][\text{PF}_6]$
43	$\text{cis-RuCl}_2(\text{P-N})(\text{PPh}_3)(\eta^1\text{-N}_2)$
44	$\text{cis-RuCl}_2(\text{P-N})(\text{PPh}_3)(\text{N}_2\text{O})$
45	$\text{cis-RuCl}_2(\text{P-N})(\text{PPh}_3)(=\text{C}=\text{CHPh})$
46	$\text{cis-RuCl}_2(\text{P-N})(\text{P}(p\text{-tolyl})_3)(=\text{C}=\text{CHPh})$
47	$\text{cis-RuCl}_2(\text{P-N})(\text{PPh}_3)(=\text{C}=\text{CHPhCH}_3)$
48	$\text{cis-RuCl}_2(\text{P-N})(\text{PPh}_3)(\text{SCHCH}_2\text{Ph})$
49	$\text{RuCl}(\text{P-N})(\text{PPh}_3)(\text{CH}_2\text{Ph})(\text{CO})$
50	$\text{RuCl}_2(\text{P-N})(\text{PPh}_3)(\text{CO})$

Acknowledgements

I offer my most sincere gratitude to my supervisor, Prof. Brian R. James for his expert guidance and support throughout this thesis work. The opportunity to work in his laboratory has provided me with invaluable experience for my career as a scientist. I would like to thank the past and present members of the James group, in particular Ian Baird, Terrance Wong, Graham Cairns, Patric Meessen, Nathan Jones, Craig Pamplin, Paul Cyr, Matt LePage, and Elizabeth Cheu for their friendship, encouragement and useful discussions. Thanks for your support and proofreading parts of this thesis.

I would also like to thank the departmental services, especially Dr. Nick Burlinson, Lianne Darge, and Marietta Austria from the NMR labs; the late Dr. Steve Rettig from the X-ray crystallography lab; Peter Borda from the microanalysis lab and Steve Rak from the glassblowing lab for their indispensable assistance. I am also grateful to Jim Sawada for assistance with the TGA/DSC instruments.

Finally, I would like to thank my parents and sisters for their support, encouragement and understanding over the years. Many thanks to Susan Ong, thanks for listening.

Chapter 1

Introduction

The reactions of H_2S with transition metal complexes have been one of the main focuses in this laboratory.¹ One aspect of such research emphasizes the development of homogeneous catalytic systems for the recovery of H_2 from H_2S .²⁻⁷ From another perspective, we are interested in studying the mechanisms of simple models in homogeneous systems and correlating these findings to those of heterogeneous catalytic systems.⁸⁻¹³ One such system is the catalytic hydrodesulfurization (HDS) of S-containing hydrocarbons in fuel (see below).

This thesis work was largely initiated by the synthesis and characterization of the stable coordinated H_2S complex, *cis*- $\text{RuCl}_2(\text{P-N})(\text{P}(p\text{-tolyl})_3)(\text{SH}_2)$ ($\text{P-N} = [o\text{-(}N,N\text{-dimethylamino)phenyl]diphenylphosphine}$).¹⁴ The discovery of this complex provided a rare opportunity to investigate the properties, including thermodynamic and kinetic aspects, resulting from the binding of H_2S to a transition metal (Ru(II)) centre.

The precursor, five-coordinate complex $\text{RuCl}_2(\text{P-N})(\text{PR}_3)$ ($\text{R} = \text{Ph}$ or *p*-tolyl), is also fascinating as a range of small molecules including H_2 , N_2 , H_2O , MeOH , CO and SO_2 can also be coordinated to the vacant sixth site.^{15,16} Thus, it was also the objective of this thesis to investigate further the reactivity of $\text{RuCl}_2(\text{P-N})(\text{PPh}_3)$ with these molecules and other small, neutral molecules, as well as with reagents such as salts and bases.

In this Chapter, the natural and industrial occurrences and implications of H_2S chemistry are briefly reviewed, some structural types of transition metal complexes containing S-moieties are presented, and the general chemistry associated with ruthenium aminophosphine complexes is discussed.

1.1 Natural and Industrial Occurrences of Sulfur Compounds

1.1.1 The Natural Sulfur Cycle

Sulfur is essential for life as it plays key roles in growth and metabolism of all organisms. Assimilatory actions of plants and animals (via plants) convert sulfur compounds to amino acids (e.g. L-methionine and L-cysteine), proteins and vitamins (e.g. thiamine and biotin) while dissimilatory processes, mediated by bacteria, involve metabolic reduction and oxidation of sulfur compounds.¹⁷ Upon death of an organism, a large portion of organic sulfur is reduced to H_2S during decomposition.¹⁸ The above biological conversions constitute the biogeochemical sulfur cycle (see Figure 1.1).¹⁸

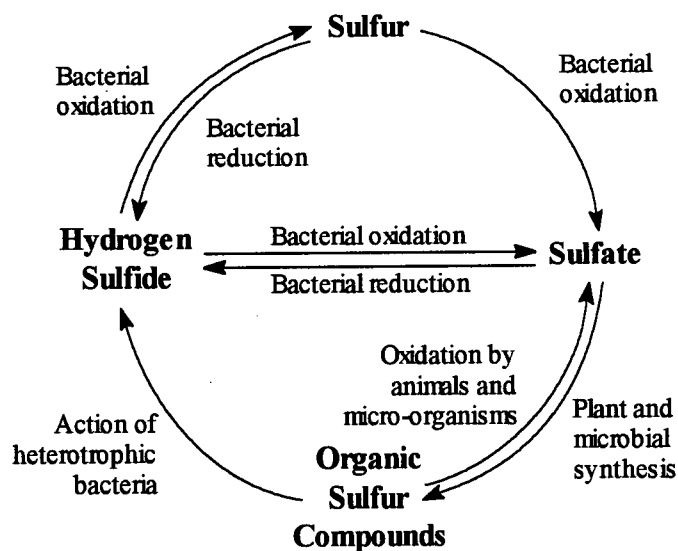


Figure 1.1 The sulfur cycle in nature (adapted from ref. 18).

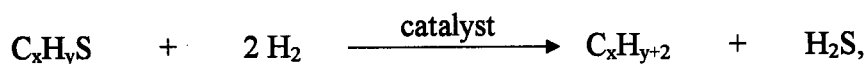
H_2S , S_8 and S-containing organics, which originate from the degradation of biological matter, are found in coal, natural gas, oil, volcanoes, soil, sulfur springs, undersea vents, swamps, marshes, and stagnant bodies of water. The natural biogenic sources account for up

to 50 % of sulfur in the atmosphere.¹⁹ In many industrial process such as HDS of petroleum²⁰⁻²⁵ (see Section 1.1.2) and the Kraft process²⁶ for chemical wood pulping, H₂S is formed as a by-product. In the Kraft process, Na₂S is added to the alkaline (NaOH) pulping liquor to strengthen wood pulp; as a result, H₂S is given off during the recovery of spent chemicals.

1.1.2 Hydrodesulfurization (HDS) and the Claus Process

The presence of S-containing hydrocarbons in petroleum causes environmental concerns because during the combustion of fuel, SO₂, a major source of anthropogenic emission, is produced. In the atmosphere, SO₂ is oxidized to SO₃ that subsequently reacts with H₂O to form H₂SO₄ which causes acid rain, smog and corrosion of materials. Acyclic and cyclic sulfides (including highly stable aromatic types such as benzothiophenes) are the major components of sulfur compounds in petroleum feedstocks. Besides environmental issues, desulfurization of oil stocks is implemented for several other reasons. Removal of sulfur in naphtha-reforming (conversion of gasoline range hydrocarbons into high-octane-number gasoline) is economically favourable as this prevents poisoning of precious metal catalysts. At high temperatures and pressures, sulfur compounds cause corrosion of burner heating equipment. Further, it is also desirable to remove offensive odours caused by volatile sulfide species.

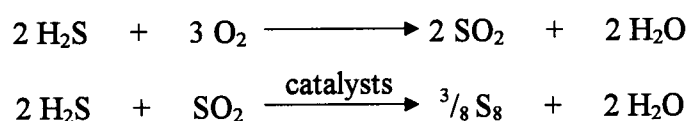
HDS is the industrial process in which sulfur is removed from organosulfur compounds found in natural gas and petroleum. This process, based on the reaction



is catalyzed by Co- or Ni-doped MoS₂ or WS₂ catalysts supported on Al₂O₃ at high temperatures (400 - 825°F) with H₂ pressures of 150-3000 psi.^{21,23,24} Sulfides of Ru, Os, Ir

and Rh have been shown to be much better catalysts than those of Co or Ni,²⁷ but are not used commercially because of their high costs. Despite the importance of HDS, details about the catalyst structures and the mechanism of the HDS reaction remain obscure. Thiophene is chosen as the model substrate in many studies because it has the simplest structure of thiophenes, which are most difficult class of compounds to desulfurize. The products of thiophene HDS are H₂S and a mixture of *n*-butane, *n*-butenes and butadiene. Continuing debate on the mechanism is centred on the bonding mode of thiophene, on the way the C-S bond is cleaved, and whether desulfurization occurs before or after hydrogenation of the thiophene ring.^{20,22,23,25,28}

The majority of the H₂S generated by HDS is converted to H₂SO₄, the largest volume inorganic substance industrially produced (43 billion kg in the US in 1995).²⁹ H₂SO₄ is used in the synthesis of fertilizers, organic sulfuric acids, plastics, explosives, batteries and refining of petroleum. For ease of transport and storage, elemental sulfur is recovered from H₂S by the Claus process.^{30,31}



The Claus reaction, catalyzed by alumina, combines H₂S and SO₂ to give S₈ and H₂O. The interactions of H₂S and SO₂ on alumina, however, are not well understood. Three models for the surface-catalyzed process have been proposed: (1) adsorbed SO₂ is attacked by H₂S, (2) adsorbed H₂S is attacked by SO₂, and (3) both gases are adsorbed on alumina before reaction.³²

It is clear that both important industrial processes, HDS and the Claus reaction, involve the interactions of H₂S with catalyst surfaces. However, the nature of these

interactions are uncertain. Thus, it is advantageous to study the reactions of H_2S and S-containing organic compounds with metal complexes in homogeneous systems and correlate these findings to those of heterogeneous systems.

1.2 Coordination Chemistry of H_2S and Thiols

1.2.1 Physical Properties of H_2S and Thiols

Perhaps the most distinguishable physical characteristic of H_2S and thiols is their unpleasant odour. H_2S , in particular, has an odour that resembles rotten eggs. Some physical properties of H_2S and thiols used in this thesis work are shown in Table 1.1. Thiols are more acidic than their corresponding alcohols by 5 to 6 pK_a units. Notably, H_2S and thiophenol are more acidic than alkanethiols. For H_2S , the greater acidity has been attributed to formation of a symmetrical solvation shell around the SH^- ion upon deprotonation, this effect being greatly reduced when the H-atom is replaced by an alkyl group. For thiophenol, the negative charge on the S-atom of the conjugate base is stabilized by the resonance effect of the aromatic ring, and thus the acidity is increased.

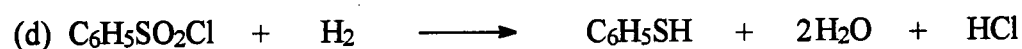
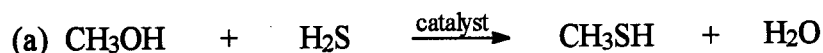
H_2S and thiols are extremely toxic. Exposure to 1400 mg/m^3 H_2S for a few minutes results in human deaths; inhalation of thiol fumes may lead to failure of the olfactory senses, headaches, nausea, and loss of consciousness.

Alkanethiols are generally prepared by acid-catalyzed (sulfuric or phosphoric acid) reactions of alcohols (Figure 1.2(a)) or alkenes (Figure 1.2(b)) with H_2S . Halide displacement is most effective in the preparation of α -toluenethiol (Figure 1.2(c)). Arenethiols such as benzenethiol are synthesized by reduction of the arene sulfonyl chloride (Figure 1.2(d)). The principal applications of thiols are in the production of synthetic rubber, agricultural chemicals and other organosulfur compounds.

Table 1.1 Some physical properties of H₂S and thiols.

Compound		Melting Point (°C) ^a	Boiling Point (°C) ^a	ΔH° formation (kJ/mol) ^a	ΔG° formation (kJ/mol) ^a	pK _a (aqueous media) ^b
Common Name(s)	Structure					
hydrogen sulfide	H ₂ S	-85.5	-60.3	-20.6	-33.6	7.0 14.9 ^c
methanethiol; methyl mercaptan	CH ₃ SH	-123.0	6.0	-22.9	-9.80	10.3
ethanethiol; ethyl mercaptan	CH ₃ CH ₂ SH	-147.9	35.0	-46.3	-4.81	10.5
1-propanethiol; <i>n</i> -propyl mercaptan	CH ₃ (CH ₂) ₂ SH	-113.2	67.7	-67.5	2.58	10.7
2-propanethiol; isopropyl mercaptan	(CH ₃) ₂ CHSH	-130.5	52.6	-75.9	2.18	10.9
1-pentanethiol; <i>n</i> -pentyl mercaptan	CH ₃ (CH ₂) ₄ SH	-75.7	126.6	-110	18.0	d
1-hexanethiol; <i>n</i> -hexyl mercaptan	CH ₃ (CH ₂) ₅ SH	-80.5	152.7	-129	27.6	d
α-toluenethiol; benzyl mercaptan	C ₆ H ₅ CH ₂ SH	-29.2	198.9	93.3	163	9.4
benzenethiol; thiophenol	C ₆ H ₅ SH	-14.9	169.1	112	148	6.5

^a(ref. 33), ΔH° and ΔG° values are for formation of gaseous product; ^b(ref. 34), pK_a values were measured at 25°C ; ^csecond dissociation constant; ^dthiol is essentially insoluble in water.

**Figure 1.2** The most widely utilized methods for the synthesis of thiols.

1.2.2 Reactions of H_2S and Thiols with Transition Metal Complexes

There are comparatively few examples of transition metal complexes containing H_2S or thiols (RSH ; $\text{R} = \text{H}$, alkyl) as ligands owing to the acidic and therefore ionic nature of the ligands.¹ A summary of the complexes reported is presented in Sections 4.1.1 and 4.1.2 (p. 110). Although coordination of RSH to transition metal centres (M) has been demonstrated, it is more often proposed as an intermediate step in reactions of RSH with M that usually result in cleavage of S-H bonds and formation of mercapto or thiolato (SR^-) complexes. The S-H bond strengths of H_2S , PhSH and alkanethiols (an average value) are 381, 314 and 362 ± 6 kJ/mol, respectively.³⁵ Structural chemistry of transition metal sulfur complexes is diverse because of the versatility of sulfur ligands to act as two-, four- or six-electron donors (Figure 1.3).

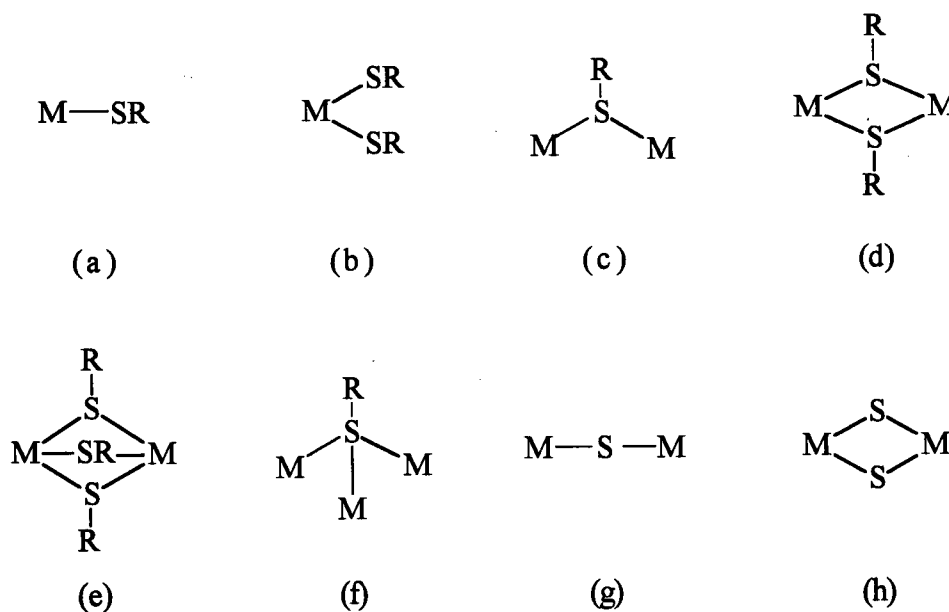


Figure 1.3 Some common coordination modes of SR^- ($\text{R} = \text{H}$ or alkyl) and S^{2-} ligands to transition metal centres (M) (adapted from ref. 36).

Literature dealing with metal mercapto and thiolato complexes is plentiful, partly because of their utilization in model studies for HDS catalysts (Section 1.1.2) and their

occurrence in metalloenzymes such as nitrogenase and ferredoxins.³⁷ While no effort is given to describe comprehensively the metal complexes containing the SR^- and S^{2-} ligands in the literature, examples of complexes with structures shown in Figure 1.3 are presented in this Chapter to display the intriguing and versatile coordination modes of SR^- . In particular, focus is given to work done in this laboratory regarding the reactions of transition metal complexes with H_2S and thiols.

1.2.2.1 Mononuclear Mercapto and Thiolato Complexes

In many cases, cleavage of the S-H bonds leads to the oxidative addition of RSH to metal complexes. James et al. showed that the reactions of $\text{Ru}(\text{CO})_2(\text{PPh}_3)_3$ or $cct\text{-Ru}(\text{H})_2(\text{CO})_2(\text{PPh}_3)_2$ ($cct = cis, cis, trans$) with H_2S in solution give (with the liberation of H_2) $cct\text{-Ru}(\text{H})(\text{SH})(\text{CO})_2(\text{PPh}_3)_2$ at -35°C and the structurally characterized $cct\text{-Ru}(\text{SH})_2(\text{CO})_2(\text{PPh}_3)_2$ at ambient conditions (Figure 1.4(a)).^{8,10,11} A similar reaction of a mixture of *cis*- and *trans*- $\text{Ru}(\text{H})_2(\text{dpm})_2$ ($\text{dpm} = \text{bis}(\text{diphenylphosphino})\text{methane}$) with H_2S gives initially *trans*- $\text{Ru}(\text{H})(\text{SH})(\text{dpm})_2$, which subsequently reacts with further H_2S to produce a mixture *cis*- and *trans*- $\text{Ru}(\text{SH})_2(\text{dpm})_2$ and H_2 (Figure 1.4(b)).^{11,12} A range of thiols RSH ($\text{R} = \text{Me}, \text{Et}, \text{Ph}, \text{CH}_2\text{Ph}, o\text{-}, m\text{-}$ and *p*-tolyl) also oxidatively add to $\text{Ru}(\text{CO})_2(\text{PPh}_3)_3$ or $cct\text{-Ru}(\text{H})_2(\text{CO})_2(\text{PPh}_3)_2$ to generate solely $cct\text{-Ru}(\text{H})(\text{SR})(\text{CO})_2(\text{PPh}_3)_2$ at 20°C with no tendency to form the bis(thiolato) species.^{8,10} The reaction of *cis*- and *trans*- $\text{Ru}(\text{H})_2(\text{dpm})_2$ with thiols generate *cis*- and *trans*- $\text{Ru}(\text{H})(\text{SR})(\text{dpm})_2$.¹² Kinetic studies showed that the rate-determining step for the reaction of $cct\text{-Ru}(\text{H})_2(\text{CO})_2(\text{PPh}_3)_2$ with RSH is the loss of H_2 , while an initial protonation of dpm precursor to give $[\text{Ru}(\text{H})(\eta^2\text{-H}_2)(\text{dpm})_2]^+$ followed by dissociation of H_2 is proposed for the dpm system; the difference in mechanism is attributed to the higher basicity of the hydride ligands in *cis*-/*trans*- $\text{Ru}(\text{H})_2(\text{dpm})_2$.¹²

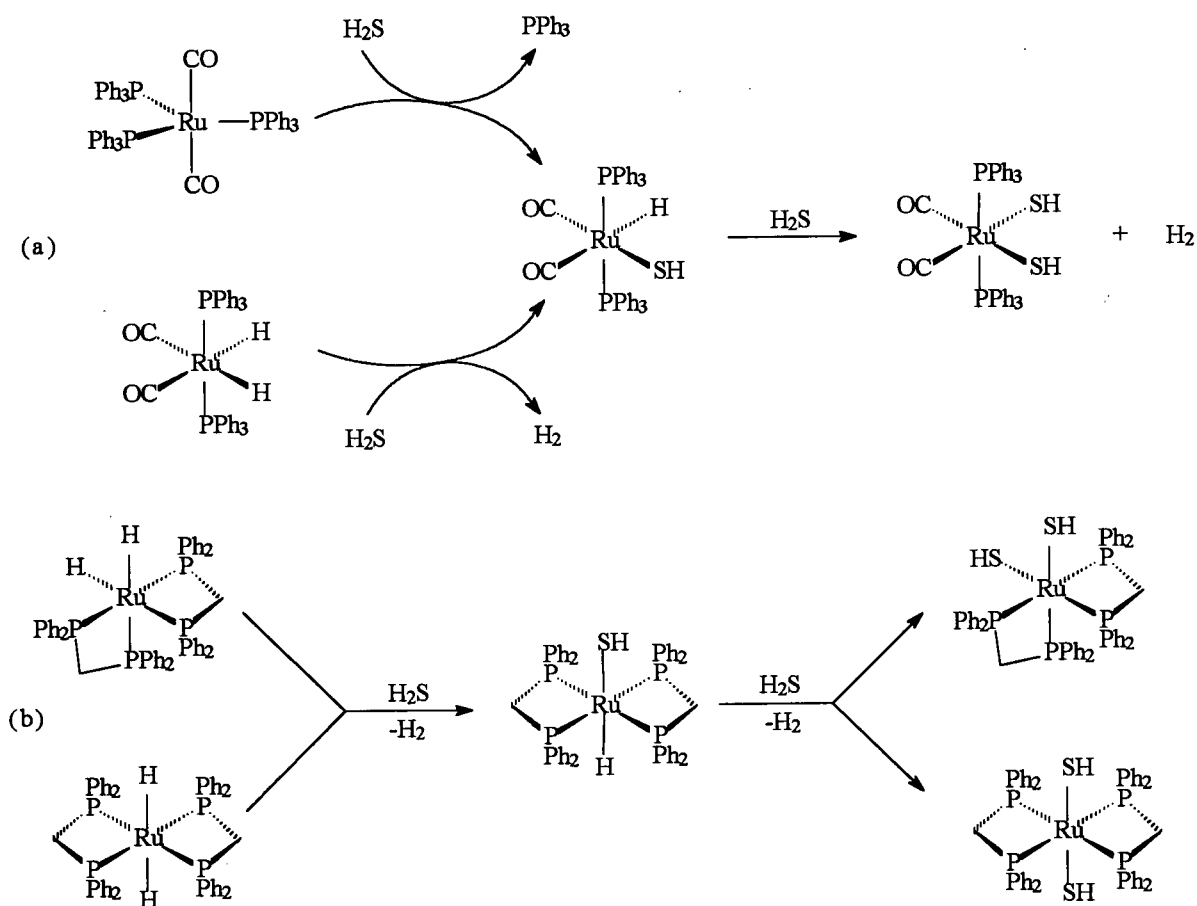


Figure 1.4 Formation of hydrido mercapto and bis(mercapto) Ru(II) phosphine complexes.

Pignolet's group has shown that H_2S also oxidatively adds to *trans*- $\text{IrCl}(\text{CO})(\text{PPh}_3)_2$ forming the crystallographically characterized $\text{IrCl}(\text{H})(\text{SH})(\text{CO})(\text{PPh}_3)_2$ (Figure 1.5).³⁸

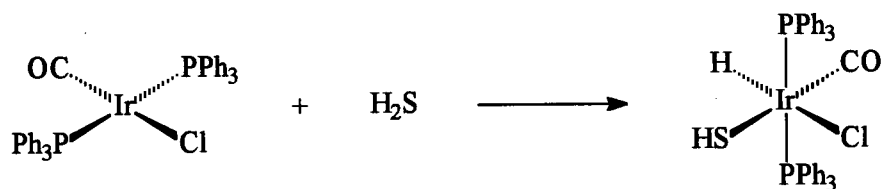


Figure 1.5 Formation of *trans*- $\text{IrCl}(\text{H})(\text{SH})(\text{CO})(\text{PPh}_3)_2$.

Reaction of *trans*-Mo(N₂)₂(dppe)₂ (dppe = bis(diphenylphosphino)ethane) with RSH (R = alkyl or aryl) generates the intermediate species *cis*-Mo(H)(SR)(dppe)₂ en route to *trans*-Mo(SR)₂(dppe)₂.³⁹ However, the intermediate species can be stabilized and isolated by using a 1:1 ratio of RSH and Mo, or a bulky RSH (R = Pr^{*i*}, Bu^{*t*}, 2,4,6-Me₃C₆H₂, 2,4,6-Pr^{*i*}₃C₆H₂, 4,2,6-BrPr^{*i*}₂C₆H₂) (Figure 1.6).⁴⁰ The mechanism is proposed as follows: dissociation of one N₂ ligand results in an equilibrium between the six-coordinate precursor and a five-coordinate species; RSH oxidatively adds to the five-coordinate species forming the hydrido thiolato species; a second N₂ ligand then dissociates, and a second RSH oxidatively adds; H₂ is finally eliminated to form the bis(thiolato) species.

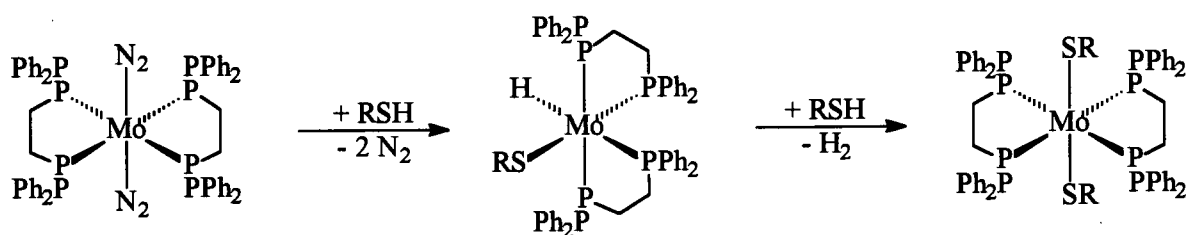


Figure 1.6 Reactions of *trans*-Mo(N₂)₂(dppe)₂ with thiols.

Stabilization of unsaturated five-coordinate complexes can be achieved by using bulky ligands such as 1,2-bis(diisopropylphosphino)ethane (dippe). Reaction of [MCl(dippe)₂][BPh₄] (M = Ru, Os) with PhSH results in [M(SPh)(dippe)₂][BPh₄] (Figure 1.7(a)), and the Ru analogue is structurally characterized.⁴¹ The formation of [M(SR)L][BPh₄] (M = Fe, Co, Ni; L = tris(2-diphenylphosphinoethyl)phosphine (PP₃), tris(2-diphenylphosphinoethyl)amine (NP₃)) further indicates that the stability of monomeric metal-sulfur complexes is influenced by sterically demanding and electron rich ligands (Figure 1.7(b)); the X-ray structures of [Fe(SH)(PP₃)] [BPh₄], [Co(MeS)(NP₃)] [BPh₄], and [Ni(SH)(PP₃)] [BPh₄] were reported.⁴²

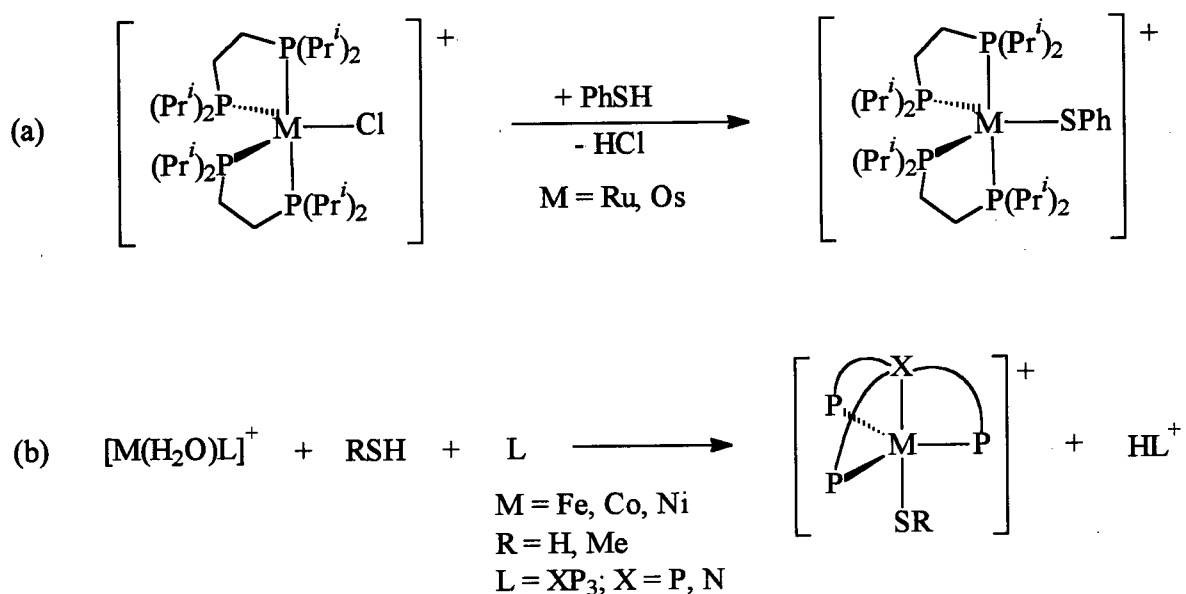


Figure 1.7 Formation of five-coordinate, trigonal bipyramidal mercapto and thiolato complexes.

1.2.2.2 Bridging Mercapto and Thiolato Ligands

The monomeric mercapto or thiolato complexes discussed above are relatively rare compared to dinuclear complexes because sulfur ligands have a tendency to utilize their lone pairs of electrons to bridge two or more metal centres.⁴³ Di- and tri- μ_2 -SR dinuclear complexes are often formed by initial oxidative addition of RSH to a monomeric metal complex followed by dimerization. H_2S reacts with $\text{RhCl}(\text{PPh}_3)_3$ ³⁸ and $\text{RhCl}(\text{triphos})(\text{C}_2\text{H}_4)$ (triphos = $\text{MeC}(\text{CH}_2\text{PPh}_2)_3$)⁴⁴ in CH_2Cl_2 solutions to form the structurally characterized, SH-bridged, dinuclear complexes $[\text{RhCl}(\text{H})(\mu_2\text{-SH})\text{PPh}_3]_2$ (Figure 1.8(a)) and $[\text{Rh}(\text{triphos})(\text{H})(\mu_2\text{-SH})]_2^{2+}$ (Figure 1.8(b)), respectively. Interestingly, the reversible elimination of 2 mol H_2 from $[\text{Rh}(\text{triphos})(\text{H})(\mu_2\text{-SH})]_2^{2+}$ to form $[\text{Rh}(\text{triphos})(\mu_2\text{-S})]_2^{2+}$ was also observed. Similar reactions of H_2S with $\text{Ru}(\text{H})_2(\text{PMe}_2\text{Ph})_4$ and $[\text{Ir}(\text{H})_2(\text{MeCO})_2(\text{PPh}_3)_2][\text{BF}_4]$ lead to the formation of the

structurally characterized $(\text{PhMe}_2\text{P})_2(\text{SH})\text{Ru}(\mu_2\text{-SH})_3\text{Ru}(\text{PhMe}_2\text{P})_3$ (Figure 1.8(c))⁴⁵ and $[(\text{PPh}_3)_2(\text{H})\text{Ir}(\mu_2\text{-H})(\mu_2\text{-SH})_2\text{Ir}(\text{H})(\text{PPh}_3)_3][\text{BF}_4]$ (Figure 1.9),⁴⁶ respectively; generation of H_2 was observed for both reactions. In the latter reaction, a minor product containing three different bridging ligands, $[(\text{PPh}_3)_2(\text{H})\text{Ir}(\mu_2\text{-H})(\mu_2\text{-SH})(\mu_2\text{-SPH})\text{Ir}(\text{H})(\text{PPh}_3)_3][\text{BF}_4]$, was also formed.

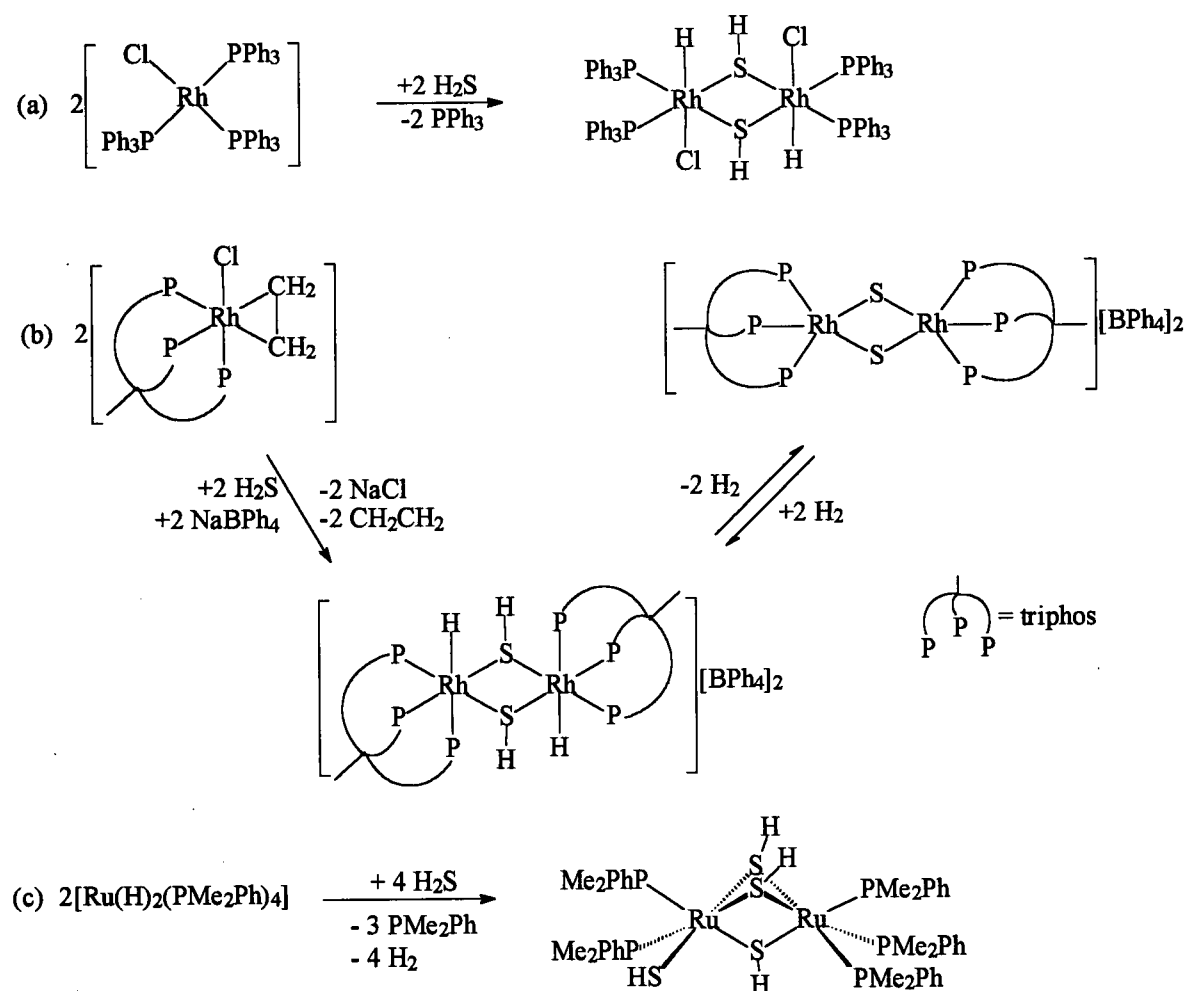


Figure 1.8 Reactions of H_2S with monomeric complexes to form di- and tri- $\mu_2\text{-SH}$ dinuclear complexes.

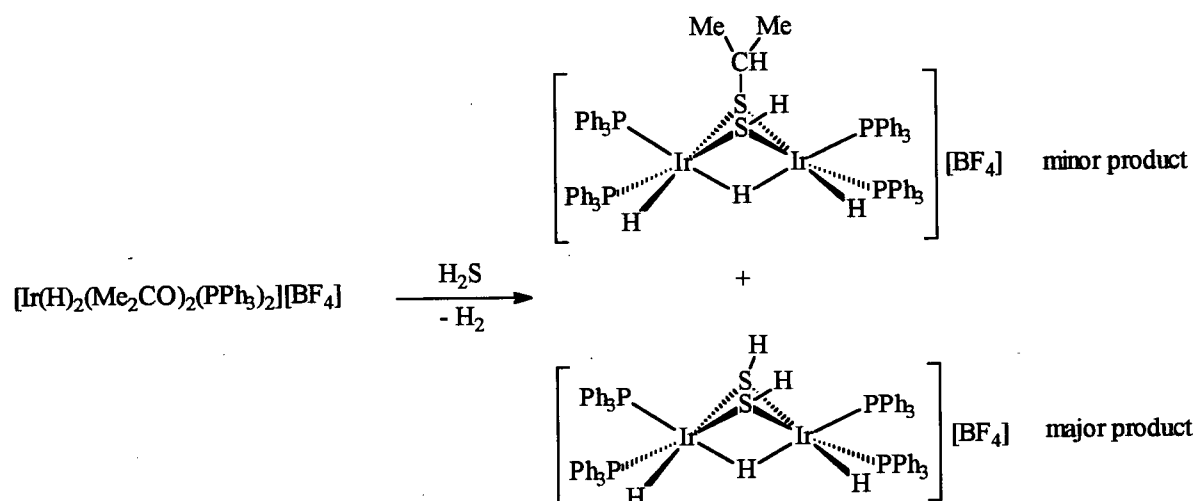


Figure 1.9 Reaction of $[\text{Ir}(\text{H})_2(\text{MeCO})_2(\text{PPh}_3)_2][\text{BF}_4]$ with H_2S .

In addition to phosphine ligands, arene ligands have also been utilized to stabilize complexes containing bridging mercapto and thiolato ligands as shown in Figure 1.10. Dinuclear molybdenum complexes $[(\eta^7\text{-C}_7\text{H}_7)\text{Mo}(\mu\text{-SR})_3\text{Mo}(\eta^7\text{-C}_7\text{H}_7)][\text{BF}_4]$ are formed by treatment of $[\text{Mo}(\eta^6\text{-C}_6\text{H}_5\text{Me})(\eta^7\text{-C}_7\text{H}_7)][\text{BF}_4]$ with RSH (Figure 1.10(a)).⁴⁷ Formation of di- $\mu_2\text{-SR}$ or tri- $\mu_2\text{-SR}$ Ir(III) dinuclear complexes is dependent on the nature of the substituent R (Figure 1.10(b)). When the precursor $[\text{Cp}^*\text{IrCl}(\mu_2\text{-Cl})_2]_2$ ($\text{Cp}^* = \eta^5\text{-C}_5\text{Me}_5$) is treated with RSH , $[\text{Cp}^*\text{Ir}(\mu_2\text{-SEt})_3\text{IrCp}^*]\text{Cl}$ is formed when $\text{R} = \text{Et}$, and $[\text{Cp}^*\text{IrCl}(\mu_2\text{-SR})_2\text{ClIrCp}^*]$ is formed when $\text{R} = \text{Pr}^i$, Cy (cyclohexyl) or CH_2Ph .⁴⁸ Reaction of the Ir(III) precursor complex with excess H_2S afforded first the doubly-bridged $\mu_2\text{-SH}$ complex $[\text{Cp}^*\text{IrCl}(\mu_2\text{-SH})_2\text{ClIrCp}^*]$ which subsequently consumes more H_2S to form the triply-bridged $\mu_2\text{-SH}$ complex $[\text{Cp}^*\text{Ir}(\mu_2\text{-SH})_3\text{IrCp}^*]\text{Cl}$.⁴⁹ As the R groups become more bulky, formation of the triply-bridged species is disfavoured, for example, when $\text{R} = \text{Bu}^t\text{SH}$.⁴⁸

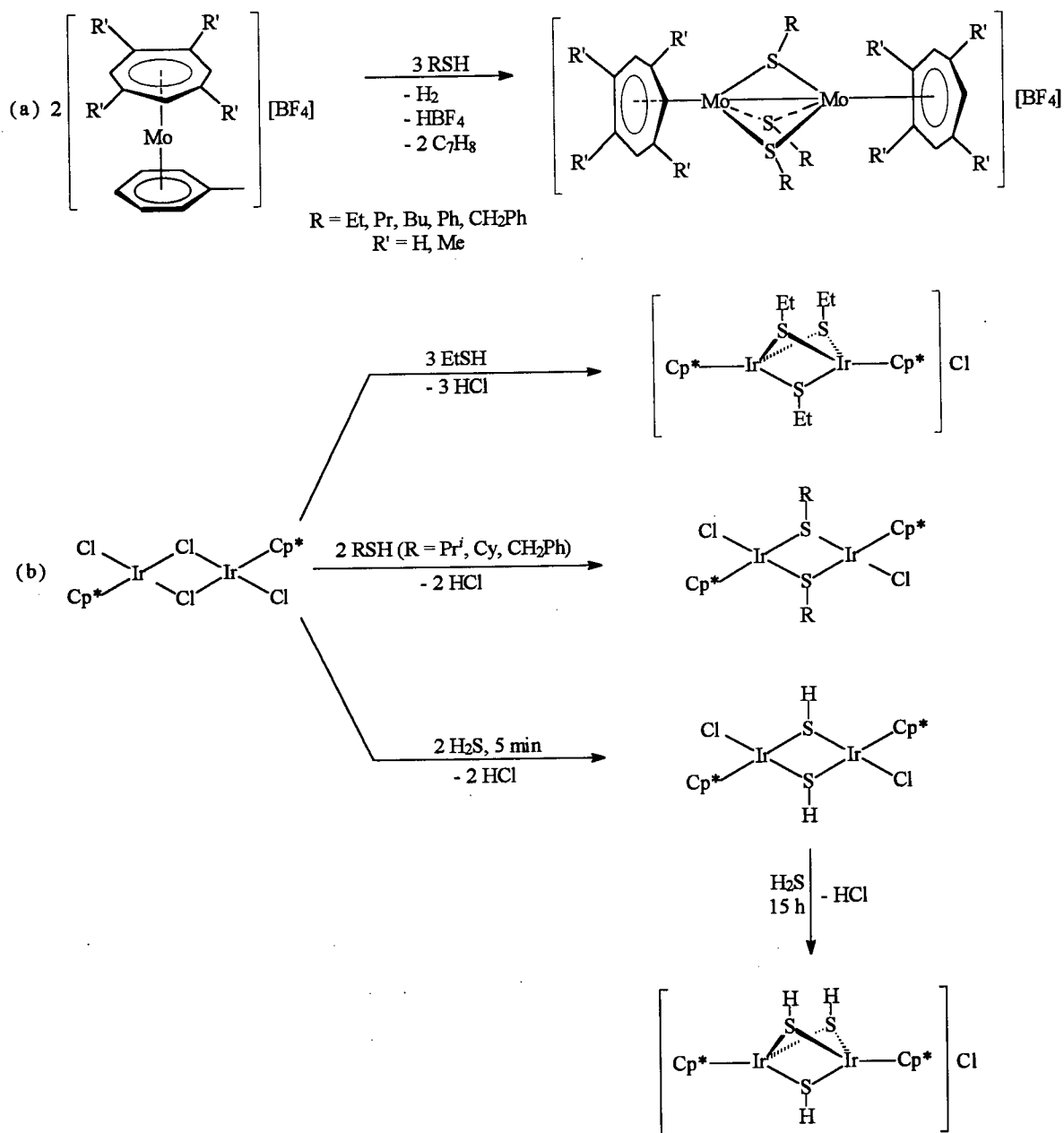


Figure 1.10 Formation of dinuclear mercapto and thiolato-bridged complexes containing arene co-ligands.

Sulfur ligands constitute the fundamental building blocks of the metal clusters found in enzymatic and industrial catalytic processes.^{50,51} Bridging thiolate ligands are used to connect metal centres in the clusters shown in Figure 1.11: (a) reaction of $\text{Co}(\text{NO}_3)_2 \cdot 6\text{H}_2\text{O}$ with PhSH

in the presence of Et_3N and Me_4NCl affords $[\text{Me}_4\text{N}]_2[\text{Co}_4(\text{SPh})_4(\mu_2\text{-SPh})_6]$;⁵⁰ (b) reaction of $\text{Co}(\text{O}_2\text{CMe})_2 \cdot 4\text{H}_2\text{O}$ with RSH ($\text{R} = \text{Me}, \text{Et}$) in the presence of PEt_3 and NaBPh_4 or TlPF_6 yields $[\text{Co}_3(\mu_2\text{-SR})_6(\text{PEt}_3)_3]\text{X}$ ($\text{X} = \text{BPh}_4, \text{PF}_6$);⁵² and (c) reaction of ZnMe_2 with Pr^iSH gives octameric $[\text{Me}_3\text{Zn}(\mu_3\text{-SPr}^i)]_8$.⁵³

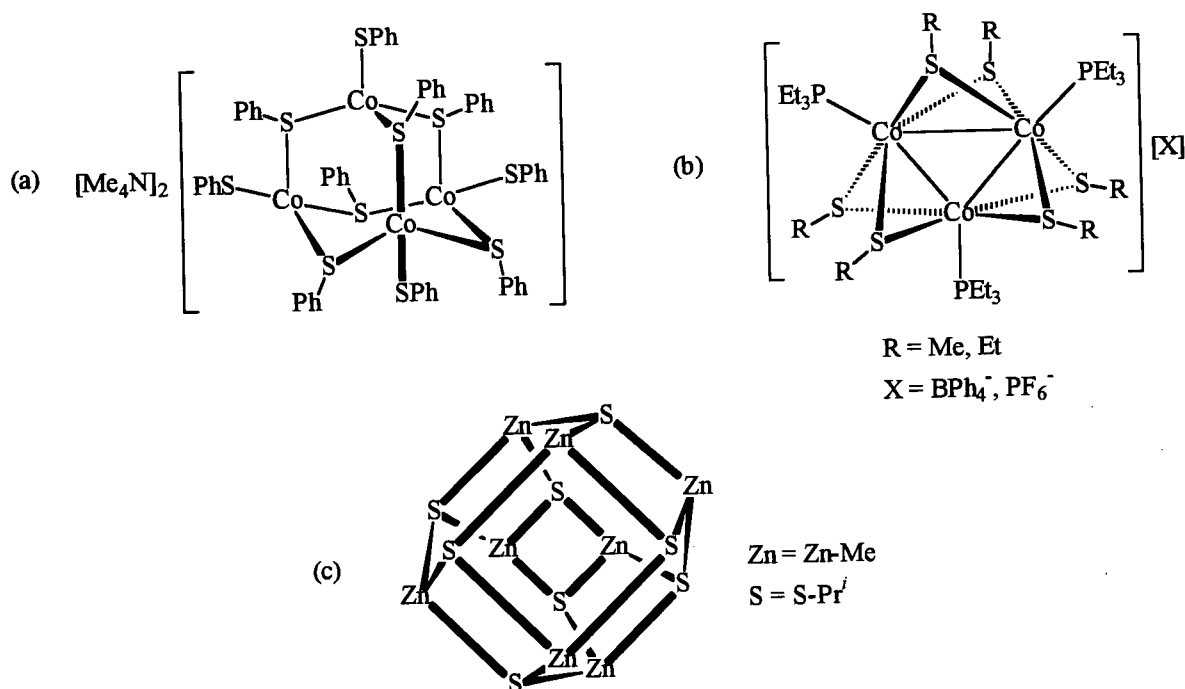


Figure 1.11 Clusters containing μ_2 - and μ_3 -SR bridged ligands.

Both H-atoms of H_2S can be cleaved from the S-atom upon reaction with metal complexes resulting in formation of species containing a bridging S^{2-} ligand. Examples include $[(\text{P}_3)\text{Ni}(\mu_2\text{-S})\text{Ni}(\text{P}_3)]^{2+}$ ($\text{P}_3 = 1,1,1$ -tris(diphenylphosphinomethyl)ethane; see Figure 1.12(a))⁵⁴ and $\text{Pd}_2\text{X}_2(\mu_2\text{-S})(\mu\text{-dpm})_2$ ($\text{X} = \text{Cl}, \text{Br}, \text{I}$; see Figure 1.12(b) and Section 1.2.2.3)² produced as shown. Cleavage of the S-C bond of alkanethiols, however, is not favoured as shown by the formation of $[\text{Pt}_2(\text{H})_2(\mu_2\text{-SMe})(\mu\text{-dpm})_2]^+$ from the reaction of $[\text{Pt}_2(\text{H})(\text{CO})(\mu\text{-dpm})_2]^+$ and

MeSH (Figure 1.12(c)).⁵⁵ Further evidence to display the different reactivities of H₂S and thiols are shown in Figure 1.13. When RhRe(CO)₄(μ-dpm)₂ is treated with H₂S, RhRe(CO)₄(μ₂-S)(μ-dpm)₂ and H₂ are generated quantitatively, while the analogous reaction with RSH (R = Et, Ph) yields RhRe(CO)₃(μ₂-H)(μ₂-SR)(μ-dpm)₂ (Figure 1.13(a)).⁵⁶ Similarly, reaction of an equal molar quantity of RSH with [Pt₃(μ₃-CO)₃(μ-dpm)₃][PF₆]₂ gives [Pt₃(H)(μ₃-S)(μ-dpm)₃][PF₆] when R = H, Bu^t, and [Pt₃(H)(μ₃-SR)(μ-dpm)₃][PF₆]₂ when R = Me, Et, CH₂Ph, CH₂CO₂Et, Ph or *p*-tolyl (Figure 1.13(b)).⁵⁷ The formation of the μ₃-S complex when Bu^tSH was used is attributed to the loss of the relatively good leaving group Bu^{t+} during the reaction.^{57b}

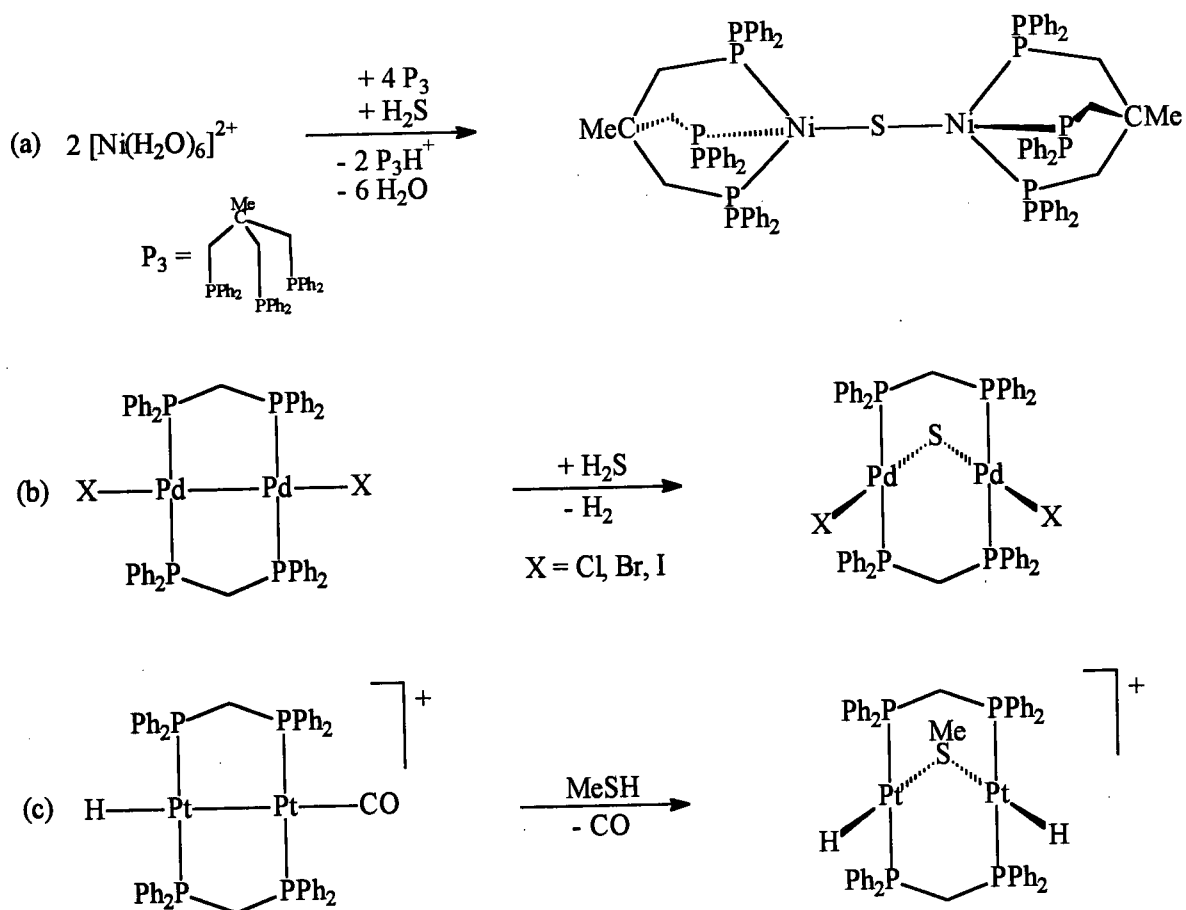


Figure 1.12 Formation of μ₂-S and μ₂-SMe dinuclear complexes.

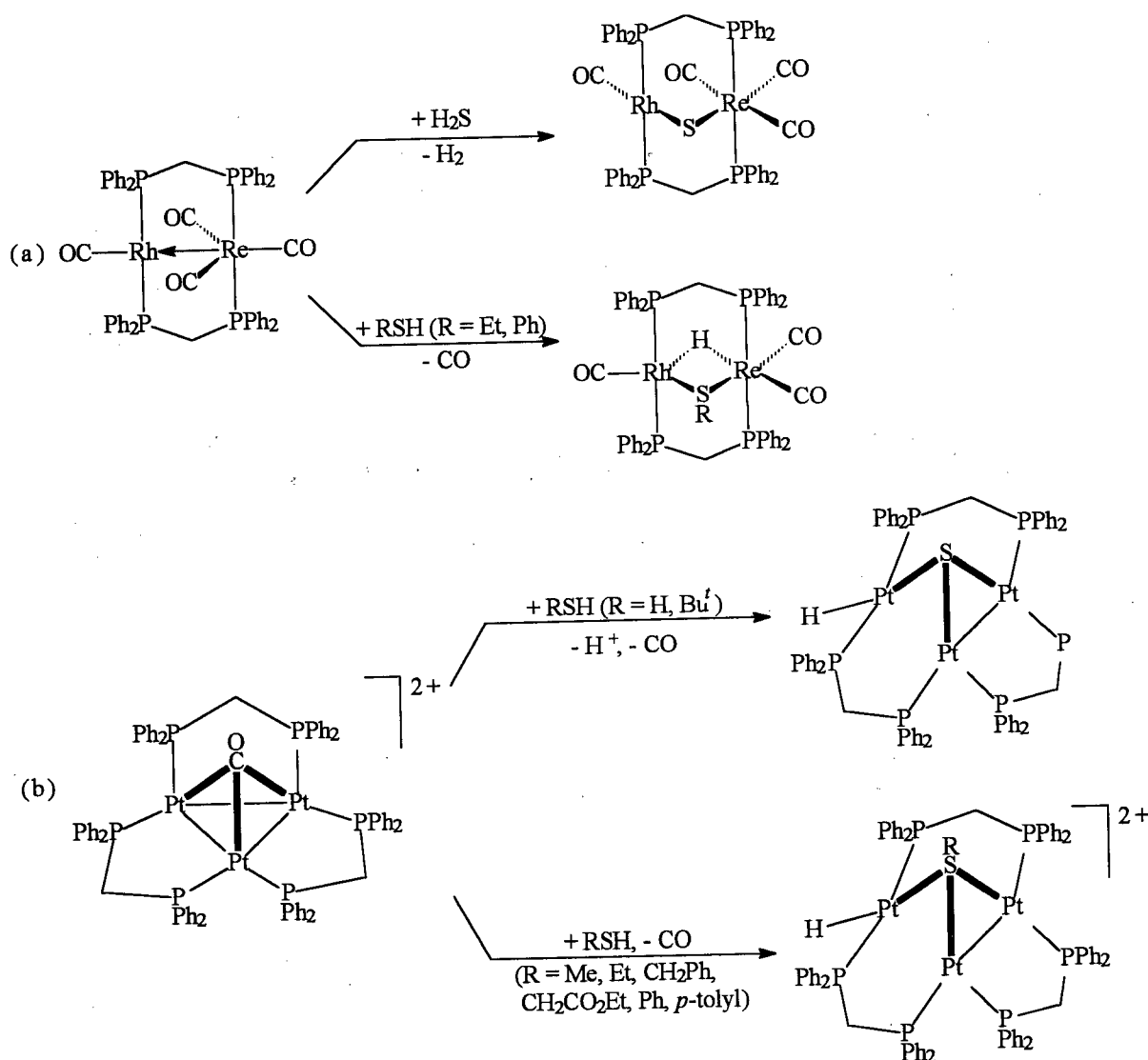


Figure 1.13 S-H bond activation in H_2S and thiols by (a) $\text{RhRe(CO)}_4(\mu\text{-dpm})_2$ and (b) $[\text{Pt}_3(\mu_3\text{-CO})(\mu\text{-dpm})_3]^{2+}$.

1.2.2.3 Recovery of H_2 from H_2S using $\text{Pd}_2\text{X}_2(\mu\text{-dpm})_2$

Study of H_2S interactions with transition metal complexes is of great interest in this laboratory because of their potential utilization in H_2 recovery.¹⁻⁷ The reaction of $\text{Pd}_2\text{X}_2(\mu\text{-dpm})_2$ with H_2S to give $\text{Pd}_2\text{X}_2(\mu_2\text{-S})(\mu\text{-dpm})_2$ and H_2 (Figure 1.12(b)) was the first homogeneous system demonstrating a 1:1 $\text{H}_2\text{S}:\text{H}_2$ stoichiometry at a metal centre.² Kinetic

and mechanistic studies showed first-order behaviour in both $\text{Pd}_2\text{X}_2(\mu\text{-dpm})_2$ and H_2S . The reaction proceeds via oxidative addition of H_2S to the Pd_2 dimer which results in formation of the hydrido mercapto dinuclear intermediate $\text{Pd}_2\text{X}_2(\text{H})(\text{SH})(\mu\text{-dpm})_2$ (Figure 1.14); which was detected at -78°C by ^1H and $^{31}\text{P}\{^1\text{H}\}$ NMR spectroscopy.^{3,4}

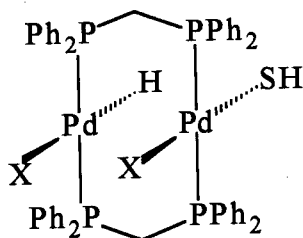


Figure 1.14 Structure of intermediate formed during the reaction of $\text{Pd}_2\text{X}_2(\mu\text{-dpm})_2$ with H_2S en route to $\text{Pd}_2\text{X}_2(\mu_2\text{-S})(\mu\text{-dpm})_2$ and H_2 .

Pursuance of a catalytic cycle for the conversion of H_2 from H_2S revealed that the bridged S-atom of $\text{Pd}_2\text{X}_2(\mu_2\text{-S})(\mu\text{-dpm})_2$ can be effectively abstracted by dpm with formation of $\text{dpm}(\text{S})$ and quantitative reconversion of $\text{Pd}_2\text{X}_2(\mu\text{-dpm})_2$ from $\text{Pd}_2\text{X}_2(\mu_2\text{-S})(\mu\text{-dpm})_2$ (Figure 1.15).⁵ This is the first reported homogeneous catalytic process that generates H_2 from H_2S .¹ Solution kinetic and mechanistic studies showed that this reaction is first-order in both $\text{Pd}_2\text{X}_2(\mu_2\text{-S})(\mu\text{-dpm})_2$ and dpm.⁵ Further, this process is thought to proceed via a transition state where a five-membered ring is formed by binding one end of the added dpm to one Pd centre and another end to $\mu_2\text{-S}$ of $\text{Pd}_2\text{X}_2(\mu_2\text{-S})(\mu\text{-dpm})_2$ as shown in Figure 1.16.⁵

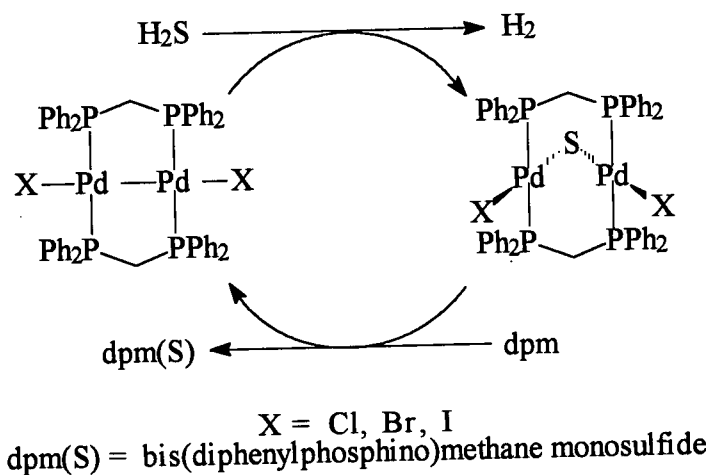


Figure 1.15 Homogeneous catalytic cycle for the recovery of H_2 from H_2S .

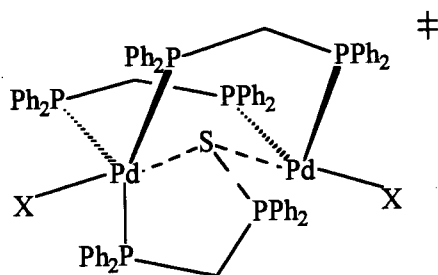


Figure 1.16 Proposed transition state for the reversion of $\text{Pd}_2\text{X}_2(\mu\text{-dppm})_2$ from $\text{Pd}_2\text{X}_2(\mu_2\text{-S})(\mu\text{-dppm})_2$.

1.3 The Chemistry of Transition Metal Aminophosphine Complexes

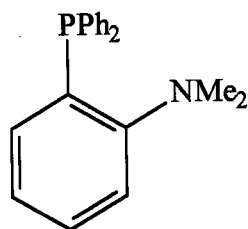


Figure 1.17 $[o\text{-(}N,N\text{-dimethylamino)phenyl}]\text{diphenylphosphine}$ (P-N).

The reactivity of [*o*-(*N,N*-dimethylamino)phenyl]diphenylphosphine (P-N; Figure 1.17) toward transition metals has been investigated since the ligand was reported in 1965.⁵⁸ The coordination chemistry of this ligand and other aminophosphine ligands to many metal centres including Ag,^{59,60} Co,^{61,62} Cr,^{63,64} Cu,^{60,65} Ir,⁶⁶⁻⁷⁰ Mo,^{63,64} Ni,^{61,71-73} Pd,^{58,61,62,70,73-76} Pt,^{61,62,70,76,77} Re,⁷⁸ Rh^{61,62,70,79,80} and Ru^{14,15,61,62,81-83} is representative of P-N type system. Aminophosphine ligands are appealing for the synthesis of complexes utilized for catalysis (e.g. hydrogen transfer reduction,^{68,69} hydrosilylation,⁷⁰ hydrogenation⁸⁰) and for inorganic medicinal studies (e.g. binding of DNA).⁸⁴ Ligands containing a tertiary phosphine group and an amine group satisfy the following desirable qualities required for effective homogeneous catalysts: (1) strong coordination of the phosphine entity stabilizes low oxidation state metal complexes; (2) the relative ease of dissociation of the metal-amine bond may generate a vacant site for which a substrate may enter the coordination sphere of the metal ion; (3) a high nucleophilicity is conferred on the metal ion through nitrogen coordination (σ -donation).^{66,79b}

The original interest of ruthenium aminophosphine complexes in this department was to evaluate the catalytic activity of $\text{RuCl}_2(\text{PPFA})(\text{PPh}_3)$ (PPFA = 1-[*N,N*- α -dimethylaminoethyl]-2-diphenylphosphinoferrocene)^{81a} with respect to that of the well-known complex $\text{RuCl}_2(\text{PPh}_3)_3$.⁸⁵ The former complex was found to be an efficient catalyst for the hydrogenation of 1-hexene under mild conditions (30-60°C, ≤ 1 atm H_2).^{81a} To further develop this chemistry, studies were extended to other ruthenium aminophosphine complexes, and this led to the discovery of the very reactive, five-coordinate, square pyramidal complexes $\text{RuCl}_2(\text{P-N})(\text{PR}_3)$ (R = Ph, *p*-tolyl).¹⁴⁻¹⁶ With the availability of a vacant sixth-coordination site, a range of small molecules (L = H_2O , MeOH, H_2S , EtSH, H_2 , N_2 ,

SO₂) were found to coordinate to yield either *trans*- or *cis*-RuCl₂(P-N)(PR₃)(L) (Figure 1.18).¹⁴⁻¹⁶

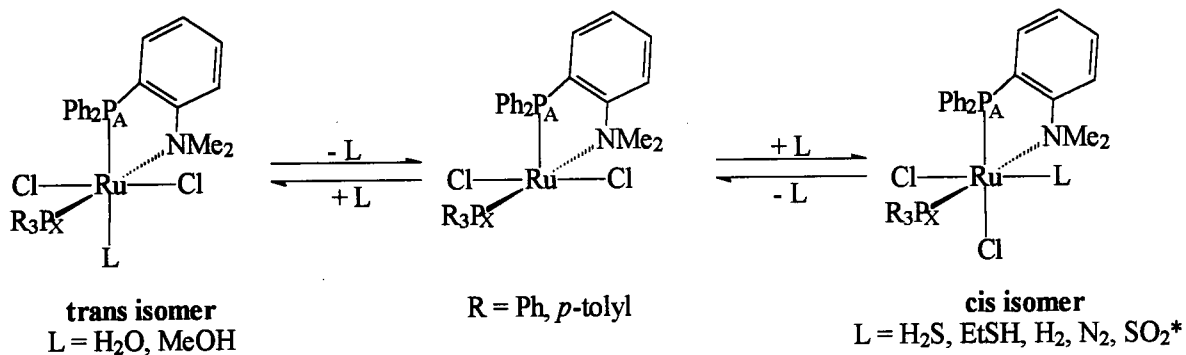


Figure 1.18 Reaction of RuCl₂(P-N)(PR₃) with small molecules L; *the formation of the SO₂ complex is not measurably reversible.

³¹P{¹H} NMR and ¹H NMR spectroscopic techniques are invaluable for the characterization of RuCl₂(P-N)(PR₃)(L) in solution. The presence of an AX coupling pattern in the ³¹P{¹H} NMR spectra are characteristic of complexes containing two distinctively different phosphorus environments. Upon addition of L to RuCl₂(P-N)(PPh₃), the positions of the P_A and P_X doublets shift with respect to those of the precursor if coordination of L takes place. In general, P_A is shifted by a greater magnitude for the *trans* isomer than the *cis* isomer because of the strong *trans* influence exerted by L on P_A; the positions of P_X are relatively unaffected for both isomers because the PR₃ groups are always *trans* to a NMe₂ group. Furthermore, the average ²J_{PP} coupling constants¹⁴⁻¹⁶ are 36 and 29 Hz for the *trans* and *cis* isomers, respectively; both values are consistent with coupling of *cis*-phosphines.⁸⁶ The NMe groups are equivalent and only one singlet is observed in the ¹H NMR spectra; thus, in solution, the five-coordinate structures have C_s symmetry. The *cis* isomers, however, have C₁ symmetry with nonequivalent NMe groups and two singlets are observed in the ¹H NMR spectra. In some cases, the *trans* and *cis* structural assignments are supported by X-ray

crystallographic data (e.g. *trans*-RuCl₂(P-N)(P(*p*-tolyl)₃)(H₂O))¹⁶ and *cis*-RuCl₂(P-N)(P(*p*-tolyl)₃)(H₂S)).¹⁴

1.4 Overview of Thesis

In this thesis work, the coordination chemistry of RuCl₂(P-N)(PR₃) and other ruthenium aminophosphine systems are further investigated. General experimental details are presented in Chapter 2, while the synthesis, characterization and reactivity of ruthenium aminophosphines complexes are discussed in Chapter 3. The solution and solid structural properties of *cis*-RuCl₂(P-N)(PPh₃)(L) (L = H₂S, RSH) and *trans*-RuCl₂(P-N)(PPh₃)(L) (H₂O, ROH) are presented and compared in Chapters 4 and 5, respectively. In Chapter 6, the binding of various small molecules other than S- or O- containing species (e.g. those have N-donor ligands) to RuCl₂(P-N)(PPh₃) are explored. Finally a summary of results and some recommendations for future work are given in Chapter 7.

1.5 References

1. James, B. R. *Pure Appl. Chem.* **1997**, *69*, 2213.
2. Lee, C.-L.; Besenyei, G.; James, B. R.; Nelson, D. A.; Lilga, M. A. *J. Chem. Soc., Chem. Commun.* **1985**, 1175.
3. Besenyei, G.; Lee, C.-L.; Gulinski, J.; James, B. R.; Nelson, D. A.; Lilga, M. A. *Inorg. Chem.* **1987**, *26*, 3622.
4. Barnabas, A. F.; Sallin, D.; James, B. R. *Can. J. Chem.* **1989**, *64*, 2009.
5. Wong, T. Y. H.; Barnabas, A. F.; Sallin, D.; James, B. R. *Inorg. Chem.* **1995**, *34*, 2278.
6. Wong, T. Y. H.; James, B. R.; Wong, P. C.; Mitchell, K. A. R. *J. Mol. Catal. A: Chem.* **1999**, *139*, 159.
7. Wong, T. Y. H.; Rettig, S. J.; James, B. R. *Inorg. Chem.* **1999**, *38*, 2143.
8. Lee, C.-L.; Chisholm, J.; James, B. R.; Nelson, D. A.; Lilga, M. A. *Inorg. Chim. Acta* **1986**, *121*, L7.
9. Jessop, P. G.; Rettig, S. J.; James, B. R. *J. Chem. Soc., Chem. Commun.* **1991**, 773.
10. Jessop, P. G.; Rettig, S. J.; Lee, C.-L.; James, B. R. *Inorg. Chem.* **1991**, *30*, 4617.
11. Jessop, P. G.; Lee, C.-L.; Rastar, G.; James, B. R.; Lock, C. J.; Faggiani, R. *Inorg. Chem.* **1992**, *31*, 4601.
12. Jessop, P. G.; Rastar, G.; James, B. R. *Inorg. Chim. Acta* **1996**, *250*, 351.
13. Jessop, P. G.; James, B. R. *Inorg. Chim. Acta* **1998**, *280*, 75.
14. Mudalige, D. C.; Ma, E. S.; Rettig, S. J.; James, B. R.; Cullen, W. R. *Inorg. Chem.* **1997**, *36*, 5426.
15. Mudalige, D. C.; Rettig, S. J.; James, B. R.; Cullen, W. R. *J. Chem. Soc., Chem. Commun.* **1993**, 830.
16. Mudalige, D. C.; Ph.D. Thesis, The University of British Columbia, 1994.

17. Trüper, H. G. In *Sulfur - Its Significance for Chemistry, for the Geo-, Bio- and Cosmosphere and Technology*; Müller, A.; Krebs, B., Eds.; Elsevier: Amsterdam, 1984, p. 351.
18. Maw, G. A. In *Sulfur in Organic and Inorganic Chemistry, Vol. II*; Senning, A., Ed.; Marcel Dekker Inc.: New York, 1972, p. 115.
19. Aneja, V. P.; Cooper, W. J. In *Biogenic Sulfur in the Environment*; Saltzman, E. S.; Cooper, W. J., Eds.; ACS: Washington, D.C., 1989, p. 2.
20. Lipsch, J. M. J. G.; Schuit, G. C. A. *J. Catal.* **1969**, *15*, 179.
21. Schuman, S. C.; Shalit, H. *Catal. Rev.* **1970**, *4*, 245.
22. Kwart, H.; Schuit, G. C. A.; Gates, B. C. *J. Catal.* **1980**, *61*, 128.
23. Angelici, R. J. *Acc. Chem. Res.* **1988**, *21*, 387.
24. Gates, B. C. *Catalytic Chemistry*; John Wiley & Sons, Inc.: Toronto, 1992, p. 406.
25. Sánchez-Delgado, R. A. *J. Mol. Catal.* **1994**, *86*, 287.
26. Genco, J. M. In *Kirk-Othmer Encyclopedia of Chemical Technology, 4th Ed., Vol. 20*; Kroschwitz, J. I.; Howe-Grant, M., Eds.; John Wiley & Sons, Inc.: Toronto, 1996, p. 524.
27. (a) Chianelli, R. R. *Catal. Rev.* **1984**, *26*, 361.
(b) Bianchini, C.; Meli, A.; Moneti, S.; Oberhauser, W.; Vizza, F.; Herrera, V.; Fuentes, A.; Sánchez-Delgado, R. A. *J. Am. Chem. Soc.* **1999**, *121*, 7071.
28. Jones, W. D.; Chin, R. M.; Hoaglin, C. L. *Organometallics* **1999**, *18*, 1786.
29. Mingos, D. M. P. *Essential Trends in Inorganic Chemistry*; Oxford University Press, Inc.: New York, 1998, p. 159.
30. (a) Grancher, P. *Hydrocarbon Process.* **1978**, *57* (July), 155.
(b) Grancher, P. *Hydrocarbon Process.* **1978**, *57* (Sept.), 257.
31. Estep, J. W.; McBride, Jr., G. T.; West, J. R. In *Advances in Petroleum Chemistry and Refining, Vol. VI*; McKetta, Jr., J. J., Ed.; Interscience Publishers: New York, 1962, p. 314.

32. Shaver, A.; El-khateeb, M.; Lehuis, A.-M. *Angew. Chem. Int. Ed. Engl.* **1996**, *35*, 2362.
33. (a) Weil, E. D.; Sandler, S. R. In *Kirk-Othmer Encyclopedia of Chemical Technology*, 4th Ed., Vol. 23; Kroschwitz, J. I.; Howe-Grant, M., Eds.; John Wiley & Sons, Inc.: Toronto, 1996, p. 275 (for H₂S data).
(b) Roberts, J. S. In *Kirk-Othmer Encyclopedia of Chemical Technology*, 4th Ed., Vol. 24; Kroschwitz, J. I.; Howe-Grant, M., Eds.; John Wiley & Sons, Inc.: Toronto, 1996, p. 19 (for thiol data).
34. (a) Crampton, M. R. In *The Chemistry of the Thiol Group, Part I*; Patai, S., Ed.; John Wiley & Sons, Ltd.: Toronto, 1974, p. 379.
(b) Danehy, J. P.; Parameswaran, K. N. *J. Chem. Eng. Data* **1968**, *13*, 386.
35. Shaw, R. In *The Chemistry of the Thiol Group, Part I*; Patai, S., Ed.; John Wiley & Sons, Ltd.: Toronto, 1974, p. 151.
36. Vahrenkamp, H. In *Sulfur - Its Significance for Chemistry, for the Geo-, Bio- and Cosmospere and Technology*; Müller, A.; Krebs, B., Eds.; Elsevier: Amsterdam, **1984**, p. 121.
37. Sellmann, D.; Barth, I. *Inorg. Chim. Acta* **1989**, *164*, 171.
38. Mueting, A. M.; Boyle, P.; Pignolet, L. H. *Inorg. Chem.* **1984**, *23*, 44.
39. (a) Chatt, J.; Lloyd, J. P.; Richards, R. L. *J. Chem. Soc., Dalton Trans.* **1976**, 565.
(b) Povey, D. C.; Richards, R. L.; Shortman, C. *Polyhedron* **1986**, *5*, 369.
40. Henderson, R. A.; Hughes, D. L.; Richards, R. L.; Shortman, C. *J. Chem. Soc., Dalton Trans.* **1987**, 1115.
41. de los Ríos, I.; Jiménez-Tenorio, M.; Puerta, M. C.; Salcedo, I.; Valerga, P. *J. Chem. Soc., Dalton Trans.* **1997**, 4619.
42. Di Vaira, M.; Midollini, S.; Sacconi, L. *Inorg. Chem.* **1977**, *16*, 1518.
43. Vahrenkamp, H. *Angew. Chem., Int. Ed. Engl.* **1975**, *14*, 322.
44. Bianchini, C.; Mealli, C.; Meli, A.; Sabat, M. *Inorg. Chem.* **1986**, *25*, 4617.
45. Osakada, K.; Yamaoto, T.; Yamaoto, A. *Inorg. Chim. Acta* **1985**, *105*, L9.

46. Mueting, A. M.; Boyle, P. D.; Wagner, R.; Pignolet, L. H. *Inorg. Chem.* **1988**, *27*, 271.
47. Green, M. L. H.; Ng, D. K. P. *J. Chem. Soc., Dalton Trans.* **1993**, 11.
48. Nishio, M.; Matsuzaka, H.; Mizobe, Y.; Hidai, M. *Inorg. Chim. Acta* **1997**, *263*, 119.
49. Tang, Z.; Normura, Y.; Ishii, Y.; Mizobe, Y.; Hidai, M. *Inorg. Chim. Acta* **1998**, *267*, 73.
50. Dance, I. G. *J. Am. Chem. Soc.* **1979**, *101*, 6264.
51. Dance, I. G. *Polyhedron*, **1986**, *5*, 1037.
52. Barbaro, P.; Cecconi, F.; Ghilardi, C. A.; Midollini, S.; Orlandini, A.; de Biani, F. F.; Laschi, F.; Zanello, P. *J. Chem. Soc., Dalton Trans.* **1996**, 4337.
53. Adamson, G. W.; Shearer, H. M. M. *J. Chem. Soc., Chem. Commun.* **1969**, 897.
54. Mealli, C.; Midollini, S.; Sacconi, L. *Inorg. Chem.* **1982**, *17*, 632.
55. Fisher, J. R.; Mills, A. J.; Sumner, S.; Brown, M. P.; Thomson, M. A.; Puddephatt, R. J.; Frew, A. A.; Manojlovic-Muir, L.; Muir, K. *Organometallics* **1982**, *1*, 1421.
56. Antonelli, D. M.; Cowie, M. *Inorg. Chem.* **1990**, *29*, 3339.
57. (a) Jennings, M. C.; Payne, N. C.; Puddephatt, R. J. *Inorg. Chem.* **1987**, *26*, 3776.
(b) Jennings, M. C.; Puddephatt, R. J. *Inorg. Chem.* **1988**, *27*, 4280.
58. Fritz, H. P.; Gordan, I. R.; Schwarzhans, K. E.; Venanzi, L. M. *J. Chem. Soc.* **1965**, 5210.
59. Del Zotto, A.; Di Bernardo, P.; Tolazzi, M.; Zanonato, P. L. *J. Chem. Soc., Dalton Trans.* **1999**, 979.
60. Crociani, L.; Anacardio, R.; Traldi, P.; Corain, B. *Inorg. Chim. Acta* **1998**, *282*, 119.
61. Khan, M. M. T.; Reddy, A. P. *Polyhedron* **1987**, *6*, 2009.
62. Rauchfuss, T. B.; Patino, F.; Roundhill, D. M. *Inorg. Chem.* **1975**, *14*, 652.
63. Knebel, W. J.; Angelici, D. J. *Inorg. Chem.* **1974**, *13*, 627.

64. Reddy, V. V. S. *Inorg. Chim. Acta* **1988**, *144*, 177.
65. Tisato, F.; Pilloni, G.; Refosco, F.; Bandoli, G.; Corvaja, C.; Corain, B. *Inorg. Chim. Acta* **1998**, *275*, 401.
66. Rauchfuss, T. B.; Clements, J. L.; Agnew, S. F.; Roundhill, D. M. *Inorg. Chem.* **1977**, *16*, 775.
67. Park, S.; Johnson, M. P.; Roundhill, D. M. *Organometallics* **1989**, *8*, 1700.
68. Bianchini, C.; Farnetti, e.; Graziani, M.; Nardin, G.; Vacca, A.; Zanobini, F. *J. Am. Chem. Soc.* **1990**, *112*, 9190.
69. (a) Farnetti, E.; Kaspar, J.; Graziani, M. *J. Mol. Catal.* **1990**, *63*, 5.
(b) Farnetti, E.; Nardin, G.; Graziani, M. *J. Organomet. Chem.*, **1991**, *417*, 163.
70. Kinting, A.; Kreuzfeld, H.-J. *J. Organomet. Chem.*, **1989**, *370*, 343.
71. Yamada, I.; Yamazaki, N.; Yamaguchi, M.; Yamagishi, T. *J. Mol. Catal. (A)* **1997**, *120*, L13.
72. (a) Crociani, L.; Refosco, F.; Tisato, F.; Gatto, S.; Corain, B. *Inorg. Chim. Acta* **1996**, *249*, 131.
(b) Crociani, L.; Tisato, F.; Refosco, F.; Giuliano, B. Corain, B. *Eur. J. Inorg. Chem.* **1998**, *11*, 1689.
73. Kreuzfeld, H.-J.; Döbler, C.; Abicht, H.-P. *J. Organomet. Chem.*, **1987**, *336*, 287.
74. de Graaf, W.; Harder, S.; Boersma, J. van Koten, G. *J. Organomet. Chem.*, **1988**, *358*, 545.
75. Crociani, L.; Bandoli, G.; Dolmella, A.; Basato, M.; Corain, B. *Eur. J. Inorg. Chem.* **1998**, *11*, 1811.
76. Albinati, A.; Lianza, F.; Berger, H.; Pregosin, P. S.; Rügger, H.; Kunz, R. W. *Inorg. Chem.* **1993**, *32*, 478.
77. Anderson, G. K.; Kumar, R. *Inorg. Chem.* **1984**, *23*, 4064.
78. Tisato, F.; Refosco, F.; Bolzati, C.; Cagnolini, A.; Gatto, S.; Bandoli, G. *J. Chem. Soc., Dalton Trans.* **1997**, 1421.

79. (a) Rauchfuss, T.; Roundhill, D. M. *J. Organomet. Chem.*, **1973**, *59*, C30.
(b) Rauchfuss, T.; Roundhill, D. M. *J. Am. Chem. Soc.* **1974**, *96*, 3098.
80. Cullen, W. R.; Einstein, F. W. B.; Huang, C.-H.; Willis, A. C.; Yeh, E.-S. *J. Am. Chem. Soc.* **1980**, *102*, 988.
81. (a) Rodgers, G. E.; Cullen, W. R.; James, B. R. *Can. J. Chem.* **1983**, *61*, 1314.
(b) Hampton, C.; Cullen, W. R.; James, B. R. *J. Am. Chem. Soc.* **1988**, *110*, 6918.
(c) Hampton, C. R. S. M.; Butler, I. R.; Cullen, W. R.; James, B. R.; Charland, J.-P.; Simpson, J. *Inorg. Chem.* **1992**, *31*, 5509.
82. Mauthner, K.; Slugovc, C.; Mereiter, K.; Schmid, R.; Kirchner, K. *Organometallics* **1997**, *16*, 1956.
83. (a) Shen, J.-Y.; Slugovc, C.; Wiede, P.; Mereiter, K.; Schmid, R.; Kirchner, K. *Inorg. Chim. Acta* **1998**, *268*, 69.
(b) Guo, Z.; Habtemariam, A.; Sadler, P. J.; James, B. R. *Inorg. Chim. Acta* **1998**, *273*, 1.
84. (a) Habtemariam, A.; Sadler, P. J. *J. Chem. Soc., Chem. Commun.* **1996**, 1785.
(b) Margiotto, N.; Habtemariam, A.; Sadler, P. J. *Angew. Chem., Int. Ed. Engl.* **1997**, *36*, 1185.
85. James, B. R. In *Comprehensive Organometallic Chemistry*, Vol. 8; Wilkinson, G., Stone, F. G. A.; Abel, E. W., Eds.; Pergamon Press: Oxford, 1982, Chapter 51.
86. (a) Krassowski, D. W.; Nelson, J. H.; Brower, K. R.; Hauenstein, D.; Jacobson, R. A. *Inorg. Chem.* **1988**, *27*, 4294.
(b) Joshi, A. M.; Thorburn, I. S.; Rettig, S. J.; James, B. R. *Inorg. Chim. Acta* **1992**, *198-200*, 283.

Chapter 2

Experimental Procedures

General Procedures

Unless otherwise stated all manipulations were performed under an oxygen-free Ar or N₂ atmosphere at r.t. using standard Schlenk techniques. All solvents were dried and purged free of oxygen prior to use.

2.1 Materials

2.1.1 Gases

Purified Ar (H.P.), N₂ (U.S.P.), H₂ (Research, extra dry) and O₂ (U.S.P.) were obtained from Union Carbide Canada Ltd., anhydrous H₂S, HCl and NH₃ from Matheson Gas Co., and N₂O from Praxair. All gases except Ar, N₂ and H₂ were used without further purification. Ar and N₂ were dried by passing through columns of CaSO₄. H₂ was passed through an Engelhard Deoxo catalytic hydrogen purifier to remove traces of O₂.

2.1.2 Solvents

All spectral or analytical grade solvents were obtained from Fisher, Eastman, Aldrich, Mallinckrodt Chemical Co., BDH, or MCB, and were refluxed and distilled over appropriate drying agents¹ under N₂ prior to use. CH₂Cl₂ was dried over CaH₂; C₆H₆, hexanes, and Et₂O over Na/benzophenone; acetone over K₂CO₃; MeOH and EtOH over Mg/I₂; isopropanol over CaO; and THF over K/Na alloy. All solvents used in reactions involving Ru complexes were purged with Ar or N₂ (for at least 10 min) to remove traces of O₂ before

being transferred into their reaction flasks via cannula. All deuterated solvents (CD_2Cl_2 , CDCl_3 , C_6D_6 , C_7D_8 , $(\text{CD}_3)_2\text{CO}$, DMSO-d_6 and D_2O) were obtained from Cambridge Isotope Laboratories (CIL), MSD Isotopes, or Isotec Inc., and stored over activated molecular sieves (Fisher, type 4 Å, 4 - 8 mesh), with the exception of D_2O . For the preparation of O_2 -sensitive samples, the deuterated solvents were de-oxygenated (via the freeze-pump-thaw method), dried over drying agents (CD_2Cl_2 , CDCl_3 and $(\text{CD}_3)_2\text{CO}$ using activated molecular sieves; C_6D_6 and C_7D_8 using Na/benzophenone), and stored under vacuum or Ar atmosphere.

2.1.3 Compounds

All commercially available compounds were supplied by Aldrich, Anachemia, BDH, Eastman, Fisher, Mallinckrodt or MCB. These materials were used as received unless otherwise specified.

Proton sponge (1,8-bis(dimethylamino)naphthalene), obtained from Aldrich, was purified by passing a solution of the amine in *n*-pentane through a column of alumina, and evaporating the eluant to yield a white solid.² Anal. Calcd. $\text{C}_{14}\text{H}_{18}\text{N}_2$: C, 78.46; H, 8.47; N, 13.07. Found: C, 78.48; H, 8.37; N, 12.78. ^1H NMR (CD_2Cl_2): δ 6.9 - 7.4 (6H, m, Ph), 2.80 (6H, s, $\text{N}(\text{CH}_3)_2$). The NMR data correspond with literature data.³

2.2 Instrumentation

2.2.1 Nuclear Magnetic Resonance Spectroscopy

NMR spectra were recorded on a Bruker AC200 (200.1 MHz for ^1H and 81.0 MHz for ^{31}P), a Varian XL300 (300.0 MHz for ^1H , 121.4 MHz for $^{31}\text{P}\{^1\text{H}\}$ and 75.0 MHz for $^{13}\text{C}\{^1\text{H}\}$ NMR), a Bruker WH400 (400.0 MHz for ^1H) or a Bruker AMX500 (500.0 MHz for ^1H and 202.5 MHz for ^{31}P) FT-NMR spectrometer. Residual protonated species in the

deuterated solvents were used as internal references (δ 5.32 for CD_2Cl_2 , δ 7.15 for C_6D_6 , δ 7.24 for CDCl_3 , and δ 2.20 for $(\text{CD}_3)_2\text{CO}$; all are reported relative to the external standard of tetramethylsilane (TMS) at δ 0.00) for ^1H NMR. NMR chemical shifts. The $^{31}\text{P}\{^1\text{H}\}$ NMR chemical shifts are reported relative to 85 % H_3PO_4 (external reference) with the downfield shifts taken as positive. For the $^{31}\text{P}\{^1\text{H}\}$ NMR spectra recorded on the Varian XL300, the chemical shifts reported were externally referenced to trimethylphosphite, $\text{P}(\text{OMe})_3$ at δ 141.0⁴ (relative to 85 % H_3PO_4). Unless otherwise specified, all variable-temperature NMR spectra were performed on the Varian XL300 or the Bruker AMX500 spectrometers.

Samples were prepared in 5 mm NMR tubes with poly(propylene) caps or rubber septa. For O_2 -sensitive samples, NMR tubes with poly(tetrafluoroethylene), J. Young valves (Aldrich) were used. Solid samples were initially placed in the NMR tubes, which were then evacuated, and deuterated solvents were subsequently vacuum transferred into the tubes maintained at liquid N_2 temperature. These samples were carefully warmed to room temperature (r.t.) and the tubes placed under 1 atm of Ar or another gas as required by the specific experiment.

2.2.2 Infrared Spectroscopy

An ATLI Mattson Genesis Series FTIR spectrophotometer was used to record all infrared spectra (range: 500 to 4000 cm^{-1}). Samples for analysis were made into KBr pellets; data are reported in cm^{-1} .

2.2.3 Ultraviolet Spectroscopy

UV-Vis spectra were recorded on a Hewlett Packard 8452A diode-array spectrophotometer (range: 190 to 820 nm) equipped with a thermostatted cell compartment

using 1 cm quartz cells. For O₂-sensitive compounds or *in situ* reactions, an anaerobic cell⁵ equipped with a side-arm flask for mixing of solutions was used. Data are reported as λ_{max} in nm (ϵ in units of M⁻¹cm⁻¹).

2.2.4 Thermal Analysis

Thermogravimetric analyses (TGA) were performed using a TA Instruments TGA 51 Thermogravimetric Analyzer. Solid samples were weighed accurately (10 - 15 mg) into an inert Pt pan. The samples were then heated in a N₂ atmosphere (flow rate = 100 cc/min) at a rate of 10°C/min to a maximum of 500°C.

Differential Scanning Calorimetry (DSC) data were collected on a TA Instruments 910S Differential Scanning Calorimeter. Solid samples were weighed accurately (2 - 5 mg) into disposable aluminum pans. The samples were then heated in a N₂ atmosphere (flow rate = 40 cc/min) at a rate of 5°C per min to a maximum of 500°C.

2.2.5 Microanalysis

Microanalyses (%C, H, N, and/or Cl, S) were performed by Mr. P. Borda of this department. A Carlo Erba Model 1106 Elemental Analyzer or a Fisons (Erba) Instruments EA 1108 CHN-O Elemental Analyzer was used and the results have an absolute accuracy within ± 0.3 %.

2.2.6 X-ray Crystallography

All single crystal X-ray, diffraction studies with the exception of data for *cis*-RuCl₂(P-N)(PPh₃)(η^2 -H₂) **36** (P-N = [*o*-(*N,N*-dimethylamino)phenyl](diphenylphosphine)), were performed by the late Dr. S. J. Rettig of this department on a Rigaku/ADSC CCD area

detector or a Rigaku AFC6S diffractometer (both with graphite monochromated Cu-K α radiation). The single crystal X-ray diffraction study of **36**, was performed by Dr. V. G. Young, Jr. of the X-Ray Crystallographic Laboratory at the University of Minnesota, using a Siemens SMART Platform CCD system (with Mo-K α radiation).

2.2.7 Gas Chromatography

Gas chromatographic analyses were performed on a temperature-programmable Hewlett Packard 5890A instrument equipped with a thermal conductivity detector, using He as the carrier gas.

2.2.8 Magnetic Susceptibility Studies

The Johnson-Matthey Magnetic Susceptibility Balance was (Gouy method) used to measure the magnetism of samples. The mass susceptibility per gram of sample, χ_g , was calculated according to the equation below. Diamagnetic contributions from Ru(III) and ligands were obtained and calculated from Pascal's constants.⁶

$$\chi_g = \frac{C_{\text{Bal}} \ell (R - R_0)}{10^9 \text{ m}}$$

where: C_{Bal} = balance calibration constant

ℓ = sample length (cm)

R = reading for tube plus sample

R_0 = reading for empty tube

m = sample mass (g)

2.2.9 Conductivity Measurements

A Serfass Conductance Bridge Model RCM15B1 (Arthur H. Thomas Co. Ltd.) connected to a 3403 cell from the Yellow Springs Instrument Company was used for conductivity measurements. The cell was thermostatted at 25°C in a water-bath. The cell

constant, $\sigma = 0.001413 \text{ ohm}^{-1} \text{ cm}^{-1}$, was determined by measuring the resistance of a 0.0100 M aqueous solution of KCl. Solutions with concentrations of $\sim 10^{-3} \text{ M}$ were used for conductance measurements. All solutions were prepared using dried and O_2 -free solvents; the most extensive set of data was obtained during studies of some reactions of complexes with NH_3 (Section 6.2).

2.3 Syntheses of Ligands

The ligands synthesized in this thesis work are shown in Figure 2.1.

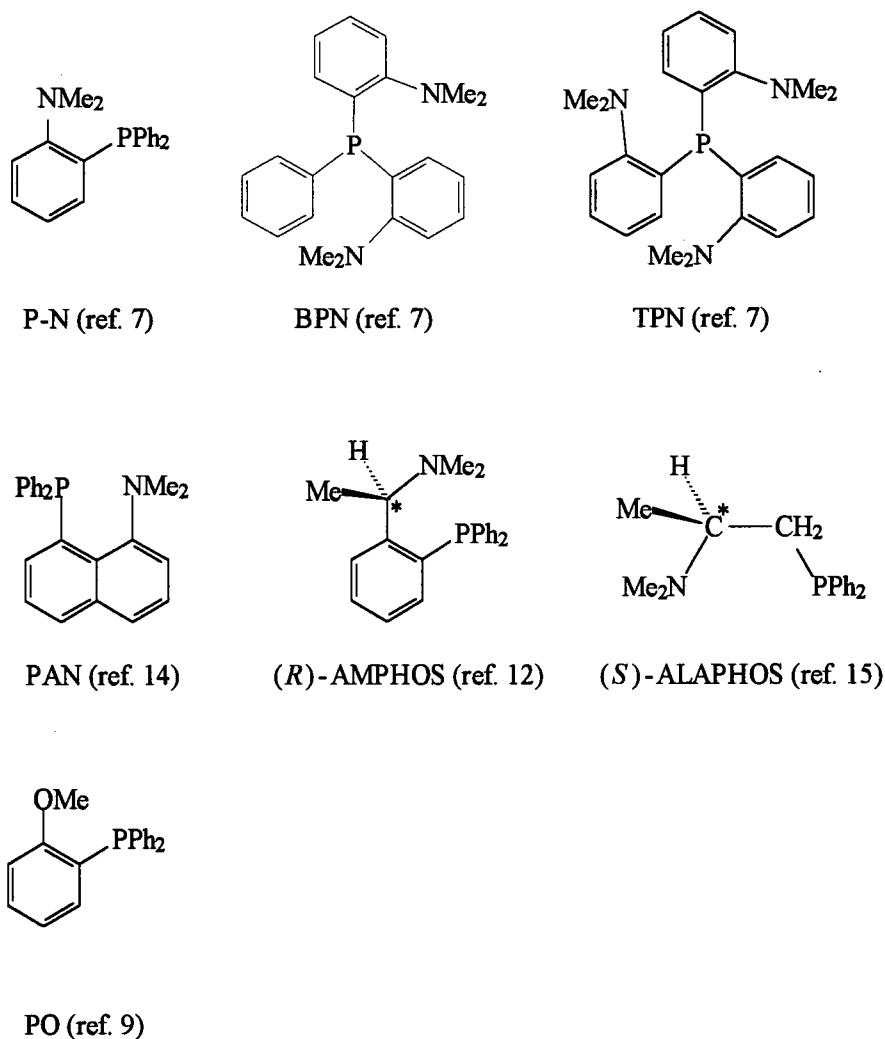


Figure 2.1 Ligands studied in this thesis work.

2.3.1 [*o*-(*N,N*-Dimethylamino)phenyl]diphenylphosphine, P-N⁷

2.3.1.1 *o*-Bromo-*N,N*-dimethylaniline⁸

The aniline was prepared by the method described by Gilman and Banner.⁸ One equiv. of dimethylsulfate (14 mL, 0.148 mol) was added to a stirring solution of *o*-bromoaniline (25 g, 0.145 mol) in water (30 mL), and the mixture was stirred for 1 h to achieve homogeneity. While cooling in an ice-bath, this solution was neutralized with 5.0 M KOH. Addition of dimethylsulfate (14 mL, 0.148 mol) and neutralization with KOH were repeated twice. After the mixture was stirred for 3 h, the organic layer was extracted with Et₂O (3 x 20 mL). The combined ethereal extracts were washed with water (3 x 20 mL) and dried over K₂CO₃. Product distillation gave a clear, colourless oil (21 g, yield: 72 %), bp 96°C (15 mm Hg). ¹H NMR (CDCl₃): δ 2.80 (6H, s, N(CH₃)₂), [6.88 (1H, t), 7.12 (1H, d), 7.27 (1H, t), 7.59 (1H, d), Ph]. The NMR data were not determined in the original reference.⁸

2.3.1.2 [*o*-(*N,N*-Dimethylamino)phenyl]diphenylphosphine, P-N⁷

P-N was prepared following the method of Fritz et al.⁷ A solution of *o*-bromo-*N,N*-dimethylaniline (3.5 g, 0.0175 mol) in Et₂O (7 mL) was added dropwise to a 1.6 M solution of ⁿBuLi in hexane (11 mL, 0.0175 mol) which had been cooled to -20°C. The mixture was warmed to r.t. and stirred for 1 h during which time a white precipitate, *o*-Li(C₆H₄)NMe₂, formed. This mixture was cooled to -40°C and a solution of Ph₂PCl (3.2 mL, 0.0175 mol) in Et₂O (3.5 mL) was added dropwise. Again, the mixture was warmed to r.t. and stirred for 1 h, when water (20 mL) was added to the turbid pale-yellow mixture. The product was extracted with Et₂O (4 x 15 mL). The combined ethereal extracts were dried over anhydrous MgSO₄. The white residue which remained after removal of the Et₂O was recrystallized from hot EtOH to give clear, colourless crystals. Yield: 3.2 g, 60 %.

Mp 122 - 123°C. Anal. Calcd. $C_{20}H_{20}NP$: C, 78.67; H, 6.60; N, 4.59. Found: C, 78.80; H, 6.47; N, 4.59. $^{31}P\{^1H\}$ NMR (C_6D_6): δ -14.4 (s). 1H NMR (C_6D_6): δ 6.8 - 7.3 (14H, m, Ph), 2.60 (6H, s, $N(CH_3)_2$). The NMR data agree with the literature data.^{7,9,10}

2.3.2 Bis[*o*-(*N,N*-dimethylamino)phenyl]phenylphosphine, BPN⁷

BPN was prepared in the same manner as described for P-N but using $PhPCl_2$ (1.2 mL, 8.75 mmol). Yield: 3.0 g, 50 %. Mp 85 - 86°C. Anal. Calcd. $C_{22}H_{25}N_2P$: C, 75.84; H, 7.23; N, 8.04. Found: C, 75.84; H, 7.26; N, 7.99. $^{31}P\{^1H\}$ NMR ($CDCl_3$): δ -22.8 (s). 1H NMR ($CDCl_3$): δ 6.6 - 7.3 (13H, m, Ph), 2.56 (12H, s, $N(CH_3)_2$). X-ray quality crystals were recrystallized from EtOH at 0°C. The ORTEP plot, selected bond lengths and angles of the crystal structure are shown and discussed in Section 3.5, while full experimental parameters and details are presented in Appendix I.

2.3.3 Tris[*o*-(*N,N*-dimethylamino)phenyl]phosphine, TPN⁷

TPN was prepared by Dr. P. Meessen of this laboratory in the same manner as described for P-N but using PCl_3 (0.5 mL, 5.83 mmol). X-ray quality crystals were recrystallized from EtOH and the structure was determined.¹¹ Yield: 0.9 g, 40 %. Mp 108 - 109°C. Anal. Calcd. $C_{24}H_{30}N_3P$: C, 73.63; H, 7.72; N, 10.73. Found: C, 73.49; H, 7.81; N, 10.53. $^{31}P\{^1H\}$ NMR ($CDCl_3$): δ -28.9 (s). 1H NMR ($CDCl_3$): δ 6.5 - 7.4 (12H, m, Ph), 2.6 (18H, s, $N(CH_3)_2$). The data given here were determined by Dr. P. Meessen.¹¹

2.3.4 (R)-(+)-*N,N*-Dimethyl-1-[*o*-(diphenylphosphino)phenyl]ethylamine, AMPHOS¹²

2.3.4.1 (R)-(+)-*N,N*-Dimethyl-1-phenylethylamine¹³

The title amine was prepared by the method described by Pine and Sanchez.¹³ A flask charged with (R)-(+)-1-phenylethylamine (30 g, 0.25 mol) was cooled to 0°C. Formic acid (90 %, 35 mL, 0.8 mol) and then formaldehyde (37 %, 56 mL, 0.75 mol) were added dropwise, and the yellow mixture was refluxed at 80°C for 24 h. It was then acidified with 6 M HCl (50 mL) while being cooled in an ice-bath. Nonbasic material was extracted from the mixture using Et₂O (3 x 50 mL) and discarded. The aqueous layer was made basic by adding 50 % NaOH and then extracted with Et₂O (2 x 50 mL). The combined ethereal extracts were washed with water (20 mL) and dried over anhydrous MgSO₄. Removal of the Et₂O resulted in a yellow liquid, the distillation of which gave a clear, colourless liquid (32°C, ~ 1 mm Hg). Yield: 20 g, 54 %. ¹H NMR (CDCl₃): δ 7.2 (4H, m, Ph), 3.1 (1H, q, CHCH₃), 2.1 (6H, s, N(CH₃)₂), 1.3 (3H, d, CHCH₃). The NMR data were not given in the original reference.¹³

2.3.4.2 AMPHOS·HCl(acetone)¹²

The AMPHOS ligand was prepared by the method described by Payne and Stephan.¹² An 1.6 M solution of ⁿBuLi in hexane (84 mL, 0.134 mol) was added dropwise to a solution of (R)-(+)-*N,N*-dimethyl-1-phenylethylamine (20 g, 0.134 mol) and Et₂O (100 mL). The yellow mixture was stirred for 24 h, and cooled in an ice-bath, before Ph₂PCl (24 mL, 0.134 mol) was added slowly. The reaction mixture was stirred for 2 h, and water (100 mL) was then added to the resultant orange solution. The organic layer was extracted with Et₂O (3 x 50 mL), and the combined organic layers were dried over anhydrous MgSO₄. HCl gas was passed through the filtered Et₂O solution for 10 min, before removal of the Et₂O resulted

in an orange oil. A minimum of acetone was added to dissolve the oil and Et₂O was slowly added to precipitate a white solid. NMR analysis of this white powder indicate a mixture of starting amine (30 %) and AMPHOS·HCl·(acetone) (70 %). The NMR data for AMPHOS·HCl·(acetone) are: ³¹P{¹H} NMR (CDCl₃): δ -17.2 (s). ¹H NMR (CDCl₃): δ 12.4 (1H, br s, -NHCl), 6.9-8.1 (14H, m, Ph), 5.04 (1H, hx, CH₃CH), 2.89, 2.45 (6H, d, N(CH₃)₂), δ 1.6 (3H, d, CH₃CH), δ 2.1 (6H, s, acetone). The NMR data correspond to those in the literature.¹²

2.3.4.3 Purification of AMPHOS¹²

Crude AMPHOS·HCl·(acetone) (3.8 g) was recrystallized from hot acetone to obtain a white powder. This was redissolved in hot EtOH and was neutralized to pH ~8 with 1 M KOH ethanolic solution. After removal of EtOH, Et₂O was added, and the mixture was filtered. An oily residue remained after the removal of the Et₂O from the filtrate. MeOH was then added to redissolve the residue. At 0°C, a white precipitate that formed was filtered off and washed with cold MeOH (2 x 10 mL). Clear, colourless crystals formed after recrystallization from hot MeOH once again. Yield: 1.0 g, 20 %. Mp 80-81°C. Anal. Calcd. C₂₂H₂₄NP: C, 79.25; H, 7.26; N, 4.20. Found: C, 79.18; H, 7.33; N, 4.22. ³¹P{¹H} NMR (CDCl₃): δ -17.2 (s). ¹H NMR (CDCl₃): δ 6.9 - 7.5 (14H, m, Ph), 4.12 (1H, qn, CH₃CH), 2.00 (6H, s, N(CH₃)₂), δ 1.20 (3H, d, CH₃CH). The above characterization data are consistent with literature data.¹²

2.3.5 1-(*N,N*-Dimethylamino)-8-(diphenylphosphino)naphthalene, PAN¹⁴

PAN was prepared by the method described by Horner and Simons with minor modifications.¹⁴ Tetramethylethylenediamine (TMEDA) was used to assist the lithiation of

1-(dimethylamino)naphthalene with *n*-BuLi. To a cooled solution (-20°C) of ⁿBuLi (1.6 M in hexane, 9.1 mL, 0.0146 mol), a solution of 1-(dimethylamino)naphthalene (2.5 g, 0.0146 mol) in hexanes (15 mL) was added dropwise. The yellow mixture was stirred for 10 min, after which TMEDA (2.2 mL, 0.0146 mol) was added. The mixture was slowly warmed to r.t. and stirred for 16 h during which time a white precipitate, 1-(dimethylamino)-8-lithionaphthalene, formed. A solution of Ph₂PCl (2.6 mL, 0.0146 mol) in Et₂O was added dropwise to the cooled (-40°C) reaction mixture. This was then warmed to r.t., stirred for 1 h, and made basic with 6 M KOH. The organic layer was extracted with Et₂O (3 x 20 mL) and the combined ethereal extracts were washed with water (20 mL) and dried over anhydrous MgSO₄. Removal of Et₂O resulted in a yellow-orange residue. Recrystallization of this solid from CH₂Cl₂ at 0°C resulted in yellow crystals. Yield: 2.6 g, 50 %. Mp 170 - 171°C. Anal. Calcd. C₂₄H₂₂NP: C, 81.10, H, 6.24; N, 3.94. Found: C, 80.83; H, 6.18; N, 3.93. ³¹P{¹H} NMR (CDCl₃): δ -2.86 (s). ¹H NMR (CDCl₃): δ 6.8 - 7.9 (16H, m, Ph), 2.57 (6H, s, N(CH₃)₂). The physical and spectroscopic data agree with those reported.¹⁴

2.3.6 [(*S*)-2-(Dimethylamino)propyl]diphenylphosphine, ALAPHOS¹⁵

2.3.6.1 (*S*)-2-(Dimethylamino)propanoic acid¹⁶

The methylation of (*S*)-2-aminopropanoic acid (alanine) was carried out according to the method described by Bowman and Stroud.¹⁶ Formaldehyde (37 %, 30 mL) was added to a stirring suspension of (*S*)-alanine (15.0 g, 0.168 mol) and Pd/C (10 %, 1.5 g) in water (400 mL, and H₂ gas was passed through the mixture for 24 h. After removal of the H₂ source, the mixture was refluxed for 15 min and was immediately filtered into a Buchner funnel containing Celite. Such filtration through Celite was repeated three times to remove any Pd/C. Removal of water resulted in a hygroscopic, white solid. Yield: 17.9 g, 90 %. ¹H

NMR (D_2O): δ 4.77 (1H, s, COH), 3.66 (1H, q, $(H_3C)CH$, $^3J_{HH} = 7.0$ Hz), 2.79 (6H, d, $N(CH_3)_2$, $^3J_{HH} = 20.7$ Hz), 1.42 (3H, d, $(H_3C)CH$, $^3J_{HH} = 7.0$ Hz). The NMR data were not given in the original reference.¹⁶

2.3.6.2 (*S*)-2-(Dimethylamino)-1-propanol¹⁵

The title alcohol was prepared by the method described by Hayashi et al.¹⁵ (*S*)-2-(Dimethylamino)propanoic acid (17.9 g, 0.153 mol) in 1 g portions was added over a period of 30 min to a stirring suspension of $LiAlH_4$ (12.4g, 0.327 mol) in THF (400 mL). The mixture was refluxed for 4 h, cooled, and stirred under N_2 for 16 h. The white precipitate that formed after the successive addition of water (25 mL), 15 % NaOH (25 mL) and water (75 mL) was removed by filtration and washed with THF (2 x 20 mL). The combined THF filtrates were dried over anhydrous $NaSO_4$. Removal of THF resulted in a yellow oil whose product distillation gave a clear, colourless oil, bp 60°C (15 mm Hg). Yield: 7 g, 45 %. 1H NMR ($CDCl_3$): δ 3.50 (1H, br s, H_2COH), 3.22 (2H, m, H_2COH), 2.61 (1H, m, $(H_3C)CH$), 2.10 (6H, s, $N(CH_3)_2$), 0.79 (3H, d, $(H_3C)CH$). The NMR data correspond to the literature data.¹⁵

2.3.6.3 (*S*)-2-(Dimethylamino)propylchloride hydrochloride¹⁵

A solution of (*S*)-2-(dimethylamino)-1-propanol (7.0 g, 0.068 mol) in EtOH (10 mL) was cooled in an ice-bath and acidified with 12 M HCl (20 mL). Evaporation of the EtOH gave the HCl salt as a clear colourless oil. $CHCl_3$ (20 mL) was then added to form two immisible layers. This mixture was cooled to 0°C and $SOCl_2$ (15 mL, 0.206 mol) was added over a period of 30 min. The resultant homogeneous, clear solution was refluxed for 2 h; removal of the solvent from the cooled solution gave an orange oil. Recrystallization of the oil from EtOH (3 times) gave clear, colourless, hygroscopic crystals. Yield: 6.7 g, 62 %. 1H

NMR (CDCl_3): δ 12.76 (1H, br s, $\text{HN}^+(\text{CH}_3)_2$), 3.96 (2H, m, H_2CCl), 3.62 (1H, m, $(\text{H}_3\text{C})\text{CH}$), 2.83 (6H, s, $\text{HN}^+(\text{CH}_3)_2$), 1.50 (3H, d, $(\text{H}_3\text{C})\text{CH}$). The NMR data were not given in the original reference.¹⁵

2.3.6.4 [(*S*)-2-(Dimethylamino)propyl]diphenylphosphine, ALAPHOS¹⁵

To a 3-neck, 200 mL flask charged with *t*-BuOK (1.8 g, 16.0 mmol) and THF (30 mL) was added Ph_2PH (1.10 mL, 6.3 mmol). A bright orange solution formed immediately. (*S*)-2-(Dimethylamino)propylchloride hydrochloride (1.0 g, 6.3 mmol) was added and the mixture was refluxed for 2 h. The mixture turned colourless and a white precipitate (KCl) formed. The solvent was removed and 3 M HCl (150 mL) was added to the residue. This cloudy mixture was extracted with C_6H_6 (50 mL). The aqueous layer was made basic by adding 15 % NaOH (50 mL) and extracted with C_6H_6 (2 x 80 mL). The combined C_6H_6 extracts were washed with a saturated NaCl solution (100 mL) and dried over anhydrous NaSO_4 . A yellow oily residue remained after the removal of C_6H_6 . Et_2O was added to dissolve the residue and the solution was passed through a neutral alumina column to remove any phosphine oxide. Evaporation of Et_2O gave a clear, colourless oil. Yield: 1.25 g, 73 %. $^{31}\text{P}\{^1\text{H}\}$ NMR (CDCl_3): δ -19.11 (s). ^1H NMR (CDCl_3): δ 7.2 - 7.7 (10H, m, Ph), 3.07 (1H, m, $(\text{H}_3\text{C})\text{CH}$), 2.87 (1H, br. d, $\text{CH}_a\text{H}_b\text{PPh}_2$), 2.56 (6H, s, $\text{N}(\text{CH}_3)_2$), 2.00 (1H, t of d, $\text{CH}_a\text{H}_b\text{PPh}_2$), 1.43 (3H, d, $(\text{H}_3\text{C})\text{CH}$). The NMR data agree with the literature data.¹⁵

2.3.7 *o*-Diphenylphosphineanisole, PO⁹

The preparation of *o*-diphenylphosphineanisole was initiated by a Grignard reaction described by Roundhill and co-workers.⁹ A 3-neck flask, equipped with an addition funnel and a condenser, was charged with Mg turnings (3.25 mg, 0.134 mol) and Et_2O (100 mL) under a flow of N_2 . *o*-Bromoanisole (25 g, 0.134 mol) was then slowly added, and the

mixture was allowed to react for 2 h. The grey-green mixture that resulted was cooled in an ice-bath and a solution of Ph_2PCl (25 mL, 0.139 mol) in Et_2O (20 mL) was added. The mixture was stirred for 20 h at 20°C during which time a white precipitate formed. Water (50 mL) was added and the product was extracted with Et_2O (2 x 50 mL). The combined ethereal extracts were washed with H_2O (2 x 20 mL) and dried over K_2CO_3 . Removal of Et_2O resulted in a white residue, whose recrystallization from hot EtOH (2 times) gave clear, colourless, crystalline needles. Yield: 15 g, 38 %. Melting point: $123\text{--}124^\circ\text{C}$. Anal. Calcd. $\text{C}_{19}\text{H}_{17}\text{OP}$: C, 78.07; H, 5.86. Found: C, 78.11; H, 5.76. $^{31}\text{P}\{^1\text{H}\}$ NMR (CDCl_3): δ -15.34 (s). ^1H NMR (CDCl_3): δ 6.6 - 7.8 (14H, m, Ph), 3.76 (3H, s, O- CH_3). The physical and spectroscopic data are consistent with the literature data.⁹

2.4 Syntheses of Ruthenium Precursors

The ruthenium as $\text{RuCl}_3 \cdot 3\text{H}_2\text{O}$ (41.5 - 43.96 % Ru) was obtained on loan from Johnson Matthey Ltd. and Colonial Metals Inc.

2.4.1 Dichlorotris(triphenylphosphine)ruthenium(II), $\text{RuCl}_2(\text{PPh}_3)_3$ (1)¹⁷

The title complex was prepared following a literature method¹⁷ with slight modifications. A solution of $\text{RuCl}_3 \cdot 3\text{H}_2\text{O}$ (2.11 g, 8.5 mmol) in MeOH (250 mL) was refluxed for 5 min, and then cooled to r.t., when PPh_3 (14.0 g, 53.4 mmol) was added. The mixture was refluxed for 3 h during which time a dark brown suspension formed. The mixture was filtered while still hot and the brown solid was washed with hot MeOH (6 x 20 mL), Et_2O (2 x 20 mL) and hexanes (2 x 20 mL) to remove excess PPh_3 . Yield: 8.0 g, 97 %. Anal. Calcd. $\text{C}_{54}\text{H}_{45}\text{Cl}_2\text{P}_3\text{Ru}$: C, 67.64; H, 4.73. Found: C, 67.50; H, 4.69.

2.4.2 Dichlorotris(tri-*p*-tolylphosphine)ruthenium(II), $\text{RuCl}_2(\text{P}(p\text{-tolyl})_3)_3$ (2)¹⁸

The title complex was prepared following a literature method.¹⁸ A solution of $\text{RuCl}_3 \cdot 3\text{H}_2\text{O}$ (1.0 g, 3.8 mmol) in MeOH (100 mL) was refluxed for 5 min, and then cooled to r.t., when $\text{P}(p\text{-tolyl})_3$ (5.0 g, 16.4 mmol) was added. The mixture was then refluxed for 24 h to give a dark purple solid which was filtered off and washed with MeOH (7 x 10 mL) and Et_2O (3 x 10 mL). Yield: 4.15 g, 74 %. Anal. Calcd. $\text{C}_{63}\text{H}_{63}\text{Cl}_2\text{P}_3\text{Ru}$: C, 69.74; H, 5.85. Found: C, 69.66; H, 5.83.

2.4.3 *Cis*-Dichlorotetrakis(dimethylsulfoxide)ruthenium(II), *Cis*- $\text{RuCl}_2(\text{DMSO})_4$ (3)¹⁹

A solution of $\text{RuCl}_3 \cdot 3\text{H}_2\text{O}$ (1.18 g, 4.5 mmol) and excess DMSO (12 mL) was refluxed for 30 min. The volume of the resulting deep red solution was reduced to 2 mL and acetone (5 mL) was added to precipitate a yellow solid, that was filtered off and washed with acetone (5 mL) and Et_2O (5 mL). Yield: 1.36 g, 62 %. Anal. Calcd. $\text{C}_6\text{H}_{12}\text{Cl}_2\text{P}_2\text{S}_4\text{Ru}$: C, 19.88; H, 4.97. Found: C, 20.02; H, 5.11.

2.4.4 Trichlorobis(triarylphosphine)(dimethylacetamide)ruthenium(III)-DMA solvate $\text{RuCl}_3(\text{PPh}_3)_2(\text{DMA}) \cdot (\text{DMA})$ (4a) and $\text{RuCl}_3(\text{P}(p\text{-tolyl})_3)_2(\text{DMA}) \cdot (\text{DMA})$ (4b)²⁰

The title complexes were prepared by Dr. D. E. Fogg, previously of this laboratory. Solid PPh_3 (4.34 g, 16.6 mmol) or $\text{P}(p\text{-tolyl})_3$ (5.05 mg, 16.6 mmol) was added to a dark brown solution of $\text{RuCl}_3 \cdot 3\text{H}_2\text{O}$ (2.0 g, 8.3 mmol) in DMA (60 mL), and the reaction mixture was stirred at r.t. for 24 h. The resulting green precipitate was filtered off, washed with DMA (2 x 5 mL) and hexanes (3 x 5 mL), and dried under vacuum. For **4a**: yield: 5.2 g, 69 %. Anal. Calcd. $\text{C}_{44}\text{H}_{48}\text{N}_2\text{O}_2\text{Cl}_3\text{P}_2\text{Ru}$: C, 58.32; H, 5.34; N, 3.09. Found: C, 58.22; H, 5.23; N, 3.01. For **4b**: yield: 5.5 g, 67 %. Anal. Calcd. $\text{C}_{50}\text{H}_{60}\text{N}_2\text{O}_2\text{Cl}_3\text{P}_2\text{Ru}$: C, 60.64; H, 6.11; N, 2.83. Found: C, 60.32; H, 6.11; N, 2.80.

2.5 Dichlorobis(*o*-diphenylphosphinoanisole)ruthenium(II), RuCl₂(PO)₂ (5)⁹

The title complex was prepared by the method described by Roundhill's group⁹ with modifications. To a suspension of RuCl₂(PPh₃)₃ (104 mg, 0.109 mmol) in acetone (5 mL) was added a solution of PO (70 mg, 0.239 mmol) in acetone (5 mL). The mixture was heated at 50°C for 3 h during which time a burgundy solid formed. This was filtered off and washed with Et₂O (2 x 5 mL). Yield: 66 mg, 80 %. Anal. Calcd. C₃₈H₃₄O₂Cl₂P₂Ru: C, 60.32; H, 4.53. Found: C, 60.12; H, 4.34. ³¹P{¹H} NMR (CDCl₃): δ 64.20 (s). ¹H NMR (CDCl₃): δ 6.8 - 7.6 (28H, m, Ph), 4.57 (6H, s, O-CH₃). The NMR data agree with the literature data.⁹

2.6 Syntheses of Ruthenium(II) Aminophosphine Complexes

2.6.1 Dichloro{[*o*-(*N,N*-dimethylamino)phenyl](diphenylphosphine)}(triphenylphosphine)ruthenium(II), RuCl₂(P-N)(PPh₃) (6a)^{2,21}

Method 1^{2,21}

To a solution of RuCl₂(PPh₃)₃ (0.30 g, 0.31 mmol) in CH₂Cl₂ (50 mL) was added P-N (0.096 g, 0.31 mmol). The dark brown solution turned dark green immediately and was stirred for 2h. After the solvent was removed *in vacuo*, 5 mL CH₂Cl₂ was added to redissolve the dark green residue. Hexanes (30 mL) was added to the solution to precipitate a dark green solid. The product was reprecipitated in CH₂Cl₂/hexanes twice more to remove excess PPh₃ and OPPh₃. Yield: 127 mg, 55 %. Anal. Calcd. C₃₈H₃₅NCl₂P₂Ru: C, 61.71; H, 4.77; N, 1.89. Found: C, 61.51; H, 4.84; N, 1.85. ³¹P{¹H} NMR (C₆D₆): δ 83.69 (d, P-N), 48.87 (d, PPh₃); ²J_{PP} = 36.54 Hz. ¹H NMR (C₆D₆): δ 7.0-7.9 (29H, m, Ph), 3.07 (6H, s, N(CH₃)₂). The NMR data correspond to those reported.^{2,21} UV-Vis (CH₂Cl₂): 454 (1100), 678 (480).

Method 2

A sample of *trans*-RuCl₂(P-N)(PPh₃)(OH₂) (**33a**) (Section 2.10.1) was placed *in vacuo* and heated to 80°C for 16 h. With the removal of H₂O, the pink solid turned green (yield: 100 %).

2.6.2 Dibromo{[*o*-(*N,N*-dimethylamino)phenyl](diphenylphosphine)} (triphenylphosphine)ruthenium(II), RuBr₂(P-N)(PPh₃) (**6b**)

A solution of P-N (135.9 mg, 0.44 mmol) in acetone (10 mL) was added to a suspension of RuCl₂(PPh₃)₃ (420.8 mg, 0.44 mmol) in acetone (10 mL), and the mixture was stirred at 50°C for 30 min. Excess NaBr (1.14 g, 11.09 mmol) was added to the resulting dark green solution. The mixture, containing a suspension of NaBr and NaCl, was stirred at r.t. for 24 h. The salts were filtered off through Celite and the volume of the filtrate was removed *in vacuo*. CH₂Cl₂ (10 mL) was then added to redissolve the dark green residue and this solution was filtered through Celite once more. The volume of the filtrate was reduced to ~5 mL before hexanes was added to precipitate a green-brown solid. This was filtered off and washed with hexanes (2 x 10 mL). Yield: 185 mg, 51 %. Anal. Calcd. C₃₈H₃₅NBr₂P₂Ru: C, 55.09; H, 4.26; N, 1.69. Found: C, 54.57; H, 4.23; N, 1.64. ³¹P{¹H} NMR (C₆D₆): δ 85.47 (d, P-N), 50.08 (d, PPh₃); ²J_{PP} = 36.30 Hz. ¹H NMR (C₆D₆): δ 6.7-7.8 (29H, m, Ph), 3.17 (6H, s, N(CH₃)₂). UV-Vis (CH₂Cl₂): 472 (1170), 706 (615).

2.6.3 Diiodo{[*o*-(*N,N*-dimethylamino)phenyl](diphenylphosphine)} (triphenylphosphine)ruthenium(II), RuI₂(P-N)(PPh₃) (**6c**)

The title complex was prepared following the same procedure used the Br analogue (Section 2.6.2) but using excess NaI (1.64 g, 10.97 mmol). A dark red solid was isolated from the acetone solution. Yield: 348 mg, 86 %. Anal. Calcd. C₃₈H₃₅NI₂P₂Ru: C, 49.47;

H, 3.82; N, 1.52. Found: C, 49.21; H, 3.78; N, 1.58. $^{31}\text{P}\{^1\text{H}\}$ NMR (CDCl_3): δ 89.18 (d, *P*-N), δ 53.62 (d, *PPh*₃); $^2J_{\text{PP}} = 35.56$ Hz. ^1H NMR (CDCl_3): δ 6.9-7.8 (29H, m, Ph), 3.48 (6H, s, $\text{N}(\text{CH}_3)_2$). UV-Vis (CH_2Cl_2): 510 (900), 774 (510).

2.6.4 Dichloro{[*o*-(*N,N*-dimethylamino)phenyl](diphenylphosphine)} (tri-*p*-tolylphosphine)ruthenium(II), $\text{RuCl}_2(\text{P-N})(\text{P}(p\text{-tolyl})_3)$ (**7a**)^{2,21}

The title complex was prepared in the same manner as described for the PPh_3 analogue (Section 2.6.1), but using $\text{RuCl}_2(\text{P}(p\text{-tolyl})_3)_3$ (335 mg, 0.31 mmol, **method 1**) or $\text{RuCl}_2(\text{P}(p\text{-tolyl})_3)_3(\text{OH}_2)$ (**method 2**). The product is a dark green solid which in the solid state is much more sensitive to O_2 than that of its PPh_3 analogue. Yield: **method 1**, 130 mg, 55 %; **method 2**, 100 %. Anal. Calcd. $\text{C}_{41}\text{H}_{41}\text{NCl}_2\text{P}_2\text{Ru}$: C, 63.00; H, 5.29; N, 1.79. Found: C, 63.03; H, 5.26; N, 1.86. $^{31}\text{P}\{^1\text{H}\}$ NMR (C_6D_6): δ 81.46 (d, *P*-N), 47.64 (d, *PPh*₃); $^2J_{\text{PP}} = 37.15$ Hz. ^1H NMR (C_6D_6): δ 6.6-8.0 (26H, m, Ph), 3.11 (6H, s, $\text{N}(\text{CH}_3)_2$), 2.00 (9H, s, *p*-(C_6H_4) CH_3). The NMR data are consistent with those reported.^{2,21} UV-Vis (CH_2Cl_2): 452 (1155), 672 (555).

2.6.5 Dibromo{[*o*-(*N,N*-dimethylamino)phenyl](diphenylphosphine)} (tri-*p*-tolylphosphine)ruthenium(II), $\text{RuBr}_2(\text{P-N})(\text{P}(p\text{-tolyl})_3)$ (**7b**)

The title complex was prepared in the same manner as the PPh_3 analogue (Section 2.6.2) but using $\text{RuCl}_2(\text{P}(p\text{-tolyl})_3)_3$ (476.0 mg, 0.44 mmol). A light orange solid was isolated. Yield: 202 mg, 53 %. Anal. Calcd. $\text{C}_{41}\text{H}_{41}\text{NBr}_2\text{P}_2\text{Ru}$: C, 56.56; H, 4.75; N, 1.61. Found: C, 57.09; H, 4.86; N, 1.75. $^{31}\text{P}\{^1\text{H}\}$ NMR (CDCl_3): δ 84.56 (d, *P*-N), 47.48 (d, *PPh*₃); $^2J_{\text{PP}} = 35.51$ Hz. ^1H NMR (CDCl_3): δ 6.6-8.0 (26H, m, Ph), 3.12 (6H, s, $\text{N}(\text{CH}_3)_2$), 2.30 (9H, s, *p*-(C_6H_4) CH_3). UV-Vis: 474 (1150), 700 (560).

**2.6.6 Diiodo{[*o*-(*N,N*-dimethylamino)phenyl](diphenylphosphine)}
(tri-*p*-tolylphosphine)ruthenium(II), RuI₂(P-N)(P(*p*-tolyl)₃) (7c)**

The title complex was prepared in the same manner as the Br analogue (Section 2.6.5) but using excess NaI (25 equiv). The solid is dark red. Yield: 300 mg, 72 %. Anal. Calcd. C₄₁H₄₁Nl₂P₂Ru: C, 51.05; H, 4.28; N, 1.45. Found: C, 51.05; H, 4.25; N, 1.48. ³¹P{¹H} NMR (CDCl₃): δ 89.27 (d, *P*-N), 51.27 (d, PPh₃); ²J_{PP} = 35.82 Hz. ¹H NMR (CDCl₃): δ 6.7-7.8 (26H, m, Ph), 3.46 (6H, s, N(CH₃)₂), 2.30 (9H, s, *p*-(C₆H₄)CH₃). UV-Vis: 512 (780), 780 (435).

2.6.7 Dichlorobis{[*o*-(*N,N*-dimethylamino)phenyl](diphenylphosphine)}ruthenium(II), RuCl₂(P-N)₂ (8)⁹

The title complex was prepared using the method described by Shen et al. for the synthesis of RuCl₂[κ²(*P,N*)-Ph₂PCH₂CH₂NMe₂]₂.²² Zn powder (66 mg, 1.00 mmol) was added to a THF (15 mL) solution containing P-N (360 mg, 1.18 mmol) and RuCl₃·3H₂O (100 mg, 0.38 mmol). The dark brown suspension was refluxed for 4 h. After the removal of the heat source, the mixture was stirred for 24 h during which time a deep red solution formed. Insoluble materials were filtered off through Celite and the volume of the filtrate was reduced to 5 mL before hexanes was added to precipitate a dark red solid. The product was filtered off and washed with hexanes (2 × 10 mL). Yield: 160 mg, 54 %. Anal. Calcd. C₄₀H₄₀N₂Cl₂P₂Ru·½(CH₂Cl₂): C, 58.95; H, 5.01, N, 3.39. Found: C, 59.19; H, 5.04; N, 3.29. ³¹P{¹H} NMR (CDCl₃): δ 58.9 (s, *P*-N). ¹H NMR (CDCl₃): δ 6.9-7.8 (28H, m, Ph), 5.32 (1H, s, CH₂Cl₂) 3.25 (12H, s, N(CH₃)₂). The NMR data agree with the literature data.⁹

2.6.8 Dichloro[(1-(*N,N*-dimethylamino)-8-(diphenylphosphino)naphthalene)(triphenyl phosphine)ruthenium(II), RuCl₂(PAN)(PPh₃) (9)

A solution of PAN (51 mg, 0.143 mmol) in CH₂Cl₂ (5 mL) was transferred to a stirring solution of RuCl₂(PPh₃)₃ (137 mg, 0.143 mmol) in CH₂Cl₂ (5 mL) via a cannula. A dark green solution was formed within 10 min. The solution was stirred for 4 h and its volume was then reduced to 2 mL. Hexanes (15 mL) was added slowly to precipitate a green solid that was filtered off and washed with hexanes (3 x 15 mL). Yield: 55 mg, 50 %. Anal. Calcd. C₄₂H₃₇NCl₂P₂Ru: C, 63.88; H, 4.72; N, 1.77. Found: C, 64.19; H, 4.84; N, 1.59. ³¹P{¹H} NMR (CDCl₃): δ 97.10 (d, *P*-N), 41.39 (d, PPh₃); ²J_{PP} = 32.05 Hz. ¹H NMR (CDCl₃): δ 6.6-8.3 (31H, m, Ph), 3.68 (3H, s, N(CH₃)), 2.96 (3H, s, N(CH₃)). UV-Vis: 450 (1210), 622 (490).

2.6.9 Dichloro[(1-(*N,N*-dimethylamino)-8-(diphenylphosphino)naphthalene)(tri-*p*-tolyl phosphine)ruthenium(II), RuCl₂(PAN)(P(*p*-tolyl)₃) (10)²

The title complex, a dark green solid, was prepared in the same manner as described for 9 (Section 2.6.8) but using RuCl₂(P(*p*-tolyl)₃)₃ (155 mg, 0.143 mmol). Yield: 58 mg, 45 %. Anal. Calcd. C₄₅H₄₃NCl₂P₂Ru: C, 64.98; H, 5.21; N, 1.68. Found: C, 64.98; H, 5.25; N, 1.66. ³¹P{¹H} NMR (C₆D₆): δ 97.71 (d, *P*-N), 39.57 (d, PPh₃); ²J_{PP} = 33.39 Hz. ¹H NMR (C₆D₆): δ 6.4-8.0 (28H, m, Ph), 3.50 (3H, s, N(CH₃)), 2.90 (3H, s, N(CH₃)), 2.00 (9H, s, *p*-(C₆H₄)CH₃). The NMR data agree with those reported.² UV-Vis: 450 (1280), 622 (520).

2.6.10 Dichloro{(*R*)-*N,N*-dimethyl-1-[*o*-(diphenylphosphino)phenyl]ethylamine} (triphenylphosphine)ruthenium(II), RuCl₂(AMPHOS)(PPh₃) (11)²

The title complex was prepared *in situ* by dissolving RuCl₂(PPh₃)₃ (12 mg, 0.013 mmol) and excess AMPHOS (5.0 mg, 0.015 mmol) in C₆D₆ (0.8 mL). The ³¹P{¹H}

NMR spectrum of the dark green solution indicates 100 % formation of **11** with 2 equiv. of PPh_3 liberated. $^{31}\text{P}\{^1\text{H}\}$ NMR (C_6D_6): δ 84.56 (d, $P\text{-N}$), 40.32 (d, PPh_3); $^2J_{\text{PP}} = 37.03$ Hz. ^1H NMR (C_6D_6): δ 6.6-8.2 (29H, m, Ph), 6.17 (1H, m, CH_3CH), 2.86 (3H, s, $\text{N}(\text{CH}_3)$), 2.33 (3H, s, $\text{N}(\text{CH}_3)$), 1.01 (3H, d, CH_3CH). The NMR data agree with those reported.² UV-Vis (*in situ*): 460 (1050), 636 (570). Repeated attempts to isolate an analytically pure product were unsuccessful. A solution of AMPHOS (35 mg, 0.105 mmol; or 70 mg, 0.210 mmol) in acetone (5 mL) was added to a solution of $\text{RuCl}_2(\text{PPh}_3)_3$ (100 mg, 0.104 mmol) in acetone (15 mL), and the mixture was stirred for 16 h. The volume of the resulting dark green solution was reduced to 5 mL and hexanes was added to precipitate a dark green/brown solid. This was filtered off and washed with hexanes (2 x 5 mL). Yield: 45 mg, 56 %. Anal. Calcd. $\text{C}_{40}\text{H}_{39}\text{NP}_2\text{Cl}_2\text{Ru}$: C, 62.58; H, 5.12; N, 1.82. Found: C, 59.99; H, 4.70; N, 1.36. $^{31}\text{P}\{^1\text{H}\}$ NMR spectrum (in CDCl_3) indicate the presence of **11**, $\text{RuCl}_2(\text{PPh}_3)_3$ (br, δ 42.5), OPPh_3 (s, δ 30.5) and PPh_3 (s, δ -4.0).

2.6.11 Attempts to Prepare Dichlorobis{[(*S*)-2-(dimethylamino)propyl] (diphenylphosphine)}ruthenium(II), $\text{RuCl}_2(\text{ALAPHOS})_2$ (**12**)

2.6.11.1 Reaction of ALAPHOS with $\text{RuCl}_2(\text{PPh}_3)_3$

A solution of (*S*)-Alaphos (30 mg, 0.110 mmol) in CH_2Cl_2 (2 mL) was added to a solution of $\text{RuCl}_2(\text{PPh}_3)_3$ (50 mg, 0.052 mmol) in CH_2Cl_2 (5 mL). The pink solution which formed immediately was stirred for 16 h. Then the volume of the solvent was reduced to 2 mL, and hexanes (10 mL) was slowly added to precipitate a pink solid (15 mg), that was filtered off and washed with hexanes (2 x 10 mL). NMR spectroscopic analysis indicates the presence of at least two Ru complexes. Reprecipitation of this solid using CH_2Cl_2 /hexanes gave a similar, impure solid. The ^1H NMR spectrum is complex and peaks could not be

assigned. $^{31}\text{P}\{^1\text{H}\}$ NMR (CDCl_3): δ 55.60 (s) is assigned to *trans*- $\text{RuCl}_2(\text{ALAPHOS})_2$ (cf. δ 57.4 (s) is due to *trans*- $\text{RuCl}_2(\text{Ph}_2\text{PCH}_2\text{CH}_2\text{NMe}_2)_2$),²² 49.7 and 43.1 (broad peaks) due to a minor product.

2.6.11.2 Reaction of ALAPHOS with *cis*- $\text{RuCl}_2(\text{DMSO})_2$

A solution of (*S*)-Alaphos (30 mg, 0.110 mmol) in CH_2Cl_2 (2 mL) was added to a solution of *cis*- $\text{RuCl}_2(\text{DMSO})_2$ (26 mg, 0.053 mmol) in CH_2Cl_2 (5 mL). The initial yellow suspension, after being stirred for 2 h, slowly turned to a pink, homogeneous solution. After 24 h the solution volume was reduced to 2 mL. Et_2O (15 mL) was added to precipitate a pale pink solid that was isolated by filtration and washed with Et_2O (2 \times 10 mL). NMR spectroscopic analysis gave similar results to those given in Section 2.6.11.1, indicating a mixture of products.

2.6.12 Dichloro{bis[*o*-(*N,N*-dimethylamino)phenyl](phenylphosphine)}(triphenylphosphine)ruthenium(II), $\text{RuCl}_2(\text{BPN})(\text{PPh}_3)$ (13)

A solution of BPN (34.8 mg, 0.100 mmol) in CH_2Cl_2 (3 mL) was added to a solution of $\text{RuCl}_2(\text{PPh}_3)_3$ (80.5 mg, 0.084 mmol) in CH_2Cl_2 (5 mL). A dark orange solution formed after the mixture was stirred for 24 h. The volume of CH_2Cl_2 was then reduced to ~3 mL and hexanes (10 mL) was added to precipitate a dark orange solid. The filtered product was reprecipitated using CH_2Cl_2 /hexanes (2 times), washed with hexanes (2 \times 10 mL) and dried *in vacuo* at 80°C. Yield: 25 mg, 38 %. Anal. Calcd. $\text{C}_{43}\text{H}_{46}\text{N}_2\text{Cl}_2\text{P}_2\text{Ru}$: C, 61.38; H, 5.15; N, 3.58. Found: C, 60.95; H, 4.87; N, 3.39. $^{31}\text{P}\{^1\text{H}\}$ NMR (CDCl_3): δ 56.00 (d, BPN), 33.67 (d, PPh_3); $^2J_{\text{PP}} = 32.05$ Hz. ^1H NMR (CDCl_3): δ 6.6-7.8 (28H, m, Ph), 3.63 (3H, s, $\text{N}(\text{CH}_3)$), 3.15 (3H, s, $\text{N}(\text{CH}_3)$), 2.60 (3H, s, $\text{N}(\text{CH}_3)$), 2.20 (3H, s, $\text{N}(\text{CH}_3)$).

**2.6.13 Dichloro{bis[*o*-(*N,N*-dimethylamino)phenyl](phenylphosphine)}
(tri-*p*-tolylphosphine)ruthenium(II), RuCl₂(BPN)(P(*p*-tolyl)₃) (14)**

The title complex was prepared using the same method as described for the PPh₃ analogue **13** (Section 2.6.12), but using RuCl₂(P(*p*-tolyl)₃)₃ (33.4 mg, 0.031 mmol) and BPN (12.3 mg, 0.035 mmol). Yield: 11 mg, 43 %. Anal. Calcd. C₄₃H₄₆N₂Cl₂P₂Ru: C, 62.62; H, 5.62; N, 3.40. Found: C, 62.37; H, 5.64; N, 3.15. ³¹P{¹H} NMR (CDCl₃): δ 56.05 (d, BPN), 31.26 (d, PPh₃); ²J_{PP} = 31.44 Hz. ¹H NMR (CDCl₃): δ 6.6-7.8 (25H, m, Ph), 3.64 (3H, s, N(CH₃)), 3.1 (3H, s, N(CH₃)), 2.57 (3H, s, N(CH₃)), 2.20 (3H, s, N(CH₃)), 2.20 (9H, s, *p*-(C₆H₄)CH₃).

2.7 Syntheses of Ruthenium(III) Aminophosphine Complexes

**2.7.1 Trichloro{[*o*-(*N,N*-dimethylamino)phenyl](diphenylphosphine)}
(triphenylphosphine)ruthenium(III), RuCl₃(P-N)(PPh₃) (15a)²**

A solution of P-N (67.0 mg, 0.22 mmol) in acetone (10 mL) was added to a stirring suspension of RuCl₃(PPh₃)₂(DMA)·(DMA) (200.0 mg, 0.22 mmol) in acetone (10 mL). The homogeneous, orange solution which formed immediately was stirred for 3 h during which time a red solid precipitated. This was collected and washed with acetone (2 x 5 mL). Yield: 140 mg, 82 %. Anal. Calcd. C₃₈H₃₅NCl₃P₂Ru: C, 58.89; H, 4.55; N, 1.81. Found: C, 58.69; H, 4.59; N, 1.81. UV-Vis (CH₂Cl₂): 336, shoulder, (1760), 398 (1875), 508 (1830). χ_g = 2.32 x 10⁻⁶ cgs, μ_{eff} = 2.0 BM. The X-ray structure of **15a** was previously determined; the UV-Vis and magnetic data were not obtained in the original reference.²

2.7.2 Trichloro{[*o*-(*N,N*-dimethylamino)phenyl](diphenylphosphine)}(tri-*p*-tolylphosphine)ruthenium(III), RuCl₃(P-N)(P(*p*-tolyl)₃) (15b)²

The title complex was prepared in the same manner as described for the PPh₃ analogue (Section 2.7.2), but using RuCl₂(P(*p*-tolyl)₃)₂(DMA)·(DMA) (220 mg, 0.22 mmol). A bright red solid was isolated. Yield: 150 mg, 84 %. Anal. Calcd. C₄₁H₄₁NCl₃P₂Ru: C, 60.26; H, 5.06; N, 1.71. Found: C, 60.30; H, 5.11; N, 1.75. UV-Vis (CH₂Cl₂): 334, shoulder, (1750), 396 (1840), 504 (1800). $\chi_g = 2.15 \times 10^{-6}$ cgs, $\mu_{\text{eff}} = 1.9$ BM. The UV-Vis and magnetic data were not determined in the original reference.²

2.7.3 *Mer*-trichloro{bis[*o*-(*N,N*-dimethylamino)phenyl](phenylphosphine)}ruthenium(III), *Mer*-RuCl₃(BPN) (16)

A solution of BPN (38.0 mg, 0.11 mmol) in CH₂Cl₂ (10 mL) was added to a solution of RuCl₃(PPh₃)₂(DMA)·(DMA) (100.0 mg, 0.11 mmol) in CH₂Cl₂ (10 mL). The reaction mixture was stirred for 2.5 h during which time an orange solution formed. The volume of CH₂Cl₂ was reduced to 3 mL and hexanes (10 mL) was added to precipitate a dark orange solid that was collected and washed with hexanes (2 × 10 mL). Yield: 55 mg, 90 %. Anal. Calcd. C₂₂H₂₅N₂Cl₃PRu: C, 47.54; H, 4.53; N, 5.04. Found: C, 50.71; H, 4.22; N, 3.47. Satisfactory elemental analysis of **16** could not be obtained even after repeated (3 times) reprecipitations with CH₂Cl₂/hexanes. $\chi_g = 1.23 \times 10^{-6}$ cgs, $\mu_{\text{eff}} = 1.5$ BM. Orange, platelet crystals of RuCl₃(BPN)·(CDCl₃) were obtained by slow evaporation from a CDCl₃ solution over 2 days in an NMR tube. The ORTEP plot, selected bond lengths and angles of this complex are shown and discussed in Section 3.6, while the full experimental parameters and details are given in Appendix II.

2.7.4 Di- μ -chloro- μ -oxo-bis{chloro[o-(*N,N*-dimethylamino)phenyl](diphenylphosphine)ruthenium(III)}, (μ -O)(μ -Cl)₂[RuCl(P-N)]₂ (17)

The title complex was prepared by stirring a suspension of RuCl₂(P-N)(PPh₃) (200 mg, 0.270 mmol) in acetone (10 mL) under 1 atm of O₂. The green precursor dissolved over 1 h to form a dark green solution. The solution was stirred for 16 h during which time a dark green solid precipitated; this was filtered off, washed with hexanes (2 x 10 mL) and dried *in vacuo* at 80°C. The green solid was insoluble in acetone, CHCl₃ or C₆H₆ and was only slightly soluble in DMSO and CH₂Cl₂. Yield: 85 mg, 32 %. Anal. Calcd. C₄₀H₄₀N₂OCl₄P₂Ru₂: C, 49.50; H, 4.15; N, 2.89. Found: C, 49.50; H, 4.16; N, 2.75. ³¹P{¹H} NMR (C₆D₆): δ 38.74 (d, *P*_A-N), 35.33 (d, *P*_B-N); ⁴J_{PP} = 10.44 Hz. ¹H NMR (C₆D₆): δ 6.6-8.4 (28H, m, Ph), 3.31 (3H, s, N(CH₃)), 2.89 (3H, s, N(CH₃)), 2.11 (3H, s, N(CH₃)), 2.02 (3H, s, N(CH₃)). UV-Vis (DMSO): 348 (15300), 652 (11200). χ_g = 0 cgs, μ_{eff} = 0 BM. Green, platelet crystals of 17 were obtained from the slow evaporation of an acetone solution of RuCl₂(P-N)(PPh₃) exposed to air over 24 h. The ORTEP plot, selected bond lengths and angles are presented and discussed in Section 3.2.1, while the full experimental parameters and details are given in Appendix III.

2.8 Syntheses of Ruthenium(II) Complexes Containing Coordinated H₂S or Thiols: *Cis*-dichloro{[*o*-*N,N*-dimethylamino)phenyl](diphenylphosphine)}(triaryl phosphine)(ligand)ruthenium(II), *Cis*-RuX₂(P-N)(PR₃)(L)

The five-coordinate RuCl₂(P-N)(PR₃) (R = Ph, *p*-tolyl) was isolated in low yield (~55 %) because many subsequent precipitations were required to remove PR₃ and OPR₃ impurities. Unless otherwise specified, RuCl₂(P-N)(PR₃) was prepared *in situ* from RuCl₂(PR₃)₃ for the syntheses of six-coordinate complexes of the type RuCl₂(P-N)(PR₃)(L), where L = a small molecule. The PR₃ (2 moles per Ru) produced is simply a spectator in the

reactions. With use of the *in situ* precursor, high yields of the six-coordinate products were obtained.

2.8.1 *Cis*-RuCl₂(P-N)(PPh₃)(SH₂)·(acetone) (18a)

The title complex was prepared using modifications of the method previously reported for synthesis of the non-solvated complex.^{2,23} A solution of P-N (64 mg, 0.21 mmol) in acetone (3 mL) was added to a suspension of RuCl₂(PPh₃)₃ (200 mg, 0.21 mmol) in acetone (8 mL), and the mixture was stirred at 50°C for 30 min to form the dark green solution of RuCl₂(P-N)(PPh₃). The reaction flask was placed under reduced pressure and 1 atm of H₂S was introduced. A yellow solution formed immediately, and this was stirred for at least 8 h during which time a yellow precipitate formed. This was filtered off, but no washings were performed as this causes the loss of H₂S. The product was dried under vacuum for 1 h at r.t. and subsequent analyses or reactions were carried out immediately. Yield: 140 mg, 80 %. Anal. Calcd. C₃₈H₃₇NCl₂SP₂Ru·(acetone): C, 59.20; H, 5.21; N, 1.68. Found: C, 58.94; H, 5.32; N, 1.69. ³¹P{¹H} NMR (C₆D₆): δ 51.28 (d, P-N), 44.53 (d, PPh₃); ²J_{PP} = 29.50 Hz. ¹H NMR (C₆D₆): δ 6.4-8.4 (29H, m, Ph), 3.67 (3H, s, N(CH₃)), 2.97 (3H, s, N(CH₃)), 1.54 (6H, s, acetone), 1.02 (2H, br s, Ru(SH₂)). UV-Vis (CH₂Cl₂, under 1 atm H₂S): 426 (830). IR: ν_{S-H} 2476, 2506 (weak), ν_{CO} 1707 (acetone, strong). Yellow-brown, prism crystals of **18a** were obtained from a saturated acetone solution of the complex left standing for 5 days. The ORTEP plot, selected bond lengths and angles are shown and discussed in Section 4.2.1, while the full experimental parameters and details are given in Appendix IV.

2.8.2 *Cis*-RuBr₂(P-N)(PPh₃)(SH₂)·(acetone) (18b)

The title complex was prepared by stirring a solution of RuBr₂(P-N)(PPh₃) (100 mg, 0.121 mmol) in acetone (3 mL) under 1 atm of H₂S. The yellow solution was stirred for 24 h during which time a yellow precipitate formed. The product was obtained by filtration and drying under vacuum for 1 h. Yield: 80 mg, 72 %. Anal. Calcd. C₃₈H₃₇NBr₂SP₂Ru·(acetone): C, 53.49; H, 4.71; N, 1.52. Found: C, 53.28; H, 4.78; N, 1.46. ³¹P{¹H} NMR (C₆D₆): δ 53.54 (d, P-N), 45.59 (d, PPh₃); ²J_{PP} = 28.41 Hz. ¹H NMR (C₆D₆): δ 6.4-8.4 (29H, m, Ph), 3.93 (3H, s, N(CH₃)), 2.87 (3H, s, N(CH₃)), 1.54 (6H, s, acetone), 1.14 (2H, br s, Ru(SH₂)). UV-Vis (CH₂Cl₂, under 1 atm H₂S): 446 (995). IR: ν_{S-H} 2506, 2476 (weak), ν_{CO} 1707 (acetone, strong). Orange prism crystals of RuBr₂(P-N)(PPh₃)(SH₂)·(C₆D₆) were obtained from a saturated C₆D₆ solution of the complex left standing in a sealed NMR tube for 2 days. The ORTEP plot, selected bond lengths and angles are shown and discussed in Section 4.2.2, while the full experimental parameters and details are given in Appendix V.

2.8.3 *In situ* Preparation of *Cis*-RuI₂(P-N)(PPh₃)(SH₂) (18c)

A dark brown solution formed after the addition of 1 atm H₂S to a CDCl₃ solution of RuI₂(P-N)(PPh₃). The ¹H NMR and ³¹P{¹H} NMR spectra were collected within 10 min of adding H₂S. ³¹P{¹H} NMR (10 min, CDCl₃): δ 56.0 (d, P-N), 49.5 (d, PPh₃); ²J_{PP} = 25.8 Hz. ¹H NMR (10 min, CDCl₃): δ 6.5-8.2 (29H, m, Ph), 4.16 (3H, s, N(CH₃)), 2.20 (3H, s, N(CH₃)), 0.95 (Ru(SH₂), signal is hidden under free H₂S signal). The *in situ* species decomposes to a paramagnetic, presumably Ru(III) species after ~1 h as indicated by noisy NMR spectra containing broad lines.

2.8.4 *Cis*-RuCl₂(P-N)(P(*p*-tolyl)₃)(SH₂)·(acetone) (19a)

The title complex was prepared in the same manner as described for the PPh₃ analogue (Section 2.8.1) but using RuCl₂(P(*p*-tolyl)₃)₃ (200 mg, 0.18 mmol) and P-N (56.3 mg, 0.18 mmol). Yield: 117 mg, 73 %. Anal. Calcd. C₄₁H₄₃NCl₂SP₂Ru·(acetone): C, 60.48; H, 5.65; N, 1.60. Found: C, 60.23; H, 5.77; N, 1.65. ³¹P{¹H} NMR (CDCl₃): δ 51.91 (d, P-N), 42.58 (d, PPh₃); ²J_{PP} = 30.41 Hz. ¹H NMR (CDCl₃): δ 6.6-8.0 (26H, m, Ph), 3.41 (3H, s, N(CH₃)), 3.05 (3H, s, N(CH₃)), 2.15 (9H, s, *p*-(C₆H₄)CH₃), 2.04 (6H, s, acetone), 0.95 (2H, br s, Ru(SH₂)). UV-Vis (CH₂Cl₂): 435 (900). IR: ν_{S-H} 2495, 2449 (weak), ν_{CO} 1707 (acetone, strong).

2.8.5 *Cis*-RuBr₂(P-N)(P(*p*-tolyl)₃)(SH₂)·(acetone) (19b)

The title complex was prepared in the same manner as described for the PPh₃ analogue (Section 2.8.2) but using RuBr₂(P-N)(P(*p*-tolyl)₃) (100 mg, 0.11 mmol). Yield: 86 mg, 78 %. Anal. Calcd. C₄₁H₄₃NBr₂SP₂Ru·(acetone): C, 54.89; H, 5.13; N, 1.45. Found: C, 55.11; H, 5.23; N, 1.49. ³¹P{¹H} NMR (CDCl₃): δ 53.41 (d, P-N), 44.58 (d, PPh₃); ²J_{PP} = 29.20 Hz. ¹H NMR (CDCl₃): δ 6.6-8.0 (26H, m, Ph), 3.68 (3H, s, N(CH₃)), 2.99 (3H, s, N(CH₃)), 2.18 (9H, s, *p*-(C₆H₄)CH₃), 2.04 (6H, s, acetone), 0.95 (2H, br s, Ru(SH₂)). UV-Vis (CH₂Cl₂): 452 (935). IR: ν_{S-H} 2495, 2449 (weak), ν_{CO} 1707 (acetone, strong).

2.8.6 *In situ* Preparation of *Cis*-RuI₂(P-N)(P(*p*-tolyl)₃)(SH₂) (19c)

An orange solution formed after adding 1 atm H₂S to a CDCl₃ solution of RuI₂(P-N)(P(*p*-tolyl)₃). Similar to 18c, 19c decomposed after ~1 h. ³¹P{¹H} NMR (10 min, CDCl₃): δ 56.2 (d, P-N), 47.5 (d, PPh₃); ²J_{PP} = 25.8 Hz. ¹H NMR (10 min, CDCl₃): δ 6.5-

8.2 (29H, m, Ph), 4.15 (3H, s, N(CH₃)), 2.91 (3H, s, N(CH₃)), δ 2.22 (9H, s, *p*-(C₆H₄)CH₃), 0.90 (Ru(SH₂), signal is hidden under free H₂S signal).

2.8.7 *Cis*-RuCl₂(P-N)(PPh₃)(MeSH)·(acetone) (20)

Methanethiol was obtained from Aldrich as a liquid and stored at 0°C. A solution of MeSH (0.5 mL, 9.0 mmol) in acetone (2 mL) was cooled to 0°C and purged with N₂ for 1 min. This solution was cannula transferred to a stirring acetone solution (5 mL) containing RuCl₂(PPh₃)₃ (100.0 mg, 0.104 mmol) and P-N (32.0 mg, 0.104 mmol). A homogeneous yellow solution formed immediately and, after being stirred for 16 h, precipitated a yellow solid. The product was filtered off and dried *in vacuo* (30 min). Yield: 72 mg, 80 %. Anal. Calcd. C₃₉H₃₉NCl₂SP₂Ru·(acetone): C, 59.64; H, 5.36; N, 1.66. Found: C, 59.46; H, 5.53; N, 1.65. ³¹P{¹H} NMR (CD₂Cl₂): δ 50.37 (d, P-N), 41.33 (d, PPh₃); ²J_{PP} = 30.17 Hz. ¹H NMR (CD₂Cl₂): δ 6.4-7.9 (29H, m, Ph), 3.35 (3H, s, N(CH₃)), 3.10 (3H, s, N(CH₃)), 2.10 (6H, s, acetone), 0.70 (4H, m, overlap of Ru(S(CH₃)H) and Ru(S(CH₃)H)). UV-Vis (CH₂Cl₂, excess MeSH): 424 (835). IR: $\nu_{\text{S-H}}$ 2533 (weak), ν_{CO} 1707 (acetone, strong). Yellow-brown, prism crystals of **20** were obtained from a saturated acetone solution of the complex left standing for 24 h. The ORTEP plot, selected bond lengths and angles are presented in Section 4.3.1, while the full experimental parameters and details are given in Appendix VI.

2.8.8 *Cis*-RuCl₂(P-N)(PPh₃)(EtSH)·(EtSH)·(acetone) (21)

The title complex was prepared in the same manner as described for **20** (Section 2.8.7) but using excess EtSH (1 mL, 19.2 mmol) at 20°C. The product was a yellow solid. Yield: 65 mg, 78 %. Anal. Calcd. C₄₀H₄₁NCl₂SP₂Ru·(EtSH)·(acetone): C, 58.62; H, 5.79; N, 1.52. Found: C, 59.08; H, 5.75; N, 1.46. ³¹P{¹H} NMR (CD₂Cl₂): δ 52.43 (d, P-N), 43.97 (d,

PPh_3); $^2J_{PP} = 30.23$ Hz. 1H NMR (CD_2Cl_2): δ 6.4-8.0 (29H, m, Ph), 3.41 (3H, s, $N(CH_3)$), 3.24 (3H, s, $N(CH_3)$), 2.10 (6H, s, acetone), 2.00 (1H, m, $Ru(S(CH_2CH_2CH_3)H)$), 0.78 (1H, m, $Ru(S(CH_2CH_2CH_3)H)$), 0.63 (1H, ddd, $Ru(S(CH_2CH_2CH_3)H)$), 0.45 (3H, dd, $Ru(S(CH_2CH_2CH_3)H)$), free EtSH signals at δ 2.55 (2H, dq, $HSCH_2CH_3$), 1.46 (1H, t, $HSCH_2CH_3$), 1.31 (3H, t, $HSCH_2CH_3$). UV-Vis (CH_2Cl_2 , excess EtSH): 424 (830). IR: ν_{S-H} 2516 (weak), ν_{CO} 1707 (acetone, strong). Yellow, prism crystals of $RuCl_2(P-N)(PPh_3)(EtSH) \cdot 1.5(C_6D_6)$ were obtained from a saturated C_6D_6 of the complex solution left standing in a sealed NMR tube for 24 h. The ORTEP plot, selected bond lengths and angles are presented in Section 4.3.2, while the full experimental parameters and details are given in Appendix VII.

2.8.9 *In situ* Preparation of *Cis*- $RuCl_2(P-N)(PPh_3)(RSH)$, $R = n\text{-Pr}$, $i\text{-Pr}$, $n\text{-Pn}$, $n\text{-Hx}$, and Bz (Pr = propyl, Pn = pentyl, Hx = hexyl, Bz = benzyl)

With use of the $RuCl_2(PPh_3)_3$ precursor, the title complexes could not be isolated for purposes of elemental analysis because they decompose during the work-up processes due to the loss of RSH ; the species are also very O_2 -sensitive and could only be observed in the $^{31}P\{^1H\}$ NMR spectra in O_2 -free conditions with the presence of excess RSH . 1H NMR spectra were not assigned due to the excess RSH . The $CDCl_3$ or C_6D_6 solutions of these species are yellow.

2.8.9.1 *Cis*- $RuCl_2(P-N)(PPh_3)(n\text{-PrSH})$ (22)

$^{31}P\{^1H\}$ NMR ($CDCl_3$): δ 51.22 (d, $P-N$), 42.46 (d, PPh_3); $^2J_{PP} = 30.05$ Hz.

2.8.9.2 *Cis*- $RuCl_2(P-N)(PPh_3)(i\text{-PrSH})$ (23)

$^{31}P\{^1H\}$ NMR (C_6D_6): (three sets of doublets, intensities of signals in parenthesis)

δ 56.76 (d, $P-N$), 46.84 (d, PPh_3); $^2J_{PP} = 36.54$ Hz (strong);

δ 49.58 (d, *P*-N), 41.68 (d, *PPh*₃); $^2J_{PP}$ = 30.23 Hz (medium);

δ 51.31 (d, *P*-N), 42.74 (d, *PPh*₃); $^2J_{PP}$ = 29.93 Hz (weak).

2.8.9.3 *Cis*-RuCl₂(*P*-N)(*PPh*₃)(*n*-PnSH) (24)

$^{31}\text{P}\{^1\text{H}\}$ NMR (C₆D₆): (two sets of doublets, intensities of signals in parenthesis)

δ 51.30 (d, *P*-N), 42.84 (d, *PPh*₃); $^2J_{PP}$ = 29.63 Hz (strong);

δ 49.57 (d, *P*-N), 46.35 (d, *PPh*₃); $^2J_{PP}$ = 36.06 Hz (weak).

2.8.9.4 *Cis*-RuCl₂(*P*-N)(*PPh*₃)(*n*-HxSH) (25)

$^{31}\text{P}\{^1\text{H}\}$ NMR (CDCl₃): δ 51.15 (d, *P*-N), 42.57 (d, *PPh*₃); $^2J_{PP}$ = 30.23 Hz.

2.8.9.5 *Cis*-RuCl₂(*P*-N)(*PPh*₃)(BzSH) (26)

$^{31}\text{P}\{^1\text{H}\}$ NMR (CDCl₃): δ 50.16 (d, *P*-N), 42.03 (d, *PPh*₃); $^2J_{PP}$ = 30.41 Hz.

2.9 *In Situ* Preparation of Ru(L)X(*P*-N)(*PPh*₃) (L = SH, OH, H) and Ru(L)₂(*P*-N)(*PPh*₃) (X = Cl, Br; L = SH, OH, H)

The title species given in this Section were not isolated and were only observed *in situ* by NMR spectroscopy. The species are O₂-sensitive and were prepared in NMR tubes equipped with poly(tetrafluoroethylene) J. Young valves. Discussion concerning their characterization is given in Section 3.3.

2.9.1 Ru(SH)Cl(*P*-N)(*PPh*₃) (27a)

The title species was observed in two different reactions:

Reaction 1: To an NMR tube containing RuCl₂(*P*-N)(*PPh*₃) (10 mg, 0.014 mmol) and NaSH·xH₂O (5 mg), d₆-acetone (0.75 mL) was vacuum transferred with the aid of liquid N₂. The resulting orange solution was stored at -78°C (dry ice/acetone), and NMR spectra were

measured at -78°C . $^{31}\text{P}\{^1\text{H}\}$ NMR (d_6 -acetone): δ 55.26 (d, $P\text{-N}$), 46.33 (d, PPh_3); $^2J_{\text{PP}} = 30.88$ Hz. ^1H NMR (d_6 -acetone): δ 6.2-8.1 (29H, m, Ph), δ 3.27 (3H, s, $\text{N}(\text{CH}_3)$), δ 3.18 (3H, s, $\text{N}(\text{CH}_3)$), δ -2.08 (1H, s, Ru-SH). This species was only observed at temperatures below -30°C .

Reaction 2: To an NMR tube containing $\text{RuCl}_2(\text{P-N})(\text{PPh}_3)$ (10 mg, 0.014 mmol) and proton sponge (3 mg, 0.014 mmol), CD_2Cl_2 (0.75 mL) was vacuum transferred. The sample was then placed under 1 atm H_2S to form an orange solution. Similar to reaction 1 above, **27a** is observed at -78°C . $^{31}\text{P}\{^1\text{H}\}$ NMR (CD_2Cl_2 , -78°C): δ 54.52 (d, $P\text{-N}$), 46.06 (d, PPh_3); $^2J_{\text{PP}} = 30.96$ Hz.

2.9.2 $\text{Ru}(\text{SH})\text{Br}(\text{P-N})(\text{PPh}_3)$ (**27b**)

Species **27b** was prepared *in situ* by the procedure described for reaction 1 in Section 2.9.1, but using $\text{RuBr}_2(\text{P-N})(\text{PPh}_3)$ (10 mg, 0.012 mmol) as precursor. $^{31}\text{P}\{^1\text{H}\}$ NMR (d_6 -acetone, -78°C): δ 56.62 (d, $P\text{-N}$), 46.16 (d, PPh_3); $^2J_{\text{PP}} = 30.48$ Hz. ^1H NMR (d_6 -acetone, -78°C): δ 6.2-8.1 (29H, m, Ph), δ 3.56 (3H, s, $\text{N}(\text{CH}_3)$), δ 3.17 (3H, s, $\text{N}(\text{CH}_3)$), δ -1.63 (1H, s, Ru-SH).

2.9.3 $\text{Ru}(\text{OH})\text{Cl}(\text{P-N})(\text{PPh}_3)$ (**28a**)

The species was observed 2 h after dissolving $\text{RuCl}_2(\text{P-N})(\text{PPh}_3)$ (10 mg, 0.014 mmol) and NaOH (~ 5 equiv) in d_6 -acetone and heating the solution at 60°C . The NMR spectra of this orange solution were measured at r.t. $^{31}\text{P}\{^1\text{H}\}$ NMR (d_6 -acetone): δ 64.09 (d, $P\text{-N}$), 50.76 (d, PPh_3); $^2J_{\text{PP}} = 42.98$ Hz. ^1H NMR (d_6 -acetone): δ 6.6-8.9 (29H, m, Ph), 3.04 (3H, s, $\text{N}(\text{CH}_3)$), 2.69 (3H, s, $\text{N}(\text{CH}_3)$).

2.9.4 Ru(OH)Br(P-N)(PPh₃) (28b)

Species **28b** was prepared in the same manner as described for **28a**, Section 2.9.3, except using RuBr₂(P-N)(PPh₃) (10 mg, 0.12 mmol) as precursor. ³¹P{¹H} NMR (d₆-acetone): δ 65.95 (d, P-N), 51.23 (d, PPh₃); ²J_{PP} = 41.22 Hz. ¹H NMR (d₆-acetone): δ 6.4-8.2 (29H, m, Ph), 3.22 (3H, s, N(CH₃)), 2.72 (3H, s, N(CH₃)).

2.9.5 Ru(H)Cl(P-N)(PPh₃) (29)^{2,21}

To a solution of RuCl₂(P-N)(PPh₃) (10 mg, 0.014 mmol) and proton sponge (3 mg, 0.014 mmol) in CD₂Cl₂, was added 1 atm H₂. A yellow-orange solution formed instantaneously. This species is stable at r.t. (20°C). ³¹P{¹H} NMR (CD₂Cl₂): δ 82.74 (d, P-N), 67.39 (d, PPh₃); ²J_{PP} = 33.20 Hz. ¹H NMR (CD₂Cl₂): δ 6.5-8.1 (29H, m, Ph), δ 3.49 (3H, s, N(CH₃)), δ 2.99 (3H, s, N(CH₃)), δ -27.2 (1H, br s, Ru-H). The NMR data correspond to those reported.^{2,21}

2.9.6 Ru(SH)₂(P-N)(PPh₃) (30)

The dithiolate species **30** was formed at r.t. when RuX₂(P-N)(PPh₃) (X = Cl, Br) was reacted with excess NaSH·xH₂O or H₂S in the presence of proton sponge (3 equiv) as described for reactions 1 and 2 of Section 2.9.1, respectively. These yellow-brown solutions were unstable at r.t. and decomposed to dark brown solutions after ~10 min. Species **30** was only observed within 10 min of sample preparation at r.t. ³¹P{¹H} NMR (d₆-acetone): δ 84.06 (d, P-N), 59.53 (d, PPh₃); ²J_{PP} = 33.75 Hz. ¹H NMR (d₆-acetone): δ 6.4-8.1 (29H, m, Ph), 3.20 (6H, s, N(CH₃)₂), δ 0.80 (2H, s, Ru-(SH)₂). The decomposed species were not identified.

2.9.7 Ru(OH)₂(P-N)(PPh₃) (31)

The dihydroxo species **31** was observed when solutions of RuCl₂(P-N)(PPh₃) (cf. Section 2.9.3) or RuBr₂(P-N)(PPh₃) (cf. Section 2.9.4) and NaOH (~5 equiv) were allowed to react for 5 h or more at 60°C. During this time, the solutions changed from orange to orange-brown colour. ³¹P{¹H} NMR (d₆-acetone): δ 79.11 (d, P-N), 73.44 (d, PPh₃); ²J_{PP} = 67.38 Hz. ¹H NMR (d₆-acetone): δ 6.4-8.2 (29H, m, Ph), 2.60 (3H, s, N(CH₃)), 2.28 (3H, s, N(CH₃)).

2.9.8 Ru(H)₂(P-N)(PPh₃) (32)

The title species **32** was observed 15 min after reacting RuCl₂(P-N)(PPh₃) or RuBr₂(P-N)(PPh₃) with NaH (~5 equiv.) in d₆-acetone at 60°C. The NMR spectra of this orange solution were measured at r.t. ³¹P{¹H} NMR (d₆-acetone): δ 61.64 (d, P-N), 50.44 (d, PPh₃); ²J_{PP} = 24.71 Hz. ¹H NMR (d₆-acetone): δ 6.5-8.1 (29H, m, Ph), δ 2.51 (6H, s, N(CH₃)₂), δ -21.16 (2H, d of d, Ru-(H)₂, ²J_{HP} = 32.70, 29.10 Hz).

2.10 Syntheses of Ruthenium(II) Complexes Containing Coordinated H₂O, MeOH, or EtOH

2.10.1 *Trans*-RuCl₂(P-N)(PPh₃)(OH₂) (33a)²

The title complex was prepared by adding a mixture of H₂O (2 mL) and acetone (2 mL) to a stirred solution of RuCl₂(PPh₃)₃ (200 mg, 0.209 mmol) and P-N (64 mg, 0.209 mmol) in acetone (5 mL). The orange-pink solution which formed instantaneously was stirred for 3 h during which time a pink solid precipitated. The product was filtered off, washed with acetone (2 x 5 mL), and dried *in vacuo* for 24 h. Yield: 115 mg, 73 %. Microanalysis indicates the presence of 1 mol acetone solvate. Anal. Calcd.

$\text{C}_{38}\text{H}_{37}\text{NOCl}_2\text{P}_2\text{Ru}\cdot(\text{acetone})$: C, 60.37; H, 5.31; N, 1.72. Found: C, 60.37; H, 5.46; N, 1.67. $^{31}\text{P}\{^1\text{H}\}$ NMR (C_6D_6): δ 73.52 (d, P-N), 49.30 (d, PPh_3); $^2J_{\text{PP}} = 38.00$ Hz. ^1H NMR (C_6D_6): δ 7.0-8.4 (29H, m, Ph), 3.05 (6H, s, $\text{N}(\text{CH}_3)_2$), 2.15 (2H, br s, Ru-OH_2), 1.55 (6H, s, acetone). UV-Vis (CH_2Cl_2 , with 0.13 M H_2O): 498 (shoulder, 270). IR: $\nu_{\text{O-H}}$ 3556, 3295, 1605 (weak), ν_{CO} 1707 (acetone, strong). Two different types of crystals of **33a** were isolated from evaporation of a saturated C_6H_6 solution of the complex over 24 h. These crystals differ in appearance as well as having different unit cells. The yellow-brown crystals (**33a** $\cdot 1.5\text{C}_6\text{H}_6$) have primitive triclinic cell dimensions, while the pink needle crystals (**33a** $\cdot 2\text{C}_6\text{H}_6$) have primitive monoclinic cell dimensions. The ORTEP plots, selected bond lengths and angles of **33a** $\cdot 1.5\text{C}_6\text{H}_6$ are presented in Section 5.3, while the full experimental parameters and details of the two structures are given in Appendix VIII.

2.10.2 *Trans*- $\text{RuCl}_2(\text{P-N})(\text{P}(p\text{-tolyl})_3)(\text{OH}_2)$ (**33b**)²

The title complex was prepared in the same manner as described for **33a** (Section 2.10.1) but using $\text{RuCl}_2(\text{P}(p\text{-tolyl})_3)_3$ (200 mg, 0.185 mmol). Yield: 122 mg, 77 %. Microanalysis indicates the presence of 1 mol acetone solvate. Anal. Calcd. $\text{C}_{41}\text{H}_{43}\text{NCl}_2\text{OP}_2\text{Ru}\cdot(\text{acetone})$: C, 61.61; H, 5.76; N, 1.63. Found: C, 61.97; H, 5.65; N, 1.77. $^{31}\text{P}\{^1\text{H}\}$ NMR (C_6D_6): δ 63.63 (d, P-N), 45.91 (d, PPh_3); $^2J_{\text{PP}} = 38.12$ Hz. ^1H NMR (C_6D_6): δ 6.8-8.2 (26H, m, Ph), 3.10 (6H, s, $\text{N}(\text{CH}_3)_2$), 2.00 (3H, s, $p\text{-(C}_6\text{H}_4)\text{CH}_3$), 2.15 (2H, br s, Ru-OH_2), 1.55 (6H, s, acetone). UV-Vis (CH_2Cl_2): 496 (shoulder, 280).

2.10.3 *Trans*- $\text{RuCl}_2(\text{P-N})(\text{PPh}_3)(\text{MeOH})$ (**34**)

A mixture of MeOH (2 mL) and acetone (1 mL) was purged with Ar and cannula transferred to a stirred solution of $\text{RuCl}_2(\text{PPh}_3)_3$ (100 mg, 0.104 mmol) and P-N (32 mg,

0.104 mmol) in acetone (5 mL) which had been heated to 50°C. The orange solution which formed instantaneously was stirred at 20°C for 24 h. The volume of the solution was then reduced to ~1 mL and hexanes (10 mL) was added to precipitate a pink solid. This was filtered off and washed with MeOH (2 x 5 mL). Yield: 45 mg, 56 %. Anal. Calcd. $C_{39}H_{39}NOCl_2P_2Ru$: C, 60.70; H, 5.09; N, 1.82. Found: C, 61.01; H, 5.12; N, 1.76. $^{31}P\{^1H\}$ NMR (CD_2Cl_2): δ 77.46 (d, P-N), 47.16 (d, PPh_3); $^2J_{PP} = 36.66$ Hz. 1H NMR (CD_2Cl_2): δ 6.9-7.9 (29H, m, Ph), 3.33 (3H, d, $Ru(O(CH_3)H)$), 3.16 (6H, s, $N(CH_3)_2$), 1.33 (1H, q, $Ru-(O(CH_3)H)$).

2.10.4 *Trans-RuCl₂(P-N)(PPh₃)(EtOH)* (35)

Attempts to prepare 35 following the method described for $RuCl_2(P-N)(PPh_3)(MeOH)$ (Section 2.10.3) were unsuccessful. Several different solvent combinations including acetone/hexanes, acetone/ Et_2O and acetone/EtOH failed to precipitate any solid. In a further attempt to prepare 35, P-N (40.5 mg, 0.133 mmol) in EtOH (2 mL) was added to a brown suspension of $RuCl_2(PPh_3)_3$ (122.8 mg, 0.128 mmol) in neat EtOH (8 mL). The suspension was stirred for 1 week during which time a pink/orange solution containing a small amount of light brown precipitate formed. This brown solid (~20 mg) was collected and washed with EtOH (5 mL), but could not be further characterized as it was found to be insoluble in common solvents (acetone, $CDCl_3$, C_6D_6 , CD_2Cl_2). Also, the EtOH was removed under vacuum from the combined pink filtrates collected earlier and hexanes (10 mL) was added to the oily residue. The solvent was once again removed and EtOH (2 mL) was added to dissolve the residue. This solution was then stirred for 15 min when a pink precipitate formed. Hexanes (10 mL) was added to precipitate more solid, which was collected by filtration and washed with hexanes (5 mL). Yield: 33 mg, 33 %. Anal. Calcd.

$C_{40}H_{41}NOCl_2P_2Ru$: C, 61.15; H, 5.26; N, 1.78. Found: C, 62.22; H, 5.06; N, 1.89. $^{31}P\{^1H\}$ NMR (CD_2Cl_2): δ 79.79 (d, *P*-N), 46.90 (d, *PPh*₃); $^2J_{PP} = 36.24$ Hz. 1H NMR (CD_2Cl_2): δ 6.9-7.9 (29H, m, Ph), 3.61 (2H, d of q, $Ru(O(CH_2CH_3)H)$), 3.18 (6H, s, $N(CH_3)_2$), 1.40 (1H, t, $Ru(O(CH_2CH_3)H)$), 1.16 (3H, t, $Ru(O(CH_2CH_3)H)$).

2.11 Syntheses of Ruthenium(II) Complexes with Other Coordinated Gases

2.11.1 *Cis*- $RuCl_2(P-N)(PPh_3)(\eta^2-H_2)$ (**36**)^{2,21}

The five-coordinate complex, $RuCl_2(P-N)(PPh_3)$ (**6a**), was prepared *in situ* by stirring a solution of $RuCl_2(PPh_3)_3$ (85.1 mg, 0.09 mmol) and *P*-N (29.2 mg, 0.09 mmol) in acetone (10 mL) at 50°C for 30 min. H_2 gas was then passed through the solution for 2 h during which time the dark green colour changed to orange. The mixture was stirred for another 48 h when a pale yellow precipitate formed. This was quickly collected and stored under Ar. This yellow solid was susceptible to loss of H_2 with re-formation of the green $RuCl_2(P-N)(PPh_3)$. Yield: 35 mg, 52 %. Anal. Calcd. $C_{38}H_{37}NCl_2P_2Ru$: C, 61.54; H, 5.03; N, 1.89. Found: C, 61.47; H, 4.89; N, 1.75. $^{31}P\{^1H\}$ NMR (C_6D_6): δ 49.30 (d, *P*-N), 45.49 (d, *PPh*₃); $^2J_{PP} = 26.83$ Hz. 1H NMR (C_6D_6): δ 6.4-8.4 (29H, m, Ph), 3.68 (3H, s, $N(CH_3)$), 3.17 (3H, s, $N(CH_3)$), -10.90 (2H, br s, $Ru(\eta^2-H_2)$). Yellow, block crystals of **36** were obtained from a saturated acetone solution of the complex left standing for 2 days. The ORTEP plot, selected bond lengths and angles are presented in Section 6.1, while the full experimental parameters and details are given in Appendix IX.

2.11.2 Reactions with NH₃

2.11.2.1 Reaction of RuCl₂(P-N)(PPh₃) with NH₃

2.11.2.1.1 Isolation of [RuCl(P-N)(PPh₃)(NH₃)₂···Cl] (37a)

To a solution of RuCl₂(P-N)(PPh₃) (50 mg, 0.068 mmol) in 5 mL C₆H₆, 1 atm of NH₃ was introduced, and the dark green solution was stirred for 1 h. Hexanes (5 mL) was added to precipitate a blue-green solid. Yield: 35 mg, 68 %. Anal. Calcd. C₃₈H₄₁N₃Cl₂P₂Ru: C, 58.99; H, 5.34; N, 5.43. Found: C, 59.14; H, 5.40; N, 5.21. Due to the loss of NH₃ when this solid was dissolved in solution (CDCl₃) (see Section 6.2), three products were observed in the NMR spectra. [37a, [RuCl(P-N)(PPh₃)(NH₃)₂···Cl], ³¹P{¹H} NMR: δ 57.20 (d, P-N), 53.24 (d, PPh₃); ²J_{PP} = 32.05 Hz. ¹H NMR: δ 6.2-8.2 (m, Ph), 3.19 (3H, s, N(CH₃)), 3.00 (3H, s, N(CH₃)), 3.72 (3H, s, Ru-NH₃), 1.70 (3H, s, Ru-NH₃). 38a, *trans*-RuCl₂(P-N)(PPh₃)(NH₃), NMR spectra are identical to those recorded in Section 2.11.2.1.2. 39a, *cis*-RuCl₂(P-N)(PPh₃)(NH₃), ³¹P{¹H} NMR: δ 59.27 (d, P-N), 51.45 (d, PPh₃); ²J_{PP} = 32.29 Hz. ¹H NMR: δ 6.2-8.2 (m, Ph), 3.61 (3H, s, N(CH₃)), 2.94 (3H, s, N(CH₃)), 0.39 (3H, s, Ru-NH₃). Of note, the integrations of the phenyl protons in the ¹H NMR spectrum were not assigned because of overlapping signals of 37a, 38a and 39a in this region. Conductivity in acetone under 1 atm NH₃: Λ_M = ~ 0.

2.11.2.1.2 Synthesis of *trans*-RuCl₂(P-N)(PPh₃)(NH₃) (38a) from a solid state reaction

Solid RuCl₂(P-N)(PPh₃) (20 mg, 0.027 mmol) was stirred under 1 atm of NH₃ for 3 h. The colour of the starting material changed from green to beige-brown. Yield: 20 mg, 100 %. Anal. Calcd. C₃₈H₃₈N₂Cl₂P₂Ru: C, 60.32; H, 5.06; N, 3.70. Found: C, 60.26; H, 5.23; N, 3.71. ³¹P{¹H} NMR (CDCl₃): δ 53.86 (d, P-N), 50.79 (d, PPh₃); ²J_{PP} = 36.48 Hz. ¹H NMR (CDCl₃): δ 6.2-8.2 (m, Ph), 2.72 (6H, s, N(CH₃)₂), 1.64 (3H, s, Ru-NH₃).

2.11.2.1.3 *In situ* reaction in the presence of excess NH_3

To a solution of $\text{RuCl}_2(\text{P-N})(\text{PPh}_3)$ (10 mg, 0.014 mmol) dissolved in 0.7 mL CDCl_3 in a NMR tube was added 1 atm NH_3 when a dark green solution formed. NMR analyses indicate the presence of one product, $[\text{RuCl}(\text{P-N})(\text{PPh}_3)(\text{NH}_3)_2\cdots\text{Cl}]$; see NMR data in Section 2.11.2.1.1 for **37a**.

2.11.2.2 Reaction of $\text{RuBr}_2(\text{P-N})(\text{PPh}_3)$ with NH_3

Reactions analogous to those for $\text{RuCl}_2(\text{P-N})(\text{PPh}_3)$ (Section 2.11.2.1) were performed on $\text{RuBr}_2(\text{P-N})(\text{PPh}_3)$.

2.11.2.2.1 NMR data for $[\text{RuBr}(\text{P-N})(\text{PPh}_3)(\text{NH}_3)_2\cdots\text{Br}]$ (**37b**) and *cis*- $\text{RuBr}_2(\text{P-N})(\text{PPh}_3)(\text{NH}_3)$ (**39b**)

All samples were prepared in CDCl_3 : $[\text{RuBr}(\text{P-N})(\text{PPh}_3)(\text{NH}_3)_2\cdots\text{Br}]$ (**37b**), $^{31}\text{P}\{^1\text{H}\}$ NMR: δ 57.40 (d, *P-N*), 56.08 (d, *PPh*₃); $^2J_{\text{PP}} = 31.81$ Hz. ^1H NMR: δ 6.2-8.2 (m, Ph), 3.34 (3H, s, *N*(*CH*₃)), 2.78 (3H, s, *N*(*CH*₃)), 3.64 (3H, s, *Ru-NH*₃), 1.75 (3H, s, *Ru-NH*₃). *Cis*- $\text{RuBr}_2(\text{P-N})(\text{PPh}_3)(\text{NH}_3)$ (**39b**), $^{31}\text{P}\{^1\text{H}\}$ NMR: δ 62.86 (d, *P-N*), 51.85 (d, *PPh*₃); $^2J_{\text{PP}} = 31.75$ Hz. ^1H NMR: δ 6.2-8.2 (m, Ph), 3.97 (3H, s, *N*(*CH*₃)), 2.74 (3H, s, *N*(*CH*₃)), 0.48 (3H, s, *Ru-NH*₃).

2.11.2.2.2 Synthesis of *trans*- $\text{RuBr}_2(\text{P-N})(\text{PPh}_3)(\text{NH}_3)$ (**38b**)

The title complex was synthesized with a 100 % yield in a solid state reaction similar to that described for **38a** (Section 2.11.2.1.2). Anal. Calcd. $\text{C}_{38}\text{H}_{38}\text{N}_2\text{Br}_2\text{P}_2\text{Ru}$: C, 53.98; H, 4.53; N, 3.31. Found: C, 53.61; H, 4.46; N, 3.05. $^{31}\text{P}\{^1\text{H}\}$ NMR (CDCl_3): δ 55.25 (d, *P-N*), 50.65 (d, *PPh*₃); $^2J_{\text{PP}} = 36.66$ Hz. ^1H NMR (CDCl_3): δ 6.2-8.2 (m, Ph), 3.01 (6H, s, *N*(*CH*₃)₂), 1.58 (3H, s, *Ru-NH*₃).

2.11.2.3 *In situ* preparation of $[\text{Ru}(\text{P-N})(\text{PPh}_3)(\text{NH}_3)_3\cdots\text{Cl}][\text{PF}_6]$ (40a)

The title species was observed *in situ* when $[\text{RuCl}(\text{P-N})(\text{PPh}_3)(\text{NH}_3)_2\cdots\text{Cl}]$ and 1 equiv of NH_4PF_6 were stirred under 1 atm of NH_3 in d_6 -acetone. $^{31}\text{P}\{^1\text{H}\}$ NMR (d_6 -acetone): δ 54.94 (d, P-N), 51.47 (d, PPh_3); $^2J_{\text{PP}} = 32.05$ Hz. ^1H NMR (d_6 -acetone): δ 6.2-8.2 (29H, m, Ph), 3.18 (3H, s, $\text{N}(\text{CH}_3)$), 3.13 (3H, s, $\text{N}(\text{CH}_3)$), 3.05 (3H, s, Ru-NH_3), 1.06 (3H, s, Ru-NH_3). Removal of excess NH_3 resulted in formation of species **41** (Section 2.11.2.5). Conductivity of **40a** after removal of NH_4Cl in acetone under 1 atm NH_3 : $\Lambda_{\text{M}} = 139 \text{ ohm}^{-1} \text{ cm}^2 \text{ mol}^{-1}$.

2.11.2.4 *In situ* preparation of $[\text{Ru}(\text{P-N})(\text{PPh}_3)(\text{NH}_3)_3][\text{PF}_6]_2$ (40b)

The title species was prepared *in situ* by dissolving $\text{RuCl}_2(\text{P-N})(\text{PPh}_3)$ (10 mg, 0.014 mmol) and 2 equiv NH_4PF_6 (2.2 mg, 0.014 mmol) in d_6 -acetone (~ 1 mL) in the presence of 1 atm NH_3 when the original solution changed from green to yellow. The reaction was allowed to proceed at r.t. for 16 h. The NH_4Cl was removed by filtration through Celite and the filtrate was subjected to NMR. $^{31}\text{P}\{^1\text{H}\}$ NMR (d_6 -acetone): δ 55.26 (d, P-N), 51.67 (d, PPh_3); $^2J_{\text{PP}} = 32.05$ Hz. ^1H NMR (d_6 -acetone): δ 6.2-8.2 (29H, m, Ph), 3.21 (3H, s, $\text{N}(\text{CH}_3)$), 3.14 (3H, s, $\text{N}(\text{CH}_3)$), 3.08 (3H, s, Ru-NH_3), 1.10 (3H, s, Ru-NH_3). Conductivity of **40b** after removal of NH_4Cl in acetone under 1 atm NH_3 : $\Lambda_{\text{M}} = 288 \text{ ohm}^{-1} \text{ cm}^2 \text{ mol}^{-1}$.

2.11.2.5 $[\text{RuCl}(\text{P-N})(\text{PPh}_3)(\text{NH}_3)_2][\text{PF}_6]$ (41)

To a solution of $[\text{RuCl}(\text{P-N})(\text{PPh}_3)(\text{NH}_3)_2\cdots\text{Cl}]$ (100 mg, 0.0013 mmol) in acetone (10 mL), a solution of NH_4PF_6 (22 mg, 0.0014 mmol) in acetone (5 mL) was added, and the pale yellow-green solution was stirred under 1 atm NH_3 for 16 h. A dark yellow solution with a suspension of NH_4Cl was formed. This mixture was filtered through Celite to remove the

insoluble salts. The dark yellow-brown residue which remained after removal of solvent from the filtrate was redissolved in 3 mL CH_2Cl_2 . Addition of Et_2O (10 mL) resulted in the formation of a yellow solid, which was collected and washed with Et_2O (2 x 5 mL). Yield: 45 mg, 39 %. Anal. Calcd. $\text{C}_{38}\text{H}_{41}\text{N}_3\text{ClF}_6\text{P}_3\text{Ru}$: C, 51.68; H, 4.68; N, 4.76. Found: C, 53.68; H, 6.41; N, 6.68. Several repeated preparations of **41** failed to give satisfactory elemental analysis data. $^{31}\text{P}\{^1\text{H}\}$ NMR (d_6 -acetone): δ 58.87 (d, *P*-N), 51.70 (d, *PPh*₃); $^2J_{\text{PP}} = 31.40$ Hz. ^1H NMR (d_6 -acetone): δ 6.2-8.2 (29H, m, Ph), 3.53 (3H, s, $\text{N}(\text{CH}_3)$), 3.02 (3H, s, $\text{N}(\text{CH}_3)$), 2.65 (3H, s, Ru-NH_3), 0.53 (3H, s, Ru-NH_3). Conductivity in acetone (with or without the presence of excess NH_3): $\Lambda_{\text{M}} = 146 \text{ ohm}^{-1} \text{ cm}^2 \text{ mol}^{-1}$.

2.11.2.6 $[\text{RuCl}(\text{P-N})(\text{PPh}_3)(\text{NH}_3)][\text{PF}_6]$ (**42**)

The title complex is a dark green solid and can be prepared by removal of NH_3 by drying a sample of $[\text{RuCl}(\text{P-N})(\text{PPh}_3)(\text{NH}_3)_2]\text{PF}_6$ (**41**) (10 mg) *in vacuo* at 80°C . The complex is O_2 -sensitive and decomposes in air to a brown solid. Yield: 10 mg, 100 %. Anal. Calcd. $\text{C}_{38}\text{H}_{38}\text{N}_2\text{ClF}_6\text{P}_3\text{Ru}$: C, 52.69; H, 4.42; N, 3.23. The inability to obtain pure **41** also led to unsatisfactory analysis for **42**. Found: C, 53.84; H, 4.92; N, 3.10. $^{31}\text{P}\{^1\text{H}\}$ NMR (d_6 -acetone): δ 48.64 (d, *P*-N), 47.85 (d, *PPh*₃); $^2J_{\text{PP}} = 36$ Hz (broad doublets). ^1H NMR signals were not assigned due to many overlapping peaks in the spectrum (δ 6.0-8.5 (m, Ph), 0.5-3.5 (br m)).

2.11.3 *Cis*- $\text{RuCl}_2(\text{P-N})(\text{PPh}_3)(\eta^1\text{-N}_2)$ (**43**)

The title complex was prepared *in situ* by the "condensation" of ~ 6 atm N_2 into an NMR tube (equipped with a poly(tetrafluoroethylene) valve) containing a solution of $\text{RuCl}_2(\text{P-N})(\text{PPh}_3)$ (10 mg) in CD_2Cl_2 (0.7 mL). ("Condensation" refers to the vacuum

transfer of 1 atm N_2 in a 18 mL vessel into a 3 mL NMR tube.) The solution was slowly warmed to r.t. when a colour change from dark green to light green-yellow was apparent. The $^{31}P\{^1H\}$ NMR spectrum indicate 100 % formation of the N_2 adduct. $^{31}P\{^1H\}$ NMR (CD_2Cl_2): δ 47.54 (d, $P-N$), 37.90 (d, PPh_3); $^2J_{PP} = 27.02$ Hz. 1H NMR (CD_2Cl_2): δ 6.6-7.9 (29H, m, Ph), 3.63 (3H, s, $N(CH_3)$), 3.04 (3H, s, $N(CH_3)$). The NMR data correspond with those previously reported, where a ν_{N_2} value of 2161 cm^{-1} was measured.²¹

2.11.4 *Cis*- $RuCl_2(P-N)(PPh_3)(N_2O)$ (**44**)

The N_2O adduct was prepared *in situ* using the same method as for the N_2 complex described in Section 2.11.3 but using ~6 atm N_2O . When the sample was warmed to r.t., a light green solution formed, but the $^{31}P\{^1H\}$ NMR spectrum was very noisy with broad peaks at δ 79.93 and δ 47.16. When this sample was cooled to -88°C , three species were observed: the starting five-coordinate complex **6a** (18 %); the N_2 adduct **43** (8 %); and the assumed N_2O adduct **43** (74 %). $^{31}P\{^1H\}$ NMR (-88°C , CD_2Cl_2) for **44**: δ 49.52 (d, $P-N$), 40.06 (d, PPh_3); $^2J_{PP} = 27.93$ Hz. 1H NMR (-88°C , CD_2Cl_2): δ 6.4-8.1 (m, Ph), 3.60 (3H, s, $N(CH_3)$), 2.85 (3H, s, $N(CH_3)$).

2.12 Synthesis and Reactions of Ruthenium(II) Carbene Complexes

The following carbene complexes were prepared employing the method described by Bianchini and co-workers for the corresponding $RuCl_2(PNP)(PPh_3)$ ($PNP = CH_3CH_2CH_2N(CH_2CH_2PPh_2)_2$) derivatives.²⁴

2.12.1 *Cis*-RuCl₂(P-N)(PPh₃)(=C=CHPh) (45)

A solution of PhC≡CH (0.60 mL, 5.46 mmol) in CH₂Cl₂ (3 mL) was added to a solution of RuCl₂(P-N)(PPh₃) (385.0 mg, 0.52 mmol) in CH₂Cl₂ (20 mL). The dark yellow solution which formed was then refluxed at 40°C for 2 h. The solution was cooled to r.t. and stirred for another 16 h at ambient conditions when a dark red solution formed. The volume of the solvent was reduced to 5 mL and hexanes (20 mL) was added to precipitate a dark orange solid that was collected and washed with hexanes (4 x 5 mL). Yield: 380 mg, 86 %. Anal. Calcd. C₄₆H₄₁NCl₂P₂Ru: C, 65.64; H, 4.91; N, 1.66. Found: C, 65.45; H, 4.92; N, 1.55. ³¹P{¹H} NMR (CDCl₃): δ 37.85 (d, *P*-N), 36.40 (d, *P*Ph₃); ²J_{PP} = 26.50 Hz. ¹H NMR (CDCl₃): δ 6.2-8.2 (34H, m, Ph), 3.60 (3H, s, N(CH₃)), 3.11 (3H, s, N(CH₃)), 2.43 (1H, d of d, CCHPh). Red-orange crystals of **45** grew over 2 days by slow evaporation of CDCl₃ from an NMR tube sample of the complex. The ORTEP plot, selected bond lengths and angles are shown in Section 6.4.1, while the full experimental parameters and details are given in Appendix X.

2.12.2 *Cis*-RuCl₂(P-N)(P(*p*-tolyl)₃)(=C=CHPh) (46)

Complex **46** was prepared in the same manner as described for the PPh₃ analogue (Section 2.12.1) but using RuCl₂(P-N)(P(*p*-tolyl)₃) (390 mg, 0.50 mmol). The product was a dark orange solid. Yield: 350 mg, 80 %. Anal. Calcd. C₄₉H₄₇NCl₂P₂Ru: C, 66.59; H, 5.36; N, 1.58. Found: C, 66.43; H, 5.29; N, 1.55. ³¹P{¹H} NMR (CDCl₃): δ 35.86 (d, *P*-N), 32.96 (d, *P*Ph₃); ²J_{PP} = 26.62 Hz. ¹H NMR (CDCl₃): δ 6.2-7.8 (31H, m, Ph), 3.54 (3H, s, N(CH₃)), 3.08 (3H, s, N(CH₃)), 2.40 (1H, d of d, CCHPh), 2.16 (9H, s, *p*-(C₆H₄)CH₃).

2.12.3 *Cis*-RuCl₂(P-N)(PPh₃)(=C=CHPhCH₃) (47)

The title complex was prepared in the same manner as described for **45** (Section 2.12.1) but using five equiv of 4-ethynyltoluene. The product is a dark yellow solid. Yield: 270 mg. 61 %. Anal. Calcd. C₄₇H₄₄NCl₂P₂Ru: C, 65.89; H, 5.18; N, 1.63. Found: C, 65.75; H, 5.02; N, 1.52. ³¹P{¹H} NMR (CDCl₃): δ 38.33 (d, *P*-N), 36.72 (d, *P*Ph₃); ²J_{PP} = 26.10 Hz. ¹H NMR (CDCl₃): δ 6.1-8.1 (33H, m, Ph), 3.59 (3H, s, N(CH₃)), 3.08 (3H, s, N(CH₃)), 2.43 (1H, dd, CCHPhCH₃), 2.16 (3H, s, CCHPhCH₃).

2.12.4 *Cis*-RuCl₂(P-N)(PPh₃)(SCHCH₂Ph) (48)

Complex **48** was prepared by bubbling H₂S through a solution of RuCl₂(P-N)(PPh₃)(=C=CHPh) (**45**) (100 mg, 0.12 mmol) in CD₂Cl₂ (15 mL) under reflux (45°C) for 5 h, when the original orange solution became brown. The solution was then concentrated to ~5 mL and hexanes (15 mL) was added to precipitate a brown solid (65 mg) which was collected and washed with hexanes (2 x 10 mL). Analytically pure **48** could not be isolated even after several reprecipitations from CH₂Cl₂/hexanes. NMR analysis, however, indicate that **48** is the major species in the brown solid. ³¹P{¹H} NMR (CDCl₃): δ 59.61 (d, *P*-N), 42.36 (d, *P*Ph₃); ²J_{PP} = 28.22 Hz. ¹H NMR (CDCl₃): δ 6.1-8.7 (29H, m, Ph), 3.04 (3H, s, N(CH₃)), 2.52 (3H, s, N(CH₃)), 3.18 (1H, t, S=CH, ³J_{HH} = 15 Hz), 1.30 (2H, d, CH₂, ³J_{HH} = 15 Hz).

2.12.5 Reaction of *Cis*-RuCl₂(P-N)(PPh₃)(=C=CHPh) (**45**) with H₂O

To a solution of **45** (100 mg, 0.12 mmol) in CH₂Cl₂ (15 mL), H₂O (1 mL) was added. This mixture was refluxed for 5 h during which time the original orange solution became brown. Hexanes (20 mL) was added to precipitate a brown solid which is composed of a

mixture of **49** and $\text{RuCl}_2(\text{P-N})(\text{PPh}_3)(\text{CO})$ (**50**) as indicated by $^{31}\text{P}\{^1\text{H}\}$ NMR data. The two species **49** and **50** were not separated for purposes of microanalysis. $^{31}\text{P}\{^1\text{H}\}$ NMR (CDCl_3): for **49**, δ 44.57 (br, P-N), 38.28 (br, PPh_3); for **50**, δ 50.55 (br, P-N), 18.74 (br, PPh_3). The $^{31}\text{P}\{^1\text{H}\}$ NMR data for **50** agree with those previously reported.² ^1H NMR spectra were not assigned because of overlapping signals due to both species (δ 6.0-8.5 (m, Ph), 1.2-3.5 (m)). IR: ν_{CO} 2046 (**49**), 1990 (**50**). **49** is thought to be $\text{RuCl}(\text{P-N})(\text{PPh}_3)(\text{CH}_2\text{Ph})(\text{CO})$ (see Section 6.4.2).

2.13 References

1. Perrin, D. D.; Armarego, W. L. F.; Perrin, D. R. *Purification of Laboratory Chemicals*; 2nd ed.; Pergamon: Oxford, 1980.
2. Mudalige, D. C. Ph.D. Thesis, The University of British Columbia, 1994.
3. Alder, R. W.; Bowman, P. S.; Steele, W. R. S.; Winterman, D. R. *J. Chem. Soc., Chem. Commun.* **1968**, 723.
4. Dixon, K. R. In *Multinuclear NMR*; Mason, J., Ed.; Plenum: New York, 1987; Chapter 13.
5. MacFarlane, K. W. Ph.D. Thesis, The University of British Columbia, 1995.
6. (a) Selwood, P. W. *Magnetochemistry*; 2nd ed.; Interscience Publishers, Inc.: New York, 1956, p. 78.
(b) Figgis, B. N.; Lewis, J. In *Modern Coordination Chemistry*; Lewis, J.; Wilkins, R. G. Eds.; Interscience Publishers, Inc.: London, 1960, p. 402.
(c) Carlin, R. L. *Magnetochemistry*; Springer-Verlag: New York, 1986, p. 3.
7. Fritz, H. P.; Gordan, I. R.; Schwarzhans, K. E.; Venanzi, L. M. *J. Chem. Soc.* **1965**, 5210.
8. Gilman, H.; Banner, I. *J. Am. Chem. Soc.* **1940**, 62, 344.
9. Rauchfuss, T. B.; Patino, F. T.; Roundhill, D. M. *Inorg. Chem.* **1975**, 14, 652.
10. Cairns, S. M.; McEwen, W. E. *Heteroatom Chem.* **1990**, 1, 9.
11. Meessen, P. H.; Rettig, S. J.; James, B. R. Unpublished data.
12. Payne, N. C.; Stephan, D. W. *Inorg. Chem.* **1982**, 21, 182.
13. Pine, S. H.; Sanchez, B. L. *J. Org. Chem.* **1971**, 36, 829.
14. (a) Horner, L.; Simons, G. *Phosphorus and Sulfur* **1983**, 15, 165.
(b) Dekker, G. P. C. M.; Buijs, A.; Elsevier, C. J.; Vrieze, K.; van Leeuwen, P. W. N. M.; Smeets, W. J. J.; Spek, A. L.; Wang, Y. F.; Stam, C. H. *Organometallics* **1992**, 11, 1937.

15. Hayashi, T.; Konishi, M.; Fukushima, M.; Kanehira, K.; Hioki, T.; Kumada, M. *J. Org. Chem.* **1983**, *48*, 2195.
16. Bowman, R. E.; Stroud, H. H. *J. Chem. Soc.* **1950**, 1342.
17. Hallman, P. S.; Stephenson, T. A.; Wilkinson, G. *Inorg. Syn.* **1970**, *12*, 237.
18. Armit, P. W.; Sime, W. J.; Stephenson, T. A.; Scott, L. *J. Organomet. Chem.* **1978**, *161*, 391.
19. (a) Evans, I.P.; Spencer, A.; Wilkinson, G. *J. Chem. Soc., Dalton Trans.* **1973**, 204.
(b) Mercer, A.; Trotter, J. *J. Chem. Soc., Dalton Trans.* **1975**, 2480.
20. (a) Stephenson, T. A.; Wilkinson, G. *J. Inorg. Nucl. Chem.* **1966**, *28*, 945.
(b) Dekleva, T. W.; Thorburn, I. S.; James, B. R. *Inorg. Chim. Acta* **1985**, *100*, 49.
(c) Fogg, D. E. Ph.D. Thesis, The University of British Columbia, 1994.
21. Mudalige, D. C.; Rettig, S. J.; James, B. R.; Cullen, W. R. *J. Chem. Soc., Chem. Commun.* **1993**, 830.
22. Shen, J.-Y.; Slugovc, C.; Wiede, P.; Mereiter, K.; Schmid, R.; Kirchner, K. *Inorg. Chim. Acta* **1998**, *268*, 69.
23. Mudalige, D. C.; Ma, E. S.; Rettig, S. J.; James, B. R.; Cullen, W. R. *Inorg. Chem.* **1997**, *36*, 5426.
24. Bianchini, C.; Innocenti, P.; Peruzzini, M.; Romerosa, A.; Zanobini, F. *Organometallics* **1996**, *15*, 272.

Chapter 3

Synthesis and Reactivity of Ruthenium Aminophosphine Precursors

3.1 Introduction

Ruthenium(II) aminophosphine (PN) complexes of the type $\text{RuCl}_2(\text{PN})(\text{PR}_3)$ ($\text{R} = \text{Ph}$, *p*-tolyl) have been prepared in this laboratory by phosphine exchange reactions of PN ligands with the well known precursor complexes $\text{RuCl}_2(\text{PR}_3)_3$.¹⁻³ A similar route involving phosphine exchange has been successful for the synthesis of Ru(II) tertiary (PR'_3), ditertiaryphosphine (P-P) and 2-pyridylmono- or diphosphine (Ppy) complexes of the types $\text{RuCl}_2(\text{PR}'_3)_3$,⁴ $\text{RuCl}_2(\text{P-P})(\text{PPh}_3)$,^{5,6} and $\text{RuCl}_2(\text{Ppy})(\text{PPh}_3)$,⁷ respectively. Synthetic methods via other precursors such as $\text{RuCl}_2(\text{DMSO})_4$,^{6,8} $[\text{RuCl}_2(\text{benzene})]_2$ ⁹ and $[\text{RuCl}_2(\text{COD})]_n$,¹⁰ that are useful in the preparation of Ru(P-P) complexes, give complex mixtures of products when PN ligands are used.² In this chapter, both successful and attempted syntheses of Ru(II) complexes containing PN ligands are described. The reactivities of these complexes are also briefly discussed.

3.2 Preparation of $\text{RuCl}_2(\text{P-N})(\text{PR}_3)$ ($\text{R} = \text{Ph}$ (6a), $\text{R} = p$ -tolyl (7a))

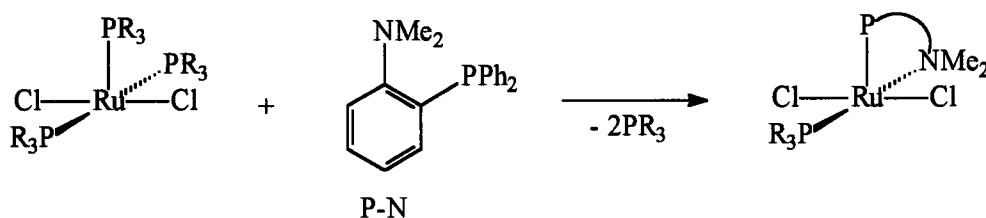


Figure 3.1 The preparation of $\text{RuCl}_2(\text{P-N})(\text{PR}_3)$ ($\text{R} = \text{Ph}$ (6a), $\text{R} = p$ -tolyl (7a)).

The title complexes were prepared by the exchange reaction of two monodentate phosphine ligands in $\text{RuCl}_2(\text{PR}_3)_3$ with one equivalent of the P-N ligand as indicated by

Figure 3.1.^{2,3} Only one P-N ligand is coordinated to the Ru centre regardless of the amounts of P-N added. The reactions of $\text{RuCl}_2(\text{PR}_3)_3$ and P-N in CH_2Cl_2 , C_6H_6 or acetone produce deep green solutions containing $\text{RuCl}_2(\text{P-N})(\text{PR}_3)$, and the liberated PR_3 species are identified by $^{31}\text{P}\{^1\text{H}\}$ NMR spectroscopy (δ -3.98 for PPh_3 and δ -4.5 for $\text{P}(p\text{-tolyl})_3$ in CDCl_3). To obtain products with high purity, as many as four repeated recrystallized steps using CH_2Cl_2 /hexanes were required. The yields of the dark green solids **6a** and **7a** were consequently low (55 %). Of note, however, use of the aquo complexes *trans*- $\text{RuCl}_2(\text{P-N})(\text{PR}_3)(\text{OH}_2)$ ($\text{R} = \text{Ph}$ (**33a**), *p*-tolyl (**33b**)) provided indirect routes to $\text{RuCl}_2(\text{P-N})(\text{PR}_3)$ of high purities and yields. Detailed discussion on the properties of **33a** and **33b** is presented in Chapter 5. The aquo complexes are readily obtained by reactions of $\text{RuCl}_2(\text{PR}_3)_3$ with P-N in solvent mixtures of H_2O /acetone (1:5 volume) with 73 to 85% yields. Heating **33a** and **33b** in the solid state *in vacuo* at 80°C leads to complete conversion to **6a** and **7a**, respectively.

X-ray quality crystals of **7a** were obtained by Mudalige, previously of this laboratory.^{2,3} The structure (Figure 3.2) reveals a distorted square pyramidal geometry with the Ru atom 0.42 Å above the plane defined by Cl(1), Cl(2), N(1), P(2). The Cl-atoms are trans to one another, the PPh_3 ligand is trans to the N arm of the P-N ligand, and the P-atom of the P-N ligand resides at the apical position. This structure is analogous to those of $\text{RuCl}_2(\text{isoPFA})(\text{PPh}_3)$ (isoPFA = 1-[α,α -dimethylethyl]-2-(diisopropylphosphino)ferrocene),¹ $\text{RuCl}_2(\text{PPh}_3)_3$,¹¹ $\text{RuBr}_2(\text{PPh}_3)_3$ ¹² and $\text{RuCl}_2(\text{dppb})(\text{PPh}_3)$ (dppb = $\text{Ph}_2\text{P}(\text{CH}_2)_4\text{PPh}_2$).¹² However, in contrast to these other structures, the vacant site trans to the apical P atom in **7a** is not occupied by an ortho H-atom of the PPh_3 ligand, and this property may contribute significantly to the highly reactive nature of **7a** (and presumably **6a**); **6a** and **7a** have similar

characteristics and reactivities (as described in succeeding chapters), and thus **6a** is presumed to have the same structure as that of **7a**.

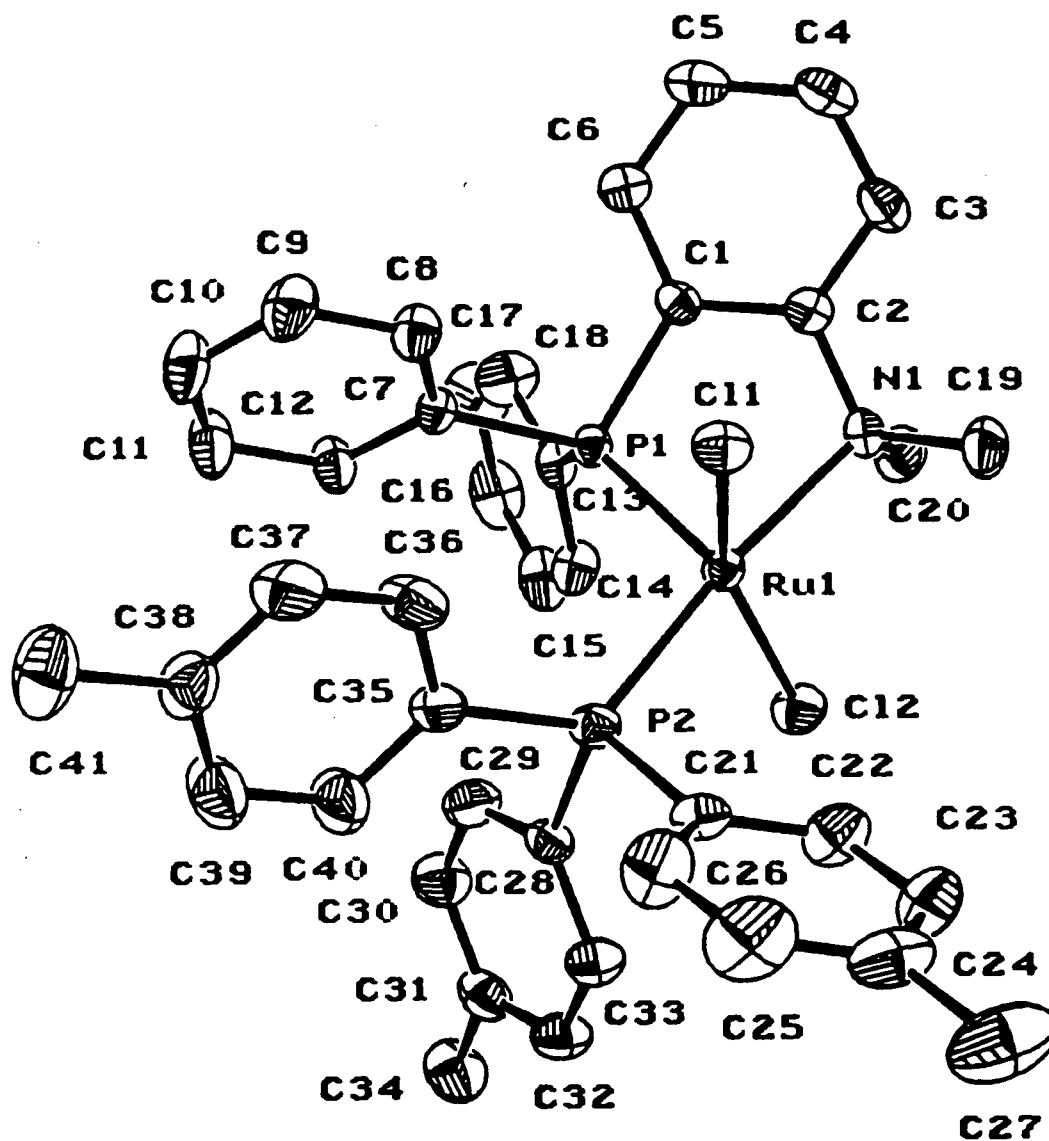


Figure 3.2 The ORTEP plot of $\text{RuCl}_2(\text{P-N})(\text{P}(p\text{-tolyl})_3)$ (**7a**).^{2,3} Thermal ellipsoids for atoms shown are drawn at 33 % probability.

NMR spectroscopic analyses show that, in solution, **6a** and **7a** remain monomeric with no phosphine dissociation. For the analogous $\text{RuCl}_2(\text{PR}_3)_3$ systems ($\text{R} = \text{Ph}$ and *p*-tolyl)¹³ and $\text{RuCl}_2(\text{P-P})(\text{PR}_3)$ ($\text{P-P} = \text{dppp}$, dppb , dppn , binap , chiraphos , and bdpp),^{5,6,12,14} the dinuclear complexes $(\mu\text{-Cl})_2[\text{RuCl}(\text{PR}_3)_2]_2$ and $(\mu\text{-Cl})_2[\text{RuCl}(\text{P-P})_2]_2$ are formed, respectively. The $^{31}\text{P}\{^1\text{H}\}$ NMR spectra (in C_6D_6) of **6a** [δ 83.69 (d, *P*-N), δ 48.87 (d, *PPh*₃), $^2J_{\text{PP}} = 36.54$ Hz] and **7a** [δ 81.46 (d, *P*-N), δ 47.64 (d, *P*(*p*-tolyl)₃), $^2J_{\text{PP}} = 37.15$ Hz] depict characteristic AX spin pattern resonances. The coupling constants are consistent with *cis* P-atom coupling.^{6,15} In the ^1H NMR spectra, the equivalent NMe groups of **6a** and **7a** are indicated by singlets at δ 3.07 and 3.13, respectively.

3.2.1 Decomposition of $\text{RuCl}_2(\text{P-N})(\text{PPh}_3)$ (**6a**) to $(\mu\text{-O})(\mu\text{-Cl})_2[\text{RuCl}(\text{P-N})]_2$ (**17**)

When CH_2Cl_2 or C_6H_6 solutions of **6a** and **7a** are exposed to air, a colour change from green to dark green-blue rapidly occurs. Addition of hexanes led to precipitation of dark green solids that were only sparingly soluble in the common organic solvents (CHCl_3 , CH_2Cl_2 , C_6H_6 , MeOH, acetone and DMSO). Dark green crystals of X-ray quality were obtained when a concentrated acetone solution of **6a** was slowly evaporated in air. The ORTEP plot for these crystals is shown in Figure 3.3 and reveals the Ru dinuclear complex $(\mu\text{-O})(\mu\text{-Cl})_2[\text{RuCl}(\text{P-N})]_2$ (**17**). Selected bond lengths and angles of **17** are given in Tables 3.1 and 3.2, respectively. Each Ru centre is coordinated in a pseudo-octahedral fashion to one P-N ligand, one terminal Cl ligand, two bridging Cl ligands and one bridging O ligand.

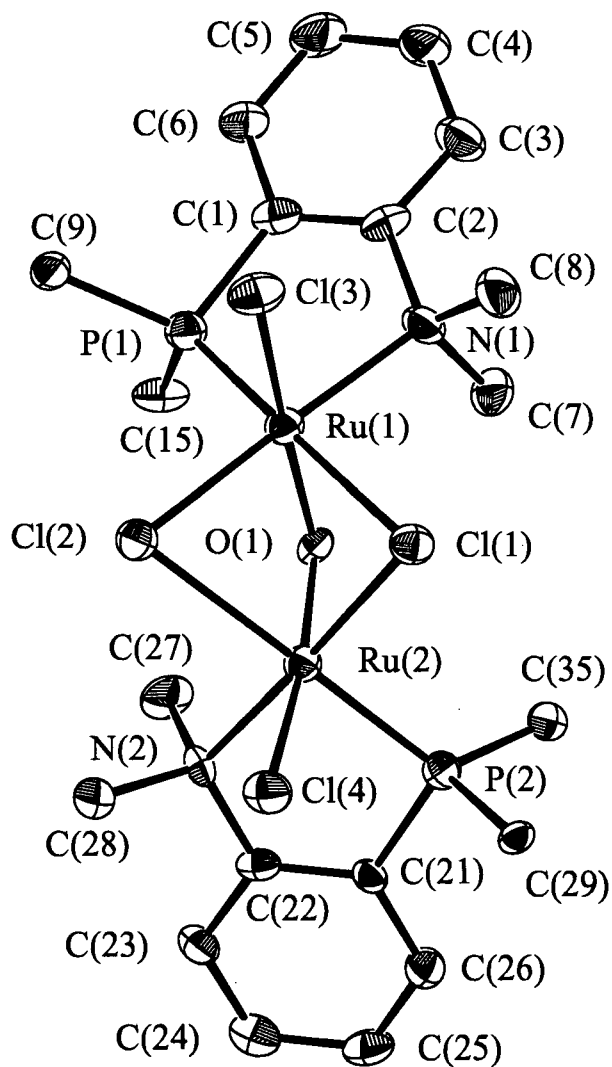


Figure 3.3 The ORTEP plot of $(\mu\text{-O})(\mu\text{-Cl})_2[\text{RuCl}(\text{P-N})]_2$ (17). Thermal ellipsoids for non-hydrogen atoms are drawn at 33 % probability (some of the phenyl carbons have been omitted for clarity). Full experimental parameters and details are given in Appendix III.

Table 3.1 Selected bond lengths (Å) for $(\mu\text{-O})(\mu\text{-Cl})_2[\text{RuCl}(\text{P-N})]_2$ (17) with estimated standard deviations in parentheses.^a

Bond	Length (Å)	Bond	Length (Å)
Ru(1)-Cl(1)	2.570(2)	Ru(2)-Cl(1)	2.3921(15)
Ru(1)-Cl(2)	2.396(2)	Ru(2)-Cl(2)	2.604(2)
Ru(1)-Cl(3)	2.411(2)	Ru(2)-Cl(4)	2.390(2)
Ru(1)-P(1)	2.224(2)	Ru(2)-P(2)	2.230(2)
Ru(1)-O(1)	1.921(4)	Ru(2)-O(1)	1.926(4)
Ru(1)-N(1)	2.193(5)	Ru(2)-N(2)	2.187(5)
Ru(1)-Ru(2)	2.9173(7)		

^aSome of the bond lengths listed here and elsewhere in the thesis are given to the 4th decimal place as provided by the crystallographers; whether such accuracy is justified is open to discussion.

Table 3.2 Selected bond angles (°) for $(\mu\text{-O})(\mu\text{-Cl})_2[\text{RuCl}(\text{P-N})]_2$ (17) with estimated standard deviations in parentheses.

Bonds	Angle (°)	Bonds	Angle (°)	Bonds	Angle (°)
Ru(1)-O(1)-Ru(2)	98.6(2)	Cl(2)-Ru(1)-N(1)	178.03(15)	Cl(1)-Ru(2)-N(2)	177.18(14)
Ru(1)-Cl(1)-Ru(2)	71.92(4)	Cl(3)-Ru(1)-P(1)	93.74(6)	Cl(2)-Ru(2)-Cl(4)	92.68(6)
Ru(1)-Cl(2)-Ru(2)	71.25(5)	Cl(3)-Ru(1)-O(1)	170.54(12)	Cl(2)-Ru(2)-P(2)	177.50(6)
Cl(1)-Ru(1)-Cl(2)	85.62(6)	Cl(3)-Ru(1)-N(1)	88.20(14)	Cl(2)-Ru(1)-O(1)	78.86(12)
Cl(1)-Ru(1)-Cl(3)	92.44(5)	P(1)-Ru(1)-O(1)	95.46(11)	Cl(2)-Ru(2)-N(2)	93.34(14)
Cl(1)-Ru(1)-P(1)	173.00(6)	P(1)-Ru(1)-N(1)	84.48(14)	Cl(4)-Ru(2)-P(2)	88.80(6)
Cl(1)-Ru(1)-O(1)	78.51(11)	O(1)-Ru(1)-N(1)	94.9(2)	Cl(4)-Ru(2)-O(1)	171.33(12)
Cl(1)-Ru(1)-N(1)	92.43(14)	Cl(1)-Ru(2)-Cl(2)	84.94(5)	Cl(4)-Ru(2)-N(2)	87.99(14)
Cl(2)-Ru(1)-Cl(3)	92.11(6)	Cl(1)-Ru(2)-Cl(4)	94.31(6)	P(2)-Ru(2)-O(1)	99.72(12)
Cl(2)-Ru(1)-P(1)	97.44(6)	Cl(1)-Ru(2)-P(2)	96.96(6)	P(2)-Ru(2)-N(2)	84.70(14)
Cl(2)-Ru(1)-O(1)	84.54(13)	Cl(1)-Ru(2)-O(1)	83.11(11)	O(1)-Ru(2)-N(2)	94.4(2)

The Ru-Ru distance of 2.9173 Å is within the range (2.632 - 3.034 Å) generally found for a Ru-Ru single bond,^{1a,16} and this leads to an electron count of 18 at each formally Ru(III) atom. The presence of a Ru-Ru bond also results in reduced Ru(1)-O-Ru(2) (98.6°), Ru(1)-Cl(1)-Ru(2) (71.92°) and Ru(1)-Cl(2)-Ru(2) (71.25°) bond angles. Complexes containing longer Ru-Ru bond distances are known to have enlarged angles between the metal atoms and the bridging ligands. For example, the Ru-Ru distance of 3.266 Å in $[\{(1\text{-MeIm})_3\text{Ru}\}_2(\mu\text{-O})(\mu\text{-O}_2\text{CMe})_2][\text{ClO}_4]_2$ (1-MeIm = 1-methylimidazole) is accompanied by the relatively large Ru-O-Ru angle of 122.3°.^{17d}

The Ru(1)-O and Ru(2)-O bond distances of 1.921 and 1.926 Å, respectively, are somewhat longer than those of other reported Ru(III) $\mu\text{-O}$ species (1.801 - 1.891 Å)¹⁷ but are significantly shorter than those of Ru(III) $\mu\text{-OH}$ (2.093 Å)¹⁸ or Ru(III) $\mu\text{-OH}_2$ (2.02 Å for $[\text{Ru}_2(\mu\text{-OH}_2)_2(\mu\text{-SO}_4)_2\text{py}_4][\text{O}_2\text{CCH}_3]_2$)¹⁹ complexes.

While the O-atom is centred equally between the Ru atoms, the bridging Cl-atoms are subjected to the *trans* influence of the P-atom of the P-N ligand. The Ru(1)-Cl(1) (2.570 Å) and Ru(2)-Cl(2) (2.604 Å) distances are significantly longer than those of the Ru(1)-Cl(2) (2.396 Å) and Ru(2)-Cl(1) (2.392 Å) bonds because the former bonds are *trans* to P(1) and P(2), respectively. This phenomenon is also observed in Ru(II)-Ru(II) dimers such as $[(\text{dppb})\text{ClRu}(\mu\text{-D}_2\text{O})(\mu\text{-Cl})_2\text{RuCl}(\text{dppb})]$.¹⁶ Here, the Ru-Cl_{terminal} bond distances (*trans* to O(1)) of 2.411 (Ru-Cl(3)) and 2.390 Å (Ru-Cl(4)) are comparable to those of the monomeric Ru(III) complex $\text{RuCl}_3(\text{P-N})(\text{PPh}_3)$ (**15a**) (2.3338 - 2.4005 Å).² The Ru-P (2.224 and 2.230 Å) and Ru-N (2.193 and 2.187 Å) distances in **17**, however, are significantly shorter than the corresponding ones in **15a** (2.3606 and 2.338 Å, respectively), and this is presumably due to the reduced steric effects in **17** as a result of the absence of PPh_3 ligands. Comparison

of the augmented bite angles (P-Ru-N) of **17** (84.48 and 84.70°) with that of **15a** (79.25°) reinforces this suggestion.

The two Ru(III) d^5 , one unpaired electron centres in **17** constitute a diamagnetic system as evidenced by a magnetic susceptibility measurement ($\chi_g = 0$). The electron-spin coupling may result from the Ru-Ru interaction but partial antiferromagnetism (superexchange mechanism) through the bridging oxo ligand (Figure 3.4) cannot not be ruled out.^{17b,20}

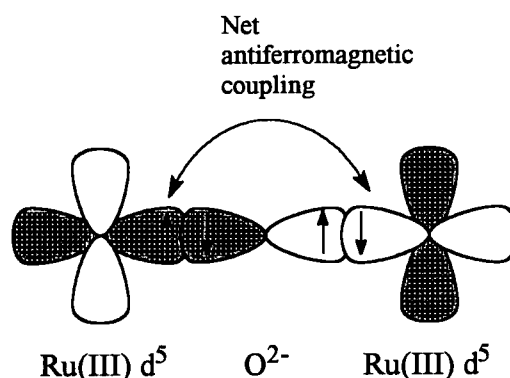


Figure 3.4 Antiferromagnetic coupling between two Ru centres through an O^{2-} ligand. Orbitals are drawn for a linear Ru-O-Ru bond.

The $^3P\{^1H\}$ and 1H NMR spectra of **17** show weak signals compared to those of related Ru(II) complexes. The $^3P\{^1H\}$ NMR spectrum shows two doublets (δ 38.74 and 35.33, $^4J_{PP} = 10.44$ Hz, in C_6D_6) and indicates coupling of the P-atoms of the two P-N ligands through four bonds. The 1H NMR spectrum (C_6D_6) reveals four inequivalent NMe groups with singlets at δ 3.31, 2.89, 2.11 and 2.02. Of note, the above NMR data were previously assigned to a speculative $\mu-O_2$ complex.²

The UV-Vis spectrum of **17** in DMSO (3.91×10^{-5} M) is shown in Figure 3.5. Strong ligand to metal charge-transfer bands are found at $\lambda_1 = 348$ nm ($\epsilon_1 = 15300$ M $^{-1}$ cm $^{-1}$) and $\lambda_2 = 652$ nm ($\epsilon_2 = 11200$ M $^{-1}$ cm $^{-1}$), the positions and magnitudes of the ϵ values of λ_1 and λ_2 being

comparable to those of complexes containing bis(μ -carboxylato or μ -phosphato)(μ -oxo) diruthenium moieties.^{17b-c,20} In particular, the low energy band at 652 nm is responsible for the intense blue-green colour of 17. [Although 17 is less soluble in CH_2Cl_2 than in DMSO, the UV-Vis spectrum in CH_2Cl_2 showed identical absorbances (λ_1 and λ_2) as in DMSO.]

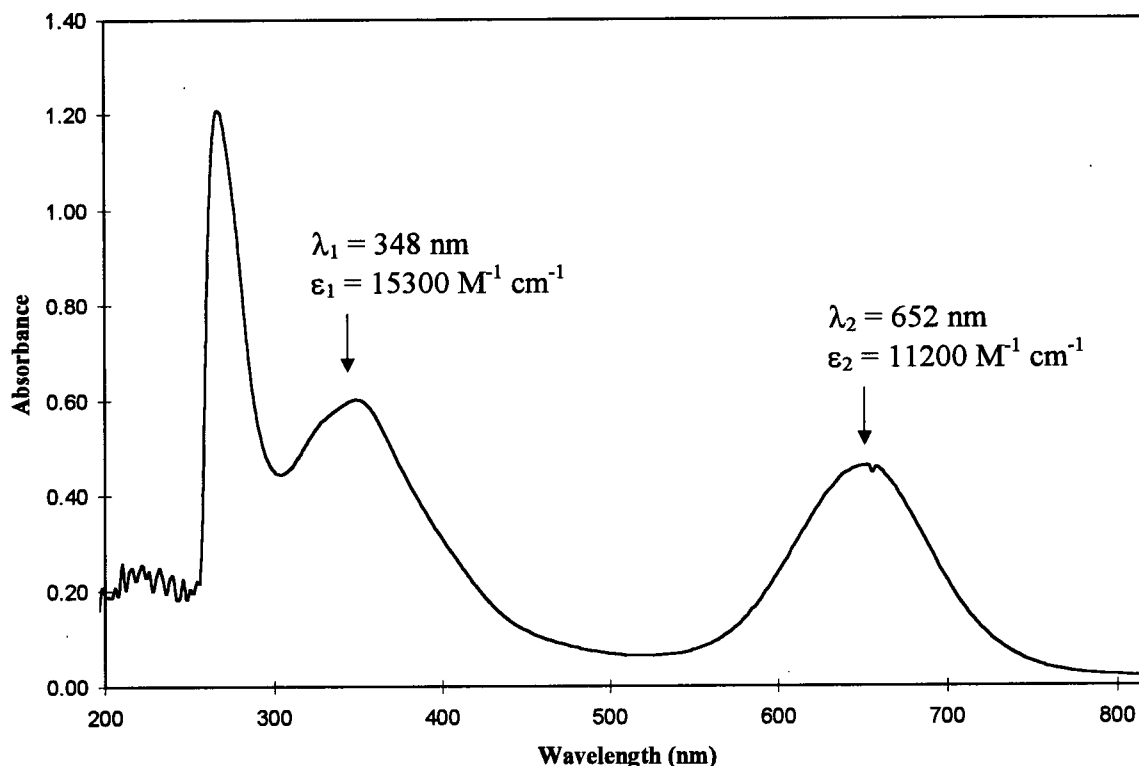


Figure 3.5 UV-Vis spectrum of $(\mu\text{-O})(\mu\text{-Cl})_2[\text{RuCl}(\text{P-N})]_2$ (17) ($3.91 \times 10^{-5} \text{ M}$) in DMSO at 25°C .

The source of the oxo ligand is O_2 . The possibility of H_2O as the origin seems less likely as 17 is formed from the reaction of 6a with O_2 in a strictly H_2O -free environment. Furthermore, 17 is not formed in the absence of O_2 . In an *in situ* reaction between 6a and O_2 in C_6D_6 at r.t., 17 and O=PPh_3 were observed by $^{31}\text{P}\{^1\text{H}\}$ NMR spectroscopy. In fact, 6a catalytically converts any excess PPh_3 added to O=PPh_3 before any 17 is observed (Figure

3.6). A plausible intermediate is an O_2 adduct formed prior to oxidation of PPh_3 to $O=PPh_3$. However, the possibility of the oxidation occurring via H_2O_2 generated within a catalytic $Ru(II)/Ru(IV)$ system requiring trace protons cannot be ruled out; a $Pt(0)/Pt(II)$ catalyzed O_2 -oxidation of PPh_3 via such a mechanism is well substantiated.²¹

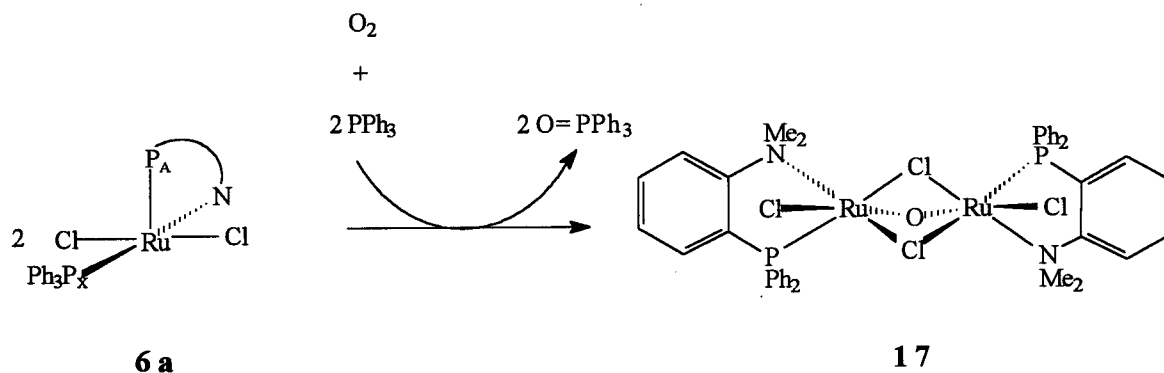
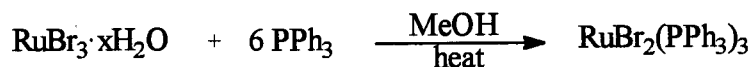
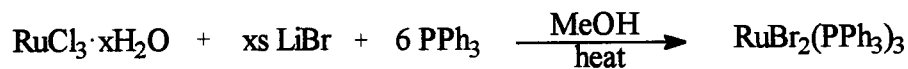


Figure 3.6 The catalytic oxidation of PPh_3 to $O=PPh_3$ by **6a** in the presence of O_2 .

3.3 Metathesis Reactions

It is desirable to prepare bromo and iodo analogues of $RuCl_2(P-N)(PPh_3)$ in order to study and compare their reactivities. A logical entry into the preparation of these analogues would be the use of the precursor complexes $RuBr_2(PPh_3)_3$ and $RuI_2(PPh_3)_3$. Unfortunately, the bromo and iodo precursor complexes could not be obtained in pure form. Two common synthetic routes to $RuBr_2(PPh_3)_3$ have been utilized:^{12b,14a,22}



However, pure product could only be obtained occasionally. For the former reaction, a mixture of the chloro and bromo complexes is often isolated while, for the latter, $RuBr_3 \cdot xH_2O$

is not a good starting material as it has limited solubility in MeOH. In this thesis work, similar difficulties were encountered when $\text{RuBr}_2(\text{PPh}_3)_3$ and $\text{RuI}_2(\text{PPh}_3)_3$ were prepared using the above methods. Thus, alternatives route to $\text{RuBr}_2(\text{P-N})(\text{PPh}_3)$ (**6b**) and $\text{RuI}_2(\text{P-N})(\text{PPh}_3)$ (**6c**) were required.

3.3.1 Synthesis and Characterization of $\text{RuBr}_2(\text{P-N})(\text{PR}_3)$ (**6b**) and $\text{RuI}_2(\text{P-N})(\text{PR}_3)$ (**6c**)

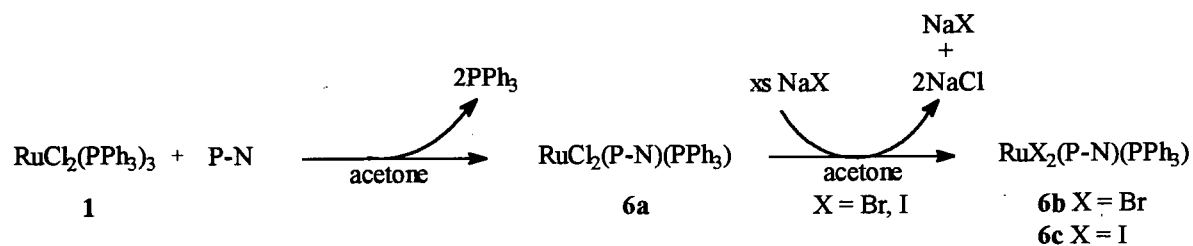


Figure 3.7 Synthesis of $\text{RuBr}_2(\text{P-N})(\text{PPh}_3)$ (**6b**) and $\text{RuI}_2(\text{P-N})(\text{PPh}_3)$ (**6c**).

Analytically pure **6b** and **6c** were obtained from the metathesis reactions of $\text{RuCl}_2(\text{P-N})(\text{PPh}_3)$ (**6a**) with NaX (X = Br, I) as shown in Figure 3.7. For good yields, **6a** is formed *in situ* by reaction of **1** with P-N. Addition of NaX is accompanied by precipitation of NaCl; acetone was used because it readily dissolves NaI, while NaBr and NaCl are slightly soluble and insoluble, respectively. Complete precipitation of NaCl drives the reactions to completion, and microanalysis and NMR spectroscopy confirm the absence of **6a**. In the solid state, **6b** is dark green while **6c** is dark red. $^{31}\text{P}\{^1\text{H}\}$ NMR spectra (C_6D_6) illustrating the P_A and P_X chemical shifts for **6a**, **6b** and **6c** are shown in Figure 3.8. The P_A and P_X resonances shift downfield with X = Cl \rightarrow Br \rightarrow I. In the ^1H NMR spectra (C_6D_6), singlets due to NMe_2 are located at δ 3.07, 3.17 and 3.33 for **6a**, **6b** and **6c**, respectively. The similarities between

the NMR spectra suggest strongly that **6b** and **6c** have the same structure as **6a**, square pyramidal about the Ru centre with the halide atoms mutually trans.

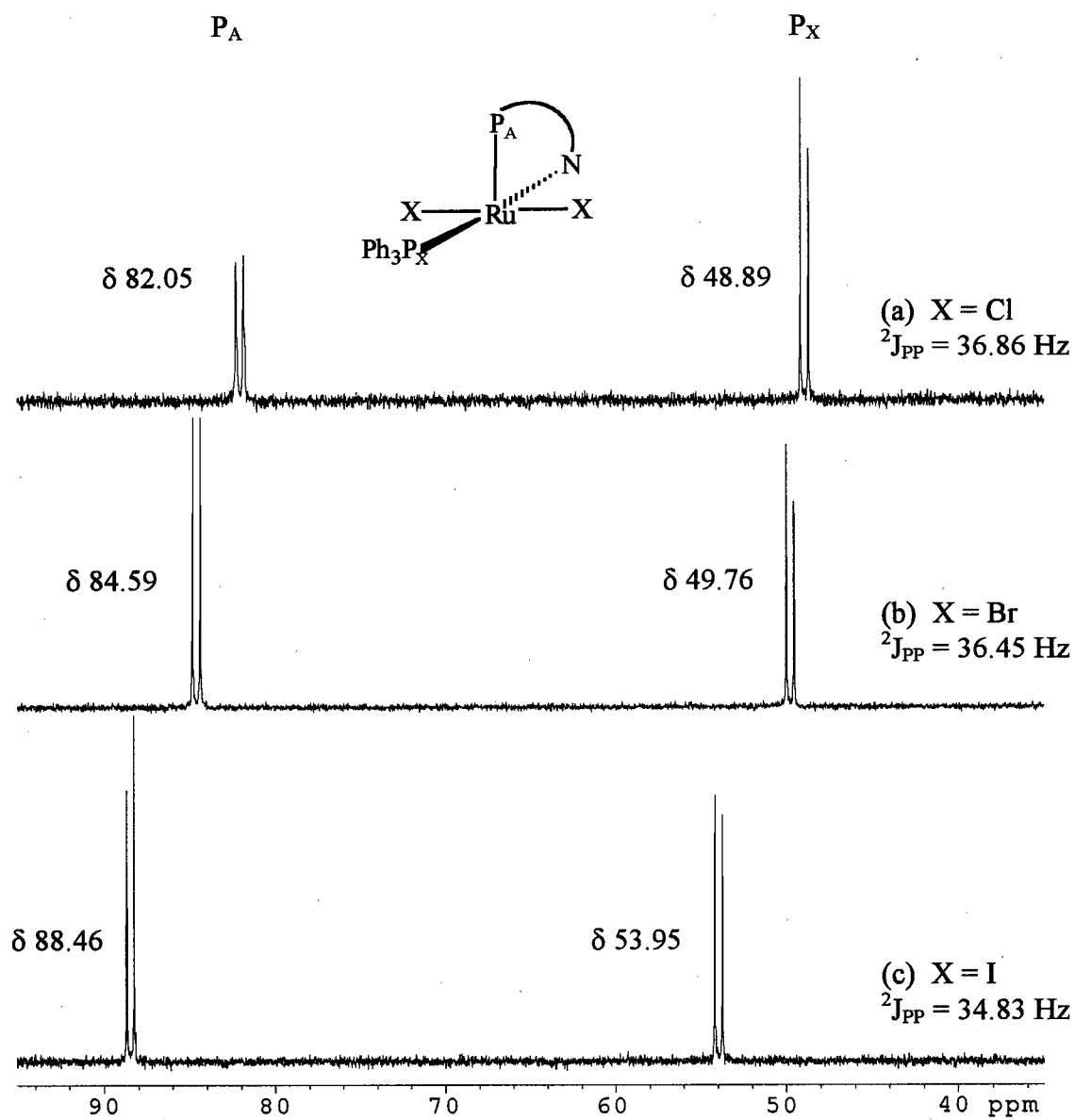


Figure 3.8 $^{31}\text{P}\{^1\text{H}\}$ NMR spectra (81.0 MHz, C_6D_6 , 20°C) for (a) $\text{RuCl}_2(\text{P-N})(\text{PPh}_3)$ (**6a**), (b) $\text{RuBr}_2(\text{P-N})(\text{PPh}_3)$ (**6b**), and (c) $\text{RuI}_2(\text{P-N})(\text{PPh}_3)$ (**6c**).

Both **6b** and **6c** are more stable in the solid state than the chloro analogue **6a** in that they do not react with the H_2O in air. The formation and characterization of *trans*- $\text{RuCl}_2(\text{P-N})(\text{PPh}_3)(\text{OH}_2)$ (**33a**), is described in Chapter 5. In solution, **6b** adds H_2O (observed *in situ* by $^{31}\text{P}\{^1\text{H}\}$ NMR spectroscopy) in the same way as **6a**, and more generally behaves like **6a**; in particular the reaction with H_2S and the syntheses and X-ray crystal structures of *cis*- $\text{RuX}_2(\text{P-N})(\text{PPh}_3)(\text{SH}_2)$ ($\text{X} = \text{Cl}$ (**18a**), Br (**18b**)) are described in Chapter 4 (Sections 4.2.1 and 4.2.2). In solution, **6c** is relatively less stable than **6a** and **6b**. For example, *cis*- $\text{RuI}_2(\text{P-N})(\text{PPh}_3)(\text{SH}_2)$ (**18c**) is initially formed when H_2S is added to a CDCl_3 solution of **6c**; however, the initially dark yellow solution decomposes to a dark brown solution containing unidentifiable species. The formation and decomposition of **18c** were monitored by $^{31}\text{P}\{^1\text{H}\}$ NMR spectroscopy (Section 4.2.3).

3.3.2 *In situ* Formation of $\text{Ru}(\text{OH})\text{X}(\text{P-N})(\text{PPh}_3)$ ($\text{X} = \text{Cl}$ (**28a**), Br (**28b**)) and $\text{Ru}(\text{OH})_2(\text{P-N})(\text{PPh}_3)$ (**31**)

Monomeric late transition metal hydroxo complexes are thought to be intermediates in catalytic processes such as Wacker oxidations and the hydration of olefins to alcohols.²³ Such complexes, however, are unstable and generally difficult to isolate, presumably due to weak metal-oxygen bonds resulting from a mismatch of hard ligands and soft metal centres.²⁴ The most common method for their preparation is via metathesis reactions. For example, Wilkinson and co-workers have prepared $\text{RuCl}(\text{OH})(\text{PPh}_3)_2(\text{H}_2\text{O})_2$ by reaction of $\text{RuCl}_2(\text{PPh}_3)_3$ with NaOH or KOH in THF, acetone or *t*-butanol in the presence of H_2O .²⁵ In this thesis work, this method was employed in the synthesis of Ru hydroxo complexes.

A bright orange solution is formed when excess NaOH is added to an d_6 -acetone solution of **6a**. $^{31}\text{P}\{^1\text{H}\}$ NMR spectroscopic analysis of this reaction *in situ* after 2 h reveals

the presence of three products, **28a** (major species), **31** (minor product) and **33a** (aquo complex) (Figure 3.9(a)). The presence of **33a** is presumably due to the reaction of **6a** with H_2O from the hygroscopic NaOH . The AX P-spin coupling is retained in **28a** and **31** as indicated by two sets of doublets at δ 64.09 (P_A) and 50.76 (P_X) with $^2J_{\text{PP}} = 42.98$ Hz and δ 79.11 (P_A) and 73.44 (P_X) with $^2J_{\text{PP}} = 67.38$ Hz, respectively, and there is no dissociation of either PPh_3 or P-N. After ~ 5 h, the concentration of **31** has increased while that of **28a** has diminished, and the conversion of **28a** to **31** is complete after ~ 20 h (Figure 3.9(b)). The species **28a** and **31** are tentatively identified (see below) as the stepwise substitution products $\text{Ru}(\text{OH})\text{Cl}(\text{P-N})(\text{PPh}_3)$ and $\text{Ru}(\text{OH})_2(\text{P-N})(\text{PPh}_3)$, respectively (Figure 3.10). Inequivalent NMe singlets for **28a** (δ 3.04, 2.69) and **31** (δ 2.60, 2.28) are also assigned in their ^1H NMR

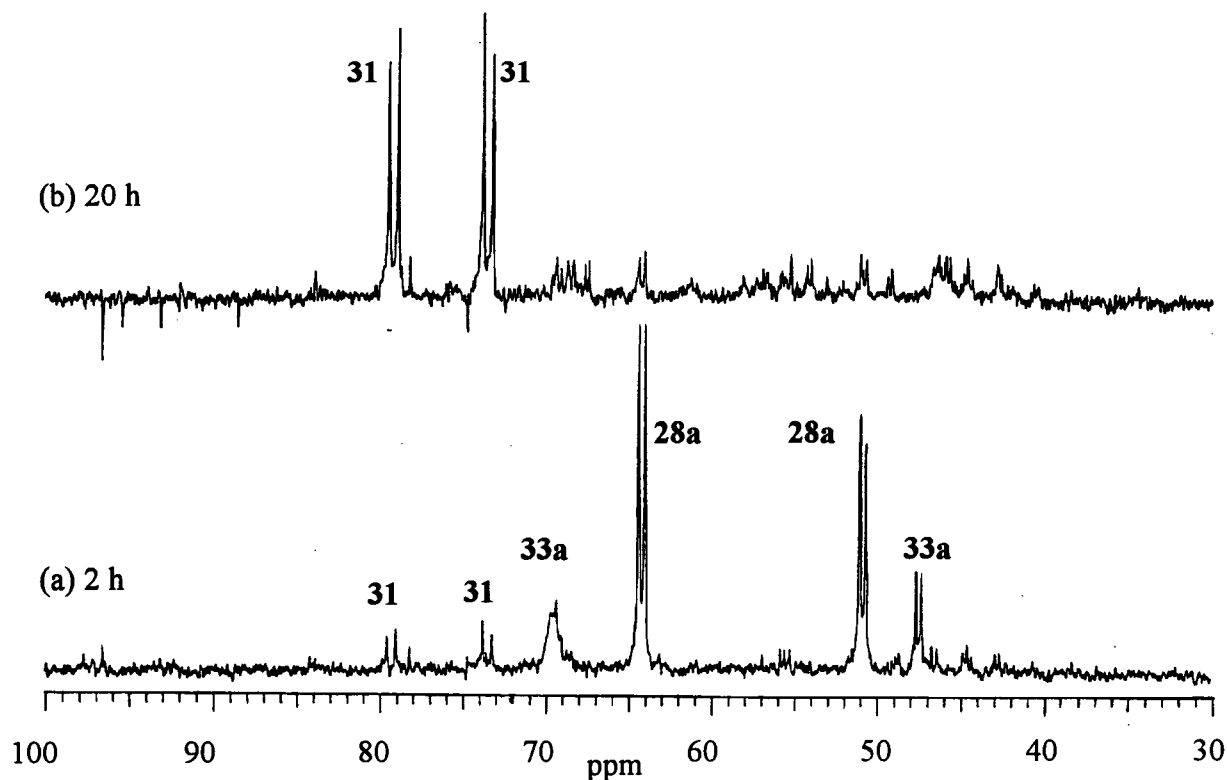


Figure 3.9 $^{31}\text{P}\{^1\text{H}\}$ NMR spectra (121.4 MHz) for the *in situ* reaction of $\text{RuCl}_2(\text{P-N})(\text{PPh}_3)$ (**6a**) with NaOH in d_6 -acetone after (a) 2 h and (b) 20 h at 25°C .

spectra. The resonance of a coordinated OH, however, has not been located, although in general, Ru(II)-OH chemical shifts are found between δ -7.0 and 0.0.²⁵⁻²⁷ In the present system, complicated ^1H NMR spectra are obtained because of the presence of H_2O and insoluble NaOH. Repeated attempts to isolate these hydroxo complexes were unsuccessful as, during work-up procedures, decomposition occurred giving dark green solutions containing uncharacterizable species. The exact structure of **31** is uncertain from the presently available data; however, the presence of two inequivalent NMe resonances in the ^1H NMR spectrum suggests, an 'unsymmetrical' five-coordinate complex.

In the above reactions H_2O probably play the role of solubilizing the NaOH. Upon addition of $\sim 10\%$ H_2O , the rates at which **28a** and **31** are formed increased significantly; in fact, **31** is now completely formed after 5 h. ^1H NMR spectra show no evidence for the coordination of H_2O to either hydroxo species.

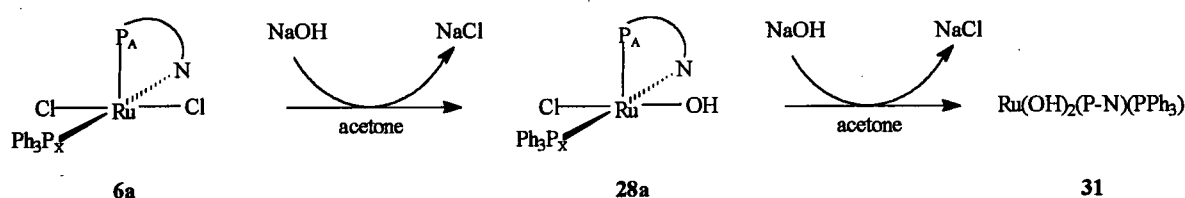


Figure 3.10 The substitution of Cl^- ligands by OH^- ligands.

Verification for the stepwise displacement of Cl^- ligands by OH^- was made by study of the analogous reaction of $\text{RuBr}_2(\text{P-N})(\text{PPh}_3)_2$ (**6b**) with NaOH. The $^{31}\text{P}\{^1\text{H}\}$ and ^1H NMR spectra for the above reaction indicate initial formation of $\text{Ru}(\text{OH})\text{Br}(\text{P-N})(\text{PPh}_3)_2$ (**28b**) after ~ 2 h, with complete conversion to **31** after 20 h. The $^{31}\text{P}\{^1\text{H}\}$ and ^1H NMR data for **28a**, **28b** and **31** are shown in Tables 3.3 and 3.4, respectively. Because of the difference in the halide ligands, NMR signals of **28b** are shifted slightly downfield from those of **28a** and this

trend parallels that observed for **6a** and **6b**. The fact that both reactions involving **6a** and **6b** with NaOH give identical species after 20 h demonstrates that the coordination sphere of **31** does not contain halide ligands.

In situ reactions of **31** with H₂S and H₂ were performed, but the resulting species could not be characterized. Addition of H₂S (1 atm) to a solution of **31** in the presence of excess NaOH resulted in a dark brown solution, that gave no ³¹P{¹H} NMR signals; this suggests that paramagnetic Ru species are formed. Similar results were observed for the reaction of **31** with H₂.

Table 3.3 ³¹P{¹H} NMR data for the *in situ* reactions of RuX₂(P-N)(PPh₃) (X = Cl, Br) with NaOH in d₆-acetone.

Reaction	Product	δ P _A	δ P _X	² J _{PP} (Hz)
RuCl ₂ (P-N)(PPh ₃) (6a) + NaOH, after 2 h	Ru(OH)Cl(P-N)(PPh ₃) (28a)	64.09	50.76	42.98
RuBr ₂ (P-N)(PPh ₃) (6b) + NaOH, after 2 h	Ru(OH)Br(P-N)(PPh ₃) (28b)	65.95	51.23	41.22
6a or 6b + NaOH, after 20 h	Ru(OH) ₂ (P-N)(PPh ₃) (31)	79.11	73.44	67.38

Table 3.4 ¹H NMR data for the *in situ* reactions of RuX₂(P-N)(PPh₃) (X = Cl, Br) with NaOH in d₆-acetone.

Reaction	Product	δ NMe
RuCl ₂ (P-N)(PPh ₃) (6a) + NaOH, after 2 h	Ru(OH)Cl(P-N)(PPh ₃) (28a)	3.04, 2.69
RuBr ₂ (P-N)(PPh ₃) (6b) + NaOH, after 2 h	Ru(OH)Br(P-N)(PPh ₃) (28b)	3.22, 2.72
6a or 6b + NaOH, after 20 h	Ru(OH) ₂ (P-N)(PPh ₃) (31)	2.60, 2.28

3.3.3 *In Situ* Reactions of **6a** or **6b** with NaSH·xH₂O

The reactions of **6a** or **6b** with NaSH·xH₂O parallel those with NaOH. The species, Ru(SH)Cl(P-N)(PPh₃) (**27a**) or Ru(SH)Br(P-N)(PPh₃) (**27b**), are initially formed when excess

NaSH·xH₂O is added to **6a** or **6b** in d₆-acetone at -78°C. At r.t., both reactions give Ru(SH)₂(P-N)(PPh₃) **30** which, unlike dihydroxo complex **31**, is thermally unstable and decomposes within 10 min of its initial formation. NMR evidence for the formations of **27a**, **27b**, and **30** will be presented in Section 4.7.

3.3.4 *In Situ* Formation of Ru(H)₂(P-N)(PPh₃) (**32**)

The metathesis reaction of **6a** with NaH *in situ* gave exclusively Ru(H)₂(P-N)(PPh₃) (**32**) as suggested by ³¹P{¹H} and ¹H NMR data. Heating a suspension of **6a** and NaH in d₆-acetone at 50°C leads to the formation of a bright orange solution. The reaction is complete after ~ 15 min, and a single product **32** is observed in the ³¹P{¹H} NMR spectrum. Doublets are found at δ 61.64 (P_A) and 50.44 (P_X) (²J_{PP} = 24.71 Hz) and indicate that P-N and PPh₃ remain coordinated to the Ru centre. The above chemical shifts differ from those of Ru(H)Cl(P-N)(PPh₃) (**29**) which are found at δ 82.74 and 67.39 (²J_{PP} = 33.20 Hz).² The monohydrido species **29** is prepared from the reaction of **6a** with PS (proton sponge) under 1 atm H₂. The ¹H NMR spectrum of **32** at 25°C shows a singlet at δ 2.51 due to the NMe₂ resonance, and a doublet of doublets at δ -21.16 (Figure 3.11) due to the dihydride is observed. The ²J_{HP} coupling constants of 29.10 and 32.70 Hz suggest that the two hydride ligands are equivalent and are coupled to P_A and P_X, although specific assignments of the coupling constants are not obvious. In comparison, the hydride chemical shift of **29** is observed as a broad signal at δ -27.6 at 25°C, while at -80°C, this is resolved into a pseudo-triplet (²J_{HP} = 28 Hz).^{2,3} Typical *cis*-hydride-phosphine coupling constants in Ru(II) complexes range from 24 to 30 Hz.^{25,28} The proposed structure for **32** is square pyramidal containing mutually trans H-ligands (Figure 3.11).

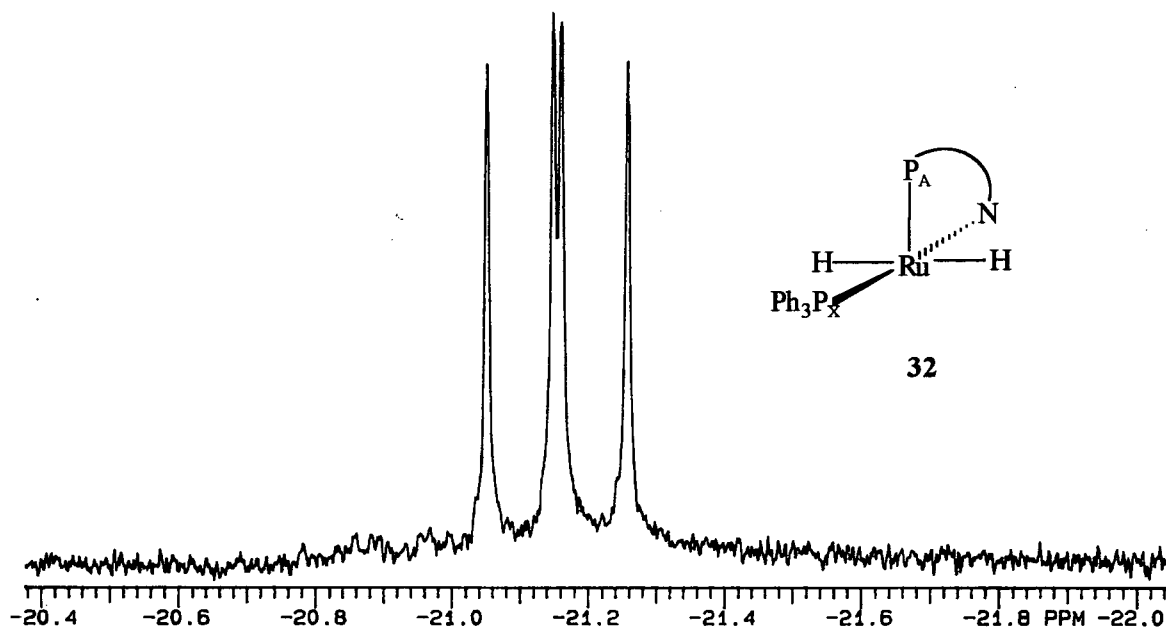


Figure 3.11 High field ^1H NMR spectrum (300 MHz) for the *in situ* reaction of **6a** with NaH in d_6 -acetone at 25°C . Proposed structure of the product **32** is shown in the inset.

As with the reactions of **6a** with NaOH and NaSH, it is reasonable to assume that the mono-hydride species **29** is an intermediate in the formation of **32**. However, attempts to observe **29** were unsuccessful as **32** is formed immediately upon addition of NaH to **6a**. Of interest, when the relatively less reactive CaH_2 was used, **29** was observed to form slowly (over 2 weeks), and indeed no **32** was detected.

3.4 Synthesis of $\text{RuCl}_2(\text{BPN})(\text{PR}_3)$ ($\text{R} = \text{Ph}$ (**13**), *p*-tolyl (**14**))

BPN contains one more dimethylamine group than P-N and is a potential tridentate ligand. Platelet crystals of BPN were obtained from saturated EtOH solutions of the compound. As expected, the ORTEP diagram (Figure 3.12) reveals trigonal pyramidal geometry about the P-atom. The average P-C bond length (1.84 \AA) of BPN is comparable to that of PPh_3 (1.83 \AA), while the bond angles for C(1)-P(1)-C(7) (103.5°), C(7)-P(1)-C(13)

(101.9°) and C(1)-P(1)-C(13) (97.9°) are slightly deviant from the average C-P-C bond angle of 103° of PPh₃, the difference being presumably because of the repulsion of the NMe₂ groups.²⁹ The dihedral angles for the P(1)-C(1)-C(2)-N(1) and P(1)-C(7)-C(8)-N(2) planes are -1.2(7) and 3.7(8)°, respectively, indicating that the two amine groups and the lone electron pair of the P-atom point essentially in the same direction.

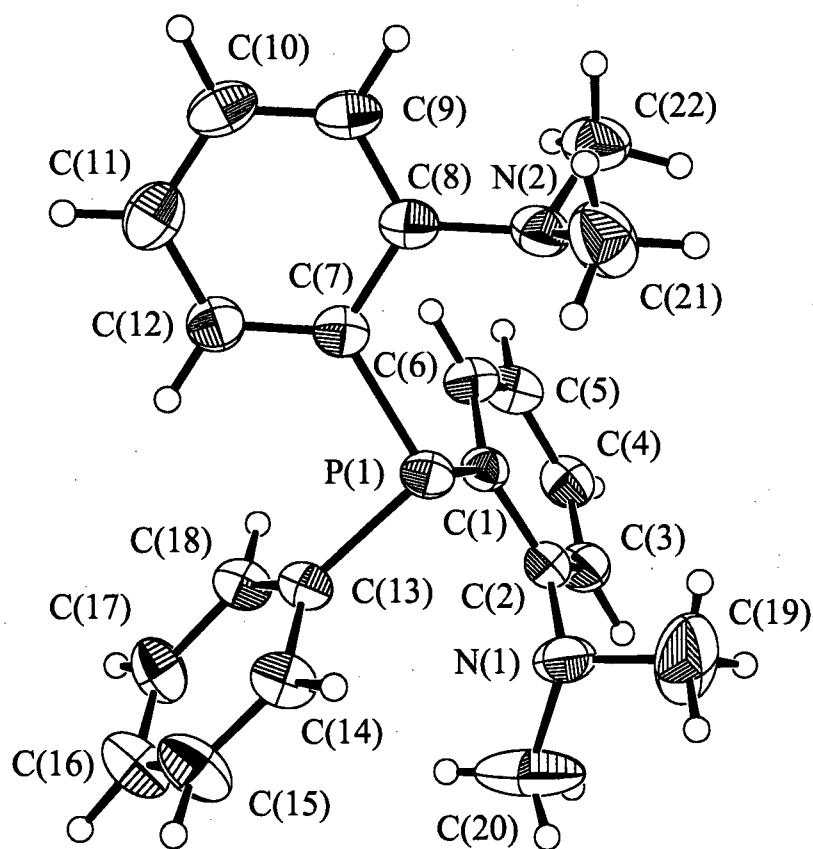


Figure 3.12 The ORTEP plot of BPN. Thermal ellipsoids for non-hydrogen atoms are drawn at 33 %. Full experimental parameters and details are given in Appendix I.

When BPN is reacted with $\text{RuCl}_2(\text{PPh}_3)_3$ or $\text{RuCl}_2(\text{P}(p\text{-tolyl})_3)_3$ in CH_2Cl_2 , dark orange solids can be isolated from the reaction mixtures. Microanalysis and NMR spectroscopic measurements are consistent with the formulations $\text{RuCl}_2(\text{BPN})(\text{PPh}_3)_3$ (**13**) and $\text{RuCl}_2(\text{BPN})(\text{P}(p\text{-tolyl})_3)_3$ (**14**). The $^{31}\text{P}\{^1\text{H}\}$ NMR resonances are given in Table 3.5, and the $^2J_{\text{PP}}$ coupling constants are consistent with the presence of cis P-atoms.^{6,15} Two possible structures for six-coordinate **13** or **14** are shown in Figure 3.13. The presence of four inequivalent NMe groups observed in the ^1H NMR spectra (Table 3.6) strongly indicates an unsymmetrical structure such as Figure 3.13(a) for **13** and **14**. The possibility of

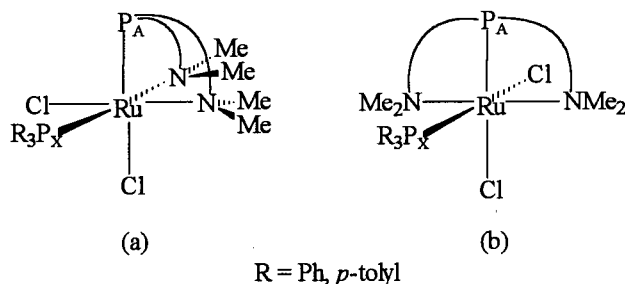


Figure 3.13 Possible structures of $\text{RuCl}_2(\text{BPN})(\text{PR}_3)_3$.

Table 3.5 $^{31}\text{P}\{^1\text{H}\}$ NMR spectroscopic data for $\text{RuCl}_2(\text{BPN})(\text{PR}_3)_3$ in CDCl_3 .

	δP_A	δP_X	$^2J_{\text{PP}}$ (Hz)
R = Ph (13)	56.00	33.67	32.05
R = <i>p</i> -tolyl (14)	56.05	31.26	31.44

Table 3.6 ^1H NMR chemical shifts for $\text{RuCl}_2(\text{BPN})(\text{PR}_3)_3$ in CDCl_3 ; assignments of the phenyl region have been omitted.

	δNMe				$\delta p\text{-(C}_6\text{H}_4\text{)CH}_3$
R = Ph (13)	3.63	3.15	2.60	2.20	-
R = <i>p</i> -tolyl (14)	3.64	3.10	2.57	2.20	2.20

five-coordinate species (with a dangling -NMe_2) cannot be ruled out entirely, but the complexes are unreactive in d_6 -acetone solution when subjected to 1 atm of H_2 , CO , H_2O or H_2S at r. t., implying six-coordinate geometry. Decomposition to paramagnetic species and phosphine oxides was observed when **13** and **14** were exposed to air for 2 days.

3.5 Synthesis of *Mer*- $\text{RuCl}_3(\text{BPN})$ (**16**)

Reaction of BPN with $\text{RuCl}_3(\text{PPh}_3)_2(\text{DMA})\cdot(\text{DMA})$ in CH_2Cl_2 gave species **16**, and platelet crystals containing one CHCl_3 per molecule of complex were obtained from saturated CHCl_3 solutions of the complex. The ORTEP plot is shown in Figure 3.14, with selected bond lengths and angles given in Tables 3.7 and 3.8, respectively. A pseudo octahedral geometry around the Ru centre with mer Cl-atoms is evident, analogous to that seen in the previously crystallographically characterized $\text{RuCl}_3(\text{P-N})(\text{PPh}_3)$ (**15a**) and $\text{RuCl}_3(\text{AMPHOS})(\text{PPh}_3)$ complexes.² Two Cl-atoms are weakly hydrogen-bonded ($\text{Cl}(2)\cdots\text{H}(26)$ 2.65 Å and $\text{Cl}(3)\cdots\text{H}(26)$ 2.86 Å) to the H-atom of the solvated CHCl_3 molecule and, as a result, the Ru-Cl(2) (2.359(2) Å) and Ru-Cl(3) (2.482(2) Å) bonds are elongated relative to Ru-Cl(1) (2.316(2) Å). The further lengthening of the Ru-Cl(3) bond results from the strong *trans* influence of the P-atom of the BPN ligand. The Ru(1)-P(1) (2.199(2) Å), Ru(1)-N(1) (2.207(5) Å) and Ru(1)-N(2) (2.209(5) Å) bond lengths are considerably shorter than the Ru-P (average 2.37 Å) and Ru-N (average 2.35 Å) bonds in **15a** and $\text{RuCl}_3(\text{AMPHOS})(\text{PPh}_3)$ probably because BPN is bonded rigidly in a meridional geometry. Furthermore, the N(1)-Ru-N(2) angle is only 160.0(2)° because of this strain.

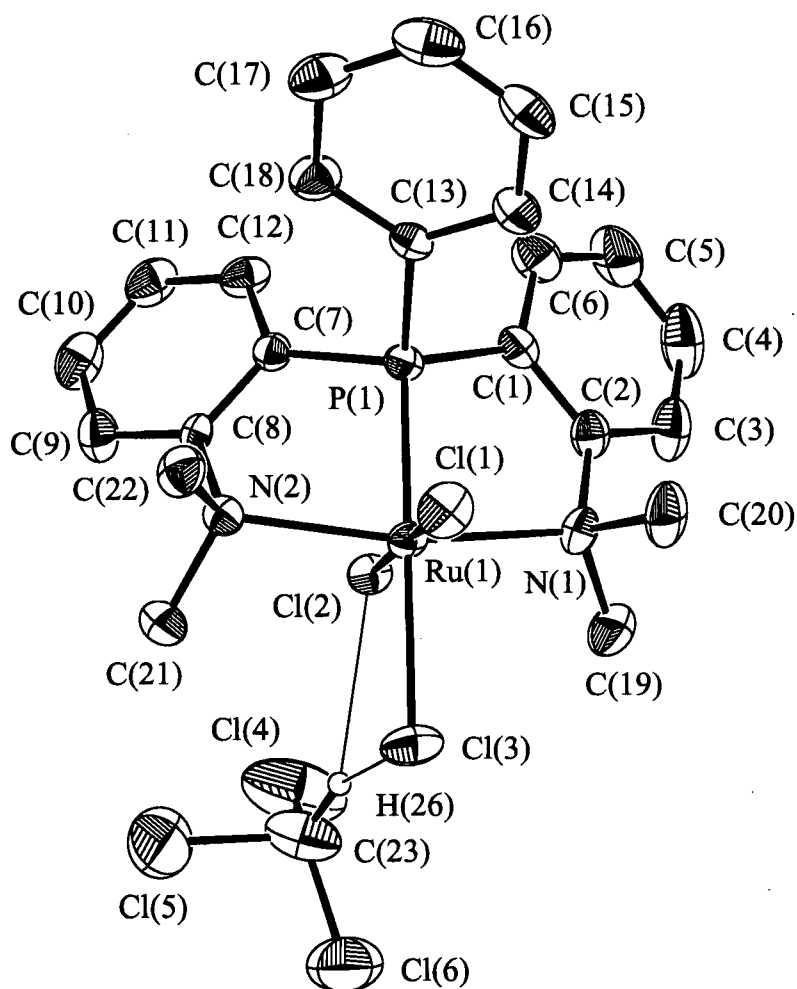


Figure 3.14 The ORTEP plot of *mer*-RuCl₃(BPN)·CHCl₃ (**16**). Thermal ellipsoids for non-hydrogen atoms are drawn at 33 % probability (some of the phenyl carbons have been omitted for clarity). Full experimental parameters and details are given in Appendix II.

Table 3.7 Selected bond lengths (Å) for *mer*-RuCl₃(BPN) (**16**) with estimated standard deviation in parentheses.

Bond	Length (Å)	Bond	Length (Å)
Ru(1)-Cl(1)	2.316(2)	Ru(1)-P(1)	2.199(2)
Ru(1)-Cl(2)	2.359(2)	Ru(1)-N(1)	2.207(5)
Ru(1)-Cl(3)	2.482(2)	Ru(1)-N(2)	2.209(5)
Cl(2)···H(26)	2.65	Cl(3)···H(26)	2.86

Table 3.8 Selected bond angles (°) for *mer*-RuCl₃(BPN) (**16**) with estimated standard deviation in parentheses.

Bonds	Angles (°)	Bond	Angles (°)
Cl(1)-Ru(1)-Cl(2)	177.65(6)	Cl(2)-Ru(1)-N(2)	83.0(1)
Cl(1)-Ru(1)-Cl(3)	87.81(7)	Cl(3)-Ru(1)-P(1)	179.88(6)
Cl(2)-Ru(1)-Cl(3)	90.03(6)	Cl(3)-Ru(1)-N(1)	95.2(2)
Cl(1)-Ru(1)-P(1)	92.12(6)	Cl(3)-Ru(1)-N(2)	98.4(1)
Cl(1)-Ru(1)-N(1)	98.6(1)	P(1)-Ru(1)-N(1)	84.7(1)
Cl(1)-Ru(1)-N(2)	96.5(1)	P(1)-Ru(1)-N(2)	81.7(1)
Cl(2)-Ru(1)-P(1)	90.05(5)	N(1)-Ru(1)-N(2)	160.0(2)
Cl(2)-Ru(1)-N(1)	82.5(1)		

The μ_{eff} value of 1.5 BM is comparable with the spin only value of 1.73 BM for a low spin, Ru(III) d⁵ structure.

3.6 The Reactions of TPN with Ru(II) and (III)

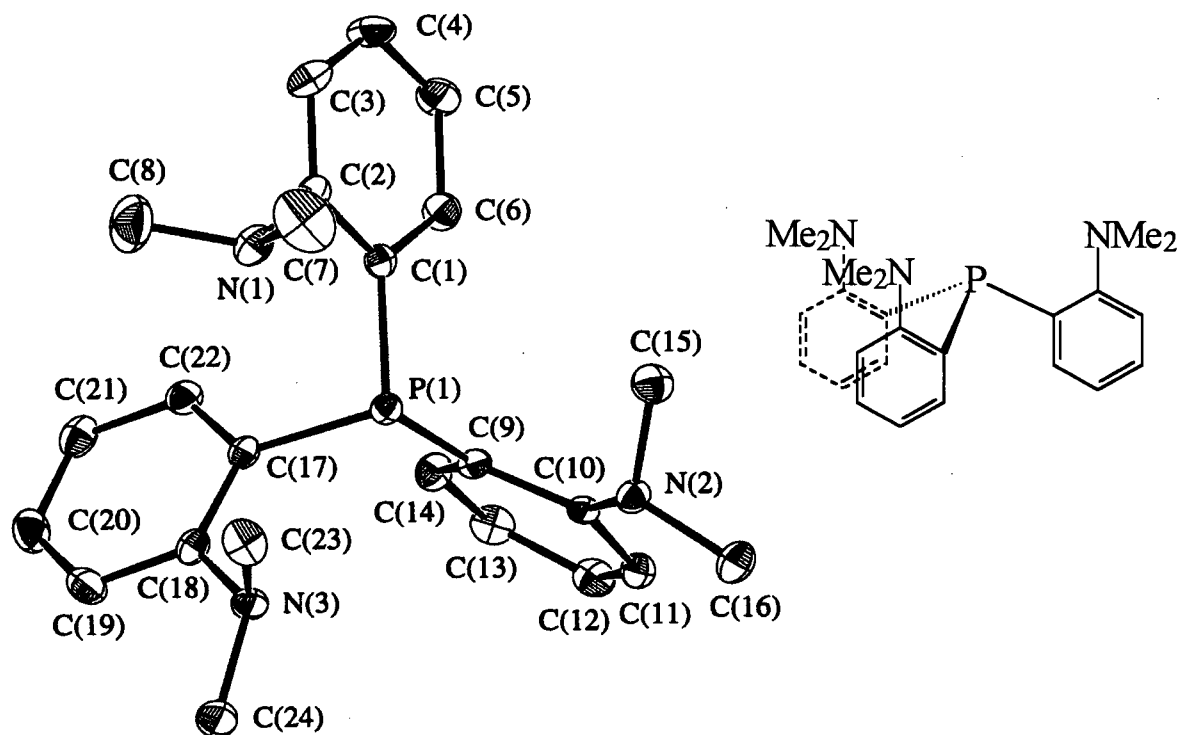


Figure 3.15 ORTEP plot of TPN, whose structure was determined by other members of this group.³⁰ Thermal ellipsoids for non-hydrogen atoms are drawn at 33 % probability.

TPN contains three dimethylamine groups and can potentially function as a tetradentate ligand. Similar to the structure of BPN (Figure 3.12), that of TPN (Figure 3.15) shows that the P-atom and the amine groups point in the same direction as indicated by the small dihedral angles of $-2.4(2)$, $-10.9(2)$ and $4.4(2)^\circ$ for the $P(1)-C(1)-C(2)-N(1)$, $P(1)-C(9)-C(10)-N(2)$ and $P(1)-C(17)-C(18)-N(3)$ planes, respectively. When TPN was added to solutions of $RuCl_2(PPh_3)_3$ or $RuCl_3(PPh_3)_2(DMA) \cdot (DMA)$, no reactions were observed. This was surprising because TPN does coordinate to Pt(II) and Pd(II) forming

Dark green solids, isolated from the reactions of $\text{RuCl}_2(\text{PPh}_3)_3$ or $\text{RuCl}_2(\text{P}(p\text{-tolyl})_3)_3$ with the bulky and rigid PAN ligand (Sections 2.6.8 and 2.6.9), analyze for the species **9** and **10**. These complexes are assumed to have square pyramidal geometries based on their NMR data which are comparable to those of **6a** and **7a**, the P-N analogues (Section 3.2). The $^3\text{P}\{^1\text{H}\}$ NMR spectra of **9** (δ 97.10 and 41.39, $^2J_{\text{PP}} = 32.05$ Hz in CDCl_3) and **10** (δ 97.71 and 39.57, $^2J_{\text{PP}} = 33.39$ Hz in C_6D_6) consist of AX cis P-spin coupling patterns, while the ^1H NMR spectra show inequivalent NMe groups with singlets at δ 3.68 and 2.96 for **9** and δ 3.50 and 2.90 for **10**. The NMR data do not distinguish between trans- or cis-Cl-atoms (Figure 3.16), but the former would require the presence of a rigid Ru(PAN) chelate ring.



Mudalige found that **10** did not react with small molecules such as H₂, H₂S, SO₂ or CH₃OH under conditions identical to those used for the reactions with RuCl₂(P-N)(PR₃).² In this present thesis work, reactions of **9** and **10** with H₂ or H₂S were re-investigated but, even with the H₂ and H₂S pressures increased from 1 to 3 atm and the mixtures heated to 80°C in C₆H₆, no reactions were observed. The inability of RuCl₂(PAN)(PR₃) to coordinate to small molecules is attributed to the steric bulk of the PAN ligand hindering access to the Ru centre.

3.8 Attempted Synthesis and Reactivity of RuCl₂(AMPHOS)(PPh₃) (**11**)

The isolation of analytically pure **11** using the preparative method for RuCl₂(P-N)(PR₃) and RuCl₂(PAN)(PR₃) was not successful. Although >99 % product formation is observed by NMR when RuCl₂(PPh₃)₃ and AMPHOS is reacted *in situ* in C₆D₆, mixtures containing **11**, RuCl₂(PPh₃)₃, OPPh₃ and PPh₃ are often isolated (Section 2.6.10). Mudalige also found such difficulties but was able to synthesis **11** employing the indirect method shown in Figure 3.17.² RuCl₃(AMPHOS)(PPh₃), initially prepared from the reaction of RuCl₃(PPh₃)₂(DMA)·(DMA) with AMPHOS, is reduced to “Ru(H)Cl(AMPHOS)(PPh₃)” by H₂ in the presence of 3 equiv. of PS. Chloride abstraction from CHCl₃ by the hydrido complex resulted in the production of **11**. However, complications also arise because of the extreme O₂-sensitivity of “Ru(H)Cl(AMPHOS)(PPh₃)” and contamination by phosphine oxides. As a result, when this procedure was followed, **11** was isolated in low yield and was not pure.

The structure of **11** is presumed to be square pyramidal with trans Cl-atoms as in the P-N analogue. The ³¹P{¹H} NMR chemicals shifts of **11** appear at δ 84.56 and 40.32 (²J_{PP} = 37.03 Hz), while the diastereotopic NMe₂ groups in AMPHOS result in the observation of two singlets at δ 2.86 and 2.33 in the ¹H NMR spectrum.

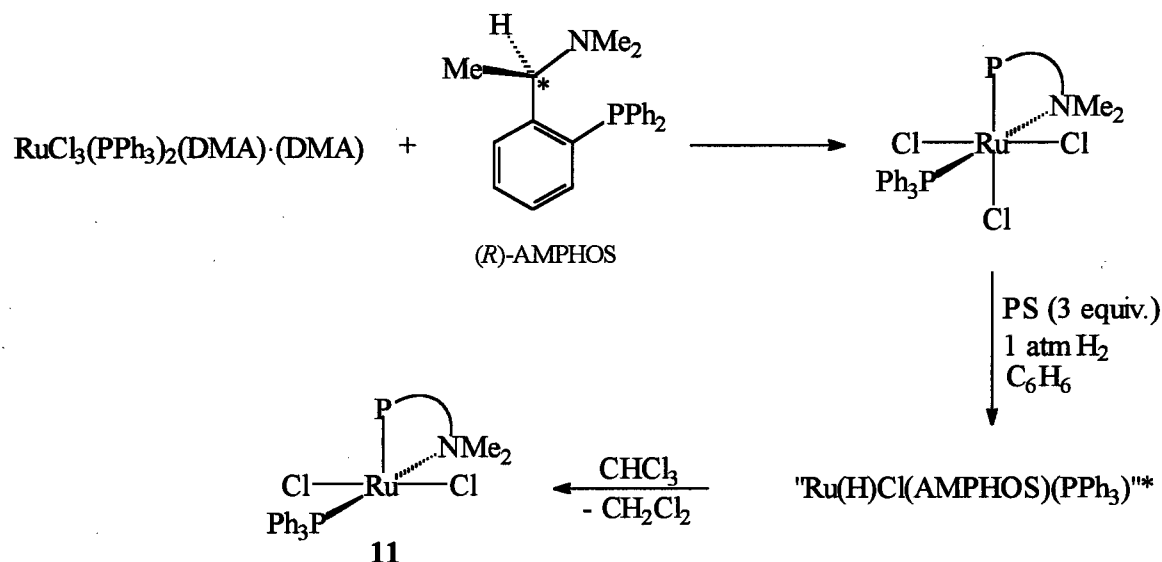


Figure 3.17 Synthesis of $\text{RuCl}_2(\text{AMPHOS})(\text{PPh}_3)$ (**11**). *The actual structure of $\text{Ru(H)Cl(AMPHOS)(PPh}_3\text{)}$ is in question as the dimeric formulation $(\mu\text{-Cl})_2[\text{Ru(H)(AMPHOS)(PPh}_3)]_2$ has also been proposed.²

The reaction of H_2 (1 atm) with an impure sample of **11** (~ 20 mg) was carried out at r. t. in C_7H_8 (~ 1 mL), when red-brown crystals were isolated from the mixture after 24 h. The $^{31}\text{P}\{^1\text{H}\}$ NMR spectrum of these crystals in C_7D_8 at 20°C shows two broad resonances at δ 71.4 and 46.4, identical to those of the previously known $[(\text{PPh}_3)_2(\eta^2\text{-H}_2)\text{Ru}(\mu\text{-H})(\mu\text{-Cl})_2\text{Ru(H)(PPh}_3)_2]$.^{1a,13c,32} A broad ^1H resonance at δ -12.9 is due to unresolved signals from the $\mu\text{-H}$, $\eta^2\text{-H}_2$ and the terminal H. The formation of the dimer is presumably due to the presence of PPh_3 , while AMPHOS is thought to act as a base and form $\text{AMPHOS}\cdot\text{HCl}$ (Figure 3.18).

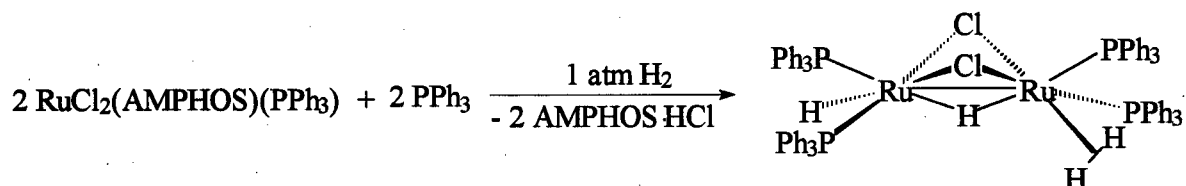


Figure 3.18 Synthesis of $[(\text{PPh}_3)_2(\eta^2\text{-H}_2)\text{Ru}(\mu\text{-H})(\mu\text{-Cl})_2\text{Ru(H)(PPh}_3)_2]$.

For preparations of $\text{RuCl}_2(\text{P-N})(\text{PR}_3)(\text{L})$ (L = small molecule, see Sections 2.8, 2.10 and 2.11) generally, L is added to a solution of $\text{RuCl}_2(\text{P-N})(\text{PR}_3)$ which is initially formed *in situ* from the reaction of $\text{RuCl}_2(\text{PR}_3)_3$ with P-N . It was thought that $\text{RuCl}_2(\text{AMPHOS})(\text{PPh}_3)(\text{L})$ might also be synthesized without the isolation of **11**. Thus, to a solution of **11**, formed *in situ* from $\text{RuCl}_2(\text{PPh}_3)_3$ (0.02 mmol) and AMPHOS (0.02 mmol) in CDCl_3 (~ 1 mL) in a NMR tube, was added 1 atm H_2 ; a dark brown solution formed immediately and dark purple crystals precipitated overnight. The $^{31}\text{P}\{^1\text{H}\}$ (δ 59.2, br) and ^1H NMR spectra (δ -17.5, q, $^2J_{\text{HP}} = 26$ Hz) of these crystals in CDCl_3 show that the compound is $\text{Ru}(\text{H})\text{Cl}(\text{PPh}_3)_3$.²⁸ The observations clearly indicate that coordination of the amine group of AMPHOS to $\text{Ru}(\text{II})$ is disfavoured, AMPHOS preferentially reacting with H_2 in the presence of $\text{RuCl}_2(\text{PPh}_3)_3$ to form $\text{AMPHOS}\cdot\text{HCl}$ (Figure 3.19). The inability to isolate pure **11** precluded studies of its reactivity with small molecules.

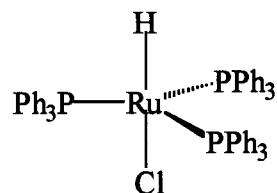
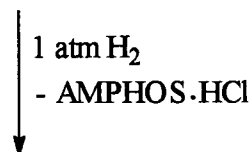
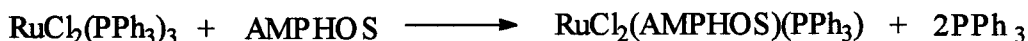


Figure 3.19 Synthesis of $\text{Ru}(\text{H})\text{Cl}(\text{PPh}_3)_3$ using AMPHOS as the base.

3.9 Attempted Preparations of $\text{RuCl}_2(\text{ALAPHOS})_2$ (12)

When one or two equiv of ALAPHOS was added to a solution of *cis*- $\text{RuCl}_2(\text{DMSO})_4$ or $\text{RuCl}_2(\text{PPh}_3)_3$ in CH_2Cl_2 , a bright pink solid was isolated after precipitation with hexanes (Section 2.6.11). The $^{31}\text{P}\{^1\text{H}\}$ NMR spectrum of this product indicated the presence of several species with the major one characterized by a $^{31}\text{P}\{^1\text{H}\}$ resonance at δ 55.60 (s) and tentatively identified as 12. The structure (Figure 3.20) is thought to be analogous to that of $\text{RuCl}_2[\kappa^2(P,N)\text{-Ph}_2\text{PCH}_2\text{CH}_2\text{NMe}_2]_2$, which has been crystallographically characterized and gives a singlet at δ 56.5 in the $^{31}\text{P}\{^1\text{H}\}$ NMR spectrum;³³ furthermore, this complex is also pink and was isolated from the reaction of *cis*- $\text{RuCl}_2(\text{DMSO})_4$ or $\text{RuCl}_2(\text{PPh}_3)_3$ with 2 equiv of $\text{Ph}_2\text{PCH}_2\text{CH}_2\text{NMe}_2$.^{33,34} The ^1H NMR spectrum of the pink solid containing 12 and other contaminants is complicated because of overlapping resonances of coordinated chiral ALAPHOS, and ^1H assignments were not made. Because 12 could not be obtained pure, further experiments to probe its reactivity were not carried out.

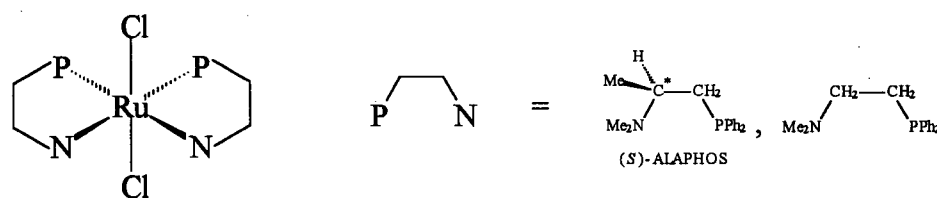


Figure 3.20 Structure of $\text{RuCl}_2(\text{ALAPHOS})_2$ (12) (proposed) and $\text{RuCl}_2[\kappa^2(P,N)\text{-Ph}_2\text{PCH}_2\text{CH}_2\text{NMe}_2]_2$.

3.10 Miscellaneous: Reactivity of *Trans*- $\text{RuCl}_2(\text{PO})_2$ (5) with H_2S

Complex 5 was prepared by the reaction of $\text{RuCl}_2(\text{PPh}_3)_3$ with 1 or 2 equiv of PO (*o*-diphenylphosphineanisole) in acetone (Section 2.5).³⁵ The $^{31}\text{P}\{^1\text{H}\}$ NMR spectrum of 5 in CDCl_3 consists of a singlet at δ 64.20 due to equivalent P-atoms, and the ^1H NMR spectrum

shows a singlet at δ 4.57 due to equivalent OMe groups. When 1 atm H_2S was added to a CDCl_3 solution of **5**, no reaction was observed even after 2 weeks at 60°C . However, when excess PPh_3 was present, **5** reacted slowly with H_2S at 60 to 100°C , and the $^{31}\text{P}\{^1\text{H}\}$ NMR spectrum of the *in situ* product mixture showed new resonances corresponding to two products, **I** and **II**. AX P-spin patterns were observed: for **I**, δ 57.38, 45.34 (d, $^2J_{\text{PP}} = 33.81$ Hz), and for **II**, δ 67.94, 56.79 (d, $^2J_{\text{PP}} = 76.60$ Hz). In the ^1H NMR spectrum, new signals at δ 4.69 (s, 3H, OMe) and δ 1.13 (br, 2H, SH_2) were seen. Unfortunately, the above reaction did not go to completion ($^{31}\text{P}\{^1\text{H}\}$ NMR data suggest $\sim 10\%$ conversion), and species **I** and **II** could not be isolated. The tentative structures for **I** and **II** are shown in Figure 3.21.

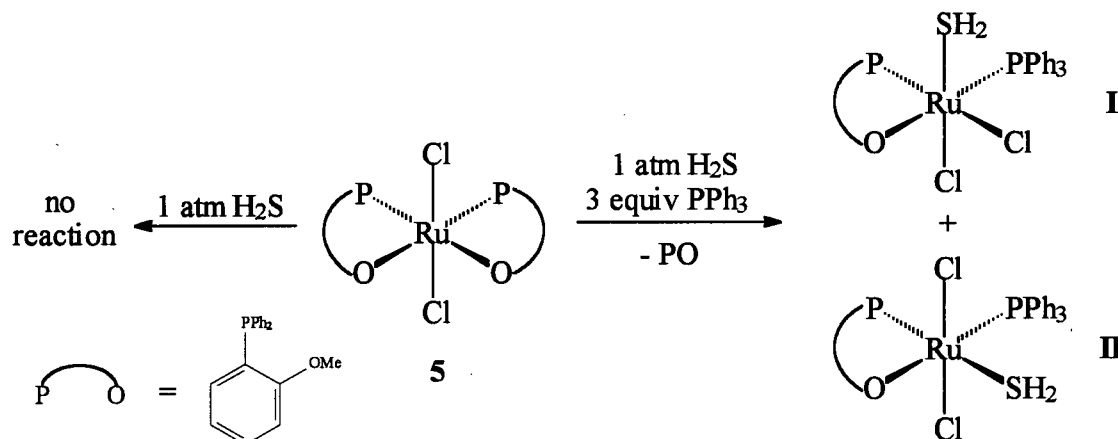


Figure 3.21 Possible reactions of $\text{RuCl}_2(\text{PO})_2$ (**5**) with H_2S .

3.11 Summary

The very reactive $\text{RuCl}_2(\text{P-N})(\text{PR}_3)$ ($\text{R} = \text{Ph}$ (**6a**), *p*-tolyl (**7a**)) complexes have been prepared and characterized. The coordination of H_2S , H_2O , H_2 , N_2 , N_2O and other small molecules to **6a** and **7a** will be discussed in Chapters 4, 5 and 6. In solution, these complexes are O_2 -sensitive and decompose to give the Ru(III) diamagnetic dinuclear $(\mu\text{-O})(\mu\text{-Cl})_2[\text{RuCl}(\text{P-N})]_2$ (**17**). The metathesis reactions of **6a** with NaX ($\text{X} = \text{Br}$, I , OH , SH

and H) result in the formation (isolated or observed *in situ*) of $\text{RuX}_2(\text{P-N})(\text{PPh}_3)$ species. Other Ru(II) aminophosphine complexes, such as $\text{RuCl}_2(\text{BPN})(\text{PR}_3)$ and $\text{RuCl}_2(\text{PAN})(\text{PR}_3)$, have also been isolated but they are unreactive toward the small molecules. The ability of aminophosphine ligands to coordinate to Ru(II) is dependent upon their steric bulk and electronic nature. For instance, the sterically hindered TPN does not react with $\text{RuCl}_2(\text{PPh}_3)_3$, while the reaction of the basic AMPHOS ligand with H_2 and $\text{RuCl}_2(\text{PPh}_3)_3$ results in the formation of $\text{Ru}(\text{H})\text{Cl}(\text{PPh}_3)_3$ and $\text{AMPHOS}\cdot\text{HCl}$.

3.12 References

1. (a) Hampton, C. R. S. M.; Ph.D. Thesis, The University of British Columbia, 1989.
(b) Hampton, C. R. S. M.; Butler, I. R.; Cullen, W. R.; James, B. R.; Charland, J.-P.; Simpson, J. *Inorg. Chem.* **1992**, *31*, 5509.
2. Mudalige, D. C. Ph.D. Thesis, The University of British Columbia, 1994.
3. Mudalige, D. C.; Rettig, S. J.; James, B. R.; Cullen, W. R. *J. Chem. Soc., Chem. Commun.* **1993**, 830.
4. Armit, P. W.; Boyd, A. S. F.; Stephenson, T. A. *J. Chem. Soc., Dalton Trans.* **1975**, 1663.
5. Jung, C. W.; Garrou, P. E.; Hoffman, P. R.; Caulton, K. G. *Inorg. Chem.* **1984**, *23*, 726.
6. (a) Joshi, A. M. Ph.D. Thesis, The University of British Columbia, 1990.
(b) Joshi, A. M.; Thorburn, I. S.; Rettig, S. J.; James, B. R. *Inorg. Chim. Acta* **1992**, *198-200*, 283.
7. Jones, N. D.; MacFarlane, K. S.; Schutte, R. P.; Smith, M. B.; Rettig, S. J.; James, B. R. *Inorg. Chem.* **1999**, *38*, 3956.
8. (a) Evans, I. P.; Spencer, A.; Wilkinson, G. *J. Chem. Soc., Dalton Trans.* **1973**, 204.
(b) Carmichael, D.; Floch, P. L.; Ricard, L.; Mathey, F. *Inorg. Chim. Acta* **1992**, *198*, 437.
9. (a) Mashima, K.; Kusano, K.; Ohta, T.; Noyori, R.; Takaya, H. *J. Chem. Soc., Chem. Commun.* **1989**, 1208.
(b) Bennett, M. A.; Ennett, J. P. *Inorg. Chim. Acta* **1992**, *198*, 583.
(c) Fogg, D. E.; James, B. R.; *J. Organomet. Chem.*, **1993**, *462*, C21.
10. (a) Bennett, M. A.; Wilkinson, G. *Chem. Ind. (London)* **1959**, 1516.
(b) Ohta, T.; Noyori, R.; Takaya, H. *Inorg. Chem.* **1988**, *27*, 566.
(c) Kawano, H.; Ikariya, T.; Ishi, Y.; Saburi, M.; Yoshikawa, S.; Uchida, Y.; Kumobayashi, H. *J. Chem. Soc., Perkin Trans. 1* **1989**, 1571.
11. LaPlaca, S. J.; Ibers, J. A. *Inorg. Chem.* **1965**, *4*, 778.

12. (a) MacFarlane, K. S. Ph.D. Thesis, The University of British Columbia, 1995.
(b) MacFarlane, K. S.; Joshi, A. M.; Rettig, S. J.; James, B. R. *Inorg. Chem.* **1996**, *35*, 7304.
13. (a) James, B. R.; Thompson, L. K.; Wang, D. K. W. *Inorg. Chim. Acta* **1978**, *29*, L237.
(b) Jardine, F. H. *Prog. Inorg. Chem.* **1984**, *31*, 265.
(c) Dekleva, T. W.; Thorburn, I. S.; James, B. R. *Inorg. Chim. Acta* **1985**, *100*, 49.
14. (a) Bressan, M.; Rigo, P. *Inorg. Chem.* **1975**, *14*, 2286.
(b) James, B. R.; Wang, D. K. W. *Inorg. Chim. Acta* **1976**, *19*, L17.
(c) Wang, D. K. W. Ph.D. Thesis, The University of British Columbia, 1978.
(d) Thorburn, I. S. Ph.D. Thesis, The University of British Columbia, 1985.
(e) James, B. R.; Pacheco, A.; Rettig, S. J.; Thorburn, I. S.; Ball, R. G.; Ibers, J. A. *J. Mol. Catal.* **1987**, *41*, 147.
15. (a) Pregosin, P. S.; Kunz, R. W. *NMR: Basic Princ. Prog.* **1979**, *16*, 28.
(b) Krassowski, D. W.; Nelson, J. H.; Brower, K. R.; Hauenstein, D.; Jacobson, R. A. *Inorg. Chem.* **1988**, *27*, 4294.
16. MacFarlane, K. S.; Thorburn, I. S.; Cyr, P. W.; Chau, D. E. K.-Y.; Rettig, S. J.; James, B. R. *Inorg. Chim. Acta* **1998**, *270*, 130.
17. (a) Smith, P. M.; Fealey, T.; Earley, J. E.; Silverton, J. V. *Inorg. Chem.* **1971**, *10*, 1943.
(b) Llobet, A.; Curry, M. E.; Evans, H. T.; Meyer, T. J. *Inorg. Chem.* **1988**, *28*, 3131.
(c) Sasaki, Y.; Suzuki, M.; Nagasawa, A.; Tokiwa, A.; Ebihara, M.; Yamaguchi, T.; Kabuto, C.; Ochi, T.; Ito, T. *Inorg. Chem.* **1991**, *30*, 4903.
(d) Sudha, C.; Mandal, S. K.; Chakravarty, A. R. *Inorg. Chem.* **1993**, *32*, 3801.
18. Orpen, A. G.; Brammer, L.; Allen, F. H.; Kennard, O.; Watson, D. G.; Raylor, R. J. *Chem. Soc., Dalton Trans.* **1989**, S1.
19. Zhilyaev, A. N.; Kuz'menko, I. V.; Fomina, T. A.; Katser, S. B.; Baranovskii, I. B. *Russ. J. Inorg. Chem. (Engl. Transl.)*, **1993**, *38*, 847.
20. Weaver, T. R.; Meyer, T. J.; Adeyemi, S. A.; Brown, G. M.; Eckberg, R. P.; Hatfield, W. E.; Johnson, E. C.; Murray, R. W.; Untereker, D. *J. Am. Chem. Soc.* **1975**, *97*, 3039.
21. Sen, A.; Halpern, J. *J. Am. Chem. Soc.* **1977**, *99*, 8337.
22. Dekleva, T. W. Ph.D. Thesis, The University of British Columbia, 1983.

23. Bryndza, H. E.; Tam, W. *Chem. Rev.* **1988**, *88*, 1163, and references therein.
24. (a) Pearson, R. G. *J. Am. Chem. Soc.* **1963**, *85*, 3533.
(b) Pearson, R. G. *J. Chem. Educ.* **1968**, *45*, 643.
(c) Pearson, R. G. *Inorg. Chem.* **1988**, *27*, 734.
25. Chaudret, B. N.; Cole-Hamilton, D. J.; Nohr, R. S.; Wilkinson, G. *J. Chem. Soc., Dalton Trans.* **1977**, 1546.
26. Bryndza, H. E.; Fong, L. K.; Paciello, R. A.; Tam, W.; Bercaw, J. E. *J. Am. Chem. Soc.* **1987**, *109*, 1444.
27. Kaplan, A. W.; Bergman, R. G. *Organometallics* **1998**, *17*, 5072.
28. Hallman, P. S.; McGarvey, B. R.; Wilkinson, G. *J. Chem. Soc. (A)* **1968**, 3143.
29. (a) Daly, J. J. *J. Chem. Soc.* **1964**, 3799.
(b) Dunne, B. J.; Orpen, A. G. *Acta Cryst. C* **1991**, *47*, 345.
30. Meessen, P. H.; Rettig, S. J.; James, B. R. unpublished data.
31. Fritz, H. P.; Gordan, I. R.; Schwarzhans, K. E.; Venanzi, L. M. *J. Chem. Soc.* **1965**, 5210.
32. (a) Hampton, C.; Dekleva, T. W.; James, B. R.; Cullen, W. R. *Inorg. Chim. Acta* **1988**, *145*, 165.
(b) MacFarlane, K. S.; Joshi, A. M.; Rettig, S. J.; James, B. R. *J. Chem. Soc., Chem. Commun.* **1997**, 1363.
33. Guo, Z.; Habtemariam, A.; Sadler, P. J.; James, B. R. *Inorg. Chim. Acta* **1998**, *273*, 1.
34. Shen, J.-Y.; Slugovc, C.; Wiede, P.; Mereiter, K.; Schmid, R.; Kirchner, K. *Inorg. Chim. Acta* **1998**, *268*, 69.
35. Rauchfuss, T. B.; Patino, F. T.; Roundhill, D. M. *Inorg. Chem.* **1975**, *14*, 652.

Chapter 4

Transition Metal H₂S and Thiol Complexes: Synthesis and Characterization of *Cis*-RuX₂(P-N)(PR₃)(L); L = H₂S, Thiols

4.1 Introduction

A recent review on the coordination chemistry and catalytic conversions of H₂S indicates that such chemistry has received little attention in the literature.¹ The synthesis and isolation of H₂S and thiol transition metal complexes are rare because they are often unstable even in an O₂-free atmosphere and at low temperatures.² The instability of these complexes is often due to the acidic nature of H₂S and thiols; upon coordination, the acidic protons are often lost and metal thiolate or sulfide-bridged complexes are formed (see Chapter 1). In this Chapter, a brief summary of the H₂S and thiol metal complexes synthesized or observed prior to this work is described; and then the preparation and characterization of *cis*-RuX₂(P-N)(PPh₃)(L) (X = Br, Cl; L = H₂S, MeSH, EtSH) are discussed.

4.1.1 Transition Metal H₂S Complexes

The first reported crystal structure of a transition metal H₂S complex is that of [Ru(SH₂)(PPh₃)('S₄')].THF ('S₄')²⁻ = 1,2-bis[(2-mercaptophenyl)thio]ethane(2-)), obtained by Sellmann and co-workers.³ This complex was isolated by the reaction of polymeric [Ru(PPh₃)('S₄')]_x with liquid H₂S at -70°C (Figure 4.1(a)). Careful recrystallization from THF/pentane gave yellow crystals that were stable at 25°C under O₂-free conditions but slowly lost H₂S when stored *in vacuo*. In the unit cell, enantiomeric units of

$[\text{Ru}(\text{SH}_2)(\text{PPh}_3)(\text{'S}_4\text{'})]$ are associated via two $\text{S-H}\cdots\text{S}$ bridges and are bound to THF molecules via $\text{S-H}\cdots\text{O}$ bridges (see Figure 4.1(b)). The coordinated H_2S ligand is stabilized by strong hydrogen bonds with $\text{H}\cdots\text{S}$ and $\text{H}\cdots\text{O}$ distances of 2.58 and 2.16 Å, respectively. The two S-H bond lengths are 1.19 and 1.21 Å, shorter than those of gaseous H_2S , 1.33 Å.⁴ The $\nu_{\text{SH}\cdots\text{S}}$ is found at 2290 cm^{-1} and the $\nu_{\text{SH}\cdots\text{O}}$ at 2410 cm^{-1} . A broad ^1H NMR signal at $\delta\ 1.96$ is attributed to the H_2S ligand. Without solvated THF, this complex is highly labile even under an H_2S atmosphere. In the presence of O_2 , both complexes (solvent-free or solvated THF) are oxidized to the bridged disulfide complex $[(\mu\text{-S}_2)\{\text{Ru}(\text{PPh}_3)\text{'S}_4\}'_2]$ (Figure 4.1(c)).

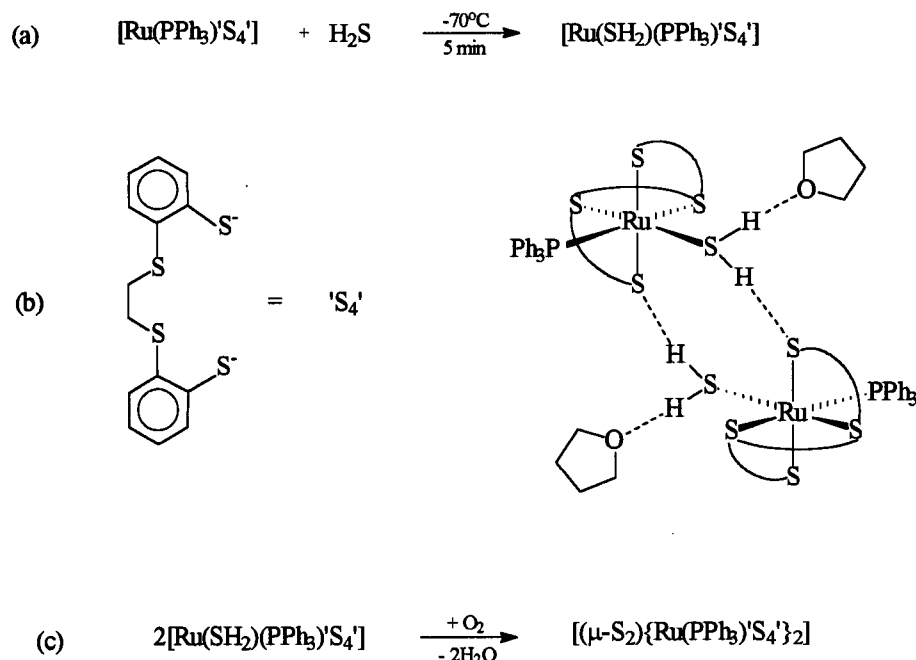


Figure 4.1 The (a) preparation, (b) structure and (c) oxidation of $[\text{Ru}(\text{SH}_2)(\text{PPh}_3)(\text{'S}_4\text{'})]$.

The unstable salts, $[\text{Ru}(\text{NH}_3)_5(\text{SH}_2)][\text{BF}_4]_2$ and *trans*- $[\text{Ru}(\text{NH}_3)_4(\text{SH}_2)(\text{isn})][\text{BF}_4]_2$ (isn = isonicotinamide), reported by Kuehn and Taube, were prepared by the displacement of H_2O or SO_4^{2-} ligands by H_2S in $[\text{Ru}(\text{NH}_3)_5(\text{OH}_2)][\text{BF}_4]_2$ and *trans*- $[\text{Ru}(\text{NH}_3)_4(\text{SO}_4)(\text{isn})]\text{Cl}$,

respectively.² Characterization included microanalysis, UV-Vis spectra and tentative assignment of a ν_{SH} band at 2547 cm^{-1} from the Raman spectrum of $[\text{Ru}(\text{NH}_3)_5(\text{SH}_2)][\text{BF}_4]_2$. Even in the absence of O_2 and H_2O , $[\text{Ru}(\text{NH}_3)_5(\text{SH}_2)][\text{BF}_4]_2$ decomposes to the Ru(III)-SH complex, $[\text{Ru}(\text{NH}_3)_5(\text{SH})][\text{BF}_4]_2$ and H_2 , the H_2 being detected by low resolution mass spectrometry. *Trans*- $[\text{Ru}(\text{NH}_3)_4(\text{SH}_2)(\text{isn})][\text{BF}_4]_2$ appeared to be indefinitely stable when stored *in vacuo*, and this was attributed to $\text{Ru}(\text{NH}_3)_4(\text{isn})^{2+}$ being less susceptible to oxidation than $\text{Ru}(\text{NH}_3)_5^{2+}$.

The Pt(0) species $[\text{Pt}(\text{PPh}_3)_2(\text{SH}_2)]$ was detected by Ugo et al.⁵ A broad ^1H NMR signal at δ 1.9 indicated the coordinated H_2S ligand, but this species is unstable and quickly formed $[\text{Pt}(\text{PPh}_3)_2(\text{SH})(\text{H})]$ via oxidative addition (Figure 4.2). The Pt(II) product was evidenced by ^1H NMR peaks at δ -1.4 (Pt-SH) and -9.2 (Pt-H).

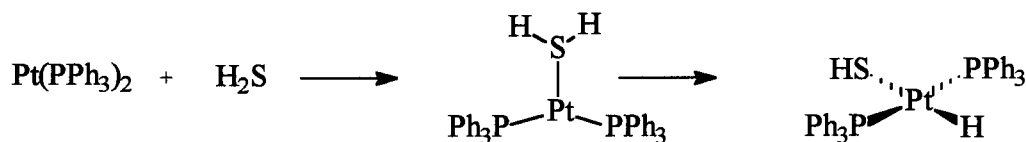


Figure 4.2 Formation of $[\text{Pt}(\text{PPh}_3)_2(\text{SH}_2)]$.

The formation of $\text{W}(\text{CO})_5(\text{SH}_2)$ can be achieved by the following methods: the photolysis of hexacarbonyltungsten(0) in the presence of H_2S ,⁶ displacement of THF with H_2S from $\text{W}(\text{CO})_5(\text{THF})$,⁶ or hydrolysis of $\text{W}(\text{CO})_5(\text{S}(\text{EMe}_3)_2)$ ($\text{E} = \text{Si}, \text{Sn}$)⁷ (Figure 4.3). Complex formation was detected by mass spectrometry (detection of the molecular ion $[\text{W}(\text{CO})_5(\text{SH}_2)]^+$); IR data (ν_{SH} at 2560 cm^{-1}); and a ^1H NMR singlet at δ 0.60 due to the H_2S ligand. The stability of this complex was attributed to the inert carbonyl fragment $\text{W}(\text{CO})_5$.

At 90°C under N₂, or at 20°C under vacuum, the green crystals of W(CO)₅(SH₂) underwent decomposition.

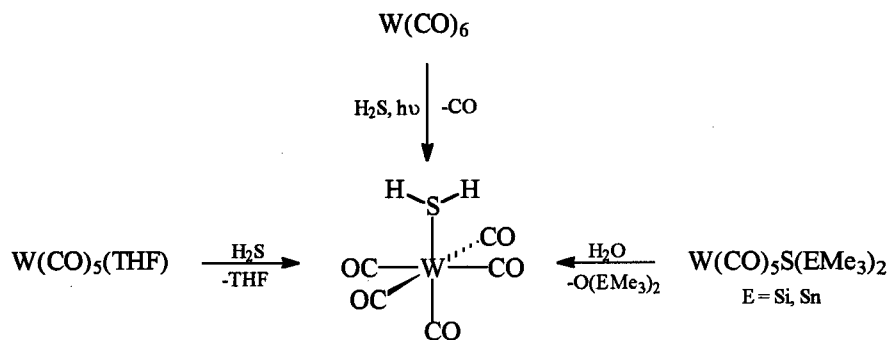


Figure 4.3 Formation of W(CO)₅(SH₂).

The displacement of H₂O by H₂S in *cis*-[Mn(CO)₄(PPh₃)(OH₂)] [BF₄] is thought to result in the formation of *cis*-[Mn(CO)₄(PPh₃)(SH₂)] [BF₄] (Figure 4.4(a)).⁸ A very weak ν_{SH} band is located at 2535 cm⁻¹ and a ¹H NMR multiplet is observed at δ -0.40 due to coordinated H₂S. Exposure of this complex to air or moisture resulted in the reformation of *cis*-[Mn(CO)₄(PPh₃)(OH₂)] [BF₄]. Previously, a similar manganese carbonyl complex, [Mn(CO)₂(η⁵-C₅H₅)(SH₂)], had been reported but was unstable and poorly characterized.⁹ Other reports of metal carbonyl H₂S complexes include [Re(CO)₅(SH₂)] [BF₄]¹⁰ (Figure 4.4(b)) and [M(CO)₃(η⁵-C₅H₅)(SH₂)]X (M = Mo, X = BF₄; M = W, X = AsF₆) (Figure 4.4(c))¹¹. The complexes are unstable at ambient conditions and their formations were supported only by IR ν_{SH} bands at 2510, 2590 and 2548 cm⁻¹, respectively.

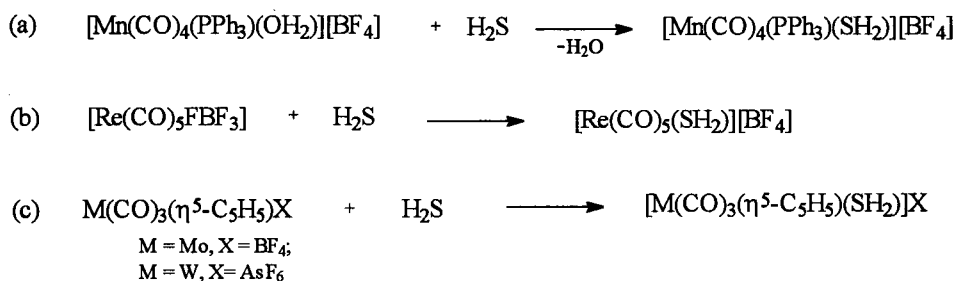


Figure 4.4 Formation of metal carbonyl H₂S salts.

The proposed unstable white product from the solid state reaction of $[\text{Ir}(\text{H})_2(\text{Me}_2\text{CO})_2(\text{PPh}_3)_2][\text{BF}_4]$ with H₂S was claimed to be $[\text{Ir}(\text{H})_2(\text{H}_2\text{S})_2(\text{PPh}_3)_2][\text{BF}_4]$,¹² although no evidence of H₂S coordination was presented.

Amarasekera and Rauchfuss observed formation of $[\text{CpRu}(\text{PPh}_3)_2(\text{SH}_2)][\text{OTf}]$ upon protonation of $\text{CpRu}(\text{PPh}_3)_2(\text{SH})$ with HOTf, or treatment of $\text{CpRu}(\text{PPh}_3)_2\text{OTf}$ with H₂S.¹³ The ¹H NMR signal of coordinated H₂S appeared at δ 3.58 (t) (³J_{HP} = 7.2 Hz), but isolation of this complex was not possible because of reversion to $\text{CpRu}(\text{PPh}_3)_2\text{OTf}$. A similar complex $[(\text{ThiCp})\text{Ru}(\text{PPh}_3)_2(\text{SH}_2)][\text{OTf}]$ was observed as the intermediate formed during the protonation of $(\text{ThiCp})\text{Ru}(\text{PPh}_3)_2(\text{SH})$ with HOTf en route to $[(\text{ThiCp})\text{Ru}(\text{PPh}_3)_2][\text{OTf}]$; conversion of the SH to H₂S provided a liable coordination site for weak ligands such as thiophenes (Figure 4.5).¹³

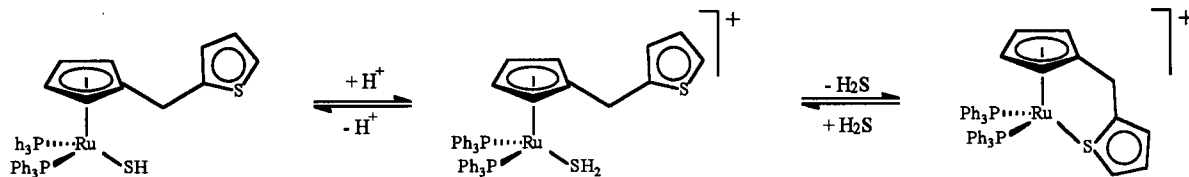


Figure 4.5 Formation of $[(\text{ThiCp})\text{Ru}(\text{PPh}_3)_2][\text{OTf}]$.

4.1.2 Transition Metal Thiol Complexes

Although thiol ligands contain one less acidic proton than H_2S , thiol complexes are also rare, and only a few have been well characterized either spectroscopically or crystallographically.

In the same report describing formation of $[\text{CpRu}(\text{PPh}_3)_2(\text{SH}_2)][\text{OTf}]$ and $[(\text{ThiCp})\text{Ru}(\text{PPh}_3)_2(\text{SH}_2)][\text{OTf}]$, the crystal structure of $[\text{CpRu}(\text{PPh}_3)_2(\text{HSP}^n)][\text{BF}_4]$ was determined.¹³ The crystals were unintentionally obtained from the reaction of $\text{CpRu}(\text{PPh}_3)_2\text{Cl}$, thiophene and AgBF_4 (Figure 4.6(a)); the HSP^n ligand is undoubtedly an impurity in the thiophene solution. The Ru-S and S-H bond distances are 2.377 and 1.25 Å, respectively. Other thiol complexes of this type were also prepared directly from the reactions of thiols with $\text{CpRu}(\text{PPh}_3)_2\text{OTf}^4$ or the alkylation of $\text{CpRu}(\text{PPh}_3)_2\text{SH}$.¹³ For example, $[\text{CpRu}(\text{PPh}_3)_2(\text{CH}_3\text{SH})][\text{OTf}]$ was prepared by treatment of $\text{CpRu}(\text{PPh}_3)_2\text{SH}$ with CH_3OTf (Figure 4.6(b)),¹³ in the ^1H NMR spectrum, the *SH* proton appears as a multiplet at δ 4.22, and the *CH*₃ protons as a doublet at δ 2.23. Draganjac and co-workers have also shown that similar thiol complexes, $[\text{CpRu}(\text{PPh}_3)_2(\text{RSH})][\text{BF}_4]$ (R = benzyl and phenethyl), can be obtained by the reaction of $\text{CpRu}(\text{PPh}_3)_2\text{Cl}$ and AgBF_4 with the appropriate mercaptan (Figure 4.6(c)).¹⁵ For $[\text{CpRu}(\text{PPh}_3)_2(\text{C}_6\text{H}_5\text{CH}_2\text{SH})][\text{BF}_4]$ and $[\text{CpRu}(\text{PPh}_3)_2(\text{C}_6\text{H}_5\text{CH}_2\text{CH}_2\text{SH})][\text{BF}_4]$, the thiol ligands are detected by IR ($\nu_{\text{SH}} = 2525$ and 2515 cm^{-1} , respectively) and ^1H NMR spectroscopy (triplet at δ 4.17 and quintet at δ 3.99 due the *SH* groups, respectively). Furthermore, the crystal structure of the phenethyl complex was solved and the thiol hydrogen was located with the Ru-S and S-H bond distances being 2.36(2) and 1.18 Å, respectively. The electron rich CpRu moiety could also stabilize sterically bulky thiols as shown by the formation of $[\text{CpRu}(\text{PPh}_3)(\text{Bu}^t\text{NC})(\text{Bu}^t\text{SH})][\text{PF}_6]$ (IR: $\nu_{\text{SH}} =$

2544 cm^{-1} ; ^1H NMR: SH doublet at δ 3.03) and $[\text{CpRu}(\text{dppm})(\text{Bu}^t\text{SH})][\text{PF}_6]$ (^1H NMR: SH triplet at δ 2.74).¹⁶ These complexes were obtained from the reaction of $\text{CpRu}(\text{PPh}_3)(\text{Bu}^t\text{NC})\text{Cl}$ or $\text{CpRu}(\text{dppm})\text{Cl}$ with Bu^tSH and NH_4PF_6 (Figure 4.6(d)). The crystal structure of $[\text{CpRu}(\text{dppm})(\text{Bu}^t\text{SH})][\text{PF}_6]$ was obtained and the Ru-S and S-H bond lengths were determined to be 2.371(2) and 1.349(77) Å, respectively. Although no spectroscopic or crystallographic evidence was provided, the air-sensitive species $[\text{CpRu}\{\text{PPh}_2(\text{OMe})\}_2(\text{Bu}^t\text{SH})][\text{PF}_6]$ ¹⁷ and $[\text{CpM}(\text{P}(\text{OMe})_3)_2(\text{PhSH})][\text{PF}_6]$ ($\text{M} = \text{Ru}, \text{Fe}$)¹⁸ were reported by Treichel et al. (Figure 4.6(f)). Oxidation in air resulted in the formation of the paramagnetic Ru(III)-thiolate complexes, $[\text{CpRu}\{\text{PPh}_2(\text{OMe})\}_2(\text{SBu}^t)][\text{PF}_6]$ and $[\text{CpM}(\text{P}(\text{OMe})_3)_2(\text{SPh})][\text{PF}_6]$. It was also found that $[\text{CpRu}(\text{P}(\text{OMe})_3)_2(\text{PhSH})][\text{PF}_6]$ could be easily deprotonated by LDA to form $\text{CpRu}(\text{P}(\text{OMe})_3)_2(\text{SPh})$.

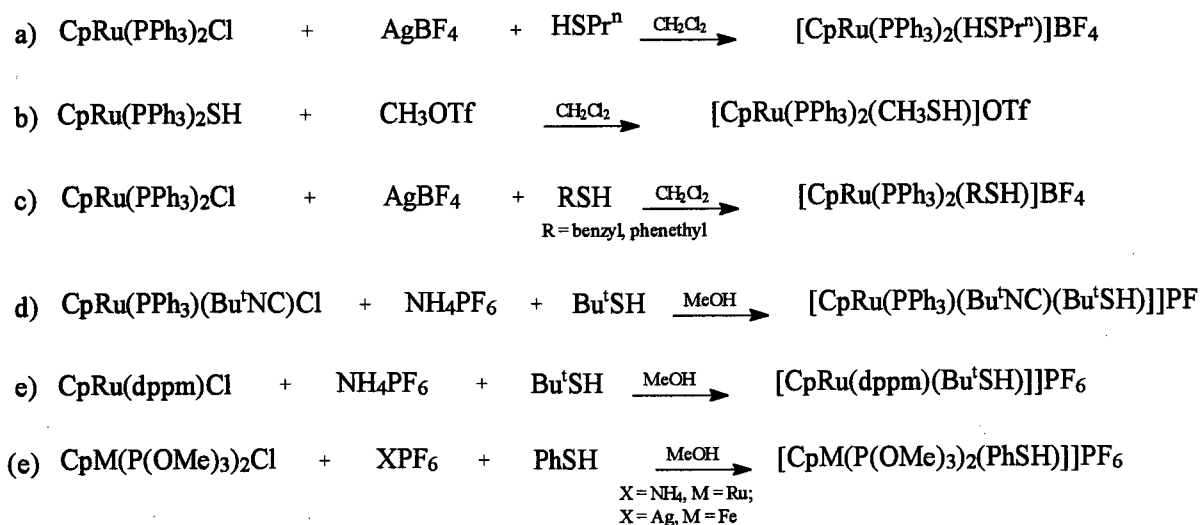


Figure 4.6 Preparation of thiol complexes containing the electron rich CpM ($\text{M} = \text{Ru}, \text{Fe}$) moieties.

More recently, Tocher's group has reported the formation of $[\text{Ru}(\eta^3\text{:}\eta^3\text{-C}_{10}\text{H}_{16})\text{Cl}_2(\text{HSR})]$ ($\text{R} = \text{Me}, \text{Et}, \text{Pr}^i, \text{Bu}^t, \text{Ph}$) from the reaction of the Ru(IV) chloro-bridged dimer $[\{\text{Ru}(\eta^3\text{:}\eta^3\text{-C}_{10}\text{H}_{16})\text{Cl}(\mu\text{-Cl})\}_2]$ with thiols (Figure 4.7).¹⁹ Supporting evidence for the coordination of thiols was given by IR and ^1H NMR data. The ν_{SH} bands for the above complexes were found at 2424, 2423, 2471, 2458 and 2460 cm^{-1} , respectively. Sharp ^1H NMR SH resonances (δ 3.46 (t), $\text{R} = \text{Et}$; δ 3.51 (q), $\text{R} = \text{Me}$) were interpreted as resulting from strong intramolecular hydrogen-bonding of the thiol hydrogen to the chlorine, while broad SH resonances (δ 3.48, $\text{R} = \text{Pr}^i$; δ 3.29, $\text{R} = \text{Bu}^t$; δ 5.56, $\text{R} = \text{HSPH}$) indicated that these thiol complexes are in dynamic equilibrium with the starting material.

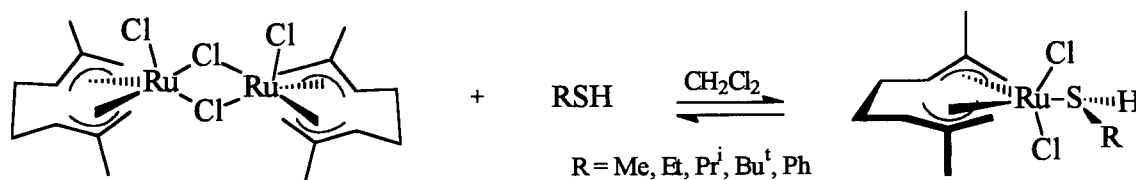


Figure 4.7 Formation of $[\text{Ru}(\eta^3\text{:}\eta^3\text{-C}_{10}\text{H}_{16})\text{Cl}_2(\text{HSR})]$.

Darensbourg et al. have reported a series of Cr(0) thiol complexes containing carbonyl ligands, $\text{Cr}(\text{CO})_4(\text{RSH})\text{L}$ ($\text{L} = \text{CO}, \text{PEt}_3$; $\text{R} = \text{Bu}^t, \text{Et}, \text{Pr}^i, \text{Ph}$), which were prepared by the reaction of $\text{Cr}(\text{CO})_5(\text{THF})$ with RSH or the protonation of $\text{Cr}(\text{CO})_4(\text{RS})\text{L}^-$ with HBF_4 .²⁰ These species were characterized by ^1H NMR SH resonances at $\delta \sim 1.0$. The crystal structure of $\text{Cr}(\text{CO})_5(\text{Bu}^t\text{SH})$ revealed Cr-S and S-H bond lengths of 2.439(2) and 1.2(1) Å, respectively.

Treatment of TiCl_4 with cyclohexane- or cyclopentanethiol afforded the moisture-sensitive, yellow solids, $[\text{TiCl}_4(\text{RSH})_2]$.²¹ In addition to sharp IR ν_{SH} bands found at

$\sim 2500\text{ cm}^{-1}$, the crystal structure of $[\text{TiCl}_4(\text{C}_6\text{H}_{11}\text{SH})_2]$ was determined, but the thiol H-atoms were not located.

The X-ray crystal structure of $\text{FeTPP}(\text{C}_6\text{H}_5)(\text{C}_6\text{H}_5\text{SH})$ (TPP = tetraphenylporphyrin), was determined by Collman et al.²² This complex was used as a dynamic model to study substrate binding in the catalytic cycle of P450 enzymes. Electronic structures based on single-crystal ESR measurements were obtained at low temperatures (77–173 K) for the above complex and the similar ferric complexes: $\text{Fe}(\text{NH}_2\text{TPP})(\text{SPh})(\text{HSPh})$, $\text{FeTPP}(\text{S-}m\text{-tolyl})(\text{HS-}m\text{-tolyl})$, $\text{FeTPP}(\text{SCH}_2\text{C}_6\text{H}_5)(\text{HSCH}_2\text{C}_6\text{H}_5)$ and $\text{FeTPP}(\text{S}(\text{CH}_2)_2\text{CH}(\text{CH}_3)_2)(\text{HS}(\text{CH}_2)_2\text{CH}(\text{CH}_3)_2)$.²³ Both types of structural determination, however, were unsuccessful in locating the thiol H-atoms.

The thiol group can also coordinate to metal centres as part of a bidentate ligand as shown by the structure of $[\text{IrH}(\text{SCH}_2\text{CH}_2\text{PPh}_2)(\text{HSCH}_2\text{CH}_2\text{PPh}_2)(\text{CO})]\text{Cl}$, formed by the reaction of *trans*- $\text{Ir}(\text{PPh}_3)_2(\text{CO})\text{Cl}$ with excess $\text{HSCH}_2\text{CH}_2\text{PPh}_2$ (Figure 4.8)²⁴. X-ray structural determination showed an S–H bond distance of $1.354(10)\text{ \AA}$. Stabilization of the S–H group was attributed to the chelating mixed P–S ligand.

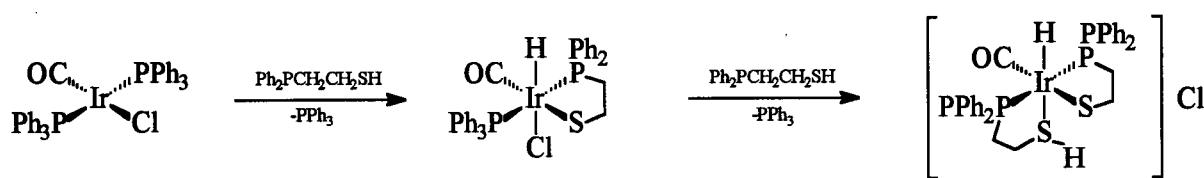


Figure 4.8 Preparation of $[\text{IrH}(\text{SCH}_2\text{CH}_2\text{PPh}_2)(\text{HSCH}_2\text{CH}_2\text{PPh}_2)(\text{CO})]\text{Cl}$.

Morris and co-workers have prepared a series of metal-thiol complexes obtained by the protonation of metal-thiolate complexes with HBF_4 . The reaction of $\text{MH}(\text{CO})(\text{N-S})(\text{PPh}_3)_2$ ($\text{M} = \text{Ru}, \text{Os}$; $\text{N-S} = \text{pyridine-2-thiolate}, \text{quinoline-8-thiolate}$) with

excess HBF_4 at 193 K gave $[\text{MH}(\text{CO})(\text{N-SH})(\text{PPh}_3)_2][\text{BF}_4]$ (Figure 4.9),²⁵ the intermediate $[\text{M}(\eta^2\text{-H}_2)(\text{CO})(\text{N-S})(\text{PPh}_3)_2][\text{BF}_4]$ being observed by NMR spectroscopy at 213 K en route to the formation of the thiol species. Both species, however, decompose at temperatures above 273 K. ^1H NMR spectroscopy located the protons of the coordinated thiol groups as doublet of doublets (coupling to two inequivalent P atoms) at $\delta \sim 4.7$. Similarly, reactions of *trans*- $\text{M}(\text{H})(\text{SPh})(\text{dppe})_2$ ($\text{M} = \text{Ru}, \text{Os}$; $\text{dppe} = 1,2\text{-bis}(\text{diphenylphosphino})\text{ethane}$) with HBF_4 resulted in *trans*- $[\text{M}(\text{H})(\text{HSPh})(\text{dppe})_2][\text{BF}_4]$.²⁶ Only the more stable Os complex was characterized by ^1H NMR where a broad resonance at δ 4.4 was assigned to the coordinated thiol.

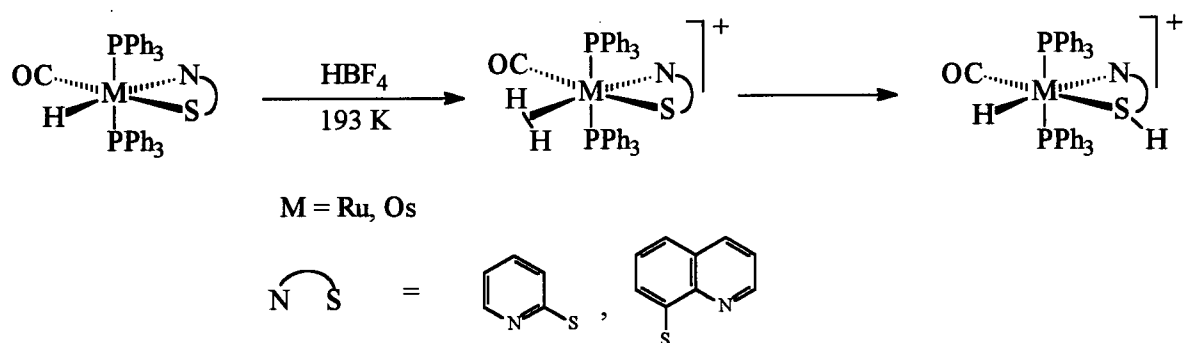


Figure 4.9 *In situ* formation of $[\text{MH}(\text{CO})(\text{N-SH})(\text{PPh}_3)_2][\text{BF}_4]$.

4.2 Synthesis and Characterization of *Cis*- $\text{RuX}_2(\text{P-N})(\text{PPh}_3)(\text{SH}_2)$, $\text{X} = \text{Cl}, \text{Br}, \text{I}$

When acetone or CD_2Cl_2 solutions of $\text{RuX}_2(\text{P-N})(\text{PPh}_3)$ are stirred under 1 atm of H_2S , the complexes *cis*- $\text{RuX}_2(\text{P-N})(\text{PPh}_3)(\text{SH}_2)$ are rapidly formed. These complexes are dark yellow, diamagnetic, stable at ambient conditions, and decompose only slowly due to the loss of H_2S . The *cis*- $\text{RuX}_2(\text{P-N})(\text{PPh}_3)(\text{SH}_2)$ species with $\text{X} = \text{Cl}$ and Br were characterized by X-ray crystallography.

4.2.1 *Cis*-RuCl₂(P-N)(PPh₃)(SH₂) (**18a**)

The prismatic crystals of *cis*-RuCl₂(P-N)(PPh₃)(SH₂) (**18a**) containing one acetone molecule per molecule of complex formed from a concentrated acetone solution containing RuCl₂(P-N)(PPh₃) (**6a**) under 1 atm H₂S. The X-ray crystal structure of **18a** (Figure 4.10) was determined and was found to be isostructural with that of *cis*-RuCl₂(P-N)(P(*p*-tolyl)₃)(SH₂) (**19a**), previously determined in this laboratory.^{27b, 28} However, contrary to the case with **19a**, where only one H-atom of the H₂S was located, both H-atoms bonded to the S-atom were isotropically refined for **18a**. Figure 4.10 reveals a pseudo-octahedral geometry around the Ru with *cis*-chloro ligands and the H₂S *trans* to one chlorine.

Selected bond lengths and angles for **18a** and **19a** are shown in Tables 4.1 and 4.2, respectively. The chelate bite angle P(1)-Ru(1)-N(1) in **18a** is 83.09(5)°, slightly larger than 81.81(8) and 81.3(3)° of the RuCl₂(P-N)(P(*p*-tolyl)₃) precursor **7a** and **19a**, respectively. For **18a**, the average *trans*-bond angle at Ru is ~172°; with the exception of 103.11(2)° for P(1)-Ru(1)-P(2) which can be attributed to the repulsion of the phenyl groups on the P-atoms, the *cis*-bond angles are approximately 89°. No significant differences were observed for the bond lengths around the Ru between **18a** and **19a**. The Ru-S bond distances, 2.3503(3) and 2.330(4) Å, are comparable to that of 2.399(5) Å in Sellmann's complex, [Ru(SH₂)(PPh₃)('S₄')],³ but are significantly shorter than those of terminal Ru-SH complexes (2.46 Å).^{29,30} However, in contrast to [Ru(SH₂)(PPh₃)('S₄')], where the H-S-H angle is 77° due to hydrogen bridges (see Figure 4.1), the 101.7(17)° angle is much larger in **18a**; the H-S-H bond angle is 92.2° for gaseous H₂S³¹. While the two S-H bond

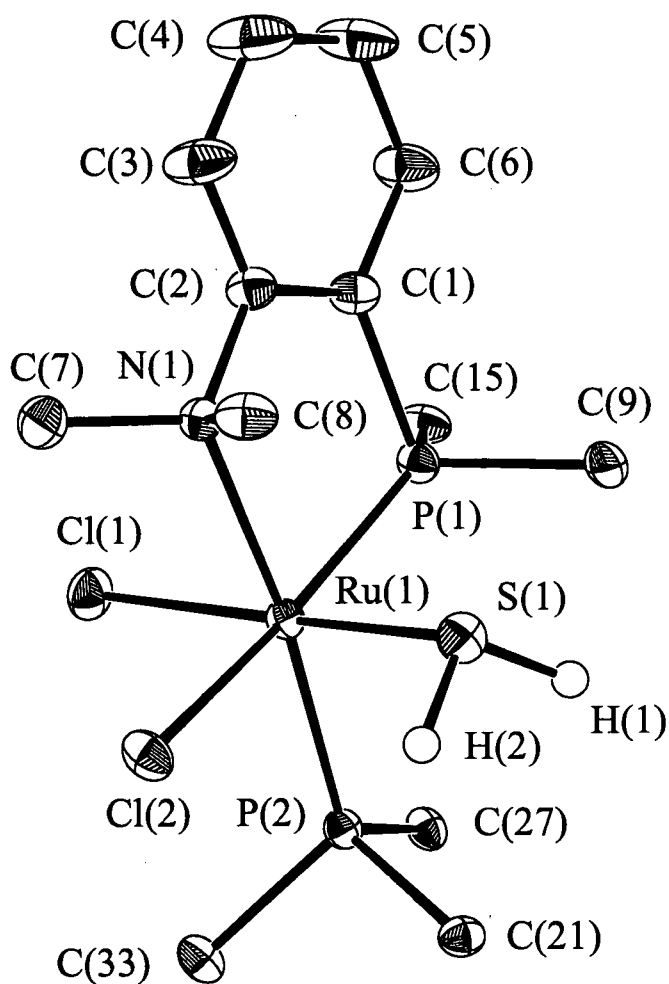


Figure 4.10 The ORTEP plot of *cis*-RuCl₂(P-N)(PPh₃)(SH₂) (**18a**). Thermal ellipsoids for non-hydrogen atoms are drawn at 33 % probability (some of the phenyl carbons have been omitted for clarity). Full experimental parameters and details are given in Appendix IV.

Table 4.1 Selected bond lengths (Å) for *cis*-RuCl₂(P-N)(PPh₃)(SH₂) (**18a**) and *cis*-RuCl₂(P-N)(P(*p*-tolyl)₃)(SH₂) (**19a**) with estimated standard deviations in parentheses.

Bond	Length (Å)		Bond	Length (Å)	
	18a	19a		18a	19a
Ru(1)-S(1)	2.3503(3)	2.330(4)	Ru(1)-Cl(1)	2.4238(6)	2.429(3)
Ru(1)-P(1)	2.2712(6)	2.256(4)	Ru(1)-Cl(2)	2.4721(5)	2.469(4)
Ru(1)-P(2)	2.3110(7)	2.304(3)	S(1)-H(1)	1.20(3)	1.25
Ru(1)-N(1)	2.338(2)	2.37(10)	S(1)-H(2)	1.30(3)	N/A

Table 4.2 Selected bond angles (°) for *cis*-RuCl₂(P-N)(PPh₃)(SH₂) (**18a**) and *cis*-RuCl₂(P-N)(P(*p*-tolyl)₃)(SH₂) (**19a**) with estimated standard deviations in parentheses.

Bond	Angles (°)		Bond	Angles (°)	
	18a	19a		18a	19a
H(1)-S(1)-H(2)	101.7(17)	N/A	S(1)-Ru(1)-P(1)	90.54(2)	93.8(1)
Ru(1)-S(1)-H(1)	110.7(12)	124.2	S(1)-Ru(1)-P(2)	93.76(2)	92.7(1)
Ru(1)-S(1)-H(2)	103.3(11)	N/A	S(1)-Ru(1)-N(1)	89.18(5)	89.8(2)
Cl(1)-Ru(1)-S(1)	175.18(2)	174.6(1)	Cl(2)-Ru(1)-P(1)	168.03(2)	170.0(1)
Cl(2)-Ru(1)-S(1)	82.63(2)	83.1(1)	Cl(2)-Ru(1)-P(2)	87.21(2)	88.0(1)
Cl(1)-Ru(1)-P(1)	91.95(2)	88.0(1)	Cl(2)-Ru(1)-N(1)	86.97(4)	89.1(3)
Cl(1)-Ru(1)-P(2)	89.70(2)	91.9(1)	P(1)-Ru(1)-P(2)	103.11(2)	101.7(1)
Cl(1)-Ru(1)-N(1)	87.03(5)	85.4(2)	P(1)-Ru(1)-N(1)	83.09(5)	81.3(3)
Cl(1)-Ru(1)-Cl(2)	94.19(2)	94.3(1)	P(2)-Ru(1)-N(1)	173.09(5)	175.9(3)

lengths are nearly identical (1.19 and 1.21 Å) in Sellmann's complex, they are slightly different in **18a** with lengths of 1.20(3) and 1.30(3) Å. Upon coordination of the H₂S to Ru, the S-H bonds are shortened with respect to those of gaseous H₂S, 1.33 Å^{4,31}. The S(1)-H(1) bond length compares with 1.25 Å of **19a**, while the longer S(1)-H(2) bond distance of 1.30 Å is attributed to intramolecular hydrogen-bonding between H(2) and Cl(2); the H...Cl distance is 2.69(3) Å, which is less than the van der Waals distance of 3.00 Å.³² The non-linear S-H...Cl angle of 100(1)° indicates that this interaction is quite weak as maximum orbital overlap is not attained. As a result of hydrogen-bonding, the Cl(2)-Ru-S and Ru-S-H(2) planes differ by only 20.85°, while H(1) is positioned at 60° under the Cl(1)-Cl(2)-S-P(1) plane. There are no apparent interactions between the coordinated H₂S and acetone solvate.

Both H-atoms of the coordinated H₂S point toward the planes of phenyl groups of PPh₃ and P-N. Osakada et al. suggested that SH/π interactions (2.69 Å and 2.63 Å) exist between bridging mercapto groups and the planes of phenyl groups in the dinuclear complex (PhMe₂P)₃Ru(μ-SH)₃Ru(SH)(PMe₂Ph)₂ (Figure 4.11).²⁹ In **18a**, the closest phenyl/SH distances are H(1)...C(9) and H(2)...C(21) with values of 2.80 and 2.97 Å, respectively. These are slightly less than the sum of 2.99 Å for the van der Waals radii of the two atoms. Therefore, weak SH/π interactions may play a role in stabilizing the H₂S in **18a**.

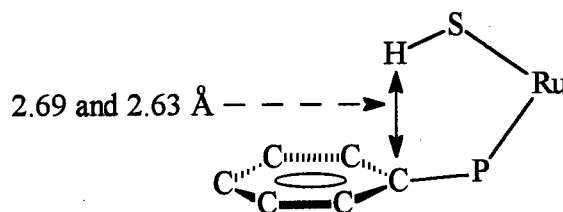


Figure 4.11 Bond distances between H-atom and nearest C-atom of phenyl ring to indicate SH/π interactions in (PhMe₂P)₃Ru(μ-SH)₃Ru(SH)(PMe₂Ph)₂.

The $^{31}\text{P}\{^1\text{H}\}$ NMR spectrum of **18a** in CD_2Cl_2 and under 1 atm H_2S gave an AX pattern at δ 49.81 and 43.30 ($^2J_{\text{PP}} = 28.78$ Hz) characteristic of *cis*-P atoms (Figure 4.12(a)).²⁷ In the ^1H NMR spectrum, the Ru-SH₂ resonances gave a broad peak at δ 1.03 in C_6D_6 (Figure 4.13) but this must be obscured by the free H_2S peak in CD_2Cl_2 (Figure 4.14(a)). The signals due to the two -N(CH₃) groups are seen at δ 3.40 and 3.13, characteristic of the symmetry imposed by the *cis*-Cl atoms. These observations are very similar to those previously found by Mudalige et al.²⁷

A variable temperature NMR study of **18a** was carried out in CD_2Cl_2 . Figure 4.12 shows the P_X signal is shifted downfield slightly, while the P_A peak is shifted upfield more significantly as the temperature is decreased from 20 to -90°C. The changes in chemical shifts are perhaps due to the diminishing rates of Ru-SH₂ bond rotation or sulfur ligand inversion at low temperatures.

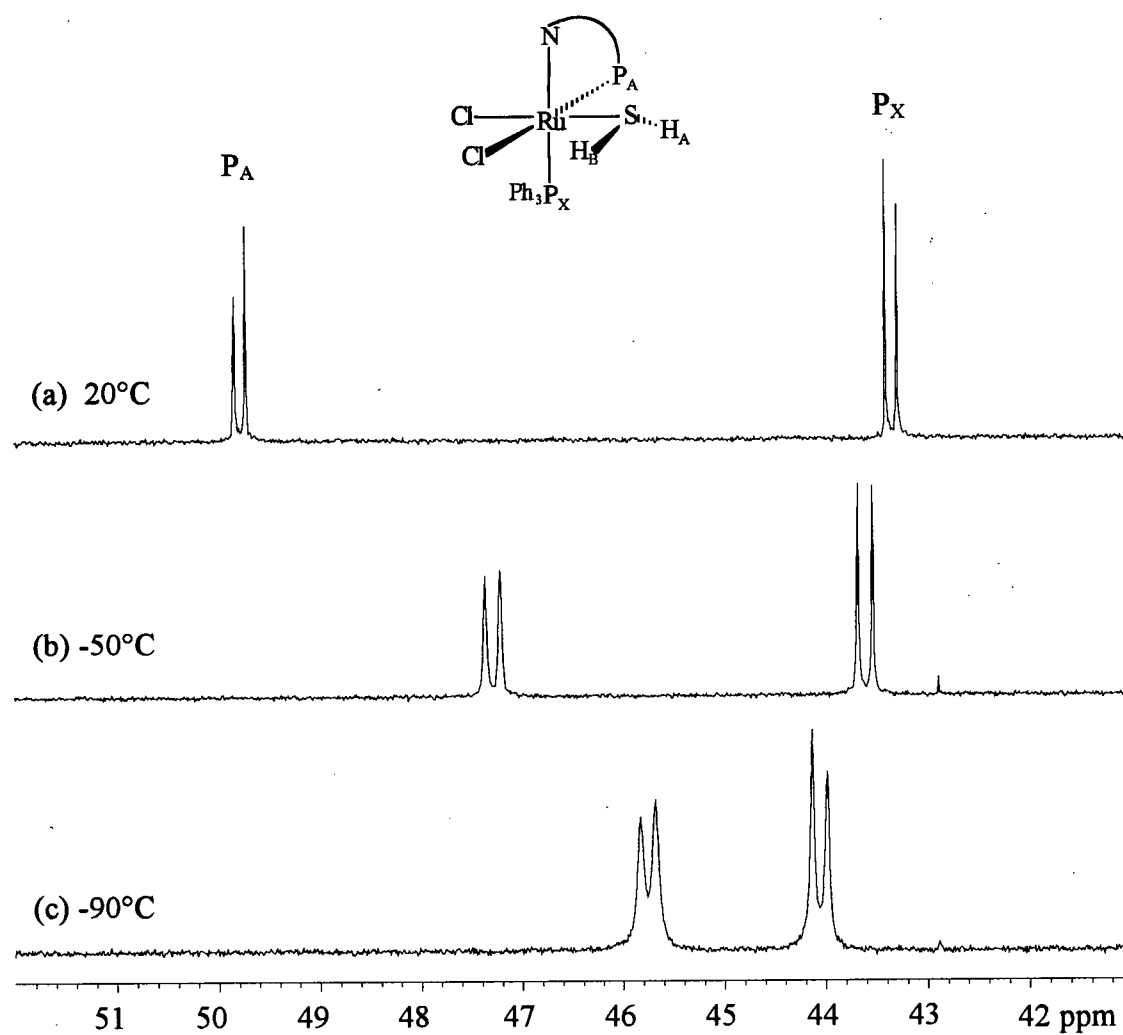


Figure 4.12 $^{31}\text{P}\{^1\text{H}\}$ NMR spectra (202.47 MHz) of *cis*-RuCl₂(P-N)(PPh₃)(SH₂) (18a) in CD₂Cl₂ at various temperatures. Sample is under 1 atm of H₂S.

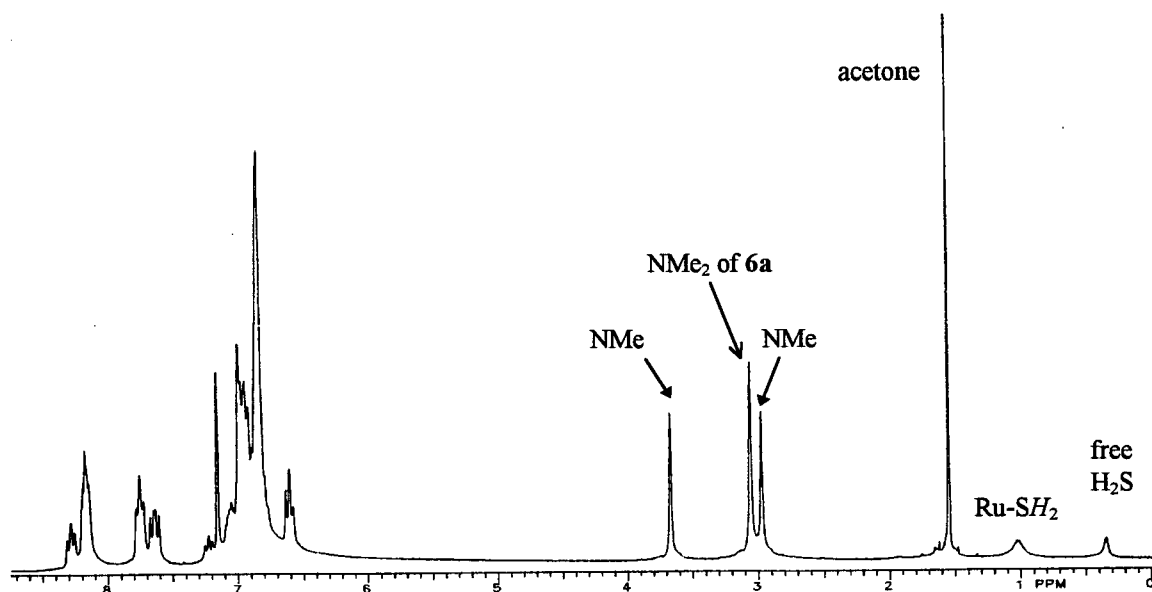


Figure 4.13 ^1H NMR spectra (121.4 MHz) of *cis*- $\text{RuCl}_2(\text{P-N})(\text{PPh}_3)(\text{SH}_2) \cdot (\text{acetone})$ (**18a**) in C_6D_6 . Note: **18a** is in equilibrium with $\text{RuCl}_2(\text{P-N})(\text{PPh}_3)$ (**6a**) (δ 3.07, NMe_2) and free H_2S (δ 0.35).

At -50°C , the ^1H NMR spectrum (Figure 4.14(b)) is the most informative, giving well resolved peaks; these became broader as the temperature approaches the freezing point of CD_2Cl_2 (-95°C). At -50°C , the signals due to the two $-\text{N}(\text{CH}_3)$ groups become closer together (δ 3.22 and 3.19) than at 20°C . The Ru-SH_2 resonances, originally hidden under the free H_2S signal at 20°C , are now resolved into a doublet of doublets at δ 1.49 (H_B) and a doublet at δ 0.30 (H_A). The doublets show that H_A and H_B are mutually coupled ($^2J_{\text{HH}} = 12.3 \text{ Hz}$), while H_B must be coupled to a P-atom while H_A is not ($^3J_{\text{HP}} = 3.50 \text{ Hz}$). The $^1\text{H}\{^{31}\text{P}\}$ NMR spectrum (Figure 4.15) was also measured at -50°C , and the H_B multiplet was reduced to a doublet while the H_A resonance remains unchanged. From these data, it was not apparent whether H_B was coupled to P_A or P_X . $^1\text{H}\{^{31}\text{P}\}$ GARP (Globally optimized Alternating-phase Rectangular Pulses)³³ NMR experiments were performed to observe

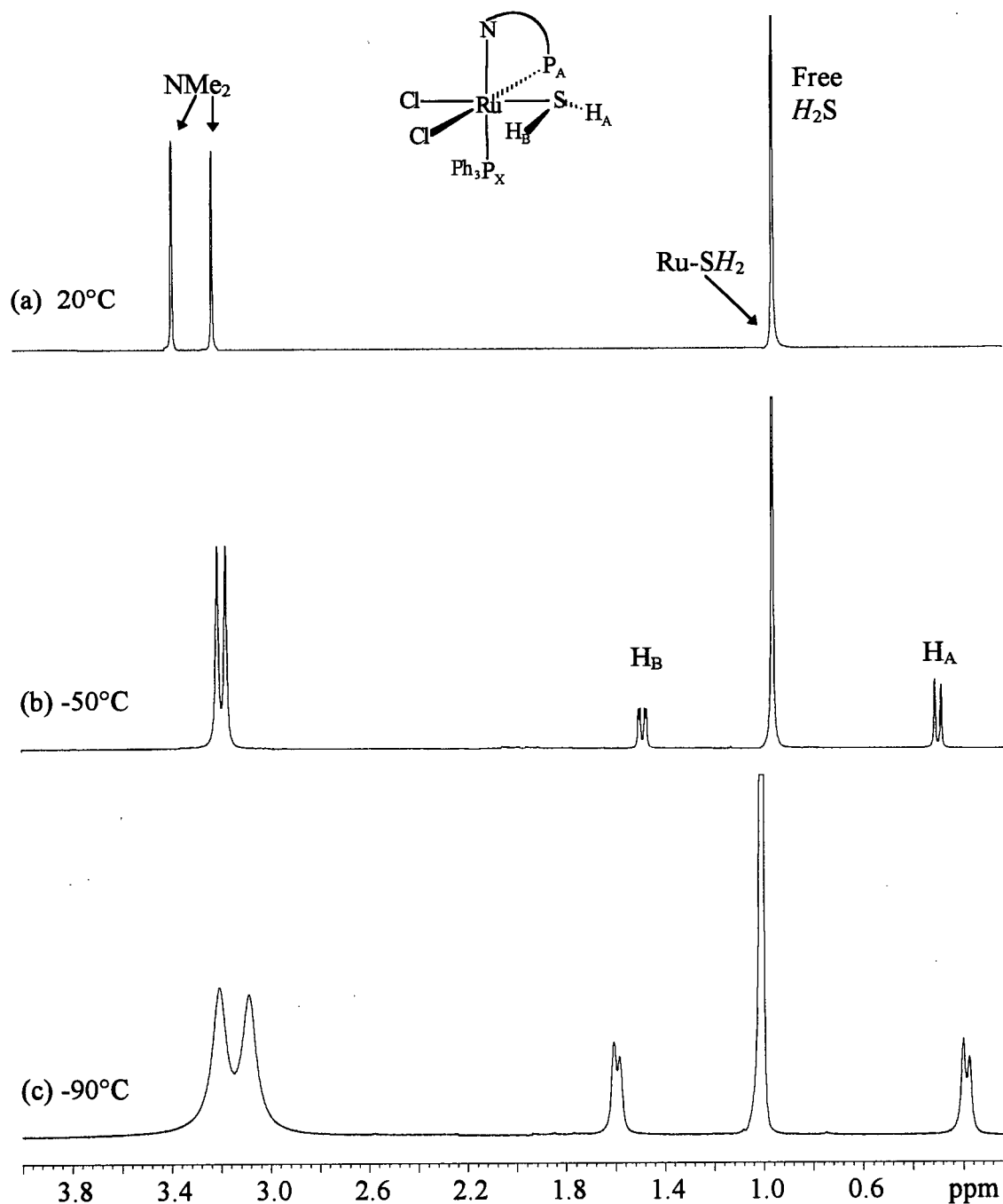


Figure 4.14 VT ^1H NMR spectra (500 MHz) of *cis*- $\text{RuCl}_2(\text{P-N})(\text{PPh}_3)(\text{SH}_2)$ (**18a**) in CD_2Cl_2 (under 1 atm H_2S) for the region δ 0.0 to δ 4.0. Note: the NMe_2 peak of $\text{RuCl}_2(\text{P-N})(\text{PPh}_3)$ (δ 3.19 in CD_2Cl_2) is no longer seen due to the presence of excess H_2S .

effects on the H_B signal. With the first scanning radiofrequency set at 500.1386730 MHz to observe the 1H region, the second irradiating frequency is centred either on the resonance of P_A at 202.4685838 MHz, δ 47.0, or P_B at 202.4677665 MHz, δ 43.0. The decoupler power was then varied by changing the attenuation (dB). With the decoupler set at δ 47.0, the H_B resonance became more decoupled to P_A as the decoupler power was increased (Figure 4.16). The above experiment was repeated with the decoupler transmitter centred at 202.4677665 MHz. However, variation of the attenuation power at this frequency had no effect on H_B . Evidently, H_B is coupled to P_A .

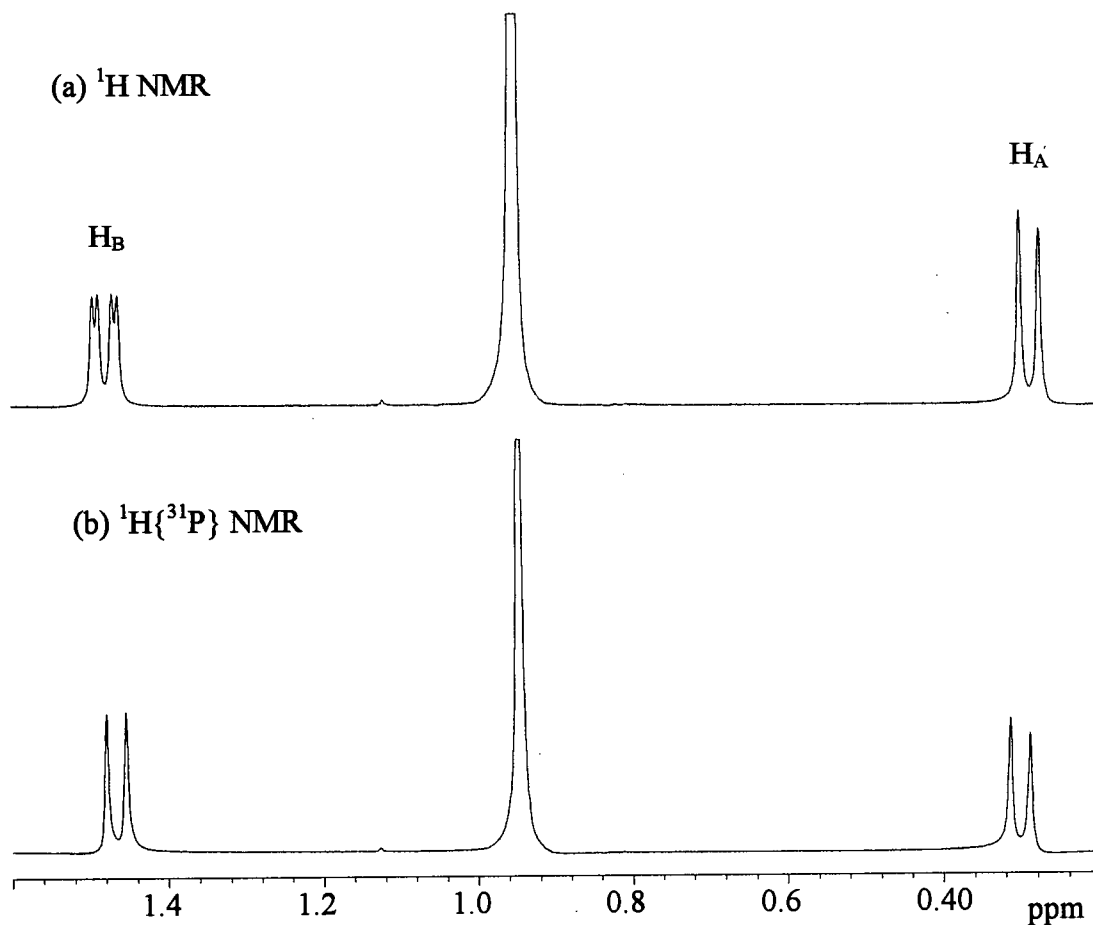


Figure 4.15 1H and $^1H\{^{31}P\}$ NMR spectra (500 MHz) of *cis*- $RuCl_2(P-N)(PPh_3)(SH_2)$ (**18a**) in CD_2Cl_2 (under 1 atm H_2S) at $-50^\circ C$ for the region δ 0.2 to 1.6.

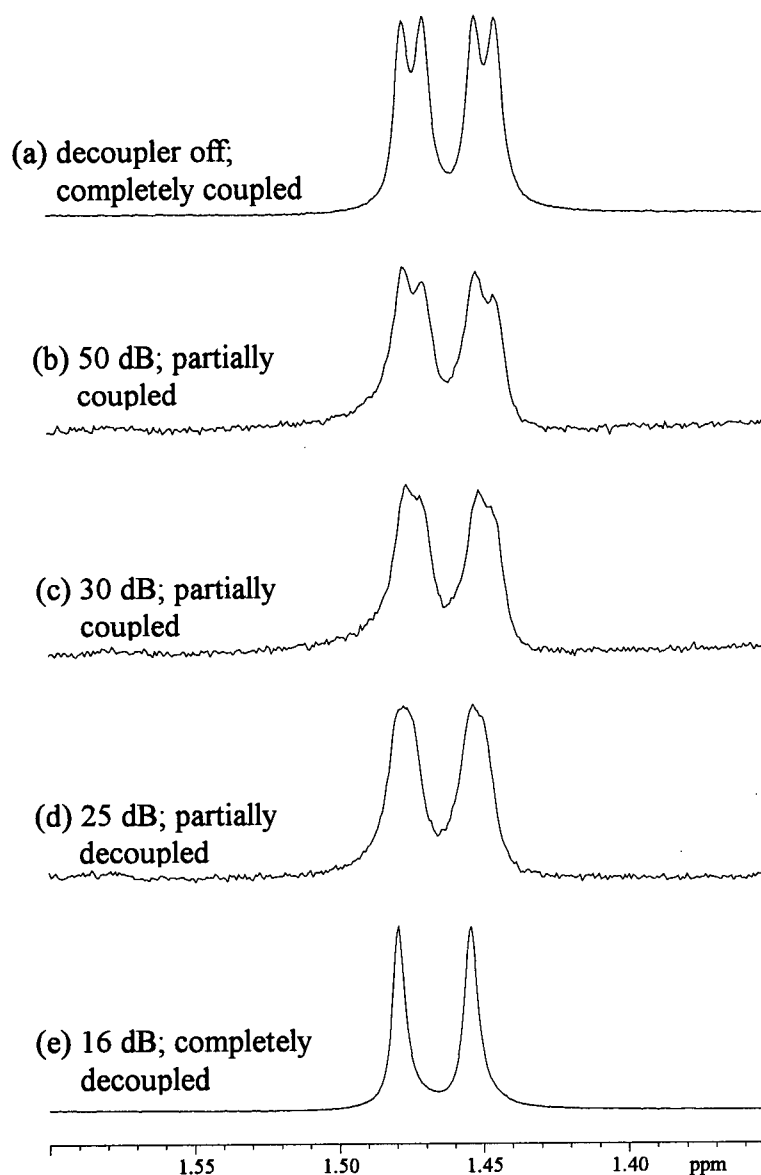


Figure 4.16 ^1H NMR (500 MHz) signal at δ 1.49 for *cis*- $\text{RuCl}_2(\text{P-N})(\text{PPh}_3)(\text{SH}_2)$ (**18a**) with decoupler transmitter centred at 202.4685838 MHz with increasing ^{31}P decoupler power (decreasing dB). Spectra recorded at -50°C and in CD_2Cl_2 .

At -50°C , the exchange of the two diastereotopic hydrogens of the coordinated H_2S diminishes (Figure 4.14(b)) and the structure of **18a** in solution presumably approaches the

solid state structure. With reference to the crystal structure of **18a** (Figure 4.10 and Table 4.1), H_B is assigned to the H(2) proton that is hydrogen-bonded to Cl(2), as this would result in a higher chemical shift due to the deshielding effect of the electron-withdrawing group. The magnitude of the $^3J_{HP}$ coupling constant (3.50 Hz) at δ 1.49 is consistent with those observed for $Ru(SH)(SR)(CO)_2(PPh_3)_2$ (6.8 Hz, $R = H$; 7.1 Hz, $R = p\text{-tolyl}$; 7.3 Hz, $R = C_6H_5$)^{34,35} and $[CpRu(PPh_3)_2(SH_2)][OTf]$ (7.2 Hz).¹³ Two logical questions to ask at this point are (1) why is H_B coupled to P_A and not P_X , and (2) why is H_A coupled to neither? Coupling between atoms on vicinal atoms depends primarily on the overlap of the orbitals within the bonding framework, and therefore the dihedral angle ϕ between the planes. In the present case, these are the P-Ru-S and Ru-S-H planes. In organic molecules, the vicinal coupling of protons (3J , $H-C-C-H$) is described by the Karplus relationship,³⁶ and this correlation may be extended to systems containing $P-C-C-H$, $P-O-C-H$, $P-N-C-H$, and $P-S-C-H$.³⁷ The Karplus curves for the $H-C-C-H$, $P-C-C-H$, and $P-O-C-H$ systems are

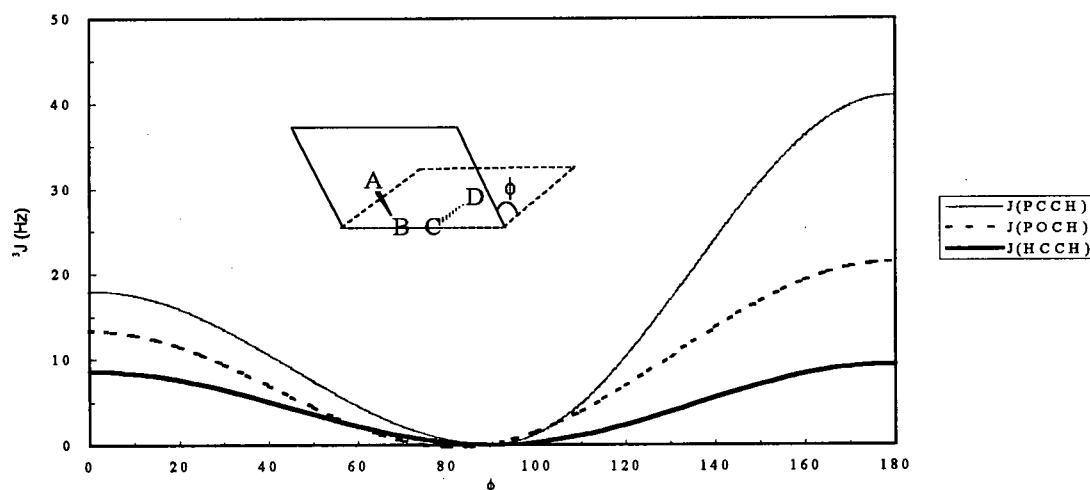


Figure 4.17 The vicinal Karplus correlation. Relationship between dihedral angle (ϕ) and 3J .

plotted in Figure 4.17. Coupling is at a maximum when ϕ is 180° when the hydrogens are antiperiplanar and orbitals are overlapping most efficiently; there is no coupling when ϕ is 90° . The magnitude of 3J is dependent on the types of atoms connected to the three bonds. For **18a**, the dihedral angles for P-Ru-S-H can be visualized by an end-on view of the Ru-S bond shown in Figure 4.18. The absolute dihedral angles for non-coupling P and H atoms are 60.79° , 42.40° and 65.84° . These correspond to P(1)-H(1), P(2)-H(1) and P(2)-H(2) interactions where the orbital overlaps are negligible. For the P(1)-H(2) coupling pair, the dihedral angle is at 169.03° where coupling is observed ($^3J_{HP} = 3.5$ Hz). Such a P(1)-Ru-S-H(2) arrangement is likely the result of interactions of H(2) with Cl(2) and a phenyl group of PPh₃.

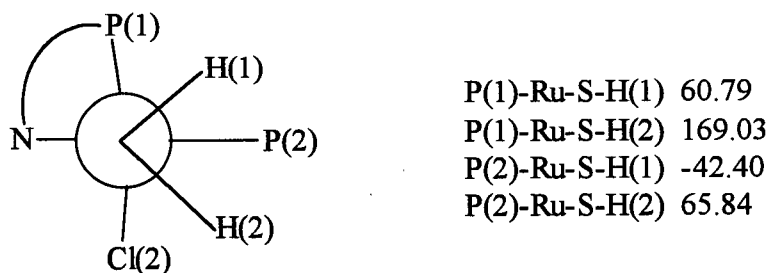


Figure 4.18 End-on schematic view of the solid state structure of **18a**, with dihedral angles ($^\circ$) corresponding to P-Ru-S and Ru-S-H planes.

4.2.2 *Cis*-RuBr₂(P-N)(PPh₃)(SH₂) (**18b**)

Orange prismatic crystals of *cis*-RuBr₂(P-N)(PPh₃)(SH₂)·(C₆H₆) (**18b**) were isolated from a saturated benzene solution of RuBr₂(P-N)(PPh₃) (**6b**) under 1 atm of H₂S. The X-ray crystal structure is shown in Figure 4.19, with selected bond lengths and angles given in Tables 4.3 and 4.4, respectively. Similar to **18a**, a pseudo octahedral geometry around the Ru centre is observed for **18b**. The two S-H bond lengths (1.25(7)) Å and 1.34(6) Å in **18b** are

inequivalent. However, contrary to **18a** where the longer S-H(2) distance (1.30 Å vs. 1.20 Å for S-H(1)) is attributed to H(2)⋯Cl(2) bonding, the H⋯Br bonding is observed between Br(1) and H(1), which is bonded to S with a shorter distance of 1.25 Å. The H⋯Br distance of 2.85(6) Å and the S(1)-H(1)⋯Br(1) angle of 94(3)° suggest weak hydrogen-bonding. The above data suggest that hydrogen-bonding has a negligible effect on the S-H bond lengths.

The H-atoms of the coordinated H₂S are situated under the Br(1)-Br(2)-P(1)-S plane and are positioned close to the planes of phenyl groups. The larger Br groups force the hydrogens close enough to the phenyl groups for possible SH/π interactions to occur. The distances of 2.52 Å and 2.59 Å found for H(1)⋯C(20) (phenyl from P-N) and H(2)⋯C(28) (phenyl from PPh₃), respectively, are considerably shorter than corresponding ones in **18a**. Such phenyl group (from thiophene rings) and mercapto proton interactions are important because they have been implicated in hydrodesulfurization mechanisms.³⁸

The ³¹P{¹H} NMR spectrum of **18b** recorded in CD₂Cl₂ under 1 atm of H₂S is very similar to that of **18a**, an AX pattern with P_A at δ 53.41 and P_B at δ 44.36 (²J_{PP} = 29.20 Hz). In the ¹H NMR spectrum, the NMe₂ resonances are located at δ 3.70 and δ 3.02 while the Ru-SH₂ protons resonate at δ 1.03 and are no longer obscured by the free H₂S signal. When the sample was cooled to -50°C, signals due to H(2) and H(1) (the H-atom bonded to Br(1)) were resolved into a doublet at δ 0.48 and a doublet of doublets at δ 1.23, respectively, with ²J_{HH} and ³J_{HP} coupling constants of 12.2 and 4.3 Hz. When the ³¹P decoupler was turned on, the signal at δ 1.23 became a doublet. Therefore, H(1), bonded to the S-atom at a distance of 1.25 Å, is coupled to P(1) of the P-N ligand, as discussed for **18a**. The absolute dihedral angle between P(1)-Ru-S and Ru-S-H(1) planes is 144.02° (see Figure 4.20).

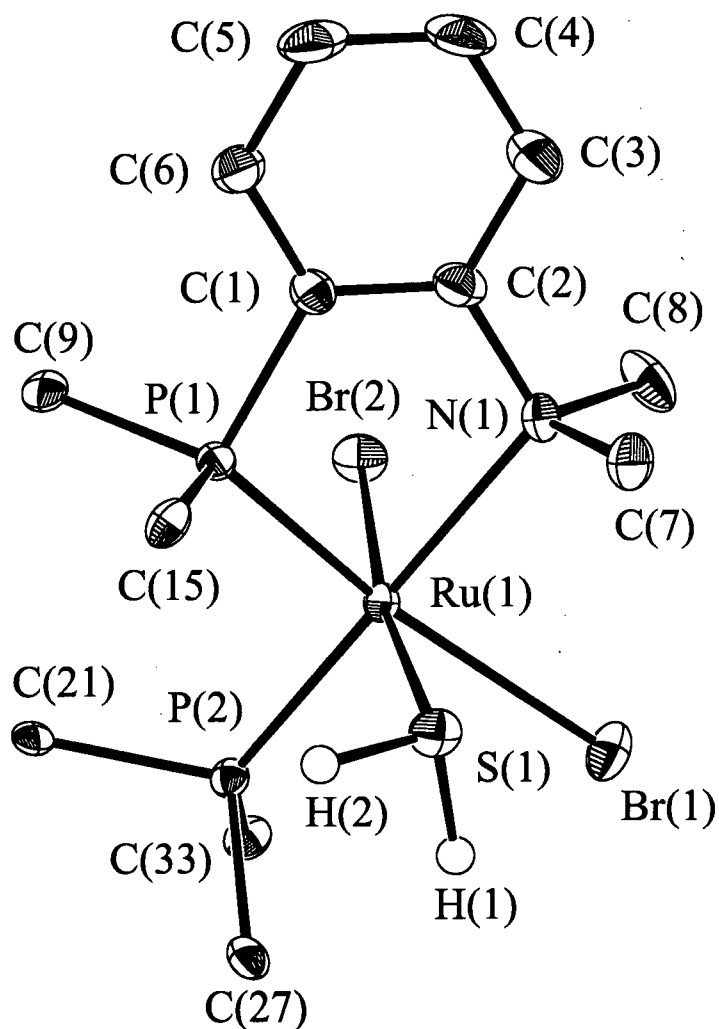


Figure 4.19 The ORTEP plot of *cis*-RuBr₂(P-N)(PPh₃)(SH₂) (**18b**). Thermal ellipsoids for non-hydrogen atoms are drawn at 33 % probability (some of the phenyl carbons have been omitted for clarity). Full experimental parameters and details are given in Appendix V.

Table 4.3 Selected bond lengths (Å) for *cis*-RuBr₂(P-N)(PPh₃)(SH₂) (**18b**) with estimated standard deviations in parentheses.

Bond	Length (Å)	Bond	Length (Å)
Ru(1)-S(1)	2.3330(10)	Ru(1)-Br(1)	2.6343(5)
Ru(1)-P(1)	2.2617(10)	Ru(1)-Br(2)	2.5540(4)
Ru(1)-P(2)	2.3011(11)	S(1)-H(1)	1.25(7)
Ru(1)-N(1)	2.372(3)	S(1)-H(2)	1.34(6)

Table 4.4 Selected bond angles (°) for *cis*-RuBr₂(P-N)(PPh₃)(SH₂) (**18b**) with estimated standard deviations in parentheses.

Bond	Angles (°)	Bond	Angles (°)
H(1)-S(1)-H(2)	98.0(39)	S(1)-Ru(1)-P(1)	93.87(4)
Ru(1)-S(1)-H(1)	100.9(26)	S(1)-Ru(1)-P(2)	93.48(4)
Ru(1)-S(1)-H(2)	115.2(22)	S(1)-Ru(1)-N(1)	89.43(9)
Br(1)-Ru(1)-S(1)	79.77(3)	Br(2)-Ru(1)-P(1)	91.57(3)
Br(2)-Ru(1)-S(1)	172.31(3)	Br(2)-Ru(1)-P(2)	90.94(3)
Br(1)-Ru(1)-P(1)	169.09(3)	Br(2)-Ru(1)-N(1)	86.01(8)
Br(1)-Ru(1)-P(2)	89.54(3)	P(1)-Ru(1)-P(2)	99.76(4)
Br(1)-Ru(1)-N(1)	89.55(8)	P(1)-Ru(1)-N(1)	81.47(8)
Br(1)-Ru(1)-Br(2)	94.00(2)	P(2)-Ru(1)-N(1)	176.75(9)

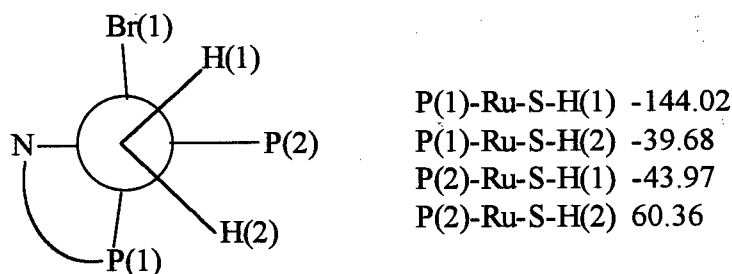


Figure 4.20 End-on schematic view of the solid state structure of **18b**, with dihedral angles corresponding to P-Ru-S and Ru-S-H planes.

4.2.3 *In situ* Preparation of *Cis*-RuI₂(P-N)(PPh₃)(SH₂) (**18c**) and *Cis*-RuI₂(P-N)(P(*p*-tolyl)₃)(SH₂) (**19c**)

The above title complexes could not be isolated as they are less stable than the Cl⁻ and Br⁻ analogues. However, formation of the H₂S adducts is observed by NMR spectroscopy when RuI₂(P-N)(PPh₃) (**6c**) or RuI₂(P-N)(P(*p*-tolyl)₃) (**7c**) in CDCl₃ are exposed to 1 atm H₂S. In the ³¹P{¹H} NMR spectra, the AX signals for **18c** and **19c** appear at δ 56.0, 49.5 (²J_{PP} = 25.8 Hz) and δ 56.2, 47.5 (²J_{PP} = 25.8 Hz), respectively. The ¹H NMR spectra show inequivalent NMe resonances (δ 4.16, 2.20 for **18c**; δ 4.15, 2.91 for **19c**) and broad Ru(SH₂) resonances (δ 0.95 for **18c**; δ 0.90 for **19c**). The dark yellow solutions of **18c** and **19c** decompose to unidentifiable brown species within 1 h of sample preparation, even in the absence of air. The instability of the iodo complexes indicates that the larger size of the iodine does not create an optimal cavity size in the five-coordinate complex with respect to H₂S coordination. Whether the iodo systems are photosensitive remains to be explored; iodo Pd(dpm) systems are known to be photosensitive.³⁹

4.3 The Synthesis and Characterization of *Cis*-RuCl₂(P-N)(PPh₃)(RSH) Species (R = alkyl)

4.3.1 *Cis*-RuCl₂(P-N)(PPh₃)(MeSH) (**20**)

Yellow-brown, prismatic crystals of *cis*-RuCl₂(P-N)(PPh₃)(MeSH)·(acetone) (**20**) were isolated from a saturated acetone solution containing RuCl₂(P-N)(PPh₃) (**6a**) and excess MeSH. In the solid state, **20** is stable in air at r.t. for ~ 24 h after which time it slowly decomposes to an uncharacterizable brown solid with the loss of MeSH (as evidenced by NMR spectra of solutions of the brown solid, as well as the smell of MeSH). The X-ray structure is shown in Figure 4.21, with selected bond lengths and angles given in Tables 4.5 and 4.6, respectively. The overall geometry, and bond lengths and angles of **20** are similar to those of *cis*-RuCl₂(P-N)(PPh₃)(SH₂) (**18a**). A search of the Cambridge Structural Database indicates that **20** is the first structure of a coordinated MeSH complex. Furthermore, the bond length of 1.03(4) Å is the shortest S-H distance yet reported for a thiol complex. There is no hydrogen bonding between the H-atom of the coordinated thiol and a Cl-atom. Both the Me and H groups of the coordinated thiol are situated below the Cl(1)-Cl(2)-P(1)-S plane. The thiol H-atom points towards the planes of phenyls bonded to P(1) and P(2); the H···C(15) and H···C(22) distances of 2.84 and 2.49 Å indicate SH/π (phenyl rings) interactions.

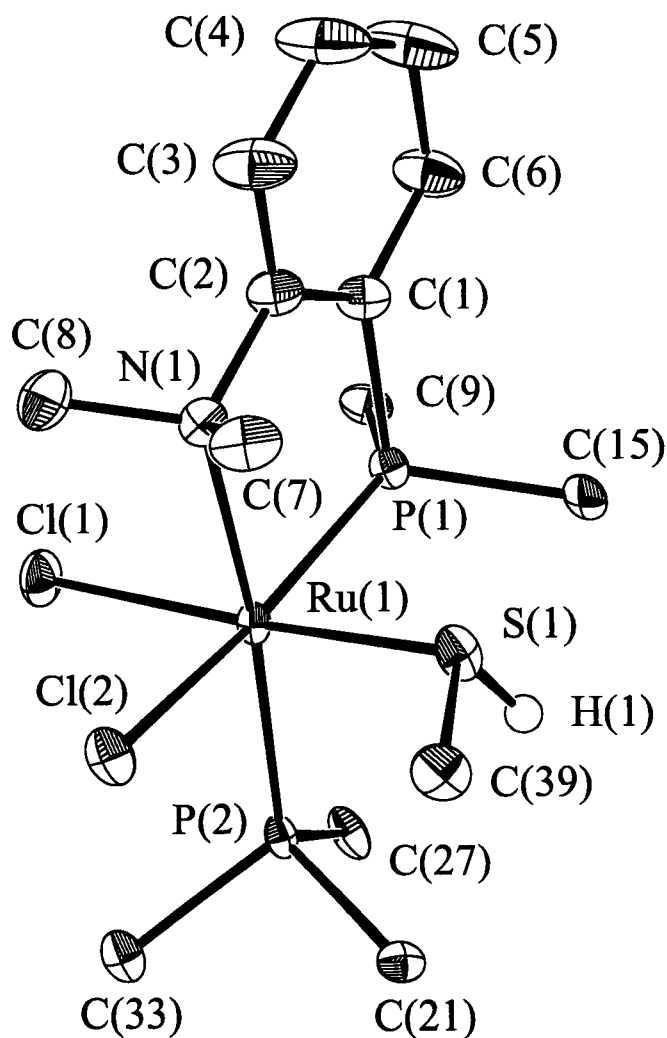


Figure 4.21 The ORTEP plot of *cis*-RuCl₂(P-N)(PPh₃)(MeSH) (**20**). Thermal ellipsoids for non-hydrogen atoms are drawn at 33 % probability (some of the phenyl carbons have been omitted for clarity). Full experimental parameters and details are given in Appendix VI.

Table 4.5 Selected bond lengths (Å) for *cis*-RuCl₂(P-N)(PPh₃)(MeSH) (**20**) with estimated standard deviations in parentheses.

Bond	Length (Å)	Bond	Length (Å)
Ru(1)-S(1)	2.3403(7)	Ru(1)-Cl(1)	2.4241(7)
Ru(1)-P(1)	2.2803(7)	Ru(1)-Cl(2)	2.4472(7)
Ru(1)-P(2)	2.3100(7)	S(1)-H(1)	1.03(4)
Ru(1)-N(1)	2.335(2)	S(1)-C(39)	1.805(3)

Table 4.6 Selected bond angles (°) for *cis*-RuCl₂(P-N)(PPh₃)(MeSH) (**20**) with estimated standard deviations in parentheses.

Bond	Angles (°)	Bond	Angles (°)
H(1)-S(1)-C(39)	100.1(18)	S(1)-Ru(1)-P(1)	86.17(3)
Ru(1)-S(1)-H(1)	101.5(21)	S(1)-Ru(1)-P(2)	94.83(3)
Ru(1)-S(1)-C(39)	116.49(11)	S(1)-Ru(1)-N(1)	87.09(6)
Cl(1)-Ru(1)-S(1)	176.61(3)	Cl(2)-Ru(1)-P(1)	169.27(3)
Cl(2)-Ru(1)-S(1)	90.07(3)	Cl(2)-Ru(1)-P(2)	86.67(3)
Cl(1)-Ru(1)-P(1)	92.50(3)	Cl(2)-Ru(1)-N(1)	86.51(6)
Cl(1)-Ru(1)-P(2)	88.51(3)	P(1)-Ru(1)-P(2)	103.65(3)
Cl(1)-Ru(1)-N(1)	89.66(6)	P(1)-Ru(1)-N(1)	83.26(6)
Cl(1)-Ru(1)-Cl(2)	90.69(3)	P(2)-Ru(1)-N(1)	172.92(6)

The ³¹P{¹H} NMR spectrum of **20** in CD₂Cl₂ shows an AX pattern with P_A and P_X signals at δ 49.77 and δ 41.22 (²J_{PP} = 30.17 Hz), respectively. The ¹H NMR spectrum at 20°C (Figure 4.22(a)), showing two inequivalent NMe groups at δ 3.42 and δ 3.17, is

consistent with the *cis* orientation of the Cl-atoms. The resonances due to the SMe and SH groups overlap giving a multiplet at δ 0.77, but at -50°C (Figure 4.22(b)) these signals resolve into a doublet for SMe at δ 0.65 ($^2J_{\text{HH}} = 6.97$ Hz) and a broad multiplet for SH at δ 0.60. The $^1\text{H}\{^{31}\text{P}\}$ NMR spectrum at -50°C is unchanged, and coupling of the thiol hydrogen to a P-atom is not evident; the Karplus correlation, for the dihedral angle of 73.89° between the P(1)-Ru-S and Ru-S-H planes, predicts only a small coupling constant between P(1) and H.

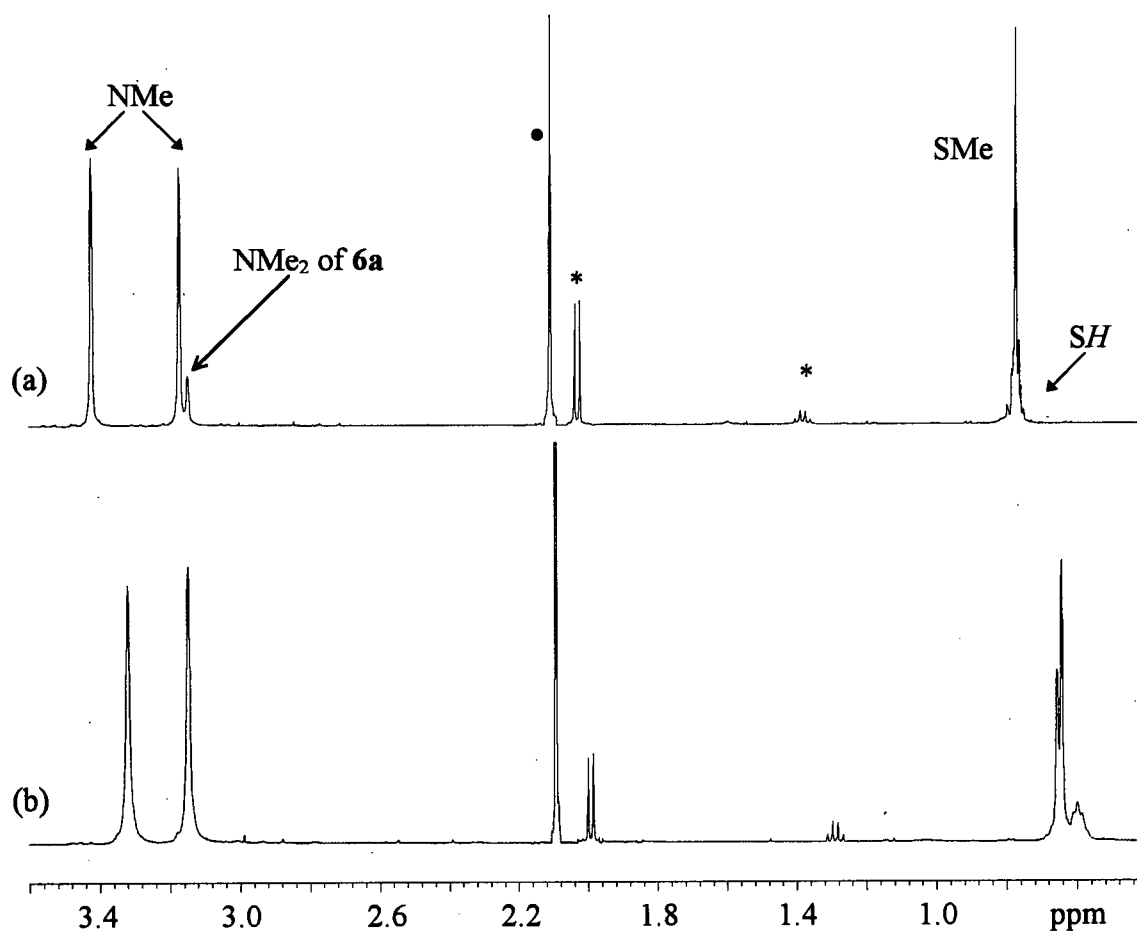


Figure 4.22 ^1H NMR spectra of *cis*- $\text{RuCl}_2(\text{P-N})(\text{PPh}_3)(\text{MeSH})\cdot(\text{acetone})$ (**20**) in CD_2Cl_2 (a) 20°C and (b) -50°C . Note: **20** is in equilibrium with $\text{RuCl}_2(\text{P-N})(\text{PPh}_3)$ (**6a**) (δ 3.08 (d, 20°C), NMe_2) and free MeSH (* δ 1.95 (d), CH_3SH ; δ 1.33 (q), CH_3SH); • = δ 2.04 ($(\text{CH}_3)_2\text{CO}$).

4.3.2 *Cis*-RuCl₂(P-N)(PPh₃)(EtSH) (**21**)

From a saturated C₆D₆ solution of RuCl₂(P-N)(PPh₃) (**6a**) in excess EtSH, yellow prismatic crystals of *cis*-RuCl₂(P-N)(PPh₃)(EtSH)·1.5(C₆D₆) (**21**) were collected. The X-ray structure of the EtSH complex is shown in Figure 4.23 with selected bond lengths and angles listed in Tables 4.7 and 4.8, respectively. The S-H bond distance is 1.27(2) Å, intermediate between the values of 1.25 Å and 1.33 Å obtained for the analogous H₂S complex **18a**. No S-H···Cl interactions were detected for **21**. One of the hydrogen atoms, H(2), bonded to C(1), the α-carbon of the ethylthiol moiety, is hydrogen-bonded to Cl(2) with a distance of 2.90 Å and angle of 97.4°. The Et and H groups of the coordinated thiol are situated below the Cl(1)-Cl(2)-P(1)-S plane with the H-atom pointing toward a phenyl group. SH/π interaction distances of 2.30 Å and 2.83 Å were found for H(1)···C(24) (a phenyl group belonging to P(1)) and H(1)···C(11) (a phenyl group belonging to P(2)), respectively.

The ³¹P{¹H} NMR spectrum of **21** in CD₂Cl₂ indicates the presence of the *cis*-dichloro isomer and approximately 10 % of the five-coordinate precursor **6a**. The P_A and P_X doublets of **21** appear at δ 52.43 and δ 43.97 (²J_{PP} = 30.23 Hz), respectively, and are consistent with the data obtained from the previous *in situ* work by Mudalige.^{27b} However, contrary to this earlier work, no trans isomer was detected. The species previously assigned as the trans isomer may be due to the use of impure EtSH. The ¹H NMR spectrum of **21** (Figure 4.24) reveals that the H_b and H_c methylene protons are inequivalent as indicated by multiplets at δ 2.00 and δ 0.88, respectively. The S-atom becomes chiral when coordinated to the Ru centre; the H_b and H_c protons are diastereotopic and therefore anisochronous.⁴⁰

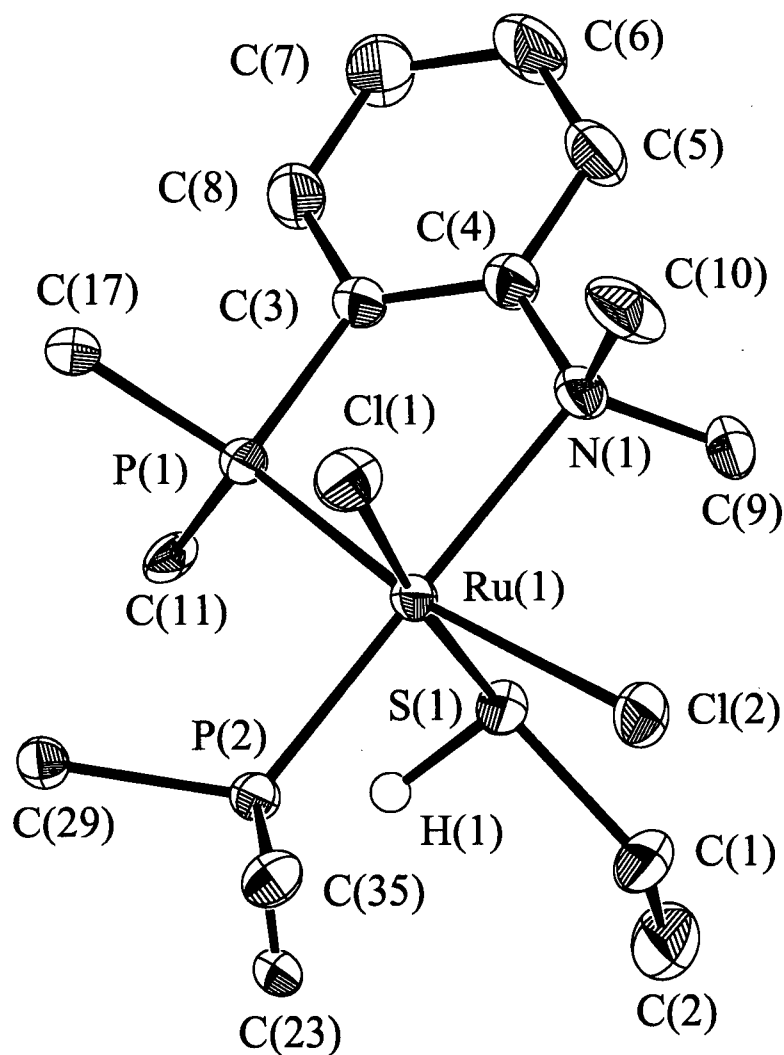


Figure 4.23 The ORTEP plot of *cis*-RuCl₂(P-N)(PPh₃)(EtSH) (**21**). Thermal ellipsoids for non-hydrogen atoms are drawn at 33 % probability (some of the phenyl carbons have been omitted for clarity). Full experimental parameters and details are given in Appendix VII.

Table 4.7 Selected bond lengths (Å) for *cis*-RuCl₂(P-N)(PPh₃)(EtSH) (**21**) with estimated standard deviations in parentheses.

Bond	Length (Å)	Bond	Length (Å)
Ru(1)-S(1)	2.3391(6)	Ru(1)-Cl(1)	2.4204(6)
Ru(1)-P(1)	2.2753(5)	Ru(1)-Cl(2)	2.4674(5)
Ru(1)-P(2)	2.3100(6)	S(1)-H(1)	1.27(2)
Ru(1)-N(1)	2.362(2)	S(1)-C(1)	1.825(2)
		C(1)-C(2)	1.502(4)

Table 4.8 Selected bond angles (°) for *cis*-RuCl₂(P-N)(PPh₃)(EtSH) (**21**) with estimated standard deviations in parentheses.

Bond	Angles (°)	Bond	Angles (°)
H(1)-S(1)-C(1)	96.0(9)	S(1)-Ru(1)-P(1)	87.37(2)
Ru(1)-S(1)-H(1)	104.1(9)	S(1)-Ru(1)-P(2)	97.16(2)
Ru(1)-S(1)-C(1)	115.84(9)	S(1)-Ru(1)-N(1)	85.33(5)
Cl(1)-Ru(1)-S(1)	174.63(2)	Cl(2)-Ru(1)-P(1)	167.88(2)
Cl(2)-Ru(1)-S(1)	87.15(2)	Cl(2)-Ru(1)-P(2)	91.78(2)
Cl(1)-Ru(1)-P(1)	96.25(2)	Cl(2)-Ru(1)-N(1)	86.18(4)
Cl(1)-Ru(1)-P(2)	86.17(2)	P(1)-Ru(1)-P(2)	99.63(2)
Cl(1)-Ru(1)-N(1)	91.19(5)	P(1)-Ru(1)-N(1)	82.61(4)
Cl(1)-Ru(1)-Cl(2)	88.54(2)	P(2)-Ru(1)-N(1)	176.71(5)
S(1)-C(1)-C(2)	109.4(2)		

The coupling constants of the protons of the coordinated EtSH group were obtained from the ¹H NMR spectrum of **21** (Figure 4.24) with the help of simulated spectrum (Figure

4.25(a)). The $\text{C}(\text{H}_\text{d})_3$ methyl protons at δ 0.46 are coupled to H_b and H_c ($^3J_{\text{H}_\text{b}\text{H}_\text{d}} = ^3J_{\text{H}_\text{c}\text{H}_\text{d}} = 7.36$ Hz) while the H_b and H_c methylene protons at δ 2.00 and δ 0.88, respectively, are coupled to each other, to the thiol H_a proton, and to H_d . The downfield shift of H_b is a result of hydrogen-bonding to a Cl-atom. The coupling constants are: $^3J_{\text{H}_\text{b}\text{H}_\text{c}} = 13.74$ Hz, $^3J_{\text{H}_\text{a}\text{H}_\text{b}} = 10.74$ Hz, $^3J_{\text{H}_\text{a}\text{H}_\text{c}} = 5.83$, $^3J_{\text{H}_\text{b}\text{H}_\text{d}} = ^3J_{\text{H}_\text{c}\text{H}_\text{d}} = 7.36$ Hz, which were also obtained from the doublet of doublet of doublets assigned to H_a . Further confirmation of

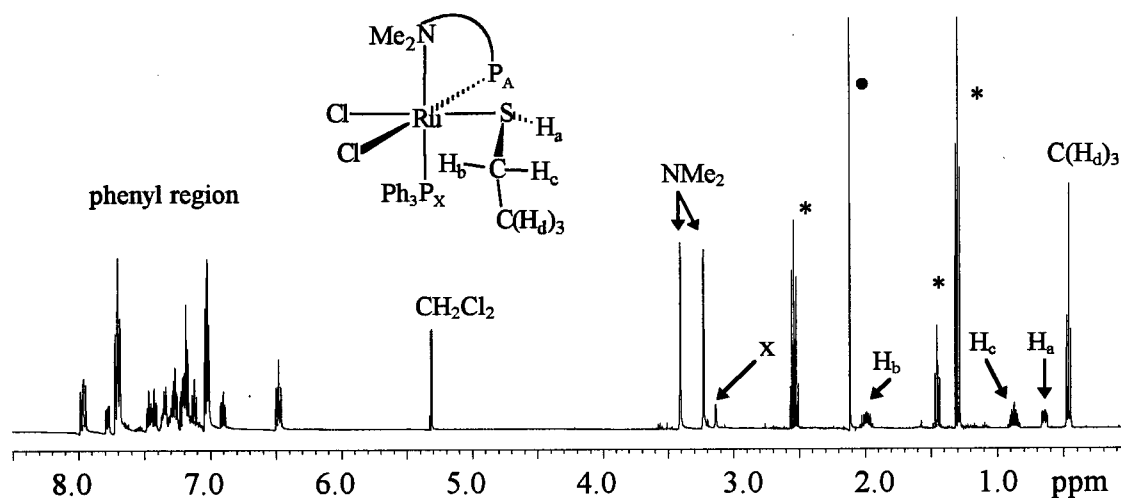


Figure 4.24 ^1H NMR spectrum (500 MHz) of **21** in CD_2Cl_2 at 20°C . Note: **21** is in equilibrium with $^*\text{6a}$ (δ 3.09, NMe_2) and free $^*\text{EtSH}$ (δ 2.55 (dq), $\text{CH}_3\text{CH}_2\text{SH}$; δ 1.46 (t), $\text{CH}_3\text{CH}_2\text{SH}$; δ 1.31 (t), $\text{CH}_3\text{CH}_2\text{SH}$); $\bullet = \delta$ 2.1 ($(\text{CH}_3)_2\text{CO}$).

these correlations was performed by a 2D COSY ^1H NMR experiment. The further splitting of the H_a doublet of doublets at δ 0.65 into doublet of doublet of doublets is due to coupling of H_a to a P-atom. As the structure of **21** is similar to that of **18a**, the H_2S analogue, H_a is assumed to be coupled to P_A with a small coupling constant $^3J_{\text{H}_\text{a}\text{P}_\text{A}} = 1.92$ Hz due to the small dihedral angle of 69.81° between the $\text{P}(1)\text{-Ru-S}$ and $\text{Ru-S-H}(1)$ planes. When a $^1\text{H}\{^{31}\text{P}\}$ NMR spectrum was measured (Figure 4.26(b)), H_a is partially decoupled to P_A .

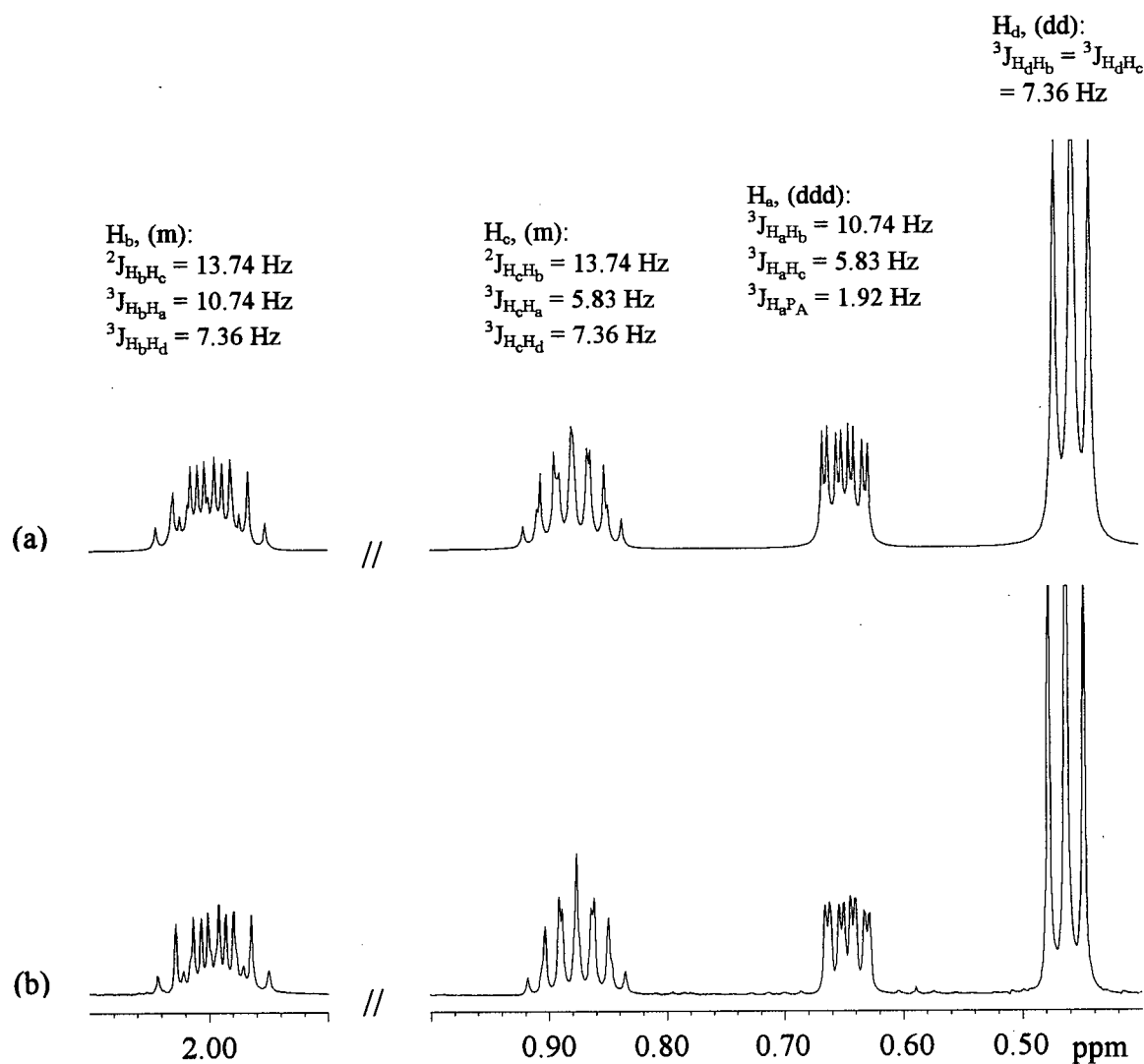


Figure 4.25 ^1H NMR spectra of **21** (500 MHz, CD_2Cl_2). Spectra only show resonances due to the protons of coordinated EtSH: (a) simulated spectrum; (b) expanded regions from actual spectrum, Figure 4.24.

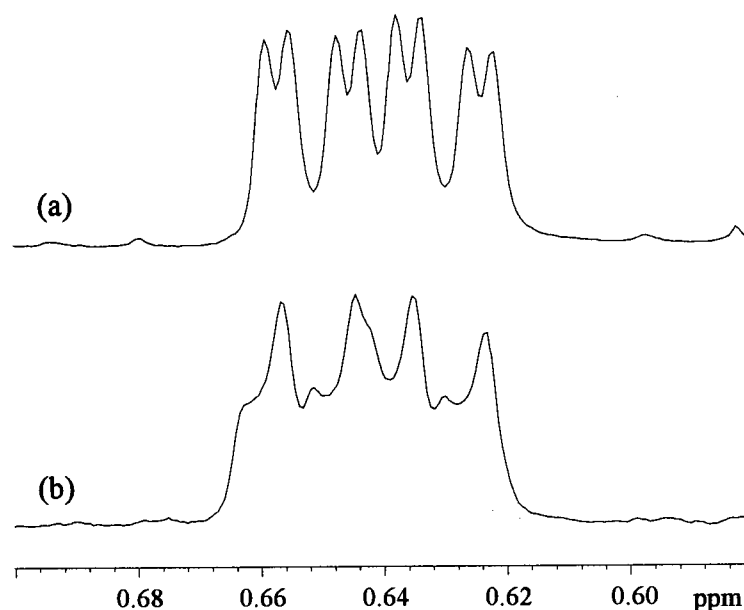


Figure 4.26 ^1H NMR resonance of Ru-S-H_4 in $\text{cis-RuCl}_2(\text{P-N})(\text{PPh}_3)(\text{EtSH})$ (**21**): (a) ^1H NMR spectrum; (b) $^1\text{H}\{^{31}\text{P}\}$ NMR spectrum (500 MHz, 20°C , CD_2Cl_2).

4.3.3 *In situ* Preparation of $\text{Cis-RuCl}_2(\text{P-N})(\text{PPh}_3)(\text{RSH})$ Species, $\text{R} = n\text{-Pr}, i\text{-Pr}, n\text{-Pn}, n\text{-Hx}, \text{Bz}$

To expand the series of coordinated thiol complexes, longer alkyl chain thiols were reacted with $\text{RuCl}_2(\text{P-N})(\text{PPh}_3)$ (**6a**). Addition of excess RSH ($\text{R} = n\text{-Pr}, i\text{-Pr}, n\text{-Pn}, n\text{-Hx}, \text{Bz}$) to a solution of **6a** in CDCl_3 or C_6D_6 yielded yellow solutions. Attempts to isolate products were unsuccessful because of the facile loss of RSH , but the $^{31}\text{P}\{^1\text{H}\}$ NMR spectra of the *in situ* reactions indicate the formation of the thiol adducts, $\text{cis-RuCl}_2(\text{P-N})(\text{PPh}_3)(\text{RSH})$ (**22 - 26**). The ^1H NMR spectra were uninformative because product peaks were obscured by those of added excess thiol required for product formation. The $^{31}\text{P}\{^1\text{H}\}$ NMR chemical shifts of $\text{RuCl}_2(\text{P-N})(\text{PPh}_3)(\text{RSH})$ depend very little on the nature of the thiol as shown in Table 4.9.

Table 4.9 $^{31}\text{P}\{^1\text{H}\}$ NMR chemical shifts (121.4 MHz) for *cis*- $\text{RuCl}_2(\text{P-N})(\text{PPh}_3)(\text{RSH})$ in the presence of added RSH (except for data labeled unknown) at 20°C.

RSH	$\delta \text{ P}_\text{A} (\text{P-N})$	$\delta \text{ P}_\text{B} (\text{PPh}_3)$	$^2\text{J}_{\text{PP}} (\text{Hz})$	Solvent
H_2S , (18a)	51.28	44.53	29.50	C_6D_6
MeSH, (20)	51.49	45.58	29.63	C_6D_6
EtSH, (21)	51.17	42.75	29.50	C_6D_6
<i>n</i> -PrSH, (22)	51.22	42.46	30.05	CDCl_3
<i>i</i> -PrSH, (23)	49.58	41.68	30.23	C_6D_6
unknown A (trans isomer ?)	56.76	46.84	36.54	C_6D_6
unknown B (impurity ?)	51.31	42.74	29.93	C_6D_6
<i>n</i> -PnSH, (24)	51.30	42.84	29.63	C_6D_6
unknown C (trans isomer ?)	49.57	46.35	36.06	C_6D_6
<i>n</i> -HxSH, (25)	51.15	42.57	30.23	CDCl_3
BzSH, (26)	50.16	42.03	30.41	CDCl_3

With the exception of *i*-PrSH and *n*-PnSH, all reactions of $\text{RuCl}_2(\text{P-N})(\text{PPh}_3)$ (**6a**) with RSH gave single products of the type *cis*- $\text{RuCl}_2(\text{P-N})(\text{PPh}_3)(\text{RSH})$. The $^{31}\text{P}\{^1\text{H}\}$ assignments were based by comparison with those for the characterized H_2S , MeSH and EtSH complexes. Figure 4.27 shows the $^{31}\text{P}\{^1\text{H}\}$ NMR spectra for reactions of **6a** with *i*-PrSH and *n*-PnSH. Unknown A and C are probably the *trans*- $\text{RuCl}_2(\text{P-N})(\text{PPh}_3)(\text{RSH})$ isomers because of the similarity of the larger coupling constants $^2\text{J}_{\text{PP}}$ (~ 36 Hz) to those of other trans complexes such as *trans*- $\text{RuCl}_2(\text{P-N})(\text{PPh}_3)(\text{L})$ ($\text{L} = \text{H}_2\text{O}$, MeOH and EtOH); see also Sections 5.3 and 5.6.^{27b} Unknown B perhaps results from impurities in the *i*-PrSH used.

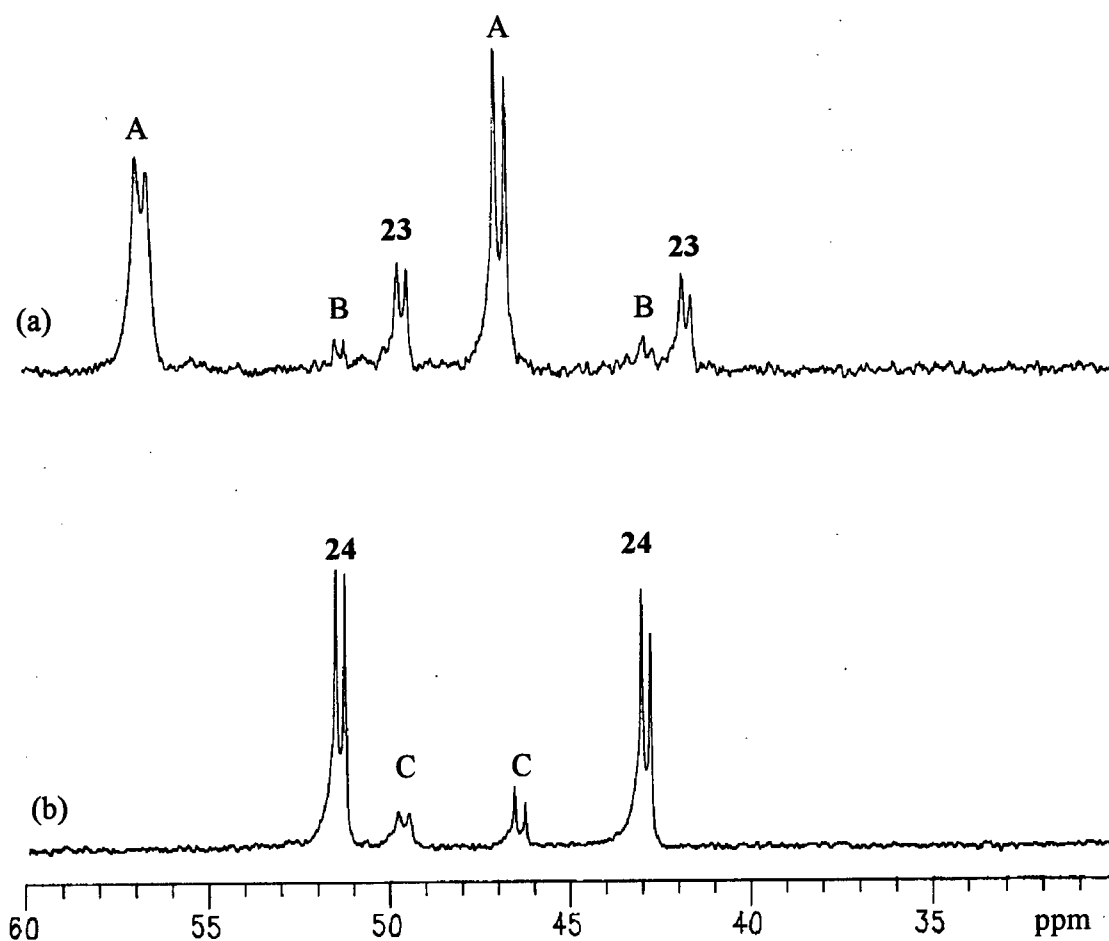


Figure 4.27 $^{31}\text{P}\{^1\text{H}\}$ NMR (300 MHz) spectra of *in situ* reactions of **6a** with (a) *i*-PrSH and (b) *n*-PnSH in C_6D_6 at 20°C .

Clearly, the steric bulk of RSH plays an important role in the coordination of thiols to **6a**, as the *cis*- $\text{RuCl}_2(\text{P-N})(\text{PPh}_3)(\text{RSH})$ complexes are not isolable as the R group becomes more bulky. No reactions were observed when excess PhSH or thiophene were added to **6a** in CDCl_3 . The reaction solutions remained green and the $^{31}\text{P}\{^1\text{H}\}$ NMR spectra showed only the presence of **6a**.

4.4 Comparison of Coordinated S-H Vibrational Frequencies for 18a, 18b, 19a, 20 and 21

The vibration modes for a triatomic molecule are shown in Figure 4.28. In the IR spectrum of gaseous H_2S , absorptions at 2629, 2615 and 1180 cm^{-1} were assigned as the

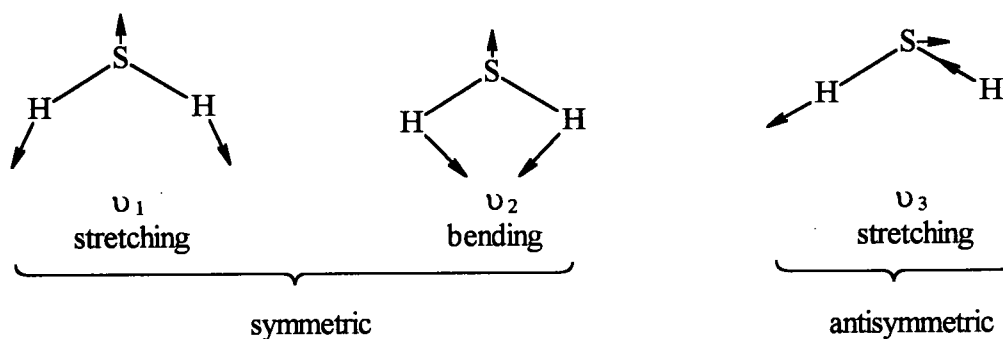


Figure 4.28 The vibrational modes for H_2S (or any bent triatomic molecules).

ν_3 , ν_1 and ν_2 bands, respectively.⁴¹ The infrared spectra of **18a**, **18b**, **19a**, **20** and **21** were obtained from solid KBr pellets of each sample. The $\nu_{\text{S-H}}$ frequencies of each complex and those of the gaseous H_2S or thiol are listed in Table 4.10. Upon coordination of H_2S , ν_1 and ν_3 can still be observed while ν_2 is obscured by other bands of the spectrum. For gaseous MeSH and EtSH , only one stretching band (ν_1) is observed for each at 2580 and 2573 cm^{-1} , respectively.³¹ In all cases but one (including literature data from Sections 4.1.1 and 4.1.2), coordination to transition metals results in lower wavenumbers that are consistently in the range of 2423 to 2590 cm^{-1} for H_2S and thiol complexes; the exception is in the much lower frequencies of 2290 and 2410 cm^{-1} reported for $[\text{Ru}(\text{SH}_2)(\text{PPh}_3)_3\text{S}_4']$ which were attributed to hydrogen-bonding to O- and S-atoms (Section 4.1.1).³

Table 4.10 $\nu_{\text{S-H}}$ (cm^{-1}) frequencies (ν_1 and ν_3 bands) for H_2S and Thiols, in the free gaseous state and upon coordination to Ru

<i>cis</i> - $\text{RuX}_2(\text{P-N})(\text{PR}_3)(\text{L})$	$\nu_{\text{S-H}}$ of Gaseous L (cm^{-1})	$\nu_{\text{S-H}}$ of Coordinated Complex (cm^{-1})
R = Ph, X = Cl, L = H_2S (18a)	2615 (ν_1), 2629 (ν_3)	2506 (ν_1), 2476 (ν_3)
R = Ph, X = Br, L = H_2S (18b)	2615 (ν_1), 2629 (ν_3)	2506 (ν_1), 2476 (ν_3)
R = <i>p</i> -tolyl, X = Cl, L = H_2S (19a)	2615 (ν_1), 2629 (ν_3)	2495 (ν_1), 2449 (ν_3)
R = Ph, X = Cl, L = MeSH (20)	2580	2533
R = Ph, X = Cl, L = EtSH (21)	2573	2516

The substitution of Cl by Br (**18a** \rightarrow **18b**) does not affect ν_1 and ν_3 , but substitution of Ph by *p*-tolyl (**18a** \rightarrow **19a**) results in significantly lower ν_{SH} stretching frequencies, possibly because of increased SH/ π interactions between H_2S protons and the ring system of the *p*-tolyl group. Unfortunately, a direct comparison between structures of **18a** and **19a** can not be made because only one H-atom of the coordinated H_2S was located in **19a**.

4.5 The UV-Vis Spectra of $\text{RuX}_2(\text{PN})(\text{PR}_3)$ (X = halogen; PN = P-N, PAN or AMPHOS; R = Ph or *p*-tolyl) and *Cis*- $\text{RuX}_2(\text{P-N})(\text{PPh}_3)(\text{L})$ (L = H_2S , MeSH or EtSH) Species

UV-Vis spectroscopy is a good tool to observe the occurrence of a reaction in this type of chemistry. The five-coordinate, square pyramidal complexes, $\text{RuX}_2(\text{PN})(\text{PR}_3)$, studied in this work have characteristic λ_1 (450 to 460 nm) and λ_2 (622 to 780 nm) bands (Table 4.11). Upon coordination of L to $\text{RuCl}_2(\text{P-N})(\text{PPh}_3)$, λ_1 shifts to a shorter wavelength and λ_2 is no longer observed in the 300 to 820 nm region.

Table 4.11 λ_1 and λ_2 UV-Vis bands for $\text{RuX}_2(\text{PN})(\text{PPh}_3)(\text{L})$ in CH_2Cl_2

$\text{RuX}_2(\text{PN})(\text{PR}_3)(\text{L})$	λ_1 (nm)	ϵ_1 ($\text{M}^{-1} \text{cm}^{-1}$)	λ_2 (nm)	ϵ_2 ($\text{M}^{-1} \text{cm}^{-1}$)
X = Cl, PN = P-N, R = Ph, L = vacant (6a)	454	1100	678	480
X = Br, PN = P-N, R = Ph, L = vacant (6b)	472	1170	706	615
X = I, PN = P-N, R = Ph, L = vacant (6c)	510	900	774	510
X = Cl, PN = P-N, R = <i>p</i> -tolyl, L = vacant (7a)	452	1155	672	555
X = Br, PN = P-N, R = <i>p</i> -tolyl, L = vacant (7b)	474	1150	700	560
X = I, PN = P-N, R = <i>p</i> -tolyl, L = vacant (7c)	512	780	780	435
X = Cl, PN = PAN, R = Ph, L = vacant (9)	450	1210	622	490
X = Cl, PN = PAN, R = <i>p</i> -tolyl, L = vacant (10)	450	1280	622	520
X = Cl, PN = AMPHOS, R = Ph, L = vacant, (12) (prepared <i>in situ</i>)	460	1050	636	570
X = Cl, PN = P-N, R = Ph, L = H_2S^a (18a)	426	830	-	-
X = Br, PN = P-N, R = Ph, L = H_2S^a (18b)	446	995	-	-
X = Cl, PN = P-N, R = <i>p</i> -tolyl, L = H_2S^a (19a)	435	900	-	-
X = Br, PN = P-N, R = <i>p</i> -tolyl, L = H_2S^a (19b)	452	935	-	-
X = Cl, PN = P-N, R = Ph, L = MeSH^a (20)	424	835	-	-
X = Cl, PN = P-N, R = Ph, L = EtSH^a (21)	424	830	-	-

^aMeasured in the presence of excess sulfur ligand.

Figure 4.29 shows the absorption spectra before and after the addition of H_2S to $\text{RuCl}_2(\text{P-N})(\text{PPh}_3)$ (**6a**). The band originally at $\lambda_1 = 454 \text{ nm}$ ($\epsilon = 1100 \text{ M}^{-1} \text{cm}^{-1}$) shifts to 426 nm ($\epsilon = 830 \text{ M}^{-1} \text{cm}^{-1}$) while the absorption at $\lambda_2 = 678 \text{ nm}$ ($\epsilon = 480 \text{ M}^{-1} \text{cm}^{-1}$) is no longer observed. Although low spin d^6 Ru(II) is a good π donor, the electronic bands observed for all the complexes are mostly likely due to halogen to metal charge transfer

transitions, as the energies decrease in the sequence $\text{Cl} > \text{Br} > \text{I}$ (Table 4.11), in parallel with the ionization energies of the halide ions. Upon coordination of the sulfur ligands, the λ_2 band may have shifted to lower energy transitions.

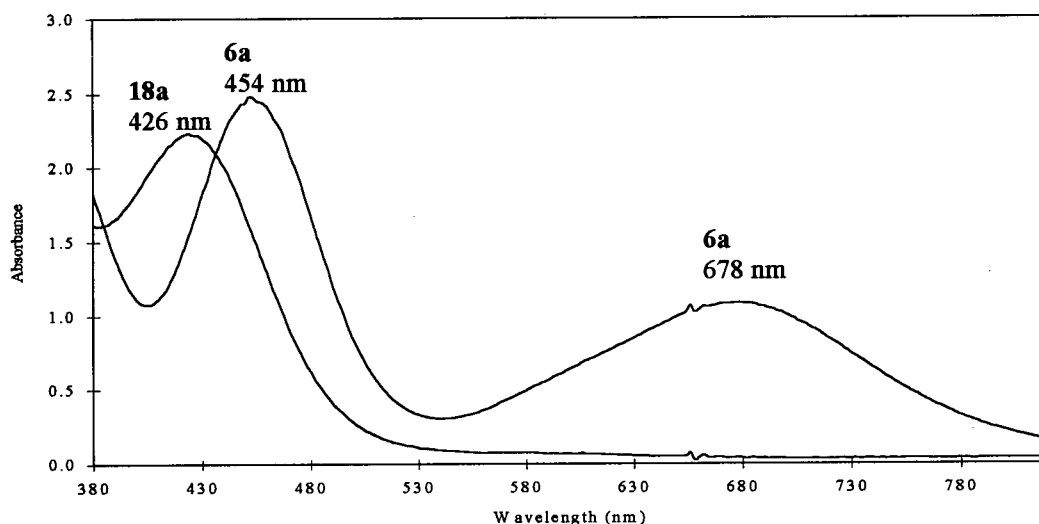


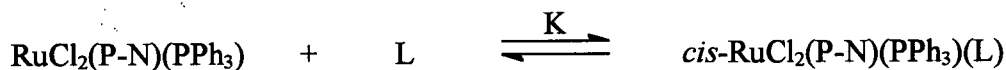
Figure 4.29 UV-Vis spectra for $\text{RuCl}_2(\text{P-N})(\text{PPh}_3)$ (**6a**) and *cis*- $\text{RuCl}_2(\text{P-N})(\text{PPh}_3)(\text{SH}_2)$ (**18a**) in CH_2Cl_2 at 20°C .

The formation of *cis*- $\text{RuCl}_2(\text{P-N})(\text{PPh}_3)(\text{SH}_2)$ (**18a**) and its distinctive UV-Vis spectrum were thought to provide an opportunity to study the kinetics and provide information on the binding of H_2S . However, formation of **18a** proved to be too fast for study by UV-Vis spectroscopy because of the 'immediate' completion of the reaction upon the addition of 1 atm H_2S to $\text{RuCl}_2(\text{P-N})(\text{PPh}_3)$ (**6a**). Repeated attempts to slow the reaction sufficiently at lower temperatures down to -10°C were also unsuccessful for monitoring the rate of formation of **18a**. Stopped-flow experiments were also performed by injections of separate, more dilute solutions of H_2S and **6a** into the spectrophotometer. However, even with rigorous exclusion of air, the samples tended to decompose and reproducible data could

not be obtained; furthermore, these experiments were not pursued because of the offensive odour and therefore non-containability of the toxic H_2S .

4.6 Solution Thermodynamics for Reversible Formation of H_2S and Thiol complexes

The affinities of $\text{RuX}_2(\text{P-N})(\text{PR}_3)$ for $\text{L} = \text{H}_2\text{S}$, MeSH and EtSH can be compared by determining the equilibrium constant, K , for the following equilibrium equation:



Equilibrium concentrations were obtained from ^1H NMR integrations of each species, the samples being prepared by dissolving $\text{cis-RuCl}_2(\text{P-N})(\text{PPh}_3)(\text{L})$ in C_6D_6 or C_7D_8 and under 1 atm Ar. K values were determined at various temperatures (within the range 10 - 70°C) and

the corresponding Van't Hoff plots (Van't Hoff equation: $\ln K = -\frac{\Delta H^\circ}{RT} + \frac{\Delta S^\circ}{R}$) are given in

Figure 4.30. As an example of the determination of K , Figure 4.31 illustrates the ^1H NMR spectra showing the region of interest for the $\text{cis-RuCl}_2(\text{P-N})(\text{PPh}_3)(\text{SH}_2)$ (**18a**) system at 20, 36 and 50°C. As the temperature is raised, the integrations of the signal due to **6a** (δ 3.07, NMe_2) and free H_2S (δ 0.30) increase while those of **18a** (δ 3.67, 2.97, NMe_2 ; δ 1.02, Ru-SH_2) decrease; that is, formation of **18a** is exothermic. The equilibrium expression for the

formation of **18a** is: $K = \frac{[\text{18a}]}{[\text{6a}][\text{H}_2\text{S}]_s}$. Because $[\text{Ru}]_{\text{total}}$ is known ($= [\text{18a}] + [\text{6a}]$), and

$$x = \frac{[\text{18a}]}{[\text{6a}]} = \frac{\alpha / 3}{(\beta - \alpha) / 6} = \frac{\varepsilon / 2}{(\beta - \alpha) / 6} \quad \text{and} \quad y = \frac{[\text{6a}]}{[\text{H}_2\text{S}]_s} = \frac{(\beta - \alpha) / 6}{\omega / 2} \quad \text{can be calculated,}$$

$$K = \frac{xy(1+x)}{[\text{Ru}]_{\text{total}}} \quad \text{can be determined } (\alpha, \beta, \varepsilon \text{ and } \omega \text{ are integrated peak areas of the resonances}$$

shown in Figure 4.31). Of note, $[\text{6a}] = [\text{H}_2\text{S}]_{\text{uncoordinated}} = [\text{H}_2\text{S}]_s + [\text{H}_2\text{S}]_{\text{hs}}$ (s refers to H_2S dissolved in solution, while hs refers to H_2S in head space of the NMR tube), although

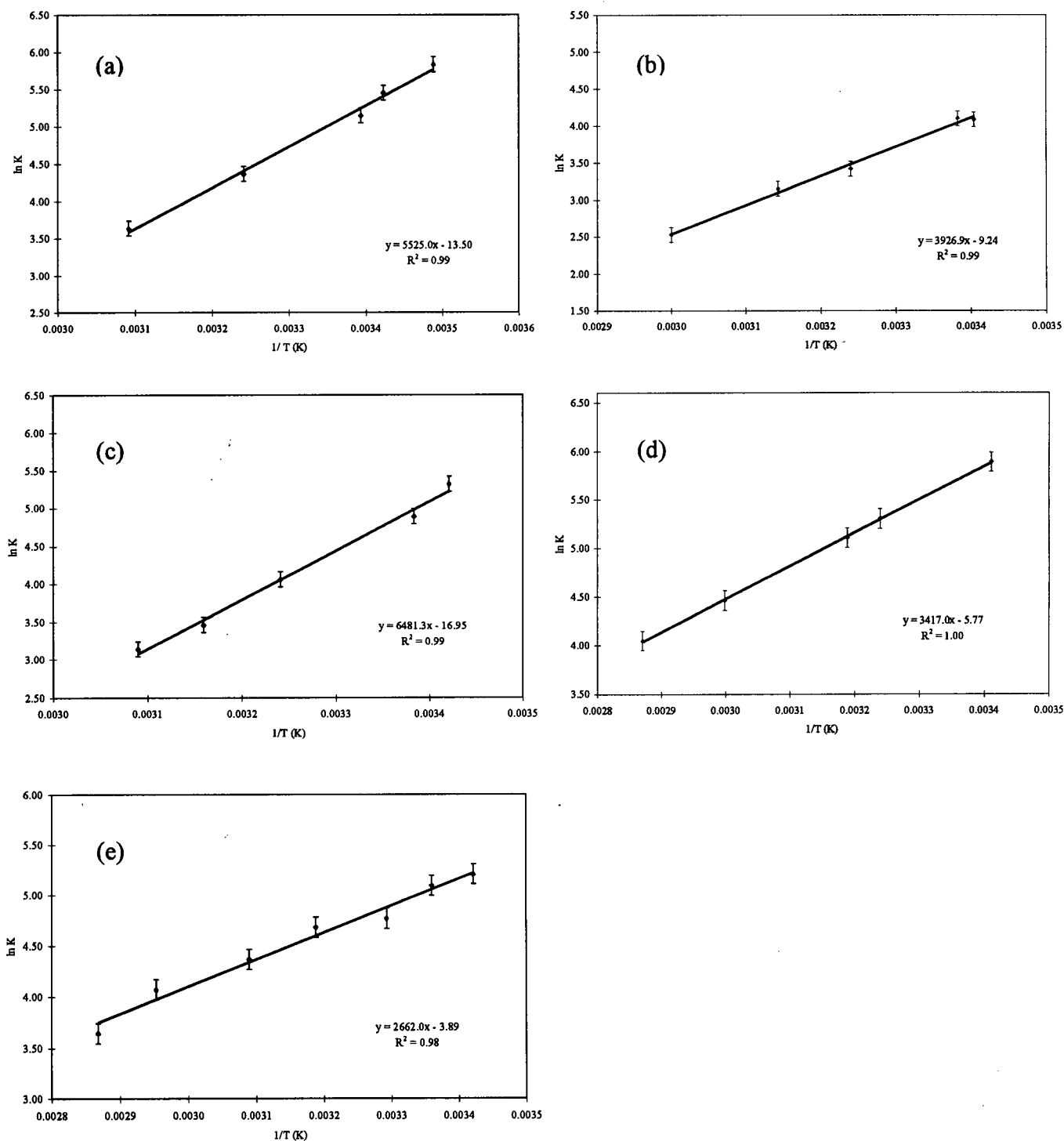


Figure 4.30 Van't Hoff plots for the K equilibria (see p. 42) for (a) 18a, (b) 18b, (c) 19a, (d) 20 and (e) 21 in C_6D_6 . Bars indicate estimated error based on repeated experiments. Data for each complex were collected from a minimum of three experiments with the average values plotted.

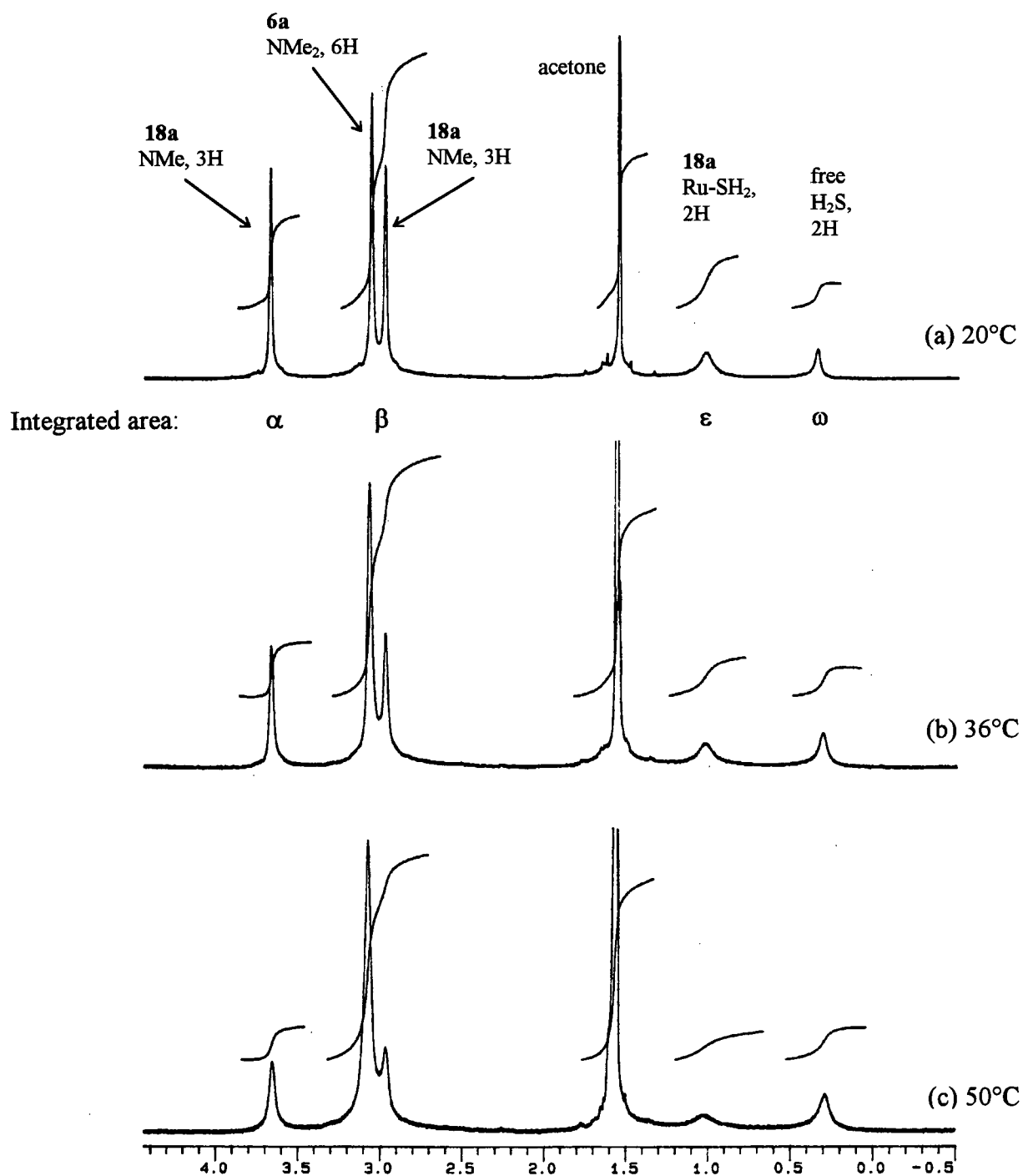


Figure 4.31 ^1H NMR spectra in the region δ -0.5 to 4.5 (300 MHz, C_6D_6) for the equilibrium between **18a**, **6a** and H_2S at (a) 20°C, (b) 36°C and (c) 50°C.

this relationship is not needed for calculation of the K values. Some raw data for the equilibrium calculations involving **18a**, **18b**, **19a**, **20** and **21** are given in Appendix XI.

Table 4.12 gives ΔH° , ΔS° and ΔG° data for the formation of **18a**, **18b**, **19a**, **20**, and **21**. Ignoring the effects of the trans to cis halide rearrangement on the thermodynamics, the negative ΔS° values are consistent with binding of a small molecule to a metal site, while the low value exothermicities imply relatively weak Ru-S bond energies. At 25°C, the relatively large magnitude of $K = 296 \text{ M}^{-1}$ ($\Delta G^\circ = -14 \text{ kJ/mol}$) indicate **20** is most thermodynamically favoured. In solution, the tendency for MeSH to dissociate is relatively weak, and this fact is confirmed by qualitative, visual observations and by UV-Vis spectroscopy: when **20** was dissolved in solution, the solution remained yellow, characteristic of *cis*-RuCl₂(P-N)(PPh₃)(L), while when **18a**, **18b**, **19a** or **21** was dissolved, the solution become green, characteristic of the five-coordinate RuX₂(P-N)(PPh₃).

Table 4.12 Thermodynamic parameters for the formation of *cis*-RuX₂(P-N)(PR₃)(L) in C₆D₆. Errors for K were estimated from repeated experiments; and errors for ΔH° and ΔS° were estimated from maximum and minimum slopes and intercepts of Van't Hoff plots, respectively.

RuX ₂ (P-N)(PR ₃)(L)	K (25°C) M ⁻¹	ΔG° (25°C) ^a kJ/mol	$\Delta H^{\circ b}$ kJ/mol	$\Delta S^{\circ c}$ J/mol K
R = Ph, X = Cl, L = H ₂ S (18a)	153 ± 5	-12.5 ± 0.1	-46 ± 4	-112 ± 14
R = Ph, X = Br, L = H ₂ S (18b)	51 ± 4	-9.7 ± 0.2	-33 ± 4	-77 ± 13
R = <i>p</i> -tolyl, X = Cl, L = H ₂ S (19a)	120 ± 15	-11.9 ± 0.3	-54 ± 9	-140 ± 35
R = Ph, X = Cl, L = MeSH (20)	296 ± 20	-14.1 ± 0.2	-28 ± 3	-48 ± 10
R = Ph, X = Cl, L = EtSH (21)	154 ± 8	-12.5 ± 0.1	-22 ± 4	-32 ± 14

^a ΔG° values are calculated from the equation $\Delta G^\circ = -RT\ln(K)$. ^b ΔH° and ^c ΔS° values are obtained from the slopes and intercepts of the Van't Hoff plots shown in Figure 4.30, respectively.

The choice to use C_6D_6 rather than chlorinated solvents such as CD_2Cl_2 or $CDCl_3$ was governed by the fact that samples in C_6D_6 gave better resolution and better separated peaks in the 1H NMR spectra for integration purposes at $0^\circ C$ or higher. Furthermore, the reproducibility of K values in the chlorinated solvents is poor.

4.7 The Ru-S Bond Strengths in the Solid State: DSC Experiments

Differential scanning calorimetry (DSC) measures the difference in temperature between a sample and an inert reference material as a function of temperature.⁴² Quantitative enthalpy changes may be obtained from a DSC cell if the sample and reference temperatures are maintained at the same temperature during heating and extra heat input into the sample (if endothermic) or to the reference (if exothermic) is measured.

When solid samples of **18a**, **20** or **21** (which exists as acetone solvated species, Section 2.8) are heated in the DSC chamber under N_2 , the enthalpy change (ΔH°) for the loss of H_2S , $MeSH$ or $EtSH$ (ignoring loss of the acetone) is measured, respectively. The DSC curves for the thermal reactions are shown in Figure 4.32. The Ru-S bond strengths in **18a** (85 ± 2 kJ/mol) and **20** (94 ± 2 kJ/mol) are comparable, while the bond is weakest in **21** (64 ± 3 kJ/mol), possibly due to the increased size of the $EtSH$ ligand. Of note, the formation of **21** from the five-coordinate precursor in solution also reveals the smallest exothermicity; however, the solid state reactions are thought to be of a somewhat different nature.

The loss of H_2S or thiols can also be visually observed when solid samples of **18a**, **20** or **21** are placed under vacuum and heated at $50^\circ C$ for 2 h. During this time, the originally yellow solids become green materials which are air-sensitive and instantaneously decompose to uncharacterizable black powders once exposed to O_2 . When the green solids are dissolved in solution (e.g. $CDCl_3$), only the five-coordinate complex *trans*- $RuCl_2(P-N)(PPh_3)$ (**6a**) is

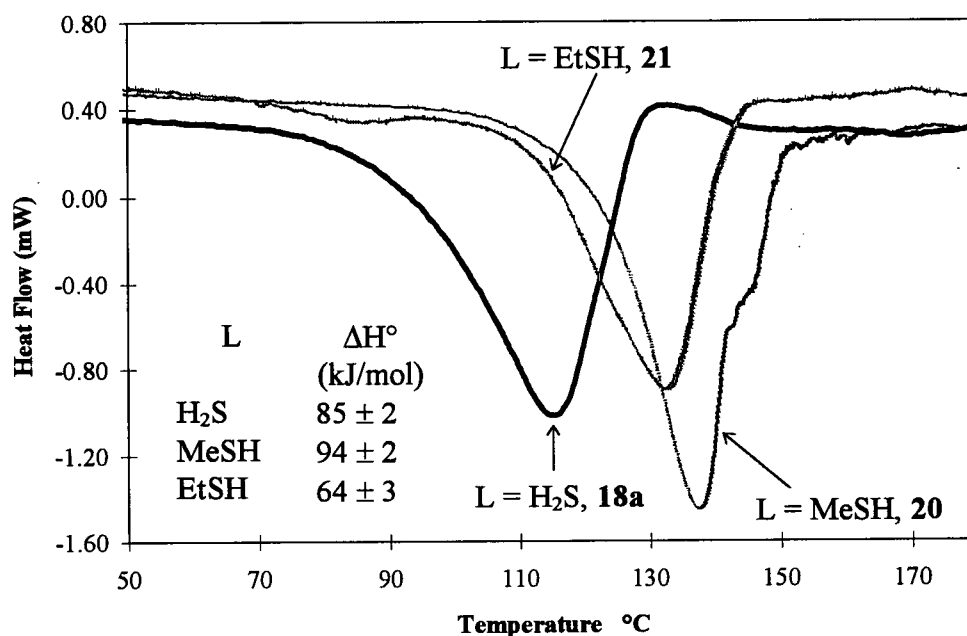


Figure 4.32 DSC curves for *cis*-RuCl₂(P-N)(PPh₃)(L) complexes. Samples are heated in an N₂ atmosphere (flow rate = 40 cc/min) at a rate of 5°C/min to 200°C.

observed by NMR spectroscopy. It is reasonable to assume that the air-sensitive, green solid is *cis*-RuCl₂(P-N)(PPh₃) and that it rearranges to the *trans* isomer in solution. A proposed scheme for the chemistry is shown in Figure 4.33. Differences in the ΔH° values determined by the solution and solid state methods are then attributed to the enthalpy change on converting this *cis*- to *trans*-isomer in the solid state. Thus, by comparison of the ΔH° values obtained from solution (ignoring any solvation effects on the 5- and 6-coordinate species) and those obtained by solid state DSC, ΔH° for the conversion of the *cis* to the more thermodynamically stable *trans*-chloro RuCl₂(P-N)(PPh₃) isomer is in the range -39 to -66 kJ/mol. These values are of the same order of magnitude as those for the solid phase

isomerizations of *trans*-RuCl₂(CO)(RP)₃ to *cis*-RuCl₂(CO)(RP)₃ (R = Ph₂Me, PhMe₂, Me₃; ΔH° values are -15, -21 and -48 kJ/mol, respectively).⁴³

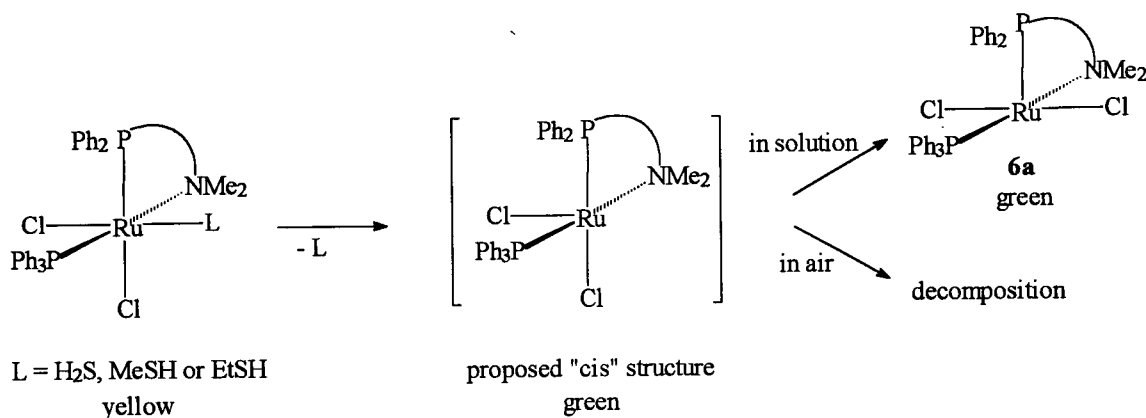


Figure 4.33 Proposed reaction scheme for the loss of L from solid *cis*-RuCl₂(P-N)(PPh₃)(L).

4.8 The Acidity of RuCl₂(P-N)(PPh₃)(H₂S): Proton Abstraction with Proton Sponge

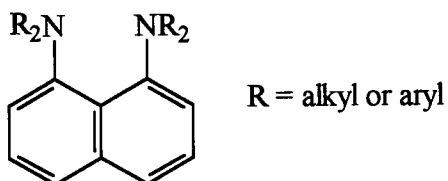


Figure 4.34 Structure of a typical proton sponge.

Proton sponges are strong bases containing a naphthalene structure with amine groups in the 1- and 8- positions (Figure 4.34). Because of their high basicity, non-coordinating behaviour towards metal ions (as a consequence of its steric bulk), and the favourable formation of strong N⋯H⋯N hydrogen bonds upon proton transfer, proton sponges abstract protons effectively from acidic moieties.⁴⁴ In fact, reactions via coordination of proton sponges to metal centres have appeared infrequently in the literature.⁴⁵ In this thesis work, 1,8-bis(dimethylamino)naphthalene (pK_a of conjugate acid = 12.3 in H₂O), herein referred to

as PS, was used. No reaction was observed spectroscopically, when PS is added to a solution of $\text{RuCl}_2(\text{P-N})(\text{PPh}_3)$ (**6a**) in CDCl_3 . In accord with the reaction of $\text{RuCl}_2(\text{PPh}_3)_3$ and H_2 in the presence of added base to produce $\text{Ru}(\text{H})\text{Cl}(\text{PPh}_3)_3$ (Figure 4.35(a)),⁴⁶ Mudalige et al. have shown that the reaction of $\text{RuCl}_2(\text{P-N})(\text{PR}_3)$ and H_2 in the presence of PS affords the hydride $\text{Ru}(\text{H})\text{Cl}(\text{P-N})(\text{PR}_3)$ via the $\eta^2\text{-H}_2$ intermediate (Figure 4.35(b)).²⁷ The use of external bases to deprotonate dihydrogen complexes has been primarily aimed at studying the thermodynamic acidity or pK_a values of such systems. Common bases used in the literature for such experiments include alkoxides (MeO^- , EtO^- , $^t\text{BuO}^-$), phosphines (P^iBu_3 , P^nBu_3 , PCy_3), amines (NEt_3), and metal hydrides ($\text{Ru}(\text{H})\text{Cp}(\text{PPh}_3)_2$, $\text{Ru}(\text{H})\text{Cp}(\text{dppm})$).⁴⁷ Analogously, in the present study, it would be beneficial to obtain $\text{Ru}(\text{SH})$ species (Figure 4.35(c)) in order to determine the acidity of $\text{RuCl}_2(\text{P-N})(\text{PPh}_3)(\text{SH}_2)$ and, in turn, evaluate the strength of the S-H bonds in the coordinated H_2S complex.

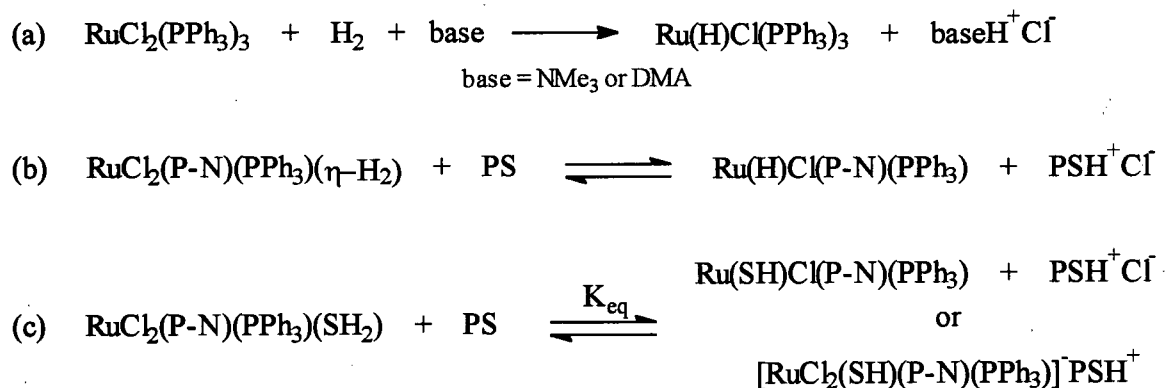


Figure 4.35 (a), (b) Dihydrogen activation by Ru(II) complexes in the presence of added base, and (c) abstraction of proton from $\text{RuCl}_2(\text{P-N})(\text{PPh}_3)(\text{SH}_2)$.

In organic solvents such as CDCl_3 , CD_2Cl_2 , C_6D_6 , or d_6 -acetone, there is no reaction observed between H_2S and PS, implying that H_2S ($\text{pK}_a = 7$ (in aqueous media)) is not a strong acid in these solvents. Similarly, PS does not deprotonate CH_3COOH ($\text{pK}_a = 4.7$ (in aqueous media)) in CDCl_3 . Although a direct comparison of acidity cannot be made between values

obtained in organic and aqueous solutions, studies have shown that pK_a values are related linearly.^{48,49} For example, the pK_a values of hydride complexes are related by the expression $pK_a(H_2O) = pK_a(MeCN) - 7.5$.⁴⁸ In the present study, CD_2Cl_2 was chosen as solvent because it dissolves all the species in equilibrium (Figure 4.35(c)) and is noncoordinating. In theory, the pK_a value of *cis*- $RuCl_2(P-N)(PPh_3)(SH_2)$ may be obtained by evaluating the equilibrium constant (Figure 4.35(c)) and applying the following equation: $pK_a = pK_{eq} + pK_{PSH^+}$, where pK_a for the H_2S complex and pK_{PSH^+} are on the same acidity scale.^{47,50} For ease of comparison, all values are discussed on the aqueous scale.

At 20°C, the addition of 1 atm H_2S to $RuCl_2(P-N)(PPh_3)$ (**6a**) in the presence of 3 equivalents PS in CD_2Cl_2 generated *in situ* a new species observed as an AX pattern at δ 82.25 and δ 57.88 ($^2J_{PP} = 34.05$ Hz) in the $^{31}P\{^1H\}$ NMR spectrum (Figure 4.36 (b)), different from that of *cis*- $RuCl_2(P-N)(PPh_3)(SH_2)$ (**18a**) (Figure 4.36 (a)). However, this new, yellow species, **30**, is only stable within 10 min of H_2S addition; after this time, the $^{31}P\{^1H\}$ NMR signals are no longer observed. **30** decomposed rapidly to a dark brown solution with formation of a white precipitate. The dark brown solid isolated from the filtrate did not give any $^{31}P\{^1H\}$ NMR signals, while broad peaks (δ 6.5 - 8.2, phenyl region and δ 1.5 - 3.8) in the 1H NMR spectrum are indicative of a paramagnetic Ru(III) species. This observation perhaps resembles the decomposition of $[Ru(NH_3)_5(SH_2)][BF_4]_2$ to $[Ru(NH_3)_5(SH)][BF_4]_2$ and H_2 (Section 4.1.1),² although in the current system no H_2 was observed. The 1H NMR spectrum of the white precipitate in $CDCl_3$ is that of PSH^+Cl^- . The 1H NMR spectra of PS (δ 7.35, 6.92 (6H, m, phenyl); δ 2.80 (12H, s, NMe)) and PSH^+Cl^- (δ 12.2 (1H, br, PSH^+); δ 7.95, 7.80, 7.65 (6H, m, phenyl); δ 3.38 (12H, s, NMe)) in $CDCl_3$ are shown in Figure 4.37. Evidently, PS does abstract proton from H_2S with concomitant decomposition of the Ru complex.

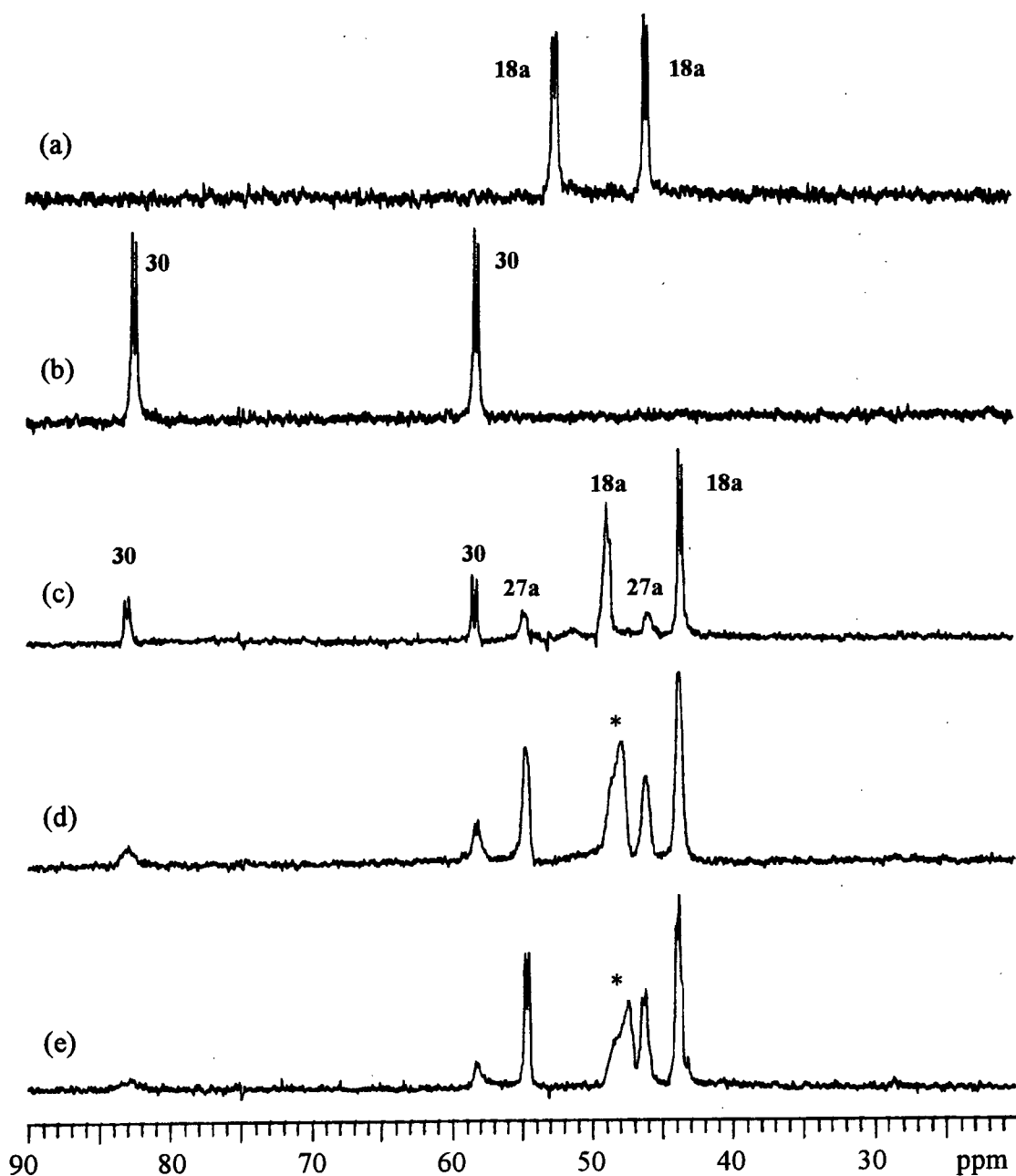


Figure 4.36 $^{31}\text{P}\{^1\text{H}\}$ NMR (300 MHz, CD_2Cl_2) spectra for various Ru(II) complexes containing sulfur ligands: (a) $\text{RuCl}_2(\text{P-N})(\text{PPh}_3)(\text{SH}_2)$ at 20°C ; $\text{RuCl}_2(\text{P-N})(\text{PPh}_3) + 3\text{PS} + 1 \text{ atm H}_2\text{S}$ at (b) 20°C , (c) -25°C , (d) -60°C and (e) -70°C (There is slow decomposition of **27a** and **30** even at low temperatures). *Broadening of the P_A peak of **18a** is only observed with the Varian XL300 spectrometer and not with the Bruker AMX500 spectrometer (Figure 4.12).

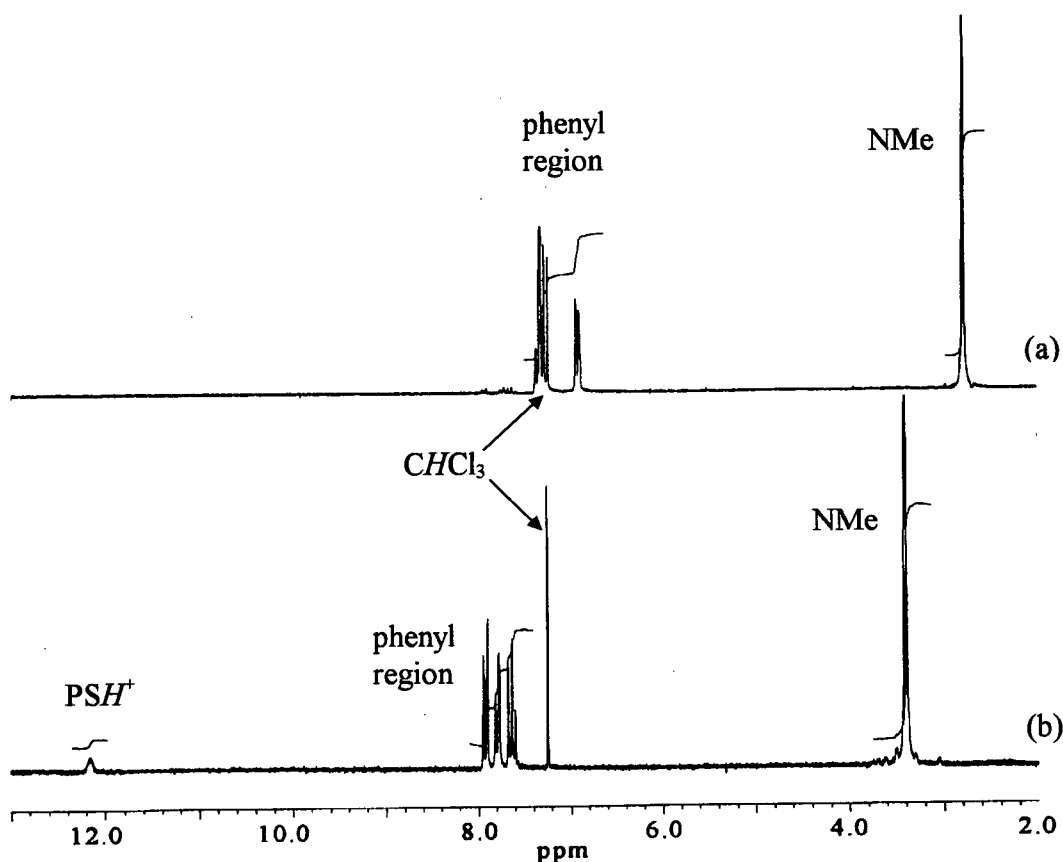


Figure 4.37 ^1H NMR spectra (200 MHz, CDCl_3 , r.t.) of (a) PS and (b) PSH^+Cl^- .

Attempts to isolate **30** were carried out at -78°C . On addition of 1 atm of H_2S to a stirring solution of $\text{RuCl}_2(\text{P-N})(\text{PPh}_3)$ (**6a**) and 1 or 3 equivalents PS in CD_2Cl_2 , a bright yellow solution formed. Addition of hexanes at -78°C resulted in the precipitation of a dark yellow-brown solid. When the suspension was filtered at $\sim -20^\circ\text{C}$, the yellow solid thermally decomposed to a dark brown powder. Of note, the $^{31}\text{P}\{^1\text{H}\}$ NMR spectrum of the above reaction *in situ* at -30°C or lower denotes the presence of three species (Figure 4.36 (c)-(e)). The three sets of AX signals indicate the presence of **18a**, **30**, and an unknown **27a** [δ 54.52 (P_A); δ 46.06 (P_X); $^2J_{\text{PP}} = 30.96$ Hz].

To rationalize the $^{31}\text{P}\{^1\text{H}\}$ NMR data, a proposed reaction scheme is shown in Figure 4.38; this suggests the formation of $\text{Ru}(\text{SH})\text{Cl}(\text{P-N})(\text{PPh}_3)$ (**27a**) as an intermediate en route

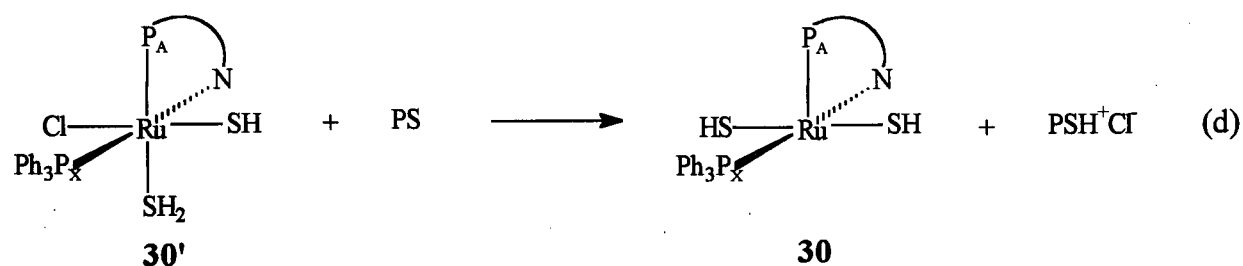
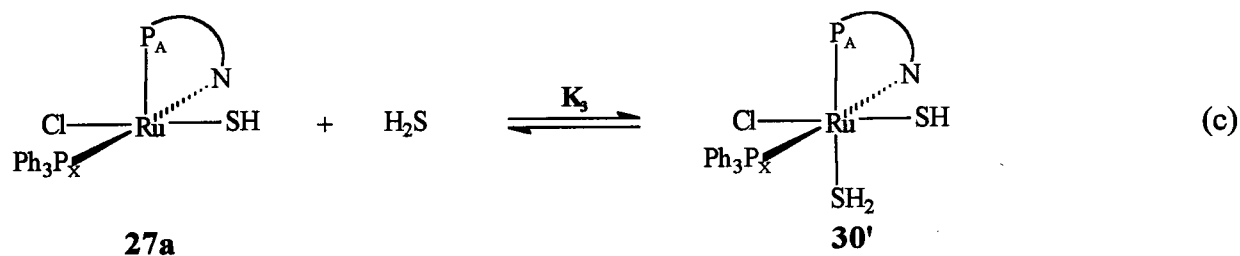
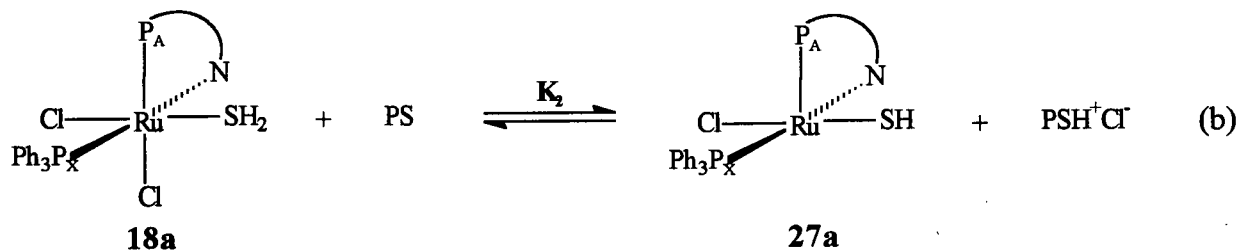
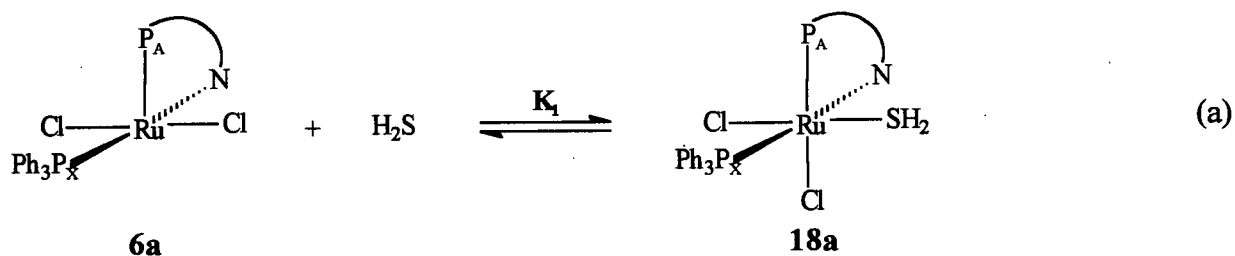


Figure 4.38 (a) Equilibrium for formation of $\text{RuCl}_2(\text{P-N})(\text{PPh}_3)(\text{SH}_2)$ (**18a**); (b), (c), (d) are subsequent equilibria en route to the formation of $\text{Ru}(\text{SH})_2(\text{P-N})(\text{PPh}_3)$ (**30**) in the presence of added PS. Note: the speculative species **30'** was not observed by NMR.

to a bis(mercapto) species $\text{Ru}(\text{SH})_2(\text{P-N})(\text{PPh}_3)$ (**30**). This scheme is supported by other *in situ* NMR data (see below). The presence of excess H_2S ensures the complete formation of $\text{RuCl}_2(\text{P-N})(\text{PPh}_3)(\text{SH}_2)$ (**18a**). K_1 has already been discussed in detail in Section 4.6.

The ^1H NMR signals of **27a** in CD_2Cl_2 or d_6 -acetone could not be assigned at -70 to -25°C because of overlapping peaks due to PS, PSH^+Cl^- and NMe_2 protons (from **18a** and **30**) in the region δ 2.5 - 3.5. Warming a d_6 -acetone solution of the low temperature samples to 20°C leads to complete formation of **30** and assignment of its ^1H NMR signals. A sharp singlet at δ 3.20 due to the NMe_2 protons suggests a symmetrical square pyramidal structure similar to that of **6a**. The SH signals were not observed even when the temperature was lowered to -70°C . Similarly, the reaction of $\text{RuBr}_2(\text{P-N})(\text{PPh}_3)$ (**6b**), PS and H_2S gives $\text{Ru}(\text{SH})\text{Br}(\text{P-N})(\text{PPh}_3)$ (**27b**) and **30**. Further evidence for the formation of **30** was provided by reaction of $\text{RuCl}_2(\text{P-N})(\text{PPh}_3)$ (**6a**) or $\text{RuBr}_2(\text{P-N})(\text{PPh}_3)$ (**6b**) with excess $\text{NaSH}\cdot x\text{H}_2\text{O}$ in d_6 -acetone at 20°C . The fact that the same product was formed regardless of the halogen involved is significant; i.e., both halogens from **6a** and **6b** are displaced by SH.

The initial formation of $\text{Ru}(\text{SH})\text{Cl}(\text{P-N})(\text{PPh}_3)$ (**27a**) and $\text{Ru}(\text{SH})\text{Br}(\text{P-N})(\text{PPh}_3)$ (**27b**) was also evident when **6a** or **6b** was reacted with excess $\text{NaSH}\cdot x\text{H}_2\text{O}$ at -70°C . The $^{31}\text{P}\{^1\text{H}\}$ NMR chemical shifts of **27a** are shifted marginally downfield from those of **27b** (Table 4.13). For these *in situ* reactions, assignment of ^1H NMR signals of **27a** (δ 3.27, 3.18 (6H, s, NMe) and δ -2.08 (2H, s, Ru-SH)) and **27b** (δ 3.56, 3.17 (6H, s, NMe) and δ -1.63 (2H, s, Ru-SH)) were possible because of the absences of overlapping peaks due to PS and free H_2S . Although there is no evidence to indicate the existence of **30'** as an intermediate, the initial coordination of an H_2S molecule to **27a** followed by deprotonation seems a logical route to the formation of **30**. The initial exchange of Cl^- for SH^- is less likely because there is no

reaction between PS and H₂S in the absence of the metal complex. Table 4.13 summarizes the ³¹P{¹H} NMR chemicals shifts for **27a**, **27b** and **30** in d₆-acetone; data for **27a** and **30** in CD₂Cl₂ are very similar (Figure 4.36). All the NMR experiments using hydrosulfide were carried out in d₆-acetone because NaSH·xH₂O is slightly soluble in d₆-acetone and insoluble in CD₂Cl₂.

Table 4.13 ³¹P{¹H} NMR chemicals shifts of Ru(II) mercapto complexes in d₆-acetone.

Complex	T (°C)	δ P _A (P-N)	δ P _B (PPh ₃)	² J _{PP} (Hz)
RuCl(SH)(P-N)(PPh ₃) (27a)	-70	55.70	45.79	31.93
RuBr(SH)(P-N)(PPh ₃) (27b)	-70	56.62	46.16	30.48
Ru(SH) ₂ (P-N)(PPh ₃) (30)	20	82.88	59.19	34.11

A variable temperature NMR study indicates that the formation of **27a** is reversible while the formation of **30** is not. The integration ratio (³¹P{¹H} NMR spectroscopy) of **27a** and **18a** decreases when the temperature is raised from -70°C to -50°C, but the same ratio re-appears when the temperature returns to -70°C. At 20°C, **30** is fully formed, and lowering the temperature gives no indications of the reversible formation of **18a** or **27a**. Repeated attempts to measure accurate equilibrium concentrations of **18a** and **27a** en route to calculating the equilibrium constant (K₂) of formation were unsuccessful. Because **27a** and **30** are thermally unstable and only observed *in situ*, their concentrations can only be measured by integrations in the ³¹P{¹H} spectra at temperatures between -70 to -25°C. However, even at these temperatures, decomposition occurs (see Figure 4.36), resulting in broadened ¹H NMR shifts and very 'noisy' ³¹P{¹H} NMR spectra. Even with long delay acquisition times of 4 s, there are discrepancies between ³¹P{¹H} NMR integrations for repeated experiments.

This matter was further complicated by the decrease in solubilities of the species involved at low temperatures. Because of these difficulties, the pK_a of *cis*-RuCl₂(P-N)(PPh₃)(SH₂) (**18a**) could not be ascertained. However, it can be predicted and concluded that the acidity of H₂S increases upon coordination to **6**. In fact, the Ru complex seems to promote the reaction between H₂S and PS; For example, the *in situ* reaction of RuCl₂(P-N)(PPh₃) (**6a**) with excess added H₂S (100 equivalents) and PS (10 equivalents) in CD₂Cl₂ after 1 h resulted in the formation of 100 % PSH⁺ (¹H NMR singlet at δ 3.38 due to NMe groups; no ¹H NMR signal at δ 2.80 due to PS was observed) and decomposition of the Ru complex. The counter anion for PSH⁺ is most likely to be Cl⁻ and SH⁻; there is a maximum of 2 equivs of Cl⁻ available for the 10 equivs PSH⁺, although no SH⁻ signal was observed in the ¹H NMR spectrum.

Other bases such as triethylamine and 2,6-lutidine were used for attempted proton abstraction from **18a**. However, the same results as described above were obtained.

No reactions were observed when PS was added to solutions containing *cis*-RuCl₂(P-N)(PPh₃)(MeSH) (**20**) and *cis*-RuCl₂(P-N)(PPh₃)(EtSH) (**21**). The pK_a values of uncoordinated MeSH (10.3)⁵¹ and EtSH (10.5)⁵² in aqueous solutions are larger than that of H₂S (7)⁵³. It thus appears that the acidities of MeSH and EtSH upon coordination to Ru are not affected to the extent required for reaction with PS. A stronger base than PS is perhaps required to deprotonate **20** and **21**; the resulting thiolate species are likely to be more stable than the corresponding mercapto species.

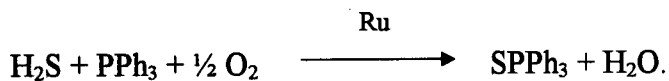
4.9 Reaction of RuCl₂(P-N)(PPh₃) with SO₂

Previous work in this laboratory has shown that **6a** reacts with SO₂ in CH₂Cl₂ to form *cis*-RuCl₂(P-N)(PPh₃)(SO₂), isolable as a yellow-orange solid.^{27(a)} The ³¹P{¹H} NMR chemical shifts (in CDCl₃) are at δ 39.02 (P_A) and δ 37.88 (P_X) (²J_{PP} = 24.77 Hz), while the ¹H

NMR data show two signals at δ 3.50 and δ 3.28 for the NMe₂ protons indicating a *cis* orientation of the Cl ligands. Unlike previous small molecule binding reactions discussed in this Chapter, the SO₂ reaction is irreversible; this, coupled with IR data for the ν_{SO} bands (1287 and 1122 cm⁻¹), suggests a co-planar bonding mode (η^1 -S) for the SO₂ ligand with the Ru.⁵⁴

4.10 Decomposition of *Cis*-RuCl₂(P-N)(PPh₃)(SH₂)

The H₂S systems are very sensitive to O₂ in solution. When O₂ is added to a bright yellow CDCl₃ solution of *cis*-RuCl₂(P-N)(PPh₃)(SH₂) (**18a**) under 1 atm H₂S, a dark green solution results. Precipitation with hexanes resulted in a green-brown solid that gave very 'noisy' ³¹P{¹H} and ¹H NMR spectra. From the filtrate, a white solid was isolated by slow evaporation of the solvents; microanalysis was consistent with the formulation S=PPh₃, and the ³¹P{¹H} NMR spectrum (in CDCl₃) showed a singlet at δ 44.8. S=PPh₃ was also isolated from the reaction of PPh₃ with S₈⁵⁵ and gave a ³¹P{¹H} NMR signal, identical to that of the above species. Of interest, when a mixture of O₂ and H₂S (1:1 by volume injection) is added to a CH₂Cl₂ solution containing **18a** and excess PPh₃, the Ru complex catalytically converts all the PPh₃ to S=PPh₃ and then decomposes. The role that O₂ plays is equivocal at this point, but the following reaction is envisioned:



4.11 Summary

In this Chapter, it was shown that Ru(II) H_2S and thiol complexes can be formed and these are stable under ambient conditions. Thermodynamic parameters indicate that Ru-S bonds are weak. Sterically hindered S-ligands do not coordinate to $\text{RuCl}_2(\text{P-N})(\text{PPh}_3)$. Although the pK_a of *cis*- $\text{RuCl}_2(\text{P-N})(\text{PPh}_3)(\text{SH}_2)$ was not determined, the acidity of H_2S does apparently increase upon coordination as shown by reactions occurring in the presence of proton sponge. Deprotonation of the coordinated thiol groups does not occur.

4.12 References

1. James, B. R. *Pure Appl. Chem.* **1997**, *69*, 2213.
2. Kuehn, C. G.; Taube, H. *J. Amer. Chem. Soc.* **1976**, *98*, 689.
3. (a) Sellmann, D.; Lechner, P.; Knoch, F. *Angew. Chem.Int. Ed. Engl.* **1991**, *30*, 552.
(b) Sellmann, D.; Lechner, P.; Knoch, F.; Moll, M. *J. Am. Chem. Soc.* **1992**, *114*, 922.
4. Edwards, T. H.; Moncur, N. K.; Snyder, L. E. *J. Chem. Phys.* **1967**, *46*, 2139.
5. Ugo, R.; La Monica, G. Cenini, S.; Segre, A.; Conti, F. *J. Chem. Soc. (A)* **1971**, 522.
6. (a) Herberhold, M.; Süss, G. *Angew. Chem. Int. Ed. Engl.* **1976**, *15*, 366.
(b) Herberhold, M.; Süss, G. *J. Chem. Res. (S)*, **1977**, 246; *J. Chem. Res. (M)* **1977**, 2720.
7. Vahrenkamp, H. In *Sulfur - Its Significance for Chemistry, for the Geo-, Bio- and Cosmosphere and Technology*; Müller, A.; Krebs, B., Eds.; Elsevier: Amsterdam, **1984**, p. 121.
8. Harris, P. J.; Knox, S. A. R.; McKinney, R. J.; Stone, F. G. A. *J. Chem. Soc. Dalton Trans.* **1978**, 1009.
9. Strohmeier, W.; Guttenberger, J. F. *Chem. Ber.* **1964**, *97*, 1871.
10. Raab, K.; Beck, W. *Chem. Ber.* **1985**, *118*, 3830.
11. Urban, G.; Sünkel, K.; Beck, W. *J. Organomet. Chem.* **1985**, *290*, 329.
12. Crabtree, R. H.; Davis, M. W.; Mellea, M. F.; Mihelcic, J. M. *Inorg. Chim. Acta* **1983**, *72*, 223.
13. Amarasekera, J.; Rauchfuss, T. B. *Inorg. Chem.* **1989**, *28*, 3875.
14. Kroener, R.; Heeg, M. J.; Deutsch, E. *Inorg. Chem.* **1988**, *27*, 558.
15. Park, H.; Minick, D.; Draganjac, M.; Cordes, A. W.; Hallford, R. L.; Eggleton, G.; *Inorg. Chim. Acta* **1993**, *204*, 195.
16. Conroy-Lewis, F. M.; Simpson, S. J. *J. Chem. Soc., Chem. Commun.* **1991**, 388.

17. Treichel, P. M.; Crane, R. A.; Haller, K. N. *J. Organomet. Chem.* **1991**, *401*, 173.
18. Treichel, P. M.; Schmidt, M. S.; Crane, R. A. *Inorg. Chem.* **1991**, *30*, 379.
19. Belchem, G.; Steed, J. W.; Tocher, D. A. *J. Chem. Soc. Dalton Trans.* **1994**, 1949.
20. Darensbourg, M. Y.; Longridge, E. M.; Payne, V.; Reibenspies, J.; Riordan, C. G.; Springs, J. J.; Calabrese, J. C. *Inorg. Chem.* **1990**, *29*, 2721.
21. Winter, C. H.; Lewkebandara, T. S.; Proscia, J. W.; Rheingold, A. L. *Inorg. Chem.* **1993**, *32*, 3807.
22. (a) Collman, J. P.; Sorrell, T. N.; Hoffman, B. M. *J. Am. Chem. Soc.* **1975**, *97*, 913.
(b) Collman, J. P.; Sorrell, T. N.; Hodgson, K. O.; Kulshrestha, A. K.; Strouse, C. E. *J. Am. Chem. Soc.* **1977**, *99*, 5180.
(c) Collman, J. P.; Sorrell, T. N. In *Concepts in Drug Metabolism*; Jerina, D. M., Ed.; Am. Chem. Soc. Symp. Series, A. C. S., Washington, D. C., 1977, p. 27.
23. Byrn, M. P.; Katz, B. A.; Keder, N. L.; Levan, K. R.; Magurany, C. J.; Miller, K. M.; Pritt, J. W.; Strouse, C. E. *J. Am. Chem. Soc.* **1983**, *105*, 4916.
24. Stephan, D. W. *Inorg. Chem.* **1984**, *23*, 2207.
25. (a) Schlaf, M.; Morris, R. H. *J. Chem. Soc., Chem. Commun.* **1995**, 625.
(b) Schlaf, M.; Lough, A. J.; Morris, R. H. *Organometallics* **1996**, *15*, 4423.
26. Bartucz, T. Y.; Golombek, A.; Lough, A. J.; Maltby, P. A.; Morris, R. H.; Ramachandran, R.; Schlaf, M. *Inorg. Chem.* **1998**, *37*, 1555.
27. (a) Mudalige, D. C.; Rettig, S. J.; James, B. R.; Cullen, W. R. *J. Chem. Soc., Chem. Commun.* **1993**, 830.
(b) Mudalige, D. C. Ph.D. Thesis, The University of British Columbia, 1994.
28. Mudalige, D. C.; Ma, E. S.; Rettig, S. J.; James, B. R.; Cullen, W. R. *Inorg. Chem.* **1997**, *36*, 5426.
29. Osakada, K.; Yamamoto, T.; Yamamoto, A. *Inorg. Chim. Acta* **1985**, *105*, L9.
30. Jessop, P. G.; Lee, C.-L.; Rastar, G.; James, B. R.; Lock, C. J. L.; Faggiani, R. *Inorg. Chem.* **1992**, *31*, 4601.
31. Csizmadia, I. G. In *The Chemistry of the Thiol Group, Part I*; Patai, S., Ed.; John Wiley & Sons: Toronto, 1974, p. 7.

32. Pauling, L. *The Nature of the Chemical Bond*; 3rd Ed.; Cornell University Press: Ithaca, N.Y. 1960.
33. Shaka, A. J.; Barker, P. B.; Freeman, R. *J. Mag. Res.* **1985**, *64*, 547.
34. Jessop, P. G.; Rettig, S. J.; Lee, C.-L.; James, B. R. *Inorg. Chem.* **1991**, *30*, 4617.
35. Jessop, P. G. Ph.D. Thesis, The University of British Columbia, 1991.
36. (a) Karplus, M. *J. Chem. Phys.* **1959**, *30*, 11.
(b) Karplus, M. *J. Am. Chem. Soc.* **1963**, *85*, 2870.
37. Bentrude, W. G.; Setzer, W. N. In *Phosphorus-31 NMR Spectroscopy in Stereochemical Analysis*; Verkade, J. G.; Quin, L. D., Eds.; VCH Publishers, Inc.: Florida, 1987, p. 365, and references therein.
38. (a) Lipsch, J. M. J. G.; Schuit, G. C. *J. Catal.* **1969**, *15*, 179.
(b) Angelici, R. *Acc. Chem. Res.* **1988**, *21*, 387.
39. Wong, T. Y. H.; Barnabas, A. F.; Sallin D.; James, B. R. *Inorg. Chem.* **1995**, *34*, 2278.
40. James, B. R.; Pacheco, A.; Rettig, S. J.; Ibers, J. A. *Inorg. Chem.* **1988**, *27*, 2414, and references therein.
41. (a) Allen, H. C.; Blaine, L. R.; Plyler, E. K. *J. Chem. Phys.* **1956**, *24*, 35.
(b) Allen, H. C.; Plyler, E. K. *J. Chem. Phys.* **1956**, *25*, 1132.
42. West, A. R. *Solid State Chemistry and its Applications*; John Wiley & Sons: New York, 1984, p. 102.
43. (a) Krassowski, D. W.; Nelson, J. H.; Brower, K. R.; Hauenstein, D.; Jacobson, R. A. *Inorg. Chem.* **1988**, *27*, 4294.
(b) Krassowski, D. W.; Reimer, K.; LeMay, Jr., H. E.; Nelson, J. H. *Inorg. Chem.* **1988**, *27*, 4307.
44. (a) Hibbert, F. *J. Chem. Soc. Perkin Trans. II* **1974**, 857.
(b) Alder, R. W.; Goode, N. C.; Miller, N. *J. Chem. Soc., Chem. Commun.* **1978**, 89.
(c) Hibbert, F.; Hunte, K. P. P. *J. Chem. Soc. Perkin Trans. II* **1983**, 1895.
(d) Benoit, R. L.; Lefebvre, D.; Frechette, M. *Can. J. Chem.* **1987**, *65*, 996.
(e) Staab, H. A.; Saupe, T. *Angew. Chem.Int. Ed. Engl.* **1988**, *27*, 865.

- (f) Brzezinski, B.; Grech, E.; Malarski, Z.; Sobczyk, L. *J. Chem. Soc. Perkin Trans. II* **1991**, 857.
45. (a) Gamage, S. N.; Morris, R. H.; Rettig, S. J.; Thackray, D. C.; Thorburn, I. S.; James, B. R. *J. Chem. Soc., Chem. Commun.* **1987**, 894.
(b) Joshi, A. M. Ph.D. Thesis, The University of British Columbia, 1990.
46. (a) Hallman, P. S.; McGarvey, B. R.; Wilkinson, G. *J. Chem. Soc. (A)* **1968**, 3143.
(b) James, B. R. *Adv. Organomet. Chem.* **1979**, *17*, 319.
(c) James, B. R. In *Comprehensive Organometallic Chemistry*, Vol. 8; Wilkinson, G.; Stone, F. G. A.; Abel, E. W., Eds.; Pergamon Press: Oxford, 1982, Chapter 51.
47. Jessop, P. G.; Morris, R. H. *Coord. Chem. Rev.* **1992**, *121*, 155, and references therein.
48. Kristjansdottir, S. S.; Norton, J. R. In *Transition Metal Hydrides: Recent Advances in Theory and Experiment*, Dedieu, A., Ed.; VCH, New York, 1991, Chapter 10.
49. Streuli, C. A. *Anal. Chem.* **1960**, *32*, 985.
50. (a) Guochen, J.; Morris, R. H. *Inorg. Chem.* **1990**, *29*, 582.
(b) Guochen, J.; Morris, R. H. *J. Am. Chem. Soc.* **1991**, *113*, 875.
(c) Guochen, J.; Lough, A. J.; Morris, R. H. *Organometallics* **1992**, *11*, 161.
51. Kreevoy, M. M.; Harper, E. T.; Stary, F. E.; Katz, E. A.; Sellstedt, J. H. *J. Org. Chem.* **1964**, *29*, 1641.
52. Danehy, J. P.; Noel, C. J. *J. Am. Chem. Soc.* **1960**, *82*, 2511.
53. Subcommittee on Hydrogen Sulfide, Committee on Medical and Biologic Effects of Environmental Pollutants, Division of Medical Services, Assembly of Life Sciences, National Research Council in 'Hydrogen Sulfide,' Univeristy Park Press, Baltimore, 1979.
54. (a) Mingos, D. M. P. *Transition Met. Chem.* **1978**, *3*, 1, and references therein.
(b) Kubas, G. J. *Inorg. Chem.* **1979**, *18*, 182.
55. (a) Olah, G. A.; Berrier, A.; Ohannesian, L. *Nouv. J. Chim.* **1986**, *10*, 253.
(b) Wong, T. Y. H. Ph.D. Thesis, The University of British Columbia, 1996.

Chapter 5

Coordination of H₂O and Alcohols to RuCl₂(P-N)(PR₃)

The coordination chemistry of H₂O has been extensively studied and is ubiquitous compared to that of H₂S, in part because it is more pleasant and tractable to work with. In addition, the more weakly acidic H₂O is more stable with respect to the formation of hydroxides and oxides. In homogeneous catalytic systems, weakly coordinating ligands such as H₂O, alcohols and other solvent molecules stabilize the vacant coordination sites of catalytic complexes prior to exchange with desired substrates.¹ The reaction of H₂O with RuCl₂(P-N)(PR₃) (R = Ph, *p*-tolyl) produces the stable H₂O adducts, *trans*-RuCl₂(P-N)(PR₃)(OH₂).² From a structural point of view, the major difference between RuCl₂(P-N)(PR₃)(SH₂) and RuCl₂(P-N)(PR₃)(OH₂) is that the former contains *cis* Cl-atoms while the Cl-atoms of the latter are *trans*. In this Chapter, the aquo complexes are reported, characterized and compared to those of the complexes containing S-ligands discussed in Chapter 4. A probable mechanism for the coordination of H₂S to RuCl₂(P-N)(PR₃) is deduced from these comparisons.

5.1 Preparation of *Trans*-RuCl₂(P-N)(PR₃)(OH₂)

The aquo complexes, *trans*-RuCl₂(P-N)(PR₃)(OH₂) (R = Ph (**33a**), *p*-tolyl (**33b**)), were initially prepared by Mudalige, previously of this laboratory, and she reported the X-ray structure of the R = *p*-tolyl complex.² Mudalige had formed *in situ* samples of **33a** and **33b** in CDCl₃ solutions of RuCl₂(P-N)(PPh₃) (**6a**) or RuCl₂(P-N)(P(*p*-tolyl)₃) (**7a**), respectively, and crystals of **33b** formed in the NMR tube.² During the course of this present thesis work, it was noted that crystals of **33a** and **33b** form easily in the presence of minute amounts of

moisture in solutions and the complexes were further investigated. The aquo complexes are most conveniently prepared by stirring **6a** or **7a** in a mixture of acetone/H₂O (4:1) under Ar (Sections 2.10.1 and 2.10.2). The precipitated and isolated pink solids analyse for the solvated species $\text{RuCl}_2(\text{P-N})(\text{PR}_3)(\text{OH}_2) \cdot (\text{acetone})$. Heating these solids *in vacuo* at 80°C results in the removal of acetone and H₂O and formation of the green, unsaturated five-coordinate precursors **6a** and **7a**. The loss of H₂O is also demonstrated by the thermogravimetric analysis (TGA) of **33a** (Figure 5.1). A weight loss of 11% between 80 to 110°C prior to thermal decomposition is a good approximation to the theoretical combined 9 % weight of acetone and H₂O present.

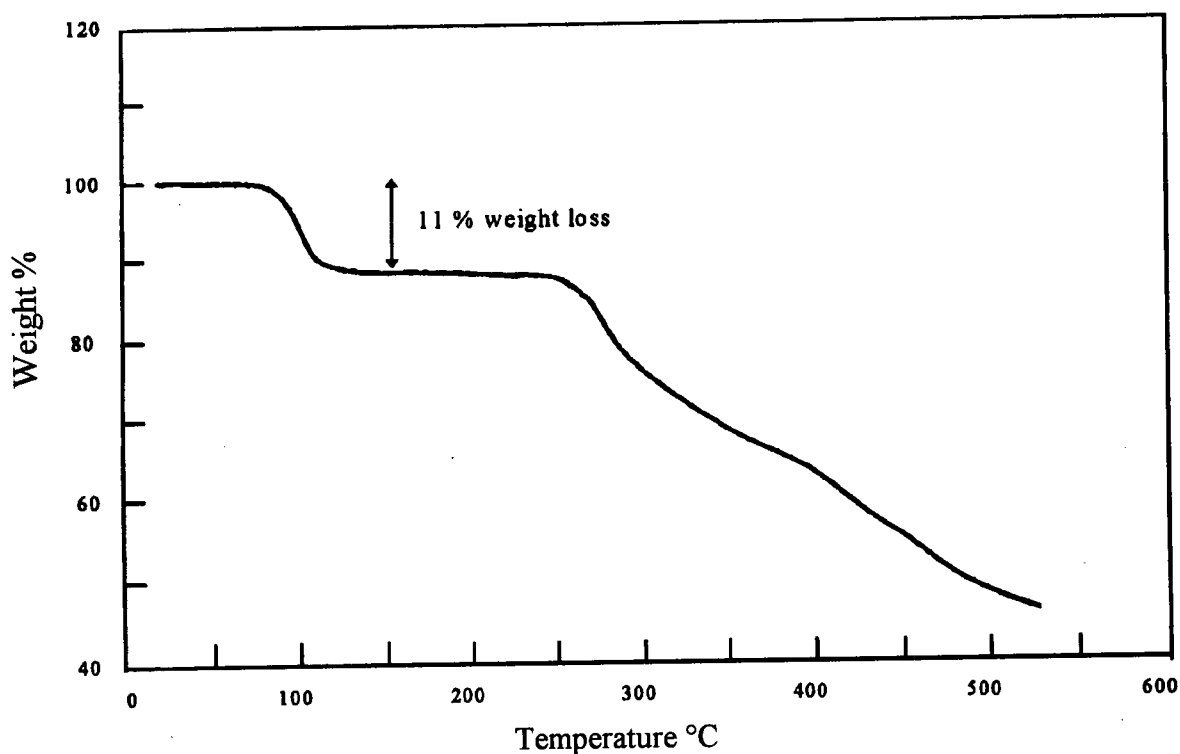


Figure 5.1 TGA spectrum of **33a**, depicting the loss of acetone and H₂O between 80° to 110°C. The sample was heated in a N₂ atm at a flow rate of 100 cc/min.

The ν_1 , ν_2 and ν_3 vibrational bands for gaseous H_2O appear at 3657, 1595 and 3756 cm^{-1} , respectively.³ Upon coordination of H_2O , these vibrations emerge as sharp and intense bands at 3295, 1605 and 3556 cm^{-1} in the IR spectrum of **33a** in the solid state (KBr). [These values differ from those of 3470 and 1739 cm^{-1} obtained by Mudalige for a CHCl_3 solution of **33a** (KBr);² perhaps she may have not recognized the extreme air-sensitivity of **33a** in solution.]

In the solid state, **33a** and **33b** can be formed reversibly by placing **6a** or **7a** in a moist atmosphere. However, the rate at which **33b** forms is approximately three times faster than that of **33a**, although this could well depend on particle size. Nevertheless, when green, powdered samples of **7a** and **6a** are placed in air, the pink solid **33b** forms in < 3 min whereas formation of **33a** takes > 15 min. The X-ray crystal structure of **7a** indicates no agostic interactions between the Ru-atom and any *ortho*-phenyl hydrogen atoms from the $\text{P}(p\text{-tolyl})_3$ ligand, and thus the species has an accessible, vacant sixth coordination site.^{2,4} Although many attempts to grow crystals of **6a** were unsuccessful, the observation that **33a** takes longer to form in the solid state perhaps infers that the sixth coordination site of **6a** is occupied by an *ortho*-phenyl hydrogen of the PPh_3 ligand. This type of agostic interaction has been observed in the very similar square pyramidal complexes $\text{RuCl}_2(\text{PPh}_3)_3$,⁵ $\text{RuBr}_2(\text{PPh}_3)_3$,^{6,7} $\text{RuCl}_2(\text{dppb})(\text{PPh}_3)$ ^{6,7} and $\text{RuCl}_2(\text{isoPFA})(\text{PPh}_3)$.⁸

5.2 X-Ray Crystal Structures of *Trans*- $\text{RuCl}_2(\text{P-N})(\text{PPh}_3)(\text{OH}_2)$ (**33a**)

Pink needle shaped crystals with a monoclinic unit cell, and yellow-brown prism shaped crystals with a triclinic unit cell, were isolated from a solution of **6a** in C_6H_6 under Ar. X-ray crystallographic analysis revealed the respective molecular formulas as *trans*- $\text{RuCl}_2(\text{P-N})(\text{PPh}_3)(\text{OH}_2) \cdot 2\text{C}_6\text{H}_6$ (**I**) and *trans*- $\text{RuCl}_2(\text{P-N})(\text{PPh}_3)(\text{OH}_2) \cdot 1.5\text{C}_6\text{H}_6$ (**II**).

The PLUTO plots for the two structures are shown in Figure 5.2. Both types of crystals yielded very similar structures for the Ru moiety, and both of these are associated with two C_6H_6 solvate molecules. The crystals of **II** were of superior X-ray quality than those of **I** and both H-atoms on the coordinated H_2O were isotropically refined in the former. While no interactions between the solvated C_6H_6 molecules and the Ru moiety in **I** were found, a distance of 2.77(3) Å between H(2) and C(40) in **II** indicates a probable OH/ π phenyl ring interaction.

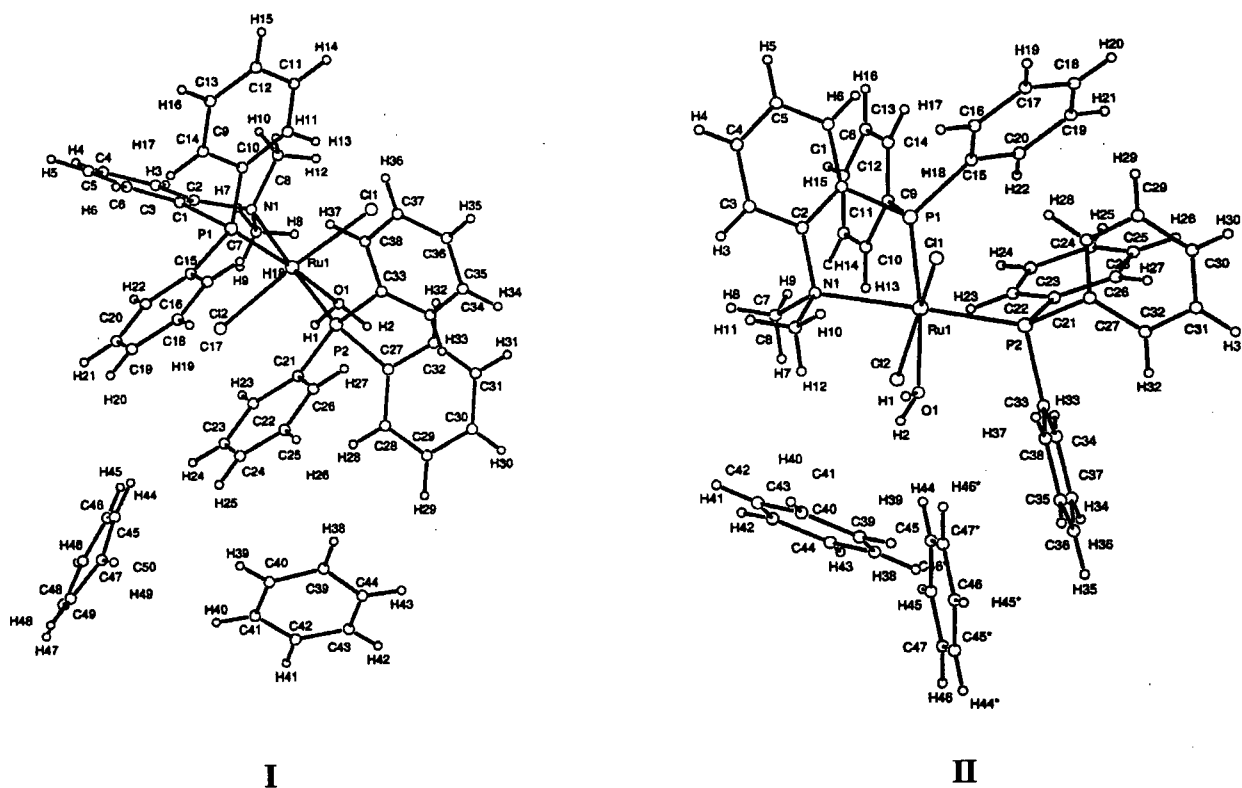
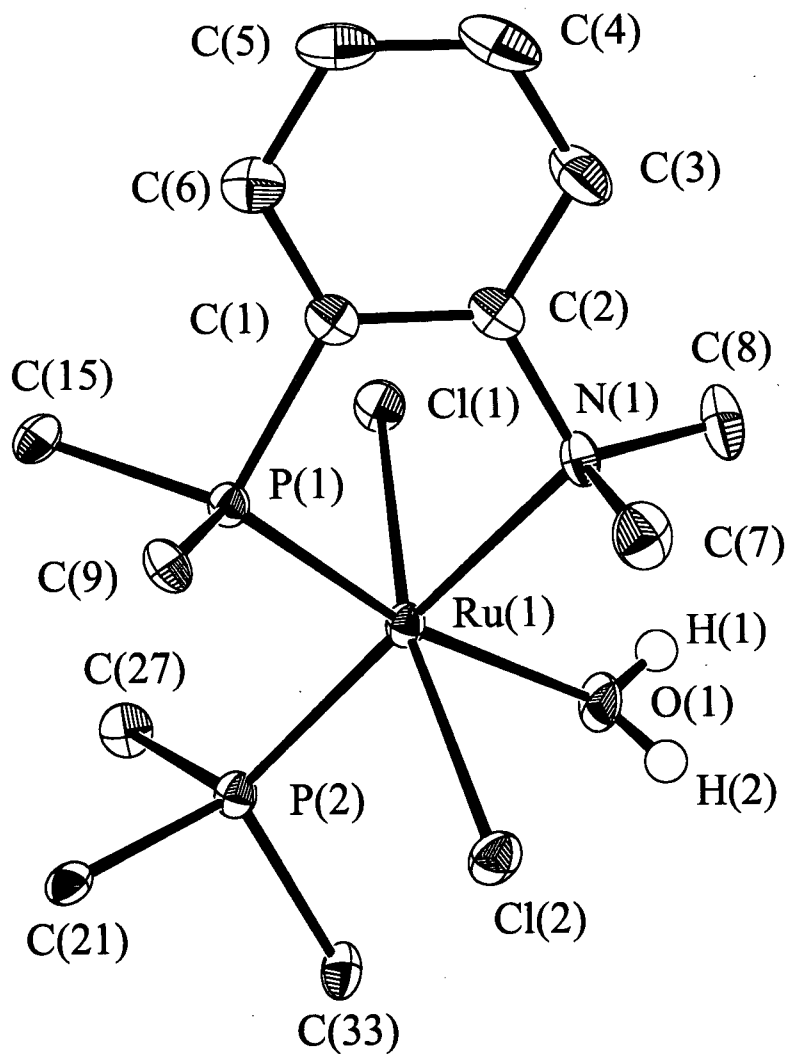


Figure 5.2 PLUTO plots: orientations of C_6H_6 molecules in the structures of **33a** (*trans*- $RuCl_2(P-N)(PPh_3)(OH_2) \cdot 2C_6H_6$ (**I**) and *trans*- $RuCl_2(P-N)(PPh_3)(OH_2) \cdot 1.5C_6H_6$ (**II**)).

The ORTEP plot of **II**, which is very similar to that of **I**, is shown in Figure 5.3 and reveals a pseudooctahedral geometry around the Ru with trans-chloro ligands and the H_2O

**Figure 5.3**

The ORTEP plot of $\text{RuCl}_2(\text{P-N})(\text{PPh}_3)(\text{OH}_2) \cdot 1.5\text{C}_6\text{H}_6$ (**33a (II)**). Thermal ellipsoids for non-hydrogen atoms are drawn at 33 % probability (some of the phenyl carbons have been omitted for clarity). Full experimental parameters and details are given in Appendix VIII.

trans to the P-atom of the P-N ligand. Selected bond lengths and angles of **I** and **II** are shown and compared with those of *trans*-RuCl₂(P-N)(P(*p*-tolyl)₃(OH₂)) (**33b**)² in Tables 5.1 and 5.2, respectively. The Ru-O(1) bond of **II** is significantly shorter (2.187 Å) than those of **I** (2.238 Å) and **33b** (2.252 Å), but is intermediate between those weakly bound aquo ligand complexes (e.g. *trans*-[Ru(H₂O)(PEt₃)₂(trpy)][ClO₄]₂ (2.218 Å, trpy = 2,2',2''-terpyridine)⁹ and [Ru(η⁶-MeC₆H₄Pr^{*i*}-*p*)(H₂O)(L)][ClO₄] (2.203 Å, HL = (S)-(α-methylbenzyl)salicylaldehydeimine)¹⁰) and strongly coordinated aquo complexes (e.g. [RuH(H₂O)(CO)₂(PPh₃)₂]₂X (2.15 Å),¹¹ [Ru(η⁶-C₆H₆)(H₂O)₃][SO₄] (2.127 Å),¹² Ru(H₂O)₂(η¹(O):η²(C,C')-OCOCH₂CH=CHCH₃)₂ (2.141 and 2.115 Å),¹³ [Ru(H₂O)₆][OTs]₂ (2.122 Å, OTs = *p*-toluenesulfonate),¹⁴ and [(cod)Ru(H₂O)₄][OTs]₂ (2.158 and 2.095 Å)¹⁵). Evidently, the close approach of the solvated benzene rings to the coordinated H₂O ligand of **II** results in the contraction of the Ru-O bond. This shorter Ru-O bond of **II** imposes the following structural consequences: (i) Strong intramolecular hydrogen bonds between the H₂O ligand and the trans-Cl-atoms are formed. The H(1)⋯Cl(1) and H(2)⋯Cl(2) bonds are 2.43 Å (2.79 Å for **33b**) and 2.76 Å (2.84 Å for **33b**), respectively. (ii) The coordinated O-H bonds are 0.74 and 0.81 Å, significantly shorter than those of free H₂O (0.956 Å) and the H-O-H angle contracts from 105° (free H₂O) to 97.5°; this is perhaps because of volume restrictions imposed by the close proximity of the Cl-atoms and the solvated benzene rings. (iii) Mutual repulsion of the O and Cl(1) atoms results in a larger Cl(1)-Ru-O angle of 85.40° (82.47° for **I** and 81.6° for **33b**) and a smaller Cl(2)-Ru-O angle of 80.63° (83.87° for **I** and 82.2° for **33b**); as a result, the Cl(1)-Ru-P(1) angle is substantially smaller at 88.02° compared to 104.11° of **I** and 104.30° of **33b**. Repulsion between Cl(2) and O also results in a smaller Cl(2)-Ru(1)-P(2) angle of 86.97° (98.88° for **I** and 96.26° for **33b**).

Table 5.1 Selected bond lengths (Å) for *trans*-RuCl₂(P-N)(PPh₃)(OH₂)·2C₆H₆ (**I**), *trans*-RuCl₂(P-N)(PPh₃)(OH₂)·1.5C₆H₆ (**II**) and *trans*-RuCl₂(P-N)(P(*p*-tolyl)₃)(OH₂) (**33b**) with estimated standard deviations in parentheses.

Bond	Length (Å)		
	33a (I)	33a (II)	33b
Ru(1)-O(1)	2.238(3)	2.187(2)	2.252(4)
Ru(1)-P(1)	2.2281(11)	2.2344(8)	2.220(1)
Ru(1)-P(2)	2.3147(12)	2.3085(7)	2.284(1)
Ru(1)-N(1)	2.308(3)	2.311(2)	2.326(4)
Ru(1)-Cl(1)	2.3941(11)	2.3976(6)	2.385(1)
Ru(1)-Cl(2)	2.4173(10)	2.4298(6)	2.418(1)
O(1)-H(1)	N/A	0.74(2)	0.69(6)
O(1)-H(2)	N/A	0.81(3)	0.96(6)
H(1)···Cl(1)	N/A	2.43(3)	2.79(7)
H(2)···Cl(2)	N/A	2.76(3)	2.84(6)

Table 5.2 Selected bond angles ($^{\circ}$) for *trans*-RuCl₂(P-N)(PPh₃)(OH₂)·2C₆H₆ (**I**), *trans*-RuCl₂(P-N)(PPh₃)(OH₂)·1.5C₆H₆ (**II**) and *trans*-RuCl₂(P-N)(P(*p*-tolyl)₃)(OH₂) (**33b**) with estimated standard deviations in parentheses.

Bond	Angle ($^{\circ}$)		
	33a (I)	33a (II)	33b
H(1)-O(1)-H(2)	N/A	97.5(28)	N/A
Ru(1)-O(1)-H(1)	N/A	126.6(23)	N/A
Ru(1)-O(1)-H(2)	N/A	116.4(25)	N/A
Cl(1)-Ru(1)-O(1)	82.47(7)	85.40(6)	81.6(1)
Cl(2)-Ru(1)-O(1)	83.87(7)	80.63(6)	82.2(1)
Cl(1)-Ru(1)-P(1)	104.11(4)	88.02(2)	104.30(5)
Cl(1)-Ru(1)-P(2)	87.05(4)	96.30(2)	89.74(5)
Cl(1)-Ru(1)-N(1)	91.01(9)	84.09(5)	90.8(1)
Cl(1)-Ru(1)-Cl(2)	165.18(4)	165.58(2)	162.91(4)
O(1)-Ru(1)-P(1)	168.33(7)	169.95(6)	168.8(1)
O(1)-Ru(1)-P(2)	90.94(8)	88.57(6)	91.4(1)
O(1)-Ru(1)-N(1)	88.85(11)	90.30(8)	90.3(1)
Cl(2)-Ru(1)-P(1)	88.45(4)	105.32(3)	90.73(4)
Cl(2)-Ru(1)-P(2)	98.88(4)	86.97(2)	96.26(5)
Cl(2)-Ru(1)-N(1)	83.01(9)	92.37(5)	83.7(1)
P(1)-Ru(1)-P(2)	98.94(4)	99.70(3)	98.04(5)
P(1)-Ru(1)-N(1)	81.48(9)	81.46(6)	80.20(9)
P(2)-Ru(1)-N(1)	178.06(9)	178.77(6)	178.24(9)

The notable structural difference between the aquo complexes and the complexes containing sulfur ligands (Chapter 4) is that the Cl-atoms in the former are mutually trans but are cis in the latter. Consequently, the P(1) (of the P-N ligand) is trans to H₂O ligand in the former and trans to a Cl-atom in the latter (see Chapter 1, Figure 1.18). The observation that the Ru-P(1) bonds in **I**, **II** and **33b** (2.2281, 2.2344 and 2.220 Å) are shorter than those in the complexes containing S ligands (2.27 Å on average) indicates that the Cl-atom has a stronger *trans* influence than that of H₂O toward phosphines. This is in agreement with *ab initio* calculations,¹⁶ and ¹J_{PP} NMR data obtained for *trans*-[Pt(H₂O)(CH₃)(dppe)]BF₄ and *trans*-[Pt(Cl)(CH₃)(dppe)].¹⁷ The correlation between ³¹P NMR data and *trans* influence will be discussed in Section 5.3.

5.3 NMR Spectra of *Trans*-RuCl₂(P-N)(PPh₃)(OH₂) (**33a**)

The ³¹P NMR spectrum of a sample of isolated **33a** shows a characteristic AX coupling pattern. The resolution and chemical shifts of these resonances, however, are dependent on the solvent, temperature and concentration of added H₂O. In solution, **33a** is in a rapid equilibrium with **6a** (Figure 5.4) and resonances of the individual species are unresolved and indistinguishable on the NMR timescale. While the chemical shifts due to P_X (sharp doublets at δ ~ 48) are relatively constant in different temperatures and solvents in the ³¹P{¹H} NMR spectra of **33a**, the P_A signals appear from δ 68 to δ 80 as broad peaks or doublets (e.g. see Figure 5.5). Table 5.3 compares the P_A and P_X chemical shifts of isolated samples of **33a** with those of **6a** in various solvents. Weakly coordinating solvent molecules compete with H₂O for the vacant sixth site on the Ru. For example, d₆-acetone is weakly coordinated to **6a**, trans to P_A, as indicated by the broad P_A signal at δ 70.5 (Figure 5.6(a)). A sharp doublet due to P_A emerges as the concentration of H₂O is increased and equilibrium

favours the formation of **33a** (Figure 5.6(b)-(e)). Coordinative competition from acetone is negligible upon addition of > 300 equiv of H₂O.

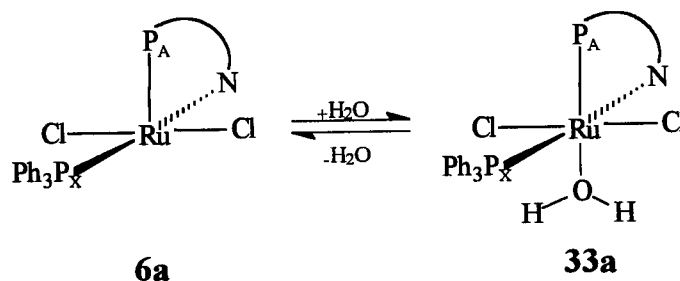


Figure 5.4 Rapid equilibrium between **6a** and **33a**.

Table 5.3 P_A and P_X chemical shifts for RuCl₂(P-N)(PPh₃) (**6a**) and *trans*-RuCl₂(P-N)(PPh₃)(OH₂) (**33a**) in various solvents at 20°C.^a

Solvent	δ P _A		δ P _X		² J _{PP} (Hz)	
	6a	33a	6a	33a	6a	33a
CD ₂ Cl ₂	80.51	80.1(br) ^b	47.00	48.40 ^b	36.54	37.39 ^b
CDCl ₃	83.23	68.5(br) ^b	48.41	45.70 ^b	34.82	37.76 ^b
C ₆ D ₆	83.69	73.52 ^b	48.87	49.31 ^b	36.54	38.00 ^b
d ₆ -acetone	70.5(br)	61.78 ^c	47.27	48.03 ^c	38.36	38.12 ^c

^aAll chemical shifts above are doublets unless otherwise specified by (br) to indicate a broad signal.

^bThe spectra are for isolated samples of **33a**, i.e. in the absence of added H₂O.

^cSpectra refer to fully formed **33a** in the presence of added H₂O.

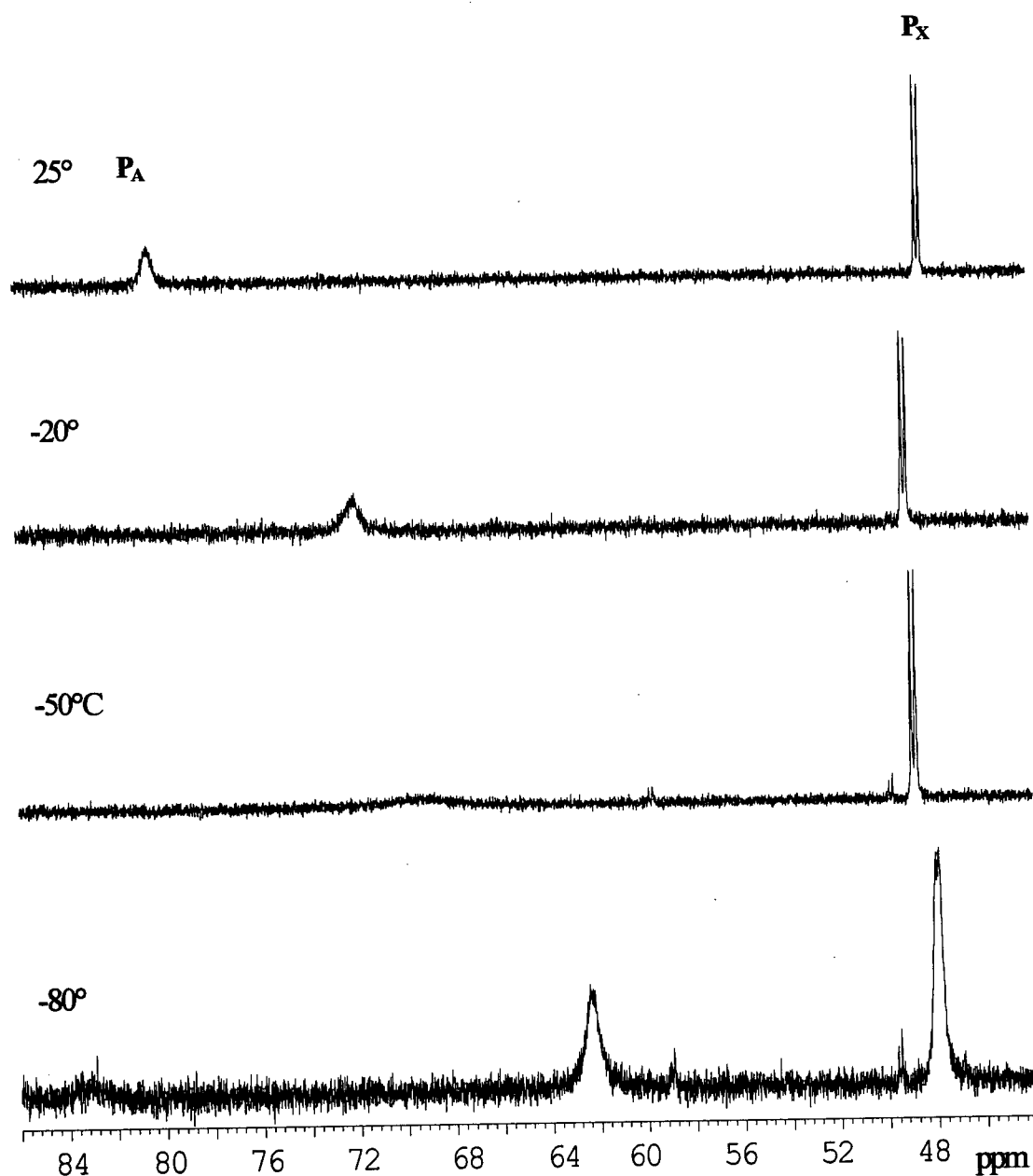


Figure 5.5 $^{31}\text{P}\{^1\text{H}\}$ NMR spectra (202.47 MHz) of *trans*- $\text{RuCl}_2(\text{P-N})(\text{PPh}_3)(\text{OH}_2)$ (33a) in CD_2Cl_2 at various temperatures. A new, unidentified species appeared between -50° and -80°C as indicated by signals at δ 49.8 and δ 59.0.

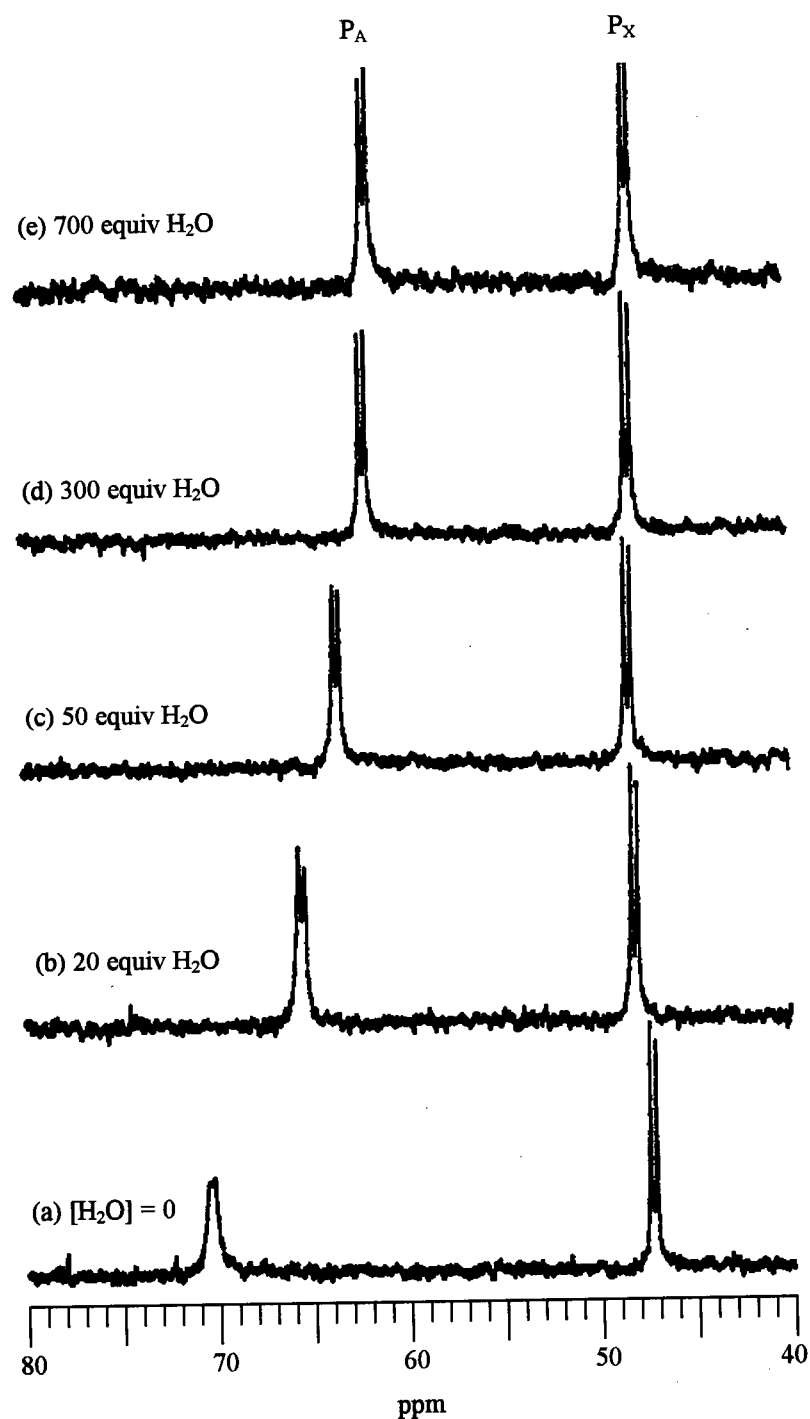


Figure 5.6 $^{31}\text{P}\{^1\text{H}\}$ NMR spectra (121.4 MHz, 20°C) of $\text{RuCl}_2(\text{P-N})(\text{PPh}_3)$ (**6a**) in d_6 -acetone with various H_2O concentrations.

The $^{31}\text{P}\{^1\text{H}\}$ NMR spectra of samples of **33a** in CD_2Cl_2 at various temperatures are shown in Figure 5.5. The rapid coordination and dissociation of the aquo ligand *trans* to the P_A atom of the aminophosphine ligands are apparent from the downfield broad signal. This type of NMR coalescence is a consequence of the *trans* effect of P_A on the H_2O ligand. Examples of this behaviour have been demonstrated by the weakly bonded H_2O complexes, *trans,mer*- $[\text{MCl}_2(\text{H}_2\text{O})(\text{PMe}_2\text{Ph})_3][\text{ClO}_4]$ ($\text{M} = \text{Rh}^{19}$ or Ir^{20}). At 25°C , equilibrium favours **6a** as indicated by the P_A chemical shift at δ 80.1. As the temperature is lowered to -50°C , concentrations of both species become equivalent and the P_A resonances coalesce into the baseline. Finally, at -80°C , the P_A signal reappears at δ 62.3 due to the dominance of the aquo complex. The ^1H NMR spectra of **33a** also agree with the above observation although the distinction between the resonances of **6a** and **33a** is not as obvious. That is, the $-\text{NMe}_2$ signals of both complexes overlap as seen in Figure 5.7. Of note, when the temperature is lowered from 25° to -80°C , the resonances due to the coordinated H_2O shift downfield from δ 2.18 to 3.42 while the $-\text{NMe}_2$ resonances shift upfield from δ 3.20 to 2.85.

The $^{31}\text{P}\{^1\text{H}\}$ and ^1H NMR spectra of the **6a/33a** equilibrium system are in marked contrast to those of the **6a/18a** (*cis*- $\text{RuCl}_2(\text{P-N})(\text{PPh}_3)(\text{SH}_2)$) system where both species are distinguished. The coalescence of the resonances of **6a** and **33a** on the NMR-timescale indicate that the aquo system is much more labile; i.e. the reversible formation of the aquo complex is faster than the H_2S species.

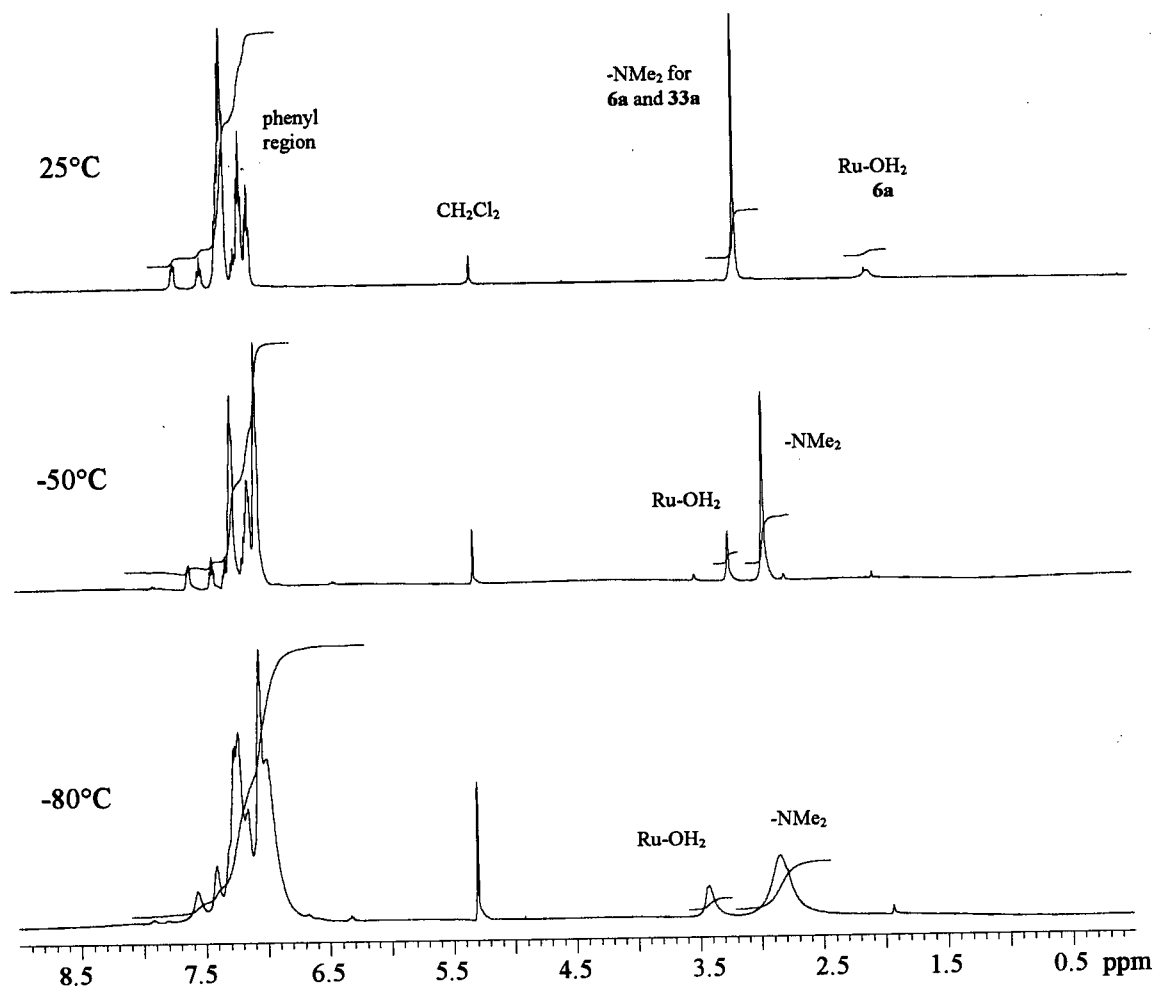


Figure 5.7 ^1H NMR spectra (500 MHz) of *trans*- $\text{RuCl}_2(\text{P-N})(\text{PPh}_3)(\text{OH}_2)$ (**33a**) in CD_2Cl_2 at various temperatures.

5.4 *Trans* Influence of Ligands and its Effect on ^{31}P NMR Chemical Shifts

The *trans* effect of the P-atom of the P-N ligand on the H_2O ligand leads to the rapid and reversible coordination of H_2O . Conversely, the *trans* influence of H_2O on P-N must weaken the Ru-P_A bond relative to its strength in the five-coordinate complex **6a**. The *trans*-influence of the ligand *trans* to the P_A atoms is exemplified by the $^{31}\text{P}\{^1\text{H}\}$ NMR spectra of the $\text{RuCl}_2(\text{P-N})(\text{PR}_3)(\text{L})$ (L = small molecule) complexes. For example, the ligand *trans* to P_A is Cl for *cis*- $\text{RuCl}_2(\text{P}_\text{A}-\text{N})(\text{P}_\text{X}\text{R}_3)(\text{H}_2\text{S})$, and H_2O for *trans*- $\text{RuCl}_2(\text{P}_\text{A}-\text{N})(\text{P}_\text{X}\text{R}_3)(\text{H}_2\text{O})$. In both cases the N-atom of the P-N ligand is *trans* to PPh_3 and the chemical shift of P_X is

relatively insensitive to the incoming ligand L or the orientation of the Cl-atoms (Table 5.4). The negligible *cis*-influence of ligands on phosphines is also demonstrated by ^{31}P NMR chemical shifts and $^1J_{\text{Pt-P}}$ coupling constants of platinum(II) phosphine systems.^{21,22} The chemical shifts of P_A , however, are dependent on the ligand at the *trans* position. A more downfield P_A signal corresponds to a higher *trans* influence of the *trans* ligand because *trans* influence is determined by the ability of this ligand to deshield P_A .^{23,24} That is, the *trans* influence is determined by the ligands effectiveness in competing for the metal orbital's s-character.^{25,26} Alternatively, the *trans* influence is also dependent on the σ -donating ability of the ligands as demonstrated by the $^1J_{\text{M-P}}$ NMR data obtained for $\text{M} = \text{Rh}(\text{I})$ ²⁵ and $\text{Pt}(\text{II})$ ^{23,27} systems. A large J value indicates a weak influence by the *trans* ligand because large NMR coupling constants reflect strong σ -bonds.^{25,28}

Table 5.4 Comparison of $^{31}\text{P}\{^1\text{H}\}$ NMR chemical shifts and Ru-P bond lengths.

Complex (in CDCl_3)	δP_A	Ru- P_A (Å)	δP_X	Ru- P_X (Å)	$^2J_{\text{PP}}$ (Hz)
<i>trans</i> - $\text{RuCl}_2(\text{P-N})(\text{P}(p\text{-tolyl})_3)$ (7a) ^a	81.46	2.170(1)	47.64	2.290(1)	37.15
<i>trans</i> - $\text{RuCl}_2(\text{P-N})(\text{P}(p\text{-tolyl})_3)(\text{OH}_2)$ (33b) ^b	71.80	2.220(1)	47.62	2.284(1)	38.12
<i>trans</i> - $\text{RuCl}_2(\text{P-N})(\text{PPh}_3)(\text{OH}_2)$ (33a , I (II)) ^b	68.50	2.2281(11) (2.2344(8))	47.70	2.3147(12) (2.3085(7))	37.76
<i>cis</i> - $\text{RuCl}_2(\text{P-N})(\text{P}(p\text{-tolyl})_3)(\text{SH}_2)$ (19a) ^c	51.91	2.2560(4)	42.58	2.3040(3)	30.41
<i>cis</i> - $\text{RuCl}_2(\text{P-N})(\text{PPh}_3)(\text{SH}_2)$ (18a) ^c	50.60	2.2712(6)	44.48	2.3110(7)	30.23
<i>cis</i> - $\text{RuBr}_2(\text{P-N})(\text{PPh}_3)(\text{SH}_2)$ (18b) ^c	53.41	2.2617(10)	44.36	2.5540(4)	29.20
<i>cis</i> - $\text{RuCl}_2(\text{P-N})(\text{PPh}_3)(\text{MeSH})$ (20) ^c	51.43	2.2803(7)	42.37	2.3100(7)	29.87
<i>cis</i> - $\text{RuCl}_2(\text{P-N})(\text{PPh}_3)(\text{EtSH})$ (21) ^c	50.97	2.2753(5)	42.48	2.3100(6)	30.05
<i>cis</i> - $\text{RuCl}_2(\text{P-N})(\text{PPh}_3)(\text{H}_2)$ (36) ^d	49.30	2.2884(7)	45.48	2.3098(6)	26.83
<i>cis</i> - $\text{RuCl}_2(\text{P-N})(\text{PPh}_3)(=\text{C}=\text{C}(\text{H})\text{Ph})$ (45) ^d	37.85	2.332(2)	36.40	2.346(2)	26.50

Discussions of the above crystal structures are found in: ^aChapter 3, ^bcurrent chapter, ^cChapter 4, and ^dChapter 6.

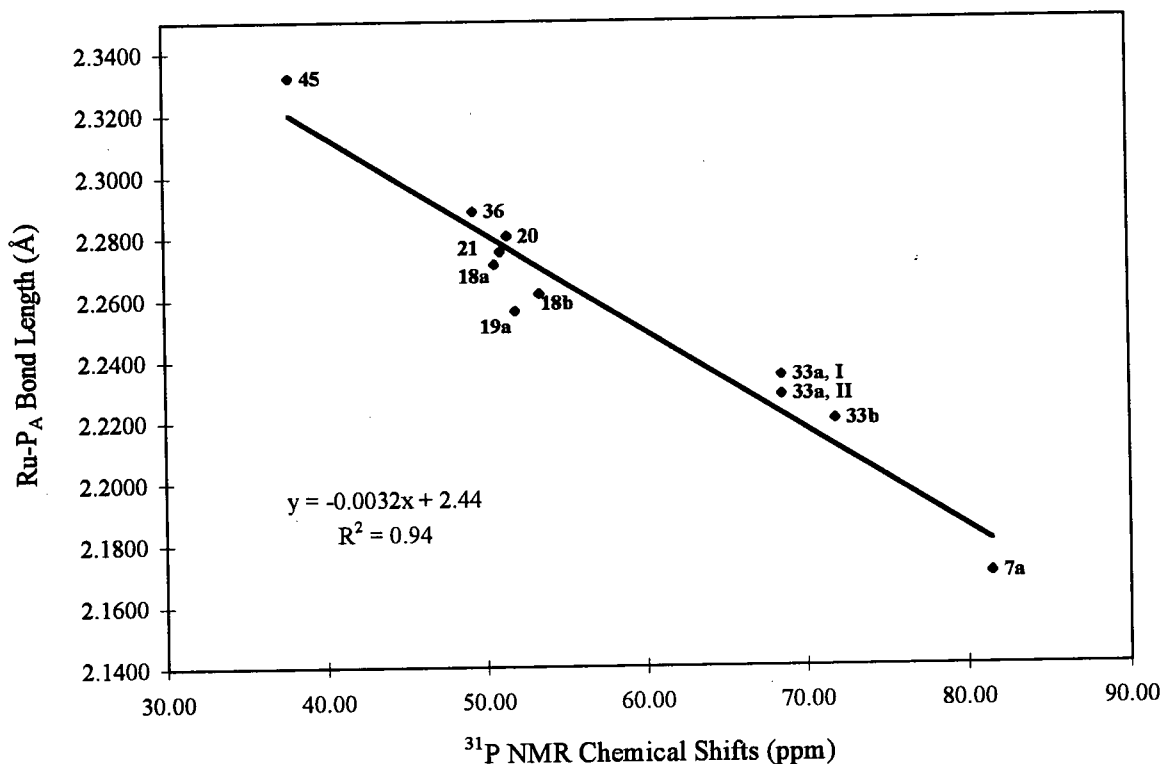


Figure 5.8 The relationship between Ru-P_A bond length (Å) and δ P_A (in CDCl₃) for the complexes containing the Ru(P-N) moiety. (Structures of **7a**, **19a**, **33b** and **45** were measured at 21°C, **18a**, **18b**, **20**, **21** and **33a** were determined at -93°C, and **36** was determined at -100°C; $^{31}\text{P}\{^1\text{H}\}$ NMR chemical shifts of P_A for all the complexes were determined at 20°C.)

Table 5.4 also compares the $^{31}\text{P}\{^1\text{H}\}$ NMR chemical shifts and Ru-P bond lengths for Ru(P-N) complexes related to this thesis work. With the exception of **45**, the δ P_X shifts for the chloro complexes are consistently at ca. δ 45 and the Ru-P_X bond lengths are ca. 2.31 Å. The inverse dependence of δ P_A on Ru-P_A is plotted in Figure 5.8, a trend that has also been observed for Ru(II) complexes containing PPh₃^{29,30} and DPPB (Ph₂P(CH₂)₄PPh₂)^{31,32} ligands. In fact, the plot for the P-N system (slope = -3.2×10^{-3} Å ppm⁻¹, intercept = 2.44 Å) is similar to that of the PPh₃ (slope = -2.9×10^{-3} Å ppm⁻¹, intercept = 2.47 Å) and DPPB (slope = -2.9×10^{-3} Å ppm⁻¹, intercept = 2.42 Å) systems.

From the plot shown in Figure 5.8, the ligands can be listed in order of decreasing *trans* influence: $\text{Cl} \sim \text{Br} > \text{H}_2\text{O}$. In accord, halides are better σ - and π -donors than H_2O . Of note, $^2J_{\text{PP}}$ values for the *trans* complexes (~ 37.7 Hz) are larger than those of the *cis* complexes (~ 29.0 Hz). Tables 5.5 and 5.6 list the Ru-Cl bond distances when the Cl-atoms are mutually *trans* and *cis*, respectively. From the comparisons of the average *trans* Ru-Cl bond distances in Table 5.5 and Ru-Cl_A bond distances in Table 5.6, it can be stated that S-ligands have a stronger *trans* influence than that of Cl. Further, the S-ligands (average Ru-Cl_A = 2.42 Å) perhaps have a slightly greater *trans* influence than that of H₂ (Ru-Cl_A = 2.41). The P_A-atom of the P-N ligand has a greater *trans* influence than that of Cl as indicated by the relatively long Ru-Cl_B bonds in Table 5.6. Greater *trans* influence of phosphine ligands over Cl has been previously observed for Pt(II)²³ and Rh(I)²⁵ complexes. Using the above observations and assuming that the *cis* effects are negligible, a *trans* influence order is derived as: $\text{P}_\text{A} > \text{SH}_2 \sim \text{thiols} > \text{H}_2 > \text{Cl} \sim \text{Br} > \text{H}_2\text{O}$.

Table 5.5 Ru-Cl bond lengths (Å) for *trans*-RuCl₂(P-N)(PR₃)(L).

<i>trans</i> -RuCl ₂ (P-N)(PR ₃)(L)	Bond Lengths (Å)	
	Ru-Cl _A	Ru-Cl _B
R = Ph, L = vacant (7a)	2.387(1)	2.379(1)
R = Ph, L = H ₂ O (33a , I)	2.3941(11)	2.4173(10)
R = Ph, L = H ₂ O (33a , II)	2.3976(6)	2.4298(6)
R = <i>p</i> -tolyl, L = H ₂ O (33b)	2.385(1)	2.418(1)

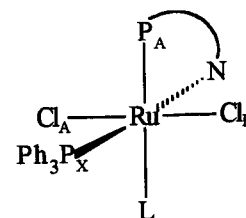
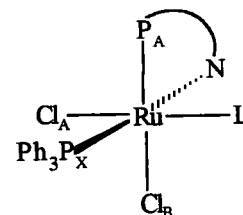
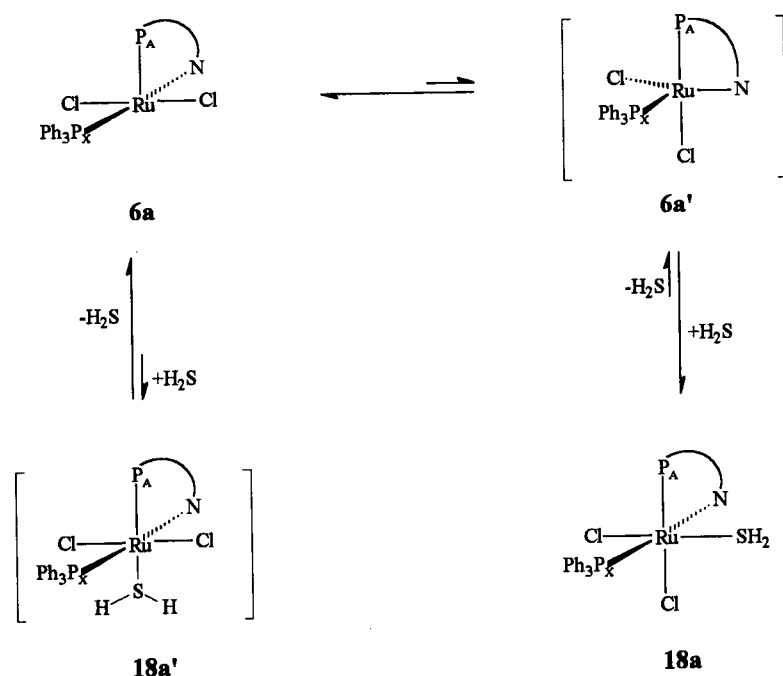


Table 5.6 Ru-Cl bond lengths (Å) for *cis*-RuCl₂(P-N)(PR₃)(L).

<i>cis</i> -RuCl ₂ (P-N)(PR ₃)(L)	Bond Lengths (Å)	
	Ru-Cl _A	Ru-Cl _B
R = Ph, L = H ₂ S (18a)	2.4238(6)	2.4721(5)
R = <i>p</i> -tolyl, L = H ₂ S (19a)	2.429(3)	2.469(4)
R = Ph, L = MeSH (20)	2.4241(7)	2.4472(7)
R = Ph, L = EtSH (21)	2.4204(6)	2.4674(5)
R = Ph, L = η ² -H ₂ (36)	2.4090(6)	2.4543(7)



Reaction of RuCl₂(P-N)(PPh₃) (**6a**) with L = H₂S and thiols (Chapter 4), H₂ (Chapter 6), and HCCPh (Chapter 6) results in the exclusive formation of the *cis* isomers, i.e., having L trans to the apical P_A atom is disfavoured. A plausible mechanism for the

**Figure 5.9** Proposed mechanism for the formation of *cis*-RuCl₂(P-N)(PPh₃)(SH₂) (**18a**).

formation of *cis*-RuCl₂(P-N)(PPh₃)(SH₂) and other *cis* isomers is shown in Figure 5.9, involving an equilibrium between the square pyramidal **6a** and minute amounts of trigonal bipyramidal **6a'** structures. The approach of the H₂S ligand towards **6a** to give the trans species **18a'** is perhaps disfavoured because of the mutual trans influences of P_A and H₂S. The approach of H₂S toward **6a'** at the equatorial position between P_X and N, presumably results in the favourable formation of the preferred *cis* isomer **18a**. The rearrangement of square pyramidal structures to trigonal bipyramidal has also been shown to exist when H₂O dissociates from *trans, mer*-[MCl₂(H₂O)(PMe₂Ph)₃][ClO₄] (M = Rh¹⁹ or Ir³³). Other routes involving initial dissociation of Cl⁻ cannot be ruled out at this stage.

5.5 UV-Vis Spectral Studies of the RuCl₂(P-N)(PPh₃)/H₂O System

The UV-Vis spectra of **6a** with increasing concentrations of H₂O in CD₂Cl₂, C₆D₆, acetone and THF are shown in Figures 11-14, respectively. Three isosbestic points at 414, 498 and 552 nm (ϵ in CH₂Cl₂ (and C₆H₆) = 560 (600), 395 (380) and 145 (115) M⁻¹ cm⁻¹) are observed in CH₂Cl₂ and C₆D₆ solutions, while only one distinct isosbestic point at 404 nm (ϵ in acetone (and THF) = 545 (655) M⁻¹ cm⁻¹) is observed in solutions of the more coordinating solvents acetone and THF. The differences in spectra changes suggest that coordinating solvents such as acetone and THF compete with H₂O for the vacant site in the coordination sphere of **6a** as shown in Figure 5.10.

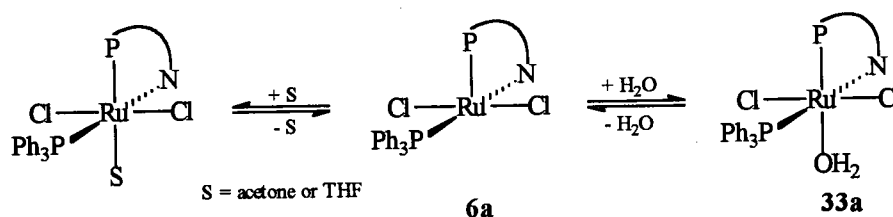


Figure 5.10 Species in equilibrium when **6a** is dissolved in a coordinating solvent in the presence of H₂O.

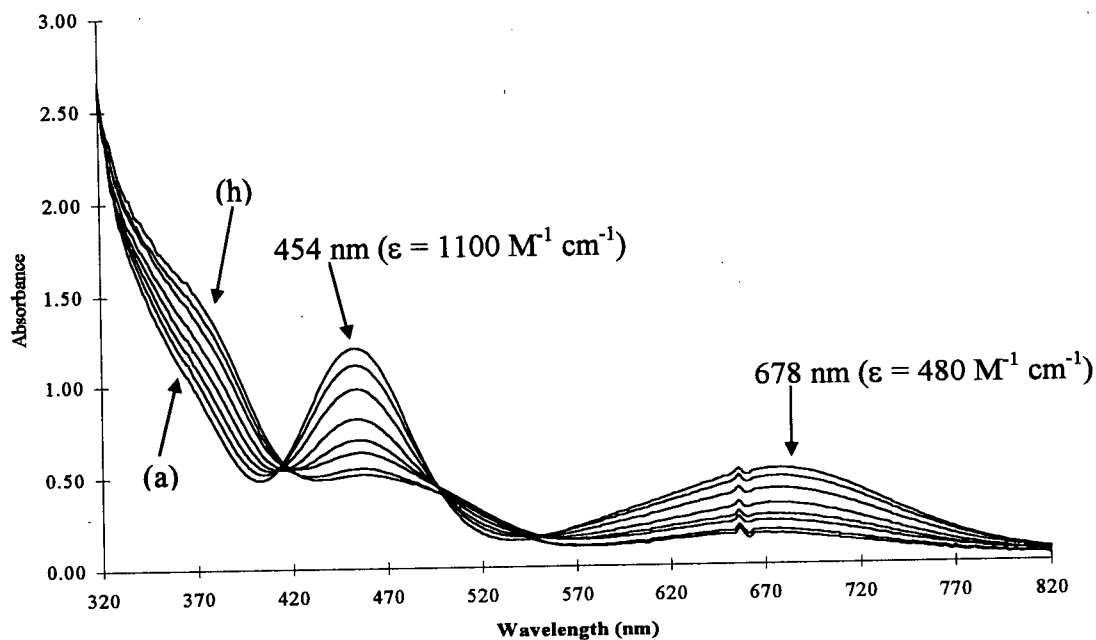


Figure 5.11 Spectral changes observed upon addition of H_2O to $\text{RuCl}_2(\text{P-N})(\text{PPh}_3)$ (**6a**) ($1.04 \times 10^{-3} \text{ M}$) in CH_2Cl_2 at 25°C . Added $[\text{H}_2\text{O}]$ = (a) 0.0, (b) 0.0056, (c) 0.0111, (d) 0.0333, (e) 0.0500, (f) 0.0666, (g) 0.0999, (h) 0.1110 M.

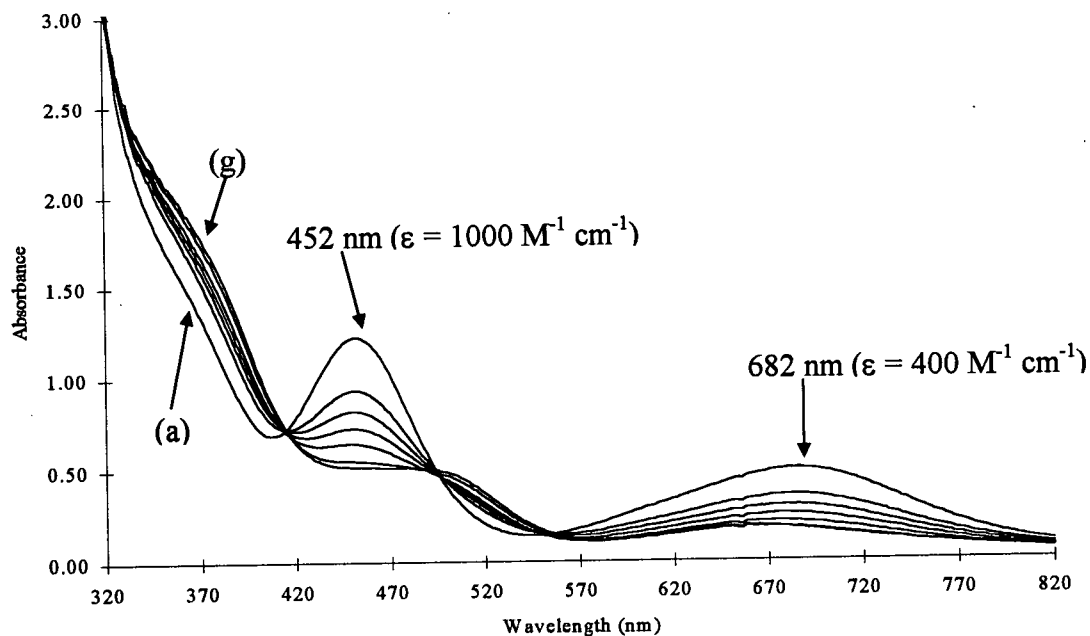


Figure 5.12 Spectral changes observed upon addition of H_2O to $\text{RuCl}_2(\text{P-N})(\text{PPh}_3)$ (**6a**) ($1.21 \times 10^{-3} \text{ M}$) in C_6H_6 at 25°C . Added $[\text{H}_2\text{O}]$ = (a) 0.0, (b) 0.0056, (c) 0.0111, (d) 0.0222, (e) 0.0333, (f) 0.0444, (g) 0.0776 M.

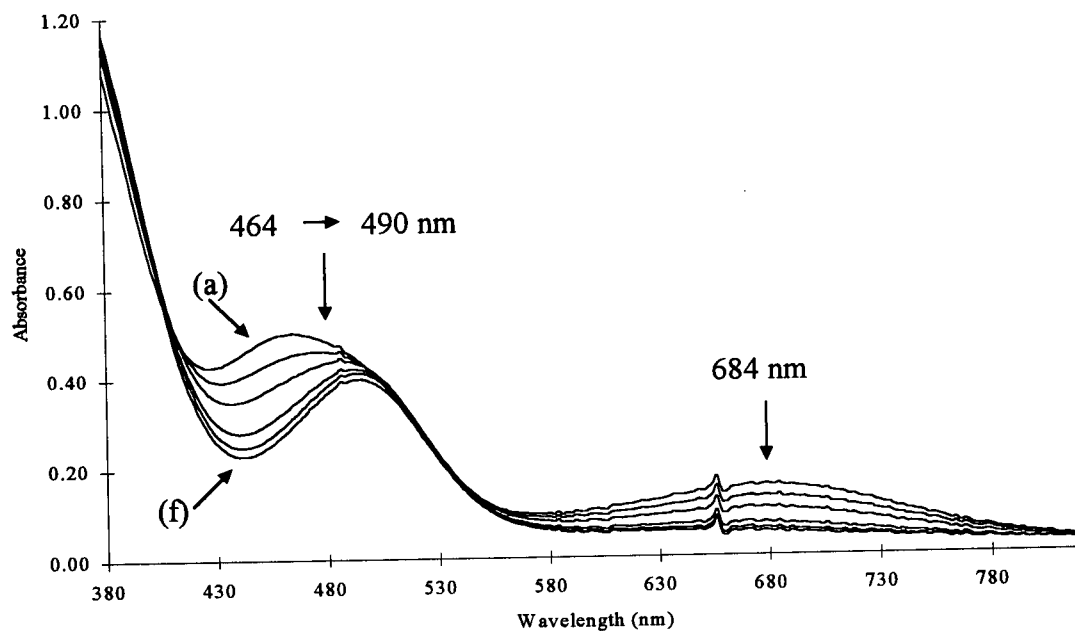


Figure 5.13 Spectral changes observed upon addition of H_2O to $\text{RuCl}_2(\text{P-N})(\text{PPh}_3)$ (**6a**) (1.12×10^{-3} M) in acetone at 25°C . Added $[\text{H}_2\text{O}]$ = (a) 0.0, (b) 0.0089, (c) 0.2652, (d) 0.9171, (e) 1.9702, (f) 3.9591 M.

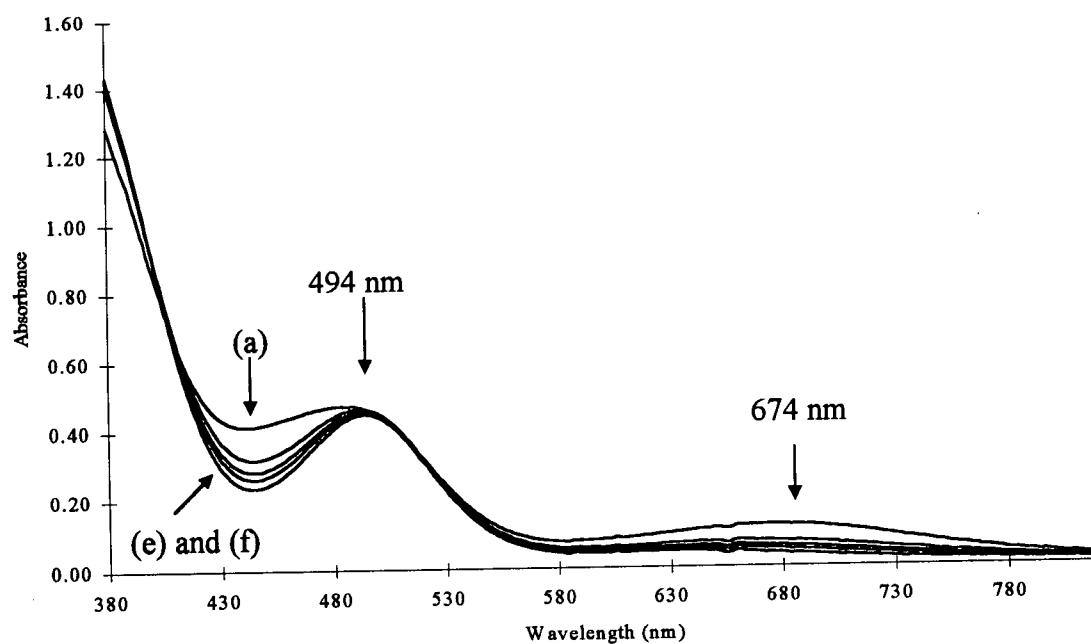


Figure 5.14 Spectral changes observed upon addition of H_2O to $\text{RuCl}_2(\text{P-N})(\text{PPh}_3)$ (**6a**) (1.19×10^{-3} M) in THF at 25°C . Added $[\text{H}_2\text{O}]$ = (a) 0.0, (b) 0.0444, (c) 0.1110, (d) 0.2220, (e) 0.9992, (f) 4.330 M.

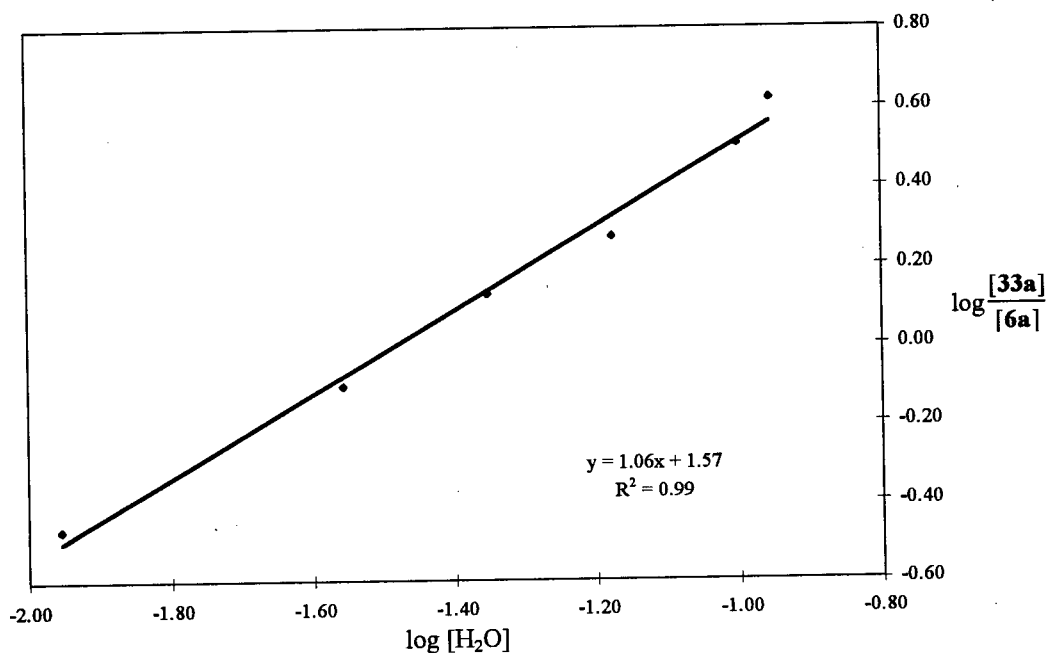


Figure 5.15 Solving K for the addition of H_2O to **6a** at 25°C . The equilibrium concentrations were obtained by monitoring the absorbance at 678 nm (Figure 5.11). Data points at higher H_2O concentrations have been omitted due to the insolubility of H_2O in CH_2Cl_2 ; solubility of H_2O in CH_2Cl_2 is 0.128 M at 25°C .³⁴

From the equation $\log \{[\mathbf{33a}]/[\mathbf{6a}]\} = \log K + \log [\text{H}_2\text{O}]$, the equilibrium constant K for the formation of **33a** in CH_2Cl_2 is obtained by plotting $\log \{[\mathbf{33a}]/[\mathbf{6a}]\}$ versus $\log [\text{H}_2\text{O}]$ (Figure 5.15). $K = 37 \pm 2 \text{ M}^{-1}$ at 25°C is calculated from the intercept of the plot, the estimated error being based on repeat experiments (see Appendix XII.1 for raw data). The slope of 1.06 is in agreement with the unity dependence on the concentration of H_2O . A value of the same order of magnitude ($K = 28 \text{ M}^{-1}$, see Appendix XII.2) was obtained for the reaction in C_6H_6 , implying that both these solvents are non-coordinating in the equilibrium system. Of note, $K \sim 10 \text{ M}^{-1}$ was estimated from the ^1H NMR spectra of **33a** in CD_2Cl_2 (at 25°C). Comparison of $K = 37 \text{ M}^{-1}$ with those obtained for H_2S and thiols (discussed in Section 4.6) insinuates that equilibrium favours the formation of $\text{RuCl}_2(\text{P-N})(\text{PPh}_3)(\text{L})$ in the

order $L = \text{MeSH} > \text{EtSH} \sim \text{H}_2\text{S} > \text{H}_2\text{O}$ at 25°C in CH_2Cl_2 solutions, with K decreasing from 296 to 37 M^{-1} .

K values in CH_2Cl_2 were measured from 10 to 38°C , but reproducible values at the extreme temperatures could not be obtained. ΔH° , ΔS° and ΔG° for the coordination of H_2O to **6a** are nevertheless estimated to be $-50 \pm 20 \text{ kJ/mol}$, $-140 \pm 40 \text{ J/mol K}$ and $-8.9 \pm 0.2 \text{ kJ/mol}$ (at 25°C , based on $K = 37 \pm 2 \text{ M}^{-1}$) (see Appendix XII.1).

Kinetic studies of ligand substitution on **33a** were attempted. Thus, H_2S or H_2 at 1 atm total pressure was added to solutions of **33a** ($1.0 \times 10^{-3} \text{ M}$) in acetone or CH_2Cl_2 containing excess H_2O ($> 1.0 \text{ M}$ in acetone, $> 0.13 \text{ M}$ in CH_2Cl_2) to insure complete formation of **33a**. However, the substitution reactions were too rapid to be measured by UV-Vis spectroscopy; for example, upon addition of 1 atm H_2S to **33a** in CH_2Cl_2 , the solution 'instantaneously' changed from a pink colour to bright yellow, the UV-Vis spectrum showing complete formation of the H_2S adduct.

5.6 The Preparation of *Trans*- $\text{RuCl}_2(\text{P-N})(\text{PPh}_3)(\text{L})$ ($\text{L} = \text{MeOH}$ (**34**) and EtOH (**35**))

The preparations of the MeOH and EtOH complexes proved to be difficult as trace moisture led to the formation of the aquo complex **33a**. *Trans*- $\text{RuCl}_2(\text{P-N})(\text{PPh}_3)(\text{MeOH})$ (**34**) was previously observed *in situ* by Mudalige from NMR experiments.² In this thesis work, **34** was isolated by stirring $\text{RuCl}_2(\text{PPh}_3)_3$ and P-N in a mixture of vigorously dried MeOH and acetone; addition of hexanes led to the precipitation of a pink solid that analysed for **34** (Section 2.10.3). The $^{31}\text{P}\{^1\text{H}\}$ NMR spectrum (in CD_2Cl_2) of an isolated sample of **34**, similar to that of **33a**, shows a broad signal at $\delta 77$ due to P_A and a resolved doublet due to P_X at $\delta 47.14$ ($^2J_{\text{PP}} = 36.66 \text{ Hz}$); upon addition of 50 equiv of MeOH to the solution, the signal due to P_A is resolved into a doublet ($\delta 77.46$, 36.66 Hz). The ^1H NMR spectrum of an

isolated sample of **34** is shown in Figure 5.16. The singlet at δ 3.16 is due to the NMe_2 resonances, the equivalence of the Me groups implying the trans structure. The doublet at δ 3.30 ($^3J_{\text{HH}} = 5.3$ Hz) is assigned to the CH_3 group while the quartet at δ 1.34 ($^3J_{\text{HH}} = 5.3$ Hz) is assigned to the OH group of the coordinated MeOH. The small singlet at δ 3.19 happens to be at the position of the resonances for the NMe_2 group of **6a**, which is in equilibrium with **34**, but the $^{31}\text{P}\{^1\text{H}\}$ NMR data imply a rapid equilibrium on the NMR-timescale.

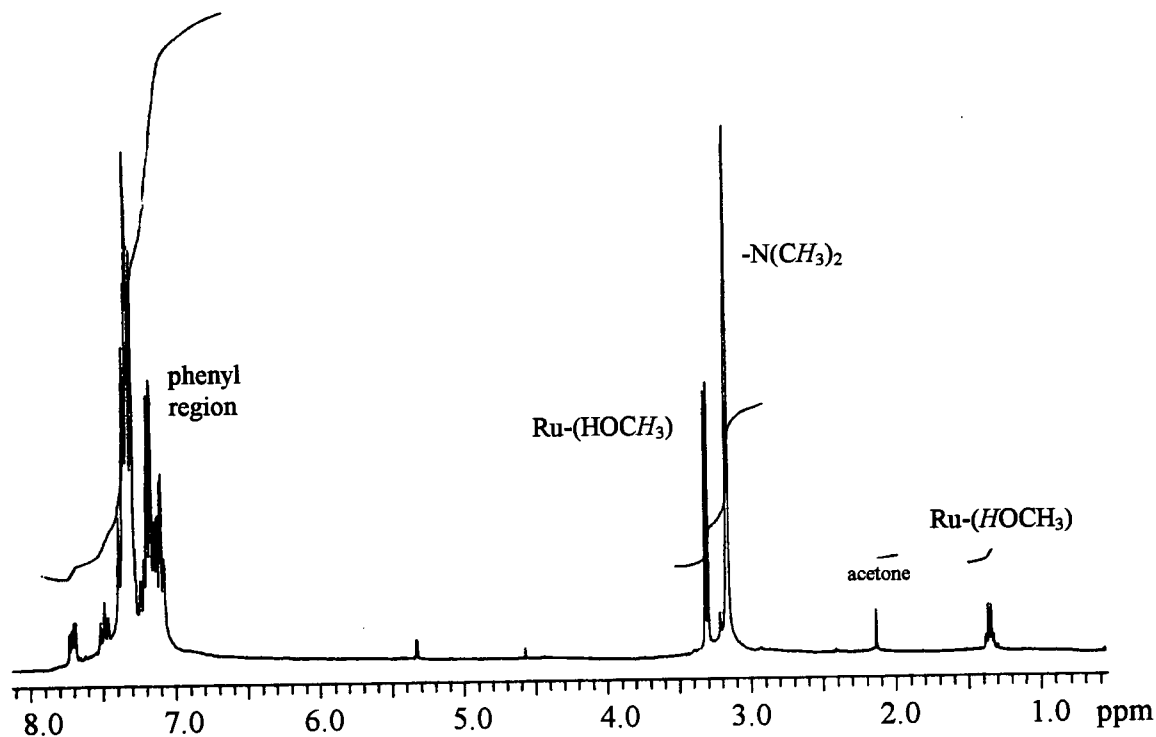


Figure 5.16 ^1H NMR spectrum (300 MHz) of *trans*- $\text{RuCl}_2(\text{P-N})(\text{PPh}_3)(\text{MeOH})$ (**34**) in CD_2Cl_2 .

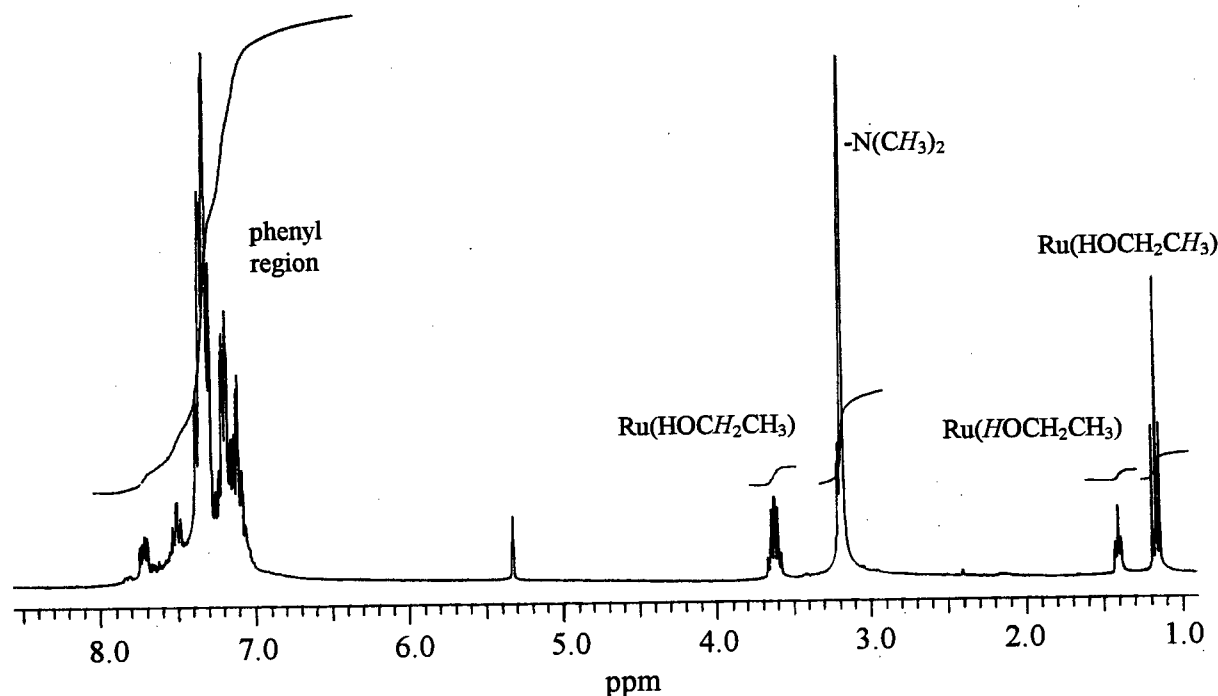


Figure 5.17 ^1H NMR spectrum (300 MHz) of *trans*- $\text{RuCl}_2(\text{P-N})(\text{PPh}_3)(\text{EtOH})$ (**35**) in CD_2Cl_2 .

The preparation of *trans*- $\text{RuCl}_2(\text{P-N})(\text{PPh}_3)(\text{EtOH})$ (**35**) required stirring a suspension of $\text{RuCl}_2(\text{PPh}_3)_3$ and P-N in neat EtOH for 1 week (Section 2.10.4), when work-up of this reaction mixture resulted in two products. Firstly, a precipitated brown solid was not characterized because of its insolubility in acetone, C_6D_6 , CDCl_3 or CD_2Cl_2 . A second work-up of the filtrate resulted in a pink solid characterized as **35**, although an analytically pure sample could not be isolated even after several repeated preparations. The $^{31}\text{P}\{^1\text{H}\}$ NMR (in CD_2Cl_2) spectrum of **35** is similar to that of **34**, and consists of a broad P_A signal at δ 80 and a doublet at δ 46.90 ($^2J_{\text{PP}} = 36.24$ Hz) due to P_X . The P_A signal is again resolved into a sharp doublet at δ 79.79 ($^2J_{\text{PP}} = 36.24$ Hz) after the addition of 50 equiv of EtOH to the above solution. The ^1H NMR spectrum of isolated **35** is shown in Figure 5.17. In addition to the singlet at δ 3.18 due to the NMe_2 group, well resolved peaks due to the

coordinated EtOH group are also depicted. The assignments are as follows: δ 3.61 (doublet of quartets) due to $\text{CH}_3\text{CH}_2\text{OH}$; δ 1.40 (triplet) due to $\text{CH}_3\text{CH}_2\text{OH}$; and δ 1.16 (triplet) due to $\text{CH}_3\text{CH}_2\text{OH}$.

The solution properties of **34** and **35** are very similar to those of the aquo complex **33a**. That is, rapid coordination and dissociation of the alcohol ligands are apparent from the broad P_A signals in the $^{31}\text{P}\{^1\text{H}\}$ NMR spectra of **34** and **35**. Furthermore, variable temperature NMR studies also display similar trends which resemble those of **33a**.

In conclusion, **34** and **35** are isolated only under absolutely anhydrous conditions. In the solid state, the complexes lose the solvent molecules rapidly even under 1 atm of Ar to regenerate the five-coordinate, green solid **6a**. Weakly coordinating solvent molecules play an important role in stabilizing complexes such as $\text{RuCl}_2(\text{EtOH})(\text{PMe}_2\text{Ph})_3$,³⁵ $[\text{RuH}(\text{PPh}_3)_2(\text{H}_2\text{O})_2(\text{MeOH})][\text{BF}_4]$,³⁶ $[\text{Ru}(\text{Y})\text{Cl}_2(\text{MeOH})(\text{PPh}_3)_2]$ ($\text{Y} = \text{CO}$ or CS),³⁷ $[\text{RuH}(\text{PMe}_2\text{Ph})_4(\text{MeOH})][\text{PF}_6]$, and $[\text{RuH}(\text{dppe})_2(\text{EtOH})][\text{PF}_6]$.³⁸ Dissociation of the solvent molecules can create vacant coordination sites for substrate binding in highly reactive catalysts. For example, $\text{Ru}(\text{BINAP})(\text{acac})(\text{MNAA})(\text{MeOH})$ ($\text{MNAA} = 2\text{-(6'-methoxynaphth-2'-yl) acrylate anion}$) plays a role in the homogeneous asymmetric hydrogenation of 2-arylacrylic acids to give high e.e. of chiral 2-arylpropionic acids, which are used as anti-inflammatory drugs.³⁹ The high activity of this species is attributed to the dissociation of the highly labile MeOH ligand as an intermediate in the catalytic cycle.

5.7 DSC Data for Complexes Containing O-Donor ligands

The enthalpy values, ΔH° , for the loss of $\text{L} = \text{H}_2\text{O}$, MeOH and EtOH from their corresponding complexes, **33a**, **34** and **35** are obtained from DSC experiments, the data being shown in Figure 5.18. When these endothermic values are compared with those of complexes

containing S-ligands (Section 4.7), the dissociation energy of L decreases in the order $\text{MeSH} > \text{MeOH} > \text{H}_2\text{S} > \text{H}_2\text{O} > \text{EtSH} > \text{EtOH}$. Thus, in the solid state, the S-ligand containing complexes have a higher dissociation energy than the corresponding O-ligand containing species, which is likely attributed to the higher thermal stability of the *cis*-chloro S-containing molecules. As previously discussed (Section 5.4), the apical P_A atom of the P-N ligand exerts a strong *trans* influence on the mutually *trans* ligand (H_2O , MeOH , EtOH). The H_2S , MeSH and EtSH ligands, however, do not experience such a strong *trans* influence from the Cl-atom. The MeSH and MeOH adducts are noticeably more thermally stable than the other complexes; perhaps the methyl mercaptan and methanol molecules are of the most compatible size and electronic structure to occupy the vacant site of the five-coordinate complex **6a**.

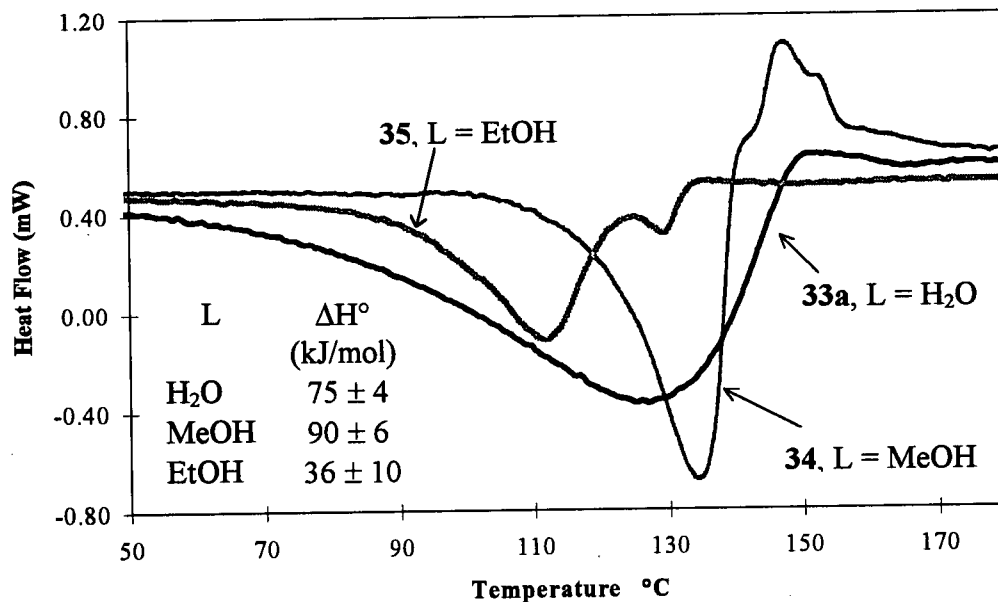


Figure 5.18 DSC curves for *trans*- $\text{RuCl}_2(\text{P-N})(\text{PPh}_3)(\text{L})$. Samples are heated in a N_2 atmosphere (flow rate = 40 cc/min) at a rate of $5^\circ\text{C}/\text{min}$ to 200°C . A more accurate ΔH° for **35** (L = EtOH) could not be determined because of the inability of obtaining an analytically pure sample.

If solution effects are negligible, the magnitude of ΔH° from solution and solid state studies should be eventually the same, as the chemistry in both cases involves no trans to cis rearrangement of the Cl-atoms. In Section 5.5, $\Delta H^\circ = -50 \pm 20$ kJ/mol was obtained for the coordination of H_2O to **6a** to give **33a** in CH_2Cl_2 , while for the dissociation of H_2O from **33a** in the solid state $\Delta H^\circ = 75 \pm 4$ kJ/mol.

DSC is also used to differentiate the Ru-O bond strengths between *trans*- $RuCl_2(P-N)(PPh_3)(H_2O)$ (**33a**) and *trans*- $RuCl_2(P-N)(P(p\text{-tolyl})_3)(H_2O)$ (**33b**). From the DSC curves shown in Figure 5.19, ΔH° values for the loss of H_2O are 75 ± 4 and 62 ± 2 kJ/mol for **33a** and **33b**, respectively; i.e., the Ru-O bond in **33a** is stronger than that in **33b** which is in agreement with the shorter Ru-O bond lengths of **33a** (2.238 Å (I), 2.187 Å(II)) versus that of **33b** (2.252 Å).

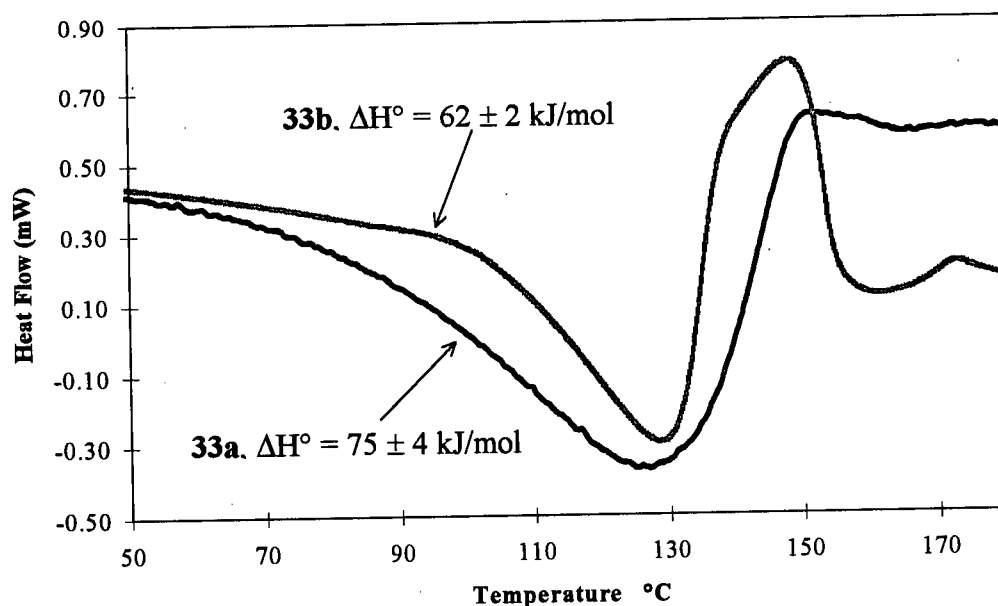


Figure 5.19 DSC curves for *trans*- $RuCl_2(P-N)(PPh_3)(H_2O)$ (**33a**) and *trans*- $RuCl_2(P-N)(P(p\text{-tolyl})_3)(H_2O)$ (**33b**). Samples are heated in a N_2 atmosphere (flow rate = 40 cc/min) at a rate of $5^\circ C/min$ to $200^\circ C$.

5.8 Summary

In this Chapter, the apical phosphine (P_A of P-N) of the five-coordinate complex $RuCl_2(P-N)(PPh_3)$ is seen to play a significant role in directing incoming monodentate ligands in a position either trans or cis to itself. The *trans* effect of P_A induces *trans*- $RuCl_2(P-N)(PPh_3)(L)$ complexes ($L = H_2O, MeOH$ and $EtOH$) into a rapid equilibrium with $RuCl_2(P-N)(PPh_3)$. The S-containing ligands ($H_2S, MeSH$ and $EtSH$), on the other hand, appear to have a stronger *trans* influence (than the O-donors) toward P_A and the *cis*- $RuCl_2(P-N)(PPh_3)(L)$ structures are more favourable.

5.9 References

1. (a) Stang, P. J.; Song, L.; Huang, Y.-H.; Arif, A. M. *J. Organomet. Chem.*, **1991**, 405, 403.
 (b) Collman, J.P.; Hegedus, L. S.; Norton, J. R.; Finke, R. G. *Principles and Applications of Organotransition Metal Chemistry*; University Science Books: Mill Valley, CA, 1987.
2. Mudalige, D. C. Ph.D. Thesis, The University of British Columbia, 1994.
3. Benedict, W. S.; Gailar, N.; Plyler, E. K. *J. Chem. Phys.* **1956**, 24, 1139.
4. Mudalige, D. C.; Rettig, S. J.; James, B. R.; Cullen, W. R. *J. Chem. Soc., Chem. Commun.*, **1993**, 830.
5. LaPlaca, S. J.; Ibers, J. A. *Inorg. Chem.* **1965**, 4, 778.
6. MacFarlane, K. S.; Joshi, A. M.; Rettig, S. J.; James, B. R. *Inorg. Chem.* **1996**, 35, 7304.
7. MacFarlane, K. S. Ph.D. Thesis, The University of British Columbia, 1995.
8. Hampton, C. R. S. M.; Butler, I. R.; Cullen, W. R.; James, B. R.; Charland, J.-P.; Simpson, J. *Inorg. Chem.* **1992**, 31, 5509.
9. Lawson, H. J.; Janik, T. S.; Churchill, M. R.; Takeuchi, K. J. *Inorg. Chim. Acta*, **1990**, 174, 197.
10. Mandal, S. K.; Chakravarty, A. R. *Inorg. Chem.* **1993**, 32, 3851.
11. Boniface, S. M.; Clark, G. R.; Collins, T. J.; Roper, W. R. *J. Organomet. Chem.*, **1981**, 206, 109.
12. Röthlisberger, M. S.; Hummel, W.; Pittet, P.-A.; Bürgi, H.-B.; Ludi, A.; Merbach, A. E. *Inorg. Chem.* **1988**, 27, 1358.
13. McGrath, D. V.; Grubbs, R. H. *J. Am. Chem. Soc.* **1991**, 113, 3611.
14. Bernhard, P.; Bürgi, H.-B.; Hauser, J.; Lehmann, H.; Ludi, A. *Inorg. Chem.* **1982**, 21, 3936.
15. Kölle, U.; Flunkert, G. Görissen, R. Schmidt, M. U.; Englert, U. *Angew. Chem., Int. Ed. Engl.* **1992**, 31, 440.

16. Basch, H.; Krauss, M.; Stevens, W. J.; Cohen, D. *Inorg. Chem.* **1985**, *24*, 3313.
17. Shinoda, S.; Koie, Y. Saito, Y. *Bull. Chem. Soc. Jpn.* **1986**, *59*, 2938.
19. Deeming, A. J.; Proud, G. P. *Inorg. Chim. Acta* **1985**, *100*, 223.
20. Deeming, A. J.; Proud, G. P.; Dawes, H. M.; Hursthouse, M. B. *J. Chem. Soc., Dalton Trans.* **1986**, 2545.
21. Malito, J.; Alyea, E. C. *Transition Met. Chem.* **1992**, *17*, 481.
22. Anderson, G. K.; Kumar, R. *J. Chem. Research (S)* **1998**, 48; *J. Chem. Research (M)* **1988**, 432.
23. Brüggeller, P. *Inorg. Chem.* **1987**, *26*, 4125.
24. Grimley, E.; Meek, D. W. *Inorg. Chem.* **1986**, *25*, 2049.
25. Gambaro, J. J.; Hohman, W. H.; Meek, D. W. *Inorg. Chem.* **1989**, *28*, 4154.
26. Pidcock, A.; Richards, R. E.; Venanzi, L. M. *J. Chem. Soc. (A)* **1966**, 1707.
27. Tau, K. D.; Meek, D. W. *Inorg. Chem.* **1979**, *18*, 3574.
28. Keiter, R. L.; Verkade, J. G. *Inorg. Chem.* **1969**, *8*, 2115.
29. Jessop, P. G.; Rettig, S. J.; Lee, C.-L.; James, B. R. *Inorg. Chem.* **1991**, *30*, 4617.
30. Dekleva, T. W. Ph.D. Thesis, The University of British Columbia, 1983.
31. (a) MacFarlane, K. S. Ph.D. Thesis, The University of British Columbia, 1995.
(b) MacFarlane, K. S.; Joshi, A. M.; Rettig, S. J.; James, B. R. *Inorg. Chem.* **1996**, *35*, 7304.
32. Queiroz, S. L.; Batista, A. A.; Oliva, G.; Gambardella, M. T. do P.; Santos, R. H. A.; MacFarlane, K. S.; Rettig, S. J.; James, B. R. *Inorg. Chim. Acta* **1998**, *267*, 209.
33. Deeming, A. J. Doherty, S.; Marshall, J. E.; Powell, J. L.; Senior, A. M. *J. Chem. Soc., Dalton Trans.* **1993**, 1093.
34. IUPAC Solubility Data Series, Volume 60, Halogenated Methanes with Water; Horváth, A. L.; Getzen, F. W., Eds.; Oxford University Press: Oxford, 1995, p. 153.

35. Young, R. J.; Wilkinson, G. *J. Chem. Soc., Dalton Trans.* **1976**, 719.
36. Chatt, J.; Leigh, G. J.; Paske, R. J. *J. Chem. Soc.(A)* **1969**, 854.
37. Armit, P. W.; Sime, W. J.; Stephenson, T. A. *J. Chem. Soc., Dalton Trans.* **1976**, 2121.
38. Ashworth, T. V.; Singleton, E. *J. Chem. Soc., Chem. Commun.* **1976**, 706.
39. Chen, C.-C.; Huang, T.-T.; Lin, C.-W.; Cao, R.; Chan, A. S. C. *Inorg. Chim. Acta* **1998**, 270, 247.

Chapter 6

Reactions of $\text{RuCl}_2(\text{P-N})(\text{PPh}_3)$ with Dihydrogen, Ammonia, Nitrous Oxide, Alkynes, and Hydrogen Chloride

In this Chapter, the coordination chemistry of $\text{RuCl}_2(\text{P-N})(\text{PPh}_3)$ is extended to small molecules other than H_2S , H_2O , thiols and alcohols, leading to greater insight into the reactivity of the compound. The potential of this five-coordinate complex as a catalyst for hydrogenation of imines is also briefly examined.

6.1 The Structure and Reactivity of *Cis*- $\text{RuCl}_2(\text{P-N})(\text{PPh}_3)(\eta^2\text{-H}_2)$ (**36**)

The formation of *cis*- $\text{RuCl}_2(\text{P-N})(\text{PPh}_3)(\eta^2\text{-H}_2)$ (**36**) has been described by Mudalige et al.^{1,2} However, this species was only observed *in situ* and its formulation established by NMR studies, including experiments to determine T_1 , the spin-lattice relaxation time of the hydrogen nuclei. The temperature dependence of T_1 gives a predicted^{3,4} V-shaped plot, and from the minimum T_1 value of 13.4 ± 0.2 ms, an intramolecular H-H bond distance of 0.87 ± 0.03 Å was calculated.^{1,2} In the present thesis work, **36** was isolated (Section 2.11.1) by reacting a suspension of $\text{RuCl}_2(\text{PPh}_3)_3$ and P-N in acetone under 1 atm H_2 gas. The microanalysis of the isolated pale yellow solid is consistent with the formulation of **36**. This solid is stable under H_2 and reasonably so under Ar, but slowly loses H_2 in air and decomposition occurs. The IR spectrum of **36** in the solid state (KBr plate) shows a band of medium intensity at 2149 cm^{-1} due to the $\nu_{\text{Ru-H}_2}$ stretching, while $\nu_{\text{H-H}}$ is not observed. Generally, $\nu_{\text{H-H}}$ bands of $\eta^2\text{-H}_2$ complexes are very weak and are only rarely located (in the 2400 to 2700 cm^{-1} range).^{3,5}

6.1.1 The Crystal Structure *Cis*-RuCl₂(P-N)(PPh₃)(η^2 -H₂) (**36**)

X-ray quality yellow crystals were crystallized from a saturated acetone solution of **36** under 1 atm H₂. The ORTEP plot of **36**, reveals a distorted octahedral structure and is shown in Figure 6.1. The dihydrogen was isotropically refined as a double-occupancy hydrogen atom, and consequently the intramolecular H-H distance was not determined. Selected bond lengths and angles of **36** are presented in Tables 6.1 and 6.2. The bond distances of Ru to the P(1), P(2), Cl(1), Cl(2) and N(1) atoms are normal, and are comparable to those of the complexes discussed in Chapters 4 and 5. Similarly, there are no significant differences between the angles around the Ru atom for **36** and those of the other *cis*-dichloro complexes containing H₂S or thiol ligands. The relatively short Ru(1)-H(1*) distance of 1.60 Å is consistent with reasonable stability with respect to loss of H₂ in the solid state. This distance is slightly longer than the Ru-(η^2 -H₂) distance (1.50 and 1.47 Å for the two Ru-H distances) reported for the dinuclear complex (isoPFA)(η^2 -H₂)Ru(μ -Cl)₂(μ -H)RuH(PPh₃)₂,⁶ but is much shorter than 1.81 Å (Ru-(η^2 -H₂)) of the labile complex *trans*-[RuH(η^2 -H₂)(dppe)₂][BPh₄].⁷ The observation that the Ru-(η^2 -H₂) distance in **36** is comparable to Ru-H distances within classical monohydrides such as RuH(SC₆H₄pCH₃)(CO)₂(PPh₃)₂ (1.58 Å),⁸ *trans*-[RuH(η^2 -H₂)(dppe)₂][BPh₄] (1.64 Å),⁷ RuH(Cl)(diop)₂ (1.65 Å; diop = 4,5-bis((diphenyl phosphino)methyl)-2,2-dimethyl-1,3-dioxolane),⁹ RuH(dmpe)₂(naphthyl) (1.67 Å),¹⁰ RuH(PPh₃)₃(O₂CCH₃) (1.68 Å),¹¹ and RuH(Cl)(PPh₃)₃ (1.70 Å)¹² is consistent with a Ru-H complex. However, NMR spectroscopic evidence and reversible solution behaviour (see Section 6.1.2) clearly show **36** to be the Ru(II)-(η^2 -H₂) adduct.

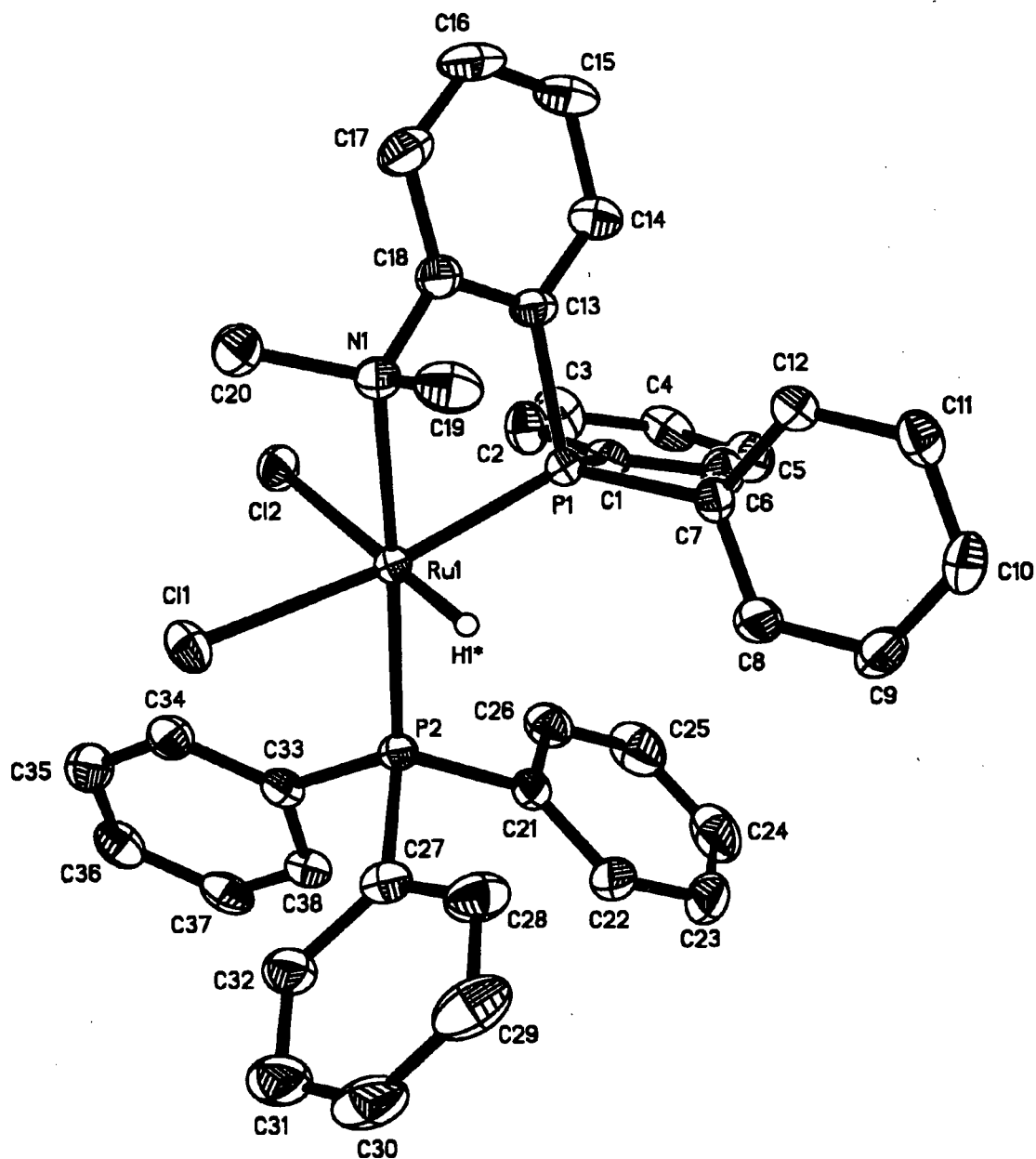


Figure 6.1 The ORTEP plot of *cis*-RuCl₂(P-N)(PPh₃)(η²-H₂) (**36**). Thermal ellipsoids for non-hydrogen atoms are drawn at 33 % probability. Full experimental parameters and details are given in Appendix IX.

Table 6.1 Selected bond lengths (Å) for *cis*-RuCl₂(P-N)(PPh₃)(η^2 -H₂) (**36**) with estimated standard deviations in parentheses. The H(1*) atomic site represents the double-occupancy hydrogen atom refined isotropically.

Bond	Length (Å)	Bond	Length (Å)
Ru(1)-H(1*)	1.60(2)	Ru(1)-N(1)	2.306(2)
Ru(1)-P(1)	2.2884(7)	Ru(1)-Cl(1)	2.4543(7)
Ru(1)-P(2)	2.3098(6)	Ru(1)-Cl(2)	2.4090(6)

Table 6.2 Selected bond angles (°) for *cis*-RuCl₂(P-N)(PPh₃)(η^2 -H₂) (**36**) with estimated standard deviations in parentheses.

Bonds	Angle (°)	Bonds	Angle (°)
P(1)-Ru(1)-N(1)	80.34(6)	Cl(1)-Ru(1)-N(1)	92.20(6)
P(1)-Ru(1)-Cl(1)	172.22(2)	Cl(2)-Ru(1)-N(1)	86.78(6)
P(1)-Ru(1)-Cl(2)	88.52(2)	P(1)-Ru(1)-H(1*)	93.6(8)
P(1)-Ru(1)-P(2)	105.27(3)	P(2)-Ru(1)-H(1*)	87.3(8)
P(2)-Ru(1)-N(1)	172.78(6)	N(1)-Ru(1)-H(1*)	87.8(8)
P(2)-Ru(1)-Cl(1)	82.34(3)	Cl(1)-Ru(1)-H(1*)	88.3(8)
P(2)-Ru(1)-Cl(2)	97.79(2)	Cl(2)-Ru(1)-H(1*)	173.8(8)
Cl(1)-Ru(1)-Cl(2)	88.86(2)		

6.1.2 Thermodynamic Studies of *Cis*-RuCl₂(P-N)(PPh₃)(η^2 -H₂) (**36**) in Solution and in the Solid State

When **36** is dissolved in solution, the η^2 -H₂ moiety quickly dissociates to form some **6a**, and the ³¹P{¹H} and ¹H NMR spectra clearly show the equilibrium between the two species (Figures 6.2 and 6.3, respectively). The ³¹P{¹H} NMR chemical shifts of **36** are located at δ 47.14 (P_A) and δ 45.33 (P_X), ²J_{PP} = 26.49 Hz, in accord with similar structures

containing cis Cl-atoms (see Table 4.9, p. 146). In the ^1H NMR spectrum, inequivalent NMe chemical shifts for **36** are located at δ 3.78 and 2.79, and the coordinated H_2 at δ -10.6. At 25°C, the equilibrium constant, K , for the formation of **36** is determined to be $261 \pm 20 \text{ M}^{-1}$, a value comparable to those of corresponding complexes containing S-ligands ($K = 51$ to 296 M^{-1} , Section 4.6). From variable temperature NMR studies, the ΔH° , ΔS° , and ΔG° (at 25°C, calculated from $\Delta G^\circ = -RT\ln K$) values are determined to be $-26 \pm 4 \text{ kJ/mol}$, $-40 \pm 15 \text{ J/mol K}$ and $-13.8 \pm 0.2 \text{ kJ/mol}$, respectively. The raw data for the calculations of these data are given in Appendix XIII. The ΔH° value for the binding of $\eta^2\text{-H}_2$ to Ru(II) is comparable to those of $(\eta^2\text{-H}_2)(\text{dppb})(\mu\text{-Cl})_3\text{RuCl}(\text{dppb})$ (-60 kJ/mol)¹³ and $\text{Ru}(\text{H}_2)(\text{H})\text{Cl}(\text{CO})(\text{P}^i\text{Pr}_3)_2$ (-32 kJ/mol).¹⁴ The relatively labile nature of the $\eta^2\text{-H}_2$ is also apparent in the solid state as shown by DSC experiments. The enthalpy, ΔH° , for the loss of H_2 in the solid state was found to be $50 \pm 3 \text{ kJ/mol}$ (Figure 6.4), and thus, $\sim -24 \text{ kJ/mol}$ is attributed to the enthalpy change for the cis to trans rearrangement of $\text{RuCl}_2(\text{P-N})(\text{PPh}_3)$; values of -39 to -66 kJ/mol were obtained from similar data for the complexes containing H_2S or RSH (see Section 4.7).

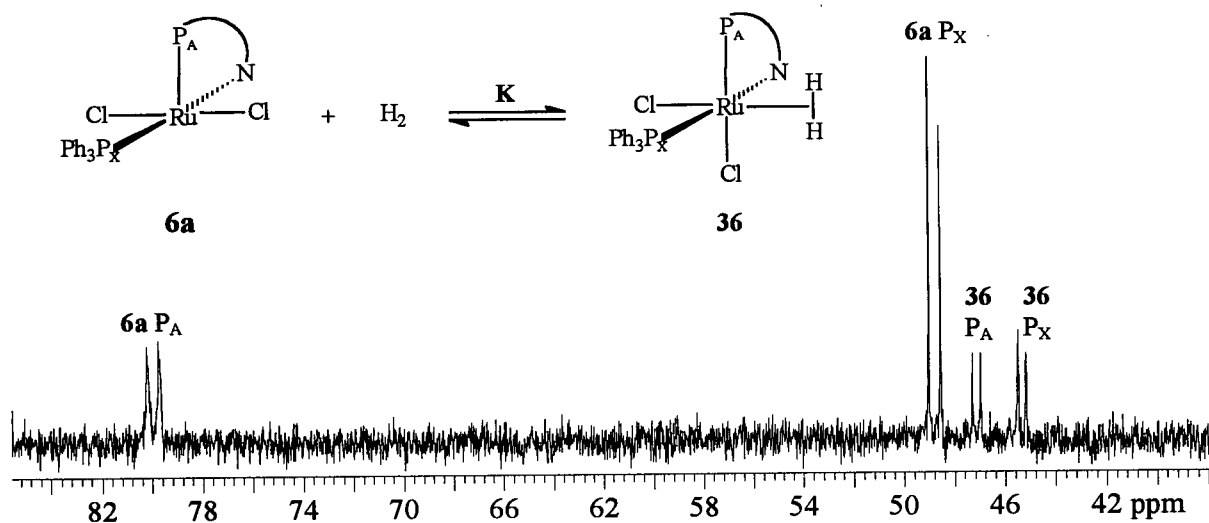


Figure 6.2 $^{31}\text{P}\{^1\text{H}\}$ NMR spectrum (81.0 MHz) of **36** in equilibrium with **6a** in C_6D_6 at 20°C , established by dissolution of a solid sample of **36**; although the signal due to P_A of **6a** is less intense than that of P_X , their integrations are the same.

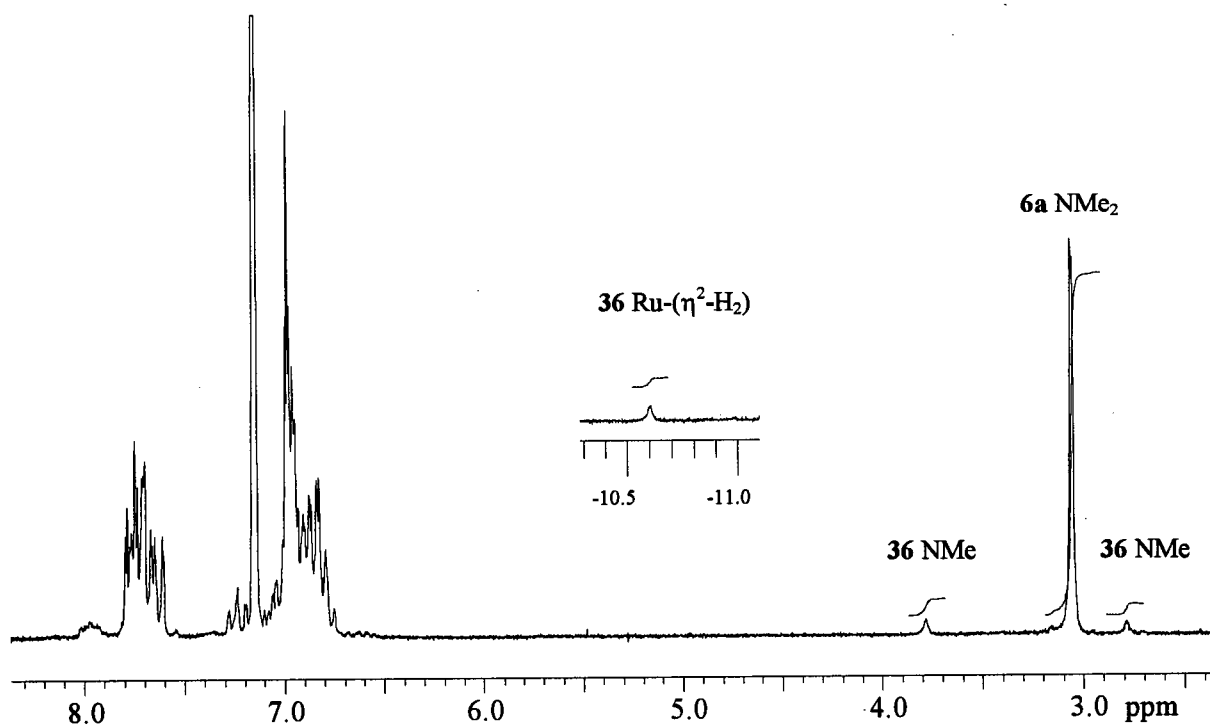


Figure 6.3 ^1H NMR spectrum (200 MHz) of **36** in equilibrium with **6a** in C_6D_6 at 20°C , established by dissolution of a solid sample of **36**; inset shows the upfield chemical shift due to $\text{Ru}(\eta^2\text{-H}_2)$ at $\delta -10.6$. The signal for free H_2 (at $\delta 4.44$) is not seen because of the low $[\text{H}_2]$.

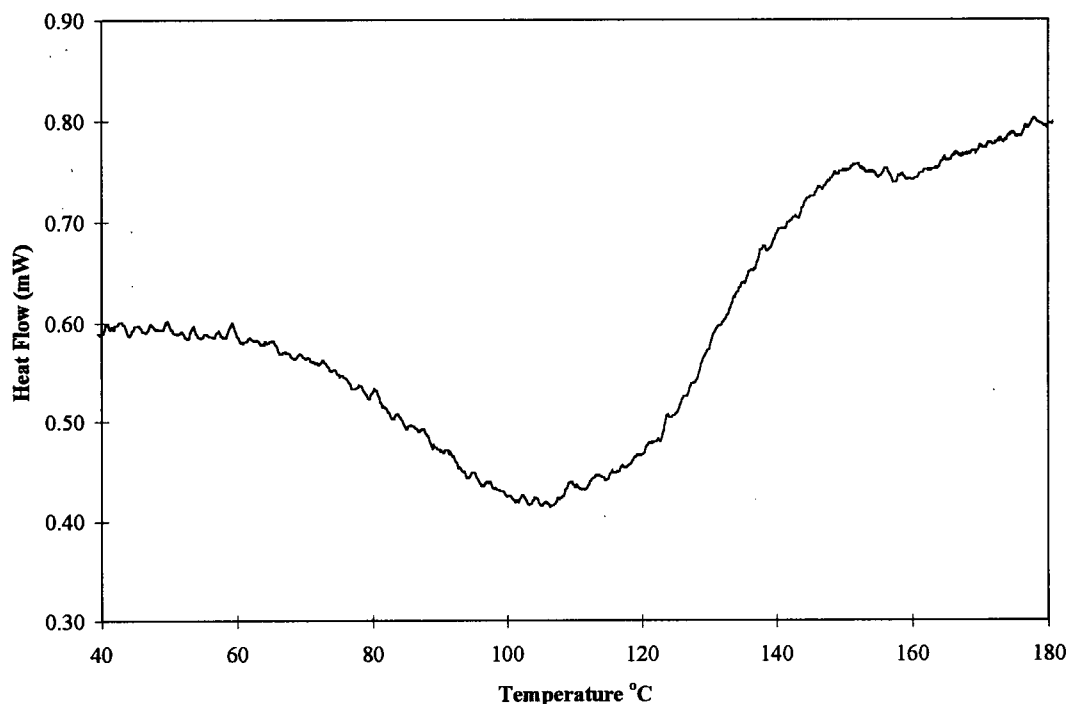
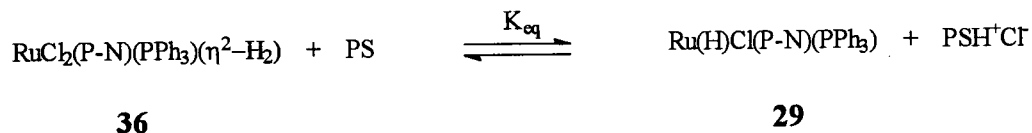


Figure 6.4 DSC curve for *cis*-RuCl₂(P-N)(PPh₃)(η^2 -H₂) (**36**). The sample is heated in a N₂ atmosphere (flow rate = 40 cc/min) at a rate of 5°C/min to 200°C.

6.1.3 The pK_a of *Cis*-RuCl₂(P-N)(PPh₃)(η^2 -H₂) (**36**)

Determination of the acidity of dihydrogen complexes leads to a better understanding of homolytic or heterolytic cleavage of dihydrogen in catalytic hydrogenation reactions. The nature of the ancillary ligands has a dramatic influence on the reactivity of η^2 -H₂,¹⁵ for example, [RuH(η^2 -H₂)(dppe)₂]⁺ is more electron-rich and therefore less acidic (pK_a = 15.0)^{15b} than [CpRu(η^2 -H₂)(dppe)]⁺ (pK_a = 7.2).¹⁶ Furthermore, the structure of a complex is also correlated to acidity; for example, within the complexes *trans*-[RuX(η^2 -H₂)(dppe)₂]⁺ (X = Cl, H),¹⁷ the chloro complex is more acidic (pK_a = 6.0) than the hydrido complex (pK_a = 15.0) because of the $\pi\pi(\text{Cl})$ - $d\pi(\text{Ru})$ repulsions which enhance the $d\pi(\text{Ru}) \rightarrow \sigma^*(\text{H}_2)$ back-bonding and thus weaken the H-H bond.

The reaction of **36** with PS (proton sponge) gives the monohydride complex $\text{Ru(H)Cl(P-N)(PPh}_3\text{)}$ (**29**) and PSH^+Cl^- (Section 4.8):^{1,2}



Accordingly, the pK_a of **36** can be determined by measuring the equilibrium concentrations of the above species. As discussed in Section 4.7, the pK_a for **36** is obtained by solving the equation $\text{pK}_a = \text{pK}_{\text{eq}} + \text{pK}_{\text{PSH}^+}$ (where $\text{pK}_{\text{PSH}^+} = 12.3$). For a typical experiment, a sample of **6a** along with 0.75 to 3.0 equiv PS are dissolved in CD_2Cl_2 ; the addition of 1 atm H_2 then produces a dark yellow-brown solution. Unlike the reaction of PS with *cis*- $\text{RuCl}_2(\text{P-N})(\text{PPh}_3)(\text{SH}_2)$ (**18a**) where the products, $\text{Ru(SH)Cl(P-N)(PPh}_3\text{)}$ (**27a**) and $\text{Ru(SH)}_2(\text{P-N})(\text{PPh}_3)$ (**30**) are unstable at r. t., the hydride complex $\text{Ru(H)Cl(P-N)(PPh}_3\text{)}$ (**29**) is stable indefinitely under inert atmospheres. The $^{31}\text{P}\{^1\text{H}\}$ and ^1H NMR spectra (Figures 6.5 and 6.6, respectively) indicate that three species, **6a**, **29**, and **36**, are in equilibrium. [The broadness of the P_A chemical shift of **6a** is due to minute amounts of H_2O in the system. (see Section 5.3)]. From the above equilibrium equation, $K_{\text{eq}} = \frac{[\mathbf{29}][\text{PSH}^+]}{[\mathbf{36}][\text{PS}]}$, and the concentrations are readily obtained, for example, from the peak integrations of the ^1H NMR (Figure 6.6); the actual concentrations are not required as only the concentration ratios are relevant. The data give $K_{\text{eq}} = 15 \pm 5$ and consequently, the pK_a of **36** is determined to be approximately 11. This value falls within a wide range of pK_a values (0 to 16) for complexes of the type $[\text{M(H}_2\text{)Cp(P-P)}]^+$ ($\text{M} = \text{Ru, Os}$; P-P = diphosphine ligand) previously reported.^{3,15-19} In order to establish a trend in the acidity of $\text{Ru(P-N)-type } \eta^2\text{-H}_2$ complexes, more studies on species with variations of the phosphines and halogens are required.

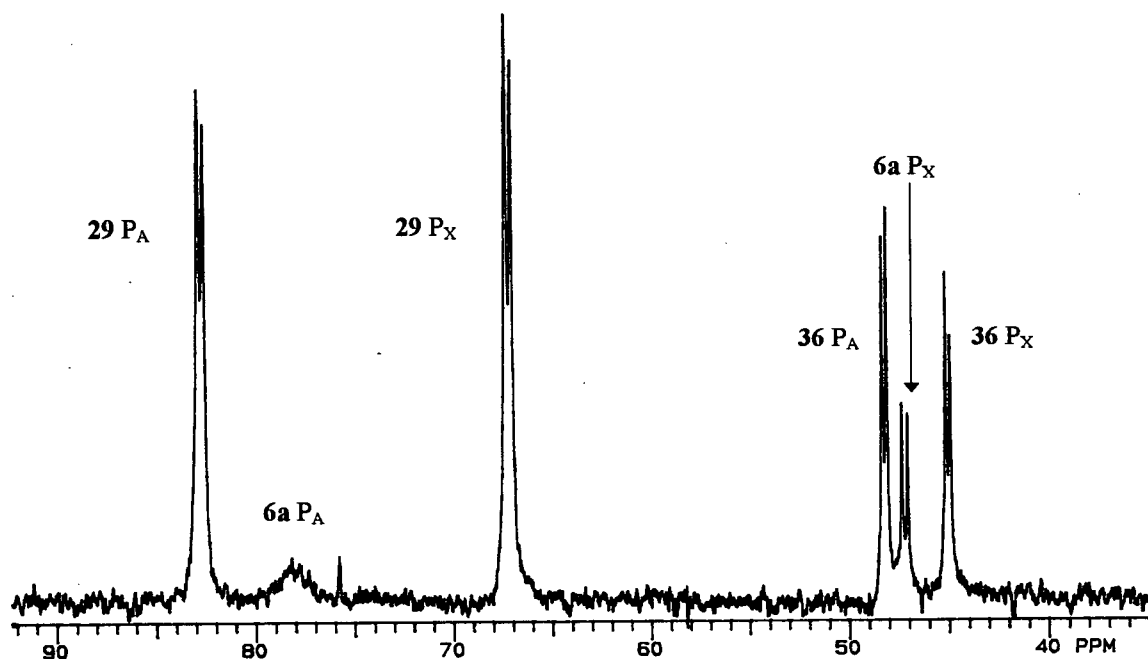


Figure 6.5 $^{31}\text{P}\{^1\text{H}\}$ NMR (121.4 MHz, 20°C, CD_2Cl_2) spectrum of the *in situ* reaction of $\text{RuCl}_2(\text{P-N})(\text{PPh}_3)$ (**6a**) with 1.5 equiv PS under 1 atm H_2 .

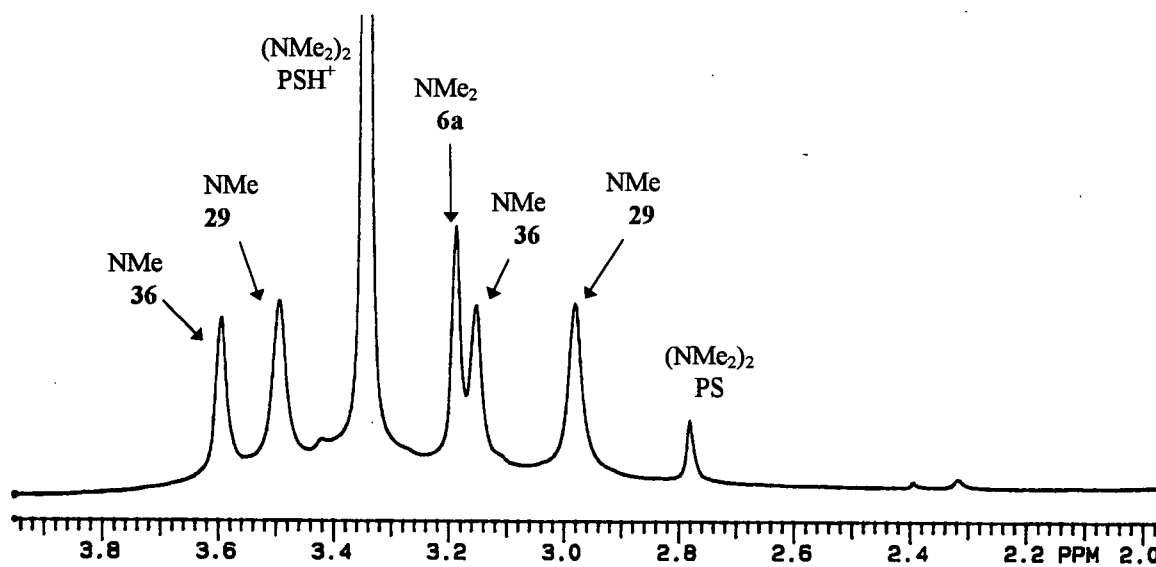


Figure 6.6 ^1H NMR (121.4 MHz, 20°C, CD_2Cl_2) spectrum in the region δ 2.0 to 4.0 of the *in situ* reaction of $\text{RuCl}_2(\text{P-N})(\text{PPh}_3)$ (**6a**) with 1.5 equiv PS under 1 atm H_2 .

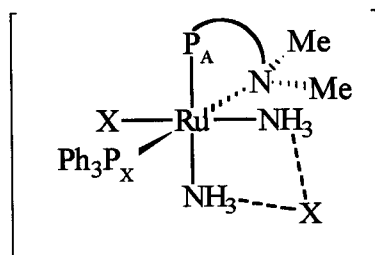
6.2 Reactions of $\text{RuX}_2(\text{P-N})(\text{PPh}_3)$ ($\text{X} = \text{Cl}, \text{Br}$) with NH_3

The reactions of NH_3 with the five-coordinate complexes $\text{RuCl}_2(\text{dppb})(\text{PPh}_3)$ and $\text{RuCl}_2(\text{PPh}_3)_3$ in solution are reported to result in the dissociation of one PPh_3 molecule and the coordination of two molecules of NH_3 , with formation of the six-coordinate species, $\text{RuCl}_2(\text{dppb})(\text{NH}_3)_2$ ^{20,21} and $\text{RuCl}_2(\text{PPh}_3)_2(\text{NH}_3)_2$,²² respectively. The reactions of NH_3 with $\text{RuX}_2(\text{P-N})(\text{PPh}_3)$ ($\text{X} = \text{Cl}$ (**6a**) or Br (**6b**)), however, do not result in the dissociation of PPh_3 as indicated by $^{31}\text{P}\{^1\text{H}\}$ NMR spectroscopy. With an equimolar concentration of NH_3 , only one NH_3 is coordinated to the vacant site of $\text{RuX}_2(\text{P-N})(\text{PPh}_3)$, with formation of *trans*- $\text{RuX}_2(\text{P-N})(\text{PPh}_3)(\text{NH}_3)$, this then rearranging to the more stable *cis* isomer. In the presence of 1 atm NH_3 , a second NH_3 displaces an X atom with formation of the complexes $[\text{RuX}(\text{P-N})(\text{PPh}_3)(\text{NH}_3)_2 \cdots \text{X}]$ (see below). All experimental details for the reactions with NH_3 or with the NH_3 complexes may be found in Section 2.11.2.

6.2.1 Isolation of $[\text{RuX}(\text{P-N})(\text{PPh}_3)(\text{NH}_3)_2 \cdots \text{X}]$ (**37**) in the Presence of Excess NH_3

When NH_3 gas is passed through a solution of $\text{RuCl}_2(\text{P-N})(\text{PPh}_3)$ (**6a**) in CH_2Cl_2 , a dark blue-green solution formed. Microanalysis of the isolated green solid corresponds to the formulation of $[\text{RuCl}(\text{P-N})(\text{PPh}_3)(\text{NH}_3)_2 \cdots \text{Cl}]$ (**37a**), with the suggested structure shown in Figure 6.7; remarkably **37a** is non-conducting in acetone or CH_2Cl_2 solutions (see Section 6.2.4), implying a “strongly associated ion-pair” formulation, possibly with the X associated via H-bonding to the NH_3 ligands as shown. In CDCl_3 solution under 1 atm NH_3 , **37a** is fully formed as indicated by the $^{31}\text{P}\{^1\text{H}\}$ NMR and ^1H NMR spectra. The ^1H NMR spectrum (Figure 6.8) shows two singlets due to $\text{Ru-N}(\text{CH}_3)_2$, δ 3.19, 3.00 and two singlets due to $\text{Ru-N}(\text{NH}_3)_2$, δ 3.72, 1.70, data consistent with a *cis* orientation of the NH_3 groups. The presence of doublets at δ 57.20 ($P_{\text{A-N}}$) and δ 53.24 (P_{XPh_3}), $^2J_{\text{PP}} = 32.05$ Hz, in the $^{31}\text{P}\{^1\text{H}\}$

NMR spectrum reveals an AX coupling pattern (Figure 6.9(a)), meaning the PPh_3 ligand remains coordinated.



$\text{X} = \text{Cl or Br}$

Figure 6.7 Proposed structure of $[\text{RuX}(\text{P-N})(\text{PPh}_3)(\text{NH}_3)_2 \cdots \text{X}]$ (37); the nature of the “associated” X remain uncertain (see text).

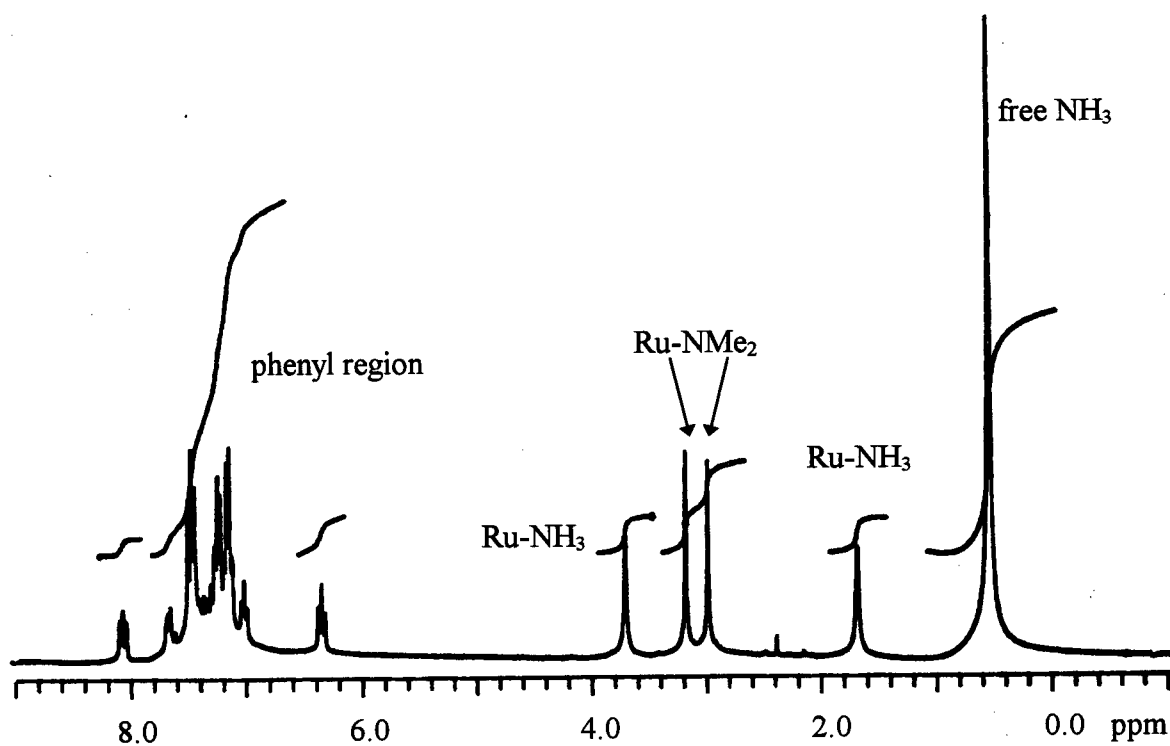


Figure 6.8 ^1H NMR spectrum (CDCl_3 , 300 MHz) of $[\text{RuCl}(\text{P-N})(\text{PPh}_3)(\text{NH}_3)_2 \cdots \text{Cl}]$ (37a) under 1 atm NH_3 at 20°C .

Similar observations were found for the reaction of 1 atm NH_3 with a solution of $\text{RuBr}_2(\text{P-N})(\text{PPh}_3)$ (**6b**). The $^{31}\text{P}\{^1\text{H}\}$ NMR spectrum for $[\text{RuBr}(\text{P-N})(\text{PPh}_3)(\text{NH}_3)_2\cdots\text{Br}]$ (**37b**) consists of doublets at δ 57.40 (P_A) and δ 56.08 (P_X), $^2J_{\text{PP}} = 31.81$ Hz, while the ^1H NMR resonances for NMe_2 are found at δ 3.34 and 2.78, and for $(\text{NH}_3)_2$ at δ 3.64 and 1.75. (Tables 6.3 and 6.4).

6.2.2 The Solution Chemistry of $[\text{RuX}(\text{P-N})(\text{PPh}_3)(\text{NH}_3)_2\cdots\text{X}]$ (**37**)

When solid $[\text{RuCl}(\text{P-N})(\text{PPh}_3)(\text{NH}_3)_2\cdots\text{Cl}]$ (**37a**) is dissolved in CDCl_3 in the absence of excess NH_3 , three species are observed in the NMR spectra (Tables 6.3 and 6.4). The starting material, $[\text{RuCl}(\text{P-N})(\text{PPh}_3)(\text{NH}_3)_2\cdots\text{Cl}]$ (**37a**), is present in a relatively small amount compared to the other two species, identified as *trans*- $\text{RuCl}_2(\text{P-N})(\text{PPh}_3)(\text{NH}_3)$ (**38a**), and *cis*- $\text{RuCl}_2(\text{P-N})(\text{PPh}_3)(\text{NH}_3)$ (**39a**). The $^{31}\text{P}\{^1\text{H}\}$ spectrum is shown in Figure 6.9(b); the presence of two doublets each for each of **38a** and **39a** shows that both P-N and PPh_3 ligands remain coordinated; the doublets at δ 53.86 and 50.79 ($^2J_{\text{PP}} = 36.48$ Hz) are assigned to the *trans* isomer **38a** because of the comparable coupling constant to that of *trans*-Cl isomers **6a** (36.54 Hz) and **33a** (37.76 Hz). The ^1H NMR singlets due to the two symmetrical NMe groups and the NH_3 are found at δ 2.72 and 1.64, respectively. For the *cis* isomer (**39a**), the $^{31}\text{P}\{^1\text{H}\}$ NMR peaks are found at δ 59.27 and 51.45 ($^2J_{\text{PP}} = 32.29$ Hz); inequivalent NMe groups are indicated by singlets at δ 3.61 and 2.94, while the NH_3 is detected at δ 0.38 in the ^1H NMR spectrum.

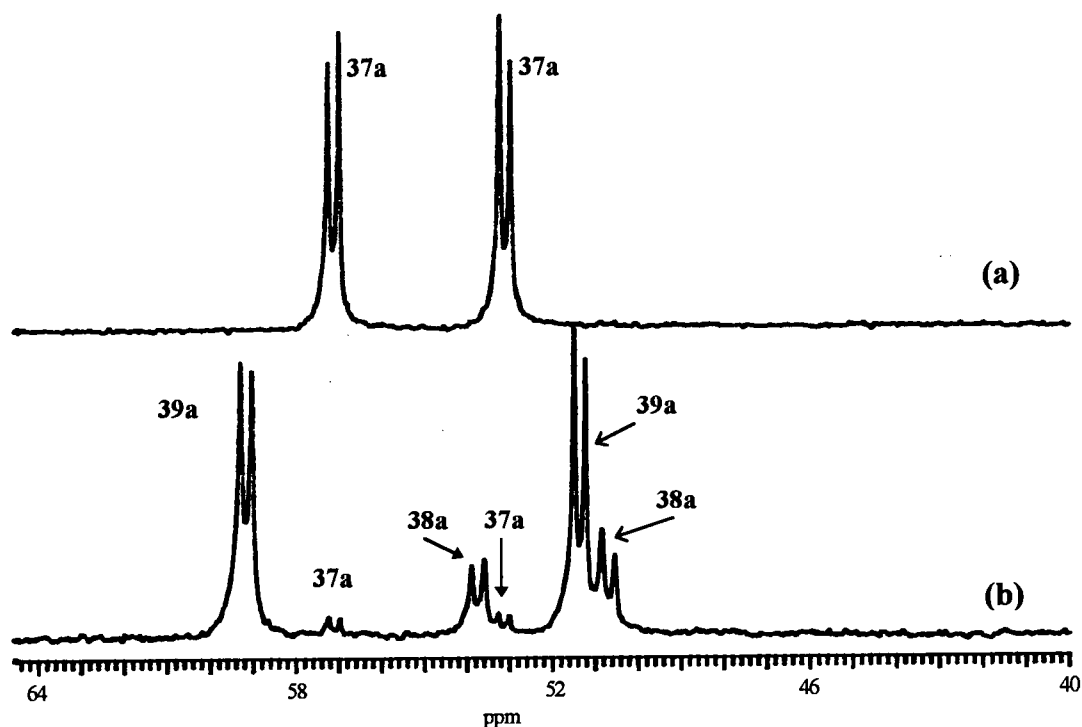


Figure 6.9 $^{31}\text{P}\{^1\text{H}\}$ spectra (121.4 MHz, 20°C, CDCl_3) for $[\text{RuCl}(\text{P-N})(\text{PPh}_3)(\text{NH}_3)_2\cdots\text{Cl}]$ (**37a**): (a) with 1 atm NH_3 and (b) absence of excess NH_3 .

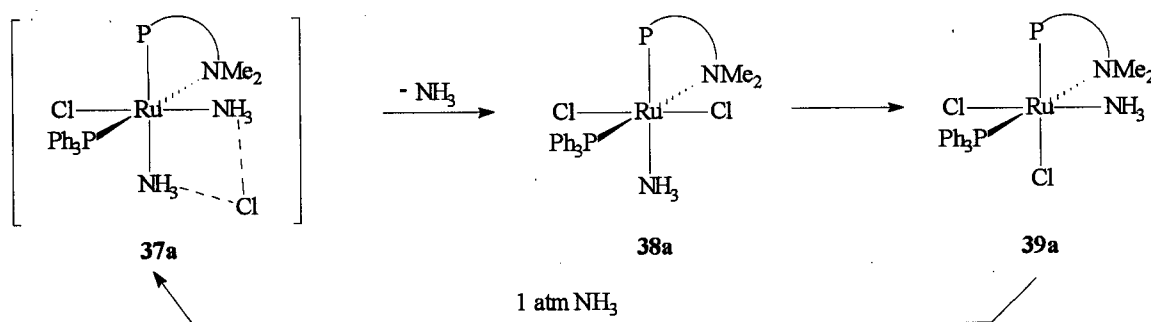
Table 6.3 $^{31}\text{P}\{^1\text{H}\}$ NMR data for Ru(II) ammonia complexes in CDCl_3 .

Complex	δ P-N	δ PPh_3	$^2J_{\text{PP}}$ (Hz)
$[\text{RuCl}(\text{P-N})(\text{PPh}_3)(\text{NH}_3)_2\cdots\text{Cl}]$ (37a)	57.20	53.24	32.05
$[\text{RuBr}(\text{P-N})(\text{PPh}_3)(\text{NH}_3)_2\cdots\text{Br}]$ (37b)	57.40	56.08	31.81
<i>trans</i> - $\text{RuCl}_2(\text{P-N})(\text{PPh}_3)(\text{NH}_3)$ (38a)	53.86	50.79	36.48
<i>trans</i> - $\text{RuBr}_2(\text{P-N})(\text{PPh}_3)(\text{NH}_3)$ (38b)	55.25	50.65	36.66
<i>cis</i> - $\text{RuCl}_2(\text{P-N})(\text{PPh}_3)(\text{NH}_3)$ (39a)	59.27	51.45	32.29
<i>cis</i> - $\text{RuBr}_2(\text{P-N})(\text{PPh}_3)(\text{NH}_3)$ (39b)	62.86	51.85	31.75

Table 6.4 ^1H NMR data for Ru(II) ammonia complexes in CDCl_3 .

Complex	δ Ru-N(CH ₃) ₂	δ Ru-NH ₃
[RuCl(P-N)(PPh ₃)(NH ₃) ₂ ⋯Cl] (37a)	3.19, 3.00	3.72, 1.70
[RuBr(P-N)(PPh ₃)(NH ₃) ₂ ⋯Br] (37b)	3.34, 2.78	3.64, 1.75
<i>trans</i> -RuCl ₂ (P-N)(PPh ₃)(NH ₃) (38a)	2.72	1.64
<i>trans</i> -RuBr ₂ (P-N)(PPh ₃)(NH ₃) (38b)	3.01	1.58
<i>cis</i> -RuCl ₂ (P-N)(PPh ₃)(NH ₃) (39a)	3.61, 2.94	0.38
<i>cis</i> -RuBr ₂ (P-N)(PPh ₃)(NH ₃) (39b)	3.97, 2.74	0.48

The presence of the three complexes can be explained by the equation shown in Figure 6.10. In the absence of excess NH_3 , the NH_3 trans to the coordinated Cl is replaced by the “associated Cl” to form the neutral *trans*-RuCl₂(P-N)(PPh₃)(NH₃) (**38a**), which then rearranges to the more stable *cis* isomer **39a**. The concentrations of the three species are time-dependent, those of **37a** and **38a** diminishing significantly within 10 min. After 1 week, [**38a**] is zero, while there are 10 % **37a** and 90 % **39a**; addition of 1 atm of NH_3 completely regenerates **37a**.

**Figure 6.10** Reversible conversion of [RuCl(P-N)(PPh₃)(NH₃)₂⋯Cl] (**37a**) to *cis*-RuCl₂(P-N)(PPh₃)(NH₃) (**39a**).

The solution chemistry of the Br analogue **37b** is identical to that of **37a**. The change of halide is reflected in changes in the chemical shifts in the NMR spectra (Tables 6.3 and 6.4).

6.2.3 The Solid State Reaction of $\text{RuX}_2(\text{P-N})(\text{PPh}_3)$ with NH_3

When a solid sample of $\text{RuCl}_2(\text{P-N})(\text{PPh}_3)$ (**6a**) is exposed to 1 atm NH_3 , a colour change from green to pink occurs in 5 min, and the microanalysis of the solid product corresponds to $\text{RuCl}_2(\text{P-N})(\text{PPh}_3)(\text{NH}_3)$. A green solution formed when this solid was dissolved in CDCl_3 , and the resulting $^{31}\text{P}\{^1\text{H}\}$ and ^1H NMR spectra (within 5 min of dissolution) indicated the presence of **37a**, **38a** and **39a** in similar concentrations (Figures 6.11 and 6.12). After 30 min, the concentrations of **37a** and **38a** significantly diminish while that of **39a** increases. The initial presence of **37a** must be due to a slight excess of NH_3 present in the solid. The data lead to the conclusion that *trans*- $\text{RuCl}_2(\text{P-N})(\text{PPh}_3)(\text{NH}_3)$ (**38a**) is initially formed in the solid state and then, in solution, it rearranges to the more stable *cis* isomer **39a**. The *trans* to *cis* rearrangement supports indirectly the formation of *trans*- $\text{RuCl}_2(\text{P-N})(\text{PPh}_3)(\text{SH}_2)$ (**18a'**) en route to *cis*- $\text{RuCl}_2(\text{P-N})(\text{PPh}_3)(\text{SH}_2)$ (**18a**) (Figure 5.9); that is, the NH_3 ligand likely initially dissociates to form the square pyramidal complex that rearranges to a trigonal bipyramidal structure prior to attack by NH_3 at the position *cis* to P_A .

The solid state reaction of $\text{RuBr}_2(\text{P-N})(\text{PPh}_3)$ (**6b**) with NH_3 produced *trans*- $\text{RuBr}_2(\text{P-N})(\text{PPh}_3)(\text{NH}_3)$ (**38b**) which also rearranges to the more stable *cis* isomer **39b** in solution.

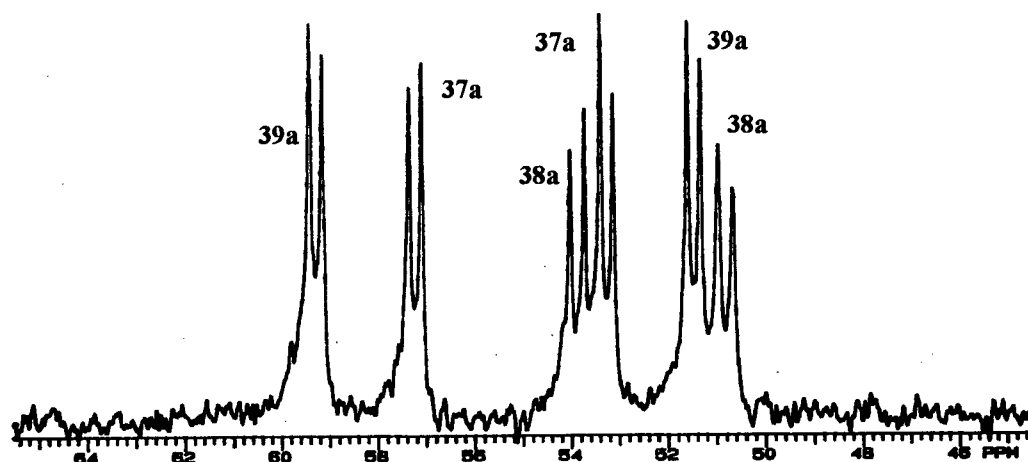


Figure 6.11 $^{31}\text{P}\{^1\text{H}\}$ NMR spectrum (121.4 MHz) of *trans*- $\text{RuCl}_2(\text{P-N})(\text{PPh}_3)(\text{NH}_3)$ (**38a**) 5 min after dissolution in CDCl_3 at 20°C .

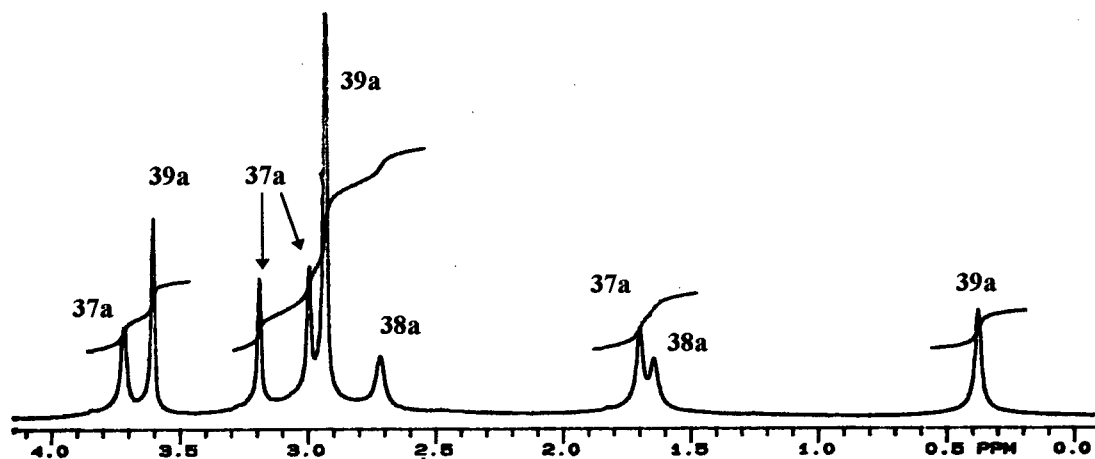


Figure 6.12 ^1H NMR spectrum (300 MHz) of *trans*- $\text{RuCl}_2(\text{P-N})(\text{PPh}_3)(\text{NH}_3)$ (**38a**) (5 min after dissolution in CDCl_3 at 20°C) in the region δ 0.0 to 4.0.

6.2.4 The Preparation of $[\text{RuCl}(\text{P-N})(\text{PPh}_3)(\text{NH}_3)_2]\text{PF}_6$ (**41**)

Conductivity measurements, performed on acetone or CH_2Cl_2 solutions of $[\text{RuX}(\text{P-N})(\text{PPh}_3)(\text{NH}_3)_2\cdots\text{X}]$ (**37**) in the absence or presence of 1 atm NH_3 , showed surprisingly that the solution species are non-conducting. Thus, these complexes are “close ion pairs” in solution, and Figure 6.7 shows a plausible formulation with H-bonding of the X-atom.

The reaction of $[\text{RuCl}(\text{P-N})(\text{PPh}_3)(\text{NH}_3)_2\cdots\text{Cl}]$ (**37a**) with NH_4PF_6 , under 1 atm of NH_3 , resulted in the displacement of the associated chlorine as Cl^- anion, and formation of a yellow solid, formulated as $[\text{RuCl}(\text{P-N})(\text{PPh}_3)(\text{NH}_3)_2][\text{PF}_6]$ (**41**); the conductivity of **41** in acetone (with or without the presence of excess NH_3) was $140 \pm 5 \text{ ohm}^{-1} \text{ cm}^2 \text{ mol}^{-1}$, consistent with a 1:1 electrolyte.²³ In the absence of excess NH_3 , the $^{31}\text{P}\{^1\text{H}\}$ NMR spectrum (in d_6 -acetone, Figure 6.13(a)) shows two doublets at δ 58.87 and δ 51.70 ($^2J_{\text{PP}} = 31.40 \text{ Hz}$), comparable to those of $[\text{RuCl}(\text{P-N})(\text{PPh}_3)(\text{NH}_3)_2\cdots\text{Cl}]$ (**37a**) [δ 57.87 and δ 52.60 ($^2J_{\text{PP}} = 31.93 \text{ Hz}$, d_6 -acetone, Figure 6.13(b))]; some trace signals at $\sim \delta$ 55.4 in Figure 6.13(a) were not identified. When the sample containing **41** is placed under 1 atm NH_3 , the only signals present are at δ 54.94 and δ 51.47 ($^2J_{\text{PP}} = 32.05 \text{ Hz}$, Figure 6.14), and are attributed to $[\text{Ru}(\text{P-N})(\text{PPh}_3)(\text{NH}_3)_3\cdots\text{Cl}][\text{PF}_6]$ (**40a**), where the coordinated Cl-atom of **41** has been replaced by another NH_3 ligand. The formation of such a tris-ammine complex was confirmed by reacting $\text{RuCl}_2(\text{P-N})(\text{PPh}_3)$ (**6a**) with 2 equiv of NH_4PF_6 under 1 atm NH_3 ; the $^{31}\text{P}\{^1\text{H}\}$ NMR chemical shifts at δ 55.26 and δ 51.67 ($^2J_{\text{PP}} = 32.05 \text{ Hz}$), which are similar to those of **40a**, are attributed to *in situ* formation of $[\text{Ru}(\text{P-N})(\text{PPh}_3)(\text{NH}_3)_3][\text{PF}_6]_2$ (**40b**). Repeated attempts to isolate **40b** yielded only dark yellow oily residues. The conductivity of **40b**, prepared *in situ* in acetone after removal of NH_4Cl , was $288 \text{ ohm}^{-1} \text{ cm}^2 \text{ mol}^{-1}$, in the range for a 1:2 electrolyte.²³ A tentative reaction scheme for the formation of the PF_6^- salts is shown in Figure 6.15. It is likely that **41** is formed by the direct reaction of **37a** with NH_4PF_6 in the absence of excess NH_3 ; however, this is difficult to demonstrate directly because in the absence of excess NH_3 , **37a** isomerizes to *cis*- $\text{RuCl}_2(\text{P-N})(\text{PPh}_3)(\text{NH}_3)$ (**39a**).

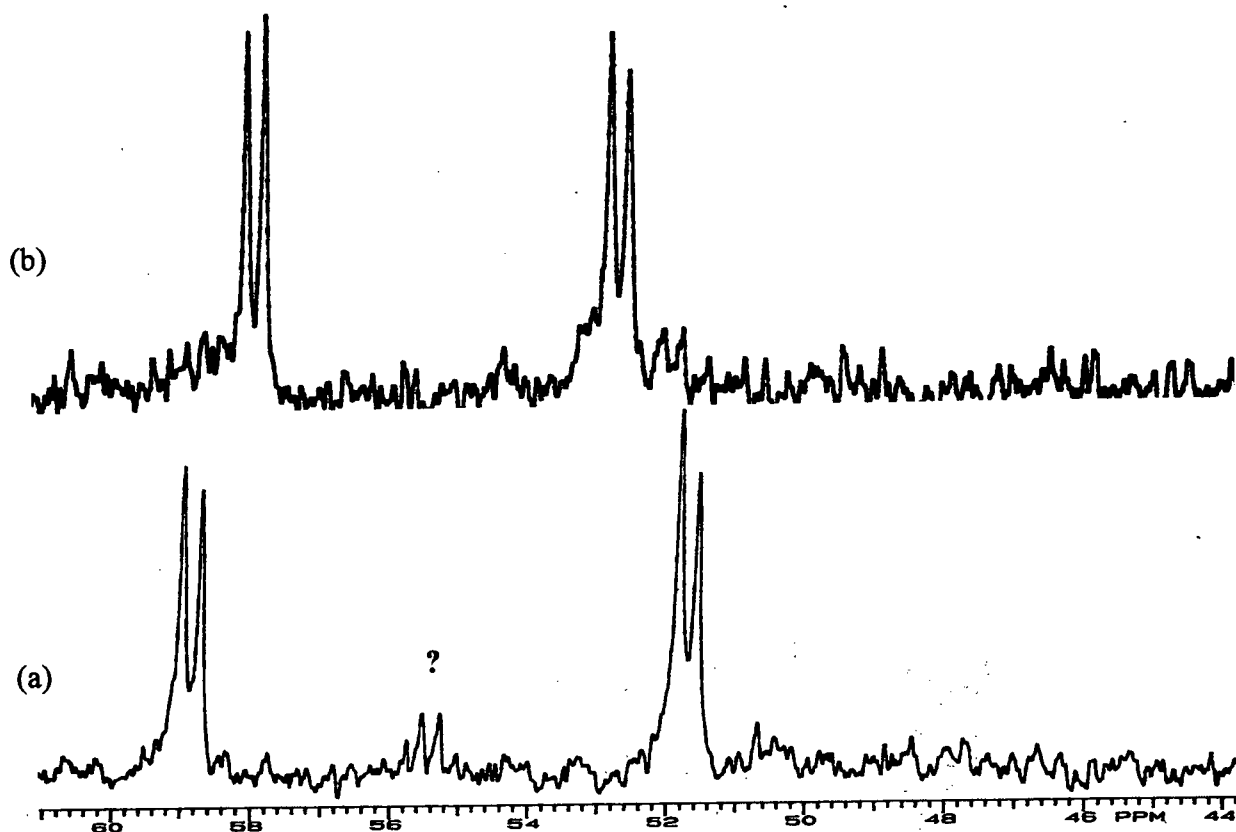


Figure 6.13 $^{31}\text{P}\{^1\text{H}\}$ NMR spectra (121.4 MHz) of (a) $[\text{RuCl}(\text{P-N})(\text{PPh}_3)(\text{NH}_3)_2][\text{PF}_6]$ (41) (a septet due to PF_6 is located at δ -143.4) and (b) $[\text{RuCl}(\text{P-N})(\text{PPh}_3)(\text{NH}_3)_2\cdots\text{Cl}]$ (37a) in d_6 -acetone at 20°C .

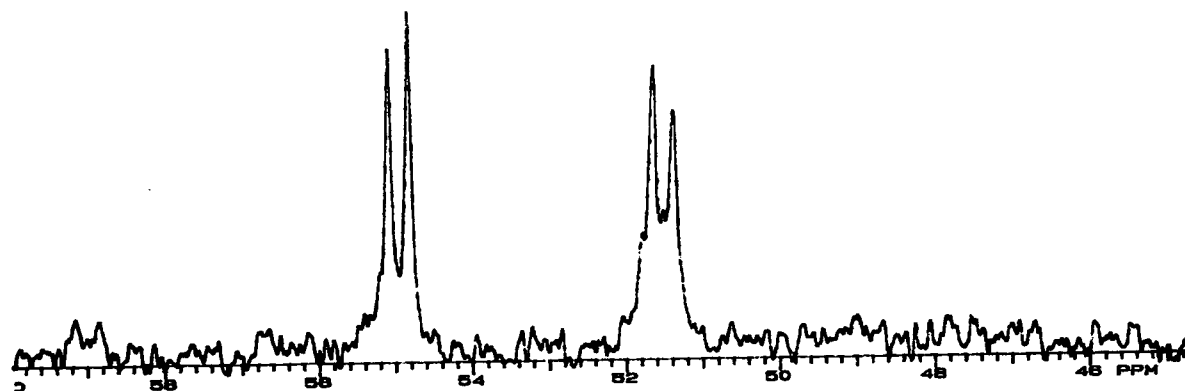


Figure 6.14 $^{31}\text{P}\{^1\text{H}\}$ NMR spectrum (121.4 MHz) for the *in situ* formation of $[\text{Ru}(\text{P-N})(\text{PPh}_3)(\text{NH}_3)_3\cdots\text{Cl}][\text{PF}_6]$ (40a) from the reaction of $[\text{RuCl}(\text{P-N})(\text{PPh}_3)(\text{NH}_3)_2][\text{PF}_6]$ (41) and 1 atm NH_3 in d_6 -acetone at 20°C (septet due to PF_6 is located at δ -143.4).

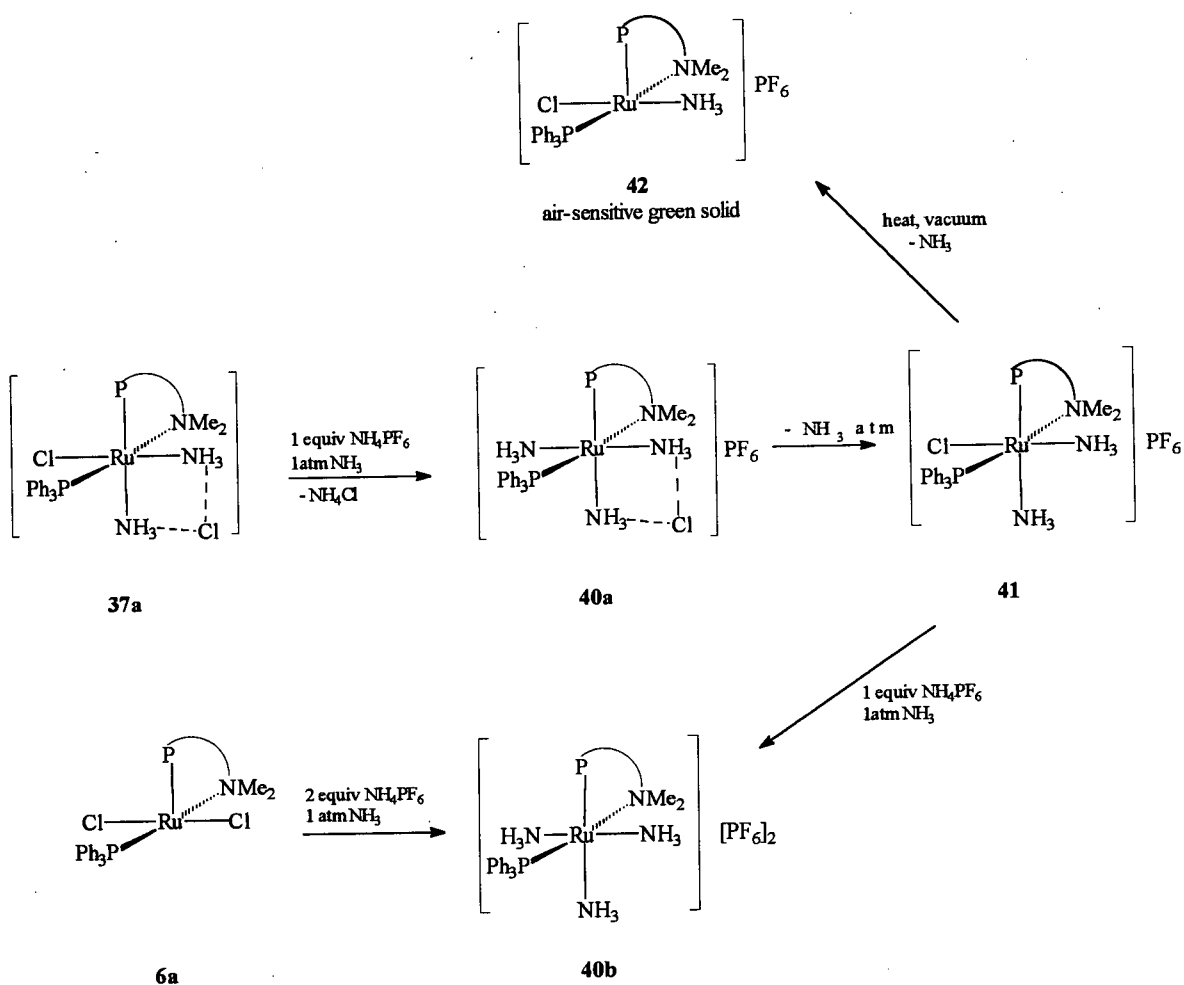


Figure 6.15 Reaction scheme for the preparation of NH_3 complexes containing PF_6^- ions.

Unfortunately, the microanalysis of **41**, a yellow solid, is not consistent (especially the high N content, see Section 2.11.2.5, p. 68) with the formulation $[\text{RuCl}(\text{P-N}(\text{PPh}_3)(\text{NH}_3)_2)][\text{PF}_6]$, in part because of the presence of unidentified species, which have ^1H NMR signals in the region δ 0.8 to 2.4 (Figure 6.16). Drying **41** *in vacuo* at 80°C resulted in a dark green solid with a microanalysis indicating the loss of an NH_3 molecule, and formation of $[\text{RuCl}(\text{P-N}(\text{PPh}_3)(\text{NH}_3))][\text{PF}_6]$ (**42**). This solid in d_6 -acetone gave new broad doublets in the $^{31}\text{P}\{^1\text{H}\}$ NMR spectrum at δ 48.64 and δ 47.85. Upon exposure to air, a solid

sample of **42** decomposed into a black powder. The reactive nature of this complex is consistent with the presence of a vacant coordination site. When the isolated yellow solid (**41**) was dissolved in CDCl_3 , all three species, **40a**, **41**, **42**, were observed in the $^3\text{P}\{^1\text{H}\}$ NMR spectrum (cf. Figure 6.15).

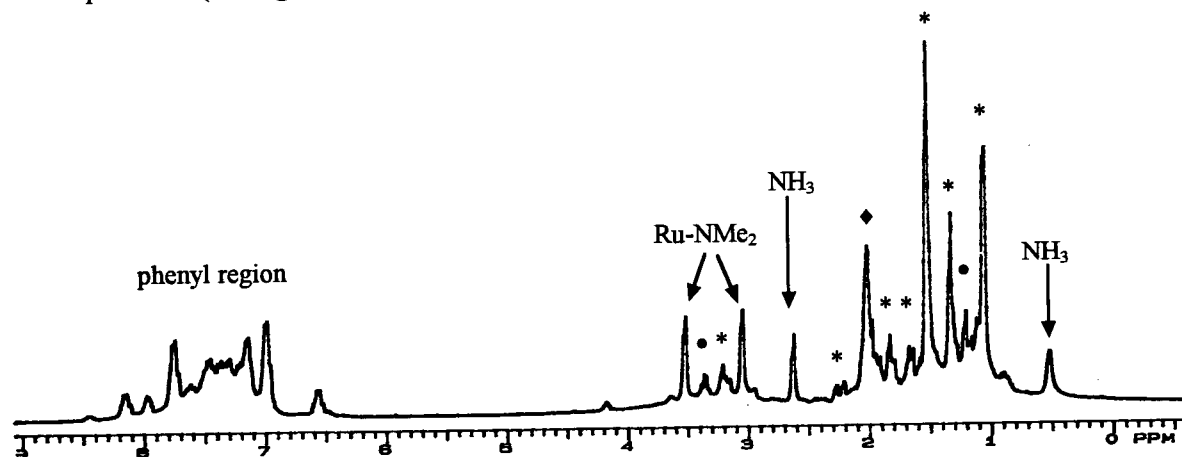


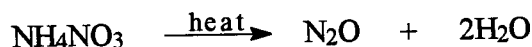
Figure 6.16 ^1H NMR spectrum of (300 MHz) of $[\text{RuCl}(\text{P-N})(\text{PPh}_3)(\text{NH}_3)_2][\text{PF}_6]$ (**41**) in d_6 -acetone at 20°C ; *, unidentified, but $\bullet\text{Et}_2\text{O}$ (δ 3.4, 1.2) and \blacklozenge acetone (δ 2.0) are present.

The conductivities of species **40a** and **41** are identical, indicating 1:1 electrolytes in both cases, and implying again that in **40a** the Cl-atom is associated strongly with the cationic complex. Perhaps hydrogen-bonding plays a role as in **37a** (Figure 6.7). Several attempts to grow crystals of **37a** and **41** were unsuccessful.

6.3 The Coordination Chemistry of N₂O

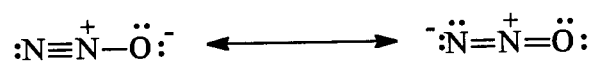
6.3.1 N₂O as a Potential Oxidant

Nitrous oxide, also known as “laughing gas” is a colourless, odourless, non-flammable, and non-toxic gas. At room temperature, it exists as a liquid at pressures of ≥ 50 atm. Commercial manufacture is from the thermal decomposition of ammonium nitrate at $\sim 270^\circ\text{C}$:

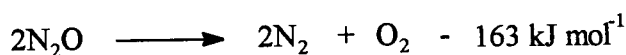


N₂O is primarily used as an inhalation anaesthetic in medicine and dentistry, and as a dispersing agent in cream whippers.

N₂O is a linear molecule as expected by the following resonance forms:²⁴



At temperatures above 600°C , N₂O is thermodynamically unstable and decomposes into its elements:²⁵



Interest in the inorganic chemistry of N₂O has advanced partly because of its potential use as an oxidant in catalytic systems. N₂O only reacts slowly with oxidizing and reducing agents and is relatively inert towards metal complexes, but is an attractive oxidant because of the following advantages: (i) Its oxidizing power is comparable to those of hydrogen peroxide and perbromate owing to the large thermodynamic driving force for the loss of N₂. (ii) In the absence of activating reagents such as metal complexes or surfaces, N₂O is kinetically inert toward organic molecules, implying oxidation by N₂O could have conceivable selectivity upon activation by catalysts. (iii) N₂O is inexpensive and non-toxic. (iv) The by-product of any potential catalytic systems involving N₂O is N₂ (Figure 6.17).²⁶⁻³⁰

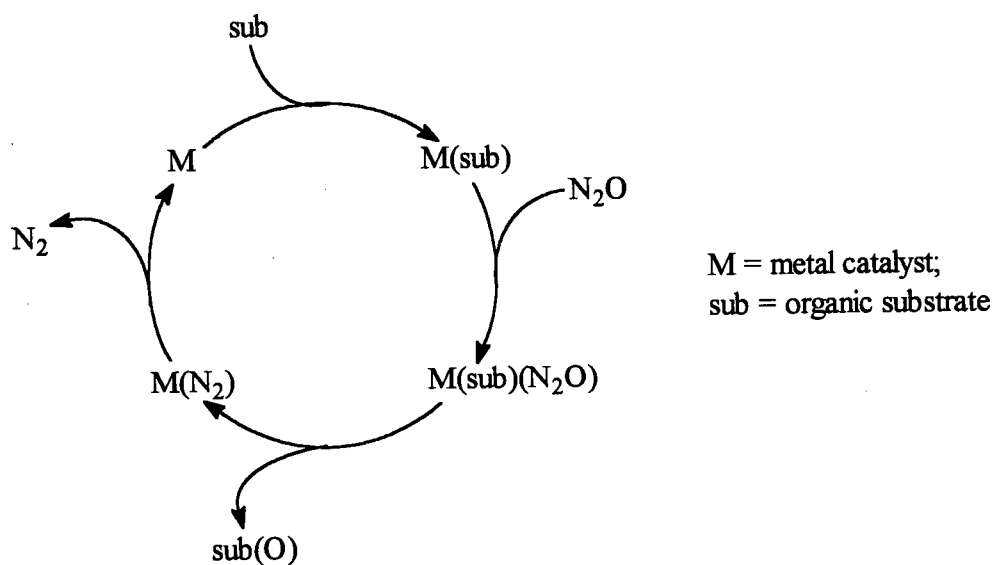


Figure 6.17 Potential catalytic cycle for the oxidation of organic substrates using N_2O .

Previous to this work, only one coordinated N_2O complex, $[\text{Ru}(\text{NH}_3)_5(\text{N}_2\text{O})]^{2+}$, has been reported with definite characterization.³¹⁻³³ The complex was first prepared by Armor and Taube by adding N_2O to an aqueous solution of $[\text{Ru}(\text{NH}_3)_5(\text{H}_2\text{O})]^{2+}$.^{31a} Whilst this route did not give a high purity product, an indirect route discovered by Bottomley and co-workers gave good yields of $[\text{Ru}(\text{NH}_3)_5(\text{N}_2\text{O})]^{2+}$.³³



Although numerous studies have been carried out to ascertain the bonding mode of N_2O in this complex, no definitive evidence has supported either the possible Ru-N-N-O ^{31b,33c} or Ru-O-N-N ^{32c,d} bonding modes. However, circumstantial evidence such as IR data, force constants, and the similarity of the electronic spectra of $[\text{Ru}(\text{NH}_3)_5(\text{N}_2\text{O})]^{2+}$ and $[\text{Ru}(\text{NH}_3)_5(\text{N}_2)]^{2+}$, strongly suggests bonding through the N-atom,^{33c} theoretical studies by Tuan and Hoffmann also indicate that N-linkage complexes are more stable than the O-linkage complexes.³⁴

Interest in the reactivity of N_2O has also involved oxygen-atom transfer from N_2O into a transition metal-ligand bond (cf. Figure 6.17). The ligand may range from hydrogen to organic substrates. The catalytic reduction of N_2O to N_2 with concomitant oxidation of PPh_3 to OPPh_3 by $\text{CoH}(\text{N}_2)(\text{PPh}_3)_3$ has been studied by Yamamoto and co-workers,³⁵ and of interest because a ligand, rather than the metal centre, was oxidized. Consequently, the N_2O -oxidation of other ligands and substrates coordinated to metal centres is worth investigation.

Hillhouse and co-workers have studied the reactions of group 4 transition-metal (Ti, Zr and Hf) complexes with N_2O that result in the oxidation of a coordinated ligand.³⁶ For example, the reaction with the diphenylacetylene zirconocene complex $\text{Cp}^*_2\text{Zr}(\text{C}_2\text{Ph}_2)$, with subsequent treatment with HCl , leads to the formation of $\text{Cp}^*_2\text{ZrCl}_2$ and deoxybenzoin, $\text{PhCH}_2\text{C}(\text{O})\text{Ph}$ (Figure 6.18).^{36b} The high strength of the group 4 M-O bonds, however, places limitations on the potential applications of the use of such metal systems with N_2O in catalytic cycles, and it is certainly of interest to study late transition metal systems as they form weaker bonds with heteroatoms (N, S, O).

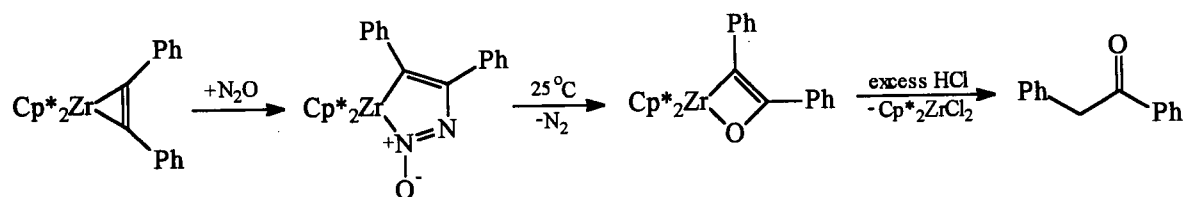


Figure 6.18 Stoichiometric formation of $\text{PhCH}_2\text{C}(\text{O})\text{Ph}$ utilizing N_2O .

N_2O reacts with cyclic and acyclic nickel alkyls to give stable nickel alkoxide complexes, with regiospecific insertion of the O-atom into the Ni-C bond (Figure 6.19).^{28,37}

Elimination of the organic moieties to form an alcohol, cyclic ether or lactone occurs via addition of HCl, I₂ and CO, respectively.²⁸

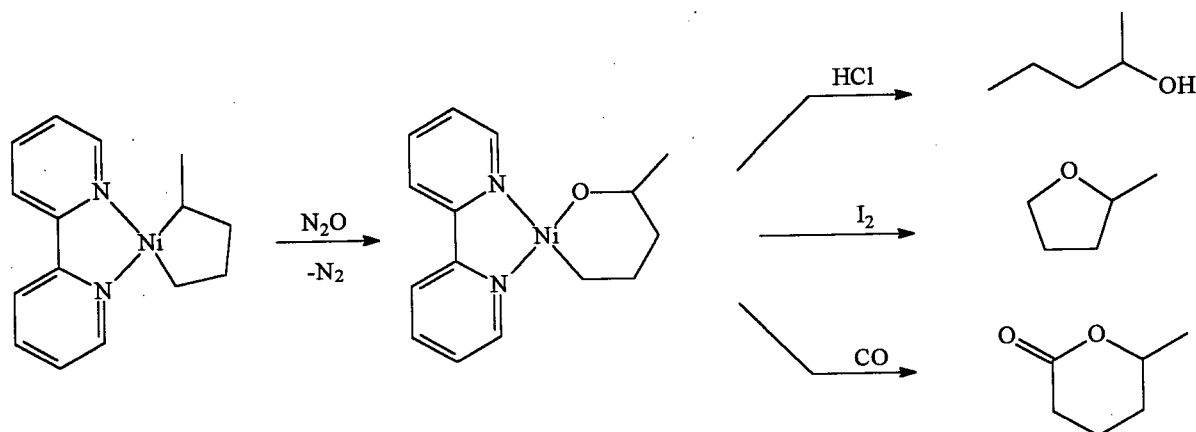


Figure 6.19 Transfer of the O-atom of N₂O into a Ni-C bond.

Monomeric late transition metal hydroxo complexes are important in catalytic processes such as hydration of olefins to alcohols, nitriles to carboxamides and the Wacker process (see Section 3.3.2, p. 88); however the synthesis and isolation of such complexes may be difficult because elevated temperatures and extended reaction times are often required.^{27,38-40} Kaplan and Bergman have shown recently that N₂O can be used to insert an O-atom into one or two Ru-H bonds of (dmpe)₂Ru(H)₂ (dmpe = 1,2-bis(dimethylphosphino)ethane) under mild conditions to form (dmpe)₂Ru(H)(OH) and (dmpe)₂Ru(OH)₂ (Figure 6.20).^{39,40}

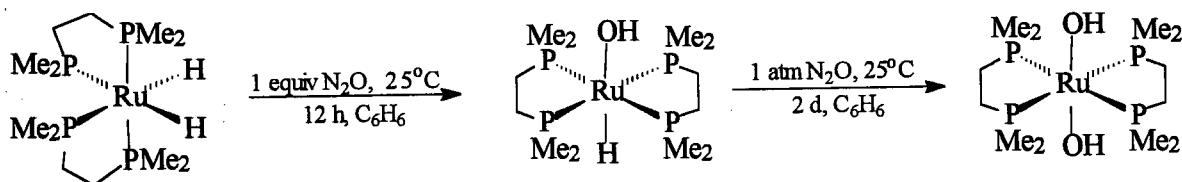


Figure 6.20 Formation of Ru-OH complexes by O-atom insertion from N₂O.

For the reactions with N_2O with the Ni and Ru complexes described above, no intermediates were observed to suggest any mechanistic pathway for O-atom insertion. However, the researchers suggest coordination of N_2O prior to N_2 loss and O-atom transfer in both cases. For the former case, a five-coordinate Ni intermediate was insinuated,²⁹ while for the Ru hydride complex, initial N_2O coordination to the Ru either via an O- or N-atom with subsequent rearrangement was suggested (Figure 6.21).⁴⁰ Despite these suggestions, the direct N_2O insertion pathway as observed for the Zr complex (Figure 6.18) cannot be ruled out.

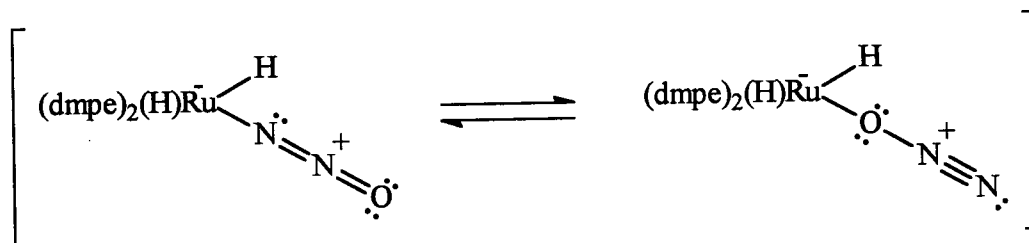


Figure 6.21 Possible coordination modes of N_2O to $(\text{dmpe})_2\text{Ru}(\text{H})_2$.

6.3.2 The Reaction of $\text{RuCl}_2(\text{P-N})(\text{PPh}_3)$ with N_2O

When 1 atm N_2O is added to a solution of $\text{RuCl}_2(\text{P-N})(\text{PPh}_3)$ (**6a**) in CD_2Cl_2 at 20°C , no immediate reaction is noted by NMR spectroscopy. After 2 days, decomposition of the Ru(II) species occurs, with identifiable species in the $^{31}\text{P}\{^1\text{H}\}$ NMR spectrum (Figure 6.22(e)) being the Ru(III) oxo complex, $(\mu\text{-O})(\mu\text{-Cl})[\text{RuCl}(\text{P-N})]_2$ (**17**) (δ 39.35, 38.21 (d, $^4J_{\text{PP}} = 10.08$ Hz)), O=PPh_3 (s, δ 27.22) and O=P-N (s, δ 25.33; signal is assigned following the preparation of O=P-N from P-N and H_2O_2).¹ Assignment of the chemical shifts in the ^1H NMR spectra proved to be difficult because the δ 2.0 - 4.0 region contains overlapping signals due to NMe resonances of the above species. As discussed in Chapter 3, **17** is formed by the oxidation of **6a** in an O_2 atmosphere, and evidently there is a slow oxidation reaction between

6a and N_2O . When the N_2O pressure was increased to 6 atm, the $^{31}\text{P}\{^1\text{H}\}$ NMR spectrum, measured within 5 min of N_2O addition, became very noisy and the chemical shifts due to **6a** became broad Figure 6.22(b). This behaviour is characteristic of the presence of a paramagnetic species, and perhaps formation of diamagnetic **17** occurs via a paramagnetic Ru(III) intermediate.

The reaction of **6a** with ~ 6 atm N_2O in CD_2Cl_2 between -90 and -40°C surprisingly produced a bright yellow solution. Two species are identified by two sets of AX doublets at δ 49.52 (P_A) and δ 40.06 (P_X), $^2J_{\text{PP}} = 27.93$ Hz, and at δ 47.54 (P_A) and δ 37.91 (P_X), $^2J_{\text{PP}} = 27.01$ Hz in the $^{31}\text{P}\{^1\text{H}\}$ NMR spectra (Figure 6.22(c) and (d)). From previous work in this laboratory, the latter species was identified as the dinitrogen complex *cis*- $\text{RuCl}_2(\text{P-N})(\text{PPh}_3)(\eta^1\text{-N}_2)$ (**43**).^{1,2} As indicated by $^{31}\text{P}\{^1\text{H}\}$ NMR data (Figure 6.23(a)), **43** is formed when **6a** is placed under 6 atm N_2 . Furthermore, **43** is in a dynamic equilibrium with **6a** and much higher pressures of N_2 are required for complete product formation. The assignment of a *cis* structure for **43** is based on the two singlets at δ 3.63 and 3.04 due to NMe_2 observed in the ^1H NMR spectrum. A direct comparison of the reactions of **6a** with N_2O and N_2 is shown in Figure 6.23. The new species, **44** is tentatively ascribed as the coordinated N_2O complex *cis*- $\text{RuCl}_2(\text{P-N})(\text{PPh}_3)(\text{N}_2\text{O})$. The assignment of a *cis* structure for **44** is based on the similar positions of the chemical shifts and coupling constants for **43** and **44** in the $^{31}\text{P}\{^1\text{H}\}$ NMR spectra, and the presence of two singlets at δ 3.60 and 2.85 due to the NMe_2 of **44** in the ^1H NMR spectrum (at -88°C). The N_2O complex is only observed and stable at temperatures at or below -40°C .

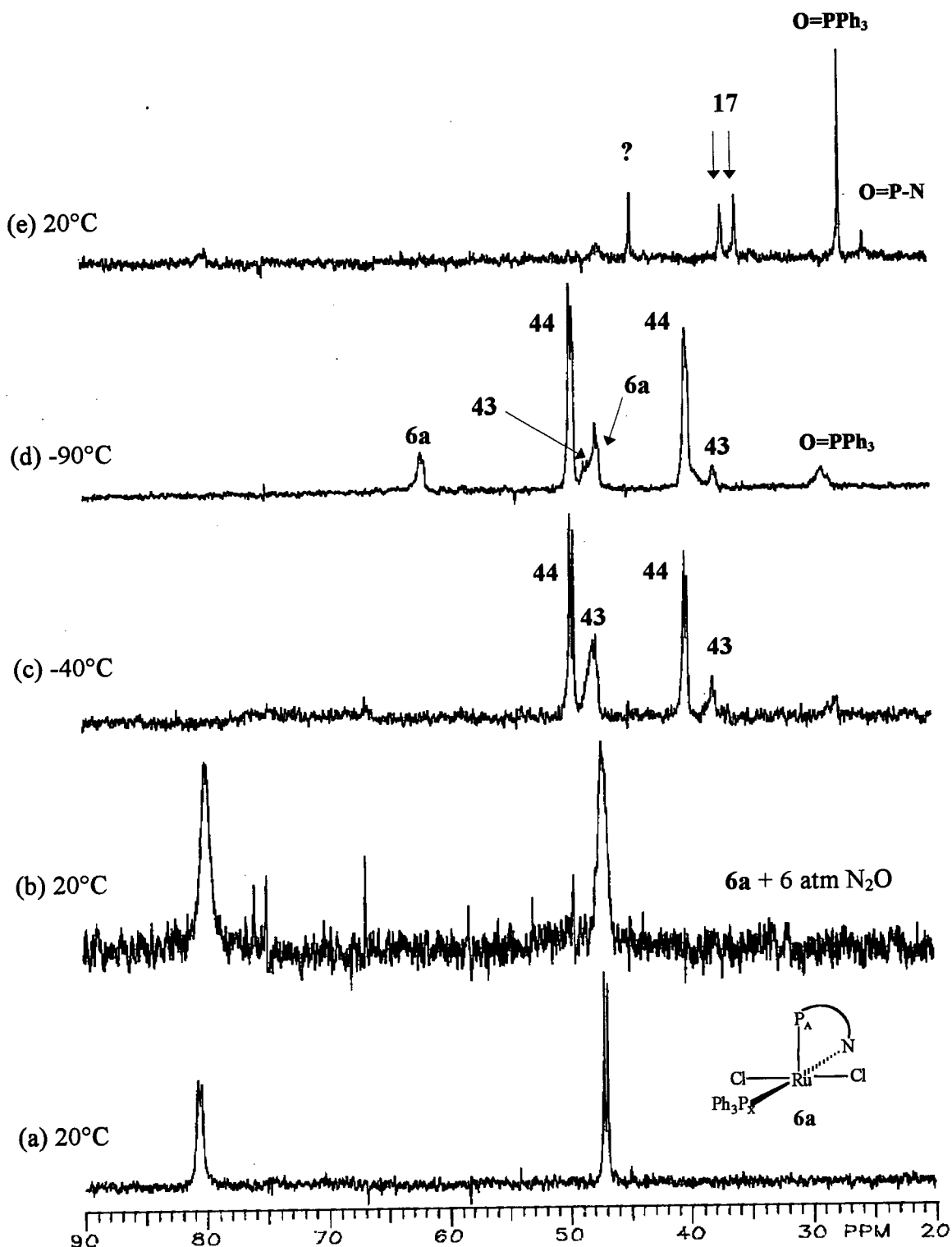


Figure 6.22 $^{31}\text{P}\{^1\text{H}\}$ NMR spectrum (121.4 MHz, CD_2Cl_2) of (a) **6a**, and the reaction of **6a** with 6 atm N_2O at (b) 20°C, (c) -40°C, (d) -90°C and (e) 20°C after reaction time of 2 days. The spectra at low temperatures are time-independent; trace $\text{O}=\text{PPh}_3$ is formed during transfer of the NMR sample from the cold temperature bath to the spectrometer probe.

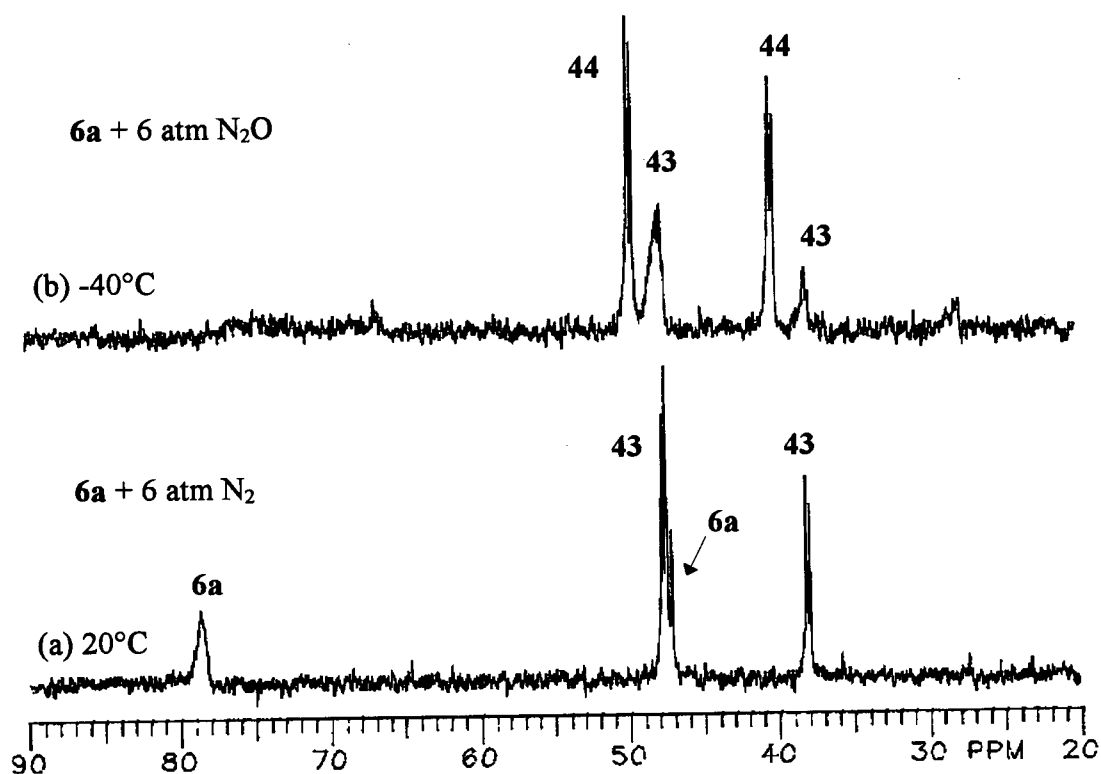


Figure 6.23 $^{31}\text{P}\{^1\text{H}\}$ NMR spectra (121.4 MHz, CD_2Cl_2) for the reaction of **6a** with (a) 6 atm N_2 at 20°C and (b) 6 atm N_2O at -40°C .

Although $^{31}\text{P}\{^1\text{H}\}$ NMR data are consistent with formation of a coordinated N_2O species **44**, the coordination mode of N_2O is not identifiable, although coordination via the N-atom seems most likely because of the formation of the $\eta^1\text{-N}_2$ adduct. The initial coordination of N_2O , followed by the cleavage of the O atom to form **43** and O_2 , seems plausible (Figure 6.24). At temperatures below -40°C , the species **6a**, **43** and **44** are stable indefinitely, and O_2 is ineffective in oxidizing the Ru(II) complexes; trace O=PPh_3 (as seen in Figure 6.22 (c) and (d)) is formed during transfer of the NMR sample from the cold temperature bath to the spectrometer probe. This was verified when a sample of **6a** was placed under 1 atm O_2 at -40°C ; no reaction was indicated by the $^{31}\text{P}\{^1\text{H}\}$ NMR spectrum. In

both systems involving N_2O and O_2 , the formation of **17** and O=PPh_3 is observed when the temperature is slowly raised to room temperature. The mechanistic aspects involving the O_2 -oxidation, however, has not been ascertained.

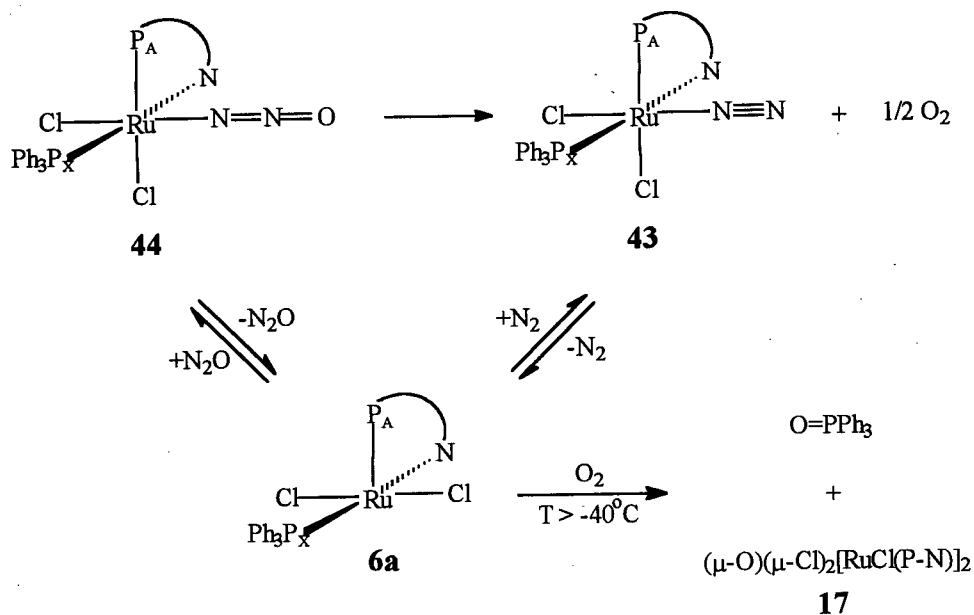


Figure 6.24 Proposed reaction scheme for the formation of **17** and O=PPh_3 , if N_2O is initially coordinated to **6a** via the terminal N atom.

If the N_2O is coordinated to **6a** via the O-atom, the direct migratory insertion of O into the Ru-PPh_3 bond is conceivable. This correlates with one mechanism proposed in Chapter 3 (Section 3.2.1) where the formation of O=PPh_3 and **17** occurs via the initial coordination of O_2 to the Ru. Of note, the oxidation of PPh_3 is catalytic. When an excess of 2 equiv of PPh_3 is added to the reaction of **6a** with N_2O , all the PPh_3 is converted to O=PPh_3 (Figure 6.25) and, only when all the PPh_3 has reacted, is the Ru(II) species oxidized to **17**.

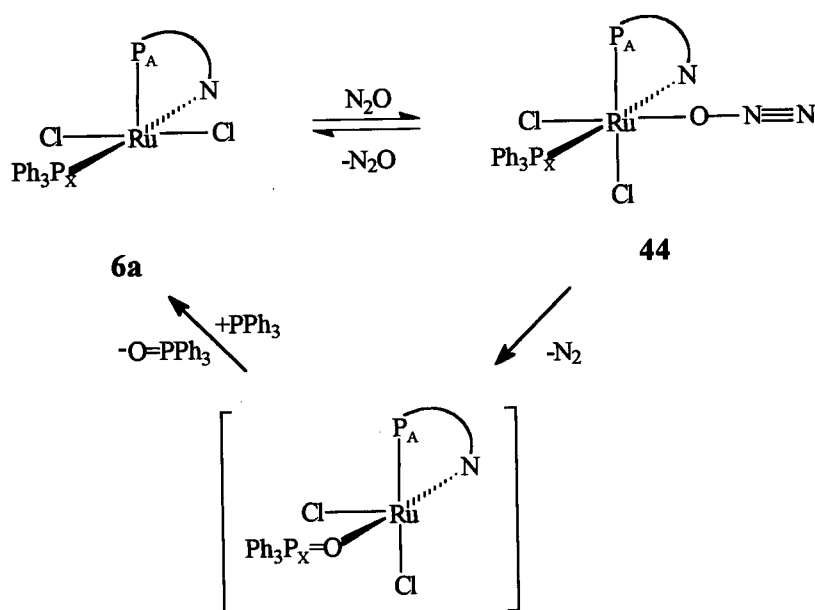


Figure 6.25 The catalytic oxidation of PPh_3 by N_2O .

The potential use of **6a** as an oxidation catalyst is promising because N_2O preferentially oxidizes PPh_3 rather than the Ru centre. However, attempts to oxidize organic substrates such as ethylene, styrene or cyclooctene at ambient conditions were unsuccessful. Even with 3 to 6 atm N_2O added to a CH_2Cl_2 or C_6H_6 solution containing **6a** and 10 equiv substrates (at -80 to 60°C), only **17** and $\text{O}=\text{PPh}_3$ were observed to form while the organic substrates remained unchanged. Of note, the substrates studied do not coordinate to **6a**, while in order for N_2O to be an effective oxidant, it is likely that the substrate in question must bind to the Ru. Furthermore, insertion of the O-atom into a Ru-substrate bond must be preferred over that of the Ru- PPh_3 bond. Fine tuning of the Ru complex is perhaps required to obtain an effective catalytic cycle using N_2O as the oxidant. These modifications may include incorporation of an alkyl ligand or the replacement of the PPh_3 with a more strongly basic phosphine.

6.4 Ruthenium Carbene Complexes: The Synthesis and Reactivity of *Cis*-RuCl₂(P-N)(PR₃)(=C=C(H)R') (R, R' = Ph, *p*-tolyl)

Carbenes are formed when monohapto, two-electron alkylidene ligands of the type CH₂, CHR and CR₂ (R = alkyl or aryl group) form M=C *d-p* double bonds within metal complexes. The first carbene complex, (CO)₅W=C(OMe)Me, was reported by Fischer and Maasböl in 1964.⁴¹ Two efficient tools for the characterization of metal carbenes are X-ray crystallography and ¹³C NMR spectroscopy. A short M-C(carbene) bond distance and a downfield shift of the carbene-carbon resonance is indicative of a M=C bond. Metal carbene complexes constitute an important area of research in organometallic and catalytic reactions,⁴² and new organic compounds of well-defined stereochemistry have been accessed from complexes with functionalized carbenes.⁴³

6.4.1 Characterization of *Cis*-RuCl₂(P-N)(PR₃)(=C=C(H)R)

Dark orange solutions were obtained when a mixture of 10 equiv of HCCPh or HCC(*p*-tolyl) and **6a** or **7a** in CH₂Cl₂ was refluxed at 40°C, and work-up yielded dark orange powders, that were identified as *cis*-RuCl₂(P-N)(PPh₃)(=C=C(H)Ph) (**45**), *cis*-RuCl₂(P-N)(P(*p*-tolyl)₃)(=C=C(H)Ph) (**46**), and *cis*-RuCl₂(P-N)(PPh₃)(=C=C(H)(*p*-tolyl)) (**47**). The formation of the vinylidene moiety is thought to occur via an η²- to η¹-alkyne slippage followed by an α,β-hydrogen shift (Figure 6.26); a repulsive 4e interaction between a d_π orbital of the Ru d⁶ system and the perpendicular filled π orbital of the alkyne destabilizes the metal η²-alkyne bond and, by localization of electron density on the Ru centre, the vinylidene complex is relatively more stable than the η²-alkyne complex.⁴⁴

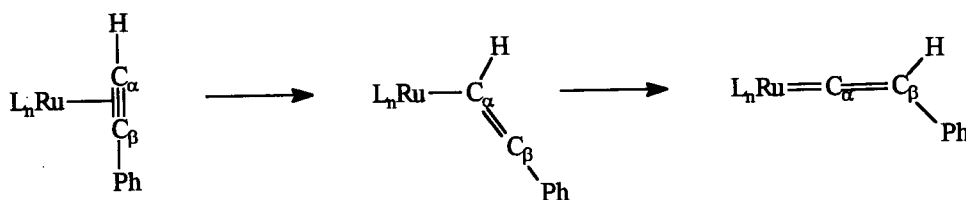


Figure 6.26 Formation of a vinylidene complex from a 1-alkyne ligand. L_n represents the auxiliary ligands of the Ru complex.

X-ray quality, red-orange crystals of **45** were obtained from the slow evaporation of a $CDCl_3$ solution of the complex in an NMR tube. The ORTEP plot, selected bond lengths and bond angles are shown in Figure 6.27, and Tables 6.5 and 6.6, respectively. The pseudo-octahedral structure contains two *cis*-Cl-atoms [$Cl(1)-Ru-Cl(2)$ 91.50°], with the P-atom of the P-N trans to one Cl-atom, and the vinylidene ($=C=C(H)Ph$) trans to the second Cl-atom [$Cl(2)-Ru-C(1)$ 172.7°]. The bond length of 1.814 \AA is indicative of a $Ru=C$ double bond, and is comparable to those observed for other Ru vinylidene complexes (1.823 to 1.86 \AA):⁴⁵ e.g. $[Ru\{=C=C(Me)R\}(\eta^5-C_9H_7)(PPh_3)_2][CF_3SO_3]$ (1.838 \AA , $R = 1\text{-cyclohexenyl}$)⁴⁶ and $[Ru\{=C=C(H)Me\}(PMe_3)_2(\eta^5-C_5H_5)][PF_6]$ (1.845 \AA).⁴⁷ The $C(1)-C(2)$ distance of 1.329 \AA is in the normal range (1.25 to 1.41 \AA)⁴⁵ for a $C=C$ bond, while the $Ru-C(1)-C(2)$ angle of 176.4° indicates the linearity of the $Ru=C=C$ moiety. All the other bonds with the exception of the $Ru-P(1)$ bond are within the range found for the other *cis*- $RuCl_2(P-N)(PPh_3)(L)$ complexes. The distance of 2.332 \AA for $Ru-P(1)$ is slightly longer than the $2.2617 - 2.2884 \text{ \AA}$ for analogous complexes previously discussed (Sections 4.2, 4.3 and 6.1), and this is attributed to the distribution of more electron density to the d-p bonding of $Ru=C$.

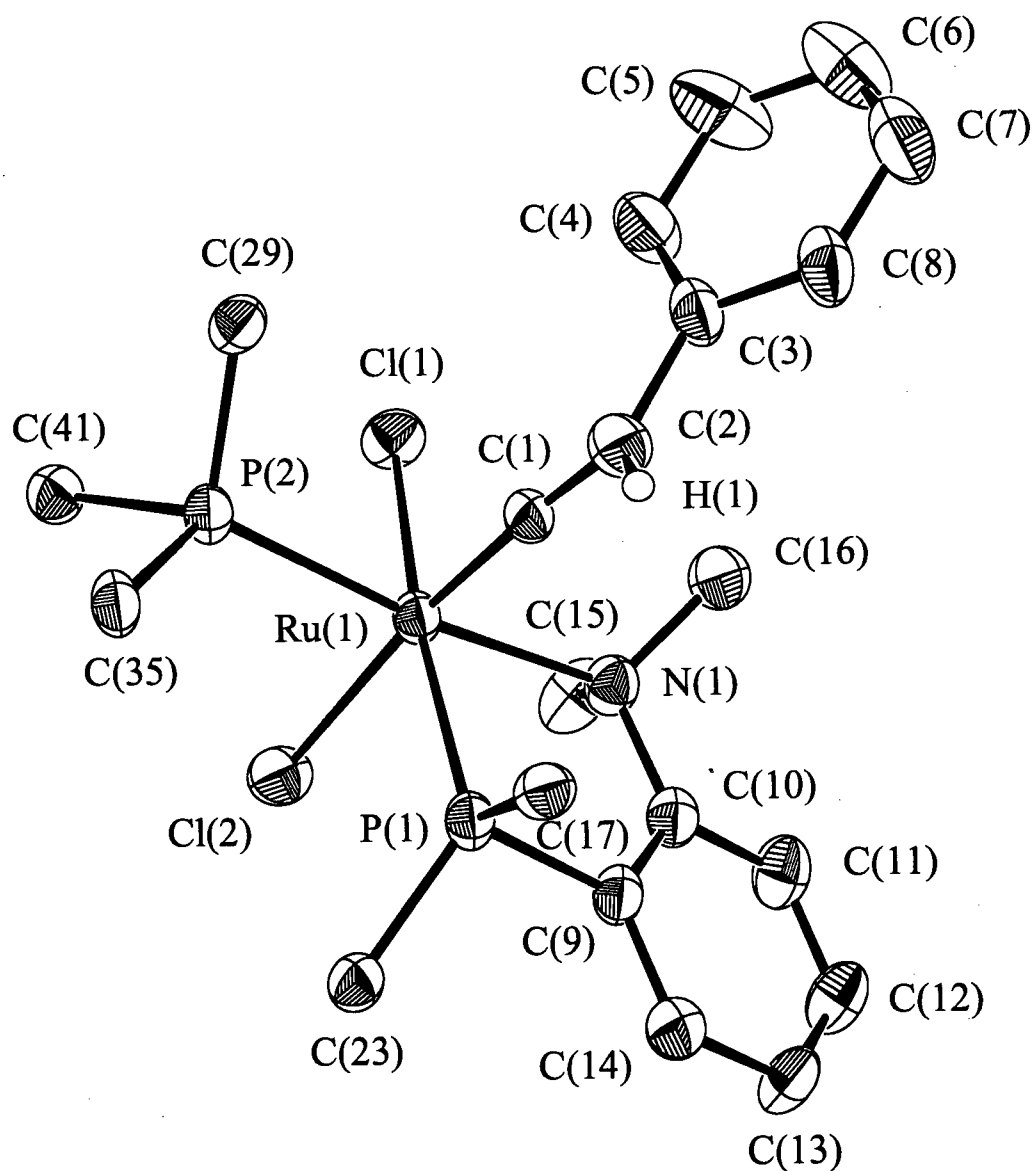


Figure 6.27 The ORTEP plot of *cis*-RuCl₂(P-N)(PPh₃)(=C=C(H)Ph) (**45**). Thermal ellipsoids for non-hydrogen atoms are drawn at 33 % probability (some phenyl carbons have been omitted for clarity). Full experimental parameters and details are given in Appendix X.

Table 6.5 Selected bond lengths (Å) for *cis*-RuCl₂(P-N)(PPh₃)(=C=C(H)Ph) (**45**) with estimated standard deviations in parentheses.

Bond	Length (Å)	Bond	Length (Å)
Ru(1)-Cl(1)	2.434(2)	Ru(1)-N(1)	2.308(7)
Ru(1)-Cl(2)	2.495(2)	Ru(1)-C(1)	1.814(8)
Ru(1)-P(1)	2.332(2)	C(1)-C(2)	1.329(12)
Ru(1)-P(2)	2.346(2)	C(2)-C(3)	1.455(13)

Table 6.6 Selected bond angles (°) for *cis*-RuCl₂(P-N)(PPh₃)(=C=C(H)Ph) (**45**) with estimated standard deviations in parentheses.

Bonds	Angle (°)	Bonds	Angle (°)
Cl(1)-Ru(1)-Cl(2)	91.50(9)	P(1)-Ru(1)-P(2)	106.94(8)
Cl(1)-Ru(1)-P(1)	169.56(8)	P(1)-Ru(1)-N(1)	82.2(2)
Cl(1)-Ru(1)-P(2)	83.15(8)	P(1)-Ru(1)-C(1)	87.3(3)
Cl(1)-Ru(1)-N(1)	87.8(2)	P(2)-Ru(1)-N(1)	170.9(2)
Cl(1)-Ru(1)-C(1)	95.6(3)	P(2)-Ru(1)-C(1)	89.9(3)
Cl(2)-Ru(1)-P(1)	85.45(8)	N(1)-Ru(1)-C(1)	89.9(3)
Cl(2)-Ru(1)-P(2)	92.61(9)	Ru(1)-C(1)-C(2)	176.4(8)
Cl(2)-Ru(1)-N(1)	88.7(2)	C(1)-C(2)-C(3)	124.3(9)
Cl(2)-Ru(1)-C(1)	172.7(3)		

The IR spectrum of **45** depicts a strong band at 1615 cm⁻¹ which is typical of the $\nu_{C=C}$ stretching of vinylidene ligands.^{45,48}

The ³¹P{¹H} and ¹H NMR spectra of **45** are shown in Figures 6.28 and 6.29, respectively. The P_A and P_X chemical shifts are found at δ 37.85 and 36.40, ²J_{PP} = 26.50 Hz,

while the inequivalent NMe groups are seen as singlets at δ 3.60 and 3.11 in the ^1H NMR spectrum. The C_β -proton is coupled to the *ortho*-protons of the phenyl ring giving a doublet of doublets at δ 2.43 ($^4J_{\text{HH}} = 6$ Hz). The $^{31}\text{P}\{^1\text{H}\}$ and ^1H NMR chemical shifts for $\text{RuCl}_2(\text{P-N})(\text{P}(p\text{-tolyl})_3)(=\text{C}=\text{C}(\text{H})\text{Ph})$ (**46**) and $\text{RuCl}_2(\text{P-N})(\text{PPh}_3)(=\text{C}=\text{C}(\text{H})(p\text{-tolyl}))$ (**47**) are nearly identical to those of **45** with the exception of an additional singlet due to the Me of the *p*-tolyl group at δ 2.16 in the ^1H NMR spectra (see Sections 2.12.2 and 2.12.3). Characteristic ^{13}C NMR data pertaining to the resonances of the four C-atoms of the $\text{RuC}_\alpha\text{C}_\beta$ and of the $\text{N}(\text{C}_\gamma\text{H}_3)_2$ units were obtained for **45**: the strongly deshielded C_α resonates at δ 358.2 (t, $^2J_{\text{CP}} = 18.6$ Hz); C_β at δ 111.0 (s); and inequivalent C_γ signals at δ 57.26 and 52.52 (s).

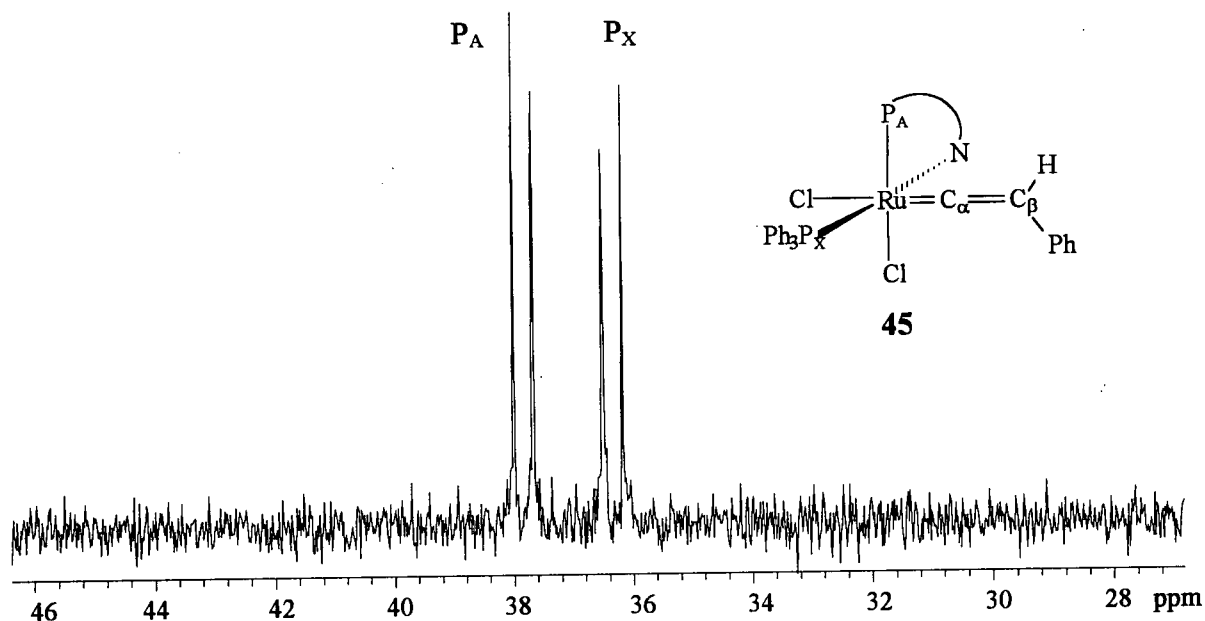


Figure 6.28 $^{31}\text{P}\{^1\text{H}\}$ NMR spectrum (81.0 MHz, 20°C) of *cis*- $\text{RuCl}_2(\text{P-N})(\text{PPh}_3)(=\text{C}=\text{C}(\text{H})\text{Ph})$ (**45**) in CDCl_3 .

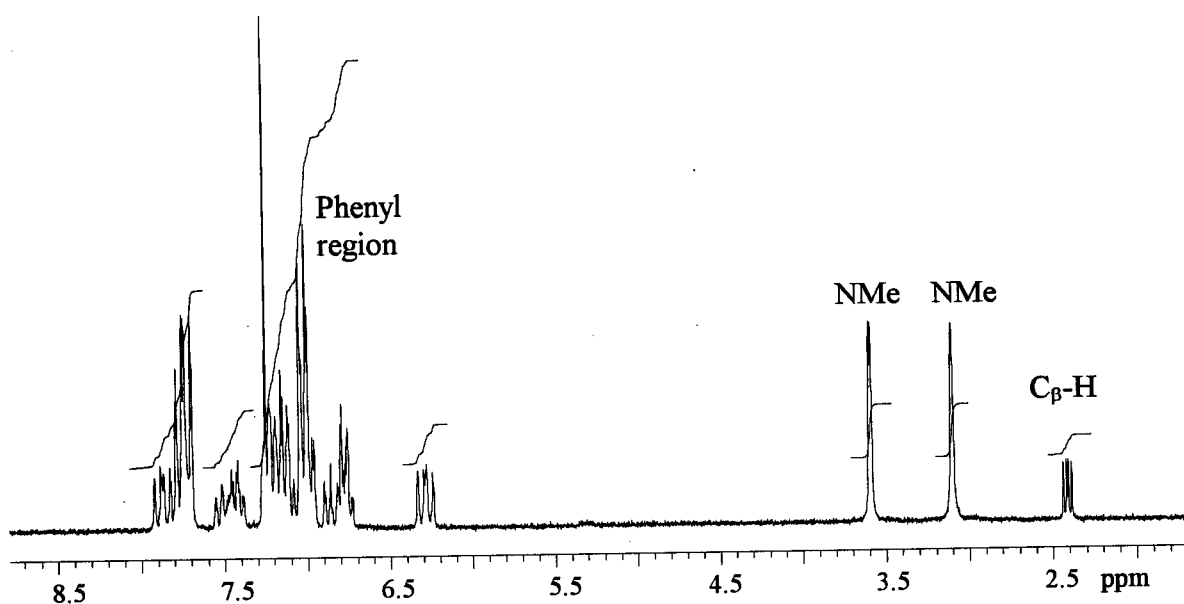


Figure 6.29 ^1H NMR spectrum (200 MHz, 20°C) of *cis*- $\text{RuCl}_2(\text{P-N})(\text{PPh}_3)(=\text{C}_\alpha=\text{C}_\beta(\text{H})\text{Ph})$ (**45**) in CDCl_3 .

6.4.2 The Reactivity of *Cis*- $\text{RuCl}_2(\text{P-N})(\text{PPh}_3)(=\text{C}=\text{C}(\text{H})\text{Ph})$ (**45**)

As a result of localization of electron density in the $\text{Ru}=\text{C}_\alpha$ bond and on the C_β atom, there is electron deficiency at the C_α atom of vinylidene complexes.⁴⁹ Consequently, electrophiles are attracted to both the $\text{Ru}=\text{C}_\alpha$ bond and the C_β atom, while nucleophiles react at the C_α atom.

Bianchini and co-workers reported the reaction of H_2S with *fac,cis*- $[(\text{PNP})\text{RuCl}_2\{\text{C}=\text{C}(\text{H})\text{Ph}\}]$ ($\text{PNP} = \text{CH}_3\text{CH}_2\text{CH}_2\text{N}(\text{CH}_2\text{CH}_2\text{PPh}_2)_2$) to give an η^1 -2-phenylethanethial complex, *fac,cis*- $[(\text{PNP})\text{RuCl}_2\{\text{S}=\text{C}(\text{H})\text{CH}_2\text{Ph}\}]$.⁵⁰ To investigate the reactivity of **45**, an analogous reaction with H_2S was carried out in this thesis work. A colour change from orange to brown resulted when H_2S was passed through a refluxing CH_2Cl_2 solution of **45**, and a dark brown solid was isolated after work-up with hexanes. The $^{31}\text{P}\{^1\text{H}\}$ and ^1H NMR spectra of this solid in CDCl_3 are consistent with the formation of a single new

product, *cis*-RuCl₂(P-N)(PPh₃)(S=C(H)CH₂Ph) (**48**) [³¹P{¹H}: doublets at δ 59.61 (P_A) and δ 42.36 (P_X) ²J_{PP} = 28.22 Hz; ¹H: δ 3.04, 2.52 (s, NMe₂), δ 3.18 (t, =CH, ³J_{HH} = 15 Hz), δ 1.30 (d, CH₂, ³J_{HH} = 15 Hz)]. However, an analytically pure solid could not be isolated even after several attempts with varying times (3 - 16 h). Figure 6.30 shows the proposed mechanism for the formation of **48**. Initially, the nucleophilic C_β is protonated by the acidic hydrogen of H₂S leading to the formation of a cationic carbyne complex (which can be observed by ³¹P{¹H} NMR spectroscopy [δ 62.80 (P_A), δ 38.36 (P_X) ²J_{PP} = 22.82 Hz] in the *in situ* reaction of **45** with excess HBF₄·Et₂O in CDCl₃; the ¹H NMR spectrum could not be assigned because of overlapping peaks due to excess Et₂O). The electrophilic C_α is then attacked by the SH⁻, and a S,C_α-hydrogen shift is followed by S-atom insertion into the Ru-C_α bond.

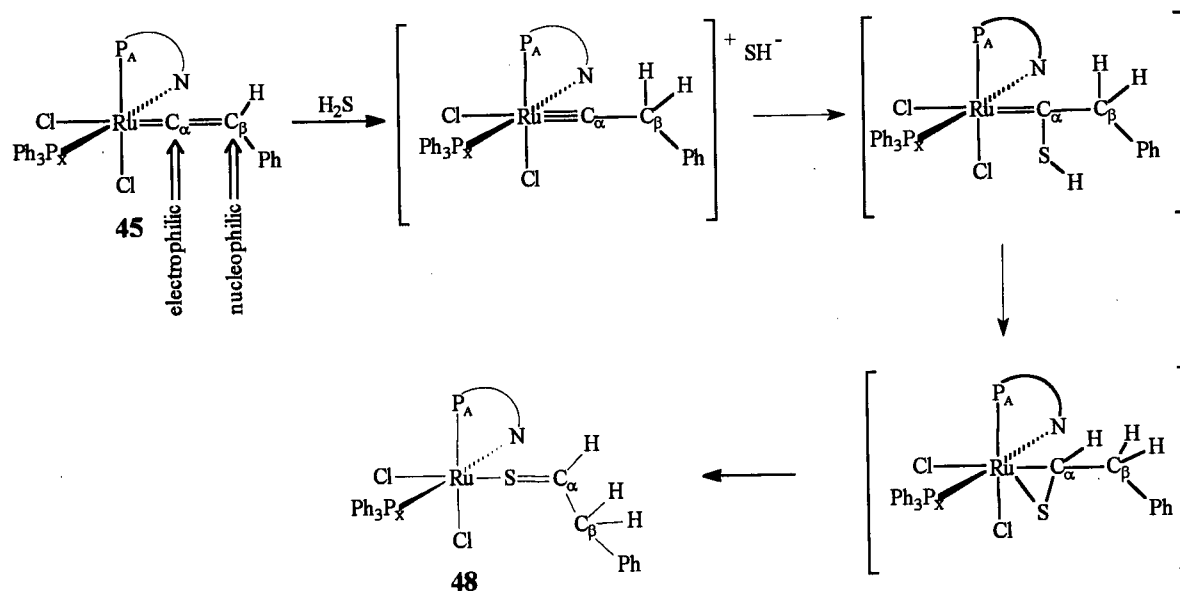


Figure 6.30 Proposed mechanism for the formation of *cis*-RuCl₂(P-N)(PPh₃)(S=C(H)-CH₂Ph) (**48**) from **45** and H₂S.

THF and CH_2Cl_2 solutions of **45** also react with H_2O under reflux conditions as implicated by changes in NMR spectra. The brown solid isolated from this reaction consists of many products as indicated by ~ 15 peaks in the $^{31}\text{P}\{^1\text{H}\}$ NMR spectrum (CDCl_3), while the ^1H NMR spectrum is uninformative because of many overlapping broad peaks in the region $\delta 1.2 - 3.5$. Repeated attempts to isolate a pure product were unsuccessful. Two major products in a 1:1 ratio were identified by two sets of broad peaks at $\delta 44.57, 38.28$ (**49**) and $\delta 50.55, 18.74$ (**50**) in the $^{31}\text{P}\{^1\text{H}\}$ NMR spectrum. By analogy to the reaction of *fac,cis*- $[(\text{PNP})\text{RuCl}_2\{\text{S}=\text{C}(\text{H})\text{CH}_2\text{Ph}\}]$ with H_2O where *fac*-(PNP) $\text{RuCl}(\text{CO})(\text{CH}_2\text{Ph})$ and *fac,cis*-(PNP) $\text{RuCl}_2(\text{CO})$ are formed,⁵¹ **49** and **50** are tentatively identified as $\text{RuCl}(\text{P-N})(\text{PPh}_3)(\text{CH}_2\text{Ph})(\text{CO})$ and $\text{RuCl}_2(\text{P-N})(\text{PPh}_3)(\text{CO})$, respectively (Figure 6.31). The IR spectrum for a mixture containing **49** and **50** showed two strong bands at 2046 and 1990 cm^{-1} , attributed to ν_{CO} . Previously in this laboratory, $\text{RuCl}_2(\text{P-N})(\text{PPh}_3)(\text{CO})$ (**50**) has been observed when CO was added to a solid state sample or a solution of **6a** at $\leq -20^\circ\text{C}$ (while at higher temperatures, the bis-CO adducts, *trans,cis*- $\text{RuCl}_2(\text{CO})_2(\text{P-N})$ and *cis,cis*- $\text{RuCl}_2(\text{CO})_2(\text{P-N})$ are formed).¹ The $^{31}\text{P}\{^1\text{H}\}$ NMR data ($\delta 51.68$ and 18.56 , $^2J_{\text{PP}} = 25.74\text{ Hz}$) for the *in situ* reaction at -20°C ¹ correspond well with the data assigned ($\delta 50.55$ and 18.74) in the current work to **50**, although the $^2J_{\text{PP}}$ coupling constants could not be obtained for **49** and **50** because the peaks were broad and the baseline noisy. The ν_{CO} value obtained by Mudalige was 1962 cm^{-1} (Nujol mull of the solid sample). Upon addition of 1 atm HCl to a mixture containing **49** and **50**, the concentration of **49** significantly diminished while that of **50** increased. This observation implies that **49** is initially formed with elimination of HCl when H_2O is reacted with **45**, while the HCl can also react with **49** to form **50** with the

elimination of toluene. The signals due to toluene could not be identified in the ^1H NMR spectrum because of the presence of other species.

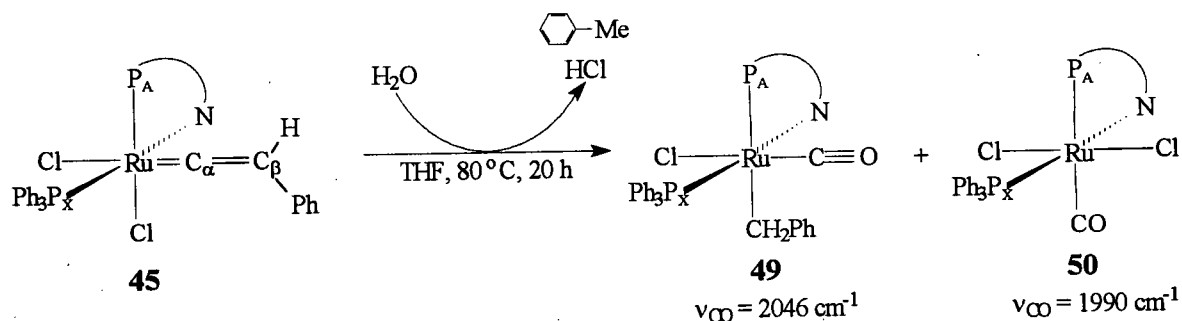


Figure 6.31 The reaction of *cis*- $\text{RuCl}_2(\text{P-N})(\text{PPh}_3)(=\text{C}=\text{C}(\text{H})\text{Ph})$ (**45**) with H_2O at 80°C in THF.

Of note, the carbene complexes **45** - **47** are stable indefinitely in air and, at ambient conditions, they do not react with H_2 , HCl , H_2S , H_2O or NEt_3 .

6.5 The Reaction of $\text{RuCl}_2(\text{P-N})(\text{PPh}_3)$ (**6a**) with HCl

When 1 atm of anhydrous HCl gas was bubbled through a dark green C_6H_6 solution of **6a** at r.t., a deep red solution formed immediately, and the isolated bright red solid had a microanalysis and UV-Vis spectrum corresponding to those of the paramagnetic $\text{RuCl}_3(\text{P-N})(\text{PPh}_3)$ (**15a**) (see Section 2.7.1). Figure 6.32 suggests the formation of **15a** via a coordinated HCl intermediate. The $^{31}\text{P}\{^1\text{H}\}$ NMR spectrum observed during the *in situ* reaction in C_6D_6 is dependent on the concentration of HCl added (Figure 6.33) and, similar to the reaction of **6a** with H_2O (Section 5.3, Figure 5.5), an upfield shift of the P_A chemical shift is observed as the concentration of HCl is increased from 1 to 5 equiv; eventually, the P_A and P_X signals vanish when more than 10 equiv of HCl are added. The formation of dihydrogen seems rational because no hydride species are observed; however, no ^1H NMR signal due to

H_2 was observed presumably because of the low concentration of H_2 formed in the reaction.

Of note, evidence for HCl complexes of Pt has been reported recently.⁵²

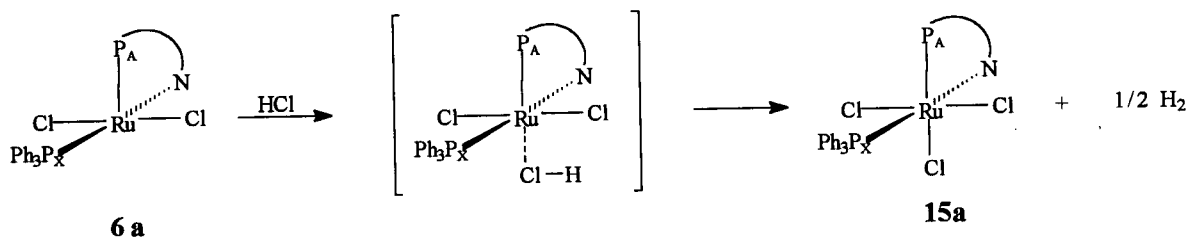


Figure 6.32 Reaction of $\text{RuCl}_2(\text{P-N})(\text{PPh}_3)$ (**6a**) with HCl to form $\text{RuCl}_3(\text{P-N})(\text{PPh}_3)$ (**15a**).

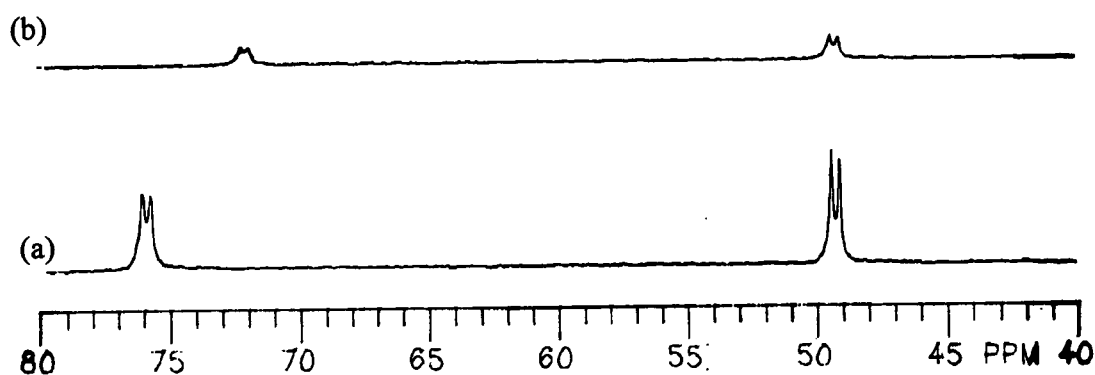
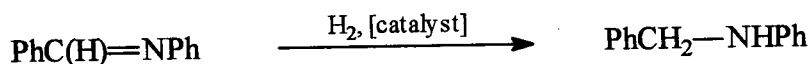


Figure 6.33 $^{31}\text{P}\{^1\text{H}\}$ NMR spectra (121.4 MHz, 20°C) for the reaction of $\text{RuCl}_2(\text{P-N})(\text{PPh}_3)$ (**6a**) with (a) 1 equiv HCl and (b) 5 equiv HCl in C_6D_6 ; spectra measured within 10 min of addition of HCl .

6.6 The Catalytic Hydrogenation of PhC(H)=NPh Using Complexes Containing the Ru(P-N) Moiety

The necessity to acquire chiral amines as precursors for the synthesis of pharmaceutical and agrochemical substances has led to accelerated interest in the homogeneous hydrogenation of imines,^{53,54} and much work has concentrated on Rh ⁵⁵ and Ir ⁵⁶ systems. Recently, Ru complexes containing phosphine ligands have also been found to hydrogenate imines effectively to the corresponding amines.^{21,53,57,58} The catalytic ability of

Ru complexes containing aminophosphine ligands to hydrogenate *N*-benzylideneaniline to *N*-benzylaniline was briefly investigated, and is described in this section:



Conditions for each hydrogenation experiment were as follows. While under the flow of Ar, the catalyst and imine, in a 1:200 ratio along with 10 mL MeOH, were placed in a glass liner equipped with a magnetic stirrer. The glass liner and its contents were then quickly placed in a machined-steel autoclave which had been previously evacuated, filled with N₂, and equipped with a high-pressure regulator connected to an H₂ cylinder. The reaction mixture was evacuated and flushed with N₂ three times before a final evacuation. The autoclave was then pressurized with 400 psi H₂ and evacuated three times before a final pressure of 1000 psi H₂ was introduced. With the stirrer turned on, the hydrogenation was allowed to proceed for 3 h. Percentage conversion was then analyzed by gas chromatography using an HP-20M (Carbowax 20M) column.

The results for the conversion of PhC(H)=NPh to PhCH₂-N(H)Ph by ruthenium aminophosphines are presented in Table 6.7. The specific substrate PhC(H)=NPh, and the chosen conditions, were used to allow for comparison between % conversions by the complexes in the present study and those by Ru phosphine complexes previously studied in this laboratory.^{21,57} The % conversions by complexes **6a**, **7a**, **15a** and **15b** are comparable to those for the most effective Ru species found to date: Ru₂Cl₅(dppb)₂ (98 % after 1 h) and Ru₂Cl₄(dppb)₂ (89 % after 1 h) (dppb = 1,4-bis(diphenylphosphino)butane).^{21,57} The Ru(II) or Ru(III) complexes which contain chlorine ligands, one P-N ligand, and a monodentate phosphine (PPh₃ or P(*p*-tolyl)₃), are comparable in effectiveness, while the complexes containing the P(*p*-tolyl)₃ ligand are somewhat better catalysts. Contrary to findings for

systems containing dppb,²¹ the chloro-containing complexes in the present study are more effective than the bromo analogue. Not surprisingly, the "less reactive" complexes containing BPN or two P-N ligands gave relatively low conversions.

Table 6.7 Hydrogenation of PhC(H)=NPh using ruthenium aminophosphine complexes. Conditions: 1000 psi H₂; [imine] = 0.153 M; [catalyst] = 0.77 mM; 20°C; 3 h; in MeOH.

Catalyst	% Conversion
RuCl ₂ (P-N)(PPh ₃) (6a)	91
RuCl ₂ (P-N)(P(<i>p</i> -tolyl) ₃) (7a)	96
RuBr ₂ (P-N)(PPh ₃) (6b)	57
RuCl ₃ (P-N)(PPh ₃) (15a)	82
RuCl ₃ (P-N)(P(<i>p</i> -tolyl) ₃) (15b)	100
RuCl ₂ (P-N) ₂ (8)	25
RuCl ₂ (BPN)(PPh ₃) (13)	56
RuCl ₃ (BPN) (16)	54

In order to evaluate further the complexes in Table 6.7 as useful catalysts, conditions for the hydrogenation such as pressure of H₂, temperature, solvent, and reaction time must be optimized. Mechanistic and kinetic studies might be of value.

6.7 Summary

RuCl₂(P-N)(PPh₃) (**6a**) forms six-coordinate complexes with H₂, NH₃, N₂, N₂O and alkynes. The η^2 -H₂ complex **36** is characterized crystallographically and its pK_a of ~ 11 is determined by NMR spectroscopy. Depending on the concentration of NH₃ and whether **6a** is in solution or the solid state, three products (**37**, **38** and **39**) containing NH₃ ligands are

identified, and salts of these complexes may be obtained by reaction with NH_4PF_6 . The formation of a coordinated N_2O complex **44** at low temperatures (below -40°C) is especially rare as only one such complex has been reported previous to this work. At higher temperatures, oxidation of **6a** by N_2O results in the formation of $\text{O}=\text{PPh}_3$ and the dinuclear species $(\mu\text{-O})(\mu\text{-Cl})_2[\text{RuCl}(\text{P-N})]_2$ (**17**). Vinylidene complexes, obtained from the reaction of **6a** with 1-alkynes, react with H_2S and H_2O . Finally, **6a** can be oxidized by HCl to form $\text{RuCl}_3(\text{P-N})(\text{PPh}_3)$ (**15a**). It has been shown in this Chapter that a wide range of small molecules binds and reacts with **6a**. Preliminary work (not documented here) has also shown that **6a** reacts with CH_3CN , NOBF_4 , NO , CH_3COOH , CH_3COSH , NaSEt , SMe_2 and $\text{C}_5\text{H}_5\text{N}$ without decomposition or oxidation; however because of the many products formed as observed by complex $^{31}\text{P}\{^1\text{H}\}$ NMR spectra, detailed investigation into these reactions was not pursued. Full characterization of the products formed would lead to even greater insight into the reactivity of **6a**.

6.8 References

1. Mudalige, D. C. Ph.D. Thesis, The University of British Columbia, 1994.
2. Mudalige, D. C.; Rettig, S. J.; James, B. R.; Cullen, W. R. *J. Chem. Soc., Chem. Commun.* **1993**, 830.
3. (a) Jessop, P. G.; Morris, R. H. *Coord. Chem. Rev.* **1992**, *121*, 155.
(b) Heinekey, D. M.; Oldham, W. J., Jr.; *Chem. Rev.* **1993**, *93*, 913.
(c) Esteruelas, M. A.; Oro, L. A. *Chem. Rev.* **1998**, *98*, 577.
4. Hamilton, D. G.; Crabtree, R. H. *J. Am. Chem. Soc.* **1988**, *110*, 4126.
5. (a) Crabtree, R. H.; Hamilton, D. G. *Adv. Organomet. Chem.* **1988**, *28*, 299.
(b) Crabtree, R. H. *Acc. Chem. Res.* **1990**, *23*, 95.
6. Hampton, C.; Cullen, W. R.; James, B. R. *J. Am. Chem. Soc.* **1988**, *110*, 6918.
7. Albinati, A.; Klooster, W. T.; Koetzle, T. F.; Fortin, J. B.; Ricci, J. S.; Eckert, J.; Fong, T. P.; Lough, A. J.; Morris, R. H.; Golombek, A. P. *Inorg. Chim. Acta* **1997**, *259*, 351.
8. Jessop, P. G. Ph.D. Thesis, The University of British Columbia, 1991.
9. Ball, R. G.; Trotter, J. *Inorg. Chem.* **1981**, *20*, 261.
10. Gregory, U. A.; Ibekwe, S. D.; Kilbourn, B. T.; Russell, D. R. *J. Chem. Soc. (A)* **1971**, 1118.
11. Skapski, A. C.; Stephens, F. A. *J. Chem. Soc., Dalton Trans.* **1974**, 390.
12. Skapski, A. C.; Troughton, P. G. H. *J. Chem. Soc., Chem. Commun.* **1968**, 1230.
13. Chau, D. E. K.-Y.; James, B. R. *Inorg. Chim. Acta* **1995**, *240*, 419.
14. Gusev, D. G.; Vymenits, A. B.; Bakhmutov, V. I. *Inorg. Chem.* **1992**, *31*, 1.
15. (a) Morris, R. H. *Inorg. Chem.* **1992**, *31*, 1471.
(b) Cappellani, E. P.; Drouin, S. D.; Jia, G.; Maltby, P. A.; Morris, R. H.; Schweitzer, C. T. *J. Am. Chem. Soc.* **1994**, *116*, 3375.

16. (a) Jia, G.; Morris, R. H. *Inorg. Chem.* **1990**, *29*, 582.
(b) Jia, G.; Morris, R. H. *J. Am. Chem. Soc.* **1991**, *113*, 875.
17. Chin, B.; Lough, A. J.; Morris, R. H.; Schweitzer, C. T.; D'Agostino, C. *Inorg. Chem.* **1994**, *33*, 6278.
18. (a) Chinn, M. S.; Heinekey, D. M.; Payne, N. G.; Sofield, C. D. *Organometallics* **1989**, *8*, 1824.
(b) Chinn, M. S.; Heinekey, D. M. *J. Am. Chem. Soc.* **1990**, *112*, 5166.
19. Baker, M. V.; Field, L. D.; Young, D. J. *J. Chem. Soc., Chem. Commun.* **1988**, 546.
20. Queiroz, S. L.; Batista, A. A.; Oliva, G.; Gambardella, M. T. do P.; Santos, R. H. A.; MacFarlane, K. S.; Rettig, S. J.; James, B. R. *Inorg. Chim. Acta* **1998**, *267*, 209.
21. MacFarlane, K. S. Ph.D. Thesis, The University of British Columbia, 1995.
22. Cenini, S.; Porta, F.; Pizzotti, M. *J. Mol. Catal.* **1982**, *15*, 297.
23. Geary, W. J. *Coord. Chem. Rev.* **1971**, *7*, 81.
24. Pauling, L. *The Natures of the Chemical Bond*, 3rd Ed.; Cornell University Press: Ithaca, N. Y. 1960.
25. Wayne, J. M. In *Nitrous Oxide*; Eger II, E. I. Ed.; Elsevier: New York, **1985**, p. 23.
26. Bottomley, F.; Lin, I. J. B.; Mukaida, M. *J. Am. Chem. Soc.* **1980**, *102*, 5238.
27. Bottomley, F.; Sutin, L. *Adv. Organomet. Chem.* **1988**, *28*, 339.
28. Matsunaga, P. T.; Mavropoulos, J. C.; Hillhouse, G. L. *Polyhedron* **1995**, *14*, 175.
29. Matsunaga, P. T.; Hillhouse, G. L. *J. Am. Chem. Soc.* **1993**, *115*, 2075.
30. Groves, J. T.; Bonchio, M.; Carofiglio, T.; Shalyaev, K. *J. Am. Chem. Soc.* **1996**, *118*, 8961.
31. (a) Armor, J. N.; Taube, H. *J. Am. Chem. Soc.* **1969**, *91*, 6874.
(b) Armor, J. N.; Taube, H. *J. Am. Chem. Soc.* **1970**, *92*, 2560.
(c) Armor, J. N.; Taube, H. *J. Am. Chem. Soc.* **1971**, *93*, 6476.

32. (a) Diamantis, A. A.; Sparrow, G. J. *J. Chem. Soc., Chem. Commun.* **1969**, 469.
(b) Diamantis, A. A.; Sparrow, G. J. *J. Chem. Soc., Chem. Commun.* **1970**, 819.
(c) Diamantis, A. A.; Sparrow, G. J. *J. Colloid Interface Sci.* **1974**, 47, 455.
(d) Diamantis, A. A.; Sparrow, G. J.; Snow, M. R.; Norman, T. R. *Aust. J. Chem.* **1975**, 28, 1231.
33. (a) Bottomley, F.; Crawford, J. R. *J. Chem. Soc., Chem. Commun.* **1971**, 200.
(b) Bottomley, F.; Crawford, J. R. *J. Am. Chem. Soc.* **1972**, 94, 9092.
(c) Bottomley, F.; Brooks, W. V. F. *Inorg. Chem.* **1977**, 16, 501.
34. Tuan, D. F.-T.; Hoffmann, R. *Inorg. Chem.* **1985**, 24, 871.
35. Yamamoto, A.; Kitazume, S.; Pu, L. S.; Ikeda, S. *J. Am. Chem. Soc.* **1971**, 93, 371.
36. (a) Vaughan, G. A.; Rupert, P. B.; Hillhouse, G. L. *J. Am. Chem. Soc.* **1987**, 109, 5538.
(b) Vaughan, G. A.; Sofield, C. C.; Hillhouse, G. L. *J. Am. Chem. Soc.* **1989**, 111, 5491.
(c) List, A. K.; Koo, K.; Rheingold, A. L.; Hillhouse, G. L.; *Inorg. Chim. Acta* **1998**, 270, 399.
37. Koo, K.; Hillhouse, G. L.; Rheingold, A. L. *Organometallics* **1995**, 14, 456.
38. Bryndza, H. E.; Tam, W. *Chem. Rev.* **1988**, 88, 1163.
39. Kaplan, A. W.; Bergman, R. G. *Organometallics* **1997**, 16, 1106.
40. Kaplan, A. W.; Bergman, R. G. *Organometallics* **1998**, 17, 5072.
41. Fischer, E. O.; Maasböl, A. *Angew. Chem., Int. Ed. Engl.* **1964**, 3, 580.
42. Weiss, K. In *Transition Metal Carbene Complexes*; Verlag Chemie GmbH: Weinheim, **1983**, p. 227.
43. (a) Dötz, K. H. In *Transition Metal Carbene Complexes*; Verlag Chemie GmbH: Weinheim, **1983**, p. 191.
(b) Dötz, K. H. In *Advances in Metal Carbene Chemistry*; Schubert, U. Ed.; Kluwer Academic Publishers: London, **1989**, p. 199.
(c) Herber, U.; Weberndörfer, B.; Werner, H. *Angew. Chem. Int. Ed.* **1999**, 38, 1609.
44. Templeton, J. L.; Winston, P. B.; Ward, B. C. *J. Am. Chem. Soc.* **1981**, 103, 7713.

45. Bruce, M. I. *Chem. Rev.* **1991**, *91*, 197.
46. Cadierno, V.; Gamasa, M. P.; Gimeno, J.; Borge, J.; García-Granda, S. *Organometallics* **1997**, *16*, 3178.
47. Bruce, M. I.; Wong, F. S.; Skelton, B. W.; White, A. H. *J. Chem. Soc., Dalton Trans.* **1982**, 2203.
48. Bianchini, C.; Innocenti, P.; Peruzzini, M.; Romerosa, A.; Zanolini, F. *Organometallics* **1996**, *15*, 272.
49. Kostic, N. M.; Fenske, R. F. *Organometallics* **1982**, *1*, 974.
50. Bianchini, C.; Glendenning, L.; Peruzzini, M.; Romerosa, A.; Zanolini, F. *J. Chem. Soc., Chem. Commun.* **1994**, 2219.
51. Bianchini, C.; Casares, J. A.; Peruzzini, M.; Romerosa, A.; Zanolini, F. *J. Am. Chem. Soc.* **1996**, *118*, 4585.
52. Kuhlman, R.; Rothfuss, H.; Gusev, D.; Streib, W. E.; Caulton, K. G. 209th Am. Chem. Soc. National Meeting, Anaheim, CA, 1995, Abstract INORG 497.
53. James, B. R. *Chem. Ind.* **1995**, *62*, 167; *Catal. Today* **1997**, *37*, 209.
54. Uematsu, N.; Fujii, A.; Hashiguchi, S.; Ikariya, T.; Noyori, R. *J. Am. Chem. Soc.* **1996**, *118*, 4916.
55. (a) Longley, C. J.; Goodwin, T. J.; Wilkinson, G. *Polyhedron* **1986**, *5*, 1625.
(b) Cullen, W. R.; Fryzuk, M. D.; James, B. R.; Kutney, J. P.; Kang, G.-J.; Herb, G.; Thorburn, I. S.; Spogliarich, R. *J. Mol. Catal.* **1990**, *62*, 243.
(c) Becalski, A. G.; Cullen, W. R.; Fryzuk, M. D.; James, B. R.; Kang, G.-J.; Rettig, S. J. *Inorg. Chem.* **1991**, *30*, 5002.
(d) Bakos, J.; Orosz, A.; Heil, B.; Laghmari, M.; Lhoste, P.; Sinou, D. *J. Chem. Soc., Chem. Commun.* **1991**, 1684.
(e) Ball, G. E.; Cullen, W. R.; Fryzuk, M. D.; Henderson, W. J.; James, B. R.; MacFarlane, K. S. *Inorg. Chem.* **1994**, *33*, 1464.
56. (a) Chan, Y. N. C.; Meyer, D.; Osborn, J. A. *J. Chem. Soc., Chem. Commun.* **1990**, 869.
(b) Chan, Y. N. C.; Osborn, J. A. *J. Am. Chem. Soc.* **1990**, *112*, 9400.
(c) Spindler, F.; Pugin, B.; Blaser, H.-U. *Angew. Chem., Int. Ed. Engl.* **1990**, *29*, 558.
(d) Bedford, R. B.; Chaloner, P. A.; Claver, C.; Fernandez, E.; Hitchcock, P. B.; Ruiz, A. *Chem. Ind.* **1995**, *62*, 181.

- (e) Spindler, F.; Pugin, B.; Jalett, H.-P.; Buser, H.-P. Pittelkow, U.; Blaser, H.-U.; *Chem. Ind. (Dekker)*, **1996**, 68, 153.
57. (a) Fogg, D. E. Ph. D. Thesis, The University of British Columbia, 1994.
(b) Fogg, D. E.; James, B. R.; Kilner, M. *Inorg. Chim. Acta* **1994**, 222, 85.
58. Oppolzer, W.; Wills, M.; Starkemann, C.; Bernardinelli, G. *Tetrahedron Lett.* **1990**, 31, 4117.

Chapter 7

General Conclusions and Recommendations for Future Research

This thesis describes for the main part the reactivity of the five-coordinate, square pyramidal complexes $\text{RuCl}_2(\text{P-N})(\text{PR}_3)$ ($\text{P-N} = [o-(N,N\text{-dimethylamino})\text{phenyl}]\text{-diphenylphosphine}$; $\text{R} = \text{Ph}$ or $p\text{-tolyl}$) which were successfully synthesized by the reaction of $\text{RuCl}_2(\text{PR}_3)_3$ with P-N . The $\text{RuCl}_2(\text{P-N})(\text{PR}_3)$ complexes are air-stable in the solid state, but in solution in the presence of O_2 are oxidized to O=PPh_3 and the crystallographically characterized, dinuclear complex $(\mu\text{-O})(\mu\text{-Cl})_2[\text{RuCl}(\text{P-N})_2]_2$. Reactions of $\text{RuCl}_2(\text{P-N})(\text{PPh}_3)$ with L give *cis*- $\text{RuCl}_2(\text{P-N})(\text{PPh}_3)(\text{L})$ ($\text{L} = \text{H}_2\text{S}$, alkanethiols, H_2 , N_2 and N_2O), *trans*- $\text{RuCl}_2(\text{P-N})(\text{PPh}_3)(\text{L})$ ($\text{L} = \text{H}_2\text{O}$, MeOH and EtOH), or both isomers ($\text{L} = \text{NH}_3$).

The H-atoms bonded to the S-ligands of the *cis*- $\text{RuX}_2(\text{P-N})(\text{PPh}_3)(\text{L})$ type complexes ($\text{X} = \text{Cl}$, $\text{L} = \text{H}_2\text{S}$, MeSH , EtSH ; $\text{X} = \text{Br}$, $\text{L} = \text{H}_2\text{S}$) were located isotropically in crystal structures and detected in ^1H NMR spectra. In particular, the ^1H NMR spectra of *cis*- $\text{RuX}_2(\text{P-N})(\text{PPh}_3)(\text{SH}_2)$ at -50°C show that one H-atom of the coordinated H_2S is coupled to the P-atom the P-N ligand, this being explained by the Karplus relationship. Solution thermodynamic parameters for the reversible formation of the H_2S and thiol complexes were obtained by variable temperature NMR measurements of equilibrated systems, and show that the Ru-S bonds are weak. Heating a solid sample of *cis*- $\text{RuCl}_2(\text{P-N})(\text{PPh}_3)(\text{SH}_2)$ results in the evolution of H_2S and suggested formation of *cis*- $\text{RuCl}_2(\text{P-N})(\text{PPh}_3)$; further characterization (e.g. by far-infrared spectroscopy) is needed to confirm this.

Trans- $\text{RuCl}_2(\text{P-N})(\text{PR}_3)(\text{OH}_2)$ was formed by the reaction of $\text{RuCl}_2(\text{P-N})(\text{PR}_3)$ in acetone solution or in the solid state with H_2O . The crystal structures of

trans-RuCl₂(P-N)(PPh₃)(OH₂)·(2C₆H₆) and *trans*-RuCl₂(P-N)(PPh₃)(OH₂)·(1.5C₆H₆) revealed that the Ru-O distance is shortened when a H-atom of the coordinated H₂O interacts with the π ring of a benzene solvate molecule. An order for the *trans* influence of the L ligands is proposed by comparison of the Ru-Cl bond lengths in the X-ray crystal structures of *trans*-RuCl₂(P-N)(PPh₃)(L) and *cis*-RuCl₂(P-N)(PPh₃)(L): P-N > H₂S ~ thiols > H₂ > Cl ~ Br > H₂O.

RuCl₂(P-N)(PPh₃) also binds H₂ reversibly, and the crystal structure of *cis*-RuCl₂(P-N)(PPh₃)(η^2 -H₂) was determined. Reaction of the dihydrogen complex with proton sponge resulted in the formation of the five-coordinate, monohydride complex Ru(H)Cl(P-N)(PPh₃), while the pK_a of *cis*-RuCl₂(P-N)(PPh₃)(η^2 -H₂) was estimated to be ~ 11 by *in situ* NMR experiments.

The reaction of RuCl₂(P-N)(PPh₃) in the solid state and in solution with excess NH₃ gave *trans*-RuCl₂(P-N)(PPh₃)(NH₃) and [RuCl(P-N)(PPh₃)(NH₃)₂···Cl], respectively. Both species dissolve in CDCl₃ solution in the absence of added NH₃ and equilibrate to the more stable *cis*-RuCl₂(P-N)(PPh₃)(NH₃). The [RuCl(P-N)(PPh₃)(NH₃)₂···Cl] formulation implies a strongly associated chlorine (possibly H-bonded to the ammine ligands), as indicated by non-conductivity of the complex. Reaction of this complex with NH₄PF₆ resulted in the expected [RuCl(P-N)(PPh₃)(NH₃)₂]PF₆ which, when subjected to vacuum and heat, subsequently gave an air-sensitive, five-coordinate species tentatively formulated [RuCl(P-N)(PPh₃)(NH₃)]PF₆. The formulation of this species requires confirmation, but in any case the species is a good candidate for study of reactions with small molecules.

At temperatures ranging from -90 to -40°C, RuCl₂(P-N)(PPh₃) reacts *in situ* with 6 atm N₂O to give apparently *cis*-RuCl₂(P-N)(PPh₃)(N₂O) which subsequently forms

cis-RuCl₂(P-N)(PPh₃)(η¹-N₂) and O₂; at temperatures above -40°C, O₂-oxidation processes yield O=PPh₃ and (μ-O)(μ-Cl)₂[RuCl(P-N)₂]₂. The formulation of the coordinated N₂O complex is based on the similarity of the ³¹P{¹H} NMR signals to those of the previously characterized η¹-N₂ complex. More positive confirmation of N₂O coordination could be realized if RuCl₂(P-N)(PPh₃) is reacted with N₂O enriched with ¹⁵N (I = 1/2, natural abundance = 0.365 %), and the reaction monitored by ¹⁵N NMR spectroscopy. Further, such data should distinguish between N- or O-atom coordination. The potential to use N₂O as an O-atom donor to organic substrates should be further investigated.

The synthesis and reactivities of Ru(II) complexes containing aminophosphines (BPN, TPN, AMPHOS, PAN and ALAPHOS) other than P-N were also examined. While Ru complexes containing BPN, AMPHOS, PAN and ALAPHOS were either formed *in situ* or isolated, TPN did not coordinate to Ru(II). The isolated species, RuCl₂(BPN)(PPh₃) and RuCl₂(PAN)(PPh₃), are relatively 'robust' and do not react with the small molecules discussed in this thesis. The electronics of the P-N ligand should be "fine-tuned" by modification of substituents on the N- or P-atom (see Figure 7.1), and/or the aromatic moiety.

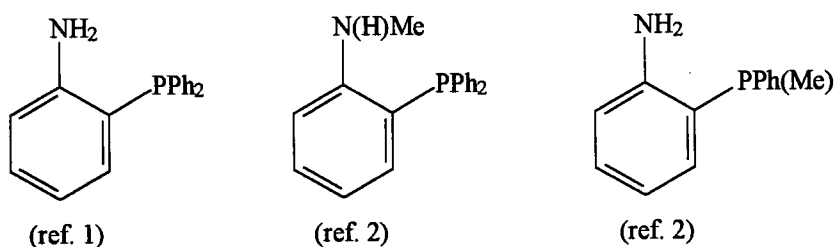


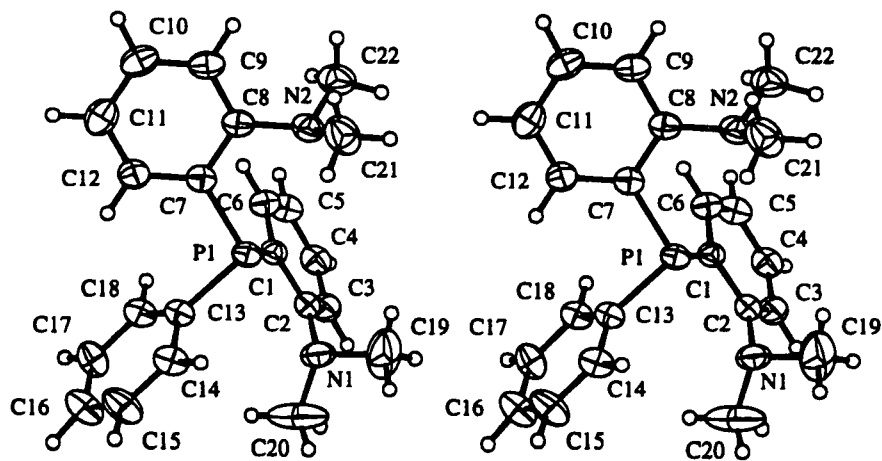
Figure 7.1 Examples for the modification of P-N.

7.1 References

1. (a) Cooper, M. K.; Downes, J. M. *Inorg. Chem.* **1978**, *17*, 880.
(b) Cooper, M. K.; Downes, J. M.; Duckworth, P. A. *Inorg. Synth.* **1989**, *25*, 129.
2. Cooper, M. K.; Downes, J. M.; Duckworth, P. A.; Tiekink, E. R. T. *Aust. J. Chem.* **1992**, *45*, 595.

APPENDICES

APPENDIX I

**X-Ray Crystallographic Analysis of Bis[*o*-*N,N*-dimethylamino)phenyl]phenylphosphine,
BPN****Figure I.1** Stereoview of the molecular structure of BPN.

EXPERIMENTAL DETAILS

A. Crystal Data

Empirical Formula	C ₂₂ H ₂₅ N ₂ P
Formula Weight	348.43
Crystal Colour, Habit	colourless, plate
Crystal Dimensions	0.04 X 0.25 X 0.30 mm
Crystal System	monoclinic
Lattice Type	C-centred
No. of Reflections Used for Unit Cell Determination (2 θ range)	25 (43.7 - 55.3°)
Omega Scan Peak Width at Half-height	0.39°
Lattice Parameters	a = 9.026(1) Å b = 14.859(2) Å c = 15.677(1) Å β = 106.119(7)°
Space Group	V = 2019.9(4) Å ³
Z value	Cc (#9)
D _{calc}	4
F ₀₀₀	1.146 g/cm ³
μ (CuK α)	744
	12.33 cm ⁻¹

B. Intensity Measurements

Diffractometer	Rigaku AFC6S
Radiation	CuK α (λ = 1.54178 Å) graphite monochromated
Take-off Angle	6.0°
Detector Aperture	6.0 mm horizontal 6.0 mm vertical
Crystal to Detector Distance	285 mm
Temperature	21.0°
Scan Type	ω -2 θ
Scan Rate	16°/min (in ω) (up to 9 scans)
Scan Width	(1.10 + 0.20 tan θ)°
2 θ_{max}	155°
No. of Reflections Measured	Total: 2271 Unique: 2124 (R_{int} = 0.024)
Corrections	Lorentz-polarization Absorption (trans. Factors: 0.692 - 1.000) Secondary Extinction (coefficient: 1.3(3) $\times 10^{-6}$)

C. Structure Solution and Refinement

Structure Solution	Direct Methods (SIR92)
Refinement	Full-matrix least-squares
Function Minimized	$\sum \omega (F_o - F_c)^2$
Least Squares Weights	$\omega = 1$
p-factor	0.0000
Anomalous Dispersion	All non-hydrogen atoms
No. Observations ($I > 3\sigma(I)$)	1667
No. Variables	225
Reflection/Parameter Ratio	7.41
Residuals: R; R _w	0.053; 0.056
Goodness of Fit Indicator	1.11
Max Shift/Error in Final Cycle	0.003
Maximum peak in Final Diff. Map	0.20 e ⁻ /Å ³
Minimum peak in Final Diff. Map	-0.19 e ⁻ /Å ³

Table I.1 Atomic coordinates and B_{eq}

atom	x	y	z	B_{eq}	atom	x	y	z	B_{eq}
P(1)	0.6306	0.2026(1)	0.3869	3.73(3)	C(11)	0.8168(10)	-0.0365(5)	0.5054(5)	5.9(2)
N(1)	0.5193(7)	0.3356(4)	0.2539(4)	5.4(1)	C(12)	0.7961(8)	0.0432(5)	0.4605(4)	4.6(2)
N(2)	0.4057(7)	0.1126(4)	0.4645(4)	4.8(1)	C(13)	0.8025(7)	0.2120(4)	0.3452(4)	4.1(1)
C(1)	0.4887(7)	0.1789(4)	0.2810(4)	3.6(1)	C(14)	0.9056(8)	0.2794(5)	0.3777(4)	4.8(2)
C(2)	0.4463(7)	0.2512(4)	0.2217(5)	4.1(1)	C(15)	1.0344(10)	0.2911(7)	0.3490(6)	7.0(2)
C(3)	0.3469(8)	0.2390(5)	0.1408(5)	4.9(2)	C(16)	1.0579(9)	0.2393(6)	0.2809(5)	6.1(2)
C(4)	0.2791(9)	0.1578(5)	0.1141(4)	4.9(2)	C(17)	0.9557(9)	0.1707(6)	0.2488(5)	5.6(2)
C(5)	0.3131(9)	0.0859(5)	0.1714(4)	4.9(2)	C(18)	0.8265(8)	0.1572(5)	0.2787(4)	4.4(2)
C(6)	0.4172(8)	0.0965(4)	0.2545(4)	4.2(1)	C(19)	0.418(1)	0.3960(7)	0.287(1)	12.3(4)
C(7)	0.6609(8)	0.0918(4)	0.4429(4)	3.9(1)	C(20)	0.594(2)	0.3789(8)	0.1949(8)	11.8(4)
C(8)	0.5442(8)	0.0604(4)	0.4782(4)	4.4(2)	C(21)	0.410(1)	0.1765(7)	0.5341(7)	7.7(3)
C(9)	0.5665(9)	-0.0181(5)	0.5266(4)	5.1(2)	C(22)	0.2645(10)	0.0618(6)	0.4420(6)	6.6(2)
C(10)	0.700(1)	-0.0665(5)	0.5409(4)	5.5(2)					

$$B_{eq} = \frac{8}{3} \pi^2 (U_{11}(aa^*)^2 + U_{22}(bb^*)^2 + U_{33}(cc^*)^2 + 2U_{12}aa^*bb^*\cos\gamma + 2U_{13}aa^*cc^*\cos\beta + 2U_{23}bb^*cc^*\cos\alpha)$$

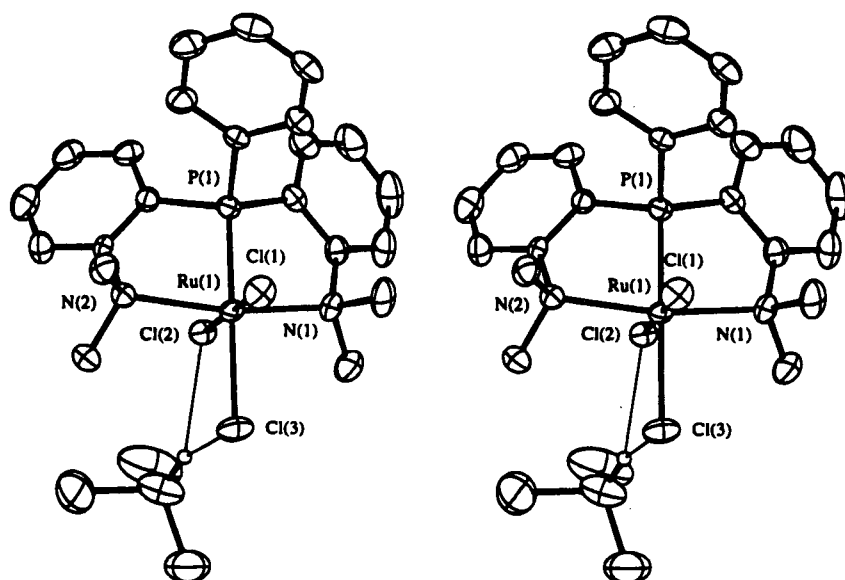
Table I.2 Bond lengths (Å) with estimated standard deviations

atom	atom	distance	atom	atom	distance
P(1)	C(1)	1.828(6)	P(1)	C(7)	1.849(6)
P(1)	C(13)	1.849(6)	N(1)	C(2)	1.441(8)
N(1)	C(19)	1.48(1)	N(1)	C(20)	1.44(1)
N(2)	C(8)	1.435(9)	N(2)	C(21)	1.44(1)
N(2)	C(22)	1.438(10)	C(1)	C(2)	1.402(8)
C(1)	C(6)	1.393(8)	C(2)	C(3)	1.347(9)
C(3)	C(4)	1.37(1)	C(4)	C(5)	1.375(10)
C(5)	C(6)	1.387(9)	C(7)	C(8)	1.400(8)
C(7)	C(12)	1.378(9)	C(8)	C(9)	1.377(9)
C(9)	C(10)	1.37(1)	C(10)	C(11)	1.40(1)
C(11)	C(12)	1.365(10)	C(13)	C(14)	1.366(8)
C(13)	C(18)	1.387(8)	C(14)	C(15)	1.368(10)
C(15)	C(16)	1.38(1)	C(16)	C(17)	1.37(1)
C(17)	C(18)	1.386(9)			

Table I.3 Bond angles (°) with estimated standard deviations

atom	atom	atom	angle	atom	atom	atom	angle
C(1)	P(1)	C(7)	103.5(3)	C(1)	P(1)	C(13)	97.9(3)
C(7)	P(1)	C(13)	101.9(3)	C(2)	N(1)	C(19)	112.6(6)
C(2)	N(1)	C(20)	114.5(7)	C(19)	N(1)	C(20)	113.8(9)
C(8)	N(2)	C(21)	113.7(6)	C(8)	N(2)	C(22)	115.5(6)
C(21)	N(2)	C(22)	111.6(7)	P(1)	C(1)	C(2)	116.6(4)
P(1)	C(1)	C(6)	126.1(4)	C(2)	C(1)	C(6)	117.2(5)
N(1)	C(2)	C(1)	114.9(6)	N(1)	C(2)	C(3)	124.5(6)
C(1)	C(2)	C(3)	120.6(6)	C(2)	C(3)	C(4)	122.2(6)
C(3)	C(4)	C(5)	119.1(6)	C(4)	C(5)	C(6)	119.7(7)
C(1)	C(6)	C(5)	121.1(6)	P(1)	C(7)	C(8)	117.1(5)
P(1)	C(7)	C(12)	124.6(5)	C(8)	C(7)	C(12)	117.9(6)
N(2)	C(8)	C(7)	118.8(6)	N(2)	C(8)	C(9)	121.9(6)
C(7)	C(8)	C(9)	119.3(7)	C(8)	C(9)	C(10)	121.6(7)
C(9)	C(10)	C(11)	119.8(7)	C(10)	C(11)	C(12)	118.2(7)
C(7)	C(12)	C(11)	123.0(7)	P(1)	C(13)	C(14)	118.4(5)
P(1)	C(13)	C(18)	122.9(5)	C(14)	C(13)	C(18)	118.6(6)
C(13)	C(14)	C(15)	121.6(7)	C(14)	C(15)	C(16)	120.7(7)
C(15)	C(16)	C(17)	117.8(6)	C(16)	C(17)	C(18)	121.7(7)
C(13)	C(18)	C(17)	119.4(6)				

APPENDIX II

X-Ray Crystallographic Analysis of *mer*-RuCl₃(BPN) (16)**Figure II.1** Stereoview of the molecular structure of 16.

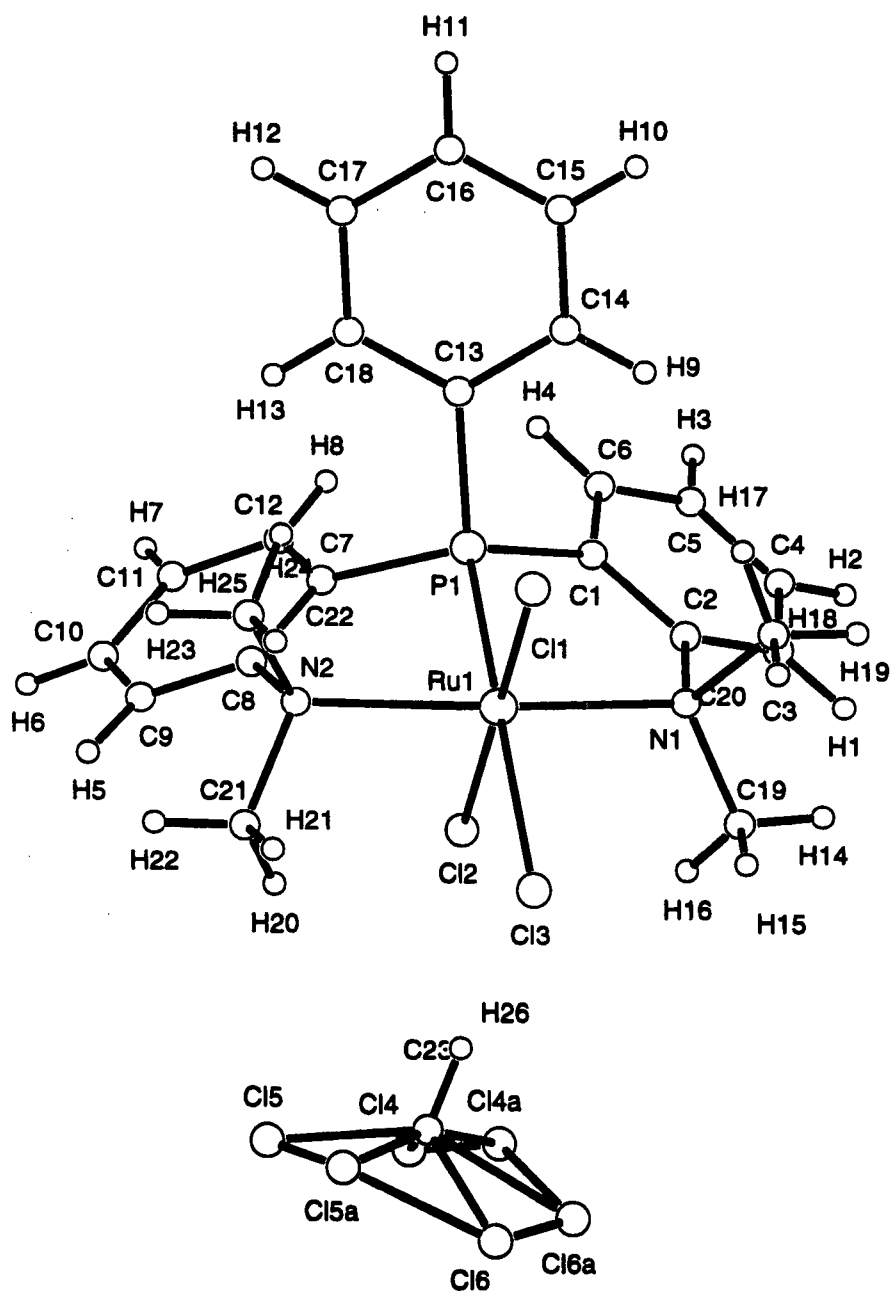


Figure II.2 Pluto plot of the molecular structure of **16**.

EXPERIMENTAL DETAILS

A. Crystal Data

Empirical Formula	C ₂₃ H ₂₆ Cl ₆ N ₂ PRu
Formula Weight	675.23
Crystal Colour, Habit	orange, plate
Crystal Dimensions	0.03 X 0.25 X 0.25 mm
Crystal System	monoclinic
Lattice Type	Primitive
No. of Reflections Used for Unit Cell Determination (2 θ range)	25 (45.3 - 72.1°)
Omega Scan Peak Width at Half-height	0.36°
Lattice Parameters	a = 13.027(3) Å b = 14.859(2) Å c = 21.221(3) Å β = 106.92(1)°
Space Group	V = 2769.1(9) Å ³
Z value	P2 ₁ /n (#14)
D _{calc}	4
F ₀₀₀	1.620 g/cm ³
μ (CuK α)	1356.00
	105.87 cm ⁻¹

B. Intensity Measurements

Diffractometer	Rigaku AFC6S
Radiation	CuK α (λ = 1.54178 Å) graphite monochromated
Take-off Angle	6.0°
Detector Aperture	6.0 mm horizontal 6.0 mm vertical
Crystal to Detector Distance	285 mm
Temperature	21.0°
Scan Type	ω -2 θ
Scan Rate	16°/min (in ω) (up to 9 scans)
Scan Width	(0.94 + 0.20 tan θ)°
2 θ_{\max}	155.4°
No. of Reflections Measured	Total: 6028 Unique: 5753 (R_{int} = 0.033)
Corrections	Lorentz-polarization Absorption (trans. Factors: 0.2193 - 1.0000)

C. Structure Solution and Refinement

Structure Solution	Patterson Methods (DIRDIF92 PATTY)
Refinement	Full-matrix least-squares
Function Minimized	$\sum \omega (F_o - F_c)^2$
Least Squares Weights	$\omega = \frac{1}{\sigma^2(F_o)} = \left[\sigma_c^2(F_o) + \frac{p^2}{4} F_o^2 \right]^{-1}$
p-factor	0.0000
Anomalous Dispersion	All non-hydrogen atoms
No. Observations ($I > 3.00\sigma(I)$)	3934
No. Variables	310
Reflection/Parameter Ratio	12.69
Residuals: R; R _w	0.049; 0.055
Goodness of Fit Indicator	2.78
Max Shift/Error in Final Cycle	0.00
Maximum peak in Final Diff. Map	0.78 e/Å ³
Minimum peak in Final Diff. Map	-0.63 e/Å ³

Table II.1 Atomic coordinates and B_{eq}

atom	x	y	z	B_{eq}	atom	x	y	z	B_{eq}
Ru(1)	0.47670(4)	0.56766(4)	0.20235(2)	2.585(9)	C(19)	0.2594(6)	0.6858(7)	0.2040(4)	5.2(2)
Cl(1)	0.6126(1)	0.7186(2)	0.22839(9)	4.24(4)	C(20)	0.4112(7)	0.7855(6)	0.2800(4)	5.2(2)
Cl(2)	0.3373(1)	0.4158(1)	0.17122(7)	3.29(3)	C(21)	0.5261(7)	0.3975(7)	0.0964(3)	4.8(2)
Cl(3)	0.4035(2)	0.6788(2)	0.09533(9)	5.08(4)	C(22)	0.6835(5)	0.4507(7)	0.1843(4)	4.1(2)
Cl(4a)	0.099(2)	0.398(2)	0.0376(10)	8.9(5)	C(23)	0.2047(8)	0.443(1)	0.0057(4)	7.5(3)
Cl(4)	0.1298(5)	0.3205(5)	0.0212(2)	13.6(2)	H(1)	0.2137	0.6541	0.3113	6.4230
Cl(5a)	0.260(2)	0.442(2)	-0.043(1)	12.6(6)	H(2)	0.2060	0.5359	0.4049	8.2484
Cl(5)	0.2856(5)	0.3493(6)	-0.0337(2)	14.6(2)	H(3)	0.3458	0.3953	0.4573	7.5466
Cl(6a)	0.098(2)	0.569(2)	-0.017(1)	12.8(7)	H(4)	0.4915	0.3695	0.4154	5.4526
Cl(6)	0.1479(4)	0.5544(4)	-0.0523(2)	10.2(1)	H(5)	0.5730	0.1717	0.1347	5.3062
P(1)	0.5415(1)	0.4696(1)	0.29727(7)	2.58(3)	H(6)	0.5592	-0.0138	0.1952	5.9504
N(1)	0.3663(4)	0.6589(5)	0.2503(3)	3.4(1)	H(7)	0.5504	0.0024	0.3042	5.5698
N(2)	0.5690(4)	0.4175(5)	0.1698(2)	3.1(1)	H(8)	0.5493	0.2040	0.3514	4.5193
C(1)	0.4373(5)	0.4911(6)	0.3367(3)	3.1(1)	H(9)	0.6147	0.6675	0.3941	4.6958
C(2)	0.3564(5)	0.5789(6)	0.3069(3)	3.5(1)	H(10)	0.7735	0.7073	0.4789	5.4268
C(3)	0.2716(7)	0.5944(7)	0.3322(5)	5.4(2)	H(11)	0.9187	0.5641	0.4974	6.5206
C(4)	0.2674(8)	0.5254(9)	0.3875(5)	6.9(3)	H(12)	0.9083	0.3847	0.4272	6.1282
C(5)	0.3487(8)	0.4426(9)	0.4180(4)	6.3(3)	H(13)	0.7488	0.3464	0.3417	4.9052
C(6)	0.4329(6)	0.4270(7)	0.3931(3)	4.5(2)	H(14)	0.2135	0.7251	0.2278	6.1805
C(7)	0.5538(5)	0.3077(5)	0.2703(3)	2.8(1)	H(15)	0.2671	0.7442	0.1695	6.1805
C(8)	0.5610(5)	0.2985(5)	0.2059(3)	2.8(1)	H(16)	0.2268	0.6057	0.1838	6.1805
C(9)	0.5655(6)	0.1795(7)	0.1792(4)	4.4(2)	H(17)	0.4809	0.7718	0.3127	6.2375
C(10)	0.5593(6)	0.0705(7)	0.2152(4)	5.0(2)	H(18)	0.4201	0.8422	0.2453	6.2375
C(11)	0.5534(6)	0.0797(6)	0.2787(4)	4.6(2)	H(19)	0.3617	0.8247	0.3014	6.2375
C(12)	0.5519(5)	0.1974(6)	0.3058(3)	3.8(2)	H(20)	0.4498	0.3753	0.0849	5.7151
C(13)	0.6660(5)	0.5001(6)	0.3614(3)	2.8(1)	H(21)	0.5349	0.4763	0.0735	5.7151
C(14)	0.6751(6)	0.6080(7)	0.4014(3)	3.9(2)	H(22)	0.5657	0.3281	0.0830	5.7151
C(15)	0.7680(6)	0.6315(8)	0.4510(3)	4.5(2)	H(23)	0.7219	0.3802	0.1708	4.9781
C(16)	0.8533(6)	0.5486(9)	0.4613(4)	5.4(2)	H(24)	0.6908	0.5281	0.1600	4.9781
C(17)	0.8470(6)	0.4426(8)	0.4206(4)	5.1(2)	H(25)	0.7138	0.4658	0.2316	4.9781
C(18)	0.7533(6)	0.4202(7)	0.3707(3)	4.1(2)	H(26)	0.2486	0.4825	0.0465	9.0503

Table II.2 Bond lengths (Å) with estimated standard deviations

atom	atom	distance	atom	atom	distance
Ru(1)	Cl(1)	2.316(2)	Ru(1)	Cl(2)	2.359(2)
Ru(1)	Cl(3)	2.482(2)	Ru(1)	P(1)	2.199(2)
Ru(1)	N(1)	2.207(5)	Ru(1)	N(2)	2.209(5)
Cl(4)	C(23)	1.70(1)	Cl(4a)	C(23)	1.77(2)
Cl(5)	C(23)	1.81(1)	Cl(5a)	C(23)	1.42(3)
Cl(6)	C(23)	1.70(1)	Cl(6a)	C(23)	1.87(3)
P(1)	C(1)	1.804(6)	P(1)	C(7)	1.811(6)
P(1)	C(13)	1.816(6)	N(1)	C(2)	1.500(8)
N(1)	C(19)	1.479(9)	N(1)	C(20)	1.510(8)
N(2)	C(8)	1.482(7)	N(2)	C(21)	1.508(8)
N(2)	C(22)	1.474(8)	C(1)	C(2)	1.403(9)
C(1)	C(6)	1.388(9)	C(2)	C(3)	1.372(9)
C(3)	C(4)	1.39(1)	C(4)	C(5)	1.38(1)
C(5)	C(6)	1.36(1)	C(7)	C(8)	1.400(8)
C(7)	C(12)	1.383(8)	C(8)	C(9)	1.378(8)
C(9)	C(10)	1.39(1)	C(10)	C(11)	1.37(1)
C(11)	C(12)	1.363(9)	C(13)	C(14)	1.398(8)
C(13)	C(18)	1.378(9)	C(14)	C(15)	1.375(9)
C(15)	C(16)	1.38(1)	C(16)	C(17)	1.39(1)
C(17)	C(18)	1.383(9)			

Table II.3 Bond angles (°) with estimated standard deviations

atom	atom	atom	angle	atom	atom	atom	angle
Cl(1)	Ru(1)	Cl(2)	177.65(6)	Cl(1)	Ru(1)	Cl(3)	87.81(7)
Cl(1)	Ru(1)	P(1)	92.12(6)	Cl(1)	Ru(1)	N(1)	98.6(1)
Cl(1)	Ru(1)	N(2)	96.5(1)	Cl(2)	Ru(1)	Cl(3)	90.03(6)
Cl(2)	Ru(1)	P(1)	90.05(5)	Cl(2)	Ru(1)	N(1)	82.5(1)
Cl(2)	Ru(1)	N(2)	83.0(1)	Cl(3)	Ru(1)	P(1)	179.88(6)
Cl(3)	Ru(1)	N(1)	95.2(2)	Cl(3)	Ru(1)	N(2)	98.4(1)
P(1)	Ru(1)	N(1)	84.7(1)	P(1)	Ru(1)	N(2)	81.7(1)
N(1)	Ru(1)	N(2)	160.0(2)	Ru(1)	P(1)	C(1)	103.1(2)
Ru(1)	P(1)	C(7)	101.2(2)	Ru(1)	P(1)	C(13)	128.7(2)
C(1)	P(1)	C(7)	114.3(3)	C(1)	P(1)	C(13)	105.0(3)
C(7)	P(1)	C(13)	105.0(3)	Ru(1)	N(1)	C(2)	110.3(4)
Ru(1)	N(1)	C(19)	112.9(4)	Ru(1)	N(1)	C(20)	110.3(4)
C(2)	N(1)	C(19)	110.8(5)	C(2)	N(1)	C(20)	105.6(5)
C(19)	N(1)	C(20)	106.6(5)	Ru(1)	N(2)	C(8)	108.0(3)
Ru(1)	N(2)	C(21)	110.5(4)	Ru(1)	N(2)	C(22)	112.1(4)
C(8)	N(2)	C(21)	110.9(5)	C(8)	N(2)	C(22)	108.1(5)
C(21)	N(2)	C(22)	107.2(5)	P(1)	C(1)	C(2)	116.2(5)
P(1)	C(1)	C(6)	124.5(5)	C(2)	C(1)	C(6)	119.4(6)
N(1)	C(2)	C(1)	119.9(6)	N(1)	C(2)	C(3)	120.9(6)
C(1)	C(2)	C(3)	119.1(7)	C(2)	C(3)	C(4)	120.1(8)
C(3)	C(4)	C(5)	120.7(8)	C(4)	C(5)	C(6)	119.3(8)
C(1)	C(6)	C(5)	121.3(8)	P(1)	C(7)	C(8)	114.2(4)
P(1)	C(7)	C(12)	126.3(5)	C(8)	C(7)	C(12)	119.4(6)
N(2)	C(8)	C(7)	118.8(5)	N(2)	C(8)	C(9)	122.0(6)
C(7)	C(8)	C(9)	119.1(6)	C(8)	C(9)	C(10)	120.0(7)
C(9)	C(10)	C(11)	120.7(7)	C(10)	C(11)	C(12)	119.2(7)
C(7)	C(12)	C(11)	121.4(6)	P(1)	C(13)	C(14)	119.8(5)
P(1)	C(13)	C(18)	121.4(5)	C(14)	C(13)	C(18)	118.8(6)
C(13)	C(14)	C(15)	120.7(7)	C(14)	C(15)	C(16)	119.9(7)
C(15)	C(16)	C(17)	120.3(7)	C(16)	C(17)	C(18)	119.2(7)
C(13)	C(18)	C(17)	121.0(7)	Cl(4)	C(23)	Cl(5)	97.2(7)
Cl(4)	C(23)	Cl(6)	120.3(6)	Cl(5)	C(23)	Cl(6)	103.1(6)
Cl(4a)	C(23)	Cl(5a)	153(1)	Cl(4a)	C(23)	Cl(6a)	71.8(10)
Cl(5a)	C(23)	Cl(6a)	107(1)				

APPENDIX III

X-Ray Crystallographic Analysis of $(\mu\text{-O})(\mu\text{-Cl})_2[\text{RuCl}(\text{P-N})_2]$ (17)

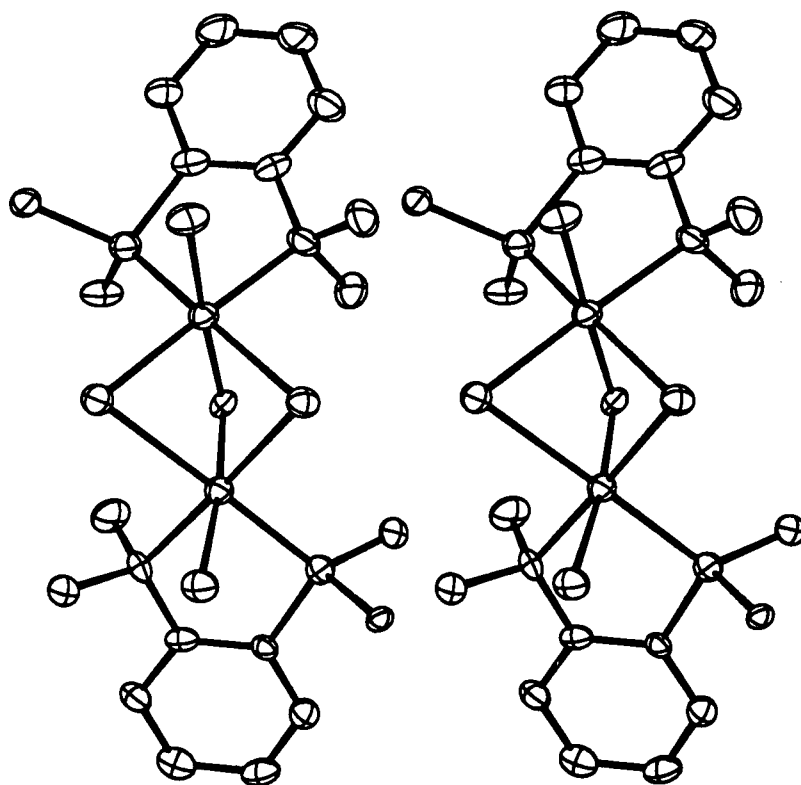


Figure III.1 Stereoview of the molecular structure of 17.

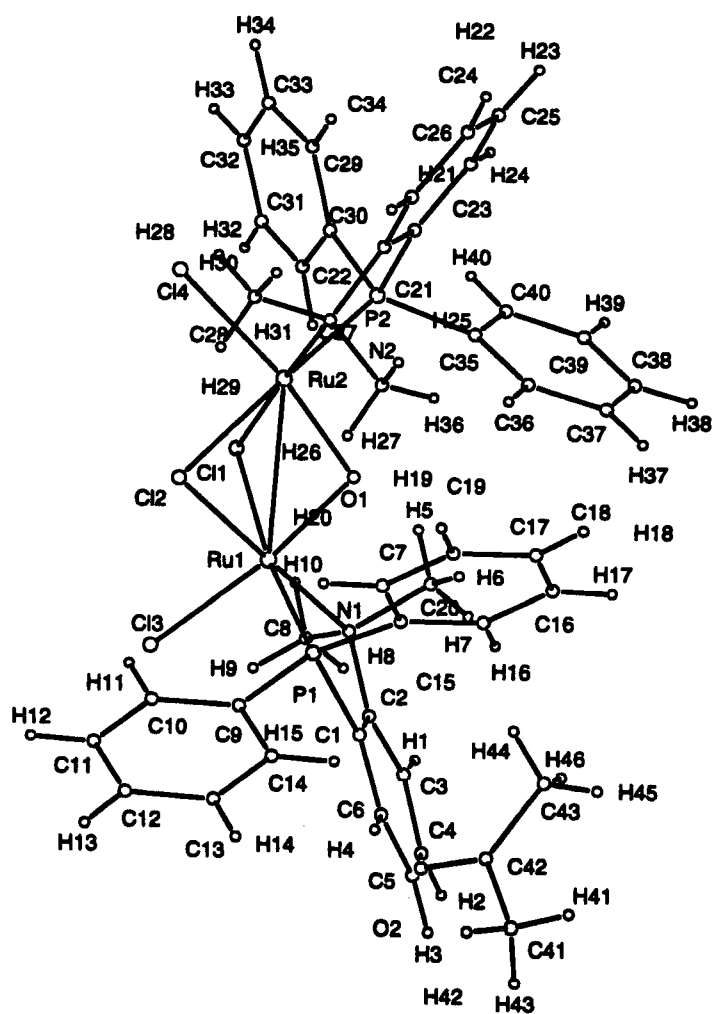


Figure III.2 Pluto plot of the molecular structure of 17.

EXPERIMENTAL DETAILS

A. Crystal Data

Empirical Formula	C ₄₃ H ₄₆ Cl ₄ N ₂ O ₂ P ₂ Ru ₂
Formula Weight	1028.75
Crystal Colour, Habit	green, plate
Crystal Dimensions	0.01 X 0.30 X 0.55 mm
Crystal System	monoclinic
Lattice Type	Primitive
Lattice Parameters	a = 18.1176(14) Å b = 9.5777(11) Å c = 25.2917(7) Å β = 100.1564(7)°
Space Group	V = 4320.0(5) Å ³ P2 ₁ /a (#14)
Z value	4
D _{calc}	1.582 g/cm ³
F ₀₀₀	2080.00
μ(MoKα)	10.59 cm ⁻¹

B. Intensity Measurements

Diffractometer	Rigaku/ADSC CCD
Radiation	MoKα (λ = 0.71069 Å) graphite monochromated
Detector Aperture	94 mm x 94 mm
Temperature	-93°C
Data Images	768 exposures of 60.0 seconds
φ oscillation Range (χ = -90)	0.0 - 189.9°
ω oscillation Range (χ = -90)	-23.0 - 17.8°
Detector Position	39.258(6) mm
Detector Swing Angle	-10.0°
2θ _{max}	60.1°
No. of Reflections Measured	Total: 39452 Unique: 11225 (R _{int} = 0.094)
Corrections	Lorentz-polarization Absorption/decay/scaling (cor. Factors: 0.6295 - 1.0000)

C. Structure Solution and Refinement

Structure Solution	Patterson Methods (DIRDIF92 PATTY)
Refinement	Full-matrix least-squares
Function Minimized	$\sum w(F_o ^2 - F_c ^2)^2$
Least Squares Weights	$w = \frac{1}{\sigma^2(F_o^2)}$
p-factor	0.0000
Anomalous Dispersion	All non-hydrogen atoms
No. Observations	11225
No. Variables	496
Reflection/Parameter Ratio	22.63
Residuals (on F ² , all data): R; Rw	0.153; 0.098
Goodness of Fit Indicator	1.35
No. Observations (I > 3σ(I))	3859
Residuals (on F ² , all data): R; Rw	0.055; 0.040
Max Shift/Error in Final Cycle	0.0006
Maximum peak in Final Diff. Map	3.00 e/Å ³ (between C(10) and Cl(3))
Minimum peak in Final Diff. Map	-3.46 e/Å ³

Table III.1 Atomic coordinates and B_{eq}

atom	x	y	z	B_{eq}	atom	x	y	z	B_{eq}
Ru(1)	0.72083(3)	0.41704(6)	0.25277(2)	1.801(12)	C(17)	0.4598(5)	0.2111(11)	0.1549(4)	6.1(3)
Ru(2)	0.64051(3)	0.57839(6)	0.32240(2)	1.685(12)	C(18)	0.4184(5)	0.3212(14)	0.1326(4)	6.9(4)
Cl(1)	0.76031(8)	0.4739(2)	0.35309(6)	2.16(4)	C(19)	0.4540(5)	0.4358(11)	0.1188(3)	5.8(3)
Cl(2)	0.69933(9)	0.6629(2)	0.24119(7)	2.43(4)	C(20)	0.5327(4)	0.4481(9)	0.1272(3)	4.0(2)
Cl(3)	0.84755(8)	0.4379(2)	0.23658(7)	2.94(4)	C(21)	0.4945(3)	0.5886(7)	0.3750(2)	1.43(13)
Cl(4)	0.67119(9)	0.7912(2)	0.37062(7)	2.42(4)	C(22)	0.4790(3)	0.6651(6)	0.3293(2)	1.64(15)
P(1)	0.67526(9)	0.3530(2)	0.16885(7)	2.01(4)	C(23)	0.4092(3)	0.7319(7)	0.3158(3)	2.00(15)
P(2)	0.58551(9)	0.5041(2)	0.38946(7)	1.78(4)	C(24)	0.3581(3)	0.7210(7)	0.3505(3)	2.3(2)
O(1)	0.6258(2)	0.4166(4)	0.27649(13)	1.68(9)	C(25)	0.3734(4)	0.6434(7)	0.3972(3)	2.4(2)
O(2)	0.5569(4)	0.2216(10)	-0.0333(4)	13.3(4)	C(26)	0.4425(3)	0.5790(7)	0.4095(2)	1.99(14)
N(1)	0.7412(3)	0.1931(5)	0.2664(2)	2.27(14)	C(27)	0.4975(3)	0.5850(8)	0.2421(2)	2.8(2)
N(2)	0.5308(3)	0.6688(5)	0.2906(2)	1.66(12)	C(28)	0.5398(4)	0.8156(7)	0.2716(3)	2.7(2)
C(1)	0.7092(3)	0.1753(7)	0.1662(3)	2.2(2)	C(29)	0.6327(3)	0.5612(7)	0.4553(2)	1.51(14)
C(2)	0.7416(3)	0.1156(7)	0.2153(3)	2.3(2)	C(30)	0.7023(4)	0.5020(7)	0.4764(3)	2.3(2)
C(3)	0.7691(4)	-0.0200(7)	0.2167(3)	2.9(2)	C(31)	0.7426(3)	0.5487(7)	0.5242(3)	2.6(2)
C(4)	0.7698(4)	-0.0899(8)	0.1697(3)	3.3(2)	C(32)	0.7171(4)	0.6571(8)	0.5517(3)	2.9(2)
C(5)	0.7389(4)	-0.0344(8)	0.1206(3)	3.5(2)	C(33)	0.6492(4)	0.7187(8)	0.5307(3)	3.5(2)
C(6)	0.7084(4)	0.0988(8)	0.1191(3)	2.8(2)	C(34)	0.6058(4)	0.6717(7)	0.4829(3)	2.6(2)
C(7)	0.6803(4)	0.1345(7)	0.2932(3)	2.6(2)	C(35)	0.5624(3)	0.3219(7)	0.3969(2)	1.84(15)
C(8)	0.8156(4)	0.1698(7)	0.3038(3)	3.0(2)	C(36)	0.5216(4)	0.2524(7)	0.3529(3)	2.6(2)
C(9)	0.7005(4)	0.4435(7)	0.1107(3)	2.3(2)	C(37)	0.4954(4)	0.1202(8)	0.3561(3)	3.0(2)
C(10)	0.7573(4)	0.5398(8)	0.1167(3)	3.1(2)	C(38)	0.5088(4)	0.0514(7)	0.4046(3)	3.5(2)
C(11)	0.7793(4)	0.6043(8)	0.0730(3)	4.2(2)	C(39)	0.5497(4)	0.1145(7)	0.4498(3)	3.1(2)
C(12)	0.7443(5)	0.5710(10)	0.0230(3)	4.9(3)	C(40)	0.5759(4)	0.2486(8)	0.4468(3)	2.8(2)
C(13)	0.6867(5)	0.4748(9)	0.0156(3)	5.0(3)	C(41)	0.4689(7)	0.1501(13)	-0.1049(5)	11.3(5)
C(14)	0.6638(4)	0.4096(8)	0.0592(3)	3.3(2)	C(42)	0.4920(7)	0.1920(12)	-0.0484(6)	8.2(4)
C(15)	0.5746(4)	0.3356(8)	0.1506(3)	2.4(2)	C(43)	0.4366(7)	0.1869(15)	-0.0121(6)	12.6(5)
C(16)	0.5387(4)	0.2209(9)	0.1646(3)	4.2(2)					

Table III.2 Bond lengths (Å) with estimated standard deviations

atom	atom	distance	atom	atom	distance
Ru(1)	Ru(2)	2.9173(7)	Ru(1)	Cl(1)	2.570(2)
Ru(1)	Cl(2)	2.396(2)	Ru(1)	Cl(3)	2.411(2)
Ru(1)	P(1)	2.224(2)	Ru(1)	O(1)	1.921(4)
Ru(1)	N(1)	2.193(5)	Ru(2)	Cl(1)	2.3921(15)
Ru(2)	Cl(2)	2.604(2)	Ru(2)	Cl(4)	2.390(2)
Ru(2)	P(2)	2.230(2)	Ru(2)	O(1)	1.926(4)
Ru(2)	N(2)	2.187(5)	P(1)	C(1)	1.815(7)
P(1)	C(9)	1.832(6)	P(1)	C(15)	1.807(6)
P(2)	C(21)	1.816(6)	P(2)	C(29)	1.816(6)
P(2)	C(35)	1.812(7)	O(2)	C(42)	1.205(11)
N(1)	C(2)	1.492(7)	N(1)	C(7)	1.504(8)
N(1)	C(8)	1.520(7)	N(2)	C(22)	1.471(7)
N(2)	C(27)	1.500(7)	N(2)	C(28)	1.504(8)
C(1)	C(2)	1.398(8)	C(1)	C(6)	1.397(8)
C(2)	C(3)	1.390(9)	C(3)	C(4)	1.367(9)
C(4)	C(5)	1.376(9)	C(5)	C(6)	1.389(9)
C(9)	C(10)	1.371(8)	C(9)	C(14)	1.392(8)
C(10)	C(11)	1.387(9)	C(11)	C(12)	1.348(9)
C(12)	C(13)	1.379(10)	C(13)	C(14)	1.393(9)
C(15)	C(16)	1.355(10)	C(15)	C(20)	1.390(9)
C(16)	C(17)	1.410(10)	C(17)	C(18)	1.358(13)
C(18)	C(19)	1.349(13)	C(19)	C(20)	1.410(10)
C(21)	C(22)	1.355(8)	C(21)	C(26)	1.395(7)
C(22)	C(23)	1.405(8)	C(23)	C(24)	1.386(8)
C(24)	C(25)	1.383(8)	C(25)	C(26)	1.381(8)
C(29)	C(30)	1.400(8)	C(29)	C(34)	1.403(8)
C(30)	C(31)	1.372(8)	C(31)	C(32)	1.375(9)
C(32)	C(33)	1.384(9)	C(33)	C(34)	1.394(9)
C(35)	C(36)	1.393(8)	C(35)	C(40)	1.427(8)
C(36)	C(37)	1.360(9)	C(37)	C(38)	1.375(9)
C(38)	C(39)	1.387(9)	C(39)	C(40)	1.375(9)
C(41)	C(42)	1.470(14)	C(42)	C(43)	1.48(2)

Table III.3 Bond angles (°) with estimated standard deviations

atom	atom	atom	angle	atom	atom	atom	angle
Cl(1)	Ru(1)	Cl(2)	85.62(6)	Cl(1)	Ru(1)	Cl(3)	92.44(5)
Cl(1)	Ru(1)	P(1)	173.00(6)	Cl(1)	Ru(1)	O(1)	78.51(11)
Cl(1)	Ru(1)	N(1)	92.43(14)	Cl(2)	Ru(1)	Cl(3)	92.11(6)
Cl(2)	Ru(1)	P(1)	97.44(6)	Cl(2)	Ru(1)	O(1)	84.54(13)
Cl(2)	Ru(1)	N(1)	178.03(15)	Cl(3)	Ru(1)	P(1)	93.74(6)
Cl(3)	Ru(1)	O(1)	170.54(12)	Cl(3)	Ru(1)	N(1)	88.20(14)
P(1)	Ru(1)	O(1)	95.46(11)	P(1)	Ru(1)	N(1)	84.48(14)
O(1)	Ru(1)	N(1)	94.9(2)	Cl(1)	Ru(2)	Cl(2)	84.94(5)
Cl(1)	Ru(2)	Cl(4)	94.31(6)	Cl(1)	Ru(2)	P(2)	96.96(6)
Cl(1)	Ru(2)	O(1)	83.11(11)	Cl(1)	Ru(2)	N(2)	177.18(14)
Cl(2)	Ru(2)	Cl(4)	92.68(6)	Cl(2)	Ru(2)	P(2)	177.50(6)
Cl(2)	Ru(2)	O(1)	78.86(12)	Cl(2)	Ru(2)	N(2)	93.34(14)
Cl(4)	Ru(2)	P(2)	88.80(6)	Cl(4)	Ru(2)	O(1)	171.33(12)
Cl(4)	Ru(2)	N(2)	87.99(14)	F(2)	Ru(2)	O(1)	99.72(12)
P(2)	Ru(2)	N(2)	84.70(14)	O(1)	Ru(2)	N(2)	94.4(2)
Ru(1)	Cl(1)	Ru(2)	71.92(4)	Ru(1)	Cl(2)	Ru(2)	71.25(5)
Ru(1)	P(1)	C(1)	102.9(2)	Ru(1)	P(1)	C(9)	122.2(2)
Ru(1)	P(1)	C(15)	117.2(2)	C(1)	P(1)	C(9)	106.3(3)
C(1)	P(1)	C(15)	103.7(3)	C(9)	P(1)	C(15)	102.8(3)
Ru(2)	P(2)	C(21)	102.5(2)	Ru(2)	P(2)	C(29)	113.6(2)
Ru(2)	P(2)	C(35)	121.9(2)	C(21)	P(2)	C(29)	108.3(3)
C(21)	P(2)	C(35)	103.4(3)	C(29)	P(2)	C(35)	105.9(3)
Ru(1)	O(1)	Ru(2)	98.6(2)	Ru(1)	N(1)	C(2)	112.2(4)
Ru(1)	N(1)	C(7)	108.6(4)	Ru(1)	N(1)	C(8)	110.4(4)
C(2)	N(1)	C(7)	108.8(5)	C(2)	N(1)	C(8)	109.1(5)
C(7)	N(1)	C(8)	107.7(5)	Ru(2)	N(2)	C(22)	113.0(4)
Ru(2)	N(2)	C(27)	107.3(4)	Ru(2)	N(2)	C(28)	110.2(4)
C(22)	N(2)	C(27)	108.6(5)	C(22)	N(2)	C(28)	110.6(5)
C(27)	N(2)	C(28)	106.8(5)	P(1)	C(1)	C(2)	116.3(5)
P(1)	C(1)	C(6)	124.7(5)	C(2)	C(1)	C(6)	118.9(6)
N(1)	C(2)	C(1)	120.0(6)	N(1)	C(2)	C(3)	119.9(6)
C(1)	C(2)	C(3)	119.9(6)	C(2)	C(3)	C(4)	119.5(7)
C(3)	C(4)	C(5)	122.1(7)	C(4)	C(5)	C(6)	118.4(6)
C(1)	C(6)	C(5)	120.9(6)	P(1)	C(9)	C(10)	121.2(5)
P(1)	C(9)	C(14)	119.7(6)	C(10)	C(9)	C(14)	119.0(7)
C(9)	C(10)	C(11)	121.9(7)	C(10)	C(11)	C(12)	119.2(8)
C(11)	C(12)	C(13)	120.4(8)	C(12)	C(13)	C(14)	121.0(7)
C(9)	C(14)	C(13)	118.5(7)	P(1)	C(15)	C(16)	121.2(6)
P(1)	C(15)	C(20)	119.2(6)	C(16)	C(15)	C(20)	119.2(7)
C(15)	C(16)	C(17)	121.8(8)	C(16)	C(17)	C(18)	119.3(9)
C(17)	C(18)	C(19)	119.1(9)	C(18)	C(19)	C(20)	123.0(9)
C(15)	C(20)	C(19)	117.5(8)	P(2)	C(21)	C(22)	117.1(5)
P(2)	C(21)	C(26)	122.3(5)	C(22)	C(21)	C(26)	120.6(5)
N(2)	C(22)	C(21)	121.4(5)	N(2)	C(22)	C(23)	118.7(5)
C(21)	C(22)	C(23)	119.6(6)	C(22)	C(23)	C(24)	119.1(6)
C(23)	C(24)	C(25)	121.7(6)	C(24)	C(25)	C(26)	118.0(6)
C(21)	C(26)	C(25)	121.0(6)	P(2)	C(29)	C(30)	118.3(5)
P(2)	C(29)	C(34)	122.4(5)	C(30)	C(29)	C(34)	119.0(6)
C(29)	C(30)	C(31)	120.5(6)	C(30)	C(31)	C(32)	121.3(6)
C(31)	C(32)	C(33)	118.8(6)	C(32)	C(33)	C(34)	121.6(7)
C(29)	C(34)	C(33)	118.9(6)	P(2)	C(35)	C(36)	118.5(5)
P(2)	C(35)	C(40)	124.0(5)	C(36)	C(35)	C(40)	117.1(6)
C(35)	C(36)	C(37)	122.6(7)	C(36)	C(37)	C(38)	119.4(7)
C(37)	C(38)	C(39)	120.7(7)	C(38)	C(39)	C(40)	120.1(6)
C(35)	C(40)	C(39)	120.0(6)	O(2)	C(42)	C(41)	117.9(14)
O(2)	C(42)	C(43)	122.9(13)	C(41)	C(42)	C(43)	119.1(12)

APPENDIX IV

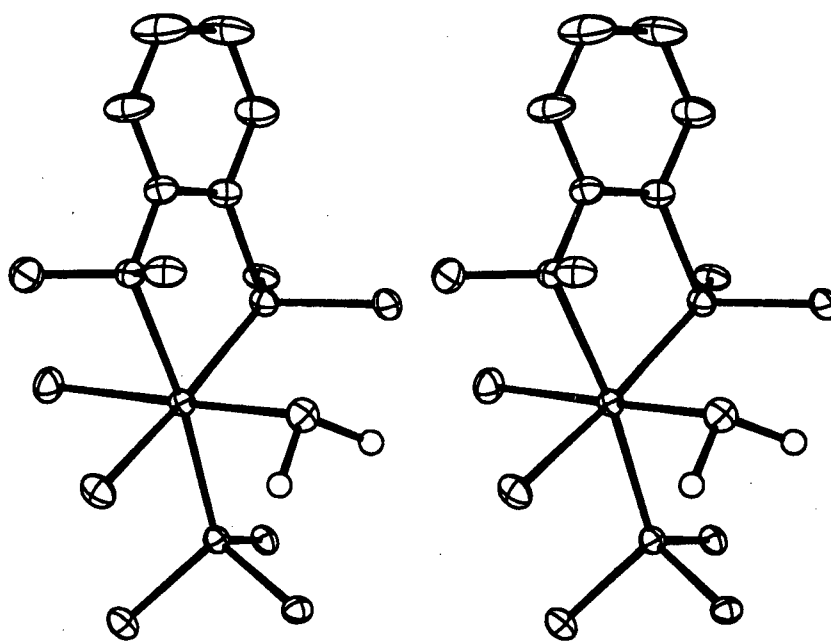
X-Ray Crystallographic Analysis of *Cis*-RuCl₂(P-N)(PPh₃)(SH₂)·(acetone) (18a)

Figure IV.1 Stereoview of the molecular structure of 18a.

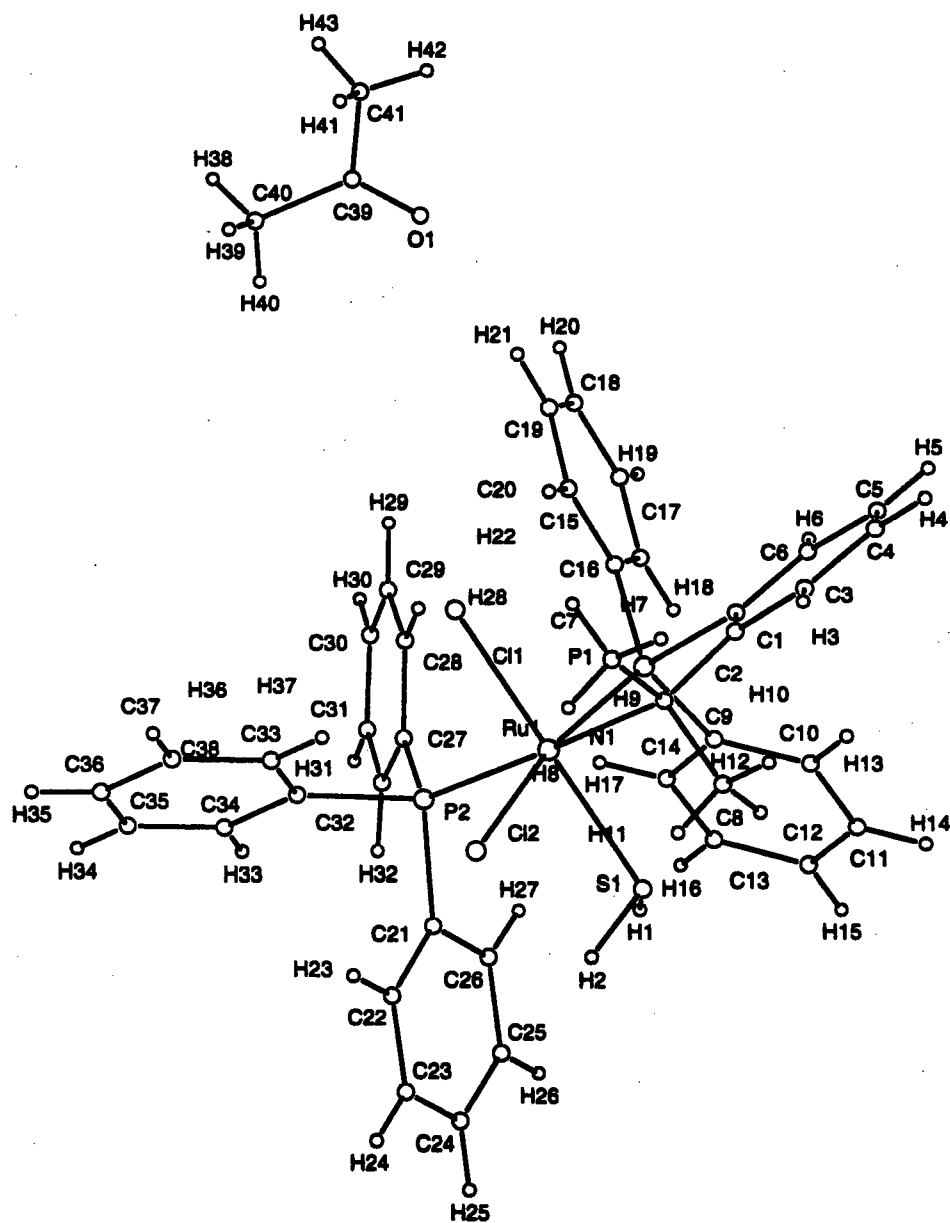


Figure IV.2 Pluto plot of the molecular structure of 18a.

EXPERIMENTAL DETAILS

A. Crystal Data

Empirical Formula	C ₄₁ H ₄₃ Cl ₂ NOP ₂ RuS
Formula Weight	831.78
Crystal Colour, Habit	yellow-brown, prism
Crystal Dimensions	0.28 X 0.30 X 0.38 mm
Crystal System	monoclinic
Lattice Type	Primitive
Lattice Parameters	a = 14.843(2) Å b = 16.0292(9) Å c = 16.0099(8) Å β = 95.286(2)°
Space Group	V = 3792.8(5) Å ³ P2 ₁ /n (#14)
Z value	4
D _{calc}	1.457 g/cm ³
F ₀₀₀	1712.00
μ(MoKα)	7.27 cm ⁻¹

B. Intensity Measurements

Diffractometer	Rigaku/ADSC CCD
Radiation	MoKα (λ = 0.71069 Å) graphite monochromated
Detector Aperture	94 mm x 94 mm
Temperature	-93°C
Data Images	462 exposures of 25.0 seconds
φ oscillation Range (χ = -90)	0.0 - 190.0°
ω oscillation Range (χ = -90)	-23.0 - 18.0°
Detector Position	39.12(2) mm
Detector Swing Angle	-10.0°
2θ _{max}	60.5°
No. of Reflections Measured	Total: 33910 Unique: 9547 (R _{int} = 0.041)
Corrections	Lorentz-polarization Absorption/decay/scaling (cor. factors: 0.6722 - 1.0000)

C. Structure Solution and Refinement

Structure Solution	Patterson Methods (DIRDIF92 PATTY)
Refinement	Full-matrix least-squares
Function Minimized	$\sum w(F_o ^2 - F_c ^2) ^2$
Least Squares Weights	$w = \frac{1}{\sigma^2(F_o^2)}$
p-factor	0.0000
Anomalous Dispersion	All non-hydrogen atoms
No. Observations	9547
No. Variables	450
Reflection/Parameter Ratio	21.22
Residuals (on F ² , all data): R; R _w	0.057; 0.053
Goodness of Fit Indicator	1.33
No. Observations (I > 3σ(I))	6176
Residuals (on F, I > 3σ(I)): R; R _w	0.028; 0.025
Max Shift/Error in Final Cycle	0.001
Maximum peak in Final Diff. Map	1.23 e ⁻ /Å ³ (1.3 Å from Ru)
Minimum peak in Final Diff. Map	-1.44 e ⁻ /Å ³

Table IV.1 Atomic coordinates and B_{eq}

atom	x	y	z	B_{eq}	atom	x	y	z	B_{eq}
Ru(1)	0.554502(13)	0.283305(11)	0.145131(11)	1.080(4)	C(19)	0.5709(2)	0.2491(2)	0.48977(15)	2.56(6)
Cl(1)	0.58901(4)	0.15775(4)	0.22620(3)	1.798(13)	C(20)	0.5824(2)	0.26798(15)	0.40674(14)	2.07(6)
Cl(2)	0.56129(4)	0.21320(4)	0.00832(3)	1.816(12)	C(21)	0.3357(2)	0.30713(13)	0.05269(13)	1.36(5)
S(1)	0.53144(5)	0.40235(4)	0.06015(4)	1.739(14)	C(22)	0.3279(2)	0.27515(15)	-0.02924(13)	1.81(5)
P(1)	0.57168(4)	0.36457(4)	0.26173(4)	1.294(13)	C(23)	0.2852(2)	0.3213(2)	-0.09406(14)	2.38(6)
P(2)	0.40269(4)	0.24894(4)	0.13544(3)	1.129(12)	C(24)	0.2500(2)	0.3995(2)	-0.0801(2)	2.60(6)
O(1)	0.5462(2)	0.11557(13)	0.64837(15)	4.94(6)	C(25)	0.2579(2)	0.43209(15)	0.0000(2)	2.26(6)
N(1)	0.71069(13)	0.30310(11)	0.14625(11)	1.38(4)	C(26)	0.3012(2)	0.38647(14)	0.06561(14)	1.83(6)
C(1)	0.6948(2)	0.37990(14)	0.27835(13)	1.50(5)	C(27)	0.3390(2)	0.26065(13)	0.22842(13)	1.23(5)
C(2)	0.7506(2)	0.34595(14)	0.22231(13)	1.59(5)	C(28)	0.3817(2)	0.22950(14)	0.30367(14)	1.62(5)
C(3)	0.6442(2)	0.3553(2)	0.23560(15)	2.67(6)	C(29)	0.3383(2)	0.23284(15)	0.37661(14)	2.05(6)
C(4)	0.8820(2)	0.3993(2)	0.3038(2)	3.49(8)	C(30)	0.2528(2)	0.26722(15)	0.37567(15)	2.29(6)
C(5)	0.8270(2)	0.4349(2)	0.3602(2)	3.09(7)	C(31)	0.2092(2)	0.29703(14)	0.3018(2)	2.11(6)
C(6)	0.7345(2)	0.4247(2)	0.34751(14)	2.29(6)	C(32)	0.2515(2)	0.29249(14)	0.22761(13)	1.67(5)
C(7)	0.7560(2)	0.2203(2)	0.13675(15)	2.31(6)	C(33)	0.3679(2)	0.14043(14)	0.10693(13)	1.44(5)
C(8)	0.7326(2)	0.35434(15)	0.07325(14)	2.01(6)	C(34)	0.2751(2)	0.12268(15)	0.09950(14)	1.98(6)
C(9)	0.5254(2)	0.46976(14)	0.24666(13)	1.56(5)	C(35)	0.2445(2)	0.0430(2)	0.07878(15)	2.49(6)
C(10)	0.5786(2)	0.5379(2)	0.2301(2)	2.58(7)	C(36)	0.3061(2)	-0.01970(15)	0.06471(15)	2.40(6)
C(11)	0.5376(2)	0.6154(2)	0.2111(2)	3.69(8)	C(37)	0.3972(2)	-0.00304(14)	0.07251(14)	2.19(6)
C(12)	0.4455(2)	0.6248(2)	0.2091(2)	3.82(8)	C(38)	0.4294(2)	0.07721(14)	0.09302(13)	1.69(5)
C(13)	0.3923(2)	0.5579(2)	0.2268(2)	3.14(7)	C(39)	0.5517(2)	0.0398(2)	0.6511(2)	3.20(7)
C(14)	0.4314(2)	0.48073(15)	0.24470(15)	2.18(6)	C(40)	0.4781(3)	-0.0132(2)	0.6113(2)	5.86(11)
C(15)	0.5477(2)	0.34172(14)	0.37028(13)	1.57(5)	C(41)	0.6293(2)	-0.0034(2)	0.6950(2)	3.72(8)
C(16)	0.5014(2)	0.39607(15)	0.41948(15)	2.38(6)	H(1)	0.466(2)	0.440(2)	0.078(2)	5.3(7)
C(17)	0.4894(2)	0.3761(2)	0.5032(2)	3.22(7)	H(2)	0.503(2)	0.372(2)	-0.013(2)	5.3(7)
C(18)	0.5238(2)	0.3028(2)	0.53796(15)	2.96(7)					

Table IV.2 Bond lengths (Å) with estimated standard deviations

atom	atom	distance	atom	atom	distance
Ru(1)	Cl(1)	2.4238(6)	Ru(1)	Cl(2)	2.4721(5)
Ru(1)	S(1)	2.3503(6)	Ru(1)	P(1)	2.2712(6)
Ru(1)	P(2)	2.3110(7)	Ru(1)	N(1)	2.338(2)
P(1)	C(1)	1.838(3)	P(1)	C(9)	1.828(2)
P(1)	C(15)	1.842(2)	P(2)	C(21)	1.836(2)
P(2)	C(27)	1.845(2)	P(2)	C(33)	1.859(2)
O(1)	C(39)	1.218(3)	N(1)	C(2)	1.474(3)
N(1)	C(7)	1.503(3)	N(1)	C(8)	1.489(3)
C(1)	C(2)	1.388(3)	C(1)	C(6)	1.403(3)
C(2)	C(3)	1.394(3)	C(3)	C(4)	1.375(3)
C(4)	C(5)	1.395(4)	C(5)	C(6)	1.380(4)
C(9)	C(10)	1.388(3)	C(9)	C(14)	1.404(3)
C(10)	C(11)	1.404(3)	C(11)	C(12)	1.372(4)
C(12)	C(13)	1.377(4)	C(13)	C(14)	1.386(3)
C(15)	C(16)	1.398(3)	C(15)	C(20)	1.395(3)
C(16)	C(17)	1.406(3)	C(17)	C(18)	1.378(4)
C(18)	C(19)	1.387(3)	C(19)	C(20)	1.389(3)
C(21)	C(22)	1.403(3)	C(21)	C(26)	1.393(3)
C(22)	C(23)	1.380(3)	C(23)	C(24)	1.385(4)
C(24)	C(25)	1.380(3)	C(25)	C(26)	1.388(3)
C(27)	C(28)	1.401(3)	C(27)	C(32)	1.395(3)
C(28)	C(29)	1.386(3)	C(29)	C(30)	1.382(3)
C(30)	C(31)	1.381(3)	C(31)	C(32)	1.396(3)
C(33)	C(34)	1.402(3)	C(33)	C(38)	1.395(3)
C(34)	C(35)	1.385(3)	C(35)	C(36)	1.391(4)
C(36)	C(37)	1.374(4)	C(37)	C(38)	1.401(3)
C(39)	C(40)	1.481(4)	C(39)	C(41)	1.467(4)
S(1)	H(1)	1.20(3)	S(1)	H(2)	1.30(3)

Table IV.3 Bond angles (°) with estimated standard deviations

Atom	atom	atom	angle	atom	atom	atom	angle
Cl(1)	Ru(1)	Cl(2)	94.19(2)	Cl(1)	Ru(1)	S(1)	175.18(2)
Cl(1)	Ru(1)	P(1)	91.95(2)	Cl(1)	Ru(1)	P(2)	89.70(2)
Cl(1)	Ru(1)	N(1)	87.03(5)	Cl(2)	Ru(1)	S(1)	82.63(2)
Cl(2)	Ru(1)	P(1)	168.03(2)	Cl(2)	Ru(1)	P(2)	87.21(2)
Cl(2)	Ru(1)	N(1)	86.97(4)	S(1)	Ru(1)	P(1)	90.54(2)
S(1)	Ru(1)	P(2)	93.76(2)	S(1)	Ru(1)	N(1)	89.18(5)
P(1)	Ru(1)	P(2)	103.11(2)	P(1)	Ru(1)	N(1)	83.09(5)
P(2)	Ru(1)	N(1)	173.09(5)	Ru(1)	P(1)	C(1)	103.33(7)
Ru(1)	P(1)	C(9)	114.09(8)	Ru(1)	P(1)	C(15)	130.13(8)
C(1)	P(1)	C(9)	104.60(11)	C(1)	P(1)	C(15)	99.52(10)
C(9)	P(1)	C(15)	101.83(10)	Ru(1)	P(2)	C(21)	112.78(7)
Ru(1)	P(2)	C(27)	119.37(8)	Ru(1)	P(2)	C(33)	119.09(8)
C(21)	P(2)	C(27)	104.30(10)	C(21)	P(2)	C(33)	100.29(10)
C(27)	P(2)	C(33)	98.17(10)	Ru(1)	N(1)	C(2)	113.11(13)
Ru(1)	N(1)	C(7)	109.41(13)	Ru(1)	N(1)	C(8)	110.90(14)
C(2)	N(1)	C(7)	110.2(2)	C(2)	N(1)	C(8)	106.9(2)
C(7)	N(1)	C(8)	106.0(2)	P(1)	C(1)	C(2)	119.9(2)
P(1)	C(1)	C(6)	121.5(2)	C(2)	C(1)	C(6)	118.6(2)
N(1)	C(2)	C(1)	119.9(2)	N(1)	C(2)	C(3)	119.7(2)
C(1)	C(2)	C(3)	120.4(2)	C(2)	C(3)	C(4)	120.3(2)
C(3)	C(4)	C(5)	120.3(3)	C(4)	C(5)	C(6)	119.3(2)
C(1)	C(6)	C(5)	121.2(2)	P(1)	C(9)	C(10)	122.6(2)
P(1)	C(9)	C(14)	118.6(2)	C(10)	C(9)	C(14)	118.6(2)
C(9)	C(10)	C(11)	119.7(3)	C(10)	C(11)	C(12)	120.9(3)
C(11)	C(12)	C(13)	119.9(3)	C(12)	C(13)	C(14)	120.0(3)
C(9)	C(14)	C(13)	120.9(2)	P(1)	C(15)	C(16)	123.8(2)
P(1)	C(15)	C(20)	117.9(2)	C(16)	C(15)	C(20)	118.3(2)
C(15)	C(16)	C(17)	120.5(2)	C(16)	C(17)	C(18)	120.3(2)
C(17)	C(18)	C(19)	119.4(2)	C(18)	C(19)	C(20)	120.6(2)
C(15)	C(20)	C(19)	120.8(2)	P(2)	C(21)	C(22)	118.8(2)
P(2)	C(21)	C(26)	122.6(2)	C(22)	C(21)	C(26)	118.2(2)
C(21)	C(22)	C(23)	120.0(2)	C(22)	C(23)	C(24)	121.2(2)
C(23)	C(24)	C(25)	119.5(2)	C(24)	C(25)	C(26)	119.8(2)
C(21)	C(26)	C(25)	121.3(2)	P(2)	C(27)	C(28)	115.6(2)
P(2)	C(27)	C(32)	125.1(2)	C(25)	C(27)	C(32)	119.1(2)
C(27)	C(28)	C(29)	120.1(2)	C(28)	C(29)	C(30)	120.3(2)
C(29)	C(30)	C(31)	120.4(2)	C(30)	C(31)	C(32)	119.9(2)
C(27)	C(32)	C(31)	120.2(2)	P(2)	C(33)	C(34)	117.3(2)
P(2)	C(33)	C(35)	123.2(2)	C(34)	C(33)	C(38)	119.4(2)
C(33)	C(34)	C(35)	120.3(2)	C(34)	C(35)	C(36)	120.0(3)
C(35)	C(36)	C(37)	120.1(2)	C(36)	C(37)	C(38)	120.8(2)
C(33)	C(35)	C(37)	119.4(2)	O(1)	C(39)	C(40)	120.8(3)
O(1)	C(39)	C(41)	122.3(3)	C(40)	C(39)	C(41)	116.8(3)
Ru(1)	S(1)	H(1)	110.7(12)	Ru(1)	S(1)	H(2)	103.3(11)
H(1)	S(1)	H(2)	101.7(17)				

APPENDIX V

X-Ray Crystallographic Analysis of *Cis*-RuBr₂(P-N)(PPh₃)(SH₂)(benzene) (18b)

EXPERIMENTAL DETAILS

A. Crystal Data

Empirical Formula	C ₄₄ H ₄₃ Br ₂ NOP ₂ RuS
Formula Weight	940.72
Crystal Colour, Habit	orange, prism
Crystal Dimensions	0.15 X 0.20 X 0.25 mm
Crystal System	monoclinic
Lattice Type	Primitive
Lattice Parameters	a = 9.6668(13) Å b = 18.976(2) Å c = 11.6270(4) Å β = 110.3292(7)°
Space Group	V = 2000.0(3) Å ³ P2 ₁ (#4)
Z value	2
D _{calc}	1.562 g/cm ³
F ₀₀₀	948.00
μ(MoKα)	25.61 cm ⁻¹

B. Intensity Measurements

Diffractometer	Rigaku/ADSC CCD
Radiation	MoKα (λ = 0.71069 Å) graphite monochromated
Detector Aperture	94 mm x 94 mm
Temperature	-93°C
Data Images	460 exposures of 90.0 seconds
φ oscillation Range (χ = -90)	-22.0 - 18.0°
ω oscillation Range (χ = -90)	0.0 - 190.0°
Detector Position	39.214(8) mm
Detector Swing Angle	-10°
2θ _{max}	60.2°
No. of Reflections Measured	Total: 18513 Unique: 5234 (R _{int} = 0.031)
Corrections	Lorentz-polarization Absorption/scaling (trans. factors: 0.7689 - 1.0119)

C. Structure Solution and Refinement

Structure Solution	Patterson Methods (DIRDIF92 PATTY)
Refinement	Full-matrix least-squares
Function Minimized	$\sum w(F_o ^2 - F_c ^2)^2$
Least Squares Weights	$w = \frac{1}{\sigma^2(F_o^2)} = [\sigma_c^2(F_o^2) + p^2 F_o^2]^{-1}$
p-factor	0.0200
Anomalous Dispersion	All non-hydrogen atoms
No. Observations	8318
No. Variables	467
Reflection/Parameter Ratio	17.81
Residuals: R; Rw	0.059; 0.074
Goodness of Fit Indicator	1.32
No. Observations (I > 3σ(I))	8318
Max Shift/Error in Final Cycle	0.01
Maximum peak in Final Diff. Map	1.10 e/Å ³ (near Ru)
Minimum peak in Final Diff. Map	-1.45 e/Å ³

Table V.1 Atomic coordinates and B_{eq}

atom	x	y	z	B_{eq}	atom	x	y	z	B_{eq}
Ru(1)	0.69024(3)	0.49960	0.48061(3)	0.974(6)	C(21)	0.3513(4)	0.5885(2)	0.3319(4)	1.13(8)
Br(1)	0.84461(5)	0.46441(3)	0.34204(4)	1.971(9)	C(22)	0.3884(5)	0.6572(2)	0.3755(4)	1.58(9)
Br(2)	0.79833(5)	0.62373(2)	0.52259(4)	1.685(9)	C(23)	0.2828(5)	0.7021(2)	0.3901(5)	2.12(10)
S(1)	0.62276(12)	0.38149(5)	0.44294(11)	1.66(2)	C(24)	0.1386(5)	0.6797(2)	0.3637(5)	2.41(11)
P(1)	0.57993(11)	0.51236(5)	0.62198(9)	1.07(2)	C(25)	0.1003(5)	0.6113(2)	0.3214(5)	2.26(10)
P(2)	0.50310(11)	0.53847(5)	0.30884(10)	1.04(2)	C(26)	0.2067(5)	0.5663(2)	0.3042(4)	1.72(9)
N(1)	0.8909(4)	0.4653(2)	0.6569(3)	1.41(7)	C(27)	0.4155(4)	0.4690(2)	0.1949(4)	1.46(8)
C(1)	0.7313(4)	0.5070(2)	0.7691(4)	1.50(8)	C(28)	0.3113(5)	0.4211(2)	0.2077(5)	2.03(10)
C(2)	0.8685(5)	0.4873(2)	0.7721(4)	1.74(9)	C(29)	0.2507(5)	0.3689(2)	0.1211(5)	2.62(11)
C(3)	0.9851(5)	0.4842(2)	0.8832(5)	2.68(11)	C(30)	0.2949(6)	0.3630(3)	0.0202(5)	3.19(12)
C(4)	0.9620(6)	0.5003(3)	0.9910(4)	3.20(11)	C(31)	0.4023(7)	0.4079(3)	0.0083(5)	3.22(13)
C(5)	0.8245(6)	0.5192(3)	0.9896(4)	2.72(11)	C(32)	0.4617(6)	0.4608(3)	0.0949(5)	2.41(10)
C(6)	0.7089(5)	0.5234(2)	0.8793(4)	2.01(10)	C(33)	0.5422(5)	0.6023(2)	0.2036(4)	1.37(8)
C(7)	0.9140(5)	0.3871(2)	0.6642(5)	2.22(10)	C(34)	0.4218(5)	0.6270(2)	0.1060(4)	1.93(9)
C(8)	1.0309(5)	0.4969(3)	0.6534(5)	2.43(10)	C(35)	0.4414(6)	0.6713(2)	0.0189(5)	2.56(11)
C(9)	0.4826(5)	0.5901(2)	0.6489(4)	1.35(8)	C(36)	0.5825(6)	0.6921(2)	0.0293(5)	2.55(11)
C(10)	0.5638(5)	0.6523(2)	0.6835(4)	1.63(9)	C(37)	0.7017(6)	0.6698(2)	0.1269(5)	2.16(10)
C(11)	0.4970(5)	0.7129(2)	0.7091(4)	1.89(10)	C(38)	0.6842(5)	0.6239(2)	0.2145(4)	1.58(9)
C(12)	0.3512(5)	0.7116(2)	0.7016(5)	2.11(10)	C(39)	0.8763(9)	0.2664(5)	0.9539(7)	5.5(2)
C(13)	0.2718(5)	0.6500(2)	0.6693(5)	2.35(11)	C(40)	0.9556(9)	0.2086(4)	1.0012(9)	5.2(2)
C(14)	0.3371(5)	0.5893(2)	0.6427(5)	1.92(10)	C(41)	1.0087(7)	0.1966(3)	1.1218(8)	4.4(2)
C(15)	0.4616(5)	0.4370(2)	0.6272(4)	1.40(9)	C(42)	0.9868(8)	0.2433(4)	1.2002(6)	4.5(2)
C(16)	0.5166(5)	0.3825(2)	0.7115(4)	1.72(9)	C(43)	0.9073(7)	0.3033(3)	1.1567(8)	4.5(2)
C(17)	0.4344(6)	0.3211(2)	0.7047(5)	2.58(12)	C(44)	0.8511	0.3161(3)	1.0317(9)	5.6(2)
C(18)	0.2979(6)	0.3135(2)	0.6141(5)	2.66(12)	H(1)	0.599(8)	0.378(3)	0.331(7)	5.6(12)
C(19)	0.2418(5)	0.3675(2)	0.5300(5)	2.06(10)	H(2)	0.686(7)	0.366(3)	0.440(5)	4.1(11)
C(20)	0.3241(4)	0.4283(2)	0.5370(4)	1.52(9)					

Table V.2 Bond lengths (Å) with estimated standard deviations

atom	atom	distance	atom	atom	distance
Ru(1)	Br(1)	2.6343(5)	Ru(1)	Br(2)	2.5540(4)
Ru(1)	S(1)	2.3330(10)	Ru(1)	P(1)	2.2617(10)
Ru(1)	P(2)	2.3011(11)	Ru(1)	N(1)	2.372(3)
P(1)	C(1)	1.827(4)	P(1)	C(9)	1.834(4)
P(1)	C(15)	1.845(4)	P(2)	C(21)	1.845(4)
P(2)	C(27)	1.852(4)	P(2)	C(33)	1.851(4)
N(1)	C(2)	1.488(6)	N(1)	C(7)	1.499(6)
N(1)	C(8)	1.494(5)	C(1)	C(2)	1.367(6)
C(1)	C(6)	1.407(6)	C(2)	C(3)	1.390(7)
C(3)	C(4)	1.382(8)	C(4)	C(5)	1.371(8)
C(5)	C(6)	1.379(7)	C(9)	C(10)	1.397(6)
C(9)	C(14)	1.383(6)	C(10)	C(11)	1.400(6)
C(11)	C(12)	1.383(7)	C(12)	C(13)	1.377(7)
C(13)	C(14)	1.399(6)	C(15)	C(16)	1.398(6)
C(15)	C(20)	1.387(6)	C(16)	C(17)	1.395(6)
C(17)	C(18)	1.380(8)	C(18)	C(19)	1.390(7)
C(19)	C(20)	1.387(6)	C(21)	C(22)	1.399(6)
C(21)	C(26)	1.386(6)	C(22)	C(23)	1.385(6)
C(23)	C(24)	1.386(7)	C(24)	C(25)	1.391(7)
C(25)	C(26)	1.405(6)	C(27)	C(28)	1.403(6)
C(27)	C(32)	1.391(6)	C(28)	C(29)	1.389(6)
C(29)	C(30)	1.385(8)	C(30)	C(31)	1.387(9)
C(31)	C(32)	1.396(7)	C(33)	C(34)	1.395(6)
C(33)	C(38)	1.396(6)	C(34)	C(35)	1.379(6)
C(35)	C(36)	1.384(7)	C(36)	C(37)	1.374(7)
C(37)	C(38)	1.394(6)	C(39)	C(40)	1.341(11)
C(39)	C(44)	1.385(12)	C(40)	C(41)	1.335(12)
C(41)	C(42)	1.339(10)	C(42)	C(43)	1.369(10)
C(43)	C(44)	1.384(11)	S(1)	H(1)	1.25(7)
S(1)	H(2)	1.34(6)			

Table V.3 Bond angles (°) with estimated standard deviations

atom	atom	atom	angle	atom	atom	atom	angle
Br(1)	Ru(1)	Br(2)	94.00(2)	Br(1)	Ru(1)	S(1)	79.77(3)
Br(1)	Ru(1)	P(1)	169.09(3)	Br(1)	Ru(1)	P(2)	89.54(3)
Br(1)	Ru(1)	N(1)	89.55(8)	Br(2)	Ru(1)	S(1)	172.31(3)
Br(2)	Ru(1)	P(1)	91.57(3)	Br(2)	Ru(1)	P(2)	90.94(3)
Br(2)	Ru(1)	N(1)	86.01(8)	S(1)	Ru(1)	P(1)	93.87(4)
S(1)	Ru(1)	P(2)	93.48(4)	S(1)	Ru(1)	N(1)	89.43(9)
P(1)	Ru(1)	P(2)	99.76(4)	P(1)	Ru(1)	N(1)	81.47(8)
P(2)	Ru(1)	N(1)	176.75(9)	Ru(1)	P(1)	C(1)	104.35(13)
Ru(1)	P(1)	C(9)	127.55(13)	Ru(1)	P(1)	C(15)	113.28(13)
C(1)	P(1)	C(9)	100.2(2)	C(1)	P(1)	C(15)	103.3(2)
C(9)	P(1)	C(15)	104.9(2)	Ru(1)	P(2)	C(21)	117.65(13)
Ru(1)	P(2)	C(27)	114.75(13)	Ru(1)	P(2)	C(33)	120.25(14)
C(21)	P(2)	C(27)	106.4(2)	C(21)	P(2)	C(33)	96.6(2)
C(27)	P(2)	C(33)	98.1(2)	Ru(1)	N(1)	C(2)	111.7(2)
Ru(1)	N(1)	C(7)	112.4(3)	Ru(1)	N(1)	C(8)	110.1(3)
C(2)	N(1)	C(7)	107.0(3)	C(2)	N(1)	C(8)	109.2(3)
C(7)	N(1)	C(8)	106.3(3)	P(1)	C(1)	C(2)	119.6(3)
P(1)	C(1)	C(6)	120.9(3)	C(2)	C(1)	C(6)	119.5(4)
N(1)	C(2)	C(1)	119.8(4)	N(1)	C(2)	C(3)	120.0(4)
C(1)	C(2)	C(3)	120.1(4)	C(2)	C(3)	C(4)	119.9(4)
C(3)	C(4)	C(5)	120.6(4)	C(4)	C(5)	C(6)	119.7(5)
C(1)	C(6)	C(5)	120.2(4)	P(1)	C(9)	C(10)	117.3(3)
P(1)	C(9)	C(14)	123.7(3)	C(10)	C(9)	C(14)	118.9(4)
C(9)	C(10)	C(11)	120.1(4)	C(10)	C(11)	C(12)	120.4(4)
C(11)	C(12)	C(13)	119.5(4)	C(12)	C(13)	C(14)	120.5(4)
C(9)	C(14)	C(13)	120.5(4)	P(1)	C(15)	C(16)	120.5(3)
P(1)	C(15)	C(20)	120.7(3)	C(16)	C(15)	C(20)	118.2(4)
C(15)	C(16)	C(17)	120.5(4)	C(16)	C(17)	C(18)	120.4(4)
C(17)	C(18)	C(19)	119.7(4)	C(18)	C(19)	C(20)	119.7(4)
C(15)	C(20)	C(19)	121.6(4)	P(2)	C(21)	C(22)	114.5(3)
P(2)	C(21)	C(26)	126.7(3)	C(22)	C(21)	C(26)	118.6(4)
C(21)	C(22)	C(23)	120.7(4)	C(22)	C(23)	C(24)	120.8(4)
C(23)	C(24)	C(25)	119.2(4)	C(24)	C(25)	C(26)	120.0(4)
C(21)	C(26)	C(25)	120.7(4)	P(2)	C(27)	C(28)	123.5(3)
P(2)	C(27)	C(32)	118.5(3)	C(28)	C(27)	C(32)	117.9(4)
C(27)	C(28)	C(29)	121.5(5)	C(28)	C(29)	C(30)	119.7(5)
C(29)	C(30)	C(31)	119.8(4)	C(30)	C(31)	C(32)	120.3(5)
C(27)	C(32)	C(31)	120.8(5)	P(2)	C(33)	C(34)	117.0(3)
P(2)	C(33)	C(38)	123.6(3)	C(34)	C(33)	C(38)	119.4(4)
C(33)	C(34)	C(35)	121.0(4)	C(34)	C(35)	C(36)	119.5(5)
C(35)	C(36)	C(37)	120.2(4)	C(36)	C(37)	C(38)	121.1(4)
C(33)	C(38)	C(37)	118.9(4)	C(40)	C(39)	C(44)	119.6(7)
C(39)	C(40)	C(41)	121.8(7)	C(40)	C(41)	C(42)	120.5(6)
C(41)	C(42)	C(43)	120.0(6)	C(42)	C(43)	C(44)	119.9(6)
C(39)	C(44)	C(43)	118.2(6)	Ru(1)	S(1)	H(1)	100.9(26)
Ru(1)	S(1)	H(2)	115.2(22)	H(1)	S(1)	H(2)	98.0(39)

APPENDIX VI

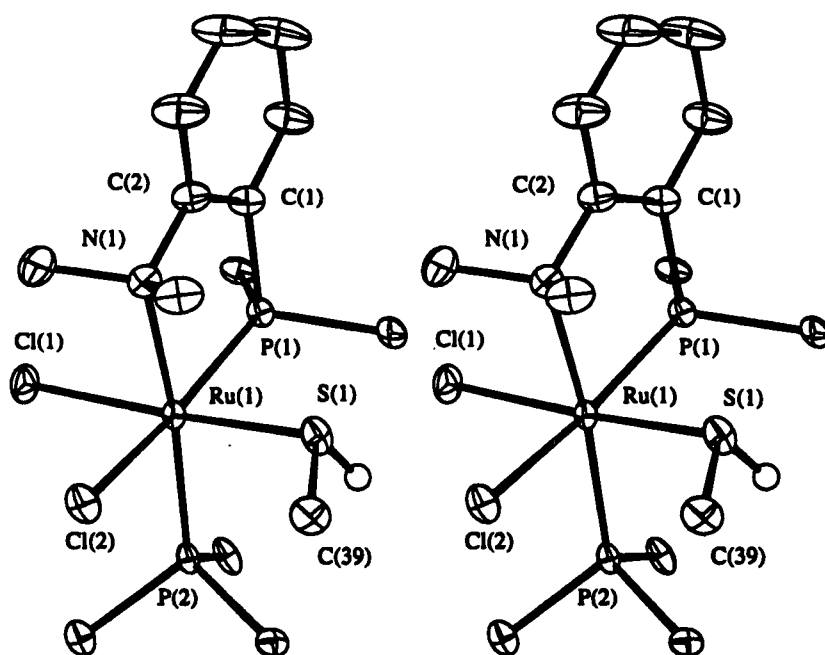
X-Ray Crystallographic Analysis of *Cis*-RuCl₂(P-N)(PPh₃)(MeSH)·(acetone) (20)

Figure VI.1 Stereoview of the molecular structure of 20.

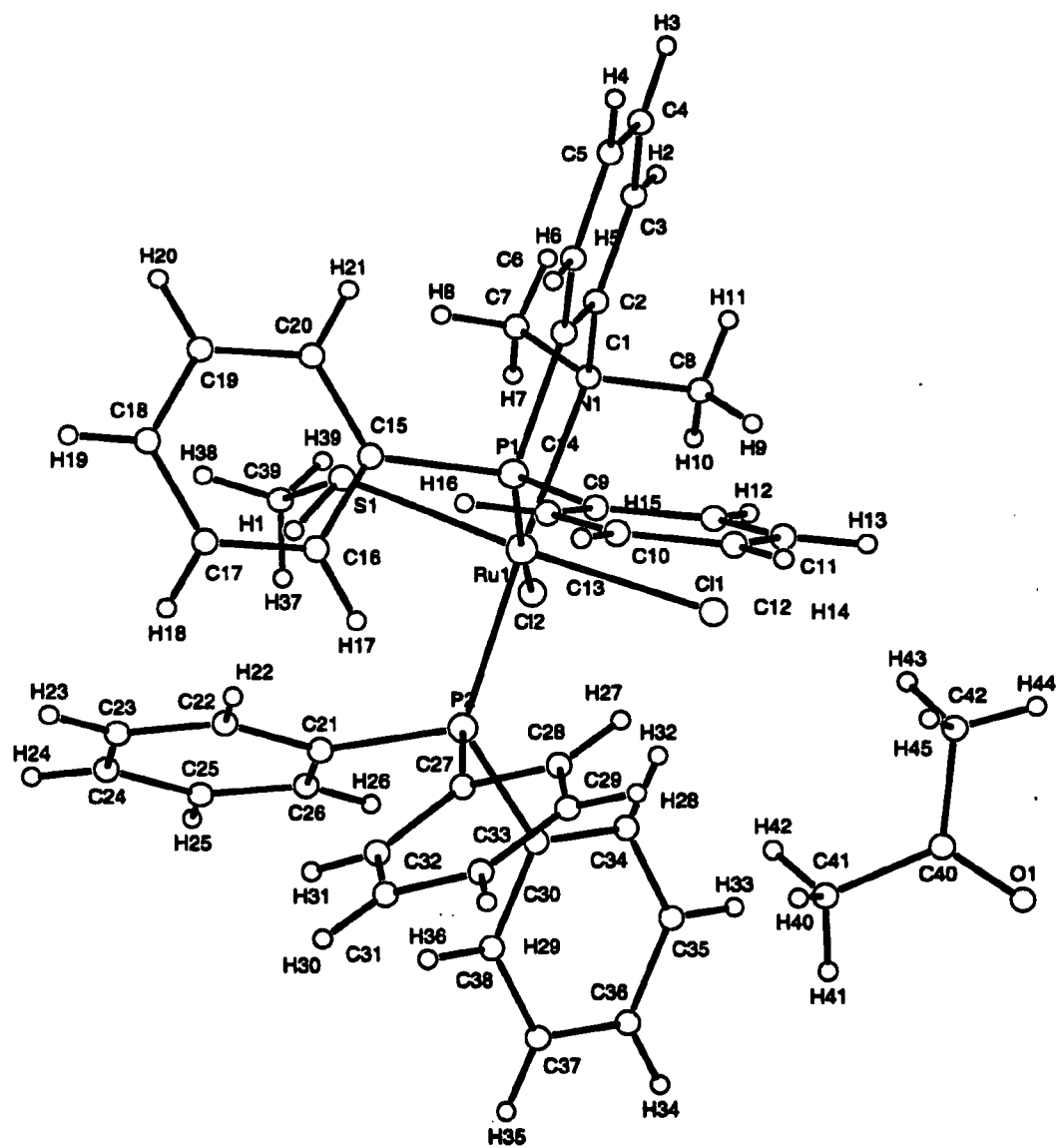


Figure VI.2 Pluto plot of the molecular structure of 20.

EXPERIMENTAL DETAILS

A. Crystal Data

Empirical Formula	C ₄₂ H ₄₅ Cl ₂ NOP ₂ RuS
Formula Weight	845.81
Crystal Colour, Habit	yellow-brown, prism
Crystal Dimensions	0.13 X 0.25 X 0.35 mm
Crystal System	monoclinic
Lattice Type	Primitive
Lattice Parameters	a = 14.2074(12) Å b = 16.275(2) Å c = 16.7122(3) Å β = 92.6672(5)°
Space Group	V = 3860.1(4) Å ³ P2 ₁ /n (#4)
Z value	4
D _{calc}	1.455 g/cm ³
F ₀₀₀	1744.00
μ(MoKα)	7.16 cm ⁻¹

B. Intensity Measurements

Diffractometer	Rigaku/ADSC CCD
Radiation	MoKα (λ = 0.71069 Å) graphite monochromated
Detector Aperture	94 mm x 94 mm
Temperature	-93°C
Data Images	462 exposures of 90.0 seconds
φ oscillation Range (χ = -90)	0.0 - 190.0°
ω oscillation Range (χ = -90)	-23.0 - 18.0°
Detector Position	39.202(6) mm
Detector Swing Angle	-10°
2θ _{max}	60.1°
No. of Reflections Measured	Total: 36449 Unique: 9917 (R _{int} = 0.062)
Corrections	Lorentz-polarization Absorption/scaling (trans. factors: 0.7658 - 1.0060)

C. Structure Solution and Refinement

Structure Solution	Patterson Methods (DIRDIF92 PATTY)
Refinement	Full-matrix least-squares
Function Minimized	$\sum w(F_o ^2 - F_c ^2)^2$
Least Squares Weights	$w = \frac{1}{\sigma^2(F_o^2)}$
p-factor	0.0000
Anomalous Dispersion	All non-hydrogen atoms
No. Observations	9917
No. Variables	455
Reflection/Parameter Ratio	21.80
Residuals (on F ² , all data): R; R _w	0.071; 0.116
Goodness of Fit Indicator	1.09
No. Observations (I > 3σ(I))	7067
Residuals (on F, I > 3σ(I)): R; R _w	0.039; 0.0525
Max Shift/Error in Final Cycle	0.001
Maximum peak in Final Diff. Map	1.60 e ⁻ /Å ³ (near Ru)
Minimum peak in Final Diff. Map	-3.08 e ⁻ /Å ³ (near Ru)

Table V.1 Atomic coordinates and B_{eq}

Atom	x	y	z	B_{eq}	Atom	x	y	z	B_{eq}
Ru(1)	0.563404(14)	0.272801(13)	0.156709(12)	0.911(5)	C(19)	0.5254(3)	0.6026(2)	0.2305(2)	2.96(8)
Cl(1)	0.58012(5)	0.14832(4)	0.23574(4)	1.84(2)	C(20)	0.5710(2)	0.5274(2)	0.2424(2)	2.14(7)
Cl(2)	0.58406(5)	0.19478(5)	0.03359(4)	1.83(2)	C(21)	0.3484(2)	0.3022(2)	0.0551(2)	1.26(6)
S(1)	0.55643(6)	0.39499(5)	0.08285(4)	1.72(2)	C(22)	0.3189(2)	0.3829(2)	0.0627(2)	1.72(6)
P(1)	0.57184(5)	0.35445(5)	0.26770(4)	1.099(14)	C(23)	0.2831(2)	0.4273(2)	-0.0030(2)	2.41(7)
P(2)	0.40451(5)	0.24444(4)	0.13879(4)	0.983(14)	C(24)	0.2779(2)	0.3902(2)	-0.0781(2)	2.82(8)
O(1)	0.4602(2)	-0.1088(2)	0.3703(2)	4.24(7)	C(25)	0.3077(2)	0.3110(2)	-0.0865(2)	2.56(8)
N(1)	0.7269(2)	0.2886(2)	0.16336(13)	1.46(5)	C(26)	0.3428(2)	0.2663(2)	-0.0214(2)	1.84(7)
C(1)	0.6987(2)	0.3746(2)	0.2826(2)	1.56(6)	C(27)	0.3280(2)	0.2622(2)	0.2229(2)	1.40(6)
C(2)	0.7607(2)	0.3402(2)	0.2315(2)	1.69(6)	C(28)	0.3627(2)	0.2345(2)	0.2978(2)	1.86(7)
C(3)	0.8571(2)	0.3553(3)	0.2429(2)	2.91(8)	C(29)	0.3093(3)	0.2439(2)	0.3645(2)	2.60(8)
C(4)	0.8905(2)	0.4047(3)	0.3055(2)	3.63(9)	C(30)	0.2218(3)	0.2808(2)	0.3582(2)	2.84(8)
C(5)	0.8288(2)	0.4382(3)	0.3577(2)	3.61(9)	C(31)	0.1867(2)	0.3075(2)	0.2841(2)	2.61(8)
C(6)	0.7334(2)	0.4225(2)	0.3471(2)	2.40(7)	C(32)	0.2385(2)	0.2970(2)	0.2161(2)	1.80(6)
C(7)	0.7609(2)	0.3252(2)	0.0872(2)	2.32(7)	C(33)	0.3648(2)	0.1390(2)	0.1112(2)	1.40(6)
C(8)	0.7711(2)	0.2057(2)	0.1698(2)	2.43(7)	C(34)	0.4244(2)	0.0732(2)	0.1004(2)	1.76(6)
C(9)	0.5441(2)	0.3309(2)	0.3727(2)	1.39(6)	C(35)	0.3880(3)	-0.0029(2)	0.0754(2)	2.49(7)
C(10)	0.5808(2)	0.2589(2)	0.4067(2)	1.80(7)	C(36)	0.2912(3)	-0.0134(2)	0.0616(2)	2.60(8)
C(11)	0.5686(2)	0.2407(2)	0.4866(2)	2.48(8)	C(37)	0.2313(2)	0.0518(2)	0.0721(2)	2.62(8)
C(12)	0.5192(3)	0.2940(3)	0.5336(2)	2.84(8)	C(38)	0.2672(2)	0.1278(2)	0.0970(2)	2.09(7)
C(13)	0.4836(3)	0.3656(2)	0.5014(2)	3.01(8)	C(39)	0.5506(2)	0.3847(2)	-0.0248(2)	2.16(7)
C(14)	0.4965(2)	0.3847(2)	0.4212(2)	2.25(7)	C(40)	0.4625(3)	-0.0350(3)	0.3664(2)	3.12(9)
C(15)	0.5186(2)	0.4568(2)	0.2558(2)	1.47(6)	C(41)	0.3850(3)	0.0114(3)	0.3244(3)	5.18(12)
C(16)	0.4213(2)	0.4630(2)	0.2568(2)	2.01(7)	C(42)	0.5446(4)	0.0127(3)	0.3996(3)	5.67(13)
C(17)	0.3765(2)	0.5384(2)	0.2456(2)	2.74(8)	H(1)	0.488(3)	0.414(2)	0.092(2)	4.2(8)
C(18)	0.4295(3)	0.6077(2)	0.2328(2)	3.13(9)					

Table VI.2 Bond lengths (Å) with estimated standard deviations

atom	atom	distance	atom	atom	distance
Ru(1)	Cl(1)	2.4241(7)	Ru(1)	Cl(2)	2.4472(7)
Ru(1)	S(1)	2.3403(7)	Ru(1)	P(1)	2.2803(7)
Ru(1)	P(2)	2.3100(7)	Ru(1)	N(1)	2.335(2)
S(1)	C(39)	1.805(3)	P(1)	C(1)	1.838(3)
P(1)	C(9)	1.856(3)	P(1)	C(15)	1.837(3)
P(2)	C(21)	1.835(3)	P(2)	C(27)	1.840(3)
P(2)	C(33)	1.858(3)	O(1)	C(40)	1.203(5)
N(1)	C(2)	1.476(4)	N(1)	C(7)	1.505(4)
N(1)	C(8)	1.489(4)	C(1)	C(2)	1.374(4)
C(1)	C(6)	1.401(4)	C(2)	C(3)	1.396(4)
C(3)	C(4)	1.387(5)	C(4)	C(5)	1.378(5)
C(5)	C(6)	1.382(4)	C(9)	C(10)	1.394(4)
C(9)	C(14)	1.390(4)	C(10)	C(11)	1.385(4)
C(11)	C(12)	1.383(5)	C(12)	C(13)	1.371(5)
C(13)	C(14)	1.396(4)	C(15)	C(16)	1.386(4)
C(15)	C(20)	1.393(4)	C(16)	C(17)	1.391(4)
C(17)	C(18)	1.378(5)	C(18)	C(19)	1.368(5)
C(19)	C(20)	1.394(5)	C(21)	C(22)	1.387(4)
C(21)	C(26)	1.405(4)	C(22)	C(23)	1.390(4)
C(23)	C(24)	1.392(5)	C(24)	C(25)	1.366(5)
C(25)	C(26)	1.382(4)	C(27)	C(28)	1.399(4)
C(27)	C(32)	1.391(4)	C(28)	C(29)	1.385(4)
C(29)	C(30)	1.381(5)	C(30)	C(31)	1.383(5)
C(31)	C(32)	1.393(4)	C(33)	C(34)	1.383(4)
C(33)	C(38)	1.408(4)	C(34)	C(35)	1.398(4)
C(35)	C(36)	1.393(5)	C(36)	C(37)	1.376(5)
C(37)	C(38)	1.394(4)	C(40)	C(41)	1.484(5)
C(40)	C(42)	1.487(5)	S(1)	H(1)	1.03(4)

Table VI.3 Bond angles (°) with estimated standard deviations

Atom	atom	atom	angle	atom	atom	atom	angle
Cl(1)	Ru(1)	Cl(2)	90.69(3)	Cl(1)	Ru(1)	S(1)	176.61(3)
Cl(1)	Ru(1)	P(1)	92.50(3)	Cl(1)	Ru(1)	P(2)	88.51(3)
Cl(1)	Ru(1)	N(1)	89.66(6)	Cl(2)	Ru(1)	S(1)	90.07(3)
Cl(2)	Ru(1)	P(1)	169.27(3)	Cl(2)	Ru(1)	P(2)	86.67(3)
Cl(2)	Ru(1)	N(1)	86.51(6)	S(1)	Ru(1)	P(1)	86.17(3)
S(1)	Ru(1)	P(2)	94.83(3)	S(1)	Ru(1)	N(1)	87.09(6)
P(1)	Ru(1)	P(2)	103.65(3)	P(1)	Ru(1)	N(1)	83.26(6)
P(2)	Ru(1)	N(1)	172.92(6)	Ru(1)	S(1)	C(39)	116.49(11)
Ru(1)	P(1)	C(1)	103.19(10)	Ru(1)	P(1)	C(9)	130.05(10)
Ru(1)	P(1)	C(15)	115.75(8)	C(1)	P(1)	C(9)	99.13(12)
C(1)	P(1)	C(15)	104.45(14)	C(9)	P(1)	C(15)	100.67(13)
Ru(1)	P(2)	C(21)	112.57(9)	Ru(1)	P(2)	C(27)	118.57(10)
Ru(1)	P(2)	C(33)	120.03(9)	C(21)	P(2)	C(27)	104.52(13)
C(21)	P(2)	C(33)	99.64(12)	C(27)	P(2)	C(33)	98.69(12)
Ru(1)	N(1)	C(2)	112.7(2)	Ru(1)	N(1)	C(7)	111.2(2)
Ru(1)	N(1)	C(8)	108.6(2)	C(2)	N(1)	C(7)	108.7(2)
C(2)	N(1)	C(8)	109.8(2)	C(7)	N(1)	C(8)	105.6(2)
P(1)	C(1)	C(2)	119.7(2)	P(1)	C(1)	C(6)	120.8(2)
C(2)	C(1)	C(6)	119.5(3)	N(1)	C(2)	C(1)	121.1(2)
N(1)	C(2)	C(3)	119.2(3)	C(1)	C(2)	C(3)	119.7(3)
C(2)	C(3)	C(4)	120.4(3)	C(3)	C(4)	C(5)	120.1(3)
C(4)	C(5)	C(6)	119.6(3)	C(1)	C(6)	C(5)	120.7(3)
P(1)	C(9)	C(10)	117.8(2)	P(1)	C(9)	C(14)	123.5(2)
C(10)	C(9)	C(14)	118.3(3)	C(9)	C(10)	C(11)	120.7(3)
C(10)	C(11)	C(12)	120.2(3)	C(11)	C(12)	C(13)	119.9(3)
C(12)	C(13)	C(14)	120.2(3)	C(9)	C(14)	C(13)	120.6(3)
P(1)	C(15)	C(16)	118.0(2)	P(1)	C(15)	C(20)	123.0(2)
C(16)	C(15)	C(20)	118.9(3)	C(15)	C(16)	C(17)	120.8(3)
C(16)	C(17)	C(18)	119.6(3)	C(17)	C(18)	C(19)	120.4(3)
C(18)	C(19)	C(20)	120.4(3)	C(15)	C(20)	C(19)	119.9(3)
P(2)	C(21)	C(22)	122.5(2)	P(2)	C(21)	C(26)	119.0(2)
C(22)	C(21)	C(26)	118.2(3)	C(21)	C(22)	C(23)	121.4(3)
C(22)	C(23)	C(24)	119.3(3)	C(23)	C(24)	C(25)	119.9(3)
C(24)	C(25)	C(26)	121.2(3)	C(21)	C(26)	C(25)	120.1(3)
P(2)	C(27)	C(28)	115.9(2)	P(2)	C(27)	C(32)	124.8(2)
C(28)	C(27)	C(32)	119.2(3)	C(27)	C(28)	C(29)	120.0(3)
C(28)	C(29)	C(30)	120.8(3)	C(29)	C(30)	C(31)	119.4(3)
C(30)	C(31)	C(32)	120.6(3)	C(27)	C(32)	C(31)	119.9(3)
P(2)	C(33)	C(34)	124.6(2)	P(2)	C(33)	C(38)	116.6(2)
C(34)	C(33)	C(38)	118.8(3)	C(33)	C(34)	C(35)	120.3(3)
C(34)	C(35)	C(36)	120.5(3)	C(35)	C(36)	C(37)	119.7(3)
C(36)	C(37)	C(38)	120.1(3)	C(33)	C(38)	C(37)	120.6(3)
O(1)	C(40)	C(41)	120.8(4)	O(1)	C(40)	C(42)	121.5(4)
C(41)	C(40)	C(42)	117.6(4)	Ru(1)	S(1)	H(1)	101.5(21)
C(39)	S(1)	H(1)	100.1(18)				

APPENDIX VII

X-Ray Crystallographic Analysis of *Cis*-RuCl₂(P-N)(PPh₃)(EtSH)·(1.5C₆D₆) (21)

EXPERIMENTAL DETAILS

A. Crystal Data

Empirical Formula	C ₄₉ H ₅₀ Cl ₂ NOP ₂ RuS
Formula Weight	918.92
Crystal Colour, Habit	yellow, prism
Crystal Dimensions	0.30 X 0.30 X 0.20 mm
Crystal System	monoclinic
Lattice Type	Primitive
Lattice Parameters	a = 16.6933(8) Å b = 12.4262(12) Å c = 21.8288(6) Å β = 106.3313(8)°
Space Group	V = 4345.3(4) Å ³ P2 ₁ /n (#14)
Z value	4
D _{calc}	1.405 g/cm ³
F ₀₀₀	1900.00
μ(MoKα)	6.41 cm ⁻¹

B. Intensity Measurements

Diffractometer	Rigaku/ADSC CCD
Radiation	MoKα (λ = 0.71069 Å) graphite monochromated
Detector Aperture	94 mm x 94 mm
Temperature	-93°C
Data Images	462 exposures of 70.0 seconds
φ oscillation Range (χ = -90)	0.0 - 190.0°
ω oscillation Range (χ = -90)	-23.0 - 18.0°
Detector Position	39.23(2) mm
Detector Swing Angle	-10.0°
2θ _{max}	60.1°
No. of Reflections Measured	Total: 39270 Unique: 11495 (R _{int} = 0.031)
Corrections	Lorentz-polarization Absorption/scaling (trans. factors: 0.7251 - 1.0060)

C. Structure Solution and Refinement

Structure Solution	Patterson Methods (DIRDIF92 PATTY)
Refinement	Full-matrix least-squares
Function Minimized	$\sum \omega (F_o^2 - F_c^2)^2$
Least Squares Weights	$\omega = \frac{1}{\sigma^2(F_o^2)}$
p-factor	0.0000
Anomalous Dispersion	All non-hydrogen atoms
No. Observations	11495
No. Variables	509
Reflection/Parameter Ratio	22.58
Residuals (on F ² , all data): R; Rw	0.056; 0.058
Goodness of Fit Indicator	1.96
No. Observations (I > 3σ(I))	7749
Residuals (on F, I > 3σ(I)): R; Rw	0.033; 0.027
Max Shift/Error in Final Cycle	0.003
Maximum peak in Final Diff. Map	1.01 e/Å ³
Minimum peak in Final Diff. Map	-0.93 e/Å ³

Table VII.1 Atomic coordinates and B_{eq}

atom	x	y	z	B_{eq}	atom	x	y	z	B_{eq}
Ru(1)	0.418466(10)	0.570955(14)	0.208292(9)	1.617(4)	C(23)	0.46229(13)	0.3100(2)	0.26619(11)	1.72(5)
Cl(1)	0.37043(3)	0.58327(5)	0.09307(3)	2.601(13)	C(24)	0.53731(13)	0.3180(2)	0.31406(11)	1.85(5)
Cl(2)	0.27352(3)	0.53219(5)	0.20834(3)	2.664(13)	C(25)	0.54974(14)	0.2641(2)	0.37205(12)	2.56(6)
S(1)	0.45307(3)	0.56662(5)	0.31981(3)	2.001(12)	C(26)	0.4856(2)	0.2017(2)	0.38268(13)	2.92(6)
P(1)	0.54808(3)	0.63933(4)	0.21880(3)	1.628(12)	C(27)	0.41101(15)	0.1924(2)	0.33560(13)	2.92(6)
P(2)	0.44387(3)	0.39156(4)	0.19320(3)	1.637(12)	C(28)	0.39846(13)	0.2459(2)	0.27738(12)	2.25(5)
N(1)	0.38559(10)	0.75368(14)	0.21865(10)	2.23(4)	C(29)	0.53372(12)	0.3589(2)	0.16258(11)	1.71(5)
C(1)	0.37686(15)	0.5025(2)	0.35372(13)	2.96(6)	C(30)	0.53938(13)	0.4141(2)	0.10888(11)	2.17(5)
C(2)	0.4146(2)	0.4868(2)	0.42421(15)	4.25(8)	C(31)	0.60449(15)	0.3941(2)	0.08185(12)	2.76(6)
C(3)	0.53772(13)	0.7826(2)	0.23543(11)	1.96(5)	C(32)	0.66430(14)	0.3189(2)	0.10925(13)	2.87(6)
C(4)	0.45912(13)	0.8249(2)	0.23178(12)	2.26(5)	C(33)	0.65814(14)	0.2609(2)	0.16161(12)	2.46(6)
C(5)	0.45044(14)	0.9361(2)	0.23961(14)	3.31(6)	C(34)	0.59347(13)	0.2800(2)	0.18855(11)	2.10(5)
C(6)	0.5190(2)	1.0021(2)	0.2518(2)	4.30(8)	C(35)	0.36373(13)	0.3085(2)	0.13691(11)	2.07(5)
C(7)	0.5975(2)	0.9604(2)	0.25654(15)	3.86(7)	C(36)	0.28266(14)	0.3435(2)	0.10819(12)	2.65(6)
C(8)	0.60632(14)	0.8517(2)	0.24811(13)	2.81(6)	C(37)	0.22415(14)	0.2740(2)	0.06924(13)	3.22(6)
C(9)	0.34489(15)	0.7699(2)	0.27102(14)	3.09(6)	C(38)	0.2455(2)	0.1712(2)	0.05829(13)	3.43(7)
C(10)	0.32383(15)	0.7897(2)	0.15837(14)	3.48(6)	C(39)	0.3260(2)	0.1356(2)	0.08558(14)	3.70(7)
C(11)	0.63106(12)	0.5926(2)	0.28861(11)	1.86(5)	C(40)	0.38463(15)	0.2035(2)	0.12465(13)	3.05(6)
C(12)	0.64354(14)	0.6398(2)	0.34871(12)	2.57(6)	C(41)	0.4097(3)	0.2249(3)	0.16161(12)	6.98(13)
C(13)	0.69956(15)	0.5943(2)	0.40198(12)	3.41(7)	C(42)	0.4784(2)	0.1826(3)	0.5610(2)	5.11(9)
C(14)	0.74447(15)	0.5036(2)	0.39619(14)	3.63(7)	C(43)	0.4715(3)	0.0864(3)	0.5852(3)	11.27(15)
C(15)	0.73424(14)	0.4578(2)	0.33736(15)	3.10(6)	C(44)	0.3948(3)	0.0346(4)	0.5678(3)	13.0(2)
C(16)	0.67789(13)	0.5009(2)	0.28361(12)	2.29(5)	C(45)	0.3318(2)	0.0694(3)	0.5223(3)	8.62(13)
C(17)	0.60383(13)	0.6527(2)	0.15717(11)	1.89(5)	C(46)	0.3373(2)	0.1666(4)	0.4959(2)	7.25(13)
C(18)	0.55905(14)	0.6784(2)	0.09574(13)	2.83(6)	C(47)	0.5458(2)	0.0922(3)	0.0024(2)	5.69(10)
C(19)	0.5985(2)	0.6926(2)	0.04784(13)	3.66(7)	C(48)	0.5394(2)	0.0452(3)	0.0584(2)	5.58(10)
C(20)	0.6839(2)	0.6798(2)	0.06154(15)	3.93(8)	C(49)	0.4943(2)	-0.0467(3)	0.0559(2)	5.66(10)
C(21)	0.73024(15)	0.6572(2)	0.12359(15)	3.42(7)	H(1)	0.5074(12)	0.493(2)	0.3353(10)	2.7(5)
C(22)	0.69093(14)	0.6441(2)	0.17145(12)	2.42(6)					

Table VII.2 Bond lengths (Å) with estimated standard deviations

atom	atom	distance	atom	atom	distance
Ru(1)	Cl(1)	2.4204(6)	Ru(1)	Cl(2)	2.4674(5)
Ru(1)	S(1)	2.3391(6)	Ru(1)	P(1)	2.2753(5)
Ru(1)	P(2)	2.3100(6)	Ru(1)	N(1)	2.362(2)
S(1)	C(1)	1.825(2)	P(1)	C(3)	1.835(2)
P(1)	C(11)	1.841(2)	P(1)	C(17)	1.846(2)
P(2)	C(23)	1.840(2)	P(2)	C(29)	1.851(2)
P(2)	C(35)	1.855(2)	N(1)	C(4)	1.474(3)
N(1)	C(9)	1.498(3)	N(1)	C(10)	1.494(3)
C(1)	C(2)	1.502(4)	C(3)	C(4)	1.395(3)
C(3)	C(8)	1.396(3)	C(4)	C(5)	1.405(3)
C(5)	C(6)	1.372(3)	C(6)	C(7)	1.386(3)
C(7)	C(8)	1.376(3)	C(11)	C(12)	1.398(3)
C(11)	C(16)	1.404(3)	C(12)	C(13)	1.391(3)
C(13)	C(14)	1.379(4)	C(14)	C(15)	1.371(4)
C(15)	C(16)	1.388(3)	C(17)	C(18)	1.377(3)
C(17)	C(22)	1.403(3)	C(18)	C(19)	1.394(3)
C(19)	C(20)	1.383(4)	C(20)	C(21)	1.386(4)
C(21)	C(22)	1.391(3)	C(23)	C(24)	1.391(3)
C(23)	C(28)	1.405(3)	C(24)	C(25)	1.395(3)
C(25)	C(26)	1.394(3)	C(26)	C(27)	1.378(4)
C(27)	C(28)	1.397(3)	C(29)	C(30)	1.384(3)
C(29)	C(34)	1.399(3)	C(30)	C(31)	1.397(3)
C(31)	C(32)	1.375(3)	C(32)	C(33)	1.379(3)
C(33)	C(34)	1.388(3)	C(35)	C(36)	1.391(3)
C(35)	C(40)	1.396(3)	C(36)	C(37)	1.398(3)
C(37)	C(38)	1.365(4)	C(38)	C(39)	1.382(4)
C(39)	C(40)	1.388(3)	C(41)	C(42)	1.380(5)
C(41)	C(46)	1.372(5)	C(42)	C(43)	1.324(5)
C(43)	C(44)	1.388(5)	C(44)	C(45)	1.300(5)
C(45)	C(46)	1.353(5)	C(47)	C(48)	1.385(5)
C(47)	C(49)*	1.382(5)	C(48)	C(49)	1.361(4)
S(1)	H(1)	1.27(2)			

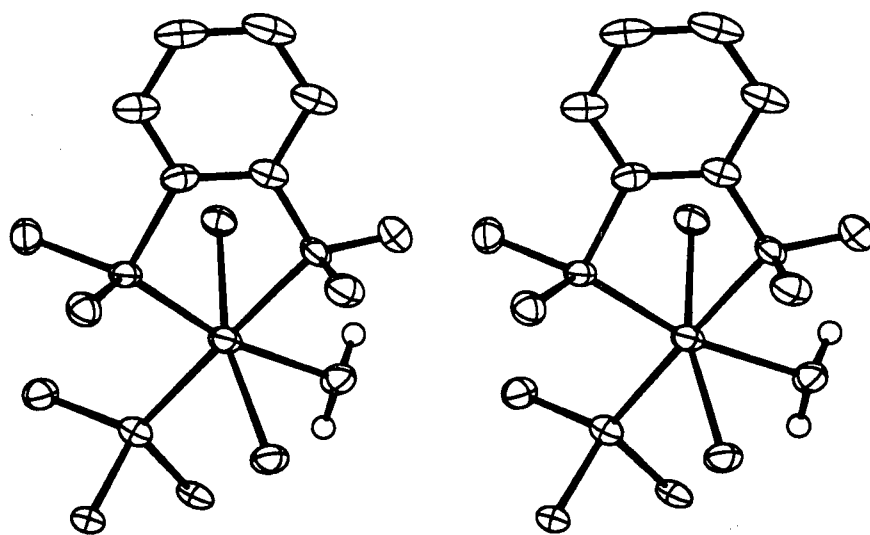
*symmetry operation: 1-x, -y, z

Table VII.3 Bond angles (°) with estimated standard deviations

atom	atom	atom	angle	atom	atom	atom	angle
Cl(1)	Ru(1)	Cl(2)	88.54(2)	Cl(1)	Ru(1)	S(1)	174.63(2)
Cl(1)	Ru(1)	P(1)	96.25(2)	Cl(1)	Ru(1)	P(2)	86.17(2)
Cl(1)	Ru(1)	N(1)	91.19(5)	Cl(2)	Ru(1)	S(1)	87.15(2)
Cl(2)	Ru(1)	P(1)	167.88(2)	Cl(2)	Ru(1)	P(2)	91.78(2)
Cl(2)	Ru(1)	N(1)	86.18(4)	S(1)	Ru(1)	P(1)	87.37(2)
S(1)	Ru(1)	P(2)	97.16(2)	S(1)	Ru(1)	N(1)	85.33(5)
P(1)	Ru(1)	P(2)	99.63(2)	P(1)	Ru(1)	N(1)	82.61(4)
P(2)	Ru(1)	N(1)	176.71(5)	Ru(1)	S(1)	C(1)	115.84(9)
Ru(1)	P(1)	C(3)	104.02(7)	Ru(1)	P(1)	C(11)	116.00(6)
Ru(1)	P(1)	C(17)	128.33(8)	C(3)	P(1)	C(11)	103.46(10)
C(3)	P(1)	C(17)	98.72(9)	C(11)	P(1)	C(17)	102.45(10)
Ru(1)	P(2)	C(23)	113.63(7)	Ru(1)	P(2)	C(29)	117.58(7)
Ru(1)	P(2)	C(35)	120.28(8)	C(23)	P(2)	C(29)	103.70(10)
C(23)	P(2)	C(35)	100.42(10)	C(29)	P(2)	C(35)	98.37(10)
Ru(1)	N(1)	C(4)	113.09(12)	Ru(1)	N(1)	C(9)	111.69(13)
Ru(1)	N(1)	C(10)	108.99(14)	C(4)	N(1)	C(9)	107.6(2)
C(4)	N(1)	C(10)	108.8(2)	C(9)	N(1)	C(10)	106.5(2)
S(1)	C(1)	C(2)	109.4(2)	P(1)	C(3)	C(4)	119.6(2)
P(1)	C(3)	C(8)	121.2(2)	C(4)	C(3)	C(8)	119.1(2)
N(1)	C(4)	C(3)	120.2(2)	N(1)	C(4)	C(5)	120.3(2)
C(3)	C(4)	C(5)	119.4(2)	C(4)	C(5)	C(6)	120.2(2)
C(5)	C(6)	C(7)	120.7(2)	C(6)	C(7)	C(8)	119.4(2)
C(3)	C(8)	C(7)	121.2(2)	P(1)	C(11)	C(12)	121.6(2)
P(1)	C(11)	C(16)	119.8(2)	C(12)	C(11)	C(16)	118.3(2)
C(11)	C(12)	C(13)	120.1(2)	C(12)	C(13)	C(14)	120.7(3)
C(13)	C(14)	C(15)	119.8(2)	C(14)	C(15)	C(16)	120.5(2)
C(11)	C(16)	C(15)	120.5(2)	P(1)	C(17)	C(18)	118.9(2)
P(1)	C(17)	C(22)	122.3(2)	C(18)	C(17)	C(22)	118.6(2)
C(17)	C(18)	C(19)	121.2(2)	C(18)	C(19)	C(20)	119.9(3)
C(19)	C(20)	C(21)	119.5(2)	C(20)	C(21)	C(22)	120.4(2)
C(17)	C(22)	C(21)	120.2(2)	P(2)	C(23)	C(24)	120.5(2)
P(2)	C(23)	C(28)	120.8(2)	C(24)	C(23)	C(28)	118.5(2)
C(23)	C(24)	C(25)	121.3(2)	C(24)	C(25)	C(26)	119.6(2)
C(25)	C(26)	C(27)	119.8(2)	C(26)	C(27)	C(28)	120.8(2)
C(23)	C(28)	C(27)	120.1(2)	P(2)	C(29)	C(30)	116.9(2)
P(2)	C(29)	C(34)	124.4(2)	C(30)	C(29)	C(34)	118.6(2)
C(29)	C(30)	C(31)	121.1(2)	C(30)	C(31)	C(32)	119.6(2)
C(31)	C(32)	C(33)	120.1(2)	C(32)	C(33)	C(34)	120.7(2)
C(29)	C(34)	C(33)	119.9(2)	P(2)	C(35)	C(36)	123.6(2)
P(2)	C(35)	C(40)	118.3(2)	C(36)	C(35)	C(40)	118.0(2)
C(35)	C(36)	C(37)	120.4(2)	C(36)	C(37)	C(38)	120.8(2)
C(37)	C(38)	C(39)	119.6(2)	C(38)	C(39)	C(40)	120.1(3)
C(35)	C(40)	C(39)	121.0(2)	C(42)	C(41)	C(46)	120.7(3)
C(41)	C(42)	C(43)	118.4(3)	C(42)	C(43)	C(44)	119.1(4)
C(43)	C(44)	C(45)	122.7(5)	C(44)	C(45)	C(46)	119.0(4)
C(41)	C(46)	C(45)	119.4(4)	C(48)	C(47)	C(49)*	120.2(3)
C(47)	C(48)	C(49)	119.9(3)	C(47)*	C(49)	C(48)	119.9(3)
Ru(1)	S(1)	H(1)	104.1(9)	C(1)	S(1)	H(1)	96.0(9)

APPENDIX VIII

(Part I)

X-Ray Crystallographic Analysis of *Trans*-RuCl₂(P-N)(PPh₃)(OH₂)·(2C₆H₆) (33a, I)**Figure VIII.1** Stereoview of the molecular structure of 33a, I.

EXPERIMENTAL DETAILS

A. Crystal Data

Empirical Formula	C ₅₀ H ₄₉ Cl ₂ NOP ₂ Ru
Formula Weight	913.87
Crystal Colour, Habit	pink, prism
Crystal Dimensions	0.08 X 0.12 X 0.30 mm
Crystal System	monoclinic
Lattice Type	Primitive
Lattice Parameters	a = 10.5773(6) Å b = 16.979(2) Å c = 24.2616(6) Å β = 90.7065(5)°
Space Group	V = 4356.9(4) Å ³ P2 ₁ /n (#14)
Z value	4
D _{calc}	1.393 g/cm ³
F ₀₀₀	1888.00
μ(MoKα)	5.94 cm ⁻¹

B. Intensity Measurements

Diffractometer	Rigaku/ADSC CCD
Radiation	MoKα (λ = 0.71069 Å) graphite monochromated
Detector Aperture	94 mm x 94 mm
Temperature	-93°C
Data Images	769 exposures of 50.0 seconds
φ oscillation Range (χ = -90)	0.0 - 190.2°
ω oscillation Range (χ = -90)	-23.0 - 17.8°
Detector Position	39.216(5) mm
Detector Swing Angle	-10.0°
2θ _{max}	60.1°
No. of Reflections Measured	Total: 38827 Unique: 10693 (R _{int} = 0.054)
Corrections	Lorentz-polarization Absorption/decay/scaling (cor. factors: 0.6090 - 1.0000)

C. Structure Solution and Refinement

Structure Solution	Patterson Methods (DIRDIF92 PATTY)
Refinement	Full-matrix least-squares
Function Minimized	$\sum w(F_o ^2 - F_c ^2)^2$
Least Squares Weights	$w = \frac{1}{\sigma^2(F_o^2)}$
p-factor	0.0000
Anomalous Dispersion	All non-hydrogen atoms
No. Observations	10693
No. Variables	514
Reflection/Parameter Ratio	20.80
Residuals (on F ² , all data): R; Rw	0.117; 0.082
Goodness of Fit Indicator	1.81
No. Observations (I > 3σ(I))	4878
Residuals (on F, I > 3σ(I)): R; Rw	0.056; 0.035
Max Shift/Error in Final Cycle	0.01
Maximum peak in Final Diff. Map	1.98 e ⁻ /Å ³ (near C(45-50) benzene)
Minimum peak in Final Diff. Map	-2.61 e ⁻ /Å ³ (near Ru)

Table VIII.1 Atomic coordinates and B_{eq}

atom	x	y	z	B_{eq}	atom	x	y	z	B_{eq}
Ru(1)	0.43571(3)	0.53463(2)	0.370059(15)	1.856(8)	C(23)	0.5213(4)	0.2267(3)	0.3686(2)	3.64(14)
Cl(1)	0.27219(8)	0.61626(7)	0.33187(5)	2.39(3)	C(24)	0.4757(4)	0.1773(3)	0.3293(2)	3.65(14)
Cl(2)	0.58439(8)	0.46816(7)	0.43054(4)	2.14(2)	C(25)	0.3817(4)	0.2000(3)	0.2931(2)	3.32(13)
P(1)	0.57846(8)	0.52747(8)	0.30347(5)	1.85(3)	C(26)	0.3338(4)	0.2759(3)	0.2965(2)	2.67(12)
P(2)	0.31168(9)	0.42776(7)	0.34521(5)	1.95(3)	C(27)	0.1829(3)	0.4090(3)	0.3952(2)	2.17(11)
O(1)	0.3252(2)	0.5512(2)	0.44726(11)	2.33(7)	C(28)	0.1727(4)	0.3401(3)	0.4259(2)	2.69(12)
N(1)	0.5543(3)	0.6440(2)	0.39354(15)	1.97(9)	C(29)	0.0703(4)	0.3288(3)	0.4605(2)	3.51(13)
C(1)	0.7103(3)	0.5847(3)	0.3314(2)	2.13(10)	C(30)	-0.0228(4)	0.3866(3)	0.4646(2)	3.40(13)
C(2)	0.6869(3)	0.6319(3)	0.3769(2)	2.07(10)	C(31)	-0.0135(3)	0.4554(3)	0.4344(2)	2.96(12)
C(3)	0.7860(4)	0.6726(3)	0.4033(2)	3.12(12)	C(32)	0.0896(3)	0.4668(3)	0.4002(2)	2.38(10)
C(4)	0.9070(4)	0.6657(3)	0.3829(2)	3.56(14)	C(33)	0.2142(3)	0.4375(3)	0.2820(2)	2.11(10)
C(5)	0.9303(4)	0.6220(3)	0.3361(2)	3.25(13)	C(34)	0.0964(4)	0.4039(3)	0.2753(2)	2.83(12)
C(6)	0.8325(4)	0.5809(3)	0.3106(2)	2.76(12)	C(35)	0.0289(4)	0.4117(3)	0.2271(2)	3.64(14)
C(7)	0.5438(4)	0.6607(3)	0.4532(2)	2.83(12)	C(36)	0.0782(4)	0.4536(3)	0.1834(2)	3.82(14)
C(8)	0.5106(4)	0.7169(3)	0.3636(2)	2.64(12)	C(37)	0.1963(4)	0.4866(3)	0.1889(2)	3.56(13)
C(9)	0.5665(4)	0.5707(3)	0.2343(2)	2.28(11)	C(38)	0.2638(4)	0.4780(3)	0.2376(2)	2.84(12)
C(10)	0.4758(4)	0.6282(3)	0.2211(2)	2.32(11)	C(39)	0.2650(12)	0.1276(5)	0.4665(4)	10.2(4)
C(11)	0.4721(4)	0.6632(3)	0.1705(2)	2.92(12)	C(40)	0.3849(8)	0.1096(5)	0.4851(4)	7.7(3)
C(12)	0.5567(5)	0.6443(3)	0.1300(2)	3.56(13)	C(41)	0.4118(6)	0.0953(4)	0.5395(3)	7.1(2)
C(13)	0.6481(4)	0.5885(3)	0.1413(2)	3.95(14)	C(42)	0.3157(7)	0.0953(4)	0.5770(3)	6.6(2)
C(14)	0.6532(4)	0.5509(3)	0.1926(2)	3.11(12)	C(43)	0.1960(7)	0.1096(4)	0.5586(4)	7.7(3)
C(15)	0.6498(4)	0.4310(3)	0.2898(2)	2.35(11)	C(44)	0.1723(9)	0.1238(5)	0.5046(5)	9.3(3)
C(16)	0.6021(4)	0.3837(3)	0.2467(2)	3.07(12)	C(45)	0.7622(9)	0.1993(10)	0.5105(5)	12.7(5)
C(17)	0.6514(5)	0.3085(3)	0.2380(2)	4.08(15)	C(46)	0.7873(7)	0.2350(5)	0.5587(5)	7.1(3)
C(18)	0.7472(5)	0.2797(3)	0.2718(3)	4.18(15)	C(47)	0.8332(8)	0.1906(7)	0.5978(4)	7.5(3)
C(19)	0.7924(4)	0.3251(3)	0.3141(2)	3.46(14)	C(48)	0.8574(12)	0.1131(9)	0.5931(8)	16.3(6)
C(20)	0.7445(4)	0.4003(3)	0.3235(2)	2.67(12)	C(49)	0.834(2)	0.0844(10)	0.5421(10)	19.3(9)
C(21)	0.3777(3)	0.3281(3)	0.3371(2)	2.23(11)	C(50)	0.772(2)	0.120(2)	0.5011(8)	23.3(10)
C(22)	0.4724(4)	0.3026(3)	0.3730(2)	2.87(12)					

Table VIII.2 Bond lengths (Å) with estimated standard deviations

atom	atom	distance	atom	atom	distance
Ru(1)	Cl(1)	2.3941(11)	Ru(1)	Cl(2)	2.4173(10)
Ru(1)	P(1)	2.2281(11)	Ru(1)	P(2)	2.3147(12)
Ru(1)	O(1)	2.238(3)	Ru(1)	N(1)	2.308(3)
P(1)	C(1)	1.823(4)	P(1)	C(9)	1.835(5)
P(1)	C(15)	1.835(4)	P(2)	C(21)	1.842(4)
P(2)	C(27)	1.861(4)	P(2)	C(33)	1.844(4)
N(1)	C(2)	1.479(4)	N(1)	C(7)	1.481(5)
N(1)	C(8)	1.505(5)	C(1)	C(2)	1.388(6)
C(1)	C(6)	1.395(5)	C(2)	C(3)	1.403(5)
C(3)	C(4)	1.382(6)	C(4)	C(5)	1.380(7)
C(5)	C(6)	1.389(6)	C(9)	C(10)	1.404(5)
C(9)	C(14)	1.414(5)	C(10)	C(11)	1.363(6)
C(11)	C(12)	1.375(6)	C(12)	C(13)	1.378(6)
C(13)	C(14)	1.400(6)	C(15)	C(16)	1.408(6)
C(15)	C(20)	1.388(6)	C(16)	C(17)	1.397(6)
C(17)	C(18)	1.385(7)	C(18)	C(19)	1.365(7)
C(19)	C(20)	1.394(6)	C(21)	C(22)	1.389(6)
C(21)	C(26)	1.400(6)	C(22)	C(23)	1.394(6)
C(23)	C(24)	1.355(7)	C(24)	C(25)	1.374(6)
C(25)	C(26)	1.388(6)	C(27)	C(28)	1.393(6)
C(27)	C(32)	1.399(5)	C(28)	C(29)	1.392(6)
C(29)	C(30)	1.395(6)	C(30)	C(31)	1.383(6)
C(31)	C(32)	1.391(5)	C(33)	C(34)	1.379(5)
C(33)	C(38)	1.387(6)	C(34)	C(35)	1.369(6)
C(35)	C(36)	1.384(6)	C(36)	C(37)	1.375(6)
C(37)	C(38)	1.381(6)	C(39)	C(40)	1.375(10)
C(39)	C(44)	1.357(12)	C(40)	C(41)	1.368(9)
C(41)	C(42)	1.373(8)	C(42)	C(43)	1.359(8)
C(43)	C(44)	1.352(11)	C(45)	C(46)	1.343(12)
C(45)	C(50)	1.37(3)	C(46)	C(47)	1.301(10)
C(47)	C(48)	1.346(13)	C(48)	C(49)	1.35(2)
C(49)	C(50)	1.33(4)			

Table VIII.3 Bond angles ($^{\circ}$) with estimated standard deviations

atom	atom	atom	angle	atom	atom	atom	angle
Cl(1)	Ru(1)	Cl(2)	165.18(4)	Cl(1)	Ru(1)	P(1)	104.11(4)
Cl(1)	Ru(1)	P(2)	87.05(4)	Cl(1)	Ru(1)	O(1)	82.47(7)
Cl(1)	Ru(1)	N(1)	91.01(9)	Cl(2)	Ru(1)	P(1)	88.45(4)
Cl(2)	Ru(1)	P(2)	98.88(4)	Cl(2)	Ru(1)	O(1)	83.87(7)
Cl(2)	Ru(1)	N(1)	83.01(9)	P(1)	Ru(1)	P(2)	98.94(4)
P(1)	Ru(1)	O(1)	168.33(7)	P(1)	Ru(1)	N(1)	81.48(9)
P(2)	Ru(1)	O(1)	90.94(8)	P(2)	Ru(1)	N(1)	178.06(9)
O(1)	Ru(1)	N(1)	88.85(11)	Ru(1)	P(1)	C(1)	102.95(14)
Ru(1)	P(1)	C(9)	127.00(13)	Ru(1)	P(1)	C(15)	117.63(14)
C(1)	P(1)	C(9)	99.8(2)	C(1)	P(1)	C(15)	103.2(2)
C(9)	P(1)	C(15)	102.4(2)	Ru(1)	P(2)	C(21)	122.25(13)
Ru(1)	P(2)	C(27)	112.44(14)	Ru(1)	P(2)	C(33)	117.09(14)
C(21)	P(2)	C(27)	101.2(2)	C(21)	P(2)	C(33)	101.7(2)
C(27)	P(2)	C(33)	98.6(2)	Ru(1)	N(1)	C(2)	109.6(3)
Ru(1)	N(1)	C(7)	110.4(2)	Ru(1)	N(1)	C(8)	112.3(2)
C(2)	N(1)	C(7)	112.1(3)	C(2)	N(1)	C(8)	105.6(3)
C(7)	N(1)	C(8)	106.8(3)	P(1)	C(1)	C(2)	117.3(3)
P(1)	C(1)	C(6)	123.3(4)	C(2)	C(1)	C(6)	119.3(4)
N(1)	C(2)	C(1)	118.5(4)	N(1)	C(2)	C(3)	120.8(4)
C(1)	C(2)	C(3)	120.5(4)	C(2)	C(3)	C(4)	119.0(5)
C(3)	C(4)	C(5)	121.0(4)	C(4)	C(5)	C(6)	119.9(4)
C(1)	C(6)	C(5)	120.2(5)	P(1)	C(9)	C(10)	121.8(3)
P(1)	C(9)	C(14)	121.4(3)	C(10)	C(9)	C(14)	116.7(4)
C(9)	C(10)	C(11)	121.4(4)	C(10)	C(11)	C(12)	121.9(4)
C(11)	C(12)	C(13)	118.7(5)	C(12)	C(13)	C(14)	120.7(4)
C(9)	C(14)	C(13)	120.6(4)	P(1)	C(15)	C(16)	120.0(4)
P(1)	C(15)	C(20)	121.6(4)	C(16)	C(15)	C(20)	118.2(4)
C(15)	C(16)	C(17)	120.2(5)	C(16)	C(17)	C(18)	120.3(5)
C(17)	C(18)	C(19)	119.6(5)	C(18)	C(19)	C(20)	121.1(5)
C(15)	C(20)	C(19)	120.6(5)	P(2)	C(21)	C(22)	119.4(4)
P(2)	C(21)	C(26)	122.3(3)	C(22)	C(21)	C(26)	118.3(4)
C(21)	C(22)	C(23)	120.4(4)	C(22)	C(23)	C(24)	119.8(5)
C(23)	C(24)	C(25)	121.7(5)	C(24)	C(25)	C(26)	119.0(5)
C(21)	C(26)	C(25)	120.8(4)	P(2)	C(27)	C(28)	123.7(3)
P(2)	C(27)	C(32)	117.4(3)	C(28)	C(27)	C(32)	118.9(4)
C(27)	C(28)	C(29)	120.3(4)	C(28)	C(29)	C(30)	120.1(5)
C(29)	C(30)	C(31)	120.1(4)	C(30)	C(31)	C(32)	119.7(4)
C(27)	C(32)	C(31)	120.9(4)	P(2)	C(33)	C(34)	123.8(3)
P(2)	C(33)	C(38)	118.5(3)	C(34)	C(33)	C(38)	117.6(4)
C(33)	C(34)	C(35)	121.4(4)	C(34)	C(35)	C(36)	120.5(4)
C(35)	C(36)	C(37)	119.0(4)	C(36)	C(37)	C(38)	120.0(4)
C(33)	C(38)	C(37)	121.4(4)	C(40)	C(39)	C(44)	115.9(9)
C(39)	C(40)	C(41)	122.4(8)	C(40)	C(41)	C(42)	119.5(7)
C(41)	C(42)	C(43)	118.5(7)	C(42)	C(43)	C(44)	120.8(8)
C(39)	C(44)	C(43)	122.7(9)	C(46)	C(45)	C(50)	125.1(16)
C(45)	C(46)	C(47)	116.1(11)	C(46)	C(47)	C(48)	125.2(12)
C(47)	C(48)	C(49)	113.4(17)	C(48)	C(49)	C(50)	127.2(21)
C(45)	C(50)	C(49)	111.2(14)				

(Part II)

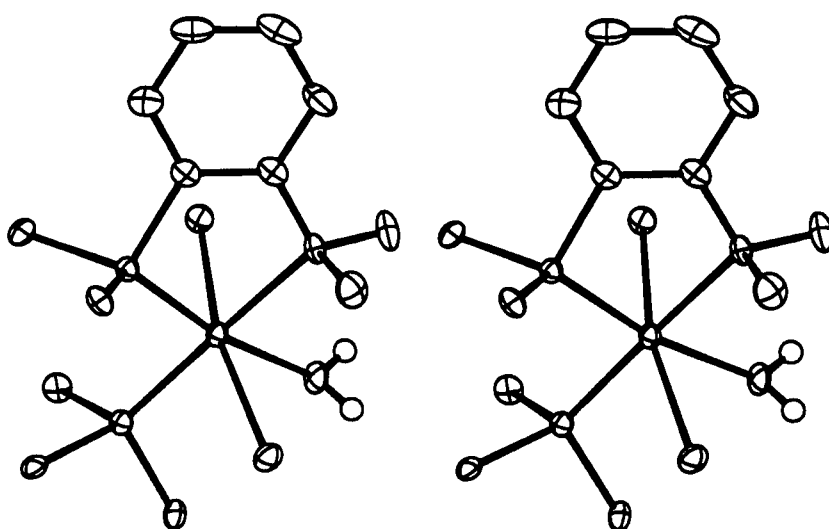
X-Ray Crystallographic Analysis of *Trans*-RuCl₂(P-N)(PPh₃)(OH₂)·(1.5C₆H₆) (33a, II)

Figure VIII.2 Stereoview of the molecular structure of 33a, II.

EXPERIMENTAL DETAILS

A. Crystal Data

Empirical Formula	C ₄₇ H ₄₆ Cl ₂ NOP ₂ Ru
Formula Weight	874.81
Crystal Colour, Habit	yellow-brown, prism
Crystal Dimensions	0.10 X 0.15 X 0.25 mm
Crystal System	triclinic
Lattice Type	Primitive
Lattice Parameters	a = 11.9020(8) Å b = 12.7647(13) Å c = 15.590(2) Å α = 106.371(5)° β = 94.400(3)° γ = 113.7903(10)°
Space Group	V = 2029.9(4) Å ³ P 1 (#2)
Z value	2
D _{calc}	1.431 g/cm ³
F ₀₀₀	902.00
μ(MoKα)	6.34 cm ⁻¹

B. Intensity Measurements

Diffractometer	Rigaku/ADSC CCD
Radiation	MoKα (λ = 0.71069 Å) graphite monochromated
Detector Aperture	94 mm x 94 mm
Temperature	-93°C
Data Images	462 exposures of 60.0 seconds
φ oscillation Range (χ = -90)	0.0 - 190.0°
ω oscillation Range (χ = -90)	-23.0 - 18.0°
Detector Position	39.229(9) mm
Detector Swing Angle	-10.0°
2θ _{max}	60.0°
No. of Reflections Measured	Total: 18577 Unique: 9139 (R _{int} = 0.039)
Corrections	Lorentz-polarization Absorption/decay/scaling (cor. factors: 0.6605 - 1.0000)

C. Structure Solution and Refinement

Structure Solution	Patterson Methods (DIRDIF92 PATTY)
Refinement	Full-matrix least-squares
Function Minimized	$\sum \omega (F_o^2 - F_c^2)^2$
Least Squares Weights	$\omega = \frac{1}{\sigma^2(F_o^2)}$
p-factor	0.0000
Anomalous Dispersion	All non-hydrogen atoms
No. Observations	9139
No. Variables	495
Reflection/Parameter Ratio	18.46
Residuals (on F ² , all data): R; Rw	0.060; 0.055
Goodness of Fit Indicator	1.20
No. Observations (I > 3σ(I))	5971
Residuals (on F, I > 3σ(I)): R; Rw	0.032; 0.025
Max Shift/Error in Final Cycle	0.004
Maximum peak in Final Diff. Map	1.18 e ⁻ /Å ³ (near Ru)
Minimum peak in Final Diff. Map	-1.02 e ⁻ /Å ³ (near Ru)

Table VIII.4 Atomic coordinates and B_{eq}

atom	x	y	z	B_{eq}	atom	x	y	z	B_{eq}
Ru(1)	0.20221(2)	0.21923(2)	0.174034(15)	1.018(5)	C(22)	0.3039(2)	0.4193(3)	0.4204(2)	1.45(6)
Cl(1)	0.02663(5)	0.17778(6)	0.06146(4)	1.477(14)	C(23)	0.3621(2)	0.5273(3)	0.4929(2)	1.82(6)
Cl(2)	0.36596(6)	0.20758(6)	0.26845(4)	1.633(15)	C(24)	0.2925(3)	0.5696(3)	0.5479(2)	2.10(7)
P(1)	0.27389(6)	0.41616(6)	0.19006(5)	1.067(15)	C(25)	0.1623(3)	0.4999(3)	0.5293(2)	2.05(7)
P(2)	0.09942(6)	0.21503(6)	0.29362(5)	1.087(15)	C(26)	0.1040(2)	0.3920(3)	0.4567(2)	1.65(6)
O(1)	0.1283(2)	0.0212(2)	0.13264(15)	1.70(5)	C(27)	-0.0658(2)	0.1927(3)	0.2804(2)	1.38(6)
N(1)	0.3051(2)	0.2195(2)	0.05420(14)	1.23(5)	C(28)	-0.1043(2)	0.2539(3)	0.2333(2)	1.52(6)
C(1)	0.2977(2)	0.4152(3)	0.0750(2)	1.35(6)	C(29)	-0.2256(2)	0.2462(3)	0.2287(2)	2.27(7)
C(2)	0.3057(2)	0.3146(3)	0.0174(2)	1.41(6)	C(30)	-0.3087(2)	0.1777(3)	0.2703(2)	2.26(7)
C(3)	0.3216(3)	0.3080(3)	-0.0709(2)	2.36(7)	C(31)	-0.2701(2)	0.1188(3)	0.3193(2)	2.67(7)
C(4)	0.3282(3)	0.4010(3)	-0.1015(2)	2.89(8)	C(32)	-0.1498(2)	0.1254(3)	0.3247(2)	2.06(7)
C(5)	0.3190(3)	0.5011(3)	-0.0458(2)	2.33(7)	C(33)	0.0834(2)	0.0876(3)	0.3324(2)	1.39(6)
C(6)	0.3056(2)	0.5089(3)	0.0429(2)	1.83(6)	C(34)	0.1527(2)	0.1048(3)	0.4156(2)	1.95(7)
C(7)	0.4405(2)	0.2494(3)	0.0856(2)	2.21(7)	C(35)	0.1348(3)	0.0054(3)	0.4427(2)	2.70(8)
C(8)	0.2462(2)	0.0974(3)	-0.0181(2)	2.16(7)	C(36)	0.0487(3)	-0.1117(3)	0.3869(2)	2.73(8)
C(9)	0.4258(2)	0.5418(3)	0.2584(2)	1.35(6)	C(37)	-0.0192(3)	-0.1288(3)	0.3035(2)	2.41(7)
C(10)	0.5203(2)	0.5183(3)	0.2964(2)	1.60(6)	C(38)	-0.0013(2)	-0.0303(3)	0.2773(2)	1.76(6)
C(11)	0.6393(2)	0.6133(3)	0.3402(2)	2.01(7)	C(39)	0.2545(3)	-0.1825(3)	0.1794(2)	3.18(8)
C(12)	0.6663(2)	0.7318(3)	0.3474(2)	2.24(7)	C(40)	0.1786(3)	-0.2298(3)	0.0923(2)	2.90(8)
C(13)	0.5734(3)	0.7560(3)	0.3107(2)	2.57(7)	C(41)	0.2299(3)	-0.2079(3)	0.0200(2)	2.73(8)
C(14)	0.4547(2)	0.6625(3)	0.2676(2)	1.99(7)	C(42)	0.3575(3)	-0.1374(3)	0.0326(2)	2.76(8)
C(15)	0.1675(2)	0.4879(2)	0.2114(2)	1.30(6)	C(43)	0.4334(3)	-0.0909(3)	0.1182(2)	2.98(8)
C(16)	0.0749(2)	0.4702(3)	0.1405(2)	1.69(6)	C(44)	0.3824(3)	-0.1122(3)	0.1912(2)	3.44(9)
C(17)	-0.0136(2)	0.5135(3)	0.1594(2)	2.43(7)	C(45)	0.5558(4)	0.1214(4)	0.5085(3)	4.57(11)
C(18)	-0.0132(3)	0.5720(3)	0.2485(2)	2.61(8)	C(46)	0.6107(3)	0.0788(5)	0.5604(3)	4.73(11)
C(19)	0.0791(3)	0.5921(3)	0.3197(2)	2.39(7)	C(47)	0.5564(4)	-0.0421(5)	0.5530(3)	4.50(12)
C(20)	0.1696(2)	0.5504(3)	0.3006(2)	1.74(6)	H(1)	0.096(2)	-0.023(3)	0.086(2)	0.7(6)
C(21)	0.1733(2)	0.3498(2)	0.3990(2)	1.27(6)	H(2)	0.178(3)	-0.004(3)	0.143(2)	4.2(8)

Table VIII.5 Bond lengths (Å) with estimated standard deviations

Atom	atom	distance	atom	atom	distance
Ru(1)	Cl(1)	2.3976(6)	Ru(1)	Cl(2)	2.4298(6)
Ru(1)	P(1)	2.2344(8)	Ru(1)	P(2)	2.3085(7)
Ru(1)	O(1)	2.187(2)	Ru(1)	N(1)	2.311(2)
P(1)	C(1)	1.834(3)	P(1)	C(9)	1.838(3)
P(1)	C(15)	1.839(2)	P(2)	C(21)	1.843(3)
P(2)	C(27)	1.856(2)	P(2)	C(33)	1.836(3)
N(1)	C(2)	1.479(3)	N(1)	C(7)	1.503(3)
N(1)	C(8)	1.482(3)	C(1)	C(2)	1.388(4)
C(1)	C(6)	1.395(4)	C(2)	C(3)	1.387(4)
C(3)	C(4)	1.376(5)	C(4)	C(5)	1.378(4)
C(5)	C(6)	1.385(4)	C(9)	C(10)	1.406(3)
C(9)	C(14)	1.398(4)	C(10)	C(11)	1.393(4)
C(11)	C(12)	1.383(4)	C(12)	C(13)	1.387(4)
C(13)	C(14)	1.383(4)	C(15)	C(16)	1.400(3)
C(15)	C(20)	1.387(3)	C(16)	C(17)	1.388(3)
C(17)	C(18)	1.378(4)	C(18)	C(19)	1.390(4)
C(19)	C(20)	1.398(3)	C(21)	C(22)	1.398(3)
C(21)	C(26)	1.406(3)	C(22)	C(23)	1.375(4)
C(23)	C(24)	1.386(3)	C(24)	C(25)	1.396(4)
C(25)	C(26)	1.374(4)	C(27)	C(28)	1.386(4)
C(27)	C(32)	1.399(4)	C(28)	C(29)	1.402(3)
C(29)	C(30)	1.372(4)	C(30)	C(31)	1.380(4)
C(31)	C(32)	1.395(3)	C(33)	C(34)	1.393(4)
C(33)	C(38)	1.390(4)	C(34)	C(35)	1.389(4)
C(35)	C(36)	1.391(4)	C(36)	C(37)	1.388(4)
C(37)	C(38)	1.372(4)	C(39)	C(40)	1.390(4)
C(39)	C(44)	1.385(4)	C(40)	C(41)	1.367(4)
C(41)	C(42)	1.380(4)	C(42)	C(43)	1.372(4)
C(43)	C(44)	1.373(4)	C(45)	C(46)	1.353(5)
C(45)	C(47)*	1.376(5)	C(46)	C(47)	1.378(6)
O(1)	H(1)	0.74(2)	O(1)	H(2)	0.81(3)

*symmetry operation: 1-x, -y, 1-z

Table VIII.6 Bond angles (°) with estimated standard deviations

Atom	atom	atom	angle	atom	atom	atom	angle
Cl(1)	Ru(1)	Cl(2)	165.58(2)	Cl(1)	Ru(1)	P(1)	88.02(2)
Cl(1)	Ru(1)	P(2)	96.30(2)	Cl(1)	Ru(1)	O(1)	85.40(6)
Cl(1)	Ru(1)	N(1)	84.09(5)	Cl(2)	Ru(1)	P(1)	105.32(3)
Cl(2)	Ru(1)	P(2)	86.97(2)	Cl(2)	Ru(1)	O(1)	80.63(6)
Cl(2)	Ru(1)	N(1)	92.37(5)	P(1)	Ru(1)	P(2)	99.70(3)
P(1)	Ru(1)	O(1)	169.95(6)	P(1)	Ru(1)	N(1)	81.46(6)
P(2)	Ru(1)	O(1)	88.57(6)	P(2)	Ru(1)	N(1)	178.77(6)
O(1)	Ru(1)	N(1)	90.30(8)	Ru(1)	P(1)	C(1)	102.15(9)
Ru(1)	P(1)	C(9)	127.19(9)	Ru(1)	P(1)	C(15)	118.76(9)
C(1)	P(1)	C(9)	99.45(11)	C(1)	P(1)	C(15)	103.65(11)
C(9)	P(1)	C(15)	101.64(11)	Ru(1)	P(2)	C(21)	116.73(8)
Ru(1)	P(2)	C(27)	121.90(9)	Ru(1)	P(2)	C(33)	112.03(8)
C(21)	P(2)	C(27)	100.05(11)	C(21)	P(2)	C(33)	104.02(12)
C(27)	P(2)	C(33)	99.38(12)	Ru(1)	N(1)	C(2)	110.19(14)
Ru(1)	N(1)	C(7)	111.16(15)	Ru(1)	N(1)	C(8)	110.46(15)
C(2)	N(1)	C(7)	106.5(2)	C(2)	N(1)	C(8)	111.4(2)
C(7)	N(1)	C(8)	107.0(2)	P(1)	C(1)	C(2)	117.7(2)
P(1)	C(1)	C(6)	123.2(2)	C(2)	C(1)	C(6)	119.1(2)
N(1)	C(2)	C(1)	118.6(2)	N(1)	C(2)	C(3)	121.2(2)
C(1)	C(2)	C(3)	120.1(3)	C(2)	C(3)	C(4)	119.8(3)
C(3)	C(4)	C(5)	121.0(3)	C(4)	C(5)	C(6)	119.2(3)
C(1)	C(6)	C(5)	120.6(3)	P(1)	C(9)	C(10)	120.8(2)
P(1)	C(9)	C(14)	121.0(2)	C(10)	C(9)	C(14)	118.0(2)
C(9)	C(10)	C(11)	120.2(3)	C(10)	C(11)	C(12)	120.8(3)
C(11)	C(12)	C(13)	119.4(3)	C(12)	C(13)	C(14)	120.4(3)
C(9)	C(14)	C(13)	121.3(3)	P(1)	C(15)	C(16)	121.4(2)
P(1)	C(15)	C(20)	119.6(2)	C(16)	C(15)	C(20)	118.7(2)
C(15)	C(16)	C(17)	120.5(3)	C(16)	C(17)	C(18)	120.3(3)
C(17)	C(18)	C(19)	120.0(2)	C(18)	C(19)	C(20)	119.7(3)
C(15)	C(20)	C(19)	120.7(2)	P(2)	C(21)	C(22)	119.1(2)
P(2)	C(21)	C(26)	123.2(2)	C(22)	C(21)	C(26)	117.5(2)
C(21)	C(22)	C(23)	121.3(2)	C(22)	C(23)	C(24)	120.6(2)
C(23)	C(24)	C(25)	118.9(3)	C(24)	C(25)	C(26)	120.5(2)
C(21)	C(26)	C(25)	121.1(2)	P(2)	C(27)	C(28)	119.5(2)
P(2)	C(27)	C(32)	121.7(2)	C(28)	C(27)	C(32)	118.5(2)
C(27)	C(28)	C(29)	120.5(3)	C(28)	C(29)	C(30)	120.8(3)
C(29)	C(30)	C(31)	119.1(2)	C(30)	C(31)	C(32)	120.9(3)
C(27)	C(32)	C(31)	120.2(3)	P(2)	C(33)	C(34)	122.3(2)
P(2)	C(33)	C(38)	119.1(2)	C(34)	C(33)	C(38)	118.7(3)
C(33)	C(34)	C(35)	120.0(3)	C(34)	C(35)	C(36)	120.5(3)
C(35)	C(36)	C(37)	119.4(3)	C(36)	C(37)	C(38)	119.8(3)
C(33)	C(38)	C(37)	121.6(3)	C(40)	C(39)	C(44)	118.6(3)
C(39)	C(4C)	C(41)	120.4(3)	C(40)	C(41)	C(42)	120.4(3)
C(41)	C(42)	C(43)	119.6(3)	C(42)	C(43)	C(44)	120.2(3)
C(39)	C(44)	C(43)	120.6(3)	C(46)	C(45)	C(47)*	119.3(4)
C(45)	C(46)	C(47)	121.3(4)	C(45)*	C(47)	C(46)	119.4(4)
Ru(1)	O(1)	H(1)	126.6(23)	Ru(1)	O(1)	H(2)	116.4(25)
H(1)	O(1)	H(2)	97.5(28)				

APPENDIX IX

X-Ray Crystallographic Analysis of *Cis*-RuCl₂(P-N)(PPh₃)(η^2 -H₂) (36)

EXPERIMENTAL DETAILS

A. Crystal Data

Empirical Formula	C ₃₈ H ₃₇ Cl ₂ NP ₂ Ru
Formula Weight	741.64
Crystal Colour, Habit	yellow, block
Crystal Dimensions	0.30 X 0.16 X 0.07 mm
Crystal System	monoclinic
Lattice Type	Primitive
Lattice Parameters	a = 8.8084(1) Å b = 17.2509(3) Å c = 11.5902(2) Å β = 105.709(1)°
Space Group	V = 1695.38(5) Å ³ P2 ₁ (#4)
Z value	2
D _{calc}	1.453 g/cm ³
F ₀₀₀	760
Absorption coefficient	0.743 mm ⁻¹

B. Intensity Measurements

Diffractometer	Siemens SMART Platform CCD
Wavelength	0.71073 Å
Temperature	-100°C
θ range for data collection	1.83 to 25.01°
Index ranges	-10 $\leq h \leq$ 10, -19 $\leq k \leq$ 20, 0 $\leq l \leq$ 13
Reflections collected	8555
Independent reflections	4935 (R _{int} = 0.0167)

C. Structure Solution and Refinement

Structure Solution	Direct methods (SHELXTL-V5.0)
Refinement	Full-matrix least-squares on F ²
Function Minimized	$\sum w(F_o ^2 - F_c ^2) ^2$
Weighting scheme	$w = [\sigma^2(F_o^2) + (AP)^2 + (BP)]^{-1}$, where P = (F _o ² + 2F _c ²)/3, A = 0.0350, and B = 0.0860
Absorption correction	SADABS (Sheldrick, 1996)
Max. and min. transmission	1.000 and 0.837
Absolute structure parameter	0.01(2)
Data/restraints/parameters	4935/1/403
Residuals (on F ² , all data): R; R _w	0.0217; 0.0537
Residuals (on F, I > 2 σ (I) = 4816): R; R _w	0.0208; 0.0532
Goodness of Fit on F ²	1.026
Maximum peak in Final Diff. Map	0.379 e/Å ³
Minimum peak in Final Diff. Map	-0.320 e/Å ³

Table IX.1 Atomic coordinates ($\times 10^4$) and U_{eq} (defined as one third of the trace of the orthogonalized U_{ij} tensor.)

atom	x	y	z	U_{eq}	atom	x	y	z	U_{eq}
Ru(1)	7078(1)	6753(1)	2103(1)	17(1)	C(19)	3392(3)	6918(2)	1287(3)	33(1)
Cl(1)	6936(1)	5463(1)	2961(1)	28(1)	C(20)	4274(4)	5770(2)	807(3)	38(1)
Cl(2)	8165(1)	6164(1)	619(1)	26(1)	P(2)	9381(1)	6824(1)	3636(1)	18(1)
P(1)	6939(1)	7900(1)	1089(1)	18(1)	C(21)	10439(3)	7746(2)	3893(2)	24(1)
C(1)	8476(3)	8368(2)	520(2)	23(1)	C(22)	10600(4)	8214(2)	4899(3)	32(1)
C(2)	9286(4)	7938(2)	-141(3)	31(1)	C(23)	11453(4)	8909(2)	5011(3)	43(1)
C(3)	10366(4)	8291(2)	-653(3)	39(1)	C(24)	12169(4)	9125(2)	4149(4)	48(1)
C(4)	10645(4)	9086(2)	-512(3)	33(1)	C(25)	12026(4)	8664(2)	3140(3)	42(1)
C(5)	9843(4)	9512(2)	142(3)	35(1)	C(26)	11156(4)	7986(2)	3008(3)	31(1)
C(6)	8771(4)	9162(2)	649(3)	29(1)	C(27)	9008(3)	6636(2)	5106(2)	25(1)
C(7)	6169(3)	8725(2)	1753(2)	21(1)	C(28)	7943(4)	7098(2)	5494(3)	37(1)
C(8)	7017(4)	8975(2)	2886(3)	31(1)	C(29)	7669(4)	6966(2)	6612(3)	47(1)
C(9)	6557(4)	9622(2)	3406(3)	34(1)	C(30)	8436(5)	6369(2)	7340(3)	46(1)
C(10)	5221(4)	10023(2)	2808(3)	33(1)	C(31)	9465(5)	5908(2)	6954(3)	43(1)
C(11)	4350(4)	9777(2)	1687(3)	32(1)	C(32)	9759(4)	6038(2)	5846(3)	32(1)
C(12)	4820(3)	9136(2)	1159(3)	26(1)	C(33)	11022(3)	6160(2)	3634(2)	22(1)
C(13)	5446(3)	7703(2)	-316(2)	23(1)	C(34)	10762(4)	5450(2)	3052(3)	27(1)
C(14)	5254(3)	8170(2)	-1332(2)	30(1)	C(35)	12009(4)	4950(2)	3090(3)	33(1)
C(15)	4129(4)	7979(2)	-2398(3)	38(1)	C(36)	13541(3)	5157(2)	3692(3)	31(1)
C(16)	3244(4)	7315(2)	-2442(3)	39(1)	C(37)	13819(3)	5864(2)	4266(3)	29(1)
C(17)	3422(3)	6849(2)	-1441(2)	33(1)	C(38)	12585(3)	6364(2)	4257(2)	25(1)
C(18)	4504(3)	7046(2)	-363(2)	24(1)	H(1*)	6189(28)	7090(13)	3026(20)	81(7)
N(1)	4641(2)	6609(1)	746(2)	23(1)					

H(1*) = double-occupancy hydrogen atom (η^2 -H₂) refined isotropically**Table IX.2** Bond lengths (Å) with estimated standard deviations

Atom	atom	distance	atom	atom	distance
Ru(1)	P(1)	2.2884(7)	Ru(1)	N(1)	2.306(2)
Ru(1)	P(2)	2.3098(6)	Ru(1)	Cl(2)	2.4090(6)
Ru(1)	Cl(1)	2.4543(7)	P(1)	C(7)	1.832(3)
P(1)	C(13)	1.827(3)	C(1)	C(2)	1.394(4)
P(1)	C(1)	1.844(3)	C(2)	C(3)	1.391(4)
C(1)	C(6)	1.395(4)	C(3)	C(4)	1.394(5)
C(7)	C(8)	1.392(4)	C(4)	C(5)	1.380(5)
C(8)	C(9)	1.381(4)	C(5)	C(6)	1.378(4)
C(9)	C(10)	1.379(4)	C(7)	C(12)	1.396(4)
C(10)	C(11)	1.385(4)	C(13)	C(18)	1.397(4)
C(11)	C(12)	1.380(4)	C(14)	C(15)	1.398(4)
C(13)	C(14)	1.399(4)	C(15)	C(16)	1.377(5)
N(1)	C(20)	1.492(4)	C(16)	C(17)	1.386(5)
P(2)	C(21)	1.827(3)	C(17)	C(18)	1.392(4)
P(2)	C(27)	1.848(3)	C(21)	C(22)	1.394(4)
C(18)	N(1)	1.466(3)	C(22)	C(23)	1.401(5)
N(1)	C(19)	1.503(3)	C(23)	C(24)	1.370(6)
P(2)	C(33)	1.845(3)	C(24)	C(25)	1.393(6)
C(21)	C(26)	1.404(4)	C(25)	C(26)	1.383(5)
C(27)	C(32)	1.388(4)	C(27)	C(28)	1.395(4)
C(28)	C(29)	1.400(4)	C(33)	C(34)	1.387(4)
C(29)	C(30)	1.386(5)	C(34)	C(35)	1.388(4)
C(30)	C(31)	1.369(5)	C(35)	C(36)	1.388(5)
C(31)	C(32)	1.396(4)	C(36)	C(37)	1.379(4)
C(33)	C(38)	1.415(4)	C(37)	C(38)	1.385(4)
Ru(1)	H(1*)	1.60(2)			

Table IX.3 Bond angles (°) with estimated standard deviations

Atom	atom	atom	angle	atom	atom	atom	angle
P(1)	Ru(1)	N(1)	80.34(6)	P(1)	Ru(1)	P(2)	105.27(3)
N(1)	Ru(1)	P(2)	172.78(6)	P(1)	Ru(1)	Cl(2)	88.52(2)
N(1)	Ru(1)	Cl(2)	86.78(6)	P(2)	Ru(1)	Cl(2)	97.79(2)
P(1)	Ru(1)	Cl(1)	172.22(2)	N(1)	Ru(1)	Cl(1)	92.20(6)
P(2)	Ru(1)	Cl(1)	82.34(3)	Cl(2)	Ru(1)	Cl(1)	88.86(2)
P(1)	Ru(1)	H(1*)	93.6(8)	N(1)	Ru(1)	H(1*)	87.8(8)
P(2)	Ru(1)	H(1*)	87.3(8)	Cl(2)	Ru(1)	H(1*)	173.8(8)
Cl(1)	Ru(1)	H(1*)	88.3(8)	C(13)	P(1)	C(7)	105.10(13)
C(13)	P(1)	C(1)	100.61(12)	C(7)	P(1)	C(1)	101.61(13)
C(13)	P(1)	Ru(1)	102.84(9)	C(7)	P(1)	Ru(1)	115.43(8)
C(1)	P(1)	Ru(1)	128.31(9)	C(2)	C(1)	C(6)	118.3(3)
C(2)	C(1)	P(1)	119.8(2)	C(6)	C(1)	P(1)	121.7(2)
C(3)	C(2)	C(1)	120.8(3)	C(2)	C(3)	C(4)	120.0(3)
C(5)	C(4)	C(3)	119.2(3)	C(6)	C(5)	C(4)	120.8(3)
C(5)	C(6)	C(1)	120.9(3)	C(8)	C(7)	C(12)	118.4(3)
C(8)	C(7)	P(1)	118.2(2)	C(12)	C(7)	P(1)	123.4(2)
C(9)	C(8)	C(7)	121.1(3)	C(10)	C(9)	C(8)	119.8(3)
C(9)	C(10)	C(11)	119.9(3)	C(12)	C(11)	C(10)	120.4(3)
C(11)	C(12)	C(7)	120.4(3)	C(18)	C(13)	C(14)	120.0(2)
C(18)	C(13)	P(1)	117.6(2)	C(14)	C(13)	P(1)	122.5(2)
C(15)	C(14)	C(13)	120.2(3)	C(16)	C(15)	C(14)	119.2(3)
C(15)	C(16)	C(17)	121.1(3)	C(16)	C(17)	C(18)	120.3(3)
C(17)	C(18)	C(13)	119.2(3)	C(17)	C(18)	N(1)	122.3(3)
C(13)	C(18)	N(1)	118.4(2)	C(18)	N(1)	C(20)	111.9(2)
C(18)	N(1)	C(19)	106.7(2)	C(20)	N(1)	C(19)	105.9(2)
C(18)	N(1)	Ru(1)	112.5(2)	C(20)	N(1)	Ru(1)	110.2(2)
C(23)	C(24)	C(25)	120.1(3)	C(21)	P(2)	C(33)	100.10(14)
C(25)	C(26)	C(21)	121.0(3)	C(33)	P(2)	C(27)	103.11(12)
C(32)	C(27)	P(2)	121.7(2)	C(33)	P(2)	Ru(1)	119.45(9)
C(27)	C(28)	C(29)	120.4(3)	C(22)	C(21)	C(26)	118.4(3)
C(31)	C(30)	C(29)	119.4(3)	C(26)	C(21)	P(2)	116.7(2)
C(34)	C(33)	P(2)	121.5(2)	C(24)	C(23)	C(22)	120.5(3)
C(37)	C(38)	C(33)	120.1(3)	C(26)	C(25)	C(24)	119.8(3)
C(34)	C(33)	C(38)	118.5(3)	C(32)	C(27)	C(28)	118.3(3)
C(38)	C(33)	P(2)	120.0(2)	C(28)	C(27)	P(2)	120.0(2)
C(34)	C(35)	C(36)	120.6(3)	C(30)	C(29)	C(28)	120.4(3)
C(36)	C(37)	C(38)	120.7(3)	C(30)	C(31)	C(32)	120.7(3)

APPENDIX X

X-Ray Crystallographic Analysis of *Cis*-RuCl₂(P-N)(PPh₃)(=C=CHPh) (45)

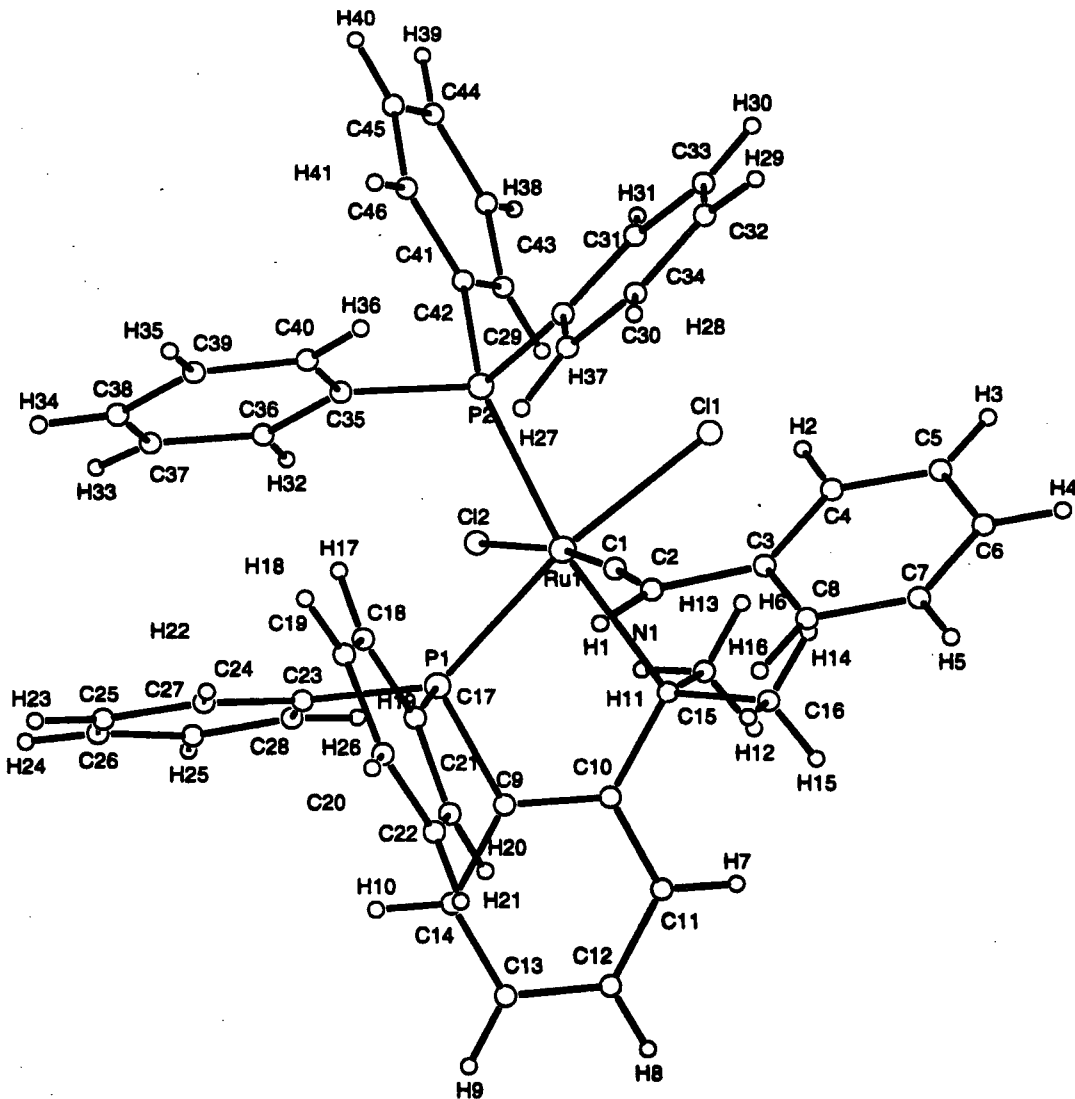


Figure X.1 Pluto plot of the molecular structure of **45**.

EXPERIMENTAL DETAILS

A. Crystal Data

Empirical Formula	C ₄₆ H ₄₁ Cl ₂ NP ₂ Ru
Formula Weight	841.76
Crystal Colour, Habit	red-orange, irregular
Crystal Dimensions	0.20 X 0.30 X 0.40 mm
Crystal System	monoclinic
Lattice Type	C-centred
No. of Reflections Used for Unit Cell Determination (2 θ range)	25 (53.0 - 73.0°)
Omega Scan Peak Width at Half-height	0.38°
Lattice Parameters	a = 10.1402(12) Å b = 21.718(2) Å c = 18.187(2) Å β = 100.329(11)°
Space Group	V = 3940.3(7) Å ³
Z value	Cc (#9)
D _{calc}	4
F ₀₀₀	1.419 g/cm ³
μ (CuK α)	1728
	54.94 cm ⁻¹

B. Intensity Measurements

Diffractometer	Rigaku AFC6S
Radiation	CuK α (λ = 1.54178 Å) graphite monochromated
Take-off Angle	6.0°
Detector Aperture	6.0 mm horizontal 6.0 mm vertical
Crystal to Detector Distance	285 mm
Voltage, Current	45kV, 25mA
Temperature	21.0°
Scan Type	ω -2 θ
Scan Rate	16°/min (in ω) (up to 9 scans)
Scan Width	(1.05 + 0.20 tan θ)°
2 θ_{max}	155.0°
No. of Reflections Measured	Total: 4271 Unique: 4137 (R_{int} = 0.066)
Corrections	Lorentz-polarization Absorption (trans. Factors: 0.624 - 1.000)

C. Structure Solution and Refinement

Structure Solution	Patterson Methods (DIRDIF92 PATTY)
Refinement	Full-matrix least-squares
Function Minimized	$\sum w(F_o - F_c)^2$
Least Squares Weights	$w = 1$
p-factor	0.0000
Anomalous Dispersion	All non-hydrogen atoms
No. Observations ($I > 3.00\sigma(I)$)	3677
No. Variables	467
Reflection/Parameter Ratio	7.87
Residuals: R; Rw	0.043; 0.048
Goodness of Fit Indicator	1.04
Max Shift/Error in Final Cycle	0.0001
Maximum peak in Final Diff. Map	0.90 e/Å ³
Minimum peak in Final Diff. Map	-0.84 e/Å ³

Table II.1 Atomic coordinates and B_{eq}

atom	x	y	z	B_{eq}	atom	x	y	z	B_{eq}
Ru(1)	0.49780	0.50642(2)	0.49750	3.056(10)	C(21)	0.2864(12)	0.3342(6)	0.2766(6)	6.4(3)
Cl(1)	0.4707(3)	0.61174(10)	0.53810(14)	4.50(5)	C(22)	0.3252(10)	0.3476(5)	0.3518(6)	5.1(3)
Cl(2)	0.6498(3)	0.48129(12)	0.61744(14)	4.76(6)	C(23)	0.6327(9)	0.3469(4)	0.5066(5)	3.7(2)
P(1)	0.4989(2)	0.40084(10)	0.47436(12)	3.27(4)	C(24)	0.6974(10)	0.3114(5)	0.4600(6)	4.4(2)
P(2)	0.6725(2)	0.54955(10)	0.44573(14)	3.43(5)	C(25)	0.7934(11)	0.2690(5)	0.4863(8)	5.6(3)
N(1)	0.3178(7)	0.4800(3)	0.5528(5)	4.0(2)	C(26)	0.8309(10)	0.2604(5)	0.5621(9)	5.8(3)
C(1)	0.3860(8)	0.5142(4)	0.4082(5)	3.4(2)	C(27)	0.7670(11)	0.2925(5)	0.6107(7)	5.5(3)
C(2)	0.3014(10)	0.5163(4)	0.3434(5)	4.3(2)	C(28)	0.6716(11)	0.3356(5)	0.5842(6)	4.8(2)
C(3)	0.2039(8)	0.5651(5)	0.3218(5)	4.2(2)	C(29)	0.6120(9)	0.6090(4)	0.3760(5)	3.9(2)
C(4)	0.2167(11)	0.6229(5)	0.3542(7)	5.8(3)	C(30)	0.5427(11)	0.5936(5)	0.3037(6)	4.8(2)
C(5)	0.122(2)	0.6674(7)	0.3332(8)	8.4(4)	C(31)	0.493(2)	0.6391(6)	0.2551(8)	5.7(3)
C(6)	0.0132(15)	0.6558(8)	0.2778(8)	7.9(4)	C(32)	0.4999(15)	0.6985(6)	0.2747(7)	7.0(4)
C(7)	-0.0005(14)	0.6011(7)	0.2443(8)	6.6(3)	C(33)	0.5651(13)	0.7150(5)	0.3477(7)	6.1(3)
C(8)	0.0954(9)	0.5547(6)	0.2644(6)	5.1(2)	C(34)	0.6162(10)	0.6700(4)	0.3960(6)	4.6(2)
C(9)	0.3707(8)	0.3718(4)	0.5228(5)	3.7(2)	C(35)	0.7749(8)	0.4969(4)	0.4023(6)	4.1(2)
C(10)	0.2925(8)	0.4128(4)	0.5536(5)	3.7(2)	C(36)	0.8417(10)	0.4519(5)	0.4474(6)	4.6(2)
C(11)	0.1919(10)	0.3901(5)	0.5902(6)	5.2(3)	C(37)	0.9252(10)	0.4089(5)	0.4212(8)	5.8(3)
C(12)	0.1702(11)	0.3289(5)	0.5953(6)	5.4(3)	C(38)	0.9334(11)	0.4091(6)	0.3460(8)	6.2(3)
C(13)	0.2464(11)	0.2874(5)	0.5636(7)	5.3(3)	C(39)	0.8676(12)	0.4534(6)	0.3001(7)	6.1(3)
C(14)	0.3481(10)	0.3093(5)	0.5273(6)	4.3(2)	C(40)	0.7885(10)	0.4984(5)	0.3270(6)	5.2(2)
C(15)	0.3390(12)	0.5037(5)	0.6302(6)	5.7(3)	C(41)	0.8057(9)	0.5927(4)	0.5065(6)	4.2(2)
C(16)	0.1952(10)	0.5107(5)	0.5118(7)	5.6(3)	C(42)	0.8048(10)	0.6060(5)	0.5812(6)	4.8(2)
C(17)	0.4427(9)	0.3778(4)	0.3766(5)	3.6(2)	C(43)	0.9096(13)	0.6399(5)	0.6215(7)	6.2(3)
C(18)	0.5226(9)	0.3942(5)	0.3254(5)	4.4(2)	C(44)	1.0134(11)	0.6608(5)	0.5906(8)	6.1(3)
C(19)	0.4869(14)	0.3802(5)	0.2495(8)	4.9(2)	C(45)	1.0140(11)	0.6479(5)	0.5153(8)	5.7(3)
C(20)	0.3648(12)	0.3499(5)	0.2266(6)	5.3(3)	C(46)	0.9135(9)	0.6137(5)	0.4757(6)	4.9(2)

Table X.2 Bond lengths (Å) with estimated standard deviations

atom	atom	distance	atom	atom	distance
Ru(1)	Cl(1)	2.434(2)	Ru(1)	Cl(2)	2.495(2)
Ru(1)	P(1)	2.332(2)	Ru(1)	P(2)	2.346(2)
Ru(1)	N(1)	2.308(7)	Ru(1)	C(1)	1.814(8)
P(1)	C(9)	1.809(9)	P(1)	C(17)	1.837(9)
P(1)	C(23)	1.808(9)	P(2)	C(29)	1.836(9)
P(2)	C(35)	1.818(9)	P(2)	C(41)	1.841(9)
N(1)	C(10)	1.480(11)	N(1)	C(15)	1.478(12)
N(1)	C(16)	1.488(13)	C(1)	C(2)	1.329(12)
C(2)	C(3)	1.455(13)	C(3)	C(4)	1.382(15)
C(3)	C(8)	1.393(12)	C(4)	C(5)	1.37(2)
C(5)	C(6)	1.38(2)	C(6)	C(7)	1.33(2)
C(7)	C(8)	1.40(2)	C(9)	C(10)	1.377(12)
C(9)	C(14)	1.383(13)	C(10)	C(11)	1.404(13)
C(11)	C(12)	1.352(15)	C(12)	C(13)	1.380(15)
C(13)	C(14)	1.404(13)	C(17)	C(18)	1.387(12)
C(17)	C(22)	1.364(12)	C(18)	C(19)	1.40(2)
C(19)	C(20)	1.40(2)	C(20)	C(21)	1.354(15)
C(21)	C(22)	1.384(14)	C(23)	C(24)	1.393(13)
C(23)	C(28)	1.418(13)	C(24)	C(25)	1.363(14)
C(25)	C(26)	1.37(2)	C(26)	C(27)	1.38(2)
C(27)	C(28)	1.370(14)	C(29)	C(30)	1.415(13)
C(29)	C(34)	1.373(13)	C(30)	C(31)	1.361(15)
C(31)	C(32)	1.34(2)	C(32)	C(33)	1.42(2)
C(33)	C(34)	1.353(14)	C(35)	C(36)	1.373(13)
C(35)	C(40)	1.401(13)	C(36)	C(37)	1.401(14)
C(37)	C(38)	1.39(2)	C(38)	C(39)	1.37(2)
C(39)	C(40)	1.408(14)	C(41)	C(42)	1.390(14)
C(41)	C(46)	1.391(13)	C(42)	C(43)	1.389(14)
C(43)	C(44)	1.36(2)	C(44)	C(45)	1.40(2)
C(45)	C(46)	1.360(13)			

Table IV.3 Bond angles (°) with estimated standard deviations

atom	atom	atom	angle	atom	atom	atom	angle
Cl(1)	Ru(1)	Cl(2)	91.50(9)	Cl(1)	Ru(1)	P(1)	169.56(8)
Cl(1)	Ru(1)	P(2)	83.15(8)	Cl(1)	Ru(1)	N(1)	87.8(2)
Cl(1)	Ru(1)	C(1)	95.6(3)	Cl(2)	Ru(1)	P(1)	85.45(8)
Cl(2)	Ru(1)	P(2)	92.61(9)	Cl(2)	Ru(1)	N(1)	88.7(2)
Cl(2)	Ru(1)	C(1)	172.7(3)	P(1)	Ru(1)	P(2)	106.94(8)
P(1)	Ru(1)	N(1)	82.2(2)	P(1)	Ru(1)	C(1)	87.3(3)
P(2)	Ru(1)	N(1)	170.9(2)	P(2)	Ru(1)	C(1)	89.9(3)
N(1)	Ru(1)	C(1)	89.9(3)	Ru(1)	P(1)	C(9)	103.1(3)
Ru(1)	P(1)	C(17)	115.6(3)	Ru(1)	P(1)	C(23)	127.3(3)
C(9)	P(1)	C(17)	104.5(4)	C(9)	P(1)	C(23)	100.3(4)
C(17)	P(1)	C(23)	102.8(4)	Ru(1)	P(2)	C(29)	112.0(3)
Ru(1)	P(2)	C(35)	117.0(3)	Ru(1)	P(2)	C(41)	119.2(3)
C(29)	P(2)	C(35)	106.8(4)	C(29)	P(2)	C(41)	100.1(4)
C(35)	P(2)	C(41)	99.6(4)	Ru(1)	N(1)	C(10)	113.6(5)
Ru(1)	N(1)	C(15)	109.7(6)	Ru(1)	N(1)	C(16)	109.0(6)
C(10)	N(1)	C(15)	109.3(8)	C(10)	N(1)	C(16)	108.4(7)
C(15)	N(1)	C(16)	106.6(8)	Ru(1)	C(1)	C(2)	176.4(8)
C(1)	C(2)	C(3)	124.3(9)	C(2)	C(3)	C(4)	122.6(9)
C(2)	C(3)	C(8)	119.4(10)	C(4)	C(3)	C(8)	117.9(9)
C(3)	C(4)	C(5)	120.9(11)	C(4)	C(5)	C(6)	120.3(14)
C(5)	C(6)	C(7)	120.2(13)	C(6)	C(7)	C(8)	120.8(13)
C(3)	C(8)	C(7)	119.7(11)	P(1)	C(9)	C(10)	119.3(7)
P(1)	C(9)	C(14)	120.8(7)	C(10)	C(9)	C(14)	119.9(8)
N(1)	C(10)	C(9)	121.3(8)	N(1)	C(10)	C(11)	119.5(8)
C(9)	C(10)	C(11)	119.1(9)	C(10)	C(11)	C(12)	121.3(10)
C(11)	C(12)	C(13)	120.3(9)	C(12)	C(13)	C(14)	119.2(9)
C(9)	C(14)	C(13)	120.3(9)	P(1)	C(17)	C(18)	117.6(7)
P(1)	C(17)	C(22)	123.6(7)	C(18)	C(17)	C(22)	118.8(9)
C(17)	C(18)	C(19)	121.9(9)	C(18)	C(19)	C(20)	117.1(11)
C(19)	C(20)	C(21)	120.9(10)	C(20)	C(21)	C(22)	120.9(10)
C(17)	C(22)	C(21)	120.3(9)	P(1)	C(23)	C(24)	124.7(8)
P(1)	C(23)	C(28)	119.6(7)	C(24)	C(23)	C(28)	115.6(9)
C(23)	C(24)	C(25)	123.1(11)	C(24)	C(25)	C(26)	119.7(11)
C(25)	C(26)	C(27)	119.9(10)	C(26)	C(27)	C(28)	120.3(11)
C(23)	C(28)	C(27)	121.4(10)	P(2)	C(29)	C(30)	121.6(7)
P(2)	C(29)	C(34)	120.3(7)	C(30)	C(29)	C(34)	117.4(9)
C(29)	C(30)	C(31)	119.7(10)	C(30)	C(31)	C(32)	122.2(13)
C(31)	C(32)	C(33)	119.1(11)	C(32)	C(33)	C(34)	119.1(10)
C(29)	C(34)	C(33)	122.3(10)	P(2)	C(35)	C(36)	116.5(8)
P(2)	C(35)	C(40)	125.0(8)	C(36)	C(35)	C(40)	118.5(9)
C(35)	C(36)	C(37)	122.3(10)	C(36)	C(37)	C(38)	118.7(10)
C(37)	C(38)	C(39)	119.8(10)	C(38)	C(39)	C(40)	121.5(11)
C(35)	C(40)	C(39)	119.1(11)	P(2)	C(41)	C(42)	124.1(7)
P(2)	C(41)	C(46)	118.0(8)	C(42)	C(41)	C(46)	117.9(9)
C(41)	C(42)	C(43)	119.2(10)	C(42)	C(43)	C(44)	122.4(12)
C(43)	C(44)	C(45)	118.6(10)	C(44)	C(45)	C(46)	119.6(11)
C(41)	C(46)	C(45)	122.3(11)				

APPENDIX XI

Thermodynamic Calculations and Data for the Reversible Formation of
***Cis*-RuX₂(P-N)(PR₃)(L) (X = Cl, Br; R = Ph, *p*-tolyl; L = H₂S, MeSH, EtSH)**

For the equilibrium:



$$K = \frac{[\text{B}]}{[\text{A}][\text{L}]} \quad (2)$$

A complete calculation of equilibrium concentrations for the *cis*-RuCl₂(P-N)(PPh₃)(SH₂) **18a** system is given in Section XI.1; sets of raw data for corresponding systems involving **18b**, **19a**, **20**, and **21** are given similarly in Sections XI.2-XI.5.

XI.1 Calculations for the *Cis*-RuCl₂(P-N)(PPh₃)(SH₂) (18a**) Equilibrium System in C₆D₆**

Table XI.1.1 Integrations Used for Equilibrium Calculations (see Figure 4.30)

Value of Integration	Signal(s), ppm	Reasonance(s)	Number of Protons
α	3.67	NMe of 18a	3
β	3.06, 2.97	NMe of 6a , NMe of 18a	6, 3
ε	1.02	Ru(SH ₂) of 18a	2
ω	0.30	free H ₂ S (in solution)	2

The calculation of equilibrium concentrations at any temperature is as follows:

[Ru]_{total} is calculated from the amount of **18a** dissolved in a known volume of solvent; this volume of solvent in the NMR tube is measured with a ruler (cm) and converted to (mL) using the calibration plot shown in Figure XI.1.

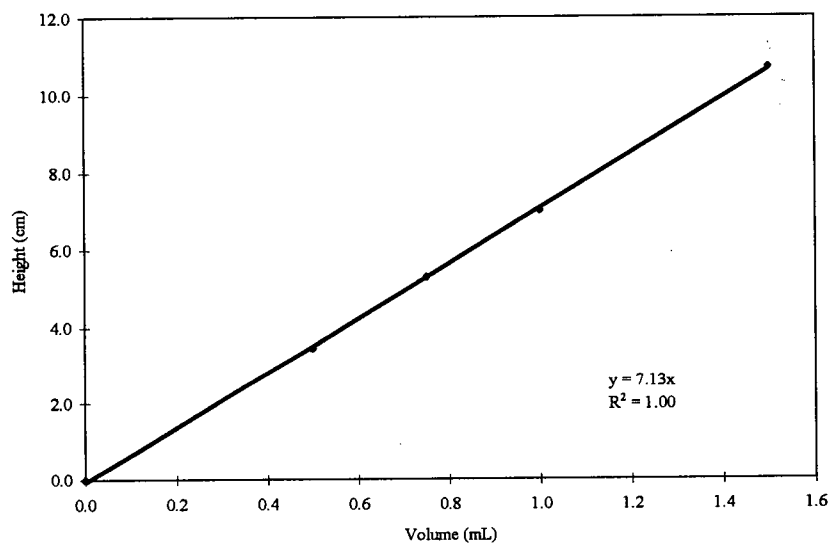


Figure XI.1 Calibration plot for measured height (cm) of solvent vs. volume (mL) in 5 mm NMR tubes (type 507-PP from Wilmad Glass Co., Inc.).

$$x = \frac{[18a]}{[6a]} = \frac{\alpha / 3}{(\beta - \alpha) / 6} = \frac{\epsilon / 2}{(\beta - \alpha) / 6} \quad (3)$$

$$y = \frac{[6a]}{[H_2S]_s} = \frac{(\beta - \alpha) / 6}{\omega / 2} \quad (4)$$

$$[6a] = \frac{[Ru]_{total}}{1 + x} \quad (5)$$

$$[18a] = [Ru]_{total} - [6a] \quad (6)$$

$$[H_2S]_s = \frac{[6a]}{y} \quad (7)$$

$$K = \frac{[18a]}{[6a][H_2S]_s} \quad (8)$$

Note: $[H_2S]_s$ (solution) = $[H_2S]_{uncoordinated} - [H_2S]_{headspace}$

Table XI.1.2 Integration Values and Equilibrium Concentration Ratios (α , β , ϵ and ω)

T (°C)	α	β	ϵ	ω	x	y
13.5	5.62	13.85	3.60	1.12	1.37	2.45
18.5 ^a	3.35	10.18	2.05	0.92	0.98	2.47
19.0 ^b	4.36	12.03	2.80	1.00	1.14	2.56
19.2	5.33	14.62	3.45	1.40	1.15	2.21
19.2 ^c	2.91	8.12	1.70	0.78	1.12	2.23
21.5	4.72	16.09	3.32	1.80	0.83	2.11
35.4	1.91	7.29	1.40	1.20	0.71	1.49
50.3	0.90	4.90	0.62	1.00	0.45	1.33

¹H NMR spectrum (of the same sample) measured ^a2 h, ^b2 d and ^c1 week after sample preparation.

Table XI.1.3 Equilibrium Concentrations and K ($[\text{Ru}]_{\text{total}} = 0.0231 \text{ M}$)

T (°C)	1/T (K)	[6a] (M)	[18a] (M)	[H ₂ S] _s (M)	K (M ⁻¹)	ln K
13.5	0.003489	0.0098	0.0133	0.0040	343	5.84
18.5 ^a	0.003429	0.0117	0.0114	0.0047	208	5.34
19.0 ^b	0.003423	0.0108	0.0123	0.0042	269	5.59
19.2	0.003421	0.0108	0.0123	0.0049	236	5.46
19.2 ^c	0.003421	0.0109	0.0122	0.0049	228	5.43
21.5	0.003394	0.0126	0.0105	0.0060	139	4.93
35.4	0.003241	0.0135	0.0096	0.0090	79	4.36
50.3	0.003092	0.0159	0.0072	0.0119	38	3.63

¹H NMR spectrum (of the same sample) measured ^a2 h, ^b2 d and ^c1 week after sample preparation.

XI.2 Calculations for the *Cis*-RuBr₂(P-N)(PPh₃)(SH₂) (18b) Equilibrium System in C₆D₆ (under 1 atm H₂S)

Table XI.2.1 Integrations Used for Equilibrium Calculations

Value of Integration	Signal(s), ppm	Reasonance(s)	Number of Protons
α	3.93	NMe of 18b	3
β	3.17, 2.87	NMe of 6b , NMe of 18b	6, 3
ϵ	1.14	Ru(SH ₂) of 18b	2
ω	0.30	free H ₂ S (in solution)	2

Table XI.2.2 Integration Values and Equilibrium Concentration Ratios (α , β , ϵ and ω)

T (°C)	α	β	ϵ	ω	x	y
20.6	9.12	16.78	5.84	17.01	2.38	0.15
22.5	9.10	15.49	5.10	19.03	2.85	0.11
35.5	8.53	19.85	5.33	24.03	1.51	0.16
45.0	6.85	19.51	4.25	20.10	1.08	0.21
60.2	4.63	17.00	2.84	21.22	0.75	0.19

Table XI.2.3 Equilibrium Concentrations and K ($[\text{Ru}]_{\text{total}} = 0.0203 \text{ M}$; under 1 atm H_2S)

T (°C)	1/T (K)	[6b] (M)	[18b] (M)	$[\text{H}_2\text{S}]_s$ (M)	K (M^{-1})	ln K
20.6	0.003404	0.0060	0.0143	0.0400	60	4.09
22.5	0.003382	0.0053	0.0150	0.0471	60	4.10
35.5	0.003240	0.0081	0.0122	0.0516	29	3.38
45.0	0.003143	0.0097	0.0106	0.0464	23	3.15
60.2	0.003000	0.0116	0.0087	0.0597	13	2.53

XI.3 Calculations for the *Cis*- $\text{RuCl}_2(\text{P-N})(\text{P}(p\text{-tolyl})_3)(\text{SH}_2)$ (**19a**) Equilibrium System in C_6D_6

Table XI.3.1 Integrations Used for Equilibrium Calculations

Value of Integration	Signal(s), ppm	Reasonance(s)	Number of Protons
α	3.76	NMe of 19a	3
β	3.10, 2.92	NMe of 7a , NMe of 19a	6, 3
ϵ	1.15	Ru(SH_2) of 19a	2
ω	0.30	free H_2S (in solution)	2

Table XI.3.2 Integration Values and Equilibrium Concentration Ratios (α , β , ϵ and ω)

T (°C)	α	β	ϵ	ω	x	y
19.0	1.94	9.14	1.31	1.20	0.54	2.00
19.3	1.00	5.10	0.55	0.52	0.49	2.63
22.4	0.79	6.43	0.45	0.7	0.28	2.69
35.4	1.37	10.62	1.00	1.45	0.30	2.13
43.4	0.30	7.13	0.25	0.85	0.09	2.68
50.5	0.24	7.60	0.20	0.91	0.07	2.70

Table XI.3.3 Equilibrium Concentrations and K ($[\text{Ru}]_{\text{total}} = 0.00808 \text{ M}$)

T (°C)	1/T (K)	[7a] (M)	[19a] (M)	[H ₂ S] _s (M)	K (M ⁻¹)	ln K
19.0	0.003423	0.0053	0.0028	0.0026	205	5.32
19.3	0.003419	0.0054	0.0026	0.0021	236	5.46
22.4	0.003384	0.0063	0.0018	0.0024	119	4.78
35.4	0.003241	0.0062	0.0018	0.0029	101	4.62
43.4	0.003159	0.0074	0.0007	0.0028	32	3.46
50.5	0.003090	0.0076	0.0005	0.0028	23	3.14

XI.4 Calculations for the *Cis*-RuCl₂(P-N)(PPh₃)(MeSH) (20) Equilibrium System in C₆D₆

Table XI.4.1 Integrations Used for Equilibrium Calculations

Value of Integration	Signal(s), ppm	Reasonance(s)	Number of Protons
α	3.63	NMe of 20	3
β	3.04 (br)	NMe of 6a, NMe of 20	6, 3
ϵ	0.78	Ru(CH ₃ SH) of 20	3
ω	1.59	free CH ₃ SH (in solution)	3

Table XI.4.2 Integration Values and Equilibrium Concentration Ratios (α , β , ϵ and ω)

T (°C)	α	β	ϵ	ω	x	y
20.0	0.76	1.80	0.80	0.45	1.46	1.16
35.5	0.85	2.30	0.85	0.80	1.17	0.91
40.4	0.70	2.05	0.72	0.75	1.04	0.90
60.3	0.52	1.95	0.49	0.90	0.73	0.79
75.2	0.39	1.80	0.35	0.92	0.55	0.77

Table XI.4.3 Equilibrium Concentrations and K ($[\text{Ru}]_{\text{total}} = 0.0115 \text{ M}$)

T (°C)	1/T (K)	[6a] (M)	[20] (M)	[MeSH] _s (M)	K (M ⁻¹)	ln K
20.0	0.003411	0.0047	0.0068	0.0040	362	5.89
35.5	0.003240	0.0053	0.0062	0.0058	201	5.30
40.4	0.003189	0.0056	0.0059	0.0063	165	5.11
60.3	0.002999	0.0067	0.0048	0.0084	87	4.46
75.2	0.002871	0.0074	0.0041	0.0097	57	4.05

Note: in this case, $x = \frac{[\text{20}]}{[\text{6a}]} = \frac{\alpha / 3}{(\beta - \alpha) / 6} = \frac{\epsilon / 3}{(\beta - \alpha) / 6}$ and $y = \frac{[\text{6a}]}{[\text{MeSH}]_s} = \frac{(\beta - \alpha) / 6}{\omega / 3}$.

XI.5 Calculations for the *Cis*-RuCl₂(P-N)(PPh₃)(EtSH) (21**) Equilibrium System in C₆D₆**

Table XI.5.1 Integrations Used for Equilibrium Calculations

Value of Integration	Signal(s), ppm	Reasonance(s)	Number of Protons
α	3.73	NMe of 21	3
β	3.17, 3.05	NMe of 6a , NMe of 21	6, 3
ϵ	0.35	Ru(CH ₃ CH ₂ SH) of 21	3
ω	1.59	free CH ₃ CH ₂ SH	2

Table XI.5.2 Integration Values and Equilibrium Concentration Ratios (α , β , ϵ and ω);
([Ru]_{total} = † 0.0171, ‡ 0.0194 M)

T (°C)	α	β	ϵ	ω	x	y
† 19.0	3.29	5.18	2.80	3.17	3.48	0.20
† 24.5	4.28	7.08	3.46	4.16	3.06	0.22
† 40.5	2.30	4.57	1.85	2.51	2.03	0.30
† 60.5	2.38	5.73	1.71	3.15	1.42	0.35
† 70.5	1.14	2.89	0.94	1.61	1.30	0.36
† 19.2	3.98	6.42	3.69	3.18	3.26	0.26
‡ 30.5	2.89	5.24	2.45	2.90	2.46	0.27
‡ 50.5	1.49	3.34	1.25	1.70	1.61	0.36
‡ 65.5	1.19	2.96	0.95	1.64	1.34	0.36
‡ 75.5	1.17	3.77	0.98	2.00	0.90	0.43

Table XI.5.3 Equilibrium Concentrations and K ([Ru]_{total} = † 0.0171, ‡ 0.0194 M)

T (°C)	1/T (K)	[6a] (M)	[21] (M)	[EtSH] _s (M)	K (M ⁻¹)	ln K
† 19.0	0.003423	0.0038	0.0133	0.0192	181	5.20
† 24.5	0.003360	0.0042	0.0129	0.0188	163	5.09
† 40.5	0.003188	0.0057	0.0114	0.0187	108	4.68
† 60.5	0.002997	0.0071	0.0100	0.0199	71	4.27
† 70.5	0.002910	0.0074	0.0097	0.0205	64	4.15
† 19.2	0.003421	0.0046	0.0148	0.0178	183	5.21
‡ 30.5	0.003293	0.0056	0.0138	0.0208	118	4.77
‡ 50.5	0.003090	0.0074	0.0120	0.0205	79	4.36
‡ 65.5	0.002953	0.0083	0.0111	0.0230	58	4.07
‡ 75.5	0.002868	0.0102	0.0092	0.0236	38	3.64

Note: in this case, $x = \frac{[\mathbf{21}]}{[\mathbf{6a}]} = \frac{\alpha/3}{(\beta - \alpha)/6} = \frac{\epsilon/3}{(\beta - \alpha)/6}$ and $y = \frac{[\mathbf{6a}]}{[\mathbf{EtSH}]} = \frac{(\beta - \alpha)/6}{\omega/2}$.

APPENDIX XII

Thermodynamic Calculations and Data for the Reversible Formation of

Trans-RuCl₂(P-N)(PPh₃)(OH₂) (33a) (UV-Vis Spectroscopic Data)

For the equilibrium:



$$K = \frac{[\text{33a}]}{[\text{6a}][\text{H}_2\text{O}]} \quad (2)$$

$$\log\left(\frac{[\text{33a}]}{[\text{6a}]}\right) = \log K + n \log[\text{H}_2\text{O}] \quad (3)$$

where $n = 1$ (slope)

plot of $\log\left(\frac{[\text{33a}]}{[\text{6a}]}\right)$ versus $\log [\text{H}_2\text{O}]$ gives intercept = $\log K$

$$A = \epsilon c \ell \quad (4)$$

where A = absorbance

ϵ = molar absorptivity ($\text{M}^{-1} \text{cm}^{-1}$)

c = concentration (M)

ℓ = pathlength = 1 cm

$$A = A_{6a} + A_{33a} = \epsilon_{6a}[\text{6a}] + \epsilon_{33a}[\text{33a}] \quad (5)$$

$$[\text{Ru}]_{\text{total}} = [\text{6a}] + [\text{33a}] \quad (6)$$

$$\epsilon_{6a} = \frac{A_0}{[\text{Ru}]_{\text{total}}} \quad (7)$$

$$\epsilon_{33a} = \frac{A_\infty}{[\text{Ru}]_{\text{total}}} \quad (8)$$

Solve for $[\text{6a}]$ and $[\text{33a}]$ by substitution of equations (6) and (7) into (5), and equations (6) and (8) into (5), respectively:

$$\frac{[\text{33a}]}{[\text{6a}]} = \frac{A - A_0}{A - A_\infty} \quad (9)$$

XII.1 Calculations in CH_2Cl_2

Trial 1 at 25°C

Table XII.1.1 Calculation of K at T = 25°C; 5.2×10^{-6} mol **6a** dissolved in 5.0 mL CH_2Cl_2 ($[\text{Ru}]_{\text{total}} = 1.04 \times 10^{-3}$ M); absorbances monitored at $\lambda_{\text{max}} = 678$ nm; $A_0 = 0.52$, $A_{\infty} = 0.078$ (estimated from a flat baseline between $\lambda = 550$ to 820 nm).

H_2O added (μL)	$[\text{H}_2\text{O}]$ (M)	$\log [\text{H}_2\text{O}]$	A at $\lambda_{\text{max}} =$ 678 nm	$\frac{[\text{33a}]}{[\text{6a}]}$	$\log \frac{[\text{33a}]}{[\text{6a}]}$
0.0	0.0000	-	0.52	-0.00052	-
0.5	0.0056	-2.26	0.47	0.11119	-0.95
1.0	0.0111	-1.95	0.41	0.33838	-0.47
2.5	0.0278	-1.56	0.33	0.78687	-0.10
4.0	0.0444	-1.35	0.27	1.34657	0.13
6.0	0.0666	-1.18	0.23	1.87686	0.27
9.0	0.0999	-1.00	0.18	3.21073	0.51
10.0	0.1110	-0.95	0.16	4.17443	0.62
17.0	0.1887	-0.72	0.15	5.22535	0.72

Plot of plot of $\log\left(\frac{[\text{33a}]}{[\text{6a}]}\right)$ versus $\log [\text{H}_2\text{O}]$ (see Figure 5.15) gives $y = 1.06x + 1.57$; $K = 37 \text{ M}^{-1}$.

Trial 2 at 25°C

Table XII.1.2 Calculation of K at T = 25°C; 3.0×10^{-6} mol **6a** dissolved in 5.0 mL CH_2Cl_2 ($[\text{Ru}]_{\text{total}} = 6.0 \times 10^{-4}$ M); absorbances monitored at $\lambda_{\text{max}} = 678$ nm; $A_0 = 0.30$, $A_{\infty} = 0.045$ (estimated from a flat baseline between $\lambda = 550$ to 820 nm).

H_2O added (μL)	$[\text{H}_2\text{O}]$ (M)	$\log [\text{H}_2\text{O}]$	A at $\lambda_{\text{max}} =$ 678 nm	$\frac{[\text{33a}]}{[\text{6a}]}$	$\log \frac{[\text{33a}]}{[\text{6a}]}$
0.0	0.0000	-	0.30	0.00252	-2.60
0.1	0.0006	-3.26	0.25	0.26758	-0.57
1.0	0.0111	-1.95	0.20	0.69199	-0.16
1.5	0.0167	-1.78	0.15	1.46377	0.17
3.5	0.0389	-1.41	0.12	2.40864	0.38
6.5	0.0722	-1.14	0.10	3.54626	0.55
8.5	0.0944	-1.03	0.09	5.07432	0.71
12.0	0.1332	-0.88	0.08	6.55556	0.82
17.0	0.1887	-0.72	0.08	6.92910	0.84

Plot of plot of $\log\left(\frac{[\text{33a}]}{[\text{6a}]}\right)$ versus $\log [\text{H}_2\text{O}]$ gives $y = 0.83x + 1.54$; $K = 35 \text{ M}^{-1}$.

Trial 1 at 10°C

Table XII.1.3 Calculation of K at T = 10°C; 4.0×10^{-6} mol **6a** dissolved in 5.0 mL CH₂Cl₂ ([Ru]_{total} = 8.1×10^{-4} M); absorbances monitored at λ_{max} = 678 nm; A_0 = 0.39, A_{∞} = 0.07 (estimated from a flat baseline between λ = 550 to 820 nm).

H ₂ O added (μL)	[H ₂ O] (M)	log [H ₂ O]	A at λ_{max} = 678 nm	$\frac{[33a]}{[6a]}$	$\log \frac{[33a]}{[6a]}$
0.0	0.0000	-	0.39	0.00000	-
0.5	0.0056	-2.26	0.35	0.14286	-0.85
1.0	0.0111	-1.95	0.31	0.33333	-0.48
1.5	0.0167	-1.78	0.27	0.60000	-0.22
2.0	0.0222	-1.65	0.25	0.77778	-0.11
3.0	0.0333	-1.48	0.21	1.28571	0.11
4.0	0.0444	-1.35	0.20	1.46154	0.16
6.0	0.0666	-1.18	0.18	1.90909	0.28

Plot of plot of $\log\left(\frac{[33a]}{[6a]}\right)$ versus log [H₂O] gives $y = 1.07x + 1.62$; $K = 42 \text{ M}^{-1}$.

Trial 2 at 10°C

Table XII.1.4 Calculation of K at T = 10°C; 4.1×10^{-6} mol **6a** dissolved in 5.0 mL CH₂Cl₂ ([Ru]_{total} = 8.2×10^{-4} M); absorbances monitored at λ_{max} = 678 nm; A_0 = 0.40, A_{∞} = 0.07 (estimated from a flat baseline between λ = 550 to 820 nm).

H ₂ O added (μL)	[H ₂ O] (M)	log [H ₂ O]	A at λ_{max} = 678 nm	$\frac{[33a]}{[6a]}$	$\log \frac{[33a]}{[6a]}$
0.0	0.0000	-	0.40	0.00000	-
0.5	0.0056	-2.26	0.34	0.22222	-0.65
1.0	0.0111	-1.95	0.30	0.43478	-0.36
1.5	0.0167	-1.78	0.25	0.83333	-0.08
2.0	0.0222	-1.65	0.22	1.20000	0.08
3.0	0.0333	-1.48	0.19	1.75000	0.24
4.0	0.0444	-1.35	0.16	2.66667	0.43
6.0	0.0666	-1.18	0.12	5.60000	0.75

Plot of plot of $\log\left(\frac{[33a]}{[6a]}\right)$ versus log [H₂O] gives $y = 1.28x + 2.18$; $K = 151 \text{ M}^{-1}$.

Trial 1 at 35°C

Table XII.1.5 Calculation of K at T = 35°C; 4.5×10^{-6} mol **6a** dissolved in 5.0 mL CH₂Cl₂ ([Ru]_{total} = 9.0×10^{-4} M); absorbances monitored at λ_{max} = 678 nm; $A_0 = 0.43$, $A_{\infty} = 0.08$ (estimated from a flat baseline between $\lambda = 550$ to 820 nm).

H ₂ O added (μL)	[H ₂ O] (M)	log [H ₂ O]	A at λ_{max} = 678 nm	$\frac{[33a]}{[6a]}$	$\log \frac{[33a]}{[6a]}$
0.0	0.0000	-	0.42	0.02609	-
1.0	0.0111	-1.95	0.34	0.32180	-0.49
2.0	0.0222	-1.65	0.30	0.60860	-0.22
3.0	0.0333	-1.48	0.25	1.08694	0.04
4.0	0.0444	-1.35	0.23	1.37176	0.14
6.0	0.0666	-1.18	0.21	1.60359	0.21
9.0	0.0999	-1.00	0.20	1.91569	0.28
12.0	0.1332	-0.88	0.19	2.14861	0.33

Plot of plot of $\log\left(\frac{[33a]}{[6a]}\right)$ versus log [H₂O] gives $y = 0.84x + 1.20$; $K = 16 \text{ M}^{-1}$.

Trial 2 at 35°C

Table XII.1.6 Calculation of K at T = 35°C; 4.8×10^{-6} mol **6a** dissolved in 5.0 mL CH₂Cl₂ ([Ru]_{total} = 9.7×10^{-4} M); absorbances monitored at λ_{max} = 678 nm; $A_0 = 0.43$, $A_{\infty} = 0.075$ (estimated from a flat baseline between $\lambda = 550$ to 820 nm).

H ₂ O added (μL)	[H ₂ O] (M)	log [H ₂ O]	A at λ_{max} = 678 nm	$\frac{[33a]}{[6a]}$	$\log \frac{[33a]}{[6a]}$
0.0	0.0000	-	0.43	-0.00591	-
1.0	0.0111	-1.95	0.37	0.20433	-0.69
2.0	0.0222	-1.65	0.32	0.43649	-0.36
3.0	0.0333	-1.48	0.28	0.70044	-0.15
4.0	0.0444	-1.35	0.26	0.94755	-0.02
6.0	0.0666	-1.18	0.23	1.36100	0.13
9.0	0.0999	-1.00	0.20	1.89962	0.28
12.0	0.1332	-0.88	0.19	2.12886	0.33

Plot of plot of $\log\left(\frac{[33a]}{[6a]}\right)$ versus log [H₂O] gives $y = 1.03x + 1.34$; $K = 22 \text{ M}^{-1}$.

Trial 1 at 38°C

Table XII.1.7 Calculation of K at T = 38°C; 5.4×10^{-6} mol **6a** dissolved in 5.0 mL CH₂Cl₂ ([Ru]_{total} = 1.08×10^{-3} M); absorbances monitored at λ_{max} = 678 nm; A_0 = 0.48, A_{∞} = 0.08 (estimated from a flat baseline between λ = 550 to 820 nm).

H ₂ O added (μ L)	[H ₂ O] (M)	log [H ₂ O]	A at λ_{max} = 678 nm	$\frac{[33a]}{[6a]}$	$\log \frac{[33a]}{[6a]}$
0.0	0.0000	-	0.48	0.00000	-
1.0	0.0111	-1.95	0.37	0.37931	-0.42
2.0	0.0222	-1.65	0.34	0.53846	-0.27
3.0	0.0333	-1.48	0.27	1.10526	0.04
5.0	0.0555	-1.26	0.25	1.35294	0.13
7.0	0.0777	-1.11	0.22	1.85714	0.27
10.0	0.1110	-0.95	0.18	3.00000	0.48
12.0	0.1332	-0.88	0.15	4.71429	0.67

Plot of plot of $\log\left(\frac{[33a]}{[6a]}\right)$ versus log [H₂O] gives $y = 0.89x + 1.29$; $K = 20 \text{ M}^{-1}$.

Trial 2 at 38°C

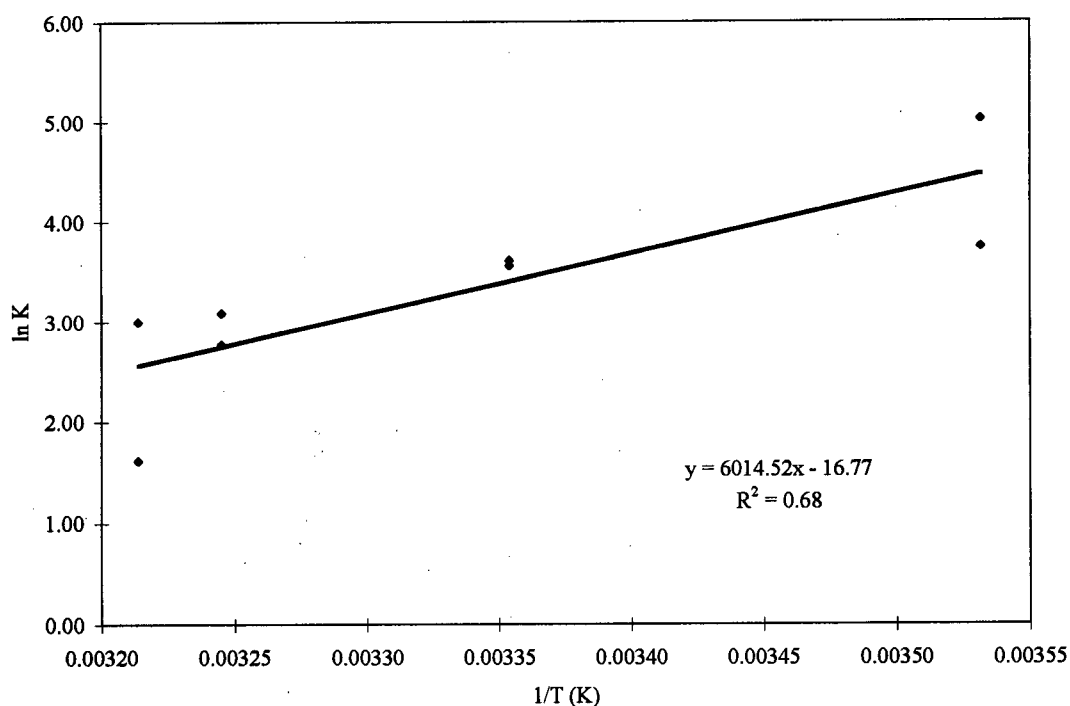
Table XII.1.8 Calculation of K at T = 38°C; 6.2×10^{-6} mol **6a** dissolved in 5.0 mL CH₂Cl₂ ([Ru]_{total} = 1.25×10^{-3} M); absorbances monitored at λ_{max} = 678 nm; A_0 = 0.60, A_{∞} = 0.085 (estimated from a flat baseline between λ = 550 to 820 nm).

H ₂ O added (μ L)	[H ₂ O] (M)	log [H ₂ O]	A at λ_{max} = 678 nm	$\frac{[33a]}{[6a]}$	$\log \frac{[33a]}{[6a]}$
0.0	0.0000	-	0.60	0.00000	-
1.0	0.0111	-1.95	0.55	0.10753	-0.97
2.0	0.0222	-1.65	0.47	0.33766	-0.47
3.0	0.0333	-1.48	0.44	0.45070	-0.35
5.0	0.0555	-1.26	0.39	0.68852	-0.16
7.0	0.0777	-1.11	0.38	0.74576	-0.13
10.0	0.1110	-0.95	0.37	0.80702	-0.09
12.0	0.1332	-0.88	0.36	0.87273	-0.06

Plot of plot of $\log\left(\frac{[33a]}{[6a]}\right)$ versus log [H₂O] gives $y = 0.78x + 0.70$; $K = 5 \text{ M}^{-1}$.

Table XII.1.9 Equilibrium constants for the reversible formation of **33a** at various temperatures (K obtained from Tables XII.1.1 - XII.1.9).

Temp (°C)	1/T (K)	K	ln K
10	0.003532	42	3.74
10	0.003532	151	5.02
25	0.003354	37	3.61
25	0.003354	35	3.56
35	0.003245	16	2.77
35	0.003245	22	3.09
38	0.003214	20	3.00
38	0.003214	5	1.61

**Figure XII.1** Van't Hoff plot for the reversible formation of $\text{RuCl}_2(\text{P-N})(\text{PPh}_3)(\text{OH}_2)$ **33a**.

Estimated thermodynamic parameters from the above plot are:

$\Delta H^\circ = -50 \pm 20 \text{ kJ/mol}$; $\Delta S^\circ = -140 \pm 40 \text{ J/mol K}$; $\Delta G^\circ = -8.9 \pm 0.2 \text{ kJ/mol}$ (25°C, based on $K = 37 \pm 2 \text{ M}^{-1}$).

XII.2 Calculations in C₆H₆

Table XII.2.1 Calculation of K at T = 25°C; 6.0×10^{-6} mol **6a** dissolved in 5.0 mL C₆H₆ ($[\text{Ru}]_{\text{total}} = 1.20 \times 10^{-3}$ M); absorbances monitored at $\lambda_{\text{max}} = 682$ nm; $A_0 = 0.50$, $A_{\infty} = 0.090$ (estimated from a flat baseline between $\lambda = 550$ to 820 nm).

H ₂ O added (μL)	[H ₂ O] (M)	log [H ₂ O]	A at $\lambda_{\text{max}} = 682$ nm	$\frac{[\text{33a}]}{[\text{6a}]}$	$\log \frac{[\text{33a}]}{[\text{6a}]}$
0.0	0.0	-	0.50	0.00001	-5.00
0.5	0.0056	-2.26	0.35	0.50333	-0.30
1.0	0.0111	-1.95	0.30	0.88328	-0.05
2.0	0.0222	-1.65	0.25	1.37334	0.14
3.0	0.0333	-1.48	0.21	2.08413	0.32
4.0	0.0444	-1.35	0.18	3.04990	0.48
7.0	0.0776	-1.11	0.17	3.4629	0.54

Plot of plot of $\log \left(\frac{[\text{33a}]}{[\text{6a}]} \right)$ versus log [H₂O] gives $y = 0.77x + 1.45$; $K = 28 \text{ M}^{-1}$.*

*Determination of K in C₆H₆ is more difficult and less accurate than in CH₂Cl₂ because water has a lower solubility in C₆H₆ (0.0356 M, 25°C)¹ than in CH₂Cl₂ (0.128 M, 25°C).²

XII.3 Calculations in Acetone (Assuming acetone is **not** involved in the aquo equilibrium system)

Table XII.3.1 Calculation of K at T = 25°C; 5.6×10^{-6} mol **6a** dissolved in 5.0 mL acetone ($[\text{Ru}]_{\text{total}} = 1.12 \times 10^{-3}$ M); absorbances monitored at $\lambda_{\text{max}} = 684$ nm; $A_0 = 0.16$, $A_{\infty} = 0.067$ (from fully formed **33a**).

H ₂ O added (μL)	[H ₂ O] (M)	log [H ₂ O]	A at $\lambda_{\text{max}} = 684$ nm	$\frac{[\text{33a}]}{[\text{6a}]}$	$\log \frac{[\text{33a}]}{[\text{6a}]}$
0.0	0.0	-	0.16	0.02119	-1.67
2.0	0.0222	-1.65	0.15	0.12414	-0.91
8.0	0.0888	-1.05	0.13	0.40271	-0.40
14.0	0.1554	-0.81	0.12	0.68784	-0.16
24.0	0.2664	-0.57	0.11	1.32908	0.12
34.0	0.3775	-0.42	0.10	1.80882	0.26
54.0	0.5995	-0.22	0.09	3.34376	0.52
84.0	0.9326	-0.03	0.07	13.32974	1.12
124.0	1.3766	0.14	0.07	83.54545	1.92

Plot of plot of $\log \left(\frac{[\text{33a}]}{[\text{6a}]} \right)$ versus log [H₂O] gives $y = 0.99x + 0.69$; $K = 5 \text{ M}^{-1}$.

1. IUPAC Solubility Data Series, Volume 37, Hydrocarbons with Water and Seawater Part I: Hydrocarbons C₅ to C₇; Kertes, A. S., Ed. Pergamon Press: Toronto, 1989, p. 95.
2. IUPAC Solubility Data Series, Volume 60, Halogenated Methanes with Water; Horváth, A. L.; Getzen, F. W., Eds.; Oxford University Press: Oxford, 1995, p. 153.

XII.4 Calculations in THF (Assuming THF is **not** involved in the aquo equilibrium system)**Table XII.4.1** Calculation of K at $T = 25^\circ\text{C}$; 5.9×10^{-6} mol **6a** dissolved in 5.0 mL THF ($[\text{Ru}]_{\text{total}} = 1.19 \times 10^{-3}$ M); absorbances monitored at $\lambda_{\text{max}} = 674$ nm; $A_0 = 0.12$, $A_\infty = 0.032$ (from fully formed **33a**).

H ₂ O added (μL)	[H ₂ O] (M)	log [H ₂ O]	A at $\lambda_{\text{max}} = 674$ nm	$\frac{[\text{33a}]}{[\text{6a}]}$	log $\frac{[\text{33a}]}{[\text{6a}]}$
0.0	0.0	-	0.119	0.00952	-2.02
2.0	0.0222	-1.65	0.083	0.70940	-0.15
4.0	0.0444	-1.35	0.074	1.10577	0.04
10.0	0.1110	-0.95	0.060	2.16775	0.34
20.0	0.2220	-0.65	0.051	3.62185	0.56
40.0	0.4441	-0.35	0.046	5.36758	0.73
90.0	0.9992	0.00	0.040	10.01377	1.00
190.0	2.1094	0.32	0.040	10.01377	1.00
390.0	4.3297	0.64	0.035	24.73099	1.39
590.0	6.5501	0.82	0.036	22.91304	1.36
890.0	9.8807	0.99	0.033	96.77778	1.99
1190.0	13.2112	1.12	0.033	134.38462	2.13

Plot of plot of $\log\left(\frac{[\text{33a}]}{[\text{6a}]}\right)$ versus $\log [\text{H}_2\text{O}]$ gives $y = 0.64x + 0.94$; $K = 9 \text{ M}^{-1}$.

APPENDIX XIII

Thermodynamic Calculations and Data for the Reversible Formation of

Cis-RuX₂(P-N)(PR₃)(η²-H₂) in C₆D₆

For the equilibrium:



$$K = \frac{[\mathbf{36}]}{[\mathbf{6a}][\text{H}_2]} \quad (2)$$

Table XIII.1 Integrations Used for Equilibrium Calculations

Value of Integration	Signal(s), ppm	Reasonance(s)	Number of Protons
α	3.78	NMe of 36	3
β	3.07	NMe ₂ of 6a	6
ω	4.44	uncoordinated H ₂	2

Sample preparation for analysis was as follows: C₆D₆ was vacuum transferred into an NMR tube containing a solid sample of **6a** (0.0163 M). The sample is warmed to r.t., and 1 atm H₂ is added; then the sample is shaken for ~ 2 min to take up H₂, when the sample is again placed under 1 atm H₂.

$$x = \frac{[\mathbf{36}]}{[\mathbf{6a}]} = \frac{\alpha / 3}{\beta / 6} \quad (3)$$

$$y = \frac{[\mathbf{36}]}{[\text{H}_2]} = \frac{\alpha / 3}{\omega / 2} \quad (4)$$

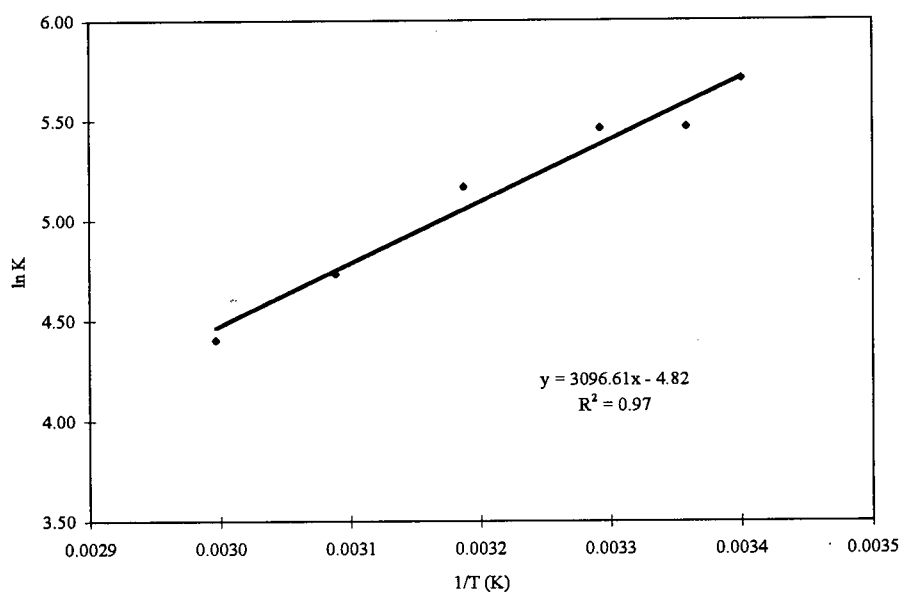
$$[\mathbf{6a}] = \frac{[\text{Ru}]_{\text{total}}}{1 + x} \quad (5)$$

$$[\mathbf{36}] = [\text{Ru}]_{\text{total}} - [\mathbf{6a}] \quad (6)$$

$$[\text{H}_2] = \frac{[\text{36}]}{y} \quad (7)$$

Table XIII.2 Integration Values and Equilibrium Concentration Ratios (α , β and ω)

T (°C)	1/T (K)	α	β	ω	x	y	[6a]	[36]	[H ₂]	K	ln K
20.9	0.00340	2.30	8.05	0.49	0.57	3.13	0.0104	0.0059	0.0019	302	5.71
24.6	0.00336	2.20	8.00	0.59	0.55	2.49	0.0105	0.0058	0.0023	236	5.47
30.6	0.00329	1.81	7.35	0.47	0.49	2.57	0.0109	0.0054	0.0021	235	5.46
40.6	0.00319	1.51	7.15	0.50	0.42	2.01	0.0115	0.0048	0.0024	176	5.17
50.6	0.00309	1.10	7.06	0.52	0.31	1.41	0.0124	0.0039	0.0027	113	4.73
60.6	0.00300	1.07	7.40	0.69	0.29	1.03	0.0126	0.0037	0.0035	82	4.40

**Figure XIII.1** Van't Hoff plot for the equilibrium $(6a + \text{H}_2 \rightleftharpoons 36)$ in C_6D_6 .